ROVIBRATIONAL CHARACTERIZATION OF INORGANIC MOLECULES AT THE INTERSECTION OF ATMOSPHERIC AND INTERSTELLAR CHEMISTRY

A Dissertation
presented in partial fulfillment of requirements
for the degree of Doctor of Philosophy
in the Department of Chemistry & Biochemistry
The University of Mississippi

by

C. Zachary Palmer

May 2025

Copyright C. Zachary Palmer 2025
ALL RIGHTS RESERVED

ABSTRACT

The chemical environments and processes of the Earth's atmosphere, the interstellar medium, and circumstellar media remain relatively understudied despite the vast molecular material available therein. Despite the advancements of emerging spectroscopic technologies, there is still a lack of reliable reference data for potential atmospheric, inter-, or circumstellar molecular species. Therefore, accurate prediction of rovibrational spectral constants is crucial for enabling current and emerging spectroscopic technologies to detect elusive inorganic molecules both within and beyond the terrestrial veil. Recent advancements in computational methodology have significantly reduced computational time while simultaneously improving the accuracy of these spectral constants. The present work highlights recent progress of computational techniques as they apply to highly accurate theoretical spectroscopy for predicting rovibrational spectral constants relevant to both interstellar and atmospheric chemistry.

DEDICATION

This work is dedicated to the students who were never given a chance ...

ACKNOWLEDGEMENTS

First and foremost, I would like to acknowledge my Lord and Savior, Jesus Christ, for His earthly and heavenly example and for His ultimate sacrifice on the cross for the sins of the world. Without my God and my Lord, I would not have had the opportunity to even attempt to understand the vast complexity of His creation. *Psalms 19:1-4*

In all honesty, my acknowledgments could be as long as this entire document, but for the sake of brevity, I can only name so many people. If you are reading this and your name is not mentioned, please know that you, too, were likely acknowledged in my thoughts.

I would like to express my deepest gratitude to my wonderful, loving, and supportive wife, Samantha. She has been by my side from the very beginning and will remain with me until the end. Samantha, I love you. Thank you for standing by me through thick and thin, especially during the long hours required for the successful completion of this work. I also want to acknowledge my incredible parents, Darren and Angie Palmer, for modeling what it means to be hardworking and dedicated, no matter the circumstances. These qualities have been, and continue to be, instrumental in shaping my journey, both to this point and wherever I go in the future. Additionally, I want to recognize my two brothers, William and Jonathan, who are not only family but also some of my best friends. You are the best brothers anyone

could ask for, and I love you both dearly. I also want to acknowledge my friends who might as well be my brothers: Connor Thom, Truett Nicholson, Taz Caldwell, and John Buchman. Each of you has supported me in your own way throughout this process, and for that, I will always be grateful. To my entire family, your ever-present love has been a constant source of strength, and I am deeply thankful for each of you. Lastly, I want to honor those I have lost along the way. Uncle Ricky, Uncle Barry, Aunt Kim, and Haley... you will never be forgotten. I look forward to seeing you again someday.

I would like to acknowledge my community of faith at The Orchard, whose support has been instrumental in my continued spiritual growth and discipline. Their constant encouragement and prayers have meant more than I can express. I am also deeply grateful to Earnie and Jane Allen, whose mentorship, guidance, prayers, and friendship transcended generations, forming a bond I will always cherish.

I want to extend my heartfelt appreciation to my advisor and friend, Dr. Ryan C. Fortenberry, for recognizing my potential and giving me the opportunity to see it for myself. Who knew that one random conversation on a September afternoon in Statesboro, GA, would mark the beginning of a lifetime in the making? Likewise, I am grateful to the rest of my committee: Dr. Nathan I. Hammer, whose physical chemistry REU program first introduced me to the University of Mississippi; Dr. Gregory S. Tschumper, who took a chance on me and funded my first summer REU, during which he and his group helped develop my computational chemistry skills; Dr. Steven R. Davis, whose vast knowledge of quantum chemistry is truly inspiring and whose lighthearted conversations always brightened my day; Dr. Breese Quinn,

whose support and kindness during my committee meetings were always appreciated.

I also want to acknowledge the past and present members of my research group, especially Brent R. Westbrook, one of my greatest friends, a great gym buddy, and my seasonal coding instructor. Brent, you truly don't know how much I value our friendship. I also appreciate former group members Taylor J. Santaloci and Megan C. Davis for their mentorship in different ways. To my friend and colleague, Dr. Vince J. Esposito, for his constant support and love. To my fellow graduate colleagues, Athena R. Flint, Rebecca A. Firth, and Taylor C. Cole, life will never quite be the same without you just feet away. Thank you all for your support and love. I hope you know it is always reciprocated. I also acknowledge the undergraduates who are still here or have since moved on to bigger and better things, namely (in no particular order) Jon R. Dotson, Ally G. Watrous, Noah R. Garrett, E. Michael Valencia, Austin M. Wallace, Nathaniel Carlson, Jacob A. Johns, and Kailey Bell. While I only had the opportunity to directly mentor some of you, it was a pleasure meeting each of you and being part of your stories. Additionally, I want to acknowledge Dr. Tschumper's former group members, Drs. Carly Rock, Morgan Perkins, Kayleigh Barlow, Jackie Mosely, and Thomas Sexton, for their love and support through both the good times and the difficult ones. I will always miss wasting time and cutting up in y'all's office.

I would like to acknowledge the funding agencies and grants that supported this work: NASA grants NNH22ZHA004C, 80NSSC24M0132, 22-A22ISFM-0009, and NNX17AH15G, and the NSF grant OIA-1757220. Additionally, I want to acknowledge the Mississippi Center for Supercomputing Research for their computa-

tional resources that made this work possible.

Finally, I want to recognize the tremendous effort and care that Dr. Brent R. Westbrook put into formulating, writing, and maintaining the push-button quartic force field (PBQFF) framework. Without PBQFF, the last three years of my life would quite literally not have been possible. I will forever be grateful for this contribution and will never take it for granted.

TABLE OF CONTENTS

LIST OF TABLES

LIST OF FIGURES

CHAPTER 1

INTRODUCTION

1.1 Motivation

In the late 1930s into 1940, the first three interstellar molecules, CH^+, CH, and CN, were detected[6–8] after comparing known, laboratory-derived, optical, molecular absorption features against interstellar cloud spectra. However, further detections of interstellar species slowed over the next 20 years as astrophysicists theorized that diatomic molecules were the only expected molecular contributors to spectral surveys of astronomical bodies.[9,10] This diatomic theory remained through the next molecular detection in 1963, the OH radical, in the radio absorption spectra of Cassiopeia A.[11] However, toward the end of the 1960s, this diatomic paradigm began to shift with the confirmed detection of polyatomic molecules, namely NH_3 and H_2O, in radio emission spectra observed towards the galactic center and Sagittarius B2, respectively.[12,13] As interstellar observations began to incorporate molecules beyond diatomics, astrophysicists and chemists devoted their efforts to determining the origin and abundance of these molecules to better understand the physical universe through the lens of chemistry.

The application of molecular spectroscopy to the field of astrochemistry bridges the gap between astrophysical sources and earth-bound laboratories.[14,15] As stated previously, radio astronomy brought about the lens change with which the universe was viewed. In fact, many of the gas-phase molecules that have been observed are mostly identified through ground-based rotational telescopes.[9,16] Notably, the largest

radio observational telescope in the world is the *Atacama Large Millimeter/submillimeter Array* (ALMA) and offers rotational spectroscopic capabilities with a high degree of resolution, sensitivity and spectral range.[17,18] Additionally, due to the nature of rotational spectroscopy, most astronomical regions provide sufficient energies to populate even the lowest of rotational levels of most molecular compounds.[19] Therefore, a rotational line survey of any given astronomical source produces a vast quantity of complex signatures painting a picture of the chemical composition within.[18]

While radio astronomy has been instrumental in detecting much of the available astronomical molecular catalog,[20] it cannot probe the entire electromagnetic spectrum. In recent years, advancements in infrared (IR) spectroscopic technologies, specifically in air- and space-based observatories, have expanded the ability to explore interstellar and circumstellar environments. This is exemplified by the *James Webb Space Telescope* (JWST), which enables more efficient and comprehensive spectral probing of astronomical sources in the near-to-mid IR.[21,22] Additionally, while radio astronomy and IR spectroscopy are distinct techniques, they provide complementary insights into the molecular composition of astronomical environments. For instance, if a molecule contains a permanent dipole moment, it can exhibit both microwave and IR transitions. As a result, spectral line lists of astrophysical sources can now be pruned of known molecular transitions in the microwave and IR regimes, painting an even fuller picture of the richer chemical composition covered up by the most abundant molecules. There is precedent for such assignments in microwave and IR regions, namely hydrogen isocyanide[23] and methyl formate.[24] However, molecules that lack permanent dipole moments will not exhibit microwave emission, though they may still undergo IR transitions. These molecules range from polycyclic aromatic hydrocarbons (PAHs) to simple gas-phase compounds that have depleted onto

the surface of dust grains or interstellar ice, both of which remain active areas of astrochemical research. Thus, IR technologies serve as an essential tool for detecting these "rotationally dark" molecules.[15,25]

The same spectroscopic techniques that assist astrochemical research are equally critical for probing Earth's atmosphere, where pollution and metal species contribute to the complex chemical environment.[26–28] Detecting and quantifying the molecular composition of the atmosphere is therefore crucial. The Cloud-Aerosol LiDAR and Infrared Pathfinder Satellite Observation (CALIPSO)[29] monitors the Earth's IR spectrum, while the Aqua satellite[30] provides rotational spectroscopic data. Together, these methods help track both known and emerging pollutants, including reactive radicals, oxidizing compounds, and metal ions that contribute to complex atmospheric chemistry. The effects of some of these metals remain uncertain, emphasizing the need for continued spectroscopic analysis to better understand their role in air quality and climate.

An inevitable consequence of the advancements in the sensitivity and resolution of rotational and IR spectroscopic technologies is the realization of the vast number of spectral lines that remain unassigned.[18] Of course, a portion of these spectral lines have been accounted for by the backlog of laboratory spectral data collected in decades past. However, even after identifying the known transitions of established molecules in spectral surveys, many of these molecules may exhibit additional transitions in other spectral regions that are challenging to characterize through laboratory studies.[15,31] Without the ability to separate these unknown transitions of known molecules, further observation of novel molecules and compounds is experimentally impeded. Thus, a technique for generating spectral data of both known and unknown molecules is warranted in order to continue answering fundamental astrochemical questions.

When laboratory experiments are unable to produce rovibrational spectral data, quantum chemical predictions often thrive in filling this gap. Even as early as the 1970s, early quantum chemical techniques, as discussed in Section 1.2, were used to predict the rotational constants of various molecules and compounds for comparison with astrophysical line surveys.[32–36] A key advantage of computational quantum chemistry is its ability to predict the pure rovibrational spectra of a given molecule without influence of impurities that may affect experimental data.[37] Furthermore, computational techniques can predict the structure and spectra of a vast array of molecules, adhering to the principles of terrestrial, interstellar, and circumstellar chemistry. These advantages make computational quantum chemistry an invaluable tool in the field of astrochemistry and atmospheric chemistry.

However, the ability to predict spectral data does not inherently guarantee its accuracy or reliability. Therefore, careful consideration must be given when selecting a level of theory that is both precise and broadly applicable for this purpose. As previously mentioned, observational and laboratory spectroscopic capabilities have significantly improved in accuracy over recent decades. As these technologies advance, computational techniques must also be refined and updated to remain effective in the prediction of spectral data. Modern computational quantum chemical methods have reached a level where their predictions closely align with experimental results,[16,18,38–42] solidifying its roles as an independent astrochemical technique. However, their continued relevance depends on rigorous benchmarking and its successful application to atmospheric and astrochemical research.

The present work showcases some of these more recent computational methods and techniques as well as how they are applied to the fields of atmospheric chemistry and astrochemistry. The first evolution showcased herein (Ch. 2) compares the accuracies of long-standing and more recent coupled cluster methods as they pertain

to providing reference rovibrational data for novel sulfur-bearing compounds in the interstellar medium (ISM) and circumstellar media (CSM). Then, in Ch. 3, these more recent coupled cluster methods are further improved upon and applied to the prediction of rovibrational reference data for a novel, elusive fluorine-containing peroxide that may be present both in the ISM and CSM as well as Earth's atmosphere. Next, Chs. 4 & 6 both explore formation pathways and rovibrational spectral predictions of aluminum nitrides within CSM. These chapters assume different starting material, but are both based on a previous experimental study of the Murchison CM2 chondritic carbonaceous meteorite.[43] Finally, Ch. 5 benchmarks 10 different levels of theory on different aluminum-bearing systems to identify a single level of theory that most accurately predicts their rovibrational spectral data, and how this level of theory affects the computational accuracy in Ch. 6. Each of the studies conducted herein represents the advancements made in computational predictions of rovibrational spectral data that serve as reference or complementary data for further astrophysical detection of molecules contributing to the chemical composition of Earth's atmosphere and the broader cosmos.

1.2 Quantum Chemistry

The rovibrational spectral data produced in this work are all based on electronic structure theory computations, which in turn are built upon by quantum chemistry. The quintessential quantum chemical problem lies in solving the Schrödinger equation:

$$\hat{H}\Psi = E\Psi. \tag{1.1}$$

The Schrödinger equation is inherently an eigenvalue equation that yields the energy E when the Hamiltonian operator $\hat{H}$ is applied to a given wave function Ψ. To effectively solve for the energy of a desired molecular system, the form of $\hat{H}$ must

adequately account for interactions of electrons and nuclei in a three-dimensional space. Thus, the form of $\hat{H}$ for N electrons and M nuclei, in atomic units, is given by:[44]

$$\hat{H} = -\sum_{i}^{N} \frac{1}{2}\nabla_i^2 - \sum_{A}^{M} \frac{1}{2M_A}\nabla_A^2 - \sum_{i}^{N}\sum_{A}^{M} \frac{Z_A}{r_{ia}} + \sum_{i}^{N}\sum_{j>i}^{N} \frac{1}{r_{ij}} + \sum_{A}^{M}\sum_{B>A}^{M} \frac{Z_A Z_B}{R_{AB}} \quad (1.2)$$

In Eq. 1.2, the Laplacian, $\nabla^2_{i\ or\ A}$ is the differentiation operator with respect to the positions of a given electron or nucleus in three-dimensional space. The first term in Eq. 1.2 corresponds to the kinetic energy of the electrons, the second term to the kinetic energy of the nuclei, the third term to the attraction between the electrons and nuclei, the fourth term to the repulsion between electrons, and the last term to the repulsion between the nuclei. Additionally, this work considers the non-relativistic, time-independent Schrödinger equation as its solutions represent physical situations where the probability density of a given wave function does not vary with time.[45] Consequently, the complete energy of a molecular system is determined without accounting for the motion of the nuclei. Within the venerated Born-Oppenheimer approximation, $\hat{H}$ can be simplified by neglecting the second term and reducing the fifth term to a constant.[44] Effectively, the electrons move within a fixed field of nuclei. This approximation yields an electronic $\hat{H}$:

$$\hat{H} = -\sum_{i}^{N} \frac{1}{2}\nabla_i^2 - \sum_{i}^{N}\sum_{A}^{M} \frac{Z_A}{r_{ia}} + \sum_{i}^{N}\sum_{j>i}^{N} \frac{1}{r_{ij}}. \quad (1.3)$$

While the Born-Oppenheimer approximation allows for a radical simplification of $\hat{H}$, Eq. 1.3 remains nontrivial when solving for the energy of wave functions beyond hydrogen-like systems.

However, further approximations can be considered for the Schrödinger equation, particularly in the choice of wave function. Since the exact wave function for

molecular systems has not yet been mathematically derived, it must be approximated by a finite set of linearly combined functions (ϕ_i) and their expansion coefficients c_i, which together serve as a mathematical representation of the atomic orbitals:

$$\Psi \approx \sum_i c_i \phi_i. \tag{1.4}$$

Early basis sets were derived from hydrogen-like orbitals but were not efficiently extrapolated to larger atomic or molecular systems. However, basis functions for Slater-type orbitals (STOs) were developed, providing a more accurate description to the atomic orbitals (AOs) around atomic or diatomic species.[46] The definition of the 1s STO is given in Eq. 1.5, where the Slater orbital exponent ζ and the center of the oribtal on the atom $\mathbf{R}_a$ are specified:[44]

$$\phi_{1s}(\zeta, \mathbf{r} - \mathbf{R}_a) = (\zeta^3/\pi)^{1/2} e^{-\zeta|\mathbf{r}-\mathbf{R}_a|} \tag{1.5}$$

While STOs are the natural choice for constructing AOs, the sheer number of the two-electron integrals that must be computed and stored for an electronic structure computation grows on the order of $K^4/8$, where K is the number of Slater functions.

Differently, utilizing Gaussian-type Orbitals (GTOs) circumvents these higher order integrals and is given in Eq. 1.6 where α is the Gaussian orbital exponent.

$$\phi_{1s}(\alpha, \mathbf{r} - \mathbf{R}_a) = (2\alpha/\pi)^{3/4} e^{-\alpha|\mathbf{r}-\mathbf{R}_a|^2}. \tag{1.6}$$

As the product of two Gaussian functions centered on different atoms results in a separate Gaussian function on a third center, the costly four-center, two-electron integrals required for STOs can be efficiently reduced to two-center, two-electron integrals.[44,46] However, a single GTO does not equate the STO's more accurate

description of electronic probability both near and far way from the nucleus.[45] The accuracy of STOs can be partially recovered by combining multiple GTOs to approximate a single STO. For example, a minimal basis set such as STO-NG[47] constructs an STO from N GTOs. Thus, approximating the exact wave function with a set of basis functions allows for the systematic improvement when a more accurate description of the electronic wave function is required. Larger basis sets, such as 6-31G, were introduced soon after the STO-NG basis set[48] but are now primarily used for very large chemical systems. In contrast, Dunning introduced basis sets like cc-pVDZ in 1989.[49] These basis sets have seen significant improvement over the years and can more accurately describe the electronic structure of molecular systems, including those in the present work.

1.2.1 The Hartree-Fock Procedure

So far in the present section, approximations have been made to both the Hamiltonian operator and the wave function to facilitate a more efficient solution to the Schrödinger equation. However, the first approximation to solving the Schrödinger equation is most often the Hartree-Fock (HF) or self-consistent field (SCF) method. Perhaps the most important approximation employed by the HF method is the further simplification of the electronic Hamiltonian, where the electron-electron repulsion term is approximated as the interaction of each electron with an average potential field created by the presence of all other electrons.

1.2.1.1 The Slater Determinant HF Procedure

Traditionally, the HF method is defined as the variational optimization of the energy expectation value of a single Slater determinant under the constraint of spin orthonormality.[44] As the HF method follows the variational principle, the expectation value of the Hamiltonian is always an upper bound to the true ground

state energy of the normalized wave function,

$$\frac{\langle \Phi | H | \Phi \rangle \geq E_0}{\langle \Phi | \Phi \rangle} \tag{1.7}$$

Physically, this implies that lower eigenvalues E_i for H provide more accurate approximations. In the context of the HF method, the variational principle ensures the iterative refinement of ground-state energies toward greater accuracy.

The variational optimization in the traditional HF method begins with a "trial" single-determinant wave function, from which the energy is computed:

$$E_0 = \langle \Phi_0 | H | \Phi_0 \rangle . \tag{1.8}$$

The eigenvalue of H for this wave function allows for the construction of the HF equation, which has the general form:

$$f(1)\chi(\mathbf{x}_i) = \epsilon\chi(\mathbf{x}_i). \tag{1.9}$$

The one-electron Fock operator $f(1)$ mimics the Hamiltonian operator from the previous section and is defined as

$$f(1) = -\frac{1}{2}\nabla_1^2 - \sum_A^M \frac{Z_A}{r_{1A}} + v^{\mathrm{HF}}(1), \tag{1.10}$$

where

$$v^{\mathrm{HF}}(1) = \sum_b J_b(1) - K_b(1). \tag{1.11}$$

In Eq. 1.11, $J_b(1)$ and $K_b(1)$ correspond to the Coulomb and exchange operators, respectively. The $J_b(1)$ operator represents the average local potential due to an electron, while the $K_b(1)$ operator naturally arises as a consequence of an antisym-

metrized single determinant wave function. Both the $J_b(1)$ and $K_b(1)$ operators are formally defined in Eqs. 1.12 & 1.13.

$$J_b(1) = \int d\mathbf{x}_2 \chi_b^*(2) r_{12}^{-1} \chi_b(2) \tag{1.12}$$

and

$$K_b(1) = \int d\mathbf{x}_2 \chi_b^*(2) r_{12}^{-1} \chi_a(2) \tag{1.13}$$

As the HF potential, in Eq. 1.11, depends upon the spin orbitals that define the wave function, the HF procedure must be solved iteratively to approximate the HF potential field until a newly generated potential field is virtually similar to the previously generated potential field according to a predetermined convergence criterion. This newly generated potential field provides optimized spin orbitals, or spatial orbitals if the linearly combined AOs (LCAO) forming the molecular orbitals (MOs) (LCAO-MOs) allow, which can then be used to satisfy Eq. 1.8 via Eq. 1.9 through self-consistency.

1.2.1.2 The Roothaan-HF Procedure

Thus far in this section, the HF equations and the self-consistent HF potential have been solved with respect to a general set of spin orbitals arising from single Slater determinant wave functions. Unfortunately, this procedure is not easily extendable to molecules,[45] which is essential for accurate spectral predictions. However, Roothaan demonstrated that spatial basis functions, like those shown in Eq. 1.4, could be easily converted into algebraic equations, solved using standard matrix techniques, and iteratively refined to determine the lowest possible SCF energy for a given trial wave function.[44,50] To leverage Roothaan's approach, a trial wave function is first chosen as a set of known basis functions that reasonably represent the LCAO-MOs

of a system, where μ are the MOs on the ith electron:

$$\psi_i = \sum_{\mu=1}^{K} C_{\mu i}\phi_\mu \qquad i = 1, 2, \cdots, K. \tag{1.14}$$

This choice of basis set follows Roothaan's impetus by reducing the calculation of the HF MOs to a simple calculation of the set of corresponding expansion coefficients from Eq. 1.14, $C_{\mu i}$. Introducing the basis functions into the HF equations yields the Roothaan-HF equation and is similar in form to Eq. 1.9:

$$f(1)\sum_{\nu} C_{\nu i}\phi_i(1) = \epsilon_i \sum_{\nu} C_{\nu i}\phi_i(1). \tag{1.15}$$

As Eq. 1.15 is itself not a matrix equation, it must be multiplied on the left by $\phi^*_\mu(1)$ and integrated to yield the matrix form

$$\sum_{\nu} C_{\nu i} \int d\mathbf{r}_1 \phi^*_\mu(1) f(1) \phi_i(1) = \epsilon_i \sum_{\nu} C_{\nu i} \int d\mathbf{r}_1 \phi^*_\mu(1)\phi_i(1). \tag{1.16}$$

However, Eq. 1.16 can be further refined by defining two more matrices,

$$S_{\mu\nu} = \int d\mathbf{r}_1 \phi^*_\mu(1)\phi_\nu(1) \tag{1.17}$$

and

$$F_{\mu\nu} = \int d\mathbf{r}_1 \phi^*_\mu(1) f(1) \phi_\nu(1). \tag{1.18}$$

With these new definitions, Eq. 1.16 can be rewritten in a similar eigenvalue equation form:

$$\mathbf{FC} = \mathbf{SC}\epsilon. \tag{1.19}$$

In Eq. 1.19, $\mathbf{C}$ is a square matrix of the expansion coefficients, $C_{\mu i}$, from Eq. 1.14

and ϵ is a diagonal matrix of the molecular orbital energies. The Fock matrix $\mathbf{F}$ is of similar form to the previous Fock operator from Eq. 1.10 but is adapted to include the choice of spatial basis functions and is defined as

$$F_{\mu\nu} = H_{\mu\nu}^{core} + G_{\mu\nu}. \tag{1.20}$$

$H_{\mu\nu}^{core}$ is the core Hamiltonian matrix and is comprised of one electron integrals describing the kinetic energy and nuclear-electron attraction

$$H_{\mu\nu}^{core} = T_{\mu\nu} + V_{\mu\nu}^{nucl}, \tag{1.21}$$

where

$$T_{\mu\nu} = \int d\mathbf{r}_1 \phi_\mu^*(1) \Big[-\frac{1}{2}\nabla_1^2 \Big] \phi_\nu(1), \tag{1.22}$$

and

$$V_{\mu\nu} = \int d\mathbf{r}_1 \phi_\mu^*(1) \Big[-\sum_A \frac{Z_A}{|\mathbf{r}_1 - \mathbf{R}_A|} \Big] \phi_\nu(1). \tag{1.23}$$

Returning to Eq. 1.20, $G_{\mu\nu}$ is the two-electron portion defined as

$$G_{\mu\nu} = \sum_{\lambda\sigma} P_{\lambda\sigma} \Big[(\mu\nu|\sigma\lambda) - \frac{1}{2}(\mu\lambda|\sigma\nu) \Big] \tag{1.24}$$

where

$$P_{\mu\nu} = 2 \sum_a^{N/2} C_{\mu a} C_{\nu a}^* \tag{1.25}$$

is the charge density matrix and is directly related to the expansion coefficients of the basis functions.

Before the Roothaan-HF can be solved for the orbital energies of the wave function, the basis set must be orthogonalized.[44] A straightforward choice for orthogonalization is to use the inverse square roots of the overlap matrix $\mathbf{S}$. This involves

the diagonalization of $\mathbf{S}$ which yields the diagonal matrix of eigenvalues $\mathbf{s}$. The new orthogonalization matrix can then be constructed by

$$\mathbf{S}^{-1/2} = \mathbf{U}\mathbf{s}^{-1/2}\mathbf{U}^{\dagger}. \tag{1.26}$$

When the basis set is orthogonalized, the initial guess to $\mathbf{F}$ from Eq. 1.20 can be made by approximating $P_{\mu\nu}$ as zero and solving

$$\mathbf{F}_0^{'} = \mathbf{S}^{\dagger -1/2}\mathbf{H}^{core}\mathbf{S}^{-1/2}. \tag{1.27}$$

Once $\mathbf{F}_0^{\prime}$ is diagonalized, a new set of orthogonal expansion coefficients, $\mathbf{C}^{\prime}$, are obtained and can be made non-orthogonal through

$$\mathbf{C} = \mathbf{S}^{-1/2}\mathbf{C}_0^{'} \tag{1.28}$$

which are now usable to recompute Eq. 1.25 and solve the initial HF energy using

$$E_0 = \sum_{\mu\nu} P_{\mu\nu}(H_{\mu\nu} + F_{\mu\nu}). \tag{1.29}$$

These new expansion coefficients can also be used in Eq. 1.25 to obtain a new guess for the two electron portion of $F_{\mu\nu}$ which then initiates the SCF procedure. With this addition of $G_{\mu\nu}$ to $F_{\mu\nu}$, Eq. 1.27 will substitute the newly constructed $\mathbf{F}^{'}$ in for $\mathbf{H}^{core}$:

$$\mathbf{F}^{'} = \mathbf{S}^{\dagger -1/2}\mathbf{F}^{'}\mathbf{S}^{-1/2}. \tag{1.30}$$

The process of diagonalizing the $\mathbf{F}$ matrix to obtain new expansion coefficients, charge density matrices, and SCF energies continues until a specified convergence criterion is met, as was the case in the previous section. A typical convergence crite-

rion for SCF convergence simply compares the difference between the total electronic energies from the last two iterations. For instance, if there is a difference of less than 10^{-6} Hartrees, the energies are considered converged. However, this threshold can be lowered if greater accuracy is required to more decimal places.[44]

1.2.2 Post HF Methods

While the Roothaan-HF equations have been instrumental as initial approximations to computational solutions of the Schrödinger equation, limitations remain in this SCF procedure. The variational nature of the HF method ensures that the SCF energy is always greater than the "exact" energy, or the solution to the nonrelativistic Schrödinger equation, regardless of the basis set size. Consequently, as the number of basis functions approaches an infinite, or complete, basis set, the difference between the SCF energy and the exact energy asymptotically converges. This convergence is known as the complete basis set (CBS) limit, or the "HF limit" for the HF method. Nevertheless, the total SCF energy (E_{HF}) will always be greater than the "exact" energy (E_0). This difference is defined as the correlation energy:[44]

$$E_{corr} = E_0 - E_{HF} \tag{1.31}$$

Additionally, this discrepancy in correlation energy arises from the way electron interactions are treated within the HF procedure. While the SCF wave function enforces the antisymmetry principle for electrons occupying the same spin orbitals, it only accounts for electron interactions through an average potential field of the other electrons in the system. Consequently, the correlation of electronic motion between electrons with opposite spins is not fully captured in the HF method.[44–46] Since the accurate prediction of rovibrational spectral data depends on the electronic energy of the system, properly accounting for electron correlation is crucial in this work.

Therefore, computational methodologies that improve upon electron correlation in the HF method, known as "correlated" methods, must be employed.

1.2.2.1 Configuration Interaction

The most straightforward improvement to the HF method is the configuration interaction (CI) approach. The CI wave function is similar to the HF wave function, and is constructed by the linear combination of excited determinant wave functions. In fact, most post-HF methods utilize the HF determinant, $|\Psi_0\rangle$, that is obtained from the SCF converged orbital energies of a given finite basis set. Thus, the CI wave function can be expressed as a linear expansion by

$$|\Phi_0\rangle = c_0 |\Psi_0\rangle + \sum_{ia} c_i^a |\Psi_i^a\rangle + \sum_{i<j,a<b} c_{ij}^{ab} |\Psi_{ij}^{ab}\rangle + \cdots, \tag{1.32}$$

where $|\Phi_0\rangle$ is the exact many-electron wave function and the Ψ functions with superscripts and subscripts represent a replacement of spin orbitals based on the number of indices and are referred to as excited determinants. For example, Ψ_i^a and Ψ_{ij}^{ab} are said to be singly- and doubly-excited determinants, respectively. For n-tuply excited states, the number of excited determinants is $\binom{N}{n}\binom{2K-N}{n}$, where N is the number of occupied spin orbitals and $2K$ is the total number of spin orbitals, which is extremely large for even modestly sized chemical systems.[44]

1.2.2.2 Perturbation Theory

As the size of an electronic system grows, so too do the electron interactions that must be correlated. That being said, even at a truncated level, the CI wave function becomes too large and cannot be easily implemented computationally. Hence, a need arises for another post HF method that can easily approximate the correlation energy of a system. The most common choice for quantum chemists

is many-body perturbation theory (PT), specifically as implemented by Møller and Plesset.[51] Essentially, the total Hamiltonian is separated into the known "zeroth-order" $\hat{H}_0$ portion and some deviation, or perturbation, $\hat{V}$.[44] In eigenvalue equation form this can be written as

$$\hat{H}_0 + V \left|\Phi_i\right\rangle = E_i \left|\Phi_i\right\rangle . \tag{1.33}$$

Since the purpose is to approximate the correlation energy of the Roothaan-HF equations, the HF Hamiltonian can be chosen as the zeroth-order $\hat{H}_0$. Now, a perturbation parameter, λ is inserted into $\hat{H}$ and allows for the expansion to the exact eigenfunctions and eigenvalues through the use of a Taylor series in λ:

$$E_i = E_i^{(0)} + \lambda E_i^{(1)} + \lambda^2 E_i^{(2)} + \cdots, \tag{1.34}$$

$$\left|\Phi_i\right\rangle = \left|\Psi_i^{(0)}\right\rangle + \lambda \left|\Psi_i^{(1)}\right\rangle + \lambda^2 \left|\Psi_i^{(2)}\right\rangle + \cdots. \tag{1.35}$$

If further constraints are imposed, such that the wave functions of $\hat{H}_0$ are normalized and $\left\langle \Psi_i^{(0)} \middle| \Phi_i \right\rangle = 1$, then Eq. 1.33 can be satisfied. As the HF Hamiltonian is taken to be $\hat{H}_0$ here, the HF energy is expressed as the zeroth- and first-order terms in the expansion. Therefore, the first correction to the HF energy can be solved for in the second-order contribution:

$$E_0^{(2)} = 2 \sum_{abrs}^{N/2} \frac{\langle ij|ab\rangle \langle ab|ij\rangle}{\epsilon_i + \epsilon_j - \epsilon_a - \epsilon_b} - \sum_{ijab}^{N/2} \frac{\langle ij|ab\rangle \langle ab|ji\rangle}{\epsilon_i + \epsilon_j - \epsilon_a - \epsilon_b}, \tag{1.36}$$

where the two-electron integrals and orbital energies come from the solutions to the SCF procedure discussed previously.

1.2.2.3 Coupled Cluster Theory

One of the most accurate post-HF methods for the computation of the electronic correlation energy is coupled cluster (CC) theory.[52] Much like CI, the goal of CC theory is to properly treat the effects of electron correlation through the expansion of the wave function. However, CI is a linear expansion to the wave function, whereas CC theory is an exponential expansion and introduces a "cluster" operator $\hat{T}$, defined as

$$\Psi_{CC} = e^{\hat{T_n}} \left|\Phi_0\right\rangle, \tag{1.37}$$

which acts on the reference wave function, typically the HF wave function, as previously stated. One of the major benefits of CC theory compared to CI is its size-extensivity. A size-extensive method is one where the total energy of the system scales linearly with the number of electrons in the system. Additionally, CC theory benefits from being size-consistent which means that the sum of the energy of two non-interacting molecular orbital fragments is equal to the total energy of the system due to the multiplicative separability of the cluster operator.[52,53]

To better understand the nature of the cluster operator, size-extensivity, and size-consistency, second-quantization is employed to describe the wave function as

$$\Psi_0 = \left|\phi_i\phi_j\cdots\right\rangle, \tag{1.38}$$

where the creation of a new orbital ϕ_a can follow the annihilation of ϕ_i by

$$\Psi_i^a = a_a^\dagger a_i \left|\phi_i\phi_j\cdots\right\rangle = \left|\phi_a\phi_j\cdots\right\rangle. \tag{1.39}$$

Qualitatively, second quantization allows for the effective excitation of electrons in orbitals ϕ_i and ϕ_j into ϕ_b and ϕ_a.

Second quantization also permits easy descriptions of the single- and double-orbital cluster operators, which are necessary for the definition of total one- and two-orbital cluster operators, Eq. 1.40 and Eq. 1.41:

$$\hat{T_1} = \hat{t_i} = \sum_a t_i^a a_a^\dagger a_i, \tag{1.40}$$

and

$$\hat{T_2} = \hat{t_{ij}} = \sum_{a>b} t_{ij}^{ab} a_a^\dagger a_b^\dagger a_j a_i. \tag{1.41}$$

The forms of $\hat{T}_1$ and $\hat{T}_2$ follow the general description of the n-orbital cluster operator as a power series

$$\hat{T_n} = \left(\frac{1}{n!}\right)^2 \sum_{ij\cdots ab\cdots}^{n} t_{ij\cdots}^{ab\cdots} a_a^\dagger a_b^\dagger \cdots a_j a_i \tag{1.42}$$

where it can be returned to Eq. 1.37 to fully define the exponential nature of the CC wave function:

$$\Psi = e^{\hat{T}_1 + \hat{T}_2 + \cdots \hat{T}_n} \Phi_0. \tag{1.43}$$

The implicit inclusion of higher excitations levels can be more clearly seen in the commonly used CCSD expansion for a four-electron system. This CCSD expansion of the wave function is written as

$$\Psi = \left(1 + \hat{T}_1 + \frac{1}{2!}\hat{T}_1^2 + \frac{1}{3!}\hat{T}_1^3 + \hat{T}_2 + \frac{1}{2!}\hat{T}_2^2 + \frac{1}{4!}\hat{T}_1^4 + \hat{T}_2\hat{T}_1 + \frac{1}{2!}\hat{T}_2\hat{T}_1^2\right), \tag{1.44}$$

where effective triple and quadruple excitations are implicitly included. While the full CI and full CC limits will produce exact wave functions, the implicit inclusions of higher excitations provides CC theory with the major benefits as described above at a given level of truncation.

Continuing with CCSD, the expression of the CC correlation energy is defined

as

$$E_{CC} = \sum_{ia} f_{ia} t_i^a + \frac{1}{4} \sum_{ijab} \langle ij||ab\rangle \, t_{ij}^{ab} + \frac{1}{2} \sum_{ijab} \langle ij||ab\rangle \, t_i^a t_j^b. \tag{1.45}$$

In Eq. 1.45, f_{ia} is the one-electron Fock operator, while $\langle ij||ab\rangle$ are constructed from the two-electron integrals obtained in the SCF procedure. The one- and two-orbital amplitude terms, t, have been explicitly formulated and defined by Stanton et al.,[54] and are not redefined herein. Like the SCF procedure, CCSD is iterative in nature. The initial guess sets the one-orbital amplitudes to zero, while the two-orbital amplitudes are taken from the MP2 energy. The amplitudes are iteratively reformulated until self-consistency is reached, allowing the CC correlation energy to be applied to the HF energy.

1.2.2.4 Perturbative Triples within Coupled Cluster Theory

Although CCSD has been widely used in computational chemistry, Noga and Bartlett demonstrated that explicit inclusion of triples excitations in the CC expansion, CCSDT ($\hat{T} = \hat{T}_1 + \hat{T}_2 + \hat{T}_3$), is necessary to model the energy for certain systems.[55] While CCSDT offered more accuracy and rapid convergence to full CI, it was also computationally expensive for all but small systems.[56,57] To address this, approximate treatments of full triples have been developed. The widely used CCSD(T) method[56,58,59] applies a perturbative triples correction to CCSD, providing a more accurate electron correlation energy while mitigating the computational cost of full triples. The total CCSD(T) energy can be expressed as

$$E_{total} = E_{SCF} + E_{CCSD} + E_{(T)}, \tag{1.46}$$

where the first two terms have been defined previously, and $E_{(T)}$ is given by

$$E_{(T)} = \frac{1}{36} \sum_{ijkabc} t_{ijk}^{abc}(c) D_{ijk}^{abc} [t_{ijk}^{abc}(c) + t_{ijk}^{abc}(d)]. \tag{1.47}$$

In Eq. 1.47, $t_{ijk}^{abc}(c)$ and $t_{ijk}^{abc}(d)$ represent approximate triples amplitudes that consist of the predetermined doubles and singles amplitudes, respectively. These are defined as

$$t_{ijk}^{abc}(c) = \frac{1}{D_{ijk}^{abc}} P(i/jk) P(a/bc) \left[\sum_{e} t_{jk}^{ae} \langle ei||bc\rangle - \sum_{m} t_{im}^{bc} \langle ma||jk\rangle \right], \tag{1.48}$$

and

$$t_{ijk}^{abc}(d) = \frac{1}{D_{ijk}^{abc}} P(i/jk) P(a/bc) t_{i}^{a} \langle jk||bc\rangle , \tag{1.49}$$

where $D_{ijk}^{abc} = f_{ii} + f_{jj} + f_{kk} - f_{aa} - f_{bb} - f_{cc}$ and the permutation $\hat{P}$ operator is defined as $P(p/qr)f(pqr) = f(pqr) - f(qpr) - f(rqp)$. When applied to the already defined CCSD process, the higher-order CCSD(T) method provides greater accuracy in the HF correlation energy than CCSD while remaining less computationally intensive than CCSDT. In terms of scaling, HF scales as N^4, where N represents the number of orbital indices. Meanwhile, CCSD, CCSD(T), and CCSDT scale as N^6, N^6 plus one non-iterative N^7 term, and N^8, respectively.[52,60]

1.2.2.5 Explicitly Correlated CCSD(T)

All post HF methods incorporate some form of implicit electron correlation with the wave function to reduce the energy gap in Eq. 1.31. However, the traditional methods discussed above have been shown to converge slowly to the CBS limit due to the inaccurate treatment of the interelectronic Coulombic repulsion.[61,62] To counteract this slow convergence, an explicit interelectronic distance term between electron 1 and 2, $\frac{1}{r_{12}}$, was introduced by Kutzelnigg and Klopper[61] as a linear ex-

pansion operator in their MP2-R12 methodology. However, Ten-no implemented an exponential explicit correlation term into MP2 that showed more efficient correlation energy convergence compared to the linear term.[63] This exponential term was later implemented into CC theory and combined with the aforementioned CCSD method yielding the explicitly correlated CCSD-F12 method.[62]

The general form of the CCSD-F12 wave function truncates Eq. 1.43 to $\Psi = e^{\hat{T}_1+\hat{T}_2}\Phi_0$ where the single excitation operator, $\hat{T}_1$, is still Eq. 1.40, but the doubles excitation operator includes an additional $\mathcal{T}_{\alpha\beta}^{ij}$ amplitude written as

$$\hat{T}_2 = \hat{t}_{ij} + \mathcal{T}_{\alpha\beta}^{ij}, \tag{1.50}$$

where

$$\mathcal{T}_{ab}^{ij} = T_{mn}^{ij}\mathcal{F}_{\alpha\beta}^{mn} \tag{1.51}$$

$$\mathcal{F}_{\alpha\beta}^{mn} = \langle mn|F_{12}\hat{Q}_{12}|\alpha\beta\rangle \tag{1.52}$$

$$\hat{Q}_{12} = (1-\hat{o}_1)(1-\hat{o}_2)(1-\hat{v}_1\hat{v}_2). \tag{1.53}$$

The indices i, j, ... refer to occupied orbitals and a, b, ... to virtual orbitals, and α, β, ... to a complete basis set. The F_{12} term in Eq. 1.52 is the correlation factor describing the short-range interactions of pairs of electrons.[64] If higher-order coupled cluster computations are desired, the perturbative triples procedure from the previous section is computed exactly the same way within the F12 formalism.[62,64] Thus, CCSD(T)-F12 is introduced to incorporate explicit electron correlation, allowing it to approach the CBS limit more quickly for a given basis set size. Moreover, CCSD(T)-F12 has been shown to achieve the same accuracy with smaller basis sets as canonical CCSD(T) with larger basis sets.[65] In terms of computational scaling, CCSD(T)-F12 scales as $4N^7$, compared to the N^7 scaling of CCSD(T). Nevertheless,

CCSD(T)-F12 captures more correlation and enables faster computations, reducing overall computational cost and making it more feasible to study larger molecular systems.

1.3 Quartic Force Fields

The electronic structure methods discussed in the previous sections provide the necessary energetic backbone for the *ab initio* computation of spectral constants via the well-established quartic force field (QFF) procedure.[66] In order to accurately describe the rovibrational profile of a given molecular system, one must return to Schrödinger equation, Eq. 1.1, and begin with the internuclear Watson Hamiltonian:[67]

$$H = \frac{1}{2}\sum_{\alpha\beta}(J_\alpha - \pi_\alpha)\mu_{\alpha\beta}(J_\beta - \pi_\beta) - \frac{1}{2}\sum_k \frac{\partial^2}{\partial Q_k^2} - \frac{1}{2}\sum_\alpha \mu_{\alpha\alpha} + V(\mathbf{Q}). \tag{1.54}$$

J corresponds to the total angular momentum of a given Cartesian direction indicated by α or β while π is the total vibrational angular momentum of the same direction; $\mu_{\alpha\beta}$ represents the inverse tensor of the moment of inertia of the $\alpha,\ \beta$-th geometric coordinate; Q_k is a single normal coordinate where $\mathbf{Q}$ is the full set of normal coordinates; and $V(\mathbf{Q})$ is the full potential energy portion of the Hamiltonian with its dependence upon the normal coordinates.[25,66] The first three terms are related to the kinetic energy and emerge from the application of perturbation theory.[68] The final term corresponds to the potential energy and is historically interpreted as an extensive global or semi-global potential energy surface (PES).[66] However, the ability to approximate the potential energy function of a molecular system has become a common tool to circumvent the more expensive computations of a PES.

A QFF is a fourth-order Taylor series expansion of the potential energy function within Eq. 1.54 with respect to its equilibrium geometry and molecular coordi-

nates. The definition of a QFF in Eq. 1.55 includes terms for force constants $F_{ij\ldots}$ and displacements of the equilibrium geometry $\Delta_i\Delta_j\cdots$.[69]

$$V \approx \frac{1}{2}\sum_{ij} F_{ij}\Delta_i\Delta_j + \frac{1}{6}\sum_{ijk} F_{ijk}\Delta_i\Delta_j\Delta_k + \frac{1}{24}\sum_{ijkl} F_{ijkl}\Delta_i\Delta_j\Delta_k\Delta_l \tag{1.55}$$

Of course, the more general form of a Taylor series would have the zeroth- and first-order terms present for completeness. However, the zeroth-order term is, by construction, zero, and the first-order term is zero if the reference geometry is a minimum on the PES, which is necessary for the accurate prediction of ground-state spectroscopic constants. The second-order term in Eq. 1.55 corresponds to the harmonic oscillator approximation to the potential energy function, which is a first approximation to the vibrational frequencies, albeit an inaccurate one. Thus, the inclusion of the third- and fourth-order terms within the QFF allows for anharmonic correction to these frequencies and the prediction of rotational spectroscopic constants for a more complete set of spectroscopic data of a molecule or compound.

However, simply computing the QFF is not enough to predict the rovibrational spectral data. The force constants (FCs) from Eq. 1.55 are must be derived to move forward. There are two numerical ways of doing so. Historically, FCs have been derived utilizing a least-squares fitting algorithm from Dateo et al.[70] This algorithm produces an analytical function for the potential energy which offers the opportunity to refit the force constants and molecular geometry to a new zero and ensure the force constants are precise as possible.[25,71] Another option is to compute the FCs directly through finite differences as described by Westbrook et al.[72] Essentially, finite differences allow for a straightforward direct computation of the FCs that requires no fitting or refitting. This reduces the overall computational time in the QFF procedure, and performs similarly to the least-squares fitting algorithm

yielding an overall improvement to the derivation of the FCs.

1.3.1 Coordinate Systems

The coordinates displaced in Eq. 1.55 can be defined using various systems, and over the years, the QFF procedure has transitioned between different coordinate schemes. Historically, most QFF computations have used symmetry-internal coordinates (SICs), which are linear combinations of simple internal coordinates based on motions such as bond stretching, bond angle bending, and torsions. A key advantage of an internal coordinate system is the reduction in total displaced coordinates from $3N$ to $3N-6$ for non-linear molecules and $3N-5$ for linear molecules, where N represents the number of atoms in the system. This reduction occurs by eliminating rotational and translational degrees of freedom. Since the QFF procedure scales geometrically with the number of coordinates, using an internal coordinate scheme can significantly reduce the number of single-point energy calculations required to construct the full QFF. Although SICs provide such a reduction, they are typically converted to Cartesian coordinates for easier input into quantum chemistry programs. The INTDER program[73] provides a valuable tool to convert between SICs and Cartersian coordinates for this purpose.

However, the definition of SICs for larger and more symmetrical molecules is notoriously difficult. Thus, one could simply use Cartesian coordinates throughout the QFF procedure. As stated previously, the later stages of the QFF procedure directly handle Cartesian coordinates which could potentially reduce the number of steps in the process. However, the full $3N$ Cartesian coordinates are reintroduced as the rotational and translation motions are no longer neglected. Due to the geometric scaling of the QFF procedure, the explicit use of Cartesian coordinates quickly becomes untenable as the size of the molecular system increases.

In recent years, advancements to the QFF procedure as conducted herein have seen the advent of normal coordinate use[72] which is what the Watson Hamiltonian was mainly formulated to use. Normal coordinates cannot be generated *ab initio*, and require the construction of a PES. However, the normal coordinates can be derived from the eigenvectors of a mass-weighted Hessian FC matrix. Thus, a harmonic force field (HFF) can be constructed and computed, first, in order to obtain the normal coordinates that fill out the rest of the cubic and quartic terms of the full QFF. Thus, the use of normal coordinates can strike a balance between the ease of definition from Cartesian coordinates in the HFF while retaining some of the computational cost savings of internal coordinates in the full QFF.

1.4 Spectroscopic Data

Once the QFF has been computed, the full Watson Hamiltonian can be used to solve the vibrational Schrödinger equation through the simple, yet effective, vibrational perturbation theory at second-order (VPT2), which is based on Rayleigh-Schrödinger perturbation theory (RSPT).[67] Within the RSPT implementation of VPT2, the harmonic oscillator acts as the zeroth-order, or unperturbed, portion of the vibrational Hamiltonian $\hat{H}_{HO}$, while the first- and second-order perturbations are based on the cubic, $\hat{H}_1$, and quartic terms, $\hat{H}_2$, from the QFF procedure. Thus, the vibrational Hamiltonian can be written as

$$\hat{H} = \hat{H}_{HO} + \hat{H}_1 + \hat{H}_2. \tag{1.56}$$

As stated by Franke, et al.,[74] diagonalization of the harmonic oscillator Hamiltonian yields the harmonic frequencies of the given molecular system. Then, the first-order correction to the harmonic frequencies can be obtained from the first-

order vibrational energy equation

$$E_i^{(1)} = \left\langle \Psi_i^{(0)} \middle| \hat{H}_1 \middle| \Psi_i^{(0)} \right\rangle, \tag{1.57}$$

where $\Psi^{(i)}$ is the harmonic oscillator wave function of a given vibrational state i. The second-order anharmonic correction equation is given by

$$E_i^{(2)} = \sum_{i \neq j} \frac{\left\langle \Psi_i^{(0)} \middle| \hat{H}_2 \middle| \Psi_j^{(0)} \right\rangle \left\langle \Psi_j^{(0)} \middle| \hat{H}_2 \middle| \Psi_i^{(0)} \right\rangle}{E_i^{(0)} - E_j^{(0)}} \tag{1.58}$$

From Eq. 1.57 & 1.58, the anharmonic energy of a given vibrational level can be given as

$$E_a = E_i^{(1)} + E_j^{(2)}. \tag{1.59}$$

In addition to anharmonic vibrational frequencies, rotational constants are also produced by VPT2 following the computation of the equilibrium rotational constants:

$$B_e = \frac{h}{8\pi^2 c I_e}, \tag{1.60}$$

where I_e is the moment of inertia tensor obtained from the optimized geometry. From there, the corrected rotational constants for a given vibrational state are

$$B_i = B_e - \sum_i \alpha_i \left(\nu_i + \frac{1}{2} \right), \tag{1.61}$$

where α_i are vibration-rotation interaction constants related to the quartic and sextic distortion constants also produced by the VPT2 procedure.[67,68,75] Again, VPT2 is one of the simplest ways to compute rovibrational spectral data for a molecule of interest. Additionally, when paired with an accurate electronic structure method, VPT2 has the ability to predict rovibrational spectroscopic data to with 1.0% of

gas-phase experimental data[40,76–81] further lending credence to its use the following work.

1.5 Closing

The methods defined in the prior sections lay the foundation for the present work insofar as it should be considered accurate predictions of rovibrational spectral data. The chapters herein provide predictions for the spectral features of novel molecules within the context of atmospheric, interstellar, and circumstellar environments. These predictions should serve as either benchmarking data for present or future laboratory and theoretical studies, or as reference data for the potential atmospheric or astrophysical detection of molecules that contribute to the complex chemical environments of the atmosphere or the cosmos as a whole.

CHAPTER 2

Spectral Signatures of Hydrogen Thioperoxide (HOSH) and Hydrogen Persulfide (HSSH): Possible Molecular Sulfur Sinks in the Dense ISM.

Reprinted with permission from Palmer, C. Z.; Fortenberry, R. C.; Francisco, J. S. *Molecules* **2022**, *27*, 3200 with permission of MDPI.
DOI: https://doi.org/10.3390/molecules27103200

Abstract

For decades, sulfur has remained underdetected in molecular form within the dense interstellar medium (ISM), and somewhere a molecular sulfur sink exists where it may be hiding. With the discovery of hydrogen peroxide (HOOH) in the ISM in 2011, a natural starting point may be found in sulfur-bearing analogs that are chemically similar to HOOH: hydrogen thioperoxide (HOSH) and hydrogen persulfide (HSSH). The present theoretical study couples the accuracy in the anharmonic fundamental vibrational frequencies from explicitly correlated coupled cluster theory with the accurate rotational constants provided by canonical high-level coupled cluster theory to produce rovibrational spectra for use in the potential observation of HOSH and HSSH. The ν_6 mode for HSSH at 886.1 cm^{-1} is within 0.2 cm^{-1} of gas phase experiment, and the B_0 rotational constant for HSSH of 6979.5 MHz is within 9.0 MHz of the experimental benchmarks implying that the unknown spectral features (such as the first overtones and combination bands) provided herein are similarly accurate. Notably, a previous experimentally-attributed $2\nu_1$ mode, at 7041.8 cm^{-1}, has been reassigned to the $\nu_1 + \nu_5$ combination band based on the present

work's $\nu_1 + \nu_5$ value at 7034.3 cm^{-1}. The most intense vibrational transitions for each molecule are the torsions, with HOSH having a more intense transition of 72 km/mol compared to HSSH's intensity of 14 km/mol. Furthermore, HOSH has a larger net dipole moment of 1.60 D compared to HSSH's 1.15 D. While HOSH may be the more likely candidate of the two for possible astronomical observation *via* vibrational spectroscopy due to the notable difference in their intensities, both HSSH and HOSH have large enough net dipole moments to be detectable by rotational spectroscopy to discover the role these molecules may have as possible molecular sulfur sinks in the dense ISM.

2.1 Introduction

Since the detection of sulfur-bearing molecules, such as carbon monosulfide,[82,83] in the 1970s in the interstellar medium (ISM), sulfur-containing species have captured the interest of astrochemists, astrophysicists, and astronomers for their analogous nature to oxygen and use in the determination of the physical structure of early stage star formation.[84,85] While volatile forms of sulfur molecules are known to exist in the diffuse ISM, the observed abundance of such molecules in the dense ISM was discovered to be less than 1% of the observed cosmic abundance.[86] This so-called sulfur depletion problem has led to the search for the missing sulfur in both the diffuse and dense regions of the ISM alike.[87,88] Since then, the majority of the sulfur that should be present in the dense ISM has still eluded detection. The majority of refractory forms of sulfur-bearing molecules have been hypothesized[89] to be depleted onto dust-grains found in the clouds of protoplanetary disks in some unknown molecule, but such a mechanism has not been supported or refuted. Alternatively, molecular forms of sulfur may simply exist in currently undetected molecular species in the ISM.

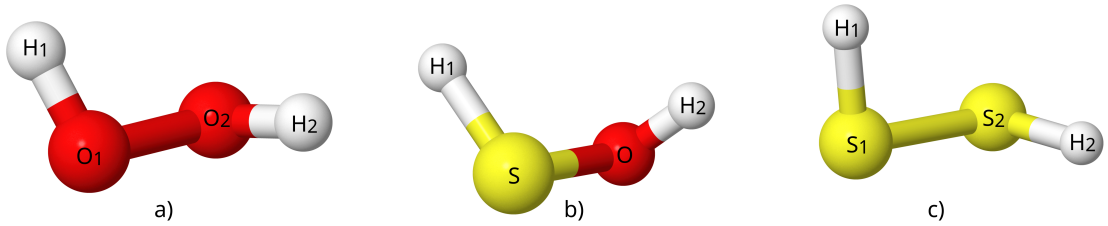

Figure 2.1: Visual depiction of the optimized structures for (a) HOOH, (b) HOSH, (c) HSSH.

Studies of sulfur-bearing molecules in the dense ISM have led to the investigation of similar molecules in cometary ices[89] due to the hypothesis that these environments mimic the chemical nature of ice found in hot core formation. Recent astrochemical models support this hypothesis and predict sulfur-containing species most likely being bound to the surface of dust grains or in volatile ices.[90] This theory is further supported by the discovery of both solid H_2S by the *Rosetta* orbiter in the Hale-Bopp comet[91] and carbonyl sulfide (OCS) in interstellar ice grain mantles of young stellar objects like AFGL 989 and Mon R2 IRS 2.[92] These discoveries set the precedent for the detection of sulfur on dust grains in protoplanetary disks, but for which particular molecules to search is still unclear.

A natural starting point into the investigation of sulfur-containing species may stem from their analogous nature to oxygen-bearing molecules that have previously been detected. In 2011, HOOH was first discovered in the ISM and is hypothesized[93] to form through the addition of H atoms onto molecular oxygen on the surface of dust grains. A straightforward analog may occur from the addition of H atoms onto sulfur monoxide (SO), which was first observed in the ISM in 1973.[93,94] Gaseous SO has been found in the remnants of type II supernovae that may contribute to the depletion of sulfur onto the dust grains found in the dense ISM.[86,95] If SO exists on the surface of dust grains, it may lead naturally to the formation of the sulfur analog hydrogen thioperoxide (HOSH). Hydrogen persulfide (HSSH) may form in

a related way, but the polymeric allotropes of sulfur imply that it may be created under different conditions. In any case, observation of either molecule would provide *in situ* comparison for such mechanisms.

Consequently, the detection of HOSH and HSSH will require rovibrational reference data which are provided herein *via* highly-accurate quantum chemical computations known as quartic force fields (QFFs). A QFF is a fourth-order Taylor series expansion of the potential portion of the internuclear molecular Hamiltonian.[66] QFFs have been used to produce highly-accurate rotational constants and fundamental anharmonic frequencies within to 1% of experimental values for numerous molecular systems.[39,40,76–78,80,96–103] The QFFs in this work are used in conjunction with high-level quantum chemical electronic structure computations and benchmarked with gas-phase experiment and previous theoretical studies where available to provide the necessary and full set of rovibrational spectral data needed for the potential detection of these sulfur-bearing molecules as possible reservoirs of sulfur in the dense region of the ISM.

2.2 Computational Details

The present work utilizes two different methods of producing QFFs for each molecule. The two methods are based on coupled cluster theory at the singles, doubles, and perturbative triples [CCSD(T)] level.[58] The first method implements the CCSD(T) level of theory within the explicitly correlated F-12b formalism along with the cc-pVTZ-F12 basis set.[62,64] This method will henceforth be abbreviated as F12-TZ. The second method is a composite method based on canonical CCSD(T) that takes into account effects from the complete basis set (CBS) limit extrapolation ("C"), core electron correlation ("cC"), and scalar relativity ("R") yielding the abbreviated "CcCR" method. F12-TZ QFFs have been used to compute accurate

anharmonic fundamental frequencies that are as, if not more, accurate than the frequencies computed using the CcCR method but at a fraction of the computational cost.[104–106] Even though F12-TZ provides highly accurate anharmonic fundamental frequencies, it cannot readily produce rotational constants at the same level of accuracy as the CcCR method, motivating the usage of both QFF methods herein.[40]

Both QFF methods utilize the MOLPRO 2020.1 quantum chemical package.[107] Both methods begin with the optimization of the molecular geometry with exceptionally tight convergence criteria. The CcCR method utilizes a geometry optimized at the CCSD(T)/aug-cc-pV5Z level of theory, but includes corrections to this geometry based on the difference between the inclusion and exclusion of the effects of core electron correlation from the Martin-Taylor[108] (MT) core-correlating basis set. The F12-TZ method, however, employs a simpler approach by only optimizing at the CCSD(T)-F12b/cc-pVTZ-F12 level of theory. Once each geometry has been optimized, the structures of each species are displaced by 0.005 Å for bond lengths and 0.005 radians for bond angles/torsions using symmetry-internal coordinates *via* the INTDER[73] program.

The simple-internal coordinate system for HOOH requires 665 points for the QFF and is defined from the atoms in Fig. 2.1A:[81,109]

$$S_1 = r(\mathrm{O}_2 - \mathrm{O}_3) \tag{2.1}$$

$$S_2 = \frac{1}{\sqrt{2}}[r(\mathrm{H}_1 - \mathrm{O}_2) + r(\mathrm{O}_3 - \mathrm{H}_4)] \tag{2.2}$$

$$S_3 = \frac{1}{\sqrt{2}}[\angle(\mathrm{H}_1 - \mathrm{O}_2 - \mathrm{O}_3) + \angle(\mathrm{O}_2 - \mathrm{O}_3 - \mathrm{H}_4)] \tag{2.3}$$

$$S_4 = \tau(\mathrm{H}_1 - \mathrm{O}_2 - \mathrm{O}_3 - \mathrm{H}_4) \tag{2.4}$$

$$S_5 = \frac{1}{\sqrt{2}}[r(\mathrm{H}_1 - \mathrm{O}_2) - r(\mathrm{O}_3 - \mathrm{H}_4)] \tag{2.5}$$

$$S_6 = \frac{1}{\sqrt{2}}[\angle(\mathrm{H}_1 - \mathrm{O}_2 - \mathrm{O}_3) - \angle(\mathrm{O}_2 - \mathrm{O}_3 - \mathrm{H}_4)] \tag{2.6}$$

The simple-internal coordinate system for HSSH is the same as the HOOH system with S atoms replacing the O atoms. The symmetry-internal system for HOSH requires 1289 points for the QFF and is based on the geometry of Fig. 2.1B:

$$S_1 = r(\mathrm{H_1 - O}) \tag{2.7}$$

$$S_2 = r(\mathrm{O - S}) \tag{2.8}$$

$$S_3 = r(\mathrm{S - H_2}) \tag{2.9}$$

$$S_4 = \angle(\mathrm{H_1 - O - S}) \tag{2.10}$$

$$S_5 = \angle(\mathrm{O - S - H_2}) \tag{2.11}$$

$$S_6 = \tau(\mathrm{H_1 - S - O - H_2}) \tag{2.12}$$

A single-point energy calculation for every displacement for either QFF method is then computed. At each displaced geometry point using the CcCR method, CCSD(T) energies are computed with the aug-cc-pV(T+d)Z, aug-cc-pV(Q+d)Z, and aug-cc-pV(5+d)Z basis sets for the extrapolation to the CBS limit.[116] Each point is also computed with the core correlation turned on and off utilizing the same MT basis set from the geometry optimization. Additionally, the Douglas-Kroll scalar relativistic corrections[117] are computed using the cc-pVTZ-DK basis set with the corrections turned either on or off. Finally, single-point energy calculations at each displaced geometry for HOSH only were computed using the CCSDT/aug-cc-pVTZ level of theory for the inclusion of the contributions of full triples in a separate, but similar, "CcCRE" composite method. For F12-TZ, each single-point energy calculation is only computed at the CCSD(T)-F12b/cc-pVTZ-F12 level of theory. Regardless of QFF method, once the single-point energy calculations are finished, the relative energies are fit to the QFF Taylor series model using a least squares fit procedure to better than 10^{-17} a.u.^{2}, then fit once again to include contributions from the com-

Table 2.1: Geometrical Parameters and Spectroscopic Constants for HOOH Compared to Previous Gas-Phase Experiment.

	Units	CcCR	F12-TZ	Prev. Theory	Prev. Expt.
R_e(H-O)	Å	0.96198	0.96348	0.963[a]	0.9617[b]
R_e(O-O)	Å	1.44803	1.45099	1.450[a]	1.4524[b]
$\angle_e$(O-O-H)	°	100.15	100.09	100.1[a]	99.76[b]
τ_e(H-O-O-H)	°	112.80	112.66	112.7[a]	113.6[b]
A_e	MHz	304899.4	303773.7		
B_e	MHz	26576.3	26472.3		
C_e	MHz	25742.3	25646.3		
$R_0(H_1\text{-}O_1)$	Å	0.96228	0.96379	0.9675[b]	
$R_0(O_1\text{-}O_2)$	Å	1.46166	1.46464	1.461[b]	
$\angle_0(H_1\text{-}O_1\text{-}O_2)$	°	100.05	99.99	100.07[b]	
A_0	MHz	302188.9	301077.7	300419[a]	301874.2654[c]
B_0	MHz	26276.2	26171.3	26030[a]	26194.08965[c]
C_0	MHz	25286.1	25194.1	25349[a]	25116.88435[c]
A_1	MHz	297349.8	296967.2		
B_1	MHz	26232.4	26128.6		
C_1	MHz	25282.6	25191.3		
A_2	MHz	305755.8	304615.1		
B_2	MHz	26093.7	25988.4		
C_2	MHz	25214.1	25121.0		
A_3	MHz	301557.4	300454.1		301,873.4973264[f]
B_3	MHz	25957.4	25853.2		26,193.0529267[f]
C_3	MHz	24962.0	24871.3		25,117.8952429[f]
A_4	MHz	300894.7	299793.5		
B_4	MHz	26290.4	26182.9		
C_4	MHz	25044.4	24958.2		
A_5	MHz	295700.7	293937.2		
B_5	MHz	26240.8	26136.4		
C_5	MHz	25284.4	25193.1		
A_6	MHz	306454.1	305307.4		306,559.6731544[e]
B_6	MHz	26215.6	26110.0		26,162.8878096[e]
C_6	MHz	25043.1	24951.8		24,836.1562867[e]
Δ_J	kHz	96.817	96.409		86.6100411[e]
Δ_K	MHz	11.027	10.914		13.7784613[e]
Δ_{JK}	MHz	1.138	1.130		1.2576293[e]
δ_J	Hz	-31.906	-14.235		
δ_K	MHz	6.812	6.780		
Φ_J	mHz	392.379 (μHz)	1.285		
Φ_K	kHz	1.765	1.729		
Φ_{JK}	Hz	77.849	74.877		
Φ_{KJ}	Hz	-228.455	-219.330		
ϕ_j	μHz	2.608 (mHz)	887.135		
ϕ_{jk}	Hz	111.163	111.449		
ϕ_k	kHz	-53.653	-55.097		
μ	D		1.75	1.746[d]	

[a] Previous theory computed at CCSD(T)-F12/cc-pVTZ-F12 from.[110]
[b] Experimental geometrical parameters from.[111]
[c] Experimental ground state rotational constants from.[112]
[d] Electric dipole moment calculated at the CCSD(T)/aug-cc-pVTZ level of theory from.[113]
[e] Experimental ν_6 rotational constant for ν_6 from.[114]
[f] Experimental rotational constants for ν_3 from.[115]

puted Hessian to construct the equilibrium geometry. The force constants generated from the least squares procedure are re-fit to produce zero gradients and then are transformed into Cartesian coordinates through the INTDER program.[73] These are then used by the SPECTRO[68] program to compute the spectroscopic constants and vibrational frequencies produced by rotational and vibrational perturbation theory at second order (VPT2).[67,75,118]

The rovibrational spectra of each species contains Fermi resonances and resonance polyads. These are treated by the SPECTRO program to provide more accurate predictions[119] of the rovibrational spectra. The spectrum for HOSH contains a $2\nu_6 = \nu_4$ and a $2\nu_6 = \nu_5$ type-1 Fermi resonance. For HSSH's spectrum, a $2\nu_5 = \nu_6$ and a $2\nu_5 = \nu_3$ type-1 Fermi resonance and ν_2/ν_1, ν_2/ν_1, and ν_2/ν_1 Darling-Dennison resonances are present, and the spectrum for HOOH includes a $\nu_6 = \nu_5$ type-1 Fermi resonance, a $\nu_6 + \nu_5 = \nu_3$ type-2 Fermi resonance and a ν_2/ν_1 and ν_4/ν_3 Darling-Dennison resonance. To further assist in possible observation, dipole moments for each species are computed at the CCSD(T)-F12b/cc-pVTZ-F12 level of theory. Anharmonic infrared intensities are calculated using the Gaussian16[120] quantum chemical package at the MP2/aug-cc-pVDZ level of theory which has been shown to produce semi-quantitative agreement with higher levels of theory for far less computational cost.[121,122]

2.3 Results and Discussion

2.3.1 HOOH

The computed rovibrational spectra for HOOH in this work provide reference benchmarks to show spectral differences between it and the sulfur analogs. As seen in Table 2.1, F12-TZ surprisingly out-performs CcCR by producing the more accurate rotational constants compared to experiment. F12-TZ's B_0 value of 26171.3 MHz is

Table 2.2: Vibrational Frequencies (cm^{-1}), and IR intensities (km/mol) given in parentheses for HOOH Compared to Previous Theory and Gas-Phase Experiment.

Mode	Desc.	CcCR	F12-TZ	Prev. Theory[a]	Prev. Theory[f]	Prev. Expt.
$\omega_1(a)$	S_5	3806.1	3798.5	3798		
$\omega_2(a)$	S_3	1441.7	1437.6	1447		
$\omega_3(a)$	S_1	915.0	911.3	911		
$\omega_4(a)$	S_4	380.3	380.4	378		
$\omega_5(b)$	S_2	3805.8	3798.4	3798		
$\omega_6(b)$	S_6	1333.3	1330.1	1330		
$\nu_1(a)$	S_5	3611.1	3607.5 (11)	3607	3611.05	3609.8[b]
$\nu_2(a)$	S_3	1398.0	1393.9 (1)	1400	1394.43	1393.5[c]
$\nu_3(a)$	S_1	878.4	875.3 (1)	875	865.77	877.93[d]
$\nu_4(a)$	S_4	314.7	319.4 (164)	315		370.89[b]
$\nu_5(b)$	S_2	3608.8	3605.2 (49)	3605	3609.73	3610.66[b]
$\nu_6(b)$	S_6	1278.4	1275.9 (119)	1283	1264.78	1273.68[e]
ZPT		5740.5	5730.6			

[a]Previous theoretical QFF computed at CCSD(T)-F12/cc-pVTZ-F12 level of theory from.[110]
[b]Previous gas-phase experimental values gathered from.,[123] [c].,[124] [d].,[115] and [e].[125]
[f]Previous theoretical values using VMP2 from.[111]

lower than the experimental[112] value of 26194.08965 MHz by 22.8 MHz, an error of 0.09%. In contrast, the B_0 rotational constant computed *via* the CcCR QFF method is 82.1 MHz higher than the experimental value with the C_0 following suit having a difference of 169.2 MHz. This, however, is not surprising as previous computational studies[110] on this molecule also fail to capture accurate rotational constants possibly due to the large amplitude motion of the torsion. Regardless, the difference between CcCR and experiment for the B_0 and C_0 constants are 0.31% and 0.67% in error, respectively.

With regard to most vibrational frequencies, the present work agrees well with both previous theory and experiment as shown in Table 2.2. The fundamental frequencies produced by the F12-TZ method compares well with gas-phase experiment[124] with the ν_2 frequency, the symmetric H−O−O bend at 1393.9 cm^{-1}, being 0.4 cm^{-1} higher than the experimental fundamental of 1393.5 cm^{-1}. CcCR compares similarly with the ν_3 frequency, the O−O stretch with a fundamental of

Table 2.3: Vibrational Frequencies (cm^{-1}), and IR intensities (km/mol) given in parentheses for two-quanta Bands of HOOH Compared to Previous Gas-Phase Experiment.

Mode	CcCR	F12-TZ	Prev. Expt.	Prev. Theory
$2\nu_1$	7131.0	7125.6 (1)		7041.8[a]
$2\nu_2$	2772.9	2764.8 (1)		
$2\nu_3$	1739.6	1734.0 (1)		
$2\nu_4$	557.8	571.5 (1)		
$2\nu_5$	7125.2	7119.8 (1)		
$2\nu_6$	2534.8	2529.7 (1)		
$\nu_1+\nu_2$	4990.7	4983.1 (1)		
$\nu_1+\nu_3$	4487.3	4480.6 (1)		
$\nu_1+\nu_4$	3930.5	3931.4 (1)		
$\nu_1+\nu_5$	7037.8	7034.3 (5)	7041.8[b], 7050[c]	
$\nu_1+\nu_6$	4879.9	4873.8 (1)	4827.49[d]	
$\nu_2+\nu_3$	2258.6	2251.4 (1)		
$\nu_2+\nu_4$	1736.0	1736.2 (1)		
$\nu_2+\nu_5$	4989.4	4981.8 (1)	4982.57[d]	
$\nu_2+\nu_6$	2663.8	2657.2 (5)		
$\nu_3+\nu_4$	1191.2	1193.0 (1)		
$\nu_3+\nu_5$	4484.9	4478.2 (1)	4487.27[d]	
$\nu_3+\nu_6$	2141.1	2135.5 (1)		
$\nu_4+\nu_5$	3926.6	3927.4 (1)		
$\nu_4+\nu_6$	1576.0	1578.6 (1)		
$\nu_5+\nu_6$	4876.7	4870.7 (1)		

[a]Previous theoretically-attributed overtone from.[126]
[b]Previous gas-phase experimentally-attributed combination band and computationally-attributed overtone from.[127] This attribution is questioned herein. See text for discussion.
[c]Previous gas-phase experimentally-attributed overtone from.[128]
[d]Previous gas-phase experimentally-attributed two-quanta modes from.[129]

878.4 cm^{-1}, being 0.5 cm^{-1} higher than gas-phase value of 877.93 cm^{-1}. The worst agreement is the ν_4 frequency, the torsion, with F12-TZ and CcCR being 51.5 and 56.2 cm^{-1} lower than experiment, respectively. Once again, as discussed in previous literature,[110] this may be attributed to the large amplitude motion of the torsion. A previous theoretical study[110] utilizes a similar QFF method also employing the CCSD(T)-F12/cc-pVTZ-F12 level of theory, but the previous work uses a different fitting model than the present work and does not mention the inclusion of resonance polyads in the VPT2 corrections. To that end, the difference between the previous theoretical study and the present work is to be expected with most fundamental fre-

quencies being within 0.5 cm^{-1}, and the worst agreement being the ν_6 fundamental with less than an 8.0 cm^{-1} difference.

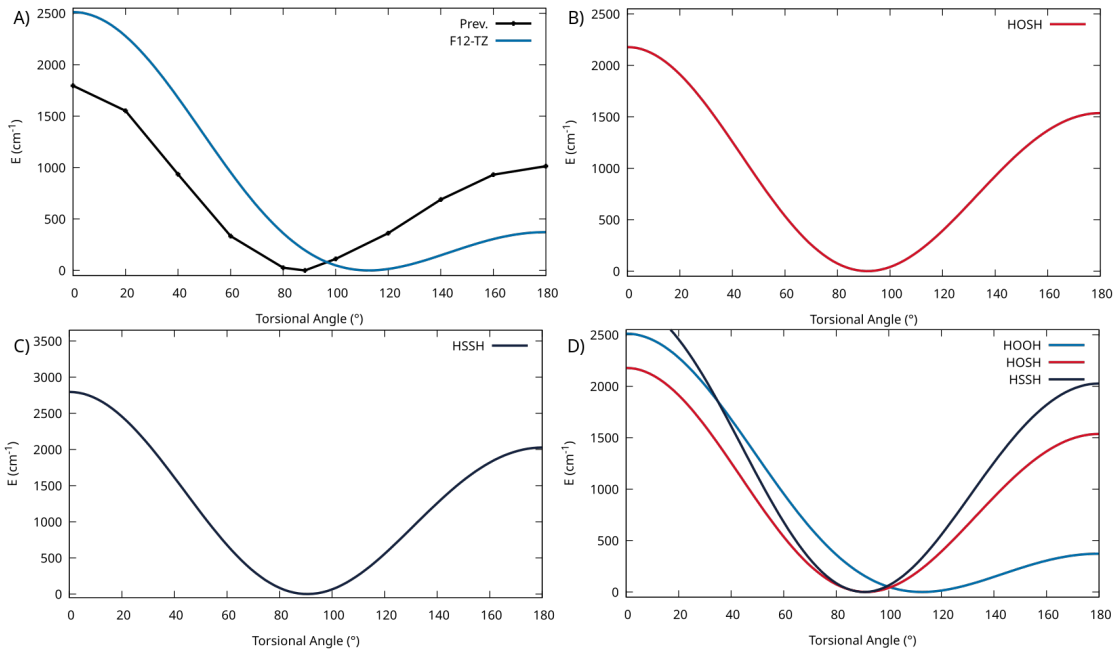

Figure 2.2: Potential Energy Scan of the Torsional Motion. **A)** HOOH Calculated at the F12-TZ Level of Theory (blue) and a Previous Theoretical Study using HF/STO (black), **B)** HOSH Calculated at the F12-TZ Level of Theory, **C)** HSSH at the F12-TZ Level of Theory, **D)** Comparison of HOOH, HOSH, and HSSH.

The inaccuracies in both the rotational constants and the anharmonic vibrational frequencies for ν_4 warrant an investigation of the potential well for this torsional motion of HOOH. As seen in Fig. 2.2A, a relaxed scan of the torsional angle produces an extremely flat potential well with a torsional *trans*-barrier of 371.9 cm^{-1} (1.06 kcal/mol). A previous theoretical study[130] also investigated the *trans*-barrier height, seen in Fig. 2.2A, and calculates the *trans*-barrier 1.17 kcal/mol higher than the current work at 2.23 kcal/mol ($\sim$780 cm^{-1}). However, a previous experimental value[131] for the *trans*-barrier at 387.07 cm^{-1} is closer to the present work's *trans*-barrier than previous theory. The previous theory utilizes the HF/STO level of theory so the inaccuracy compared to experiment is to be expected. In any case,

a molecule with a mode that exhibits a flat potential can be notorious for its inability to be accurately modeled with VPT2 corrections as used in the present work. As stated previously, CcCR QFF methods generally provide more accurate ground state rotational constants. However, due to the composite nature of the method, there are conflicting minima for the potential energy surface thus introducing additional inaccuracy. This same inaccuracy has been seen as well for [Al, N, C, O] isomers.[132] While there is still considerable accuracy to experiment for the remainder of the fundamentals, the large amplitude motion of the torsion decreases the overall accuracy of the ground state rotational constants seemingly preventing the accurate rovibrational modeling of this molecule.

Further, several two-quanta vibrational overtones and combination bands for HOOH have not been reported in the current literature. In order to assist in further potential astrophysical observation, the present work introduces the missing overtones and combination bands for HOOH, as seen in Table 2.3. In current literature, two previous studies attribute the same value of 7041.8 cm^{-1} to either the $2\nu_1$ or $\nu_1 + \nu_5$ two-quanta band, Halonen[126] and Redington et al.[129], respectively. The present work's F12-TZ value for the $\nu_1 + \nu_5$ combination band is 7034.3 cm^{-1} falling in a similar region with the value attributed to the value from Redington et al.[129] with only a difference of 7.5 cm^{-1}. Another previous experimental value, from Dzugan et al.[128], for the $\nu_1 + \nu_5$ combination band, at 7050 cm^{-1}, also falls within the same region as the present work's theoretical value along the work from both Halonen[126] and Redington et al.[129]. Based on the agreement between the present work's value and each of the previous studies values for the band in question, this band is attributed to the $\nu_1 + \nu_5$ combination band for HOOH.

With regard to other two-quanta modes, previous gas-phase experimental work is available for comparison.[129] The previous experimental $\nu_1 + \nu_6$ combination

band, at 4827.49, does not compare favorably to the present F12-TZ value of 4873.8, or a 46.3 cm^{-1} difference. Both the $\nu_2 + \nu_5$ and $\nu_3 + \nu_5$ two-quanta bands from previous gas-phase experiment,[129] however, compare exceptionally well to the present theoretical study. The previous gas-phase $\nu_2 + \nu_5$ value of 4982.57 cm^{-1} is 0.8 cm^{-1} higher than the present F12-TZ combination band. Similarly, the previous gas-phase $\nu_3 + \nu_5$ value of 4487.27 cm^{-1} is 2.4 cm^{-1} higher than the present CcCR value of 4484.9 cm^{-1}. While some two-quanta modes compare well to experiment, the slight inaccuracy compared to experiment for other two-qaunta bands is not unexpected as the available previous gas-phase experiment was conducted in 1962. Therefore, the present work's theoretical values will serve as a benchmark for any further, current laboratory analysis even for the overtones and combination bands.

Analysis of the computed two-qaunta modes' intensities show far weaker transitions than the anharmonic vibrational frequencies with the brightest two transitions, the $\nu_1 + \nu_5$ and $\nu_2 + \nu_6$ combination bands, at a mere 5.0 km/mol. Outside of these modes, no two-quanta modes are present that exhibit intensities greater than 1.0 km/mol. Though these transitions are weak, the $\nu_1 + \nu_5$ and $\nu_2 + \nu_6$ band fall within the elusive, and consequently understudied, near- to mid-IR spectrum, 1.4 μm and 3.7 μm range, respectively. With the recently launched *James Webb Space Telescope* (JWST), the proper instrumentation to analyze this region of the IR spectrum is now achievable with its Near Infrared Spectrograph. Since these fall within the region of the IR dominated by polycyclic aromatic hydrocarbons (PAHs), the data provided in this work will be instrumental in identifying molecules in this region that are unrelated to these PAHs but have yet to be identified.

Table 2.4: Geometrical Parameters and Spectroscopic Constants for HOSH Compared to Previous Theory and Gas-Phase Experiment

	Units	CcCRE	CcCR	F12-TZ	Prev. Theory	Prev. Expt.
$R_e(H_1\text{-}O)$	Å	0.95700	0.96012	0.96152	0.9601[a]	0.9606[c]
R_e(O-S)	Å	1.65350	1.66051	1.66370	1.6614[a]	1.6616[c]
$R_e(S\text{-}H_2)$	Å	1.33758	1.34273	1.34423	1.3413[a]	1.3420[c]
$\angle_e(H_1\text{-}O\text{-}S)$	°	107.53	107.21	107.20	107.0[a]	107.19[c]
$\angle_e(O\text{-}S\text{-}H_2)$	°	98.38	98.45	98.43	98.6[a]	98.57[c]
$\tau_e(H_1O\text{-}S\text{-}H_2)$	°	91.58	91.31	91.42	91.3[a]	90.41[c]
A_e	MHz	205070.3	203373.2	202852.8	203624[a]	
B_e	MHz	15546.3	15420.7	15362.9	15406[a]	
C_e	MHz	15116.1	14995.6	14940.2	14985[a]	
$R_0(H_1\text{-}O)$	Å	0.95493	0.95805	0.95947		
R_0(O-S)	Å	1.66203	1.66926	1.67248		
$R_0(S\text{-}H_2)$	Å	1.34726	1.35227	1.35379		
$\angle_0(H_1\text{-}O\text{-}S)$	°	107.80	107.51	107.49		
$\angle_0(O\text{-}S\text{-}H_2)$	°	98.44	98.50	98.49		
A_0	MHz	203686.6	202021.5	201494.3	202199[a]	202069[b]
B_0	MHz	15428.1	15299.9	15242.2	15285[a]	15282[b]
C_0	MHz	14983.2	14860.4	14805.3	14847[a]	14840[b]
A_1	MHz	201230.6	199597.1	199079.8	199769.9[d]	199532.6[d]
B_1	MHz	15403.5	15275.4	15217.9	15255.6[d]	15260.0[d]
C_1	MHz	14971.9	14849.0	14794.0	14829.6[d]	14833.2[d]
A_2	MHz	199585.2	197980.8	197464.1		
B_2	MHz	15447.6	15318.6	15260.6		
C_2	MHz	14982.9	14859.6	14804.2		
A_3	MHz	206750.4	205046.1	204484.5		
B_3	MHz	15386.9	15257.9	15200.6		
C_3	MHz	14986.0	14861.5	14806.5		
A_4	MHz	206017.2	204343.0	203808.7		
B_4	MHz	15414.9	15286.0	15228.1		
C_4	MHz	14920.8	14797.9	14742.9		
A_5	MHz	203499.1	201823.1	201296.5		
B_5	MHz	15299.2	15168.7	15111.4		
C_5	MHz	14855.8	14730.7	14675.9		
A_6	MHz	202269.5	200635.4	200115.3		
B_6	MHz	15384.1	15255.2	15197.5		
C_6	MHz	14912.1	14789.6	14734.6		
Δ_J	kHz	23.614	23.535	23.346		24.528463[b]
Δ_K	MHz	5.604	5.495	5.473		5.989715[b]
Δ_{JK}	kHz	388.724	385.632	382.477		0.3904340 (MHz)[b]
δ_J	Hz	682.725	678.344	671.200		
δ_K	MHz	-0.811	-0.823	-0.816		
Φ_J	mHz	-12.453	-14.415	-14.509		
Φ_K	Hz	448.475	433.966	429.934		
Φ_{JK}	Hz	-8.868	-9.067	-8.931		
Φ_{KJ}	Hz	58.332	58.290	57.557		
ϕ_j	μHz	484.538	407.691	394.947		
ϕ_{jk}	mHz	-862.352	-710.680	-699.524		
ϕ_k	kHz	-7.755	-7.988	-7.893		
μ_a	D			1.41		
μ_b	D			0.76		
μ_c	D			0.05		
μ_{net}	D				1.66[a]	

[a] Previous theoretical geometrical parameters calculated at the CCSD(T,full)/cc-pwCVQZ level of theory, ground state rotational constants calculated at the CCSD(T, full)/cc-pwCVQZ level of theory with vibration rotation corrections from the CCSD(T)/cc-pV(T+d)Z level of theory, and theoretical dipole moment calculated at the CCSD(T, full)/cc-pwCVQZ level of theory from.[133]

[b] Previous gas-phase ground state rotational constants and centrifugal distortion constants from.[134]

[c] Previous empirical equilibrium geometrical parameters from.[135]

[d] Previous theoretical rotational constants at the CCSD(T)/cc-pVQZ level of theory with CCSD(T)/cc-pVTZ vibrational correction and experimental rotational constants from.[136]

2.3.2 HOSH

Considering HOSH's analogous nature and similar geometry to HOOH, a potential energy scan of the torsional motion for this molecule is also investigated. In Fig. 2.2B, a considerably deeper potential well, with a *trans*-barrier height of 1536.4 cm^{-1} for the torsion, is seen compared to the potential well for HOOH. With this deeper well, the rovibrational spectra of HOSH will not suffer from the same inaccuracies in its VPT2 corrections. For this reason, the geometrical parameters and rotational constants, given in Table 2.4, show a much higher accuracy compared to experiment than that of HOOH. The CcCR value for B_0 of 15299.9 MHz is in good agreement with the experimental gas-phase value of 15282 MHz,[134] giving a difference of only 17.9 MHz which is only an error of 0.12%.[40] The F12-TZ value is less accurate, as expected, with a difference of ∼40 MHz, an error of 0.26%, further supporting the accuracy of rotational constants computed using CcCR versus F12-TZ when compared to experiment. Similarly, the C_0 rotational constant shares a 20.4 MHz difference, 0.14% error, between the CcCR value and the previous experimental value of 14840 MHz, while the F12-TZ C_0 value is 34.7 MHz lower than the experimental method, an error of 0.23%. A previous theoretical study,[133] however, performs more accurately when compared to experiment and calculates rotational constants at the CCSD(T, full)/cc-pwCVQZ level with vibration-rotation corrections from the CCSD(T)/cc-pV(T+d)Z level of theory and finds the B_0 and C_0 to be within 7.0 and 3.0 MHz, respectively. The difference in accuracy for these rotational constants may largely be due to the previous computational study's implementation of the CCSD(T, full)/cc-pwCVQZ level of theory with vibrational corrections at the CCSD(T)/cc-pV(T+d)Z level, which is considered to be a more theoretically rigorous composite method.

Additionally, a previous theoretical study[137] simulates the full rotational line

Table 2.5: Vibrational Frequencies (cm^{-1}), and IR intensities (km/mol) given in parentheses for HOSH Compared to Previous Theory and Gas Phase Experiment.

Mode	Desc.	CcCRE	CcCR	F12-TZ	Prev. Theory	Prev. Gas Phase	Prev. Ar Matrix
ω_1	S_1	3854.6	3825.8	3819.6	3829 (69)[a]		
ω_2	S_3	2672.4	2662.2	2656.1	2649 (16)[a]		
ω_3	S_4	1210.4	1210.9	1211.0	1228 (41)[a]		
ω_4	S_5	1043.8	1033.7	1032.8	1029 (2)[a]		
ω_5	S_2	794.1	786.0	784.7	777 (52)[a]		
ω_6	S_6	487.1	479.8	479.6	490 (75)[a]		
ν_1	S_1	3650.8	3628.9	3626.7 (67)	3646.5[b]	3625.6[b]	3608.3[b]
ν_2	S_3	2556.8	2547.0	2544.9 (8)	2533.3[b]	2538[b]	2550.1[b]
ν_3	S_4	1173.5	1174.8	1176.7 (36)	1183.5[b]		1175.7[b]
ν_4	S_5	1018.8	1009.3	1008.3 (2)	1006.6[b]		
ν_5	S_2	772.2	763.7	763.4 (47)	764.4[b]		762.5[b]
ν_6	S_6	441.9	438.0	447.4 (72)	448.1[b]		445.3[b]
ZPT		4951.8	4922.8	4920.2			

[a]Previous computed harmonic frequencies conducted at the CCSD(T)/cc-pV(T+d)Z level of theory from [133]

[b]Previous theory, conducted at CCSD(T)/cc-pVTZ level of theory, gas-phase experiment, and Ar Matrix data from. [5]

spectrum of HOSH at the CCSD(T)/aug-cc-pV(Q+d) level of theory through the use of the TROVE program. [138] While the present study utilizes VPT2 to generate accurate rovibrational constants and fundamental frequencies, TROVE implements a variational method for generating accurate rotational energies. The present CcCR B_0 rotational constant of 15299.9 MHz is 16.1 MHz higher than the previous theory's B_0 of 15283.8 MHz, which is only in error of 0.11%. The comparable ground state rotational constants are derived from the rotational energies provided in the previous study. Furthermore, the CcCR C_0 value of 14860.4 MHz is 22.1 MHz greater than the previous theoretical C_0 value of 14838.3, only a 0.15% error. While the previous theoretical ground state rotational constants are more accurate compared to experiment, the small margin of error between the present and previous methods still suggests the validity and accuracy of the current VPT2 methodology for generating accurate rotational constants for systems of this type.

Presently, HOSH only has two observed fundamental frequencies by previous

Table 2.6: Vibrational Frequencies (cm^{-1}), and IR intensities (km/mol) given in parentheses for Two-Quanta Bands of HOSH Compared to Previous Gas-Phase Experiment.

Mode	CcCR	F12-TZ	Prev. Theory
$2\nu_1$	7075.6	7074.7 (5)	
$2\nu_2$	4986.7	4985.7 (1)	
$2\nu_3$	2330.8	2334.7 (4)	
$2\nu_4$	2010.7	2008.8 (1)	
$2\nu_5$	1524.8	1522.5 (1)	
$2\nu_6$	839.1	864.0 (3)	846.269[a]
$\nu_1+\nu_2$	6174.8	6170.5 (1)	
$\nu_1+\nu_3$	4781.8	4782.1 (1)	
$\nu_1+\nu_4$	4637.1	4633.8 (1)	
$\nu_1+\nu_5$	4394.2	4390.7 (1)	
$\nu_1+\nu_6$	4063.4	4071.3 (1)	
$\nu_2+\nu_3$	3721.6	3721.4 (1)	
$\nu_2+\nu_4$	3537.0	3533.9 (1)	
$\nu_2+\nu_5$	3315.6	3312.2 (1)	
$\nu_2+\nu_6$	2988.3	2997.4 (1)	
$\nu_3+\nu_4$	2178.7	2179.4 (1)	
$\nu_3+\nu_5$	1935.8	1936.2 (1)	
$\nu_3+\nu_6$	1612.0	1626.5 (1)	
$\nu_4+\nu_5$	1768.6	1766.2 (1)	
$\nu_4+\nu_6$	1448.0	1456.5 (1)	
$\nu_5+\nu_6$	1202.3	1209.7 (1)	

[a]Previous theoretically-attributed overtone at the CCSD(T)/aug-cc-pV(Q+d)Z level of theory from.[139]

gas-phase experiment,[5] as seen in Table 2.5: the O−H stretch at 3625.6 cm^{-1} and the, tentatively assigned, S−H stretch at 2538 cm^{-1}. The present F12-TZ ν_1 fundamental of 3626.7 cm^{-1} compares favorably with the gas-phase value of 3625.6 cm^{-1}. Both the present work and previous theory compare similarly with the gas-phase ν_2 fundamental at 2538 cm^{-1} with the F12-TZ fundamental being 6.9 cm^{-1} higher than experiment, and previous theory at 4.7 cm^{-1} lower than the experimental value.

In a previous experimental work conducted by Beckers et al.,[5] the IR spectrum of the S−H stretch is investigated and shown to be just above the $\nu_1 + \nu_3$ combination band from the SO_2 byproduct from the experiment. Due to the overlap from this combination band on the lower J branches, the previous work was unable to confirm the full assignment of this fundamental mode. In 2009, Yurchenko et al.[139]

simulated an IR spectrum for the S−H stretching region, utilizing the TROVE program at the aug-cc-pV(Q+d)Z level of theory, to explain perturbations found in the experimental S−H stretching frequency. The previous simulated spectrum is in good qualitative agreement with the region around the band center of the S−H stretching region, but lacks any comparison to the lower or higher frequency bands. The present study provides a simulated IR spectrum generated through PGOPHER's[140] vibrational spectrum simulation software. In Fig. 2.3, the S−H stretching fundamental frequency is centered on the previous experiment's fundamental at 2538 cm^{-1} in order to compare the overall rovibrational structure from the presently-computed vibrationally-excited rotational constants provided by the use of the VPT2 methodology in this work with that from the previously-reported laboratory spectrum. The bands align closely with the lower J bands of the previous experimental IR spectrum, only deviating after the third band. These deviations from higher frequencies can be attributed to the present work's rotational constants being lower than experiment which is expected.

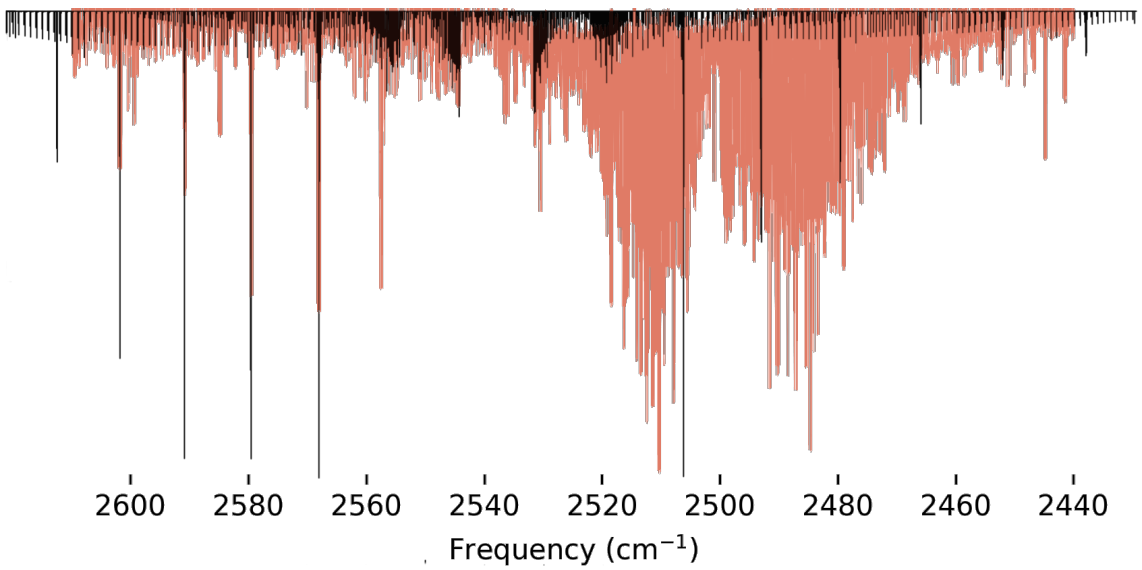

Figure 2.3: Simulated IR spectrum (black) of the S−H stretch for HOSH with the gas-phase IR spectrum from[5] (red) of the same mode containing the contamination from the $(\nu_1 + \nu_3)$ combination bands.

Moving toward detectability, the anharmonic intensities, seen in Table 2.5, show two relatively high intensity vibrational transitions. HOSH's most intense transition is, again, the ν_6 torsion at 72 km/mol, while the second is the ν_1, O−H stretch, fundamental transition at 67 km/mol. Compared to what is considered the intense transition of the anti-symmetric stretch of water at 70 km/mol, the two aforementioned transitions of HOSH are of similar intensity suggesting these are readily detectable. An additional benefit of the use of the QFF methods in this work is their ability to produce not only highly accurate ground vibrational state rotational constants, but also vibrationally excited rotational constants. The present work introduces such rotational constants for multiple fundamentals that serve to assist in accurate rovibrational modeling of HOSH as is discussed above for ν_2. These models are constructed to support further laboratory analysis or potential astronomical observation through the use of vibrationally-excited rotational spectroscopy as is the case for the detection of vibrationally excited states of the SiS[141] and C_6H[142] molecules observed in IRC+10216.

Similarly to HOOH, current literature discussing the two-quanta vibrational overtones and combination bands for HOSH is limited. To aid in this regard, the present work introduces such two-quanta modes for the purpose of benchmarking, assistance in potential astrophysical detection, and further laboratory analysis, as seen in in Table 2.6. Comparing to previous literature, a previous theoretical value[139] for the first overtone of the torsional motion, $2\nu_6 = 846.269$ cm^{-1}, is only 7.2 cm^{-1} higher the the present work's CcCR value of 839.1 cm^{-1}. This further suggests the reliability of the present theoretical methodology for generating two-quanta bands for molecules of this type. With regard to the detectability of these two-quanta transitions, much like in HOOH, the relative intensities are exceptionally lower than that of the anharmonic vibrational frequencies. The brightest transitions are the

first overtone of both the O−H stretch and the O−S−H bend at 5 km/mol and 4 km/mol, respectively. Once again, these two-quanta modes fall within the near- to short-wavelength mid-IR spectrum that the JWST will be able to probe more efficiently. Thus, the present work provides the necessary benchmark data for the potential astrophysical detection of HOSH *via* investigation of its overtones and combination bands.

2.3.3 HSSH

For much the same reason as HOSH, a potential energy scan of the torsion for HSSH is investigated to probe viability with the current QFF methods. In Fig. 2.2C, an even deeper potential well for this motion is shown compared to both HOSH and HOOH. This comparison can be clearly seen in Fig. 2.2C where the torsional PES scans of all three molecules are given. The *trans*-barrier height of 2026.6 $cm^{-1}$is the highest seen for each of the three molecules investigated in this work and is considerably higher than the HOOH *trans*-barrier height of 371.9 cm^{-1}. That being said, as with HOSH, the current rovibrational spectrum for this molecule should not suffer from the inaccuracies in the VPT2 corrections that are a byproduct of the shallow potential well.

With regard to the rotational constants of HSSH, provided in Table 2.7, considerable agreement is demonstrated in the present study's F12-TZ B_0 rotational constant of 6979.5 MHz being only 9.0 MHz above the gas-phase value, an error of 0.13%.[143] The same agreement is not present for the CcCR method's value of 7010.6 MHz being nearly 40.0 MHz above previous gas-phase experiment; nevertheless this difference is only 0.58% in error. With regard to the C_0 rotational constant, the CcCR method produces a value of 6938.1 MHz which is only 30.0 MHz below the 6967.68832 MHz gas-phase constant. The F12-TZ C_0 does not fare similarly, how-

Table 2.7: Geometrical Parameters and Spectroscopic Constants for HSSH Compared to Previous Gas Phase Experiment.

	Units	CcCR	F12-TZ	Prev. Theory	Prev. Expt.
r_e(H-S)	Å	1.34066	1.34213	1.3395[e]	1.3421[c]
r_e(S-S)	Å	2.05016	2.05579	2.0503[e]	2.0564[c]
$\angle_e$(H-S-S)	°	98.19	98.17	98.18[e]	97.88[c]
τ_e(H-S-S-H)	°	90.63	90.59	90.64[e]	90.34[c]
A_e	MHz	147873.5	147533.6		
B_e	MHz	7023.8	6986.4		
C_e	MHz	7022.3	6984.9		
$r_0(H_1\text{-}S_1)$	Å	1.34588	1.34733	1.34[b]	1.327[c]
$r_0(S_1\text{-}S_2)$	Å	2.05883	2.06453	2.082[b]	2.055[c]
$\angle_0(H_1\text{-}S_1\text{-}S_2)$	°	98.23	98.21	97.8[b]	91.33[c]
A_0	MHz	146754.2	146415.8		146858.1473[a]
B_0	MHz	7010.6	6979.5		6970.42953[a]
C_0	MHz	6938.1	6894.1		6967.68832[a]
A_1	MHz	144632.3	144299.4		
B_1	MHz	7016.9	6985.7		
C_1	MHz	6945.2	6901.1		
A_2	MHz	149577.8	156292.4		
B_2	MHz	7001.9	7029.5		
C_2	MHz	6924.8	6880.8		
A_3	MHz	146685.6	146348.2		146799.077[g]
B_3	MHz	6969.5	6938.4		6928.53044[g]
C_3	MHz	6898.1	6854.0		6926.67937[g]
A_4	MHz	145893.9	145559.8		
B_4	MHz	6982.3	6951.3		
C_4	MHz	6903.0	6859.0		
A_5	MHz	144698.0	144365.9	144702.2[f]	
B_5	MHz	7016.2	6985.0	6977.638[f]	
C_5	MHz	6944.5	6900.5	6975.508[f]	
A_6	MHz	146799.1	139393.7		
B_6	MHz	6980.1	6890.5		
C_6	MHz	6914.5	6870.6		
Δ_J	kHz	5.342	5.295		5.39849[d]
Δ_K	MHz	2.268	2.261		2.42355[d]
Δ_{JK}	kHz	85.417	84.400		85.5254[d]
δ_J	Hz	-8.572	-8.395		
$^g\delta_K$	MHz	17.569	20.809		
Φ_J	mHz	-1.211	-1.270		
Φ_K	Hz	103.985	106.134		
Φ_{JK}	Hz	5.649	6.891		
Φ_{KJ}	Hz	-15.461	-19.644		
ϕ_j	μHz	6.012	5.185		
ϕ_{jk}	Hz	449.754	638.243		
μ	D		1.15	1.30[b]	

[g a]Previous gas-phase ground state rotational constants from.[143]
[b]Previous theoretical geometry and dipole moment at the CCSD(T)/cc-pVTZ level of theory from.[144]
[c]Previous experimental structural data from.[145]
[d] Previous experimental centrifugal distortion constants from.[146]
[e] Previous theoretical geometrical parameters at the HF/VnZ(Q,5,6)+fc-CCSD(T)/VnZ(q,5)+CV/CCSD(T)/CVQZ level of theory with full-T,Q corrections and DPT2 corrections from.[147]
[f]Previous experimental rotational constants from.[148]
[g]Previous experimental rotational constants from.[149]

Table 2.8: Vibrational Frequencies (cm^{-1}), and IR intensities (km/mol) given in parentheses for HSSH Compared to Previous Gas Phase Experiment.

Mode	Desc.	CcCR	F12-TZ	Prev. Expt.
ω_1 (a)	S_2	2680.6	2674.8	
ω_2 (a)	S_3	908.1	907.9	
ω_3 (a)	S_1	529.9	528.0	
ω_4 (a)	S_4	443.7	441.1	
ω_5 (b)	S_5	2683.1	2677.2	
ω_6 (b)	S_6	907.3	907.7	
ν_1 (a)	S_2	2566.3	2563.5 (1)	2555.78[a]
ν_2 (a)	S_3	887.2	889.7 (1)	883[b]
ν_3 (a)	S_1	518.2	516.8 (1)	515.92230[b]
ν_4 (a)	S_4	405.8	417.6 (14)	416[a]
ν_5 (b)	S_5	2569.7	2566.2 (1)	2558.64[a]
ν_6 (b)	S_6	884.1	886.1 (2)	886[a]
ZPT		4020.2	4018.1	

[a]Previous gas phase experimental values from.[150]
[b]Previous gas phase experimental values from.[148]

ever, with its computed value being nearly 74.0 MHz lower than that from gas-phase experiment. As expected, the CcCR method produces a more accurate C_0 value only in error of 0.42%, while the F12-TZ value is in error of roughly 1.1%. Additionally, the current QFF methodology provides the computation of the vibrationally excited rotational constants that have not been previously investigated possibly offering supplemental data that may be necessary in the potential detection of this molecule rotationally or rovibrationally in the infrared.

Shown in Table 2.8, exceptional agreement can be seen between the two present QFF methods for the anharmonic vibrational frequencies of HSSH. The S−S stretch, fundamental ν_3, shows the best agreement between the computational values with F12-TZ's value of 516.8 cm^{-1} being within 2.0 cm^{-1} of CcCR. All fundamentals for HSSH are within 4.0 cm^{-1} between QFF methods, except for the CcCR torsional motion of ν_4 being 11.0 cm^{-1} below that of the F12-TZ method. When comparing to experiment, F12-TZ performs better with the best agreement being the H−S−S anti-symmetric bend, ν_6, at 886.1 cm^{-1}, being less than 0.2 cm^{-1} above previous

gas-phase experiment ν_3.[150] There is also considerable agreement between the previous gas-phase experiment's S−S stretching frequency and that from F12-TZ being within 0.9 cm^{-1} of one another. The same agreement with experiment is not suggested with regard to CcCR as almost every mode differs by more than 10.0 cm^{-1}, save for the ν_6 mode with a difference of 2.0 cm^{-1}. The difference between the CcCR QFF and experiment re-illustrates the high accuracy of the F12-TZ QFF method for anharmonic fundamental vibrational frequencies molecules of this type.

The anharmonic intensities of the vibrational transitions for HSSH are reported in Table 2.8. While the highest intensity transition, like HOSH, is the torsion, HSSH has by far the lowest intense of the molecules investigated in this work. HSSH's torsional motion has a calculated intensity of 14 km/mol, while it's second highest intensity transition is the ν_6 S−S−H bend at 2.0 km/mol. These are glaringly less intense than HOSH's 72 km/mol intensity for its ν_6, torsional, transition suggesting that HSSH is not nearly as observable *via* IR spectroscopy. Both gas-phase experiment or theoretical study, appears to be lacking with regard to the dipole moment. For this reason, while the present computed dipole moment of HSSH (1.15 D) is relatively small compared to the other sulfur-analog investigated in this work, it should nonetheless serve as a basis for potential radioastronomical observation.

Furthermore, the present work introduces calculated two-quanta vibrational overtones and and combination bands that appear to be missing from current literature, as seen in Table 2.9. There is previous experimental work[143] for the first overtone of the torsional motion, $2\nu_4$ = 808.0 cm^{-1}, that is only 3.8 cm^{-1} lower than the present work's F12-TZ value. Unlike HOOH and HOSH, HSSH exhibits no overtone or combination band transitions that have intensities over 1.0 km/mol potentially reducing its chance of detection through the use of IR spectroscopy and explaining why sulfur-containing molecules may be underdetected in astrophysical

Table 2.9: Vibrational Frequencies (cm^{-1}), and IR intensities (km/mol) given in parentheses for Two-Quanta Bands of HSSH Compared to Previous Gas-Phase Experiment.

Mode	CcCR	F12-TZ	Prev. Expt.
$2\nu_1$	5085.8	5080.2 (1)	
$2\nu_2$	1762.5	1766.1 (1)	
$2\nu_3$	1031.8	1029.2 (1)	
$2\nu_4$	776.8	811.8 (1)	808.0[a]
$2\nu_5$	5078.4	5074.3 (1)	
$2\nu_6$	1760.7	1765.1 (1)	
$\nu_1+\nu_2$	3447.1	3445.2 (1)	
$\nu_1+\nu_3$	3087.9	3082.9 (1)	
$\nu_1+\nu_4$	2977.8	2985.0 (1)	
$\nu_1+\nu_5$	5028.9	5025.5 (1)	
$\nu_1+\nu_6$	3447.0	3445.9 (1)	
$\nu_2+\nu_3$	1398.6	1399.0 (1)	
$\nu_2+\nu_4$	1290.7	1306.7 (1)	
$\nu_2+\nu_5$	3443.0	3442.4 (1)	
$\nu_2+\nu_6$	1763.5	1767.2 (1)	
$\nu_3+\nu_4$	919.1	930.3 (1)	
$\nu_3+\nu_5$	3084.3	3080.1 (1)	
$\nu_3+\nu_6$	1398.0	1398.6 (1)	
$\nu_4+\nu_5$	2973.8	2982.5 (1)	
$\nu_4+\nu_6$	1281.3	1298.1 (1)	
$\nu_5+\nu_6$	3444.2	3443.4 (1)	

[a]Previous gas-phase experimentally-attributed overtone from.[143]

sources. Nonetheless, the present works introduction of the two-quanta modes provides reference data for further laboratory benchmarking or potential astrophysical detection.

2.4 Conclusions

HOSH is the more likely candidate for potential astronomical detection as a possible sulfur sink in the dense ISM than HSSH. While the vibrational spectrum for HSSH contains more experimentally observed frequencies, the calculated intensities of those transitions are markedly lower than that of HOSH including the first overtones and combination bands. Each molecule investigated in this work shows the most intense and lowest energy anharmonic vibrational frequency to be the torsional

mode. For the investigation of the two sulfur-bearing analogs, the computed anharmonic intensities and dipole moments presented in this work shows that the more intense torsional transition belongs to HOSH at 72 km/mol which noticeably outshines HSSH's torsional transition of a mere 14 km/mol. Additionally, HOSH's net dipole moment of 1.60 D is almost 0.5 D greater than HSSH's 1.15 D further supporting HOSH as the more readily detectable sulfur-bearing molecule both rotationally and in the infrared.

Additionally, the present work has investigated the potential energy wells of the torsional motion for HOOH, HOSH, and HSSH. HOOH exhibits a relatively flat potential that diminishes the accuracy of the torsional fundamental as well as the ground state rotational constants when compared to both experiment and previous theory. The potential energy scans for HOSH and HSSH, however, show much deeper potential wells for this torsional motion, and the rovibrational spectra indicates that these molecules do not suffer from the same inaccuracies in their fundamentals and rotational constants. To that end, the present work includes not only ground state rotational constants, but also introduces vibrationally excited rotational constants for numerous fundamentals for both HOSH and HSSH that should exhibit the same level of accuracy. Additionally, the present work includes novel two-quanta modes for HOOH that have yet to be reported in literature and are included for the first time. This accuracy for the vibrationally-excited rotational constants is demonstrated for HOSH through their use alongside a previous experimental IR spectrum for the S−H stretching fundamental[5] centered at 2538 cm^{-1} simulates an IR spectrum that aligns well with previous gas-phase experiment for the lower J values, especially. This semi-quantitative agreement from the use of the vibrationally excited rotational constants provided in this work suggests that the rovibrational spectra for HOSH produced *via* the present QFF methodology can be trusted to serve as a basis and a benchmark

for any future comparison to or assignments from gas-phase IR spectroscopy.

The anharmonic fundamental vibrational frequencies, and their intensities, will be particularly useful for current observatories such as the *Stratospheric Observatory for Infrared Astronomy*. With the torsional frequency being the most intense and the lowest energy transition, the inclusion of the vibrationally excited rotational constants will be beneficial for detection from spaced-based observatories that will have the capability for both high-resolution and high sensitivity spectroscopy, notably the recently launched JWST. Similarly, the two-quanta modes introduced in the present work provide overtones and combination bands for each molecule investigated in this work, and have been utilized to confirm the assignment of the precious gas-phase value of 7041.8 cm^{-1} to the $\nu_1 + \nu_5$ combination band. The provided first overtones and combination bands fall in regions of the IR spectrum that have been understudied but can now be efficiently probed through the use of JWST, most notably its NIRSpec instrument. In this regard, the present work provides the necessary reference data to assist in the astrophysical detection of HOSH and perhaps HSSH. Finally, the rotational spectroscopic constants provided in this work will be essential for ground-based radio telescopic observation from facilities such as the *Atacama Large Millimeter/submillimeter Array*. Consequently, the investigation of HOSH and HSSH may provide a clue as to where the molecular sulfur in the dense ISM has been eluding detection for the past 50 years.

CHAPTER 3

Fluoro Hydrogen Peroxide: A Plausible Molecular Form of Naturally-Occuring Fluorine.

Reproduced from Palmer, C. Z.; Fortenberry, R. C.

ACS Earth & Space **2022**, *6*, 2032-2040. © 2022 American Chemical Society

DOI: 10.1021/acsearthspacechem.2c00114

Abstract

Fluorine's hostile nucleosynthetic environment makes it one of the least common elements, and, consequently, understudied both on the earth and in the interstellar medium (ISM). However, the presence of fluorine-containing species in both the ISM and in the earth's atmosphere necessitates the existence of a pathway out of this environment to form fluorine-containing molecules. To that end, the presence of fluorine and hydroperoxyl radical (HO_2) in either of these environments may lead to the formation of fluorinated molecules like fluoro hydrogen peroxide (HOOF) on dust grains of protoplanetary disks in the planet-forming regions of ρ Oph and in the earth's atmosphere as a sink for other fluorine pollutants that have yet to be detected. This theoretical study utilizes explicitly correlated coupled cluster theory computed with core correlation and corrections from scalar relativity, to provide the first anharmonic fundamental vibrational frequencies and rotational constants of HOOF for use as reference benchmarking of any further computational or experimental study, as well as potential astrophysical observation. The ν_6 bending frequency for HOOF at 454.4 cm^{-1} exhibits an anharmonic transition intensity of 78 km/mol,

while the ν_4 frequency at 738.2 cm^{-1} is 66 km/mol. Additionally, HOOF has a large net dipole moment of 2.12 D compared to the previously detected HF and HOOH molecules, 1.82 and 1.85 D respectively, resulting from the electronegativity of the fluorine. Consequently, HOOF is a likely candidate for possible detection *via* vibrational and rotational spectroscopy to further the understanding of fluorine's small, but important, role in astrochemical and atmospheric environments.

3.1 Introduction

Other than H and He, which make up approximately 99% of the universe, the eight most abundant elements in the interstellar medium (ISM) are O, C, Ne, N,[151] Mg,[152] S,[153] Si,[154] and Fe.[155] However, astrochemically important molecules exist that are comprised of elements that are far less abundant. Fluorine, for example, is the 24th most common element in the ISM[156,157] and has only been uniquely, astronomically observed in three chemical species. The first unique observation of fluorine was its monatomic form toward δ Sco region of the ISM in 1981.[158] The first interstellar fluorine-containing molecule observed was aluminum fluoride (AlF) with its presence in the ISM confirmed in 1994 towards IRC+10216.[159] Since fluorine is one of the most reactive elements known, it interacts with the abundant H in the universe to form the strong bond found in hydrogen fluoride (HF) which was first observed near Sgr B2 in 1997.[160] With the abundance of atomic fluorine in the ISM being $\sim 3.0 \times 10^{-10}$ compared to H_2, most gaseous fluorine in the ISM is theorized to be locked up in the HF molecule.[160,161] This census, however, does not account for fluorine that may have been depleted onto interstellar dust grains and may contribute to the production of further, unique fluorine-containing species. Additionally, while not necessarily another unique observation, the ^{26}AlF isotopologue was first observed towards CK Vul more recently in 2018.[162] The presence of fluorine and a radioactive

isotope of aluminum implies the unique chemistry present in the region of CK Vul where such a region could be a vital source of less common astrochemicals.

Mystery still surrounds the formation of molecules containing fluorine in the ISM due to this element's relatively low abundance. This low abundance arises from fluorine nuclei succumbing to annihilation by surrounding H and He atoms almost as soon as it is created in stellar nucleosynthesis. However, the presence of fluorine-containing species in the ISM suggests that this highly reactive halogen escapes such a hostile environment. Fluorine's nucleosynthesis is the subject of ongoing debate, but three theories have been proposed that may provide insight as to how fluorine atoms circumvent this annihilation. The first theory is that a burst of neutrinos from type II supernovae breakdown ^{20}Ne atoms stored within a massive star into the stable ^{19}F atom that are then carried away before collisions with H and He can further break them down.[163,164] The next theory involves the catalytic CNO-cycle that governs the hydrogen-to-helium fusion reaction yielding helium, neutrinos, fluorine, and gamma-rays in massive stars like Wolf-Rayet stars.[165] The last theory involves the re-ignition of the helium shell in late-stage asymptotic giant branch (AGB) star[166] in a process known as a helium-shell flash. Each of the three theories presented will produce ^{19}F and blow it away faster than the surrounding He can annihilate it. For this reason, the detection of more fluorine-containing species in the ISM may provide the necessary observational data to confirm or improve one of the three theorized nucleosynthetic processes.

Conveniently, within the planet-forming regions of ρ Oph A, the hydroperoxyl radical, HO_2, was first observed in 2012[167] following the observation of HOOH in 2011.[93] The formation pathway of HOOH in this region is believed to be the successive addition of H atoms onto O_2 molecules present on the surface of the dust grains found in these regions. Similarly, the formation pathway for the HO_2 radical is

theorized to be singular addition of an H atom onto O_2. If a jettisoned monatomic fluorine atom depletes onto dust grains in these planet-forming regions, the interaction between fluorine (instead of the typical hydrogen atom) and HO_2 radical may lead to the formation of the understudied fluoro hydrogen peroxide (HOOF) molecule. If HOOF can be found in the ISM, it may provide the necessary data for investigating the unknown nucleosynthetic processes of fluorine found in the ISM.

Terrestrially, fluorine is found in many naturally occurring minerals such as fluorite, fluorapatite, and cryolite. While fluorine's abundance on Earth is vastly lower than other elements like oxygen, its presence within these minerals suggests that some amount must exist in protoplanetary disks. This implies that at least part of the abundance of fluorine in the ISM has depleted from the gas-phase onto dust grains found within the ISM. As a result, if a newly generated fluorine nucleus can escape its demise by any of the previously mentioned proposed pathways, fluorine atoms would likely reach some planet-forming region. This is especially the case for the planet-forming regions near δ Sco where, as mentioned previously, monatomic fluorine was first observed in the ISM[158] and other relatively close planet-forming regions like in the ρ Oph A stellar complex where fluorine nucleosynthesis may occur. Thus, the detection of new fluorine-containing species may be found from unique mechanisms involving fluorine atoms and other molecules found on the surface of interstellar dust grains.

Within the Earth's atmosphere, both fluorine-containing species and HO_2 radical have been classified as pollutants.[26,168] Additionally, the most common form of fluorine in the atmosphere, chlorofluorocarbons (CFCs), are known to cause degradation to the ozone layer and trap heat within the atmosphere. Recent studies, however, show that CFC emission has been steadily decreasing over the years[26] while other forms of fluorine pollutants are still large contributors. HF is a toxic gas that has

made its way into the atmosphere and still has limited information known about it[169] insinuating that other fluorinated pollutants may exist that have yet to be classified. Additionally, HO_2 is considered a toxic oxidant that is known to generate HOOH in the Earth's atmosphere contributing to plant cell damage. Furthermore, the HO_2 radical is also known to assist in the production of other toxic gases such as NO_x, SO_x, and ClO_x.[168,170] If the HO_2 radical oxidizes fluorinated pollutants, the resulting interactions may lead to the formation of HOOF in the Earth's atmosphere. Furthermore, there are forms of peroxides that are known already to contain fluorine here on the Earth. For example, Bis[trifluoromethyl] peroxide has been historically used as an etching agent for silicon etching, and sets a precedent for peroxide environments that contain fluorine readily here on the Earth.[171] If HOOF can be classified in the Earth's atmosphere, it may offer another fluorine-containing species that can be investigated as a possible contributor to pollution present in the atmosphere.

To that end, detecting HOOF in the ISM, the atmosphere, or even in the laboratory will require rovibrational reference data which are provided herein *via* highly-accurate quantum chemical calculations known as quartic force fields (QFFs). A QFF is a fourth-order Taylor series expansion to the potential portion of the internuclear Watson Hamiltonian.[66] QFFs have been used to produce rotational constants and fundamental anharmonic frequencies within 1% of experimental values for many molecular systems.[39,40,76–78,80,97,99–101,103] The QFFs computed herein are coupled with high-level quantum chemical electronic structure computations to provide the set of reference rovibrational spectral data required for potential astrophysical[98,102,172,173] or atmospheric detection of these fluorine-containing species as another unique molecular form of the limited fluorine present in the ISM or the Earth's terrestrial veil.

3.2 Computational Details

The QFF methods implemented in this work are based on coupled cluster theory at the singles doubles and perturbative triples [CCSD(T)] level.[58] The first method uses the CCSD(T) level of theory within the explicitly correlated F12b[62,64] formalism along with the cc-pVTZ-F12 basis set.[174,175] This CCSD(T)-F12b/cc-pVTZ-F12 level of theory (furthermore abbreviated as F12-TZ) has shown to produce exceptionally accurate fundamental vibrational frequencies at far less computational cost compared to other QFF methods.[104,105,176] The second method utilized in this work is related to both the highly-accurate and establish composite approach involving a complete basis limit extrapolation and corrections for relativity and core electron correlation (CcCR) and the F12-TZ level of theory previously mentioned. Much like the first method, this second QFF method utilizes CCSD(T)-F12b, but includes core correlation *via* the cc-pCVTZ-F12 basis set.[177] The addition of the core correlation in the explicitly correlated basis set is an attempt at mimicking both the corrections to the complete basis set limit extrapolation[116] and the core electron correlation[108] present in the CcCR composite method.[178] Additionally, the scalar relativistic corrections[117] present in the CcCR methodology are included in the second QFF method in this work. With these corrections applied to the F12-TZ QFF method, this second QFF methodology will henceforth be abbreviated F12-TZ-cCR.[179] The F12-TZ-cCR QFF method has been shown to find a sweet-spot between the significantly reduced computational cost of F12-TZ and the accuracy of CcCR.[179,180]

Regardless of QFF method, the molecular geometry of HOOF is first optimized with exceptionally tight convergence criteria *via* the MOLPRO 2020.1 quantum chemical package.[107] The F12-TZ QFF optimizes its geometry at the CCSD(T)-F12b/cc-pVTZ-F12 level of theory, while the F12-TZ-cCR optimizes the geometry

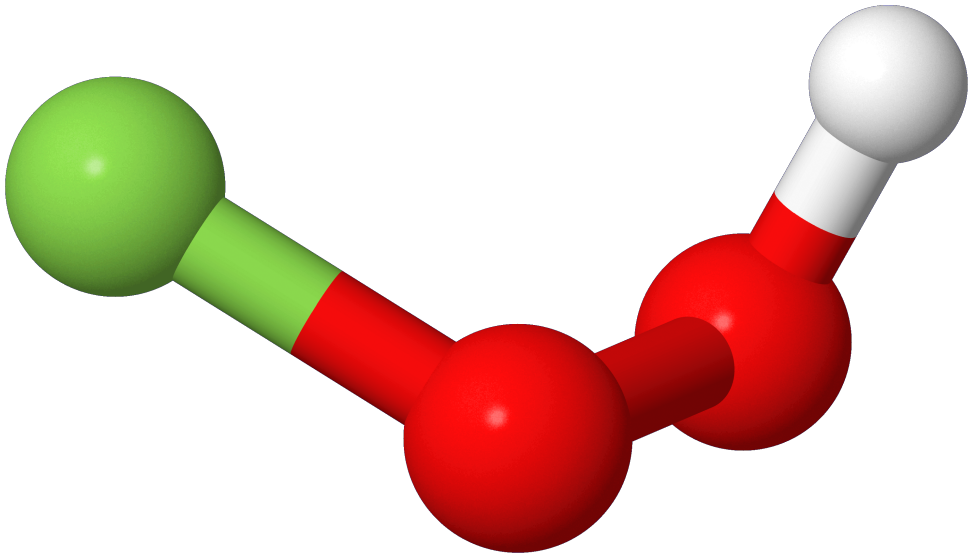

Figure 3.1: Visual depiction of the optimized structure for HOOF

at the CCSD(T)-F12b/cc-pCVTZ-F12 level. These optimized geometries are then displaced at 0.005 Å for bond lengths and 0.005 radians for bond angles/torsions using symmetry-internal coordinates *via* the INTDER[73] program. The simple-internal coordinate system for HOOF requires 1289 points for the QFF and is defined from the atoms in Fig. 3.1:

$$S_1 = r(\mathrm{H}-\mathrm{O}) \tag{3.1}$$

$$S_2 = r(\mathrm{O}-\mathrm{O}) \tag{3.2}$$

$$S_3 = r(\mathrm{O}-\mathrm{F}) \tag{3.3}$$

$$S_4 = \angle(\mathrm{H}-\mathrm{O}-\mathrm{O}) \tag{3.4}$$

$$S_5 = \angle(\mathrm{O}-\mathrm{O}-\mathrm{F}) \tag{3.5}$$

$$S_6 = \tau(\mathrm{H}-\mathrm{O}-\mathrm{O}-\mathrm{F}). \tag{3.6}$$

Single-point energy calculations for every displacement are then computed utilizing both QFF methods. The F12-TZ methodology simply computes the ener-

gies at the CCSD(T)-F12b/cc-pVTZ-F12 level of theory. The F12-TZ-cCR QFF first computes these single-point energies at the CCSD(T)-F12b/cc-pCVTZ-F12 level of theory. Then the Douglas-Kroll scalar relativistic corrections[117] are added by computing the difference in energies at the CCSD(T)/cc-pVTZ-DK level of theory with said corrections turned either on or off. Once the single-point energy calculations for either QFF method are finished, their relative energies are fit to the QFF Taylor series model utilizing a least squares fit procedure to better than 10^{-17} a.u.[2]. The QFF is then re-fit once again to include the corrections from the computed Hessian that will construct the final equilibrium geometry. The force constants that are generated from the least-squares re-fitting produce zero-gradients and are transformed into Cartesian coordinates through the INTDER[73] program. Finally, the new Cartesian-based force constants are utilized by SPECTRO[68] to generate the fundamental vibrational frequencies and spectroscopic constants produced by rotational and vibrational perturbation theory at second-order (VPT2).[67,75,118] The produced spectroscopic constants include the ground state and vibrationally-excited rotational constants and the quartic and sextic distortion constants, Δ and Φ, respectively, from the A-reduced Watson Hamiltonian.[67]

For the purpose of comparison between the two QFF methods employed in this work, a mean absolute difference (MAD) formula is used and follows the standard form:

$$\bar{x} = \frac{1}{n}\sum_{i=0}^{i}|x_i - y_i|. \tag{3.7}$$

For example, when this is applied to the rotational constants, "n" is the total number of values for a given rotational constant, and "x" and "y" are the F12-TZ and F12-TZ-cCR values, respectively, for the rotational constant in question. Additionally,

the mean absolute percent difference (MA%D) is also used and changes the above formula as follows:

$$\bar{x} = \frac{1}{n} \sum_{i=0}^{i} \frac{|x_i - y_i|}{x_i}. \tag{3.8}$$

The aforementioned formulae have been applied to the rotational constants and anharmonic vibrational frequencies produced by the QFF methods discussed in this work.

Additionally, the rovibrational spectra for HOOF contain Fermi resonances and resonance polyads that are treated by the SPECTRO program to correct the predictions[119] of the rovibrational spectra. The spectrum for HOOF contains a $2\nu_4{=}\nu_5+\nu_3{=}\nu_5+\nu_4{=}\nu_6+\nu_3{=}\nu_2$ and a $2\nu_5{=}2\nu_6{=}\nu_6+\nu_5{=}\nu_3$ Fermi resonance polyad. Further, dipole moments for HOOF are computed using the F12-TZ QFF method. Anharmonic infrared intensities are calculated using the Gaussian16[120] quantum chemical package at the MP2/cc-pVDZ level of theory.[51] The values at this level of theory have been shown to yield semi-quantitative agreement with higher at levels of theory for less computational cost.[121,122,181,182] These transition intensities are proportional to the change in the dipole moment at a particular vibrational frequency, i.e. the greater the change in the dipole moment from a given vibrational transition, the greater the intensity of that transition.

3.3 Results and Discussion

3.3.1 Spectroscopic Data & Astrophysical/Atmospheric Implications

As mentioned previously, HOOF is an understudied fluorine-containing species that has little, if any, previous experimental or theoretical data. Therefore, the computed spectroscopic constants and fundamental anharmonic vibrational frequencies

Table 3.1: Geometrical Parameters and Spectroscopic Constants for HOOF.

	Units	F12-TZ	F12-TZ-cCR	F12-TZ-cCR[a]
R_e(H-O_1)	Å	0.96940	0.96864	0.96864
R_e(O_1-O_2)	Å	1.37112	1.36969	1.36969
R_e(O_2-F)	Å	1.46187	1.46121	1.46121
$\angle_e$(H-O_1-O−2)	°	102.68	102.71	102.71
$\angle_e$(O_1-O_2-F)	°	105.42	105.43	105.43
τ_e(H-O_1-O_2-F)	°	84.70	84.71	84.71
A_e	MHz	55485.9	55586.3	55586.3
B_e	MHz	10775.1	10788.6	10788.6
C_e	MHz	9293.9	9306.2	9306.2
R_0(H-O_1)	Å	0.96715	0.96638	0.96638
R_0(O_1-O_2)	Å	1.38059	1.37917	1.37918
R_0(O_2-F)	Å	1.46887	1.46820	1.46818
$\angle_0$(H-O_1-O−2)	°	102.87	102.90	102.90
$\angle_0$(O_1-O_2-F)	°	105.40	105.42	105.41
A_0	MHz	55250.2	55350.3	55352.4
B_0	MHz	10687.6	10700.9	10700.8
C_0	MHz	9199.3	9211.5	9211.5
A_1	MHz	55122.6	55222.5	55224.4
B_1	MHz	10678.3	10691.5	10691.3
C_1	MHz	9197.7	9209.8	9209.7
A_2	MHz	55177.3	55276.6	55276.2
B_2	MHz	10659.5	10672.9	10672.5
C_2	MHz	9185.9	9198.1	9197.8
A_3	MHz	55014.1	55112.8	55115.1
B_3	MHz	10640.0	10653.3	10653.3
C_3	MHz	9177.2	9189.3	9189.5
A_4	MHz	54915.5	55016.3	55017.4
B_4	MHz	10615.4	10628.7	10628.7
C_4	MHz	9111.5	9123.6	9123.6
A_5	MHz	55188.5	55289.2	55299.0
B_5	MHz	10692.1	10705.3	10705.8
C_5	MHz	9180.6	9192.7	9193.4
A_6	MHz	55612.4	55712.0	55714.0
B_6	MHz	10664.6	10677.9	10677.5
C_6	MHz	9154.0	9166.1	9165.9
Δ_J	kHz	14.947	15.000	15.001
Δ_K	MHz	1.286	1.291	1.291
Δ_{JK}	kHz	-56.703	-56.715	-56.670
δ_J	kHz	2.923	2.931	2.931
δ_K	kHz	47.784	47.993	47.987
Φ_J	mHz	15.791	15.820	15.746
Φ_K	Hz	99.638	100.288	100.190
Φ_{JK}	mHz	119.945	121.794	125.587
Φ_{KJ}	Hz	-15.277	-15.368	-15.368
ϕ_j	mHz	9.527	9.557	9.516
ϕ_{jk}	mHz	-45.417	-45.680	-46.407
ϕ_k	Hz	14.904	15.007	15.016
μ_a	D	1.75		
μ_b	D	0.45		
μ_c	D	1.35		
μ_{net}	D	2.12		

[a]Geometrical parameters and spectroscopic constants computed using the F12-TZ-cCR QFF method but utilizing a looser energy convergence threshold for the geometry optimization.

for HOOF in this work provide the necessary reference benchmark data for potential astrophysical and atmospheric observation and laboratory analysis. To that end, the spectroscopic data computed from QFF methods are given in Tables 3.1 and 3.2. For the rotational constants, found in Table 3.1, there is a general trend when comparing the two QFF methods utilized in this work. For example, the vibrationally-averaged B rotational constants for F12-TZ-cCR are higher than the F12-TZ values by a MAD of 13.3 MHZ. Similarly, the vibrationally-averaged C rotational constants for F12-TZ-cCR are higher than the F12-TZ QFF with a MAD of 12.2 MHz. Regardless of the trend, both the B and C rotational constants agree exceptionally well between the two QFF methods with the MAD between them being well within the accepted 20 MHz difference for comparison of these rotational constants to experiment.[40,76,77] This systematic trend is not unexpected, however, as the biggest difference between the two QFF methods are the scalar relativistic corrections since the core correlation matters most when the molecule in question has a bond order grater than one, which is not the case for HOOF. Regardless, the differences between the two QFF methods are meant to improve the rovibrational data collected from the F12-TZ QFF method. In fact, previous studies[41,180] utilizing the F12-TZ-cCR QFF report that the rotational constants generated contain, on average, less error when compared to previous gas-phase experiment than that of either F12-TZ or CcCR QFFs. Therefore, the rotational constants introduced in this work via the F12-TZ-cCR QFF methodology will provide the necessary data for benchmarking, laboratory analysis, and potential atmospheric or astrophysical detection via rotational spectroscopy.

The fundamental anharmonic vibrational frequencies of HOOF produced by the two QFF methods utilized in this work are introduced in Table 3.2 with a visual description of each mode given in Fig. 3.2. The vibrational frequencies compare well between F12-TZ and F12-TZ-cCR with the worst comparison being the ν_1 mode,

Table 3.2: Vibrational Frequencies (cm^{-1}) and IR intensities (km/mol) given in parentheses for HOOF.

Mode	Desc.	F12-TZ	F12-TZ-cCR	F12-TZ-cCR[a]
ω_1	S_1	3710.1	3711.7	3711.6
ω_2	S_4	1463.1	1464.4	1464.4
ω_3	$0.83S_2$+$0.09S_3$-$0.07S_5$	979.0	979.4	979.3
ω_4	$0.72S_3$-$0.16S_2$-$0.11S_5$	759.9	759.7	759.72
ω_5	$0.79S_6$-$0.14S_5$-$0.07S_3$	543.5	543.5	543.3
ω_6	$0.68S_5$+$0.20S_6$+$0.11S_3$	465.7	465.8	465.8
ν_1	S_1	3508.8 (31)	3510.6	3509.0
ν_2	S_4	1420.5 (42)	1421.7	1423.0
ν_3	$0.83S_2$+$0.09S_3$-$0.07S_5$	938.2 (27)	938.7	954.9
ν_4	$0.72S_3$-$0.16S_2$-$0.11S_5$	738.2 (66)	738.2	723.4
ν_5	$0.79S_6$-$0.14S_5$-$0.07S_3$	516.6 (27)	517.0	578.5
ν_6	$0.68S_5$+$0.20S_6$+$0.11S_3$	454.5 (78)	454.8	433.3
ZPT		3899.7	3901.5	3910.3

[a]Vibrational frequencies computed using the F12-TZ-cCR QFF method but utilizing a looser energy convergence threshold for the geometry optimization.

the O-H stretch, at only a difference of 1.8 cm^{-1} or 0.05%. The best comparison, however, is the ν_4 mode, the O-F stretch, having almost no difference. Additionally, the MAD for the anharmonic fundamental vibrational frequencies is 0.7 cm^{-1} with a MA%D of a mere 0.06%. Furthermore, fundamental vibrational frequencies generated from the F12-TZ methodology in previous studies[104–106,178,183] suggest exceedingly high accuracy for comparison to previous experiments. However, much like the rotational constants, previous theoretical work[41,180] utilizing the new F12-TZ-cCR QFF methods show almost as, if not more, accurate fundamentals than F12-TZ when compared to previous gas-phase experimental studies. The high accuracy exhibited by both QFF methods in previous studies further suggests their validity for application in generating highly accurate vibrational frequencies for a molecule such as HOOF. Finally, with both QFF methods exhibiting low differences between produced spectroscopic data, the provided fundamental frequencies can serve as the reference data for any further benchmarking whether theoretical, experimental, atmospheric classification, or astrophysical observation via IR spectroscopy.

Regarding the detectability, the anharmonic intensities of HOOF, given in

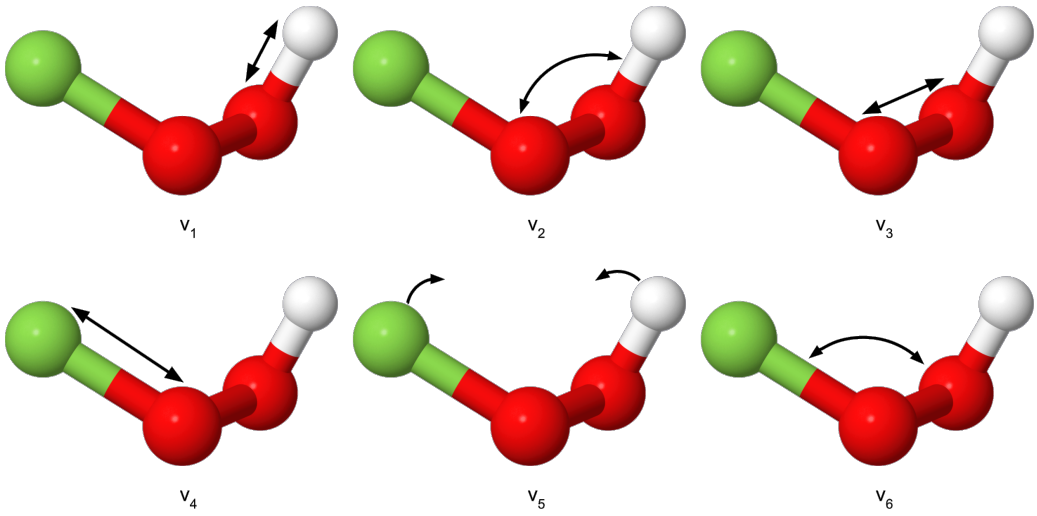

Figure 3.2: Visual depiction of the motions for each vibrational mode.

Table 3.2, show two relatively large vibrational intensities. The most intense vibrational transition is found in ν_6, the O-O-F bend at 454.5 cm^{-1}, and exhibits a vibrational transition of 78 km/mol. Comparing this transition to the O-H antisymmetric stretch of water at 70 km/mol, which is considered to be an intense vibrational transition, suggests that this mode should be detectable even with the assumed lower abundances of the fluorine-containing molecule. Additionally, ν_4, the O-F stretch at 738.2 cm^{-1} exhibits a transition of 66 km/mol. This is only slightly under the 70 km/mol transition of water but should still be considered relatively intense in terms of observation via IR spectroscopy for organic molecules or those comprised of second-row atoms. Also, HOOF possesses a large net dipole 2.12 D which is noticeably large compared to the dipole moment of water at 1.85 D and even hydrogen peroxide at 1.82 D more than likely due to the presence of the fluorine atom. For this reason, the computed net dipole moment for HOOF reported herein should be considered large enough to warrant potential radioastronomical observation or atmospheric microwave spectroscopy.

In order to assess the viability and persistence of the HOOF molecule for

potential astronomical or atmospheric observation, the bond strengths of the HOOF are computed in this work, in kcal/mol, at the F12-TZ level and given in the following scheme:

$$\begin{aligned}
&\mathrm{HO}\cdot + \cdot\mathrm{OF} \rightarrow \mathrm{HOOF} && = -44.96\\
&\mathrm{H}\cdot + {}^2A^{"}\cdot\mathrm{OOF} \rightarrow \mathrm{HOOF} && = -69.21\\
&\mathrm{HOO}\cdot + \cdot\mathrm{F} \rightarrow \mathrm{HOOF} && = -31.53\\
&\mathrm{HO}\cdot + \cdot\mathrm{OH} \rightarrow \mathrm{HOOH} && = -48.09\\
&\mathrm{FO}\cdot + \cdot\mathrm{OF} \rightarrow \mathrm{FOOF} && = -44.02\\
&\mathrm{F}\cdot + {}^2A^{"}\cdot\mathrm{OOF} \rightarrow \mathrm{FOOF} && = -17.20.
\end{aligned}$$

Table 3.3: F12-TZ fundamental anharmonic vibrational frequencies (cm^{-1}) with IR intensities (km/mol) given in parentheses and dipole moments for HOOF, HOOH, and HOSH.

Mode	HOOF	HOOH[a]	HOSH[a]
ω_1	3710.1	3798.5	3819.6
ω_2	1463.1	1437.6	2656.1
ω_3	979.0	911.3	1211.0
ω_4	759.9	380.4	1032.8
ω_5	543.5	3798.4	784.7
ω_6	465.7	1330.1	479.6
ν_1	3508.8 (31)	3607.5 (11)	3626.7 (67)
ν_2	1420.5 (42)	1393.9 (1)	2544.9 (8)
ν_3	938.2 (27)	875.3 (1)	1176.7 (36)
ν_4	738.2 (66)	319.4 (164)	1008.3 (2)
ν_5	516.6 (27)	3605.2 (49)	763.4 (47)
ν_6	454.5 (78)	1275.9 (119)	447.4 (72)
ZPT	3899.7	5730.6	4920.2
μ_a	1.75		1.41
μ_b	0.45		0.76
μ_c	1.35		0.05
μ_{net}	2.12	1.75	1.60

[a]Previous theoretical values for the vibrational frequencies and dipole moments from Ref. 184

Comparing the O−O bond strength in HOOF to the previously computed[184] O−O bond strength of HOOH, first observed in the ISM in 2011[93] shows good agree-

ment with a difference of only 3.0 kcal/mol, suggesting this bond will persist after formation. The O−F bond strength, however, is much weaker at -31.53 kcal/mol which is a 30% difference from the O−O bond strength of HOOH calling into question its persistence. However, when compared to F_2O_2, a previously-characterized molecular fluorine-containing peroxide species,[185] the O−O bond strength is within 1.0 kcal/mol of HOOF's O−O bond strength suggesting that it may still persist. Furthermore, the O−F bond strength of HOOF is -31.53 kcal/mol is 14 kcal/mol stronger than the O−F bond in F_2O_2 at -17.20 kcal/mol. Consequently, HOOF should persist long enough for potential astrophysical and atmospheric detection.

Additionally, a comparison of the vibrational frequencies and dipole moments between HOOF and other peroxides such as HOOH and the theorized hydrogen thioperoxide (HOSH) molecule are given in Table 3.3. The data for both HOOH and HOSH come from a previous theoretical study[184] that also utilizes the F12-TZ QFF method to compute accurate vibrational frequencies. HOOH exhibits more intense vibrational transitions than either HOSH and HOOF with HOOH's largest being the torsional motion, ν_4 at 164 km/mol and its second largest being the anti-symmetric H−O−O bend, ν_6, at 119 km/mol. HOSH and HOOF do not contain any transitions that are as intense as HOOH. However their two most intense vibrational transitions are fairly similar in magnitude suggesting they are both as detectable as the other with regard to IR spectroscopy. To the dipole moments, HOOF contains the largest net dipole moment of either HOOH and HOSH at 2.12 D. This is not unexpected given the greater electronegativity of the fluorine atom compared to either sulfur or oxygen further suggesting its assistance in potential radioastronomical observation in the ISM or atmospheric detection *via* rotational spectroscopy.

3.3.2 Theoretical Implications

One of the major improvements introduced through the F12-TZ-cCR method is the significant reduction in the time needed to produce the spectroscopic data when compared to previously used composite methods like CcCR. In an effort to save even more computational time, the convergence threshold that governs at what point the geometry optimization *via* MOLPRO has reached the lowest energy has been reduced from the standard 10^{-12} E_h to 10^{-8} E_h. The resulting spectroscopic data produced from this "loose F12-TZ-cCR" (i.e. that with 10^{-8} E_h convergence) QFF can also be seen in Tables 3.1 and 3.2. With regard to the rotational constants seen in Table 3.1, the loose F12-TZ-cCR QFF shows only minor discrepancies. For example, the loose F12-TZ-cCR A_5 rotational constant shows the largest difference of 9.8 MHz, less than 0.03%, while multiple other rotational constants show almost no difference at all when compared to the same rotational constants from the F12-TZ-cCR QFF with the tight energy convergence threshold. The total time saved from using the loose F12-TZ-cCR compared to the tight F12-TZ-cCR QFF method is approximately 148 hours, a reduction of 27.5%, and it introduces negligible error in the rotational constants. Consequently, loose F12-TZ-cCR QFF is a time-saving, alternative QFF method that produces rotational data that is just as accurate as its more time-costly partner.

This is not the case, however, with regard to the fundamental vibrational frequencies. As shown in Table 3.2, the fundamentals produced from the loose F12-TZ-cCR show considerable difference compared to the F12-TZ-cCR and F12-TZ fundamentals. The worst comparison between the loose F12-TZ-cCR and F12-TZ is the torsional motion, ν_5 at 578.5 cm^{-1}, being nearly 62 cm^{-1} higher than the F12-TZ value of 516.6 cm^{-1}, an error of 12%. The ν_5 anharmonic frequency also exhibits a positive anharmonicity highlighting that the underlying potential surface

Table 3.4: Vibrational Frequencies (cm^{-1}) with corrections relative to F12-TZ parentheses for HOOF.

Mode	Desc.	F12-TZ	F12-TZ-cCR	ΔR	ΔcC	F12-TZ-cCR[a]	ΔR[a]	ΔcC[a]
ω_1	S_1	3710.1	3711.7	−4.8	+6.3	3711.6	−4.8	+6.3
ω_2	S_4	1463.1	1464.4	−1.0	+2.4	1464.4	−1.0	+2.0
ω_3	$0.83S_2$+$0.09S_3$-$0.07S_5$	979.0	979.4	−2.1	+2.4	979.3	−2.1	+2.4
ω_4	$0.72S_3$-$0.16S_2$-$0.11S_5$	759.9	759.7	−1.0	+0.8	759.72	−1.0	+0.5
ω_5	$0.79S_6$-$0.14S_5$-$0.07S_3$	543.5	543.5	−0.9	+0.9	543.3	−0.9	+0.6
ω_6	$0.68S_5$+$0.20S_6$+$0.11S_3$	465.7	465.8	−1.3	+1.4	465.8	−1.3	+1.2
ν_1	S_1	3508.8	3510.6	−3.0	+5.9	3509.0	−7.0	+6.4
ν_2	S_4	1420.5	1421.7	−1.4	+2.6	1423.0	+9.6	+9.3
ν_3	$0.83S_2$+$0.09S_3$-$0.07S_5$	938.2	938.7	−1.8	+2.4	954.9	+24.1	+20.8
ν_4	$0.72S_3$-$0.16S_2$-$0.11S_5$	738.2	738.2	−0.6	+0.9	723.4	−5.4	−12.5
ν_5	$0.79S_6$-$0.14S_5$-$0.07S_3$	516.6	517.0	−1.0	+1.4	578.5	−35.6	+95.9
ν_6	$0.68S_5$+$0.20S_6$+$0.11S_3$	454.5	454.8	−1.0	+1.4	433.3	−3.6	−11.6
ZPT		3899.7	3901.5	−4.9	+7.2	3910.3	−16.6	+27.8

[a]Vibrational frequencies from lowered energy convergence threshold QFF.

is not even properly described with the loose convergence criteria. In fact, only two vibrational frequencies produced by the loose F12-TZ-cCR are less than 1.0% in error: the O-H stretch, ν_1, and the H-O-O bend, ν_2. Overall, the MA%D for the fundamentals from the loose F12-TZ-cCR QFF is 3.4% when comparing to the F12-TZ QFF. While there is considerable time saved from using the loose F12-TZ-cCR QFF compared to the tight F12-TZ-cCR QFF, the degradation in the fundamental vibrational frequencies by such a large margin of error does not suggest its feasibility for investigating vibrational molecular spectra.

In order to investigate this behavior, QFFs are conducted piecewise utilizing the loose convergence criteria with either the scalar relativistic or the core correlation corrections removed. This data has been provided in Table 3.4 with corrections relative to F12-TZ QFF values. One obvious conclusion from these loose F12-TZ-cCR piecewise QFFs is that the contributions from the core correlation corrections radically overshoots the ν_5 torsional mode. The scalar relativistic corrections fortuitously corrects for this but still is not enough to bring the frequencies within an acceptable margin of error. Consequently, the MA%D for the additions of only core

correlation is 4.3%, while the scalar relativistic corrections produce a 2% MA%D. The greater likely error introduced from just the inclusion of the core correlation over the scalar relativity is not unexpected as scalar relativistic corrections are generally more important for larger atoms and would, therefore, have less impact on the fundamentals for second-row atoms. Regardless, the large error introduced from the loose F12-TZ-cCR QFF method, again, seems infeasible for benchmarking the fundamental vibrational frequencies of any subsequent theoretical or experimental study.

3.4 Conclusions

The low margin of difference exhibited in the rovibrational spectroscopic data of HOOF between the accurate, well documented F12-TZ QFF and the relatively new F12-TZ-cCR QFF suggest that the data provided herein are accurate and reliable. Additionally, based on previous studies utilizing the F12-TZ-cCR QFF method, any discrepancies between it and the F12-TZ QFF method may suggest that F12-TZ-cCR's computed rotational constants and vibrational frequencies are more accurate. Additionally, with no previous theoretical or experimental data provided in the literature, the present rovibrational spectrum for HOOF provides novel reference benchmark data that can be be used in future benchmarking studies and possible astrophysical and atmospheric classification.

For the investigation of HOOF, the computed anharmonic intensities and net dipole moment presented herein show that two frequencies exhibit relatively large vibrational transition intensities. The largest intensity at 78 km/mol belongs to the O-O-F bend while the next largest is the O-F stretch at 66 km/mol. Even though the O-F stretch is not as intense of a transition as the O-O-F bend, the 68 km/mol transition is still intense enough to be a notable characteristic of its IR spectrum.

This is further suggested when comparing HOOF to HOSH and HOOH. While the most intense frequencies for HOOF are not nearly as intense as HOOH, they are slightly more intense than HOSH. Furthermore, both the O-O-F bend at 738.2 cm^{-1} and the O-F stretch at 454.4 cm^{-1} fall within the >12 μm region of the IR that are typically not hindered by the unidentified infrared bands dominated by the spectral features of polycyclic aromatic hydrocarbons. Additionally, HOOF has a larger net dipole moment of 2.12 D compared to the lower dipole moments of HOOH and HOSH, 1.75 D and 1.60 D, respectively, suggesting that HOOF is a viable candidate for microwave spectroscopic observation in the Earth's atmosphere and in the ISM.

In an effort to produce less costly QFFs, the lowered geometrical optimized energy convergence F12-TZ-cCR QFF investigated in this work provides further time savings than the boasted time-savings of its tighter energy convergence F12-TZ-cCR counterpart. While the loose F12-TZ-cCR shows excellent agreement with the tight F12-TZ-cCR in terms of the rotational constants, the extreme reduction in the accuracy of the fundamentals suggests that utilizing the loose F12-TZ-cCR QFF would be unwise for the analysis of the full rovibrational spectra. To that end, using the poor accuracy in the rovibrational spectroscopic data that utilizes lowered convergence criteria provides more evidence as to why higher convergence criteria are needed in quantum chemical calculations in order to achieve the accuracy necessary for a full comparison of the rovibrational spectra to other theoretical work or laboratory analysis. However, if only the rotational constants are desired for benchmarking or potential radioastronomical observation, then the loose F12-TZ-cCR can likely be recommended. Thus, further theoretical work on new QFF methods that may offer further time-savings is necessary in order to produce QFFs that provide highly-accurate full rovibrational spectra for further benchmarking, and potential astrophysical and atmospheric detection.

The reported rotational spectroscopic data provided in this work will be fundamental for ground-based radiotelescopic observatories such as the *Atacama Large Millimeter/submillimeter Array*. Also, the regions of the IR spectrum that the brightest transitions fall in can now be more effectively probed with the recent launch of the *James Webb Space Telescope*. Additionally, the reported spectral data herein will be useful for current observatories such as the *Stratospheric Observatory for Infrared Astronomy*. Hence, the investigation of HOOF may provide the evidence to confirm any of the proposed nucleosynthetic processes that have been suggested, as well as uncovering more unique fluorine-containing species as of yet detected in the ISM. Additionally, highly-oxidizing pollutants, like HO_2 radical, and fluorine-containing species in the earth's atmosphere may be progenitors for HOOF or, perhaps, vis versa. With the classification of HOOF in the earth's atmosphere, more pathways of formation for fluorine-containing pollutants may be elucidated in an effort to further characterize the roll they may play in atmospheric change. Consequently, HOOF is a plausible, and worthwhile, fluorine-containing candidate for atmospheric and astronomical detection to classify possible fluorine-containing pollutants in the Earth's atmosphere and to make clear the still unknown properties of fluorine in the ISM.

CHAPTER 4

Reaction Pathway and Rovibrational Analysis of Aluminum Nitride Species as Potential Dust Grain Nucleation Agents.

Reproduced from Palmer, C. Z.; Fortenberry, R. C.
Astrophys. J. **2024**, *962*, 148, with the permission of AAS Publishing.
DOI:10.3847/1538-4357/ad182e

Abstract

A dust nucleating agent may be present in interstellar or circumstellar media that has gone seemingly undetected and unstudied for decades. Some analyses of the Murchison CM2 meteorite suggest that at least some of the aluminum present within condensed as aluminum nitrides instead of the long studied, but heretofore undetected suite of aluminum oxides. The present theoretical study utilizes explicitly correlated coupled cluster theory and density functional theory to provide a pathway of formation from alane (AlH_3) and ammonia to the cyclic structure, $Al_2N_2H_4$ which has the proper Al/N ratio expected of bulk aluminum nitrides. Novel rovibrational spectroscopic constants are computed for alane and the first two formed structures, $AlNH_6$ and $AlNH_4$, along the reaction pathway for use as reference in possible laboratory or observational studies. The ν_8 bending frequency for $AlNH_6$ at 755.7 cm^{-1} (13.23 μm) presents a vibrational transition intensity of 515 km mol^{-1}, slightly more intense than the anti-symmetric C$-$O stretch of carbon dioxide, and contains a dipole moment of 5.40 D, which is $\sim 3\times$ larger than that of water. Thus,

the present reaction pathway and rovibrational spectroscopic analysis may potentially assist in the astrophysical detection of novel, inorganic species which may be indicative of larger dust grain nucleation.

4.1 Introduction

Previous study[43] of the Murchison CM2 chondritic meteorite seems to suggest the aluminum present within condensed as a form of aluminum nitride rather than the more commonly assumed aluminum oxides. However, aluminum nitride clusters must compete with these aluminum oxides during dust grain nucleation and further formation. Alumina (Al_2O_3) is a common aluminum oxide that has been theorized as a major contributor to both bulk aluminum oxides and their use in dust grain nucleation and formation in the interstellar medium (ISM) and in circumstellar media (CSM).[186–188] One of the most commonly attributed spectral features for bulk alumina's Al−O vibrational stretching and bending motions is seen at 13 μm.[189,190] Additionally, previous studies[187,190] attribute emission features at 11, 20, 28, and 32 μm to the same carrier as the 13 μm feature. Despite this, monomeric forms of aluminum oxides like Al_2O_3 have yet to be detected as their formation seems to be unfavorable due to many pathways hindered by endothermicities.[189,191,192] Further, bulk-phase aluminum oxides exhibit high condensation temperatures that lead to reaction timescales that are too rapid to adequetly detect such clusters.[193] The presence of Al_2O_3 in chondritic meteorite studies suggests its existence in these stellar environments; without astronomical detection, though, their potential role in dust grain nucleation to formation cannot be confirmed.[194,195] Thus, an investigation into an alternative Al-containing species that may not condense on timescales as quickly as Al_2O_3 is warranted to elucidate long-sought-after dust formation pathways containing Al that have eluded astrochemists and astrophysicists to date.

While Al condensates show high refractory character,[193] not all of its forms, in CSM, condense into large bulk solids early in stellar evolution and evade detection. Within the circumstellar envelope of IRC+10216, amongst other oxygen-rich sources, two Al-halide species have been observed in the form of AlCl and AlF.[159,196–198] These Al-halides have also been observed within circumstellar envelopes with C/O $\sim$ 1.[199] While these have been observed closer to the star, upon their ejection to the cooler regions of the stellar envelope, they are thought to deplete onto dust grains eluding any further detection. However, this is not the case for AlNC, which has been detected in larger concentrations within the cooler regions of the envelope and under the condensation temperature of the elusive Al_2O_3 molecule and other aluminum oxide clusters.[200] The presence of the Al-halides and AlNC suggests that Al-containing species are not solely locked up into aluminum oxide clusters or grains. Thus, O-deficient, Al-containing species can be formed within the warmer regions of the stellar envelope and persist long enough in the cooler, outer circumstellar dust clouds before depositing or aggregating and disappearing from rovibrational detection.

Additionally, a radioisotope of Al, ^{26}Al, was identified in its fluorinated form, ^{26}AlF, near the stellar merger of CK Vulpus.[162] ^{26}AlF is believed to have been introduced into the surrounding stellar region during the collision of the binary system yet persisted on a timescale long enough for detection.[201] Much like the elusive Al_2O_3, both the stable ^{27}Al and an extinct form of ^{26}Al, which later decayed into the ^{26}Mg isotope based on isotopic abundance studies, were found within the Murchison CM2 chondritic meteorite. An investigation of the ratio of ^{26}Al/^{27}Al suggests that the ^{26}Al present is in larger abundance in at least this meteorite compared to the ratio in the solar system at large. In any case, the presence of an aluminum nitride system within Murchison CM2 is suggested *via* a comparison of the SiC abundance and

CN^-/C^- ratio and the Al and N present within. Such a correlation suggests that the Al in the meteorite condensed not as some form of aluminum oxide, like Al_2O_3, but rather as some form of aluminum nitride system.[43] As discussed previously, the Al−N moiety is not unheard of in CSM from the presence of AlNC. Previous computational studies have calculated an Al−N bond strength of −105.0 kcal mol^{-1}, which is stronger than the bond strength of the N−C bond at −77.8 kcal mol^{-1}.[202] This larger bond strength of the Al−N bond, relative to the N−C bond in AlNC, suggests the stability of Al−N bonds in CSM and the ISM.

The study of the Murchison CM2 meteorite implies that the aluminum nitride systems present within play a key role in the nucleation of the graphite that composes the bulk of the carbonaceous material within the meteor by catalyzing the graphite's inhibited nucleation.[43,203,204] With that, these new Al-containing species may be instrumental for the nucleation of aggregated material onto other solar system bodies, such as comets, asteroids, and other meteors. That being said, these conclusions justify an investigation into the presence of unreported aluminum nitride molecular systems in CSM and the ISM that may potentially assist in elucidating the processes of how Al-bearing species get from the gas phase into their bulk solid-phase dust grain counterparts.

As aluminum nitride systems have not been characterized in any stellar environment, no gas-phase observational or experimental spectroscopic data are available to begin the search for such species. Thus, the present quantum chemical study provides reference data for a proposed pathway of formation from the aluminum hydride, alane, (AlH_3) and ammonia (NH_3) into the first cyclic species along said pathway. Regardless of the AlH_3 molecule's lack of interstellar detection, the present study utilizes AlH_3 as the main source of aluminum given its simplicity as a metal hydride and its closed-shell configuration. The AlH_3 molecule is used in place of the more

simple, and previously detected,[205] aluminum mono-hydride (AlH) as previous computational studies suggest that access to more hydrogen atoms assists the progress of the reaction pathway.[206,207] The rovibrational spectroscopic data herein will be instrumental in supporting the currently available spectroscopic telescopes and observational technologies like the *James Webb Space Telescope* (JWST) for its efficiency in probing the near- to mid-IR spectrum with its Near-Infrared Spectrograph (NIRSpec) and Mid-Infrared Instrument (MIRI) instruments. Where available, the provided rotational data will assist microwave spectroscopic observatories like the *Atacama Large Millimeter/sub-millimeter Array* (ALMA). To that end, the rovibrational spectroscopic analysis provided should aid in the potential astrophysical identification of aluminum nitride species that have yet to be characterized and may contribute to the dust grain nucleation and formation processes present in CSM and the ISM.

4.2 Computational Methods

4.2.1 Reaction Mechanism Methods

Unless otherwise stated, all geometry optimizations, single-point energy (SPE) computations, and zero-point vibrational energy corrections for the reactants, intermediates, and products of the aluminum nitride reaction pathway are conducted utilizing coupled cluster theory at the singles, doubles, and perturbative triples level [CCSD(T)].[58,208,209] For an additional gain in accuracy, the CCSD(T) level of theory is corrected within the explicitly correlated F12b formalism[62,64] along with its corresponding cc-pVTZ-F12 basis set.[174,175] The aforementioned level of theory will henceforth be abbreviated as "F12-TZ." Geometry optimization and harmonic frequency computations for all transition states along the pathway are conducted with the B3LYP density functional[210,211] along with the aug-cc-pVTZ correlation consistent

Dunning basis set.[212] After the transition states are optimized at the B3LYP/aug-cc-pVTZ level of theory, single-point energy computations are computed at the F12-TZ level,[213] and are subsequently corrected with B3LYP/aug-cc-pVTZ zero-point vibrational energies (ZPVEs). All minima along the reaction pathway are computed *via* the MOLPRO 2022.2 suite of quantum chemical packages.[107] Finally, all transition state computations on the pathway are conducted *via* GAUSSIAN16.[120]

4.2.2 Rovibrational Spectroscopic Methods

The highly accurate rovibrational spectroscopic constants are computed utilizing the quartic force field (QFF) approach. A QFF is a fourth-order Taylor series expansion of the potential energy portion of the internuclear Watson Hamiltonian.[66] QFFs as employed herein have been able to produce rovibrational spectroscopic constants within 1% of experimental values for many molecular systems.[39,40,76–78,80,97,99–101,103] F12-TZ has been shown to produce accurate fundamental vibrational frequencies and rotational constants at far less computational cost compared to other QFF methods.[104,106,176,214,215] Additionally, the QFF implemented in this work is conducted within the recently developed automated PBQFF framework.[72] The PBQFF procedure begins with a geometry optimzation utilizing MOLPRO[107] at the F12-TZ level of theory with tight convergence criteria. From there, the optimized Cartesian geometry is displaced by 0.005 Å respective of bond lengths or angles, to mimic a QFF but is truncated to the second-order yielding a Cartesian harmonic force field. SPE computations for every displacement are computed and used to generate a harmonic force constant (FC) matrix. The normal coordinates are then extracted from the resulting mass-weighted Hessian matrix for the given molecular species. The optimized molecular geometry is then displaced along these normal coordinates to compute the rest of the semi-diagonal QFF, and SPE computations are performed

at each normal coordinate displacement.

Once the SPE computations are finished, the final normal FCs are computed directly utlizing a finite differences procedure. The normal coordinate FCs are then passed to a second-order vibrational and rotational perturbation theory (VPT2)[67,74,75,118] algorithm within the PBQFF framework itself. From this, the harmonic frequencies, fundamental anharmonic vibrational frequencies, vibrationally-averaged rotational constants, singly-vibrationally-excited rotational constants, quartic distortion constants, and sextic distortion constants are produced. Additionally, if present in the analysis, the type-1 and -2 Fermi resonances and Coriolis resonances are taken into account as it has been shown to increase the accuracy of the computed rovibrational spectroscopic constants.[119,216] To further assist in potential astrophysical detection, dipole moments for $AlNH_6$ and $AlNH_4$ are computed at the F12-TZ level within MOLPRO 2022.2.[107] Finally, double-harmonic infrared intensities computed using GAUSSIAN16[120] at the MP2/cc-pVDZ[49,51] level of theory are included to assist in the detection of these species in the infrared (IR). Computed intensities at this level of theory have been show to produce semi-quantitative agreement with higher levels of theory for far less computational costs.[121,122,182]

In addition to IR intensities, absorption cross sections, σ, are given for all applicable vibrational frequencies. The absorption cross sections are derived utilizing the formula in EQ. 4.1, where "N_a" is Avogadro's number, and "ϵ" is the molar absorption coefficient.

$$\sigma = \frac{ln(10) \times 10^3}{N_a} \times \epsilon \tag{4.1}$$

The molar absorption coefficients for each vibrational frequency are computed following the formula in EQ. 4.2,[217] where "I_{IR}" is the IR intensity computed above and "w" is the resolving power of the given observing telescope.

Table 4.1: Symbol definitions and chemical formulae for the species in the present reaction pathway.

Symbol	Definition	Chemical Formula
R_1	Reactant 1	AlH_3
R_2	Reactant 2	NH_3
I_1	Intermediate 1	$AlNH_6$
TS_1	Transition State 1	$AlNH_6$
P_1	Product 1	$AlNH_4$
$N{-}I_2$	Nitrogen Intermediate 2	AlN_2H_7
$Al{-}I_2$	Aluminum Intermediate 2	Al_2NH_7
$N{-}TS_2$	Nitrogen Transition State 2	AlN_2H_7
$Al{-}TS_2$	Aluminum Transition State 2	Al_2NH_7
$N{-}P_2$	Nitrogen Product 2	AlN_2H_5
$Al{-}P_2$	Aluminum Product 2	Al_2NH_5
$N{-}I_3$	Nitrogen Intermediate 3	$Al_2N_2H_8$
$Al{-}I_3$	Aluminum Intermediate 3	$Al_2N_2H_8$
$N{-}TS_3$	Nitrogen Transition State 3	$Al_2N_2H_8$
$Al{-}TS_3$	Aluminum Transition State 3	$Al_2N_2H_8$
$N{-}P_3$	Nitrogen Product 3	$Al_2N_2H_6$
$N{-}TS_4$	Nitrogen Transition State 4	$Al_2N_2H_6$
$Al{-}P_3$	Aluminum Product 3	$Al_2N_2H_6$
$N{-}P_4$	Nitrogen Product 4	$Al_2N_2H_6$
$Al{-}TS_4$	Aluminum Transition State 4	$Al_2N_2H_6$
$N{-}TS_5$	Nitrogen Transition State 5	$Al_2N_2H_6$
$Al{-}P_4$	Aluminum Product 4	$Al_2N_2H_4$
$N{-}P_5$	Nitrogen Product 5	$Al_2N_2H_4$

$$\epsilon = 27.648 \times \frac{I_{IR}}{w} \tag{4.2}$$

The resolution, "R," of the NIRSpec and MIRI on the *JWST*, at their respective operating wavelengths, are provided and are trivially converted to the resolving power in EQ. 4.3.[21,22]

$$R = \frac{\lambda}{\Delta\lambda} \tag{4.3}$$

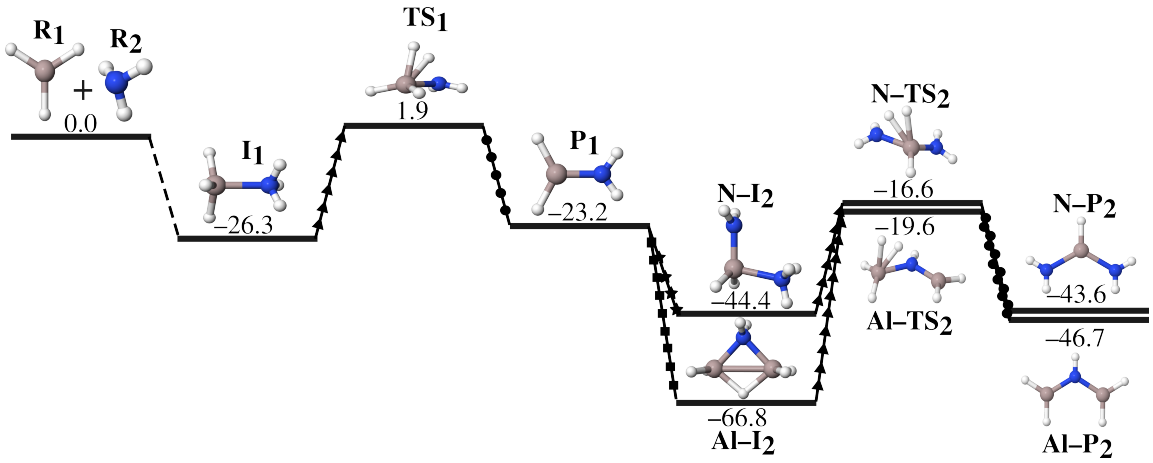

Figure 4.1: Reaction coordinate diagram from AlH_3 and NH_3 to N− and Al−P_2. The arrowed lines indicate isomerization, the circular lines indicate H_2 departure, the starred lines indicate NH_3 addition, and the squared lines indicate AlH_3 addition. Relative energies are in kcal mol^{-1}. White atoms indicate H, blue atoms indicate nitrogen, and grey beige indicate Al.

4.3 Results and Discussion

4.3.1 Reaction Pathway Analysis

The reaction coordinate profile shown in Figs. 4.1 and 4.2 along with their corresponding equilibrium geometries, and definitions and chemical formulae in Table 4.1, shows the continual addition of equivalents of AlH_3 and NH_3. Additions of AlH_3 and NH_3 produce progressively larger datively-bonded structures but contain an initially raised transition barrier from I_1 to the P_1. In order for the reaction to progress to larger aluminum nitride systems, I_1 must overcome the aforementioned barriered TS_1 that sits 1.9 kcal mol^{-1} higher than the reactants and lose an H_2 molecule to form P_1. This is in stark contrast with previous computed reaction schemes[189,206] on AlH_3 and water that produce aluminum oxides with submerged barriers of formation. These barrierless formation most likely govern the short timescales of leading to the underdetection of a suitable carrier of the Al−O features, like Al_2O_3 in CSM or the ISM. Regardless, overcoming this barrier requires sufficiently high temper-

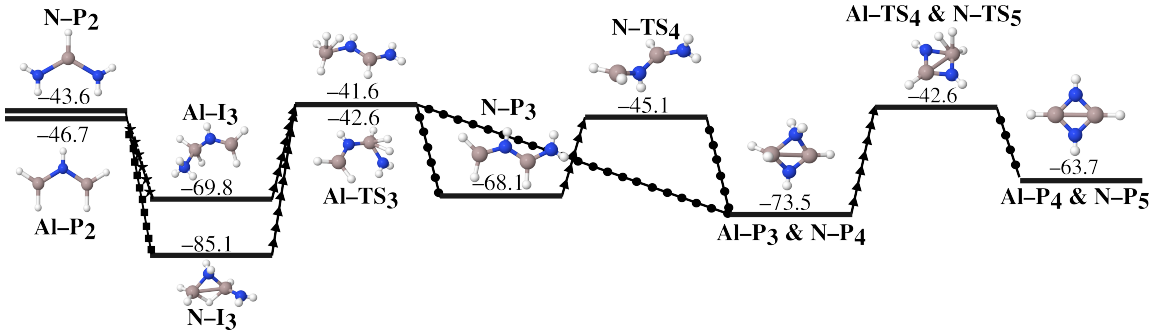

Figure 4.2: The continued reaction coordinate diagram from N− and Al−P_2 to cyclic-$Al_2N_2H_4$. The arrowed lines indicate isomerization, the circular lines indicate H_2 departure, the starred lines indicate NH_3 addition, and the squared lines indicate AlH_3 addition. Relative energies are in kcal mol^{-1}. White atoms indicate H, blue atoms indicate nitrogen, and grey beige indicate Al.

atures, ∼960 K, in the aluminum nitride species' formation environment from the surrounding stellar environments to begin forming larger clusters.

Obviously, the cold, diffuse ISM at ∼10−40 K is not a likely region for the formation of P_1 to occur. However, as stated earlier, the previous work on Murchison CM2[43] suggests that the theorized aluminum nitride systems present in the meteorite may have nucleated the meteorite's dust grain formation. If this is the case, then the aluminum nitride system would have been formed in some region warm enough for its own production and for dust grain formation to occur. The warm environments of inner protoplanetary disks can achieve a range of temperatures anywhere from 500−1500 K[218] and contain ample material for molecular synthesis to begin that may potentially lead to seeding and nucleating processes of dust grain formation. Additionally, highly evolved asymptotic giant branch (AGB) stars are known to exhibit much higher temperatures within 1−2 stellar radii at 2000−3000 K compared to the warm inner protoplanetary disks.[219] AGB stars also contribute considerable dust forming material to their surrounding environment, and the ISM at large, given the stars substantial mass-loss rates.[220,221] If a region of CSM or the ISM contains sufficient temperatures and has the necessary material, the proper conditions toward

formation the aluminum nitride species along the reaction pathway proposed herein will be satisfied. Once these aluminum nitrides have been formed, they may likely go on to contribute to dust grain nucleation and formation as suggested in the study of the Murchison CM2 meteorite.

Once the transitional barrier, shown in Fig. 4.1, is overcome there will be enough latent energy within the system to further progress through the now relatively submerged pathway of formation. Thus, the reaction pathway is no longer nearly as limited by the surrounding temperature and can further condense into larger and larger dust grains in both the warmer and cooler regions of the CSM or ISM. In any case, from the P_1 structure, additions of AlH_3 or NH_3 lead to either the $N{-}I_2$ or the $Al{-}I_2$ structure. The addition of the AlH_3 leads to a lower energy cyclic structure with a three-center two-electron bond commonly seen in trivalent species containing an empty *p*-orbital like aluminum and boron.[222] Upon the loss of the H_2 molecule, seen in the $N/Al{-}TS_2$ species, both pathways lead to their respective products (P_2) of similar structure. Interestingly, if an equivalent of AlH_3 is added to $N{-}P_2$, it stabilizes into $N{-}I_3$, which is structurally similar to Al-I_2 with a three-center two-electron bond. The extra stability of the three-center two-electron bond in $N{-}I_3$ yields the lowest energy structure of the present reaction pathway. While $N{-}I_3$ is the lowest energy structure, the reaction pathway should still progress further not only due to the energy from the ambient temperature of its formation environments but also from collision with other molecular citizens present within the same regions.

Further departure of an H_2 molecule from (N or Al)$-I_3$ yields the cyclic $Al{-}P_3$ structure, whereas $N{-}P_3$ is an open chain structure. The open-chain $N{-}P_3$ structure must overcome a torsional barrier before it becomes the cyclic $N{-}P_4$. At this point along the pathway, the paths of additions of AlH_3 and NH_3 converge to the same structure. After a final loss of and H_2 molecule in $Al{-}TS_4$ and $N{-}TS_5$, the

proposed reaction pathway concludes with the final cyclic structure of Al$-$P$_4$ and N$-$P$_5$ ($Al_2N_2H_4$). This $Al_2N_2H_4$ species may then go on to form larger aluminum nitride clusters that potentially contribute to the nucleation and formation of dust grains in the universe. Given that the above reaction pathway contains no carbon- or oxygen-containing species, the present reaction pathway may contribute to the aluminum dust grain nucleation pathways in regions where the C/O ratio is ~ 1. However, in oxygen-rich environments it may compete with the aluminum-oxygen pathways described in previous studies.[186,187,189] This may not be the case for carbon-dominated environments, C/O ≥ 1, given the lack of oxygen and the aluminum-carbon motif has yet to be characterized in CSM or the ISM in any form other than AlNC. Therefore, the reaction pathway investigated in this work may assist in the potential detection of aluminum-containing dust grain nucleation species that that have gone undetected, and understudied, in the literature for decades.

4.3.2 Rovibrational Spectroscopic Analysis

As stated previously, some of the aluminum nitride systems investigated in this work have little-to-no previous experimental or observational data of any type. Therefore, the computed rovibrational spectroscopic constants for R_1 (AlH_3), I_1 ($AlNH_6$), and P_1 ($AlNH_4$) as shown in Fig. 4.1 reported herein are reference data necessary for laboratory analysis and potential astrophysical detection. Presently, AlH_3 and $AlNH_4$ have Ar matrix spectroscopic data in the literature, and $AlNH_4$ and $AlNH_6$ have had previous theoretical studies conducted. Several of the previous theoretical studies[223–225] for $AlNH_4$ and $AlNH_6$ only provide an analysis of the harmonic frequencies and their structural character. However, The work herein provides anharmonic vibrational frequencies and rotational spectroscopic constants at a more rigorous level of theory.

Table 4.2: Rotational Constants for AlH_3, $AlNH_4$, and $AlNH_6$

Consts.	Units	AlH_3	$AlNH_4$	$AlNH_6$
A_e	MHz	133833.5	95478.0	49434.0
B_e	MHz	133833.5	13074.1	9048.5
C_e	MHz	66916.7	11499.5	9048.4
A_0	MHz	132407.6	95063.3	49154.6
B_0	MHz	132407.6	13015.9	8916.2
C_0	MHz	66034.4	11430.3	8916.4
A_1	MHz	131376.9	94810.8	49090.3
B_1	MHz	131376.9	12994.8	8913.7
C_1	MHz	65518.7	11412.4	8913.9
A_2	MHz	131652.0	94636.1	49025.6
B_2	MHz	131652.0	12999.7	8914.2
C_2	MHz	66346.6	11411.6	8914.4
A_3	MHz	131457.8	94432.1	48865.1
B_3	MHz	131457.8	13009.1	8920.6
C_3	MHz	65043.4	11418.4	8920.8
A_4	MHz	132824.6	94214.4	48926.0
B_4	MHz	132824.6	13012.7	8922.5
C_4	MHz	66244.7	11415.5	8922.7
A_5	MHz		95436.9	49035.0
B_5	MHz		13034.2	8927.4
C_5	MHz		11420.7	8927.6
A_6	MHz		95225.2	49144.2
B_6	MHz		12981.5	8881.5
C_6	MHz		11369.6	8881.7
A_7	MHz		95582.8	49064.1
B_7	MHz		13017.0	8918.3
C_7	MHz		11441.5	8918.5
A_8	MHz		97565.1	49309.6
B_8	MHz		13052.9	8904.7
C_8	MHz		11398.1	8904.9
A_9	MHz		93906.6	49191.6
B_9	MHz		12981.2	8878.7
C_9	MHz		11444.4	8878.9
A_{10}	MHz		94707.4	49146.8
B_{10}	MHz		12977.0	8807.8
C_{10}	MHz		11433.0	8808.0
A_{11}	MHz		93227.5	49487.3
B_{11}	MHz		12975.5	8900.9
C_{11}	MHz		11429.1	8901.0
A_{12}	MHz		96185.7	49145.0
B_{12}	MHz		13038.4	8875.0
C_{12}	MHz		11430.9	8875.3
μ	D	0.0	1.08	5.40

Table 4.3: Quartic and sextic distortion constants in the Watson A-reduced Hamiltonian for $AlNH_4$ and $AlNH_6$

Const.	$AlNH_4$	$AlNH_6$
Δ_J	12.151 (kHz)	16.330 (kHz)
Δ_K	1.630 (MHz)	76.397 (kHz)
Δ_{JK}	192.297 (kHz)	55.756 (kHz)
δ_J	1.621 (kHz)	149.664 (mHz)
δ_K	140.576 (kHz)	−36.525 (kHz)
Φ_J	2.955 (mHz)	−33.349 (mHz)
Φ_K	122.517 (Hz)	−188.055 (Hz)
Φ_{JK}	2.261 (Hz)	−79.589 (Hz)
Φ_{KJ}	−9.071 (Hz)	268.269 (Hz)
ϕ_j	2.638 (mHz)	18.738 (μHz)
ϕ_{jk}	1.188 (Hz)	−9.396 (Hz)
ϕ_k	81.816 (Hz)	−57.226 (MH)

Table 4.4: Quartic and sextic distortion constants in the Watson S-reduced Hamiltonian for AlH_3, $AlNH_4$, and $AlNH_6$

Const.	AlH_3	$AlNH_4$	$AlNH_6$
D_J	6.338 (MHz)	11.486 (kHz)	16.330 (kHz)
D_{JK}	−11.275 (MHz)	196.288 (kHz)	55.756 (kHz)
D_K	5.287 (MHz)	1.627 (MHz)	76.397 (kHz)
d_1	−31.927 (Hz)	−1.621 (kHz)	−149.664 (mHz)
d_2	158.915 (Hz)	−332.607 (Hz)	8.511 (mHz)
H_J	885.237 (Hz)	−3.890 (mHz)	−33.344 (mHz)
H_{JK}	−3.292 (kHz)	862.837 (mHz)	374.006 (mHz)
H_{KJ}	3.939 (kHz)	−4.307 (Hz)	1.725 (Hz)
H_K	−1.530 (kHz)	119.158 (Hz)	−1.474 (Hz)
h_1	−23.100 (mHz)	1.787 (mHz)	23.397 (μHz)
h_2	−34.752 (mHz)	3.422 (mHz)	−2.245 (μHz)
h_3	−52.810 (Hz)	851.524 (μHz)	−4.658 (μHz)

Table 4.5: Vibrational frequencies (cm^{-1}), IR Intensities (km mol^{-1}) with absorption cross sections in parentheses (10^{-14} cm^2), and wavelength (μm) for D_{3h} AlH_3

Mode	Symm.	Desc.	Harm.	Anharm.	f (σ)	λ	Expt.[a]
ν_1	A_1'	AlH Stretch	1951.4	1890.7	0 (0)	5.29	
ν_2	A_2"	OPB	710.5	707.8	387 (200)	14.13	697.8
ν_3	E'	Anti-sym. AlH Stretch	1955.7	1889.7	251 (40)	5.29	1882.8
ν_4	E'	HAlH Anti-sym. Bend	798.6	789.1	234 (100)	12.67	783.4
ZPT				4052.6			

[a]Experimental Ar matrix FTIR spectroscopy.[2]

In order to provide a full rovibrational profile for the aluminum nitride species investigated herein, the equilibrium, vibrationally averaged, and vibrationally excited rotational constants are reported in Table 4.2. Also, the quartic and sextic distortion constants from the A- and S-reduced Watson Hamiltonians are given in Tables 4.3 and 4.4, respectively. Additionally, the formation pathways to larger aluminum nitride species assume the presence of AlH_3 in the same regions. As AlH_3 has not yet been observed in CSM or the ISM, perhaps a consequence of its rapid reaction with ammonia or water, the present study also provides the reference data for this species for completeness. To that end, the vibrational profile for AlH_3, $AlNH_6$, and $AlNH_4$ are given in Tables 4.5, 4.6, and 4.7, respectively.

As stated above, previous Ar matrix spectroscopic data[2] exists for AlH_3 and characterizes three of the four vibrational frequencies available, shown in Table 4.5. The out-of-plane bending mode, ν_2, differs the furthest from experiment at 10 cm^{-1} or 1.4%. The closest to experiment is ν_4, the H−Al−H anti-symmetric bending motion, differing by 5.7 cm^{-1} or 0.7%. While the F12-TZ anharmonic vibrational frequencies exhibit relatively large differences compared to experiment, it should be noted that Ar matrix spectroscopy is known to cause a shift in the true vibrational frequency.[226] Thus, most of the discrepancy between the current high-level quantum chemical computations and experiment should be attributed to the Ar matrix shifts. Further, previous computational studies of Al-containing species utilizing the

F12-TZ methodology have produced vibrational frequencies within 0.4% of the gas-phase experimental value.[227] Given the higher-order, D_{3h} symmetry exhibited by AlH_3 the permanent dipole of this molecule is zero, thus rendering it undetectable *via* rotational spectroscopy. For this reason, the anharmonic vibrational frequencies computed in this work are even more crucial for potential spaced-based IR spectroscopic telescopes.

Further, AlH_3 exhibits very intense vibrational transitions with the ν_2, out-of-plane bend being the most intense at 387 km mol^{-1}. Compared to the anti-symmetric stretch of H_2O at 70 km mol^{-1} and CO_2 at $\sim$475 km mol^{-1}, which are both considered to be intense transitions, the present ν_2 intensity should be considered intense enough for detection *via* IR spectroscopy even at low concentrations. Additionally, the other vibrational fundamentals of AlH_3 with intensities of 251 and 234 km mol^{-1} are also substantially greater than the aforementioned stretches in water and carbon dioxide. Looking at the spectral profile, ν_4 sits at 12.67 μm putting it around the 13 μm spectral feature that is typically used as an identifier for Al_2O_3. While this does not really question Al_2O_3's presence based on this spectral feature, it does posit the existence of another carrier of said spectral feature in CSM or the ISM that may be attributed to the present aluminum nitride system. Nevertheless, the computed vibrational data herein should be especially important for the detection of AlH_3 that would be supportive for confirming the reaction pathway of formation proposed in this work and from previous computational reaction pathways.[206,207]

The first intermediate, $AlNH_6$, exhibits the most notable vibrational transition intensities of the two formed structures studied herein, shown in Table 4.6. $AlNH_6$'s ν_8 frequency, the H$-$Al$-$N symmetric bending motion, at 515 km mol^{-1}is 30 km mol^{-1} larger than the CO_2 motion mentioned above. Further, $AlNH_6$ ν_4, ν_6, and ν_7 exhibit transition intensities of 331, 135, and 271 km mol^{-1}, respectively.

Table 4.6: Vibrational frequencies (cm^{-1}), IR intensities (km mol^{-1}) with absorption cross sections in parentheses (10^{-14} cm^2), and wavelength (μm) for C_{3v} $AlNH_6$

Mode	Symm.	Desc.	Harm.	Anharm.	f (σ)	λ
ν_1	E	NH Stretch	3588.9	3411.8	45 (5)	2.93
ν_2	A_1	Sym. NH Stretch	3468.8	3322.4	16 (2)	3.01
ν_3	A_1	Sym. AlH Stretch	1885.7	1819.2	36 (6)	5.50
ν_4	E	AlH Stretch	1865.1	1800.4	331 (50)	5.55
ν_5	E	NH2 Rocking	1665.3	1624.4	19 (3)	6.16
ν_6	A_1	HNAl Sym. Bend	1269.0	1207.8	135 (30)	8.28
ν_7	E	HAlN Rocking	790.8	779.1	271 (100)	12.84
ν_8	A_1	HAlN Sym. Bend	773.9	755.7	515 (200)	13.23
ν_9	E	OPB	706.8	666.1	15 (10)	15.01
ν_{10}	A_1	AlN Stretch	426.4	389.3	11 (20)	25.69
ν_{11}	E	OPB	372.6	352.2	2 (-)	28.40
ν_{12}	A_2	Torsion	119.4	21.4	1 (-)	467.29
ZPT				12724.7		

While $AlNH_6$ exhibits multiple intense vibrational transitions, due to the nature of its synthesis, it may be a short-lived species as it will likely progress to $AlNH_4$ or regress back to the reactants. However, even with a relatively small concentration, its intense transitions may still be seen in the IR. Rotationally, $AlNH_6$ also exhibits the largest permanent dipole moment of the three molecules studied, at 5.40 D. Compared to the previously detected[228] AlOH molecule with a permanent dipole of 1.11 D,[227] $AlNH_6$ may be a suitable candidate for potential radioastronomical observation, but may be limited by shorter lifetimes as discussed above. Regardless, like AlH_3, $AlNH_6$ also exhibits spectral features in and around the 13 μm dust feature as well as the associated 11, 20 and 28 μm. Namely, the aformentioned ν_8 frequency, with the 515 km mol^{-1} intensity, sits directly at 13.23 μm, as shown in Table 4.6. It should be noted that the mid- to far-IR regions where these features are located are dominated by larger dust grains than present potential grain nucleating species. Regardless, a laboratory and observational study of $AlNH_6$ is warranted utilizing the novel reference data provided herein in order to assist in the astrophysical detection of the first intermediate along an alternative pathway for formation for dust grains

in CSM or the ISM.

Table 4.7: Vibrational frequencies (cm^{-1}), IR intensities (km mol^{-1}) with absorption cross sections in parentheses (10^{-14} cm^2), and wavelength (μm) for C_{2v} $AlNH_4$

Mode	Symm.	Desc.	Harm.	Anharm.	f (σ)	λ	Prev.[a/b]
ν_1	b_2	Anti-symm. NH stretch	3673.6	3495.9	27 (3)	2.86	–/3496.8
ν_2	a_1	Symm. NH Stretch	3582.7	3421.5	31 (4)	2.92	3499.7/3421.7
ν_3	b_2	Anti-symm. AlH stretch	1961.2	1895.3	257 (40)	5.28	1899.3/1895.5
ν_4	a_1	Symm. AlH Stretch	1957.5	1893.5	81 (10)	5.28	1891.0/1894.7
ν_5	a_1	Symm. HNAl stretch	1582.0	1552.1	28 (5)	6.44	1541.6/1552.7
ν_6	a_1	AlN stretch	836.9	822.5	217 (90)	12.16	818.7/822.7
ν_7	a_1	Symm HAlN stretch	757.2	747.1	51 (20)	13.39	755.0/747.9
ν_8	b_2	Anti-symm. HNAl stretch	732.6	717.5	145 (90)	13.94	769.8/715.9
ν_9	b_1	Al OPB	614.4	606.0	165 (100)	16.50	608.7/611.3
ν_{10}	a_2	Anti-symm. Torsion	495.0	469.5	0 (0)	21.30	–/465.8
ν_{11}	b_1	N OPB	448.9	442.9	236 (300)	22.58	518.3/426.1
ν_{12}	b_2	Anti-symm. HAlN stretch	426.0	422.8	19 (30)	23.65	–/431.4
ZPT				8427.6			

[a] Previous Ar matrix attributions.[3]
[b] Previous F12-TZ anharmonic vibrational data.[179]

The $AlNH_4$ molecule has both previous Ar matrix spectroscopic data[3] and theoretical vibrational frequency computations.[179] The previous vibrational frequency studies are computed at the F12-TZ level of theory much like the rovibrational spectroscopic data provided herein. While the present computational study utilizes a normal coordinate system to compute the QFF procedure, the previous study utilizes a symmetry internal coordinate system that is comparable to the present normal coordinate system. Any deviation between the two methods should be considered an effect of the difference between the construction of the two coordinate systems. In any case, while, $AlNH_6$ contains more intense vibration transitions, $AlNH_4$ still exhibits exceptionally intense transitions. Shown in Table 4.7, the $AlNH_4$ molecule's most intense transition is its anti-symmetric Al−H stretching motion, ν_3, of 257 km mol^{-1}. Like $AlNH_6$, $AlNH_4$ also contains multiple intense vibrational transitions such as ν_6, ν_8, ν_9, and ν_{11} at 217, 145, 165, and 236 km mol^{-1}, respectively. Again, while most of the these transitions are less intense than $AlNH_6$, the above

intensities are still relatively intense suggesting $AlNH_4$ is a strong candidate for potential astrophysical detection utilizing IR spectroscopy. Additionally, this species may be longer-lived in its formation environment in CSM making it an even stronger candidate for astronomical observational detection, perhaps, than $AlNH_6$ itself.

In terms of its dipole moment, the $AlNH_4$ molecule's is much smaller at 1.08 D. While $AlNH_4$ can still be observed rotationally given a high enough column density, with such a small dipole moment $AlNH_4$ may be better suited for detection via high resolution IR spectroscopy which can be achieved *via* the JWST. Also, $AlNH_4$ contains multiple spectral features that fall in or around the 13 μm feature and other associated spectral lines. Specifically, ν_7 and ν_8 have wavelengths at 13.39 and 13.94 μm, respectively, shown in Table 4.7. Again, this suggests that more than Al_2O_3 or the other associated suspected carriers exhibit this spectral feature, but this does suggest that species containing aluminum may contribute to the features more than initially observed or speculated. To that end, the novel vibrational spectroscopic data provided herein are necessary for further laboratory and possible astronomical observational investigations into the proposed formation pathway that will potentially assist in characterizing another potential player in dust grain formation.

4.4 Conclusions

The reaction pathway of AlH_3 and NH_3 leads to the formation of larger aluminum nitride molecular systems. This pathway must first overcome a barrier of 1.9 kcal mol^{-1} which is fully achievable in high temperature environments ($\sim$1000 K) such as warmer inner protoplanetary disks and circumstellar envelopes of AGB stars, but not necessary to begin the process of formation. The rest of the pathway is submerged compared to the reactants and is available given the latent energy present in the molecular system. The final step of the presently studied pathway involves the

formation of a four-membered cyclic ring that is also the only step on the pathway to have a submerged product over its preceding intermediate. Even so, the present reaction pathway provides a novel, potential formation mechanism for Al-bearing dust grains containing nitrogen as suggested in the studies of the Murchison CM2 chondritic meteorite and gives a hint at where such nucleation can take place in protoplanetary disks.

The $AlNH_4$ molecule investigated herein is the most likely candidate for potential astronomical observation *via* current rovibrational spectroscopic technologies in order to support this proposed reaction pathway. $AlNH_4$ contains multiple vibrational transitions with exceptionally large intensities, notably the 1895.3 cm^{-1} frequency with the 257 km mol^{-1} intensity and the 442.9 cm^{-1} frequency with the 236 km mol^{-1} intensity. While $AlNH_4$ has a smaller dipole moment of 1.08 D, if there is sufficient column density, this species should still be observable utilizing current radioastronomical telescopes. The rovibrational analysis of $AlNH_6$ suggests that the most intense vibrational transition studied here is the 515 km mol^{-1} intensity corresponding to the 755.7 cm^{-1} frequency. Additionally, the 5.40 D dipole moment feature calculated is the largest of the three studied. However, given the $AlNH_6$ molecule's likely shorter timescales within the reaction pathway, it may not be a suitable candidate for rovibrational detection in CSM or the ISM. The AlH_3 molecule also exhibits exceptionally intense vibrational transitions, especially the 707.8 cm^{-1} frequency with an intensity of 387 km mol^{-1}. Like the $AlNH_6$ molecule, the AlH_3 molecule may react too quickly, with ammonia, water, or other circumstellar or interstellar denizens before it can be detected. However, the spectral features give it a strong chance of observation with *JWST*. That being said, while all three species contain strong IR features and some strong rotational features, $AlNH_4$ may be the most likely candidate for potential astronomical observation.

The three Al-containing molecules studied in the present work contain vibrational frequencies that fall in or around the 13 μm spectral feature attributed to Al−O class of molecules. Additionally, the computed vibrational profile shows the presence of vibrational frequencies at the associated 11, 20, and 28 μm carrier features. The spectral features found in the present Al-containing species imply that dust containing some form of aluminum oxide may not be the only source of the 13 μm dust feature, and the aluminum nitride species studied herein may provide other alternative answers to the question of the origins of such features. These computed vibrational analyses warrant further laboratory, theoretical, and observational investigations into the present reaction profile and other, higher-order aluminum nitride clusters. These investigations will assist in the search for Al-containing species that may be present in CSM and the ISM, but have been uncharacterized and understudied in the present literature.

CHAPTER 5

Computing Accurate Rovibrational Spectral Data for Relevant Aluminum-bearing Species in Interstellar and Atmospheric Chemistry

Reprinted with permission from Palmer, C. Z.; Firth, R. A. ; Fortenberry, R. C.
J. Comp. Chem. **2024**, *46*, 25524. © 2024 John Wiley and Sons
DOI: 10.1002/jcc.27524

Abstract

The difficulty of quantum chemically computing vibrational, rotational, and rovibrational reference data via quartic force fields (QFFs) for molecules containing aluminum appears to be alleviated herein using a hybrid approach based upon CCSD(T)-F12b/cc-pCVTZ further corrected for conventional CCSD(T) scalar relativity within the harmonic terms and simple CCSD(T)-F12b/cc-pVTZ for the cubic and quartic terms: the F12-TcCR+TZ QFF. Aluminum containing molecules are theorized to participate in significant chemical processes in both the Earth's upper atmosphere as well as within circumstellar and interstellar media. However, experimental data for the identification of these molecules are limited, showcasing the potential for quantum chemistry to contribute significant amounts of spectral reference data. Unfortunately, current methods for the computation of rovibrational spectral data have been shown previously to exhibit large errors for aluminum-containing molecules. In this work, ten different methods are benchmarked to determine a method to produce experimentally-accurate rovibrational data for theorized aluminum species. Of the benchmarked methods, the explicitly correlated, hybrid

F12-TcCR+TZ QFF consistently produces the most accurate results with respect to both gas-phase and Ar-matrix experimental data. This method combines the accuracy of the composite F12-TcCR energies along with the numerical stability of non-composite anharmonic terms where the non-rigid nature of aluminum bonding can be sufficiently treated.

5.1 Introduction

Aluminum (Al) and its constituent species have long been hypothesized as a major contributor to the chemistry of Earth's upper atmosphere[27,28,229] as well as, differently, dust grain formation in interstellar and circumstellar media.[186–189] To date, only one chemical substance containing Al has been identified in the Earth's atmosphere, the Al^+ atomic cation.[230] However, previous thermodynamic[229] and kinetic[231] studies suggest that Al in the atmosphere may exist in some form of aluminum oxide material before rapidly reacting to form other unobserved molecular compounds. Beyond the Earth's atmosphere, only five unique Al-containing species have been observed in interstellar or circumstellar media: AlF and AlCl,[196,198,232] AlNC,[200] AlO,[233] and AlOH.[228] However, these have yet to shed light onto the theorized dust grain formation pathways within astronomical regions like circumstellar envelopes that may contribute material to protoplanetary disks.[186,195,234,235]

The relatively few observations of Al-bearing molecules in either environment may result from a lack of appreciable data, whether experimental or theoretical, in the current literature.[4] Thus, the ability to compute rovibrational spectral data for novel Al-bearing chemical species is imperative to assist in potential astrophysical, atmospheric, and laboratory studies and observations. Modern computational quantum chemical techniques can compute rovibrational spectral data to a high-level of accuracy employing the quartic force field (QFF)[66] in conjunction with vi-

brational perturbation theory at second order (VPT2).[67,74,75] A QFF is a fourth-order Taylor series expansion of the potential portion of the internuclear Watson Hamiltonian. The QFF procedure has been used historically to predict rovibrational spectral data to within 1% or better of experimental values for many molecular systems.[39,76–78,80,97,99–101,103] Though many levels of theory have been benchmarked in tandem with the QFF procedure[40–42,105] on diverse sets of molecular systems, few, if any, forms of molecular Al have been included. Thus, previously benchmarked levels of theory may not accurately model the potential energy surface (PES) for prediction of rovibrational spectral data of molecular Al for both atmospheric and extraterrestrial applications.

In fact, a well-known issue in the QFF procedure is the improper treatment of PESs of large-amplitude motions[122,184,236–238] associated with flat potential wells leading to "floppy" modes. Even though these "floppy" modes are more evident in weaker interactions, they have been observed in molecules that exhibit high bond strengths within sets of bond angles, such as Al−O and Al−N bonds.[202] Previous computational studies on the "floppy" AlOH and OAlOH molecules[227] and [Al, N, O_2] complexes[239] suggest that this behavior with QFF procedures fails to compute accurate rovibrational data of bending modes for these Al systems when compared to gas-phase experiment. While some of this failure may be due to the nature of the QFF procedure,[66] as is the case for AlOH and OAlOH, some contribution to the error exhibited by "floppy" molecules may also stem from the choice of the level of theory and how such a level may influence the resulting QFF. As stated previously, little to no previous benchmarking papers have investigated the efficacy for various levels of theory for Al-containing molecules presenting an immediate gap in the literature.

That being said, the work herein benchmarks different levels of theory across a subset of Al-bearing molecules exhibiting common bonding motifs found in interstel-

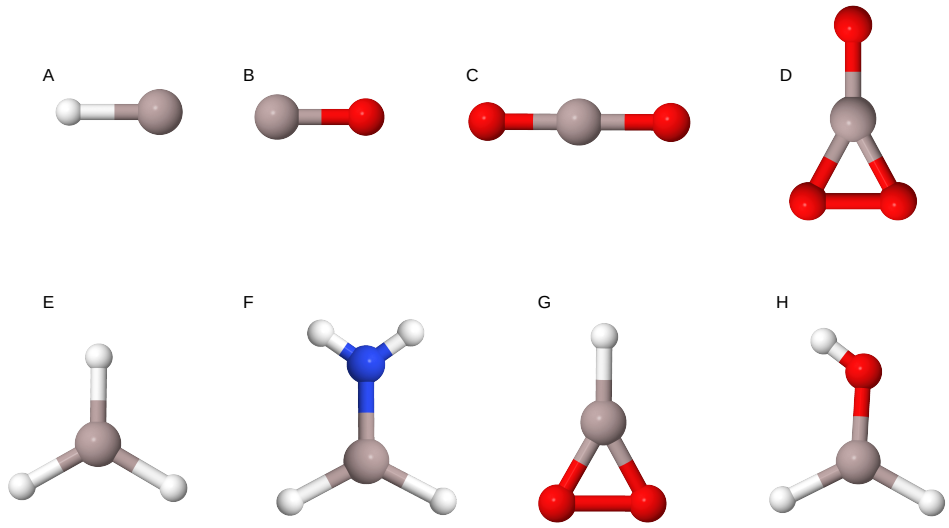

Figure 5.1: Optimized geometries for the molecules studied: (A) AlH, (B) AlO, (C) AlO_2^-, (D) AlO_3^-, (E) AlH_3, (F) $AlNH_4$, (G) $HAlO_2$, and (H) AlH_2OH. Al (grey), O (red), N (blue), and H (white).

lar and circumstellar media as well as the Earth's atmosphere. Notably these include Al−H, Al−O, and Al−N bonds. Figure 5.1 displays the optimized geometries for the nine molecules in the present test set; Figure 5.1B depicts both the AlO and AlO^- geometries. Where available, gas-phase experimental and Ar matrix data are used as a comparison to verify a given level of theory. Thus, the present study may yield new understanding for various levels of theory that should be instrumental in providing accurate rovibrational spectral data as a reference for potential astrophysical and atmospheric observation as well as further laboratory studies. The vibrational data computed herein may assist current infrared (IR) spectroscopic telescopes like JWST for interstellar and circumstellar observation in addition to terrestrial missions such as the CALIPSO satellite for probing the IR spectrum of Earth's atmosphere. Additionally, the included rotational data may be utilized by ground-based rotational spectroscopic telescopes like ALMA for interstellar observations and the Aqua satellite for Earth's atmosphere, respectively.

Table 5.1: Levels of theory computing accurate rovibrational spectral data for the Al-bearing species investigated in this work

Method	Basis Set	Ref.	Abbrev.
CCSD(T)	aug-cc-pVTZ	212,240	aTZ
...	aug-cc-pCVTZ	241,242	aCTZ
...	aug-cc-pwCVTZ	241,242	awCTZ
CCSD(T)-F12b	cc-pVTZ-F12	174,175	F12-TZ
...	cc-pVTZ-F12 + [a]cc-pVTZ-DK	174,175,243,244	F12-TZR
...	cc-pCVTZ-F12	245	F12-TcC
...	cc-pCVTZ-F12 + [a]cc-pVTZ-DK	243–245	F12-TcCR
...	(cc-pCVTZ-F12 + [a]cc-pVTZ-DK) + cc-pVTZ-F12	174,175,243,244	F12-TcCR + TZ
...	Al, cc-pVTZ-F12 & cc-pCVTZ-F12	174,175,245	Split basis TcC
...	Al, cc-pVTZ-F12 & cc-pCVTZ-F12 + [a]cc-pVTZ-DK	174,175,243,244	Split basis TcCR

[a]Douglas-Kroll scalar relativistic basis sets are used in conjunction with conventional CCSD(T).

5.2 Computational Methods

The levels of theory utilized in the present QFF work are given in Table 5.1 along with their abbreviations and references. Additionally, all levels of theory employed herein are based on coupled cluster theory at the singles, doubles, and perturbative triples level [CCSD(T)].[58,208,209] However, conventional CCSD(T) computations are known to converge slowly to the complete basis set (CBS) limit,[65] which is most notable in the previously used and well-documented CcCR composite method.[40,246] In order to speed up the convergence to the CBS limit, a majority of the CCSD(T) methods are further corrected within the explicitly-correlated F12b formalism.[62,64] The CCSD(T)-F12b methodology is shown to converge to the CBS limit more quickly and provide similar higher-order accuracies for smaller basis sets when compared to gas-phase experiment.[105,106,183,214,247]

As a portion of the QFF methods in the present work are based on composite energies, the equations for their energy computations are provided for the sake of completeness. The first composite method listed in Table 5.1 is the F12-TZR level. This level is a composite of the F12-TZ energy with the addition of Douglas-Kroll scalar relativistic corrections[117,243,244] with the relativity Hamiltonian toggled

on (E_{DKr}) and off (E_{DK}).

$$E_{TZR} = E_{F12-TZ} + \Delta_R \tag{5.1}$$

$$\Delta_R \equiv E_{DKr} - E_{DK} \tag{5.2}$$

The next composite method is the F12-TcCR method and exchanges the cc-pVTZ-F12 basis set for the explicit core correlation cc-pCVTZ-F12 basis set[245] along with the aforementioned scalar relativistic corrections. The composite energy definition is defined as:

$$E_{F12-TcCR} = E_{cc-pCVTZ-F12} + \Delta_R. \tag{5.3}$$

The "Split basis" TcCR and TcC levels of theory are related to Eq. 5.3, but do not include the core-electron correlation in the basis set for only the Al atoms in the system. In the case of Split basis TcC, the Douglas-Kroll scalar relativistic corrections are also removed. The Split basis levels of theory are defined as follows in the following equations:

$$E_{\text{Split Basis TcCR}} = E_{cc-pVTZ-F12(\text{Al})+cc-pCVTZ-F12(\text{N, O, or H})} + \Delta_R \tag{5.4}$$

$$E_{\text{Split Basis TcC}} = E_{cc-pVTZ-F12(\text{Al})+cc-pCVTZ-F12(\text{N, O, or H})}. \tag{5.5}$$

Regardless of the level of theory, the QFFs in this work are implemented *via* the "push-button quartic force field" (PBQFF) framework.[72] The QFF procedure begins with the geometry of each Al molecule being optimized in MOLPRO 2023.2[107,248,249] at each level of theory specified above. For open-shell molecules, the restricted open-shell Hartree-Fock program is utilized as the reference followed by the unrestricted program of the aforementioned levels theory. The Cartesian coordinates of the optimized geometry is then displaced by 0.005 Å for bond lengths. These

displacements mimic a QFF but truncate the expansion at second-order yielding a Cartesian harmonic force field (HFF). Each displacement then undergoes a single-point energy (SPE) computation and is subsequently used to generate a harmonic force constant (FC) matrix. The subsequent mass-weighted Hessian matrix provides the normal coordinates for each molecular species in question. The optimized geometry is then displaced along these normal coordinates to compute the semi-diagonal QFF, and SPE computations are performed at each of these displacements.

Finally, the SPE energy computations are then used to compute the final normal FCs directly using a finite differences procedure. The normal coordinate FCs are passed to a VPT2 algorithm with the PBQFF framework itself.[67,74,75,118] In order to improve the spectral data produced, type-1 & -2 Fermi and Coriolis resonances are taken into account as this has shown to increase the accuracy of the computed rovibrational data.[68,72,119,216] Finally, in an effort to assist laboratory study or potential astrophysical and atmospheric detection, dipole moments for each Al compound are computed at the F12-TZ level of theory also utilizing MOLPRO2023.2. Similarly, double-harmonic infrared intensities are computed at the B3LYP/aug-cc-pVTZ[210,211] level of theory within MOLPRO2023.2.[107,248,249]

The F12-TcCR+TZ hybrid method is also included in Table 5.1. This hybrid method takes advantage of the computation of a HFF before the subsequent QFF within the PBQFF framework. Therefore, a blend of higher and lower-levels of theory can be utilized to the reduce computational cost of the full QFF process for no signifcant decrease in the over all accuracy of the rovibrational spectral data for the given molecule.[42,250,251] The TcCR+TZ hybrid method utilizes the more theoretically rigorous F12-TcCR level of theory to compute the HFF. Then, the cubic and quartic terms are computed at the lower F12-TZ level of theory and combined with the higher-level harmonic terms to flesh out the full QFF. This allows for even greater

Table 5.2: Vibrational frequencies (cm^{-1}), calculated percent error (%E) for AlH, AlO^-, and AlO, and overall mean absolute percent error (MA%E).

	AlH		AlO^-		AlO		
Level of Theory	ν	%E	ν	%E	ν	%E	MA%E
aTZ	1610.1	0.8	931.6	2.7	990.9	2.7	2.1
aCTZ	1609.0	0.9	940.2	1.8	956.4	0.9	1.2
awCTZ	1612.6	0.7	948.8	0.9	958.3	0.7	0.8
F12-TZ	1631.5	0.5	955.2	0.2	980.0	1.6	0.8
F12-TcC	1634.2	0.6	950.9	0.6	978.5	1.4	0.9
F12-TZR	1629.2	0.3	951.0	0.6	994.9	3.1	1.3
F12-TcCR	1629.3	0.3	945.2	1.2	986.5	2.2	1.2
F12-TcCR+TZ	1626.3	0.1	958.5	0.2	981.4	1.7	0.7
Split basis TcC	1631.5	0.5	977.6	2.2	992.3	2.8	1.8
Split basis TcCR	1628.6	0.3	954.5	0.3	979.3	1.5	0.7
Expt.[a]	1623.9		957		965		

[a] Previous gas-phase experimental data from Ref. 252 for AlH, Ref. 1 for AlO^-, and Ref. 253 for AlO

time savings than the full F12-TcCR composite method while still maintaining a higher degree of accuracy compared to the F12-TZ method alone.

5.3 Results and Discussion

5.3.1 Diatomic Molecules with Gas-Phase Data

All three of the diatomic molecules studied herein, $\tilde{X}\ ^1\Sigma^+$ AlH, $\tilde{X}\ ^1\Sigma_g^+$ AlO^-, and $\tilde{X}\ ^2\Sigma^+$ AlO, have gas-phase experimental vibrational data to benchmark the performance of the various levels of theory explored in this work. Computed fundamental anharmonic frequencies, experimental frequencies, and the percent error with respect to experiment are listed in Table 5.2. The experimental gas-phase data for these two molecules are from Refs. 252, 1, and 253 for AlH, AlO^-, and AlO, respectively. The simple bonding motif between aluminum and hydrogen in AlH lends itself to strong agreement with experimental gas-phase data for all levels of theory with all computed frequencies lying within 1% of experiment at 1623.9 cm^{-1}. The lack of core electrons in hydrogen, and thus the lack of internuclear core elec-

tron interaction in the Al−H bond, results in minimal changes to the deviation from experiment regardless of the choice of core electron correlation included. The inclusion of relativistic effects tends to contribute to closer agreement with experiment regardless of whether or not the core electrons are included in the computation. The method that is the closest to experiment for AlH is the hybrid F12-TcCR+TZ with only 0.1% error (3.6 cm^{-1}).

The computed vibrational data for AlO^-, shown in the middle columns of Table 5.2 retain the closed shell characteristics of AlH while the bonding motif is more complicated due to the interaction of core electrons between the aluminum and oxygen atoms. This more complicated bonding environment leads to more variance in the error across all tested QFFs and levels of theory. The inclusion of core electrons in the computations improves the agreement with experiment for the methods that do not include explicit correlation, while the opposite effect occurs with inclusion of explicit correlation. The inclusion of relativistic effects results in greater error for F12-TcCR compared to F12-TcC where all of the core electrons are included. When only the core electrons in oxygen are included but not aluminum, relativistic effects improve the agreement with experiment significantly between the Split basis TcCR and Split basis TcC QFFs. Despite this, the best agreement with experiment is once again the hybrid method F12-TcCR+TZ with only 0.2% MA%E (2 cm^{-1}).

The neutral radical AlO diatomic molecule has similar bonding as its corresponding anion, but the open-shell nature of this radical presents a slightly different interaction between aluminum and oxygen. Computed vibrational data for AlO are also listed in Table 5.2 along with the gas-phase experimental frequency. The inclusion of core electrons and relativistic effects produce larger error in the computed values for the open-shell system compared to closed-shell AlO^-. Relativistic effects without core correlation added in F12-TZR show the largest deviation from

Table 5.3: Rotational spectroscopic and distortion constants (MHz unless otherwise specified), calculated percent error (%E) for AlH and AlO, and overall mean absolute percent error (MA%E)

	AlH				AlO				
Level of Theory	B_0	%E	D_e	%E	B_0	%E	D_e (kHz)	%E	MA%E
aTZ	186333.4	0.2	10.843	1.5	18609.9	2.3	31.686	2.2	1.5
aCTZ	187788.6	1.0	11.128	4.1	18832.6	1.2	33.095	2.1	2.1
awCTZ	188761.9	1.5	11.256	5.3	18963.3	0.5	33.294	2.8	2.5
F12-TZ	188294.2	1.2	10.886	1.9	18973.4	0.4	32.007	1.2	1.2
F12-TcC	189360.6	1.8	11.080	3.7	19106.5	0.3	32.621	0.7	1.6
F12-TZR	188292.0	1.2	10.904	2.0	18986.4	0.3	31.981	1.3	1.2
F12-TcCR	189357.0	1.8	11.098	3.8	19117.7	0.3	32.639	0.7	1.7
F12-TcCR+TZ	189285.2	1.8	11.098	3.8	19115.2	0.3	32.639	0.7	1.6
Split basis TcC	188289.2	1.2	10.904	2.0	18988.8	0.3	31.986	1.3	1.2
Split basis TcCR	188294.2	1.2	10.886	1.9	18975.4	0.4	32.014	1.2	1.2
Expt.[a]	191588.4		10.688		19239		32.4		

[a] Previous gas-phase experimental data from Ref. 252 for AlH and Ref. 253 for AlO

experiment with 3.1% error. The explicitly correlated methods that perform the best for AlO are F12-TZ, F12-TcCR, F12-TcCR+TZ, and Split basis TcCR. All of which exhibit errors of 1.4-1.7%. Of these four methods, the hybrid F12-TcCR+TZ method is the furthest from experiment with a deviation of 1.7% (16 cm^{-1}). Despite this, F12-TcCR+TZ, along with Split basis TcCR, displays the best agreement with experiment with a MA%E of 0.7%.

Experimental rotational spectroscopic results have also been provided for AlH and AlO. Table 5.3 contains the computed B_0 and D_e rotational and centrifugal distortion constants along with the experimental results from Ref. 252 and 253 for AlH and AlO, respectively. For the B_0 rotational constant of the simple AlH system, the error to experiment varies between 1.2 or 1.8%. The levels of theory that predict the rotational constants slightly less accurately compared to experiment (F12-TcC, F12-TcCR, and F12-TcCR+TZ) include some form of core electron correlation in the QFF definition. This likely occurs from the lack of hydrogen core electrons where the additional terms in the Hamiltonian provide no improvement to the overall accuracy of the given level of theory and likely introduce some numerical noise. This is further

suggested by the increased accuracy in the prediction of B_0 seen in the F12-TZ, F12-TZR, and both split basis levels of theory that freeze the Al core electrons. However, the prediction of B_0 for AlO suggests that F12-TcC, F12-TZR, F12-TcCR, and F12-TcCR+TZ all perform with similar accuracy with an error of a meager 0.3% (57 MHz out of 19115 MHz). The B_0 accuracy for AlO suggests that the additional core electron correlation and scalar relativistic corrections are necessary for the accurate prediction of rotational constants for Al-bearing species bonded to other heavy atoms or, especially, with higher bond orders.

The centrifugal distortion constants (D_e) exhibit more error for both AlH and AlO as expected.[254,255] Some of the same methods (F12-TcC, F12-TcCR, and F12-TcCR+TZ) for AlO that produce the lowest error in the B_0 values also show the lowest error in the D_e values with agreement to within 0.7% of experiment. In contrast with AlO, the D_e values for AlH do not show the same trend for accuracy. Of the explicitly correlated methods, F12-TcC, F12-TcCR and F12-TcCR+TZ exhibit the most error (3.7-3.8%). However, F12-TZ displays the smallest error in D_e at 1.9%. Again, the inaccuracies seen in the prediction of D_e for AlH may stem from the lack of core electron correlation from the hydrogen atom decreasing the accuracy in the QFF levels of theory that include these terms. With regards to the MA%E, the methods with the lowest overall error for rotational data are F12-TZ, F12-TZR, Split basis TcC, and Split basis TcCR with 1.2% overall error. This does not seem to follow the trend for accuracy seen in the calculated accuracy of the overall vibrational frequencies for the diatomic species. F12-TcCR+TZ exhibits the lowest error with respect to the vibrational frequency accuracies as well as the rotational data accuracy for AlO. This suggests that for species containing Al and heavier atoms than H, F12-TcCR+TZ will produce overall more accurate rovibrational spectral data. Finally, the computed rotational constants (B_0), centrifugal distortion constants (D_e), and

Table 5.4: Anharmonic vibrational frequencies (in cm^{-1}) and IR intensities (in parentheses in km mol^{-1} computed at B3LYP/aTZ) for AlO_2^- compared to previous gas-phase experiment from Ref. 1 with calculated percent error (%E).

Mode	Symm.	Desc.[a]	Expt.[a]	aTZ	%E	aCTZ	%E
ν_1	b_{1u}	AS (AlO)	1134	1111.6 (177)	2.0	1109.0	2.0
ν_2	a_g	S (AlO)	–	772.9 (0)	–	778.8	–
ν_3	b_{2u}	Bend (OAlO)	–	280.2 (88)	–	262.8	–
awCTZ	%E	F12−TZ	%E	F12−TcC	%E	F12−TZR	%E
1116.8	1.5	1126.4	0.7	1039.8	8.3	1124.1	0.9
785.7	–	787.0	–	895.2	–	787.1	–
265.1	–	263.9	–	171.0	–	269.9	–
F12−TcCR	%E	F12−TcCR+TZ	%E	Split Basis TcC	%E	Split Basis TcCR	%E
1255.9	10.7	1132.9	0.1	1128.9	0.4	1120.5	1.2
828.2	–	794.2	–	793.5	–	783.7	–
418.8	–	264.1	–	285.1	–	259.7	–

[a] "S" refers to the symmetric stretch, and "AS" is the antisymmetric stretch.

the dipole moment (D) for AlO^- are provided in the supplemental materials. While there are no experimental data available for AlO^-, the trend of F12-TcCR+TZ producing highly accurate results suggests this method will also be accurate for AlO^-.

5.3.2 Tri- and Tetratomic Molecules with Gas-Phase Data

5.3.2.1 AlO_2^-

Moving from diatomic molecules, the present work also benchmarks the given levels of theory on larger Al complexes as they exhibit interatomic effects that may be more common in the Earth's atmosphere as well as the interstellar medium and circumstellar media. To that end, the computed anharmonic vibrational frequencies for $\tilde{X}\ ^1\Sigma_g^+$ AlO_2^-, and comparison to previous gas-phase work,[1] are given in Table 5.4. The previous gas-phase experimental study[1] only observes the 1134 cm^{-1} frequency for the ν_1 anti-symmetric (AS) stretching mode for AlO_2^-. Hence, this frequency is the only available comparable to assess the accuracy of the levels of theory benchmarked for AlO_2^-. Immediately, the same trend seen in the diatomic molecules is further suggested here with the F12-TcCR+TZ hybrid method computing the most accu-

rate vibrational frequency for the AlO_2^- molecule, an error of 0.1% (1.1 cm^{-1} out of 1134 cm^{-1}). The split basis TcC level of theory follows closely behind at 0.4% error. Of the ten levels of theory benchmarked, the F12-TcCR composite method and the F12-TcC method exhibit the least accuracy compared to experiment at 10.7% and 8.3% error, respectively. This seems to follow the inaccuracies of the F12-TcC and F12-TcCR computed fundamental for AlO^-. Although, the overall MA%E for the diatomic computed anharmonic frequencies suggest F12-TZR to produce the least accurate QFF. That being said, the present computed anharmonic vibrational frequency data suggest that the F12-TcCR+TZ hybrid method can accurately predict the vibrational frequencies of the AlO_2^- molecule as well as the Al-bearing diatomics studied herein.

As mentioned previously, there is a lack of literature data for many Al-containing chemical compounds that may be present in Earth's atmosphere and beyond. The AlO_2^- species is no exception, and a direct comparison between the computed rotational data, shown in the supplemental materials, and previous experiment cannot be made. However, the accuracy of a given level of theory with respect to the rotational data may be inferred based on its performance for the Al diatomic compounds discussed above. Shown in Table 5.3, several levels of theory perform similarly suggesting that the accuracy in the rotational spectrum is not as hindered by the choice of the level of theory as the vibrational frequencies are. The F12-TcCR+TZ level of theory behaves similarly to F12-TcCR and F12-TZR in the diatomics despite the latter's inability to compute accurate vibrational spectral data. Of course, the accuracy in the diatomic Al-bearing species cannot be fully extrapolated to the performance of larger Al compounds, but an overall trend can be applied as a heuristic while laboratory data are absent. Therefore, the level of theory that best computes the rotational data can be deferred to the level of theory that performs

best for the vibrational frequencies given the similar performance across the levels of theory in the diatomic rotational data.

Table 5.5: Anharmonic vibrational frequencies (in cm^{-1}) and IR intensities (in parentheses in km mol^{-1} computed at B3LYP/aTZ) for AlO_3^- compared to previous gas-phase experiment from Ref. 1 with calculated %E.

Mode	Symm.	Desc.[a]	Expt.	aTZ	%E	aCTZ	%E
ν_1	a_1	AlO	1098	1073.5	2.3	1062.2	3.4
ν_2	b_2	S (O_2)	842	725.2	–	720.2	–
ν_3	a_1	AS (AlO_2)	685[b]	643.1	5.0	579.6	16.5
ν_4	a_1	S (AlO_2)	526	526.2	0.0	517.4	1.7
ν_5	b_1	OPB (AlO_3)	–	304.4	–	113.9	–
ν_6	b_2	Wag ($OAlO_2$)	–	229.4	–	85.0	–
MA%E					2.4		7.2
awCTZ	%E	F12-TZ	%E	F12-TcC	%E	F12-TZR	%E
1041.6	5.4	1093.9	0.4	1104.9	0.6	1089.3	0.8
707.3	–	747.4	–	746.8	–	723.4	–
653.7	3.3	680.5	0.8	636.5	6.0	661.7	2.0
356.0	47.8	531.0	0.9	586.3	10.3	514.0	2.3
253.9	–	295.8	–	385.0	–	243.4	–
185.3	–	277.9	–	189.8	–	274.8	–
	18.8		0.7		5.7		1.7
F12-TcCR	%E	F12-TcCR+TZ	%E	Split Basis TcC	%E	Split Basis TcCR	%E
1201.1	8.6	1096.0	0.2	1093.5	0.4	1038.1	5.8
1119.3	24.8	742.6	–	744.0	–	765.1	–
1228.5	44.2	680.0	0.7	693.5	2.7	680.8	0.9
778.6	32.4	525.2	0.2	530.9	0.9	516.5	1.8
1358.6	–	270.5	–	338.4	–	307.6	–
1198.7	–	258.9	–	305.7	–	226.6	–
	28.4		0.4		1.3		2.8

[a] "S" and "AS" are once more symmetric and antisymmetric with "OPB" referring to the out-of-plane bend.
[b] Previous experiment suggests 685/675 cm^{-1} for this mode. Further discussion is in the text.

5.3.2.2 AlO_3^-

The tetratomic $\tilde{X}\ ^1A_1$ AlO_3^- anharmonic vibrational frequencies are given alongside a comparison to previous gas-phase experimental data[1] in Table 5.5. While the previous experiment observes four fundamental vibrational frequencies for AlO_3^-, the spectrum provided therein suggests an 842 cm^{-1} frequency corresponding to the ν_2 O_2 stretching mode. However, given the presently-computed frequencies and the CCSD(T) harmonic frequencies reported in that work for this same fundamental, the

frequency at 842 cm^{-1} may be a misattribution of what is likely noise resulting from the previous experimental set-up. The levels of theory in the present work compute the frequency for this mode to lie between 700−747 cm^{-1} with the corresponding harmonic IR intensity of a meager 1 km mol^{-1}. That being said, the present computational work will not consider the experimental 842 cm^{-1} frequency for comparison to the computed frequencies.

The comparison of the levels of theory computed herein to the previous gas-phase data further suggests that the hybrid F12-TcCR+TZ method provides the most accurate anharmonic vibrational frequencies with an MA%E of 0.4. This is followed closely by the F12-TZ level, at 0.7 MA%E, which is similar to the accuracy seen in the linear AlO_2^- molecule. In contrast, the F12-TcCR level, again, performs the least accurate compared to experiment with an MA%E of 28.4, which is also similar to this level's performance for AlO_2^-. This may suggest that computing the full QFF at the F12-TcCR level of theory introduces some numerical instability in the computation of the third- and fourth-order constants leading to errors in the overall vibrational frequencies. In the case of the hybrid QFF, these errors seem to be mitigated significantly as the only difference is the computation of the third- and fourth-order force constants at the lower F12-TZ level of theory. Thus, the higher-level harmonic force constants seemingly provide higher accuracy and retain numeric stability whereas the anrharmonic force constants degrade. These F12-TcCR harmonic force constants can then be enhanced with the numeric stability from the computed F12-TZ third- and fourth-order force constants which correct the F12-TcCR harmonics in line with experiment.

Shown in Table 5.5, previous gas-phase experiment [1] attributes both 675 cm^{-1} and 685 cm^{-1} to the ν_3 AS AlO_2 mode corresponding to a split peak in the previous experimental IR spectrum given therein. However, the splitting in the peaks is likely

due to the presence of the $AlO_2{}^{18}O^-$ isotopologue. This is further confirmed by the computation of vibrational frequency of said isotopologue at the F12-TcCR+TZ level revealing a frequency for ν_3 at 672 cm^{-1}Às this level of theory has performed accurately for the diatomic and triatomic species, as well as the standard isotopologue of AlO_3^-, the computation of this isotopologue's frequency of 672 cm^{-1}should be considered as an explanation for the splitting seen in the previous gas-phase IR spectrum.

Like AlO_2^-, no previous gas-phase rotational data are available for comparison to the computed rotational spectroscopic data of AlO_3^- provided in the supplemental materials. However, as shown for the diatomic species, the accuracy for the rotational constants of a given level of theory compared to experimental data is coupled to that of the vibrational frequencies. Since the hybrid method performs with high accuracy in the vibrational frequencies for AlO_3^-, the same level of accuracy can be expected for the rotational spectral constants for this level of theory.

5.3.3 Al Molecules with Ar Matrix Data

Several Al-bearing species investigated herein have little-to-no gas-phase experimental data outside of an Ar Matrix. As interaction with a matrix is known to cause shifts in the observed frequencies compared to the true gas-phase data,[226] a numerical accuracy comparison of the theoretical work herein is not possible. However, matrices are known to redshift the frequencies between $\Delta\nu = 9 - 20$ cm^{-1} on average.[226] That being said, a simple comparison of the difference between the provided theoretical data and the previous Ar matrix spectroscopic data can be analyzed. Thus, the levels of theory that perform best for the aforementioned Al-containing molecules with Ar matrix data will reasonably offset the redshifted vibrational frequencies by the prescribed $9 - 20$ cm^{-1}.

Table 5.6: Comparison of computed anharmonic vibrational frequencies with previous Ar matrix experimental frequencies (in cm^{-1}) from Ref. 2 with B3LYP/aTZ IR intensities in parentheses (in km mol^{-1}) for AlH_3.

Mode	Symm.	Desc.	Expt.[a]	aTZ	$\Delta\nu$	aCTZ	$\Delta\nu$
ν_1	A_1'	S (AlH)	–	1873.4 (0)	–	1879.7	–
ν_2	A_2"	OPB (AlH_3)	697.8	710.8 (387)	13.0	710.9	13.1
ν_3	E'	AS (AlH)	1882.8	1874.1 (251)	−8.7	1879.3	−3.5
ν_4	E'	AS (HAlH)	783.4	781.0 (234)	−2.4	785.7	2.3
awCTZ	$\Delta\nu$	F12−TZ	$\Delta\nu$	F12−TcC	$\Delta\nu$	F12−TZR	$\Delta\nu$
1886.4	–	1891.0	–	1859.5	–	1885.9	–
712.4	14.6	708.3	10.5	665.5	−32.2	700.6	2.8
1886.0	3.2	1890.0	7.2	1901.2	18.4	1885.4	2.6
789.9	6.5	788.9	5.5	728.8	−54.6	780.3	−3.1
F12−TcCR	$\Delta\nu$	F12−TcCR+TZ	$\Delta\nu$	Split Basis TcC	$\Delta\nu$	Split Basis TcCR	$\Delta\nu$
1917.6	–	1896.1	–	1890.3	–	1888.8	–
771.6	73.8	714.1	16.3	707.6	9.8	719.8	22.0
1900.9	18.1	1895.2	12.4	1889.2	6.4	1890.3	7.5
828.2	44.8	794.9	11.5	788.2	4.8	797.0	13.6

5.3.3.1 AlH_3

As shown in Table 5.6, the computed anharmonic vibrational frequencies for AlH_3 are provided with the Ar matrix experimental frequencies and the differences between them, $\Delta\nu$. As the ν_1 stretching mode is the totally symmetric irrep for AlH_3, previous Ar matrix data are not reported for this fundamental. It has been included in the present work for completeness sake and to serve as a reference for future laboratory work. Regardless, the difference between the computed and Ar matrix data varies substantially across the different levels of theory for AlH_3. Of the 10 levels of theory benchmarked on AlH_3, the F12-TcCR+TZ hybrid method computes a sufficient difference to offset the matrix effects for each mode within the aforementioned $9 - 20$ cm^{-1} range. This seems to follow a similar trend seen in the above diatomic species, especially AlH and AlO^-, where the hybrid method provides the most accurate rovibrational data when compared to gas-phase experiment. Again, this gain in accuracy is discussed in a previous benchmark study utilizing this F12-TcCR+TZ hybrid method[42] where the more theoretically rigorous

method (F12-TcCR) is applied to the harmonic portion of the QFF procedure to lay a more accurate foundation for the lower-level computation (F12-TZ) of the cubic and quartic terms to build upon.

Most other levels of theory all perform similarly relative to one another. The conventional aTZ and aCTZ levels perform almost identically, where awCTZ performs similar to F12-TZ. That is to say, provides sufficient correction for the ν_2 bending mode, but does not compute the same correction for the other modes. The F12-TZR composite method does not produce accurate shifts for any mode but is not as substantially different compared to Ar matrix data as the F12-TcC method and the F12-TcCR composite method. The F12-TcC performance for AlH_3 seems to mimic, though not as significantly, that of the singly-hydrogenated AlH molecule, where F12-TcC exhibits the most inaccuracy for the explicitly correlated methods. As the bonding environment within AlH_3 does not include contribution from Al core electrons, the F12-TcC method may suffer from some numerical instability that may be contributing to the large differences seen for at least AlH_3.

The F12-TcCR composite QFF exhibits the largest differences across the levels of theory for AlH_3 compared to Ar matrix data and substantially blueshifts the ν_2 and ν_4 bending fundamentals. While the F12-TcCR method has historically been utilized as a highly-accurate QFF method,[41,215] molecules that exhibit very "floppy" vibrational modes are known to suffer from the use of composite methods due to conflicting minima at every point of the potential well.[110,132,184] Thus, the F12-TcCR composite method may be an undesirable QFF method when applied to Al-bearing species. However, when the F12-TcCR composite method is relegated to only the harmonic terms within the QFF procedure and the rest of the terms are computed at the F12-TZ level, the correction of the matrix shifting effect seems to fall entirely within the aforementioned offset of $9 - 20$ cm^{-1}. Thus, the F12-

TcCR+TZ level, again, seems to provide accurate anharmonic vibrational spectral data for AlH_3.

5.3.3.2 $AlNH_4$

The computed anharmonic vibrational frequencies along with the calculated difference from previous Ar matrix experimental data[3] are shown in Table 5.7. Like AlH_3, the rotational spectral constants can be found in the supplementary materials as there are no experimental rotational data for comparison. In the previous Ar matrix experiment, the b_2 ν_1 AS N−H stretch at 3499.7 cm^{-1} was attributed to the a_1 S N−H stretch, but all presently computed QFFs report frequencies that correspond to the b_2 mode. Thus, the work herein attributes that the previous a_1 frequency at 3499.7 cm^{-1} to the b_2 mode hereafter. Additionally, the previous Ar matrix study attributes a frequency of 518.3 cm^{-1} to the ν_{11} NH_2 OPB. Given that most levels of theory herein do not compute a vibrational frequency in this region, this may suggest that the frequency of 518.3 cm^{-1} is also a misattribution or is unrelated to the molecule entirely. Thus, this frequency will not be considered when examining the accuracies of the various QFFs. Additionally, the large difference present in every level of theory, ≈50 cm^{-1}, for the ν_8 AS in-plane NH_2 bend may be indicative of the QFF procedure's inability to accurately describe certain "floppy" modes as discussed previously. That being said, the failure to describe this mode may not be inherent to the choice of the level of theory and should not discredit the QFF predictions of the vibrational frequencies for the $AlNH_4$ species.

Again, for Ar matrix data, the most accurate level of theory will be the level that reasonably offsets the matrix shift. For $AlNH_4$, both the F12-TcC and F12-TcCR+TZ hybrid method provide the most reasonable difference from the Ar matrix data. This is in stark contrast to the F12-TcC performance for AlH_3 which exhibits a large error likely associated with the lack of core electron correlation. However,

Table 5.7: Computed anharmonic vibrational frequencies (in cm^{-1}) with IR intensities (in parentheses in km mol^{-1}computed at B3LYP/aTZ) for $AlNH_4$ compared to previous Ar matrix experiment from Ref. 3

Mode	Symm.	Desc.	Expt.	aTZ	$\Delta\nu$	aCTZ	$\Delta\nu$
ν_1	b_2	AS (NH)	3499.7[a]	3487.3 (31)	-12.4	3491.8	-7.9
ν_2	a_1	S (NH)	–	3414.0 (27)	–	3418.3	–
ν_3	b_2	AS (AlH)	1899.3	1884.0 (257)	-15.3	1889.1	-10.2
ν_4	a_1	S (AlH)	1891.0	1881.1 (81)	-9.9	1887.2	-3.8
ν_5	a_1	S (NH_2)	1541.6	1548.3 (28)	6.7	1552.3	10.7
ν_6	a_1	AlN	818.7	810.5 (217)	-8.2	818.6	-0.1
ν_7	a_1	S(AlH_2)	755.0	742.4 (51)	-12.6	747.4	-7.6
ν_8	b_2	AS (NH_2)	769.8	714.4 (145)	-55.4	715.2	-54.6
ν_9	b_1	OPB (AlH_2)	608.7	611.9 (165)	3.2	612.4	3.7
ν_{10}	a_2	τ	–	473.1 (0)	–	474.8	–
ν_{11}	b_1	OPB (NH_2)	518.3[b]	424.0 (236)	–	434.3	–
ν_{12}	b_2	AS (AlH_2)	–	427.6 (19)	–	428.5	–
awCTZ	$\Delta\nu$	F12-TZ	$\Delta\nu$	F12-TcC	$\Delta\nu$	F12-TZR	$\Delta\nu$
3492.4	-7.3	3496.0	-3.7	3516.6	16.9	3495.2	-4.5
3419.4	–	3421.3	–	3432.8	–	3421.0	–
1893.3	-6.0	1895.3	-4.0	1920.2	20.9	1894.7	-4.6
1891.5	0.5	1893.3	2.3	1904.0	13.0	1893.6	2.6
1552.8	11.2	1552.1	10.5	1548.5	6.9	1556.3	14.7
821.3	2.6	819.7	1.0	811.2	-7.5	825.9	7.2
749.6	-5.4	747.0	-8.0	749.1	-5.9	753.7	-1.3
714.6	-55.2	715.4	-54.4	715.8	-54.0	724.3	-45.5
611.5	2.8	609.2	0.5	769.8	161.1	613.7	5.0
473.5	–	466.5	–	380.5	–	478.6	–
437.7	–	441.9	–	505.7	–	447.0	–
427.1	–	424.5	–	438.0	–	438.4	–
F12-TcCR	$\Delta\nu$	F12-TcCR+TZ	$\Delta\nu$	Split Basis TcC	$\Delta\nu$	Split Basis TcCR	$\Delta\nu$
3433.3	-66.4	3503.1	3.4	3497.6	-2.1	3495.9	-3.8
3375.9	–	3427.8	–	3423.1	–	3420.4	–
1869.1	-30.2	1901.5	2.2	1895.7	-3.6	1892.7	-6.6
1743.5	-147.5	1900.8	9.8	1895.0	4.0	1892.2	1.2
1413.4	-128.2	1553.1	11.5	1555.4	13.8	1554.8	13.2
494.1	-324.6	823.7	5.0	825.9	7.2	822.0	3.3
567.1	-187.9	752.8	-2.2	751.6	-3.4	751.9	-3.1
345.2	-424.6	717.6	-52.2	718.6	-51.2	716.4	-53.4
85.3	-523.4	612.9	4.2	609.5	0.8	611.9	3.2
376.8	–	471.0	–	474.4	–	483.9	–
−236.2	–	442.8	–	451.5	–	445.9	–
−338.3	–	432.2	–	434.4	–	432.2	–

[a] This was attributed to an a_1 symmetry label in the previous Ar matrix data. Further discussion provided in text.

[b] This is may not be associated with this molecule. Further discussion provided in text.

with the presence of the Al−N bond, this is no longer the case. However, the ν_9 AlH_2 OPB is substantially redshifted which suggests there is still some error present in the F12-TcC prediction of the vibrational frequencies. For the F12-TcCR+TZ level, though they are not all within the $9 - 20$ cm^{-1} offset, there is no further redshifting of the ν_9 mode and the other corrections appear well-behaved. While the F12-TcC level offsets the matrix shift for this molecular species more sufficiently than the F12-TcCR+TZ hybrid method, its inability to do so for many other species herein suggests that it may not be suitable in every case for computing accurate rovibrational spectral data.

5.3.4 Al Molecules without Experimental Data

$HAlO_2$

Harmonic and anharmonic frequencies are listed in Table 5.8 at all ten levels of theory benchmarked in this work. In general, the inclusion of explicit correlation introduces positive anharmonic corrections to several frequencies with the corrections to ν_5 and ν_6 typically being the most severe. For F12-TZ, the positive anharmonicities are fairly small at only 3.5 cm^{-1}, and the frequencies are in line with those computed previously with a very similar approach. The exception is for ν_6 which was not computed to have positive anharmonicities utilizing symmetry-internal coordinates.[256] Even so, these positive anharmonic corrections become especially severe with the inclusion of core correlation in F12-TcC where the anharmonic frequencies are 129.4 and 382.0 cm^{-1} larger than the harmonic frequencies for ν_5 and ν_6, respectively. Inclusion of Douglas-Kroll relativistic effects on their own in F12-TZR produces much smaller positive anharmonic corrections of only 30.7 and 26.7 cm^{-1} for ν_5 and ν_6, respectively. Combining core correlation and relativistic effects with F12-TcCR creates similar behavior in that ν_5 and ν_6 still are untrustworthy in the

anharmonic portion.

In contrast with the other methods, the F12-TcCR+TZ hybrid approach generates no positive anharmonicities, implying that this method is reliable for $HAlO_2$. The hybrid QFF is also consistent with the two Split basis QFFs in Table 5.8. This outcome combined with the previous benchmarks above points to this level of theory generating the best predictions for the IR spectrum of this molecule. Previous F12-TZ and CcCR values computed with symmetry-internal coordinates 256 are also listed in Table 5.8. The F12-TZ results are consistent with each other across both coordinate systems with more variation in the low-frequency fundamentals. The CcCR data are similar to the F12-TcCR+TZ data with the exception of CcCR producing a large anharmonic correction for the ν_6 frequency. Presently, the F12-TcCR+TZ values indicate that the notably intense (138 km mol^{-1}) out-of-plane b_1 ν_6 fundamental frequency lies closer to its harmonic value than the previous computations indicate.[256]

The calculated rotational constants for $HAlO_2$ are given in the supplementary materials. The rotational constants are in much better agreement across the methods than the vibrational frequencies as they are less susceptible to anharmonic variation. The largest difference arises when core electrons are excluded which is known to decrease the accuracy of the methods.[41,105,106] However, the F12-TcCR+TZ rotational constants are in close agreement ($\sim$ 20 MHz) with previous CcCR results as shown in Table 5.9, especially the B and C constants, implying that the rotational constants of the current method are just as accurate[40] as the previous or potentially moreso.[41]

5.3.4.1 AlH_2OH

Table 5.10 lists all of the harmonic and anharmonic vibrational frequencies for AlH_2OH for all ten benchmarked QFFs and their respective levels of theory, along with the previously computed data at F12-TZ and CcCR with symmetry-internal

Mode	Symm.	Desc.	aTZ	aCTZ	awCTZ	F12-TZ	F12-TcC
ω_1	a_1	S(AlH)	2049.7 (63)	2053.3	2061.3	2057.1	2069.4
ω_2	a_1	SS (AlO)	923.0 (51)	931.0	937.7	943.2	950.0
ω_3	b_2	AS (AlO)	758.0 (24)	768.2	774.8	777.9	784.9
ω_4	a_1	S (OO)	512.6 (24)	516.4	519.3	525.0	526.7
ω_5	b_2	Bend (HAlO)	521.7 (86)	521.2	522.6	520.9	523.3
ω_6	b_1	OPB (HAlO)	487.5 (138)	484.9	482.2	477.1	479.3
ν_1	a_1	S(AlH)	1987.1	1990.7	1995.4	1994.8	2089.8
ν_2	a_1	SS (AlO)	905.9	912.3	918.6	929.2	940.5
ν_3	b_2	AS (AlO)	750.9	762.4	767.6	772.1	799.6
ν_4	a_1	S (OO)	494.8	496.2	499.7	511.9	510.9
ν_5	b_2	Bend (HAlO)	521.8	520.6	522.5	524.4	652.5
ν_6	b_1	OPB (HAlO)	487.2	481.4	479.4	480.6	861.3

Mode	F12-TZR	F12-TcCR	F12-TcCR+TZ Split	Basis	TcC Split	Basis	TcCR	F12-TZ[a]	CcCR[a]
ω_1	2055.8	2068.2	2068.2	2057.1	2055.8			2057.2	2070.0
ω_2	941.8	948.5	948.5	943.3	941.9			942.8	950.8
ω_3	776.2	783.2	783.2	777.9	776.2			776.5	783.8
ω_4	526.5	528.2	528.2	525.2	526.7			529.9	534.6
ω_5	523.1	525.6	525.6	521.0	523.2			520.5	521.4
ω_6	478.3	480.5	480.5	477.1	478.2			477.1	473.6
ν_1	1996.0	2042.1	2005.3	1995.6	1993.6			1994.0	2006.1
ν_2	934.8	935.3	926.5	928.2	921.2			926.0	933.8
ν_3	789.2	783.9	771.8	769.1	770.2			766.8	773.6
ν_4	529.3	534.0	508.2	514.4	508.4			508.5	513.8
ν_5	553.8	823.7	520.2	520.5	532.0			518.2	518.3
ν_6	505.0	556.0	474.0	484.2	490.7			439.3	430.3

[a]Previous computations from Ref. 256.

Table 5.8: Harmonic and anharmonic vibrational frequencies (in cm^{-1}) and IR intensities (in parentheses in km mol^{-1} computed at B3LYP/aTZ) for $HAlO_2$

Const.	Units	F12-TZ	F12-TcCR+TZ	F12-TZ[a]	CcCR[a]
A_e	MHz	23033.5	23091.1	23117.3	23216.5
B_e	MHz	13367.8	13519.3	13346.5	13499.4
C_e	MHz	8458.7	8527.0	8461.3	8536.0
A_0	MHz	22838.3	22898.0	22916.1	23020.8
B_0	MHz	13356.0	13506.2	13335.6	13487.6
C_0	MHz	8404.8	8472.3	8407.3	8482.0
A_1	MHz	22824.2	22883.4	22901.0	23005.5
B_1	MHz	13323.4	13472.2	13303.2	13454.4
C_1	MHz	8390.0	8456.9	8392.4	8466.8
A_2	MHz	22768.5	22828.3	22846.1	22951.3
B_2	MHz	13306.0	13453.4	13285.6	13436.9
C_2	MHz	8377.0	8443.6	8379.4	8453.9
A_3	MHz	22935.9	22996.6	23014.3	23118.2
B_3	MHz	13287.7	13434.4	13267.5	13418.5
C_3	MHz	8404.0	8470.6	8407.4	8482.1
A_4	MHz	22421.4	22484.1	22505.0	22617.0
B_4	MHz	13470.5	13622.7	13447.4	13599.0
C_4	MHz	8428.8	8561.2	8375.6	8436.9
A_5	MHz	22873.4	22933.4	22945.8	23052.4
B_5	MHz	13377.1	13528.6	13357.8	13509.6
C_5	MHz	8303.8	8306.7	8361.6	8449.4
A_6	MHz	22815.8	22876.0	22882.3	22989.1
B_6	MHz	13348.1	13499.2	13330.6	13483.2
C_6	MHz	8417.5	8485.7	8419.5	8494.5
κ		−0.314	−0.302	−0.32064	−0.31141
Dipole	D	4.55		4.55	

[a]Previous computations from Ref. 256.

Table 5.9: Comparison of rotational constants and dipole moment at select levels of theory with previous computations for $HAlO_2$

coordinates.[179] As with $HAlO_2$, the methods with explicit correlation introduce either positive or very large, non-physical anharmonic corrections, particularly in the low frequency range. The positive anharmonicities for AlH_2OH are not as extreme as for $HAlO_2$ with F12-TZ only displaying one positive anharmonicity of 1.4 cm^{-1} for ν_7. However, the addition of core correlation in F12-TcC does not produce any positive anharmonicities, but ν_8 and ν_9 show exceptionally large anharmonic corrections with magnitudes of 382.8 and 105.5 cm^{-1}, respectively. Inclusion of only Douglas-Kroll relativistic effects in F12-TZR result in positive anharmonicities in ν_4, ν_5, ν_7, and ν_8 that range from 0.4-12.4 cm^{-1}. The combination of core correlation and relativity in F12-TcCR once again does not produce any positive anharmonic corrections, but the corrections are even larger than F12-TcC with ν_4 through ν_9 all having corrections of larger than 100 cm^{-1}. The ν_6 and ν_9 corrections are the worst with magnitudes of 335.2 and 488.2 cm^{-1}, respectively. The anharmonic correction for ν_9 is larger than the harmonic frequency, resulting in a non-physical anharmonic frequency of -53.6 cm^{-1}.

The hybrid method F12-TcCR+TZ follows the performance for $HAlO_2$ and does not produce any positive anharmonicities or abnormally large anharmonic corrections. The data from both Split basis QFFs are consistent with the hybrid F12-TcCR+TZ data. This, once again, suggests F12-TcCR+TZ as the most reliable method for this molecule. As has been the case for all aluminum species studied herein, F12-TcCR+TZ is likely to generate the most accurate predictions for the IR spectrum of AlH_2OH. In comparison with the previously computed data, the F12-TZ data are consistent across both the use of normal and symmetry-internal coordinates. The previous CcCR data are in close agreement with F12-TcCR+TZ with the exception of the lower-frequency fundamentals. F12-TcCR+TZ suggests the ν_9 torsion may be higher than previously predicted.

Mode	Symm.	Desc.	aTZ	aCTZ	awCTZ	F12-TZ	F12-TcC
ω_1	a'	S (OH)	3922.5 (73)	3927.2	3930.7	3946.3	3952.7
ω_2	a'	S (AlH)	1971.5 (176)	1977.3	1985.7	1984.7	1995.7
ω_3	a'	S (AlH)	1941.0 (163)	1946.1	1954.5	1954.2	1964.5
ω_4	a'	S (AlO)	851.1 (160)	860.9	868.4	868.2	874.9
ω_5	a'	Bend (HAlH)	767.2 (96)	773.5	778.5	774.8	780.7
ω_6	a'	Bend (HOAl)	674.9 (212)	666.6	666.3	665.0	665.5
ω_7	a''	OPB (HAlH)	630.6 (224)	630.3	631.5	624.8	628.7
ω_8	a'	Bend (HAlH)	492.9 (81)	493.9	495.9	494.0	496.6
ω_9	a''	τ (HOAl)	435.9 (104)	436.4	439.4	434.4	437.7
ν_1	a'	S (OH)	3748.4	3753.8	3755.6	3769.5	3784.4
ν_2	a'	S (AlH)	1907.3	1912.2	1917.6	1920.0	1842.9
ν_3	a'	S (AlH)	1878.5	1883.2	1888.6	1892.1	1801.5
ν_4	a'	S (AlO)	839.9	848.3	855.2	858.9	675.4
ν_5	a'	Bend (HAlH)	762.0	759.4	765.6	767.0	616.3
ν_6	a'	Bend (HOAl)	621.8	610.5	614.2	615.7	396.8
ν_7	a''	OPB (HAlH)	625.6	624.7	626.3	626.2	460.4
ν_8	a'	Bend (HAlH)	489.1	485.3	489.1	493.8	113.8
ν_9	a''	τ (HOAl)	405.9	405.2	408.9	412.6	332.2

Mode	F12-TZR	F12-TcCR	F12-TcCR+TZ Split Basis TcC	Split Basis TcCR	F12-TZ[a]	CcCR[a]
ω_1	3943.4	3949.8	3949.8	3946.7	3943.8	3946.6	3953.2
ω_2	1982.4	1993.3	1993.3	1984.7	1982.4	1984.8	1998.3
ω_3	1951.8	1962.0	1962.0	1954.2	1951.8	1954.2	1966.9
ω_4	866.9	873.5	873.5	868.3	867.0	868.2	875.1
ω_5	775.6	781.5	781.5	774.8	775.7	774.8	781.0
ω_6	665.0	665.6	665.6	664.8	664.7	665.5	668.1
ω_7	626.4	630.2	630.2	624.8	626.4	624.7	626.6
ω_8	494.8	497.4	497.4	494.0	494.8	494.3	496.6
ω_9	431.2	434.6	434.6	434.4	431.3	433.5	436.4
ν_1	3767.3	3725.5	3772.3	3769.0	3764.9	3768.7	3773.6
ν_2	1914.5	1932.2	1926.0	1918.0	1914.0	1918.4	1929.2
ν_3	1893.0	1802.4	1897.3	1890.0	1886.8	1892.5	1906.3
ν_4	867.3	682.2	859.6	854.4	849.8	855.7	864.7
ν_5	780.4	559.5	766.4	761.9	760.5	766.3	782.5
ν_6	627.9	330.4	613.2	611.3	599.4	616.1	590.9
ν_7	636.7	328.1	627.7	621.1	616.3	621.9	626.0
ν_8	507.2	261.7	488.8	487.8	467.4	486.3	494.0
ν_9	416.3	-53.6	403.3	406.6	375.2	424.1	310.0

[a]Previous computations from Ref. 179.

Table 5.10: Harmonic and anharmonic vibrational frequencies (in cm^{-1}) and IR intensities (in parentheses in km mol^{-1} computed at B3LYP/aTZ) for AlH_2OH

All calculated rotational constants are listed in the supplementary material. As was the case with $HAlO_2$, the rotational constants across all methods are in close agreement with each other as they are less affected by anharmonic variation. The most variation in the rotational constants depends on the inclusion of core correlation. As previously stated, inclusion of core correlation is known to increase the accuracy of the methods.[41,105,106] As shown in Table 5.11, F12-TcCR+TZ produces rotational constants within 10 MHz of the previously computed CcCR data for the B/C constants and within $\sim$ 30 MHz for the A rotational constants. This suggests the rotational constants from the hybrid F12-TcCR+TZ method are just as[40] or even more[41] accurate than the previous data.

5.4 Conclusion

Of the ten QFFs and their defined levels of theory that are benchmarked in the present work, the F12-TcCR+TZ hybrid QFF most consistently outperforms the other levels of theory in terms of accuracy for molecules containing Al. This is the case for the diatomic molecules all the way to the six-atom, Al-bearing species and showcases the effects of composite inclusion of core electron correlation and scalar relativity in defining PESs such as QFFs. This trend is not only predicted in molecules with comparable gas-phase data, but also in comparison to Ar matrix data. The accuracy of the rovibrational spectral data suggests that for species containing Al−N and Al−O bonds, the added core electron correlation and scalar relativistic corrections are necessary in some manner as is accomplished through F12-TcCR+TZ. These additional corrections provide the needed accuracy in the computation of the harmonic force constants while the lower-level F12-TZ cubic and quartic force constants ensure numeric stability in these portions of the overall QFF. In the case of the conventional CCSD(T) QFFs (excluding the diatomic species), these levels of

Const.	Units	F12-TZ	F12-TcCR+TZ	F12-TZ[a]	CcCR[a]
A_e	MHz	113030.1	113969.8	113031.4	113935.5
B_e	MHz	14284.5	14414.8	14284.8	14416.1
C_e	MHz	12681.8	12796.4	12682.1	12796.9
A_0	MHz	113739.0	114677.1	113732.6	114629.3
B_0	MHz	14230.6	14358.7	14230.1	14361.4
C_0	MHz	12614.2	12727.0	12614.5	12729.0
A_1	MHz	112456.8	113374.0	112450.4	113333.9
B_1	MHz	14207.1	14334.7	14206.5	14337.7
C_1	MHz	12579.6	12691.8	12580.0	12694.1
A_2	MHz	112809.4	113714.8	112802.5	113692.0
B_2	MHz	14222.3	14350.0	14221.7	14353.0
C_2	MHz	12597.8	12709.8	12598.1	12712.4
A_3	MHz	112647.7	113545.2	112641.1	113522.4
B_3	MHz	14225.6	14353.5	14225.0	14356.4
C_3	MHz	12598.0	12710.1	12598.3	12712.6
A_4	MHz	113785.9	114715.0	113780.5	114665.3
B_4	MHz	14178.5	14304.1	14177.9	14308.0
C_4	MHz	12547.5	12657.3	12547.8	12661.4
A_5	MHz	114353.3	115304.2	114347.2	115233.3
B_5	MHz	14235.4	14363.1	14234.8	14366.5
C_5	MHz	12597.9	12710.1	12598.2	12712.5
A_6	MHz	118134.6	119068.9	118116.3	119040.8
B_6	MHz	14278.1	14405.1	14277.2	14408.1
C_6	MHz	12608.9	12720.9	12609.2	12723.3
A_7	MHz	112851.2	113803.4	112844.2	113730.2
B_7	MHz	14191.9	14319.3	14191.3	14323.7
C_7	MHz	12630.3	12743.8	12630.6	12745.5
A_8	MHz	117991.0	119092.3	117906.1	119019.2
B_8	MHz	14255.6	14383.0	14255.1	14386.5
C_8	MHz	12608.8	12723.0	12608.9	12724.1
A_9	MHz	110039.3	110890.4	110107.3	110814.0
B_9	MHz	14173.1	14303.4	14171.9	14303.9
C_9	MHz	12623.9	12737.2	12623.7	12738.3
κ		−0.968	−0.968	−0.97	
Dipole	D	1.21		1.22	

[a]Previous computations from Ref. 179.

Table 5.11: Comparison of rotational constants and dipole moment at select levels of theory for AlH_2OH.

theory predict less accurate data in comparison to the explicitly correlated levels of theory. This further suggests the corrections offered by explicit electron correlation and its faster approach to the CBS limit are useful for the accurate prediction of the rovibrational spectral data. This will allow computational chemistry to assist in the potential astrophysical and atmospheric detection of Al-bearing species that may contribute to dust grain formation or unique atmospheric chemistry. Further, this will provide reference data to assist in laboratory studies of said species that are noticeably lacking from the present literature.

CHAPTER 6

Investigating the Spectral Constants and Formation Pathway of Aluminum Nitrides from AlH and NH_3

Reprinted from Palmer C. Z.; Johns, J. A.; Fortenberry, R. C. *submitted* **2025**, DOI: *TBD*

Abstract

Reactions of AlH and NH_3 are shown to produce Al-N containing species that could potentially contribute to the composition of dust grains, like the Murchison CM2 chondritic meteorite. The present computational study couples explicitly correlated coupled cluster theory and density functional theory to produce a gas-phase chemical formation pathway from AlH and NH_3 to $Al_4N_4H_8$, a stable, cubic structure with the proper Al/N ratio expected of larger aluminum-nitride species. Rovibrational spectroscopic analyses of $HAlNH_3$, $AlNH_2$, $Al_2N_2H_4$, and $Al_4N_4H_8$ reveal consistently intense vibrational transitions and large absorption cross-sections of modes associated with spectral features typically associated with dust grain formation in circumstellar media. The ν_5 wagging frequency for $Al_4N_4H_8$ at 748.8 cm^{-1} (13.35 μm) exhibits a vibrational transition intensity of 428 km mol^{-1}, more than 5$\times$ larger than the antisymmetric stretch in water. Hence, the present formation pathway and rovibrational analysis should assist in the potential detection of a class of inorganic molecules that may contribute to the nucleation and formation of dust in protoplanetary disks and stellar outflows of AGB stars.

6.1 Introduction

Aluminum nitrides (AlNs) are a promising molecular class that may contribute to the nucleation and formation of dust grains in astronomical regions, ultimately leading to the development of larger rocky bodies in warmer inner protoplanetary disks or circumstellar envelopes of AGB stars. These stand in contrast to the long-theorized alumina (Al_2O_3) species.[186–188] Through laboratory examinations of samples of the Murchison CM2 chondritic meteorite,[43] the abundances of aluminum (Al) and nitrogen (N) therein were seemingly correlated to such a degree that the Al in the silicon-carbide samples were present as AlN or even AlN inclusions. The suggested presence of the AlN inclusions posits that in carbon-rich protoplanetary environments, Al and N species can form favorably as nucleating species to begin the dust formation process. Although alumina (Al_2O_3) is theorized to be the primary Al-containing compound contributing to dust grain nucleation,[186–188] the lower oxygen abundances in C-rich regions may reduce competition for the available Al. Without major competition, the formation of AlN may be more likely, similar to the formation of CH_3^+ in H_2O-poor regions of the ISM.[257,258] Furthermore, since a monomeric form of Al_2O_3 has yet to be astrophysically observed despite searches for it,[189,191,192] an investigation of other Al-bearing species is warranted to further study the mechanism of formation for dust grains in protoplanetary regions within circumstellar media (CSM) and the interstellar medium (ISM).

While previous studies on the formation of AlN clusters are limited, a previous computational study[259] has shown that successive additions of AlH_3 and NH_3 must overcome an initially raised energetic barrier of $\sim$2.0 kcal mol^{-1} ($\sim$1000 K). Once surpassed, this process can lead to the formation of larger aluminum nitride clusters, such as $AlNH_4$, $AlNH_6$, and even cyclic $Al_2N_2H_4$. However, the $\sim$2.0 kcal mol^{-1} barrier suggests that AlN species may form favorably only in the warmer inner

regions of protoplanetary disks, where dust grain nucleation and formation are already taking place. Furthermore, the aforementioned computational study predicts fundamental anharmonic vibrational frequencies for AlH_3, $AlNH_6$, and $AlNH_4$ that fall within the 13 μm spectral feature typically associated with elusive contributors to dust grains.[187,189] Additionally, these AlN species exhibit spectral features at 11, 20, and 28 μm, which are considered correlating, or potentially competing, features for contributing to the 13μm dust emission feature, similar to Al_2O_3.[190]

Although the previously predicted AlN formation pathway culminates in a cyclic AlN structure, AlH_3 has yet to be detected in the ISM potentially limiting the validity of the aforementioned reaction mechanism. Though access to more hydrogen atoms has been shown to benefit the progress of reaction pathways,[206,207] the previously observed aluminum monohydride (AlH) species detected toward Mira variable stars such χ Cyg and o Ceti[205] may serve as a more realistic reactant with NH_3 to form the cyclic $Al_2N_2H_4$ species. Thus, this present quantum chemical study proposes a novel formation pathway for larger AlN dust-nucleating species, starting from AlH and NH_3. The first product along the pathway, $AlNH_2$, is isoelectronic with the previously studied[227,228] and detected AlOH molecule which has been considered a dust precursor.[189] As such, this pathway would support the formation of AlN species that may contribute to dust grain nucleation and growth within protoplanetary disks or the circumstellar envelopes of AGB stars.

To support the proposed formation pathway of larger AlN species, the present quantum chemical work provides the rovibrational spectroscopic data necessary for comparison to observation for key species along the pathway. These rovibrational spectroscopic data are computed utilizing the quartic force field (QFF)[25,66] approach in conjunction with vibrational perturbation theory at second order (VPT2).[67,74,75,118] A QFF is a fourth-order Taylor series expansion of the potential energy portion of

the internuclear Watson Hamiltonian and, when combined with an accurate quantum chemical method, has historically produced rovibrational spectral constants to within 0.1% of experimental values for numerous molecular systems.[40,76,80,97,98,101,184,260,261] Thus, the spectral data provided herein will provide support for infrared (IR) and radioastronomical observations with tools such as the *James Webb Space Telescope* (JWST) and the *Atacama Large Millimeter/sub-millimeter Array* (ALMA), respectively. Consequently, the formation pathway and rovibrational analysis will assist the potential astrophysical detection of AlN as an alternative species that are potentially contributing to dust grain nucleation and propagation in CSM and the ISM.

6.2 Computational Methods

6.2.1 Reaction Mechanism Methods

For the minima along the reaction pathways presented herein, geometry optimizations, single-point energies (SPE), and zero-point vibrational energies are computed utilizing coupled cluster theory at the singles, doubles, and perturbative triples level [CCSD(T)].[52,58,208] The CCSD(T) method further incorporates the explicitly correlated F12b formalism[62,64] along with the corresponding cc-pVTZ-F12 basis set;[174,175] this CCSD(T)-F12b/cc-pVTZ-F12 level of theory is abbreviated "F12-TZ" hereafter. Each of the minima computations are conducted using the MOLPRO 2024.1 suite of quantum chemical packages.[262] To accurately describe the energetic profile of the formation pathway, geometry optimizations of the transition states and larger species are first conducted with the B3LYP density functional[210,211] at the aug-cc-pvtz (aTZ) level of theory.[212] Following this, an F12-TZ SPE and harmonic vibrational frequency computation are conducted for each optimized transition-state structure,[213] with corrections applied using the zero-point vibrational energy (ZPVE) from the harmonic frequency computation. Finally, all transition-state computations

are conducted *via* GAUSSIAN16.[120]

6.2.2 Rovibrational Spectroscopic Methods

The QFFs computed herein are conducted utilizing a hybrid methodology that is based on the aforementioned F12-TZ level of theory referred to as "F12-TcCR+TZ" defined below. The use of a hybrid method indicates that the harmonic and anharmonic force constants (FC) are computed at different levels of theory.[42] In this case, the "+TZ" portion specifies that the anharmonic FCs are computed at the F12-TZ level of theory. However, the harmonic FCs are computed at a composite level of theory that includes corrections from explicit core electron correlation "cC" and Douglas-Kroll scalar relativity "R"[117] from the cc-pCVTZ-F12 basis set[245] and the cc-pVTZ-DK basis set,[243,244] respectively. A recent computational benchmarking study[263] has shown that the use of hybrid methodologies, like F12-TcCR+TZ, predicts accurate rovibrational spectroscopic data to within 0.2% error compared to experimental gas-phase data for Al-containing species with higher bond orders much like the AlN species investigated herein. The hybrid procedure is preferred over the composite F12-TcCR level of theory as it fails for the large amplitude motions typically found in aluminum bonds.[15] However, as the size of the AlN molecules of interest increases, the computational cost of the triple-ζ basis sets become untenable even for the hybrid methodology. Thus, for the final product along the pathway, the full QFF is computed at the comparable double-ζ F12-DcCR+DZ hybrid level of theory.[42]

Regardless of the level of theory, the QFF procedure is conducted within the automated PBQFF framework.[72] The PBQFF procedure begins with a geometry optimization of the species at the chosen level of theory using the MOLPRO program[262] with tight convergence criteria. Next, the optimized geometry in Cartesian coor-

dinates is displaced by 0.005 Åand mimics a QFF but the expansion is truncated to the second order yielding a Cartesian harmonic force field (HFF). Each of these displacements then has a SPE computation performed, subsequently producing a harmonic force constant (FC) matrix. The eigenvectors of this Hessian matrix correspond to the normal coordinates for the molecule in question. Then, the optimized geometry is displaced along these normal coordinates, and SPE computations are performed for each displacement to fill out the semi-diagonal QFF. Once the SPE computations are completed, the final, normal FCs are computed utilizing a finite difference procedure.

These normal FCs are then passed to a VPT2 algorithm[67,74,75,118] within the PBQFF framework originally based on the SPECTRO program.[68] The VPT2 algorithm yields harmonic and fundamental anharmonic vibrational frequencies, vibrationally-averaged and singly-vibrationally-excited rotational constants, and quartic and sextic distortion constants. Finally, the rovibrational spectral data are further improved by the inclusion of type-1 & and -2 Fermi and Coriolis resonances in the computation of the rovibrational spectra. The inclusion of these resonances have been shown to increase the accuracy of computed rovibrational spectral data.[72,119,216,264] The descriptions of the fundamental vibrational frequencies are defined as symmetric (S) and anti-symmetric (AS) stretches or bends and out-of-plane bends (OPB). Finally, in order to assist in the potential laboratory or astrophysical observation of a new class of dust grain nucleating species, dipole moments for applicable AlN species are computed with F12-TZ in MOLPRO 2024.1, and anharmonic IR intensities are computed with B3LYP/aTZ in GAUSSIAN16. Finally, absorption cross-sections are calculated for each applicable vibrational frequency in order to assess a given fundamental's probability of IR absorption as described in the previously mentioned AlN formation pathway study.[259]

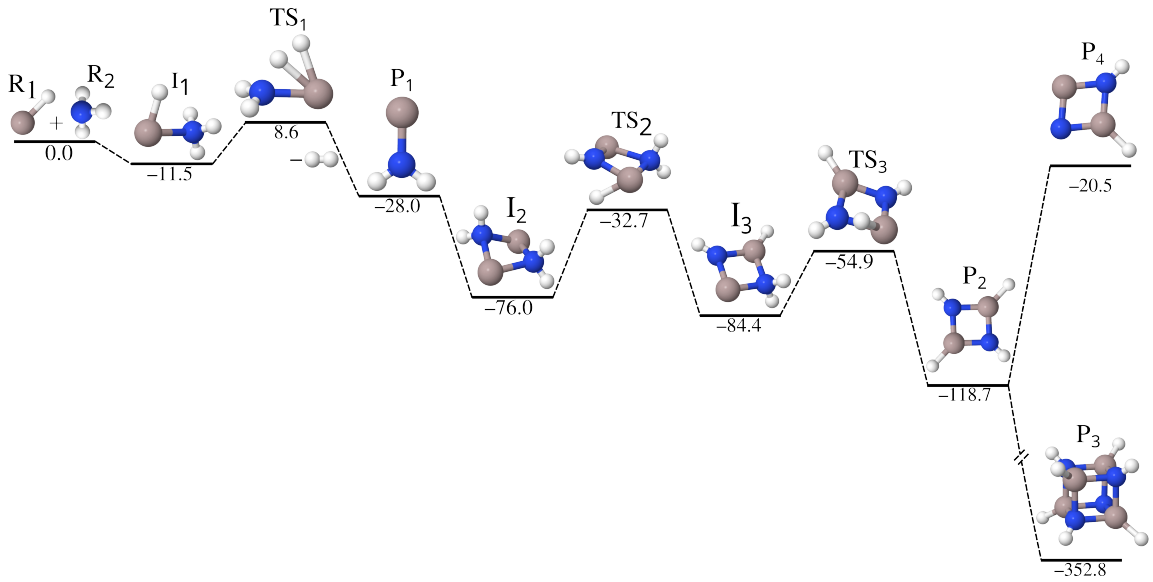

Figure 6.1: Reaction formation profile from AlH and NH_3 to T_d $Al_4N_4H_8$. Relative energies are in kcal mol^{-1}. White atoms indicate H, blue atoms indicate nitrogen, and gray beige indicate Al.

6.3 Results and Discussion

The formation pathway of larger, cyclic AlN species, along with their corresponding equilibrium geometries is shown in Fig. 6.1. The first step along the formation pathway involves the dative bonding of R_1 (AlH) and R_2 (NH_3) to form I_1 ($HAlNH_3$), which is lower in energy by ∼11.5 kcal mol^{-1}. This initiating step then means that subsequent chemical species can be produced from these reactants including the first product, P_1. While the P_1 species ($AlNH_2$) is lower in energy relative to the reactants by 28.0 kcal mol^{-1}, $HAlNH_3$ must first overcome a raised transition barrier of ∼8.6 kcal mol^{-1} relative to the reactants. This initially raised barrier mimics the behavior of the previously computed formation pathway on AlH_3 and NH_3[259] but is higher in energy than the previous pathway by a factor of roughly 4.5. Consequently, much like the previous work on AlH_3 and NH_3, the computed formation pathway is unlikely to commence in the diffuse, cold ISM.

Since the theorized presence of condensed AlN within the Murchison CM2

meteorite suggests its presence before the condensing of the full meteorite,[43] the AlN within would have likely condensed in a warmer environment supporting dust grain formation. While warmer, inner protoplanetary disks may be suitable regions for some AlN dust grain formation, the blackbody radiation from young stars (∼500 to 1500 K)[218] alone, at face value, is insufficient to directly facilitate the production of the larger AlN species proposed in the present pathway. However, a Boltzmann distribution for the population of TS_1 created from the reactants reveals that at least 1.00% of TS_1 is generated at ∼940 K. This energy requirement is within the previously mentioned ambient temperature range of protoplanetary disk for limited production of $AlNH_2$. In order to produce a more appreciable population of $AlNH_2$, the 8.6 kcal mol^{-1} barrier must be overcome in larger numbers. In contrast to protoplanetary environments, many highly evolved asymptotic giant branch (AGB) stars are known to exhibit significantly high blackbody radiation (1250−8500 K)[219,265] that can easily overcome the energy requirement necessary for the proposed pathway. Additionally, AGB stars are known to undergo significant mass loss regularly contributing ample amounts of dust-forming material to the surrounding interstellar and circumstellar environments.[220,221] Therefore, dust-forming environments around AGB stars, where ejecta accumulate, may be more suitable for the appreciable production of the proposed AlN species than protoplanetary disks.

Provided that TS_1 can be overcome in such environments, the successful production of $AlNH_2$, again in Fig. 6.1, is highly likely since all subsequent steps along the proposed pathway are submerged relative to $AlNH_2$. Hence, barrierless formation of larger AlN species is achievable much like previously computed pathways forming aluminum oxides.[189,206] In contrast, the previously computed AlN pathway starting from AlH_3 contains multiple instances of barriered transitions between products and their preceding intermediates.[259] Therefore, the present formation pathway may be

more likely to occur since such phenomena are not present. Regardless, I_2 shows the dimerization of $AlNH_2$ into a bent, cyclic structure due to the interaction between the nitrogen atom's lone pair and the empty *p*-orbitals on the Al atom in the presence of its lone pair. From there, I_2 undergoes an intramolecular hydrogen migration through TS_2 to I_3, seemingly stabilizing the structure by delocalizing the electron density into the overall cyclic structure. I_3 then follows a similar intramolecular hydrogen migration through TS_3 further stabilizing the overall structure forming the cyclic P_2 ($Al_2N_2H_4$) species. However, the hydrogen migration could be subverted if H-atom tunneling occurs further enhancing the population of P_2 relative to I_2 or I_3. Tunneling is more common at lower temperatures, but such behavior of the H-atom is not limited to those temperatures.[266] Regardless, the previous computational formation pathway[259] also concludes with formation of this cyclic $Al_2N_2H_4$ structure (P_2) but implies that it may go on to form larger structures. That being said, a natural, larger structure would be the dimerized form of $Al_2N_2H_4$. This structure is realized and included in the reaction pathway as the concluding molecular species herein, P_3 ($Al_4N_4H_8$). This species is the largest AlN molecule of the pathway and forms a cube-like structure $\sim$325 kcal mol^{-1} below $AlNH_2$. As the energy of the $Al_4N_4H_8$ is nearly triple the total energy of $Al_2N_2H_4$ further suggesting the stability of $Al_4N_4H_8$ such that it may not back-dissociate allowing some radiative association to take place to produce observable amounts of this material. Additionally, if an H_2 were to dissociate from $Al_2N_2H_4$ similar to the transition from $HAlNH_3$ and $AlNH_2$, the resulting energy of $Al_2N_2H_2$ would sit $\sim$ 90 kcal mol^{-1} higher in energy than $Al_2N_2H_4$, as shown in the upper-right of Fig. 6.1. Thus, the energetically favorable last step in this reaction is the dimerization of $Al_2N_2H_4$into $Al_4N_4H_8$.

Table 6.1: Rotational Constants (in MHz) and for $AlNH_2$, $HAlNH_3$, and $Al_2N_2H_4$ at the F12-TcCR+TZ level of theory following the same order as the vibrational frequencies. Dipole moments (in D) for $AlNH_2$ and $HAlNH_3$ are also provided. Previous theoretical data in parentheses from Ref. 4

Const.	$AlNH_2$	$HAlNH_3$	$Al_2N_2H_4$	$Al_4N_4H_8$
A_e	372521.1 (371964)	94963.1	8961.0	1446.4
B_e	14208.0 (14059)	9073.1	4997.1	1446.4
C_e	13686.0 (13547)	8658.6	3208.1	1438.9
A_0	371856.6 (371383)	94305.0	8880.3	1438.8
B_0	14180.2 (14030)	8815.0	4994.7	1438.5
C_0	13626.4 (13487)	8419.8	3195.8	1431.6
A_1	368308.0	94179.4	8874.6	1438.2
B_1	14154.6	8823.1	4986.7	1437.7
C_1	13600.9	8426.8	3191.8	1430.9
A_2	365483.1	93975.8	8874.5	1438.1
B_2	14161.6	8837.6	4986.7	1437.8
C_2	13600.6	8440.2	3191.8	1430.9
A_3	377425.8	93837.6	8880.3	1438.6
B_3	14204.8	8831.5	4989.4	1438.2
C_3	13615.8	8435.2	3193.6	1431.2
A_4	371671.4	93994.9	8880.1	1438.6
B_4	14068.5	8838.5	4989.6	1438.2
C_4	13524.1	8426.3	3193.7	1431.2
A_5	386936.5	93750.3	8852.5	1439.7
B_5	14283.0	8823.0	5021.8	1439.3
C_5	13655.8	8440.1	3198.3	1431.8
A_6	359985.7	92854.3	8897.5	1438.5
B_6	14152.6	8830.6	4981.3	1438.1
C_6	13642.0	8425.4	3188.6	1431.9
A_7		94234.3	8871.5	1438.9

Continued on next page

Table 6.1 – continued from previous page

Const.	$AlNH_2$	$HAlNH_3$	$Al_2N_2H_4$	$Al_4N_4H_8$
B_7		8735.9	4986.0	1438.5
C_7		8348.5	3194.5	1431.8
A_8		94794.3	8860.7	1438.7
B_8		8724.7	5018.3	1438.3
C_8		8317.1	3194.5	1431.2
A_9		98803.7	8858.8	1437.9
B_9		8746.3	4996.3	1437.5
C_9		8364.5	3190.8	1430.9
A_{10}		91463.8	8868.8	1437.9
B_{10}		8728.8	4987.5	1437.5
C_{10}		8320.0	3188.2	1430.8
A_{11}		94404.6	8906.1	1438.4
B_{11}		8624.1	4992.3	1438.0
C_{11}		8243.4	3193.7	1431.2
A_{12}		94050.4	8857.7	1438.5
B_{12}		8720.2	4992.0	1438.1
C_{12}		8372.2	3197.2	1431.4
A_{13}			8876.9	1439.3
B_{13}			4997.1	1438.9
c_{13}			3194.4	1430.5
A_{U4}			8858.7	1438.4
B_{14}			4992.7	1437.9
C_{14}			3197.4	1431.3
A_{15}			8876.7	1441.8
B_{15}			5006.9	1439.3
C_{15}			3198.0	1430.9
A_{16}			8890.9	1435.1
B_{16}			4984.3	1436.1

Continued on next page

Table 6.1 – continued from previous page

Const.	$AlNH_2$	$HAlNH_3$	$Al_2N_2H_4$	$Al_4N_4H_8$
C_{16}			3194.0	1430.7
A_{17}			8847.7	1438.6
B_{17}			4994.9	1438.2
C_{17}			3197.6	1431.3
A_{18}			8849.7	1438.6
B_{18}			4996.3	1438.2
C_{18}			3201.5	1431.3
μ	1.21 (1.21)	5.04	3201.5	1431.3

6.3.1 Rovibrational Spectroscopic Analysis

In order to confirm the validity of the formation pathway, these molecules must be observed in progression. As such, the computed rovibrational spectroscopic constants for the minima of Fig. 6.1 ($HAlNH_3$, $AlNH_2$, $Al_2N_2H_4$, and $Al_4N_4H_8$) are reported herein and will serve as reference data for further laboratory analysis and potential astrophysical detection. To that end, the rotational spectroscopic constants are reported in Table 6.1, the quartic and sextic distortion constants from the A- and S-reduced Watson Hamiltonian are reported in Tables 6.3 & 6.4, and the fundamental vibrational frequencies are reported in Tables $6.2 - 6.7$. Of the four molecular species further investigated herein, $AlNH_2$ is the only molecule with previous theoretical[4] rovibrational and experimental[267] Ar matrix vibrational data for comparison. Ar matrices are known to redshift the observed vibrational frequencies of a given species from their gas phase value by as much as $\Delta\nu = 9 - 20$ cm^{-1}.[226] However, based on the prior benchmarking studies,[42,263,268] the present F12-TcCR+TZ level of theory is shown to predict rovibrational spectroscopic data for molecules containing the Al−N moiety that reasonably correct the redshifted vibrational frequencies typically seen in

Table 6.2: Harmonic and anharmonic vibrational frequencies (cm^{-1}), f IR intensities (km mol^{-1}) with absorption cross sections in parentheses (10^{-25} cm^2), λ wavelength (μm), and μ dipole moment (D) for C_s $HAlNH_3$.

Mode	Symm.	Desc.	Harm.	Anharm.	f	λ
ν_1	a'	S stretch (NH_2)	3604.4	3426.3	28 (3)	2.92
ν_2	a''	AS stretch (NH_2)	3580.3	3401.0	17 (2)	2.94
ν_3	a'	S stretch (NH_3)	3460.2	3313.9	3 (0.4)	3.02
ν_4	a''	Wag (HNH_2)	1661.2	1641.6	13 (2)	6.09
ν_5	a'	S $\angle$(NH_2)	1660.8	1609.6	20 (4)	6.21
ν_6	a'	AlH stretch	1620.4	1557.3	654 (100)	6.42
ν_7	a'	OPB (NH_3)	1208.8	1149.9	135 (40)	8.70
ν_8	a'	S $\angle$(HAlNH)	773.3	734.2	75 (50)	13.62
ν_9	a''	Wag ($AlNH_3$)	441.2	430.5	1 (1)	23.23
ν_{10}	a'	AS $\angle$(HAlNH)	430.8	414.0	4 (6)	24.15
ν_{11}	a'	AlN stretch	288.5	266.8	22 (0)	37.48
ν_{12}	a''	τ	161.6	131.1	1 (0)	76.28
μ	5.04					
ZPT				9277.7		

Table 6.3: Quartic and sextic distortion constants in the Watson A-reduced Hamiltonian for $AlNH_2$, $HAlNH_3$, and $Al_2N_2H_4$ at the F12-TcCR+TZ level of theory and $Al_4N_4H_8$ at the F12-DZ level of theory.

Const.	$AlNH_2$	$HAlNH_3$	$Al_2N_2H_4$	$Al_4N_4H_8$
Δ_J	20.676 (kHz)	35.284 (kHz)	1.161 (kHz)	52.101 (Hz)
Δ_K	42.430 (MHz)	987.824 (kHz)	5.876 (kHz)	−12.928 (Hz)
Δ_{JK}	1.917 (MHz)	50.531 (kHz)	−1.232 (kHz)	17.538 (Hz)
δ_J	799.281 (Hz)	1.692 (kHz)	432.213 (Hz)	2.305 (Hz)
δ_K	1.058 (MHz)	−241.295 (kHz)	1.534 (kHz)	−22.568 (Hz)
Φ_J	−44.049 (mHz)	−220.065 (mHz)	781.282 (μHz)	2.036 (μHz)
Φ_K	417.398 (kHz)	−15.763 (Hz)	20.620 (mHz)	288.623 (μHz)
Φ_{JK}	458.720 (Hz)	854.246 (mHz)	−2.178 (mHz)	125.771 (μHz)
Φ_{KJ}	14.427 (kHz)	−10.371 (Hz)	−9.787 (mHz)	−412.484 (μHz)
ϕ_j	20.437 (mHz)	−9.352 (mHz)	387.504 (μHz)	0.717 (μHz)
ϕ_{jk}	233.663 (Hz)	2.573 (Hz)	−1.328 (μHz)	−5.424 (μHz)
ϕ_k	116.515 (kHz)	−7.827 (Hz)	10.996 (mHz)	18.430 (μHz)

Ar matrix data. That being said, the present spectral data presented herein should be considered accurate and reliable to serve as reference data for further laboratory analysis and potential astrophysical detection.

6.3.1.1 $HAlNH_3$

In the warm, inner portion of a protoplanetary disk, $HAlNH_3$ may be a more likely species for detection, given the energy needed to overcome the first transition state barrier. The $HAlNH_3$ molecule's fundamental vibrational frequencies, shown

Table 6.4: Quartic and sextic distortion constants in the Watson S-reduced Hamiltonian for $AlNH_2$, $HAlNH_3$, and $Al_2N_2H_4$ at the F12-TcCR+TZ level of theory and $Al_4N_4H_8$ at the F12-DZ level of theory. Previous theoretical data in brackets from Ref. 4

Const.	$AlNH_2$	$HAlNH_3$	$Al_2N_2H_4$	$Al_4N_4H_8$
D_J	20.291 (kHz)	35.575 (kHz)	1.019 (kHz)	63.384 (Hz)
D_{JK}	1.919 (MHz) [1.872]	48.788 (kHz)	−384.751 (Hz)	−50.161 (Hz)
D_K	42.428 (MHz) [44.239]	989.276 (kHz)	5.170 (kHz)	43.488 (Hz)
d_1	−799.281 (Hz)	−1.692 (kHz)	−432.213 (Hz)	−2.305 (Hz)
d_2	−192.468 (Hz)	145.225 (Hz)	−70.601 (Hz)	5.642 (Hz)
H_J	−129.406 (mHz)	−218.587 (mHz)	596.596 (μHz)	−1.575 (μHz)
H_{JK}	327.615 (Hz)	−160.733 (mHz)	−3.804 (mHz)	−183.408 (μHz)
H_{KJ}	14.865 (kHz)	−7.009 (Hz)	−1.596 (mHz)	672.266 (μHz)
H_K	417.091 (kHz)	−18.111 (Hz)	14.241 (mHz)	−483.339 (μHz)
h_1	14.450 (mHz)	−9.503 (mHz)	356.043 (μHz)	−19.959 (μHz)
h_2	42.679 (mHz)	−738.685 (μHz)	92.343 (μHz)	1.805 (μHz)
h_3	5.987 (mHz)	151.384 (μHz)	31.461 (μHz)	20.676 (μHz)

in Table 6.2, contains intense vibrational transitions, with the ν_6 Al−H stretch being the most intense at 654 km mol^{-1}. This is substantially more intense than the antisymmetric (AS) stretches of H_2O at 70 km mol^{-1} and CO_2 at ∼475 km mol^{-1}, which are known to be intense vibrational transitions. Hence, even if this molecule is transient, it may produce detectable signals. Additionally, the ν_7 NH_3 OPB and ν_8 ∠HAlNH bend are also more intense than the AS stretch in water with intensities of 135 and 75 km mol^{-1}, respectively. Additionally, ν_8 at 734.2 cm^{-1} falls in a wavelength range within the 13 μm dust grain feature that the Al−O stretching motion to which Al_2O_3 is also attributed.[186–188] In terms of rotational observation, the rotational constants and dipole moment for $HAlNH_3$ are presented in Table 6.1. $HAlNH_3$ possesses a substantial permanent dipole moment of 5.04 D that is on par with previously studied AlN species[259] such as $AlNH_6$ at 5.40 D. A permanent dipole moment of 5.04 D is notably larger than known species like H_2O at 1.84 D or even previously detected AlOH at 1.11 D.[227,228]

$HAlNH_3$ also exhibits three relatively large absorption cross-sections with the largest being the ν_6 AlH stretching mode at 100 $\times 10^{-25}$ cm^2 followed by the ν_8 ∠HAlNH bend at 50 $\times 10^{-25}$ cm^2. Previous experimental absorption cross-sections

Table 6.5: Vibrational frequencies (cm^{-1}), IR intensities (km mol^{-1}) with absorption cross sections in parentheses (10^{-25} cm^2), wavelength (μ), and dipole moment (D) for C_{2v} $AlNH_2$

Mode	Symm.	Desc.	Harm.	Anharm.	f	λ	Expt.[a] ($\Delta\nu$)	Prev. Theory[b]
ν_1	b_2	AS (NH)	3624.8	3441.7	12 (1)	2.91	3495.1 (−53.4)	3433.8
ν_2	a_1	S (NH)	3529.5	3364.0	1 (0.1)	2.97	–	3356.5
ν_3	a_1	S $\angle(NH_2)$	1557.9	1526.0	43 (8)	6.55	1520.3 (5.7)	1525.7
ν_4	a_1	AlN	753.9	739.5	107 (50)	13.52	726.5 (13.0)	734.9
ν_5	b_2	AS $\angle(NH_2)$	460.3	450.0	1 (1)	22.22	–	444.3
ν_6	b_1	OPB	425.3	423.1	163 (200)	23.64	406.5 (16.6)	398.2
μ				1.21				1.21
ZPT				5104.6				5077.4

[a] Ar matrix frequencies from Ref. 267
[b] Previous theoretical data from Ref. 4

for IR transitions in water have been found to range between 1.6 $\times 10^{-25}$ cm^2 and 8.4 $\times 10^{-25}$ cm^2.[269] As absorption cross-sections are a function of the wavelength of the transition, there cannot be a direct comparison for accuracy. However, the water cross-sections are on a similar order of magnitude suggesting semi-quantitative agreement, and, therefore, the presently computed absorption cross-sections for the AlN species investigated herein are accurate and reliable probabilities of IR absorption. Hence, considering the intense vibrational transitions, large absorption cross-sections, and large permanent dipole moment, $HAlNH_3$ should be considered a viable candidate for radioastronomical and IR detection in warmer inner protoplanetary disks as it may persist long enough for appreciable observation and could be a marker for this species participation in the nucleation of carbonaceous dust grains.

6.3.1.2 $AlNH_2$

As mentioned previously, $AlNH_2$ is the only species with previous rovibrational data for comparison[4,267] The rotational and vibrational data for $AlNH_2$ are shown in Tables 6.1 & 6.5, respectively. The previous theoretical data are computed at the CCSD(T)/aug-cc-pV(Q+d)Z level of theory which is a lower level compared to the F12-TcCR+TZ level of theory utilized herein. The difference between the present and previously computed equilibrium and ground-state rotational constants

is small with less than a ∼1% difference. However, as the present work is conducted at a higher level of theory, any difference between the present and previous data should be considered an improvement over the CCSD(T)/aug-cc-pV(Q+d)Z level of theory. In terms of the dipole moment, $AlNH_2$ contains a small dipole moment of 1.21 D, which is corroborated by the previous theoretical work.[4] While not as large as the 5.04 D dipole moment from $HAlNH_3$, $AlNH_2$'s dipole moment is larger than the aforementioned and astronomically-observed AlOH molecule's dipole moment of 1.11 D.[227,228]

Some of the vibrational frequencies between the present and previous are fairly similar with others varying to slightly larger degrees. The closest is the ν_3 S $\angle NH_2$ bend at 1526.0 cm^{-1}, which is 0.3 cm^{-1} higher than the previously computed value. However, again, any difference between the present and previous theoretical vibrational frequencies should indicate and increase in accuracy from the present F12-TcCR+TZ hybrid level of theory. Toward the experimental data, there are only four Ar matrix vibrational frequencies for comparison in Table 6.5. While three of these four frequencies are sufficiently corrected by the F12-TcCR+TZ level of theory, as suggested by the previous benchmarking study,[263] the AS N−H stretch is predicted to be further redshifted from experiment by 53.4 cm^{-1}. However, the previous Ar matrix study used harmonic frequencies calculated with the B3LYP density functional and the relatively small 6-311G(d) basis set to guide the frequency assignment of the Ar matrix data to the $AlNH_2$ species. However, the previous theoretical vibrational frequency at 3433.8 cm^{-1} is in a similar range to the presently computed frequency at 3441.7 cm^{-1}. Additionally, this previously assigned AS N−H mode exhibits a relatively low transition intensity. Therefore, the Ar matrix frequency for the AS N−*H* stretch, at 3495.1cm^{-1}, may have been a misattribution. The excellent prediction of rovibrational spectroscopic constants in the previous benchmarking study[263] for the

F12-TcCR+TZ level of theory further suggests this assessment. Thus, the present computed anharmonic vibrational frequencies should be accurate reference data in further laboratory analysis of the $AlNH_2$ species as well as potential astrophysical detection.

Additionally, $AlNH_2$ exhibits two intense vibrational transitions when compared to the aforementioned water transition. The ν_6 OPB is the most intense of the two at 163 km mol^{-1} followed closely by the ν_4 AlN stretch at 107 km mol^{-1}. Of these two intense transitions, the AlN stretch at 739.5 cm^{-1} also falls within the aforementioned 13 μm dust feature[186,189] and carries the second highest absorption cross-section for the molecule at 50 $\times 10^{-25}$ cm^2. While the ν_6 OPB at 423.1 cm^{-1} has a substantially larger absorption cross-section, 200 $\times 10^{-25}$ cm^2, the IR resolving power of the instruments onboard *JWST* is diminished below $\sim$400 cm^{-1}. Therefore, the ν_6 OPB may not be suitable for observation compared to the less intense ν_4 AlN stretch.

In terms of viability, the production of $AlNH_2$ follows a relatively high energy barrier, which may be more efficiently overcome in the warmer ambient temperatures surrounding stellar outflows of advanced AGB stars, as discussed previously. However, while $AlNH_2$ is produced, the present pathway suggests its dimerization and the subsequent barrierless formation of larger AlN species. If $AlNH_2$ production in these AGB outflows is sufficiently efficient, larger AlN species may exist at higher population densities than $AlNH_2$, making them more appreciable for observation. Regardless, the rovibrational spectral data for $AlNH_2$ is presented for completeness and will serve as reference data for further laboratory and computational analysis, if not for astrophysical detection.

Table 6.6: Vibrational frequencies (cm^{-1}), IR intensities (km mol^{-1}) with absorption cross sections in parentheses (10^{-25} cm^2), wavelength (μ), and dipole moment (D) for D_{2h} $Al_2N_2H_4$

Mode	Symm.	Desc.	Harm.	Anharm.	f	λ
ν_1	b_{2u}	AS (NH)	3695.7	3537.6	38 (4)	2.83
ν_2	a_g	S (NH)	3694.6	3528.7	0 (0)	2.83
ν_3	a_g	S (AlH)	1991.1	1925.6	0 (0)	5.19
ν_4	b_{1u}	AS (AlH)	1983.2	1926.2	425 (60)	5.19
ν_5	b_{1u}	S ∠(AlNH)	873.5	845.0	232 (100)	11.83
ν_6	b_{2u}	AS (AlN)	862.6	939.9	0 (0)	11.59
ν_7	a_g	AS ∠(AlNH)	845.1	808.3	399 (200)	12.37
ν_8	b_{3g}	Ring Breathing	838.5	839.5	0 (0)	11.91
ν_9	b_{1u}	S (AlN)	745.5	726.3	127 (80)	13.77
ν_{10}	b_{3g}	AS ∠(NAl_2)	681.5	642.0	0 (0)	15.58
ν_{11}	b_{2u}	S ∠(NAlH)	583.7	662.5	56 (40)	15.09
ν_{12}	b_{3u}	S Wag (NH)	574.6	541.9	144 (200)	18.45
ν_{13}	b_{3g}	AS ∠(NAlH)	557.1	582.9	0 (0)	17.16
ν_{14}	b_{3u}	S Wag (AlH)	502.7	548.3	226 (300)	18.24
ν_{15}	b_{2g}	AS Wag (AlH)	495.5	463.2	0 (0)	21.59
ν_{16}	a_g	S ∠(NAl_2)	483.8	459.0	0 (0)	21.79
ν_{17}	b_{1g}	AS Wag (NH)	392.0	374.4	0 (0)	26.71
ν_{18}	b_{3u}	OPB	205.1	322.0	2 (0)	31.06
	μ	0.00				
ZPT				9958.4		

6.3.1.3 $Al_2N_2H_4$

Upon the successful hydrogen migrations in TS_2 and TS_3 as shown in Fig. 6.1, the cyclic D_{2h} $Al_2N_2H_4$ is formed and, due to its D_{2h} symmetry, exhibits no permanent dipole moment. The lack of a permanent dipole moment leaves it entirely undetectable *via* rotational spectroscopy. Consequently, the anharmonic vibrational frequencies computed herein are crucial for assisting laboratory studies and potential space-based IR observations of $Al_2N_2H_4$, and the computed, anharmonic fundamental vibrational frequencies for $Al_2N_2H_4$ are shown in Table 6.6. Much like $HAlNH_3$, $Al_2N_2H_4$ exhibits multiple exceedingly intense vibrational transition intensities. The ν_4 AS Al−H stretch at 1926.2 cm^{-1} is the most intense transition at 425 km mol^{-1} followed closely by the ν_7 AS ∠AlNH bending mode at 808.3 cm^{-1} with a transition intensity at 399 km mol^{-1}. While these are not as intense as the AS stretch in CO_2, they are markedly more intense than that of water.

Additionally, $Al_2N_2H_4$ exhibits six vibrational frequencies with large absorp-

Table 6.7: Vibrational frequencies (cm^{-1}), IR intensities (km mol^{-1}) with absorption cross sections in parentheses (10^{-25} cm^2), wavelength (μ), and dipole moment (D) for T_d $Al_4N_4H_8$

Mode	Symm.	Desc.	Harm.	Anharm.	f	λ
ν_1	t_2	AS (NH)	3592.5	3419.4	24 (3)	2.92
ν_2	a_1	S (NH)	3590.1	3415.9	0 (0)	2.93
ν_3	a_1	S (AlH)	1976.2	1911.8	0 (0)	5.23
ν_4	t_2	AS (AlH)	1964.8	1885.6	345 (50)	5.30
ν_5	t_2	S Wag (NH)	837.9	748.8	428 (200)	13.35
ν_6	e	AS Wag (NH)	826.7	779.3	0 (0)	12.83
ν_7	t_1	AS ∠(HNAL)	764.8	756.9	0 (0)	13.21
ν_8	t_2	S (AlN) + AS (NN)	748.8	684.3	354 (200)	14.61
ν_9	a_1	S (AlN)	738.2	692.5	0 (0)	14.44
ν_{10}	t_2	AS (AlN)	641.4	635.0	93 (60)	15.75
ν_{11}	e	AS (AlN) + AS (NN)	608.0	471.3	0 (0)	21.22
ν_{12}	t_1	AS (AlN)	541.1	481.4	0 (0)	20.77
ν_{13}	a_1	S (Al Breathing)	521.4	484.6	0 (0)	20.64
ν_{14}	t_2	AS Wag (AlH)	507.0	447.3	21 (30)	22.36
ν_{15}	e	AS (AlN)	468.1	278.4	0 (0)	35.92
ν_{16}	t_1	AS ∠(NAlN)	462.3	341.8	0 (0)	29.26
ν_{17}	t_2	S ∠(NAlN)	344.5	245.8	1 (0)	40.68
ν_{18}	e	τ	300.4	301.0	0 (0)	33.22
	μ	0.00				
ZPT				20466.0		

tion cross-sections. The largest of which is associated with ν_{14} at 300 $\times 10^{-25}$ cm^2, but, like $AlNH_2$, the detection of this frequency may be hindered by the loss in resolving power as mentioned previously. However, ν_5, ν_7, and ν_9 all exhibit intense vibrational transitions and relatively large absorption cross-sections that are also attributed to wavelengths associated with dust grain formation between $11-13$ μm. Thus, $Al_2N_2H_4$ likely exhibit a sufficient amount of observable data. Therefore, $Al_2N_2H_4$ should be considered a suitable candidate for potential astrophysical observation in the IR of an undetected dust grain nucleation species that may contribute to the formation of carbonaceous dust in the envelope of advanced AGB stars if not warmer, inner protoplanetary disks.

6.3.1.4 $Al_4N_4H_8$

Finally, upon the successful dimerization of $Al_2N_2H_4$, the stable, cubic $Al_4N_4H_8$ species is formed, and, much like $Al_2N_2H_4$, exhibits no permanent dipole moment given its higher-order T_d symmetry. Again, this makes the anharmonic vibrational

frequencies computed in this work, shown in Table 6.7, that much more crucial in order to assist potential astrophysical characterization of AlN species in the ISM or CSM. Another consequence associated with the higher-order symmetry of $Al_4N_4H_8$, similar to $Al_2N_2H_4$, is the reduced number of IR-active fundamental vibrational modes. However, what few IR-active modes there are exhibit intense vibrational transitions. For example, the ν_5 N−H wagging mode at 748.8 cm^{-1} exhibits a vibrational transition intensity of 428 km mol^{-1} followed closely by ν_8, a coupled S Al−N and AS N−N stretching mode, and ν_4, S Al−H stretching, at 354 and 345 km mol^{-1}, respectively. Again, compared to water, these vibrational transitions are exceedingly intense and should be considered sufficient for potential astrophysical detection. Furthermore, ν_5 is an intense transition within the 13 μm region much like the other AlN species investigated here. Additionally, both ν_5 and ν_8 have large absorption cross-sections, 200 $\times 10^{-25}$ cm^2, indicating that $Al_4N_4H_8$ is highly likely to absorb IR radiation significant enough to produce these intense transitions in circumstellar environments such as AGB stellar outflows.

6.4 Conclusions

Aluminum nitride clusters exhibit intense vibrational transitions and large absorption cross-sections in the IR regime, specifically in the 13 μm dust feature as well as the correlated 11, 20, and 28 μm features all associated with dust emission. As such, AlN clusters may contribute to these features most often associated with AlO clusters. Additionally, the present formation pathway suggests the formation of AlN species in both protoplanetary disks as well as stellar ejecta of advanced AGB stars. Within protoplanetary disks, for appreciable population densities of larger AlN species, the formation pathway must initiate in the inner circumstellar envelope to overcome the $\sim$ 8.6 kcal mol^{-1} transition barrier. However, a more efficient

production of $AlNH_2$, and subsequently $Al_2N_2H_4$ and $Al_4N_4H_8$, can be achieved in the stellar outflows of AGB stars, as they contain both ample material and higher ambient temperatures compared to protoplanetary disks. Hence, the present computational study provides a potential formation pathway of AlN molecular clusters as theorized in the study of the Murchison CM2 silicon-carbide meteorite[43] and consequently, a more robust understanding of the dust grain nucleating processes in and around circumstellar envelopes.

While the rovibrational spectral data of the first intermediate and three products along the present formation pathway have been computed presently, the first product, $AlNH_2$, serves as the key species in the pathway; its production enables the subsequent barrierless formation of $Al_2N_2H_4$ and $Al_4N_4H_8$. Not only does $AlNH_2$ contain intense vibrational transitions and relatively large absorption cross-sections, $AlNH_2$ is the last species along the proposed pathway that contains a dipole moment that is larger than the previously observed, isoelectronic AlOH species. Conversely, $Al_2N_2H_4$ and $Al_4N_4H_8$ exhibit vibrational transitions that are significantly more intense than those of $AlNH_2$ with absorption cross-sections that are comparable to or even larger than those of $AlNH_2$. Although $HAlNH_3$ contains the most intense vibrational transition at 654 km mol^{-1} around 6.42 μm and the strongest dipole moment of 5.04 D, it may not persist on timescales long enough for appreciable detection. Nevertheless, the rovibrational spectral data computed herein for each molecule will be instrumental in aiding the potential laboratory observation or astrophysical detection of species indicative of larger AlN species production through both ALMA and JWST.

Each of the AlN species investigated herein exhibits observable anharmonic vibrational frequencies in spectral ranges that are associated with dust grains as well as aluminum oxide, namely the 13 μm feature. This further suggests that AlN

species may also contribute to the composition of dust grains and could potentially assist in elucidating the still relatively unknown molecular pathways to the formation of larger rocky bodies in circumstellar regions of the cosmos. Thus, the presently computed rovibrational spectral data will serve as novel reference data for further laboratory, theoretical, and observational studies to assist in the detection of understudied alternative Al-containing species that may be present in the CSM and ISM.

CHAPTER 7

CONCLUSION

The work herein showcases that QFFs, when applied to highly accurate electronic structure methods, yield rovibrational spectral data that serves as reference or complementary data for further laboratory study and astrophysical or atmospheric detection of molecules. In Ch. 2, the explicitly correlated F12-TZ level of theory was compared to the long-standing CcCR level of theory for predicting rovibrational spectral constants of sulfur-bearing molecules. The results show that F12-TZ achieves significantly lower computational cost than CcCR, with a slight decrease in accuracy for rotational constants but improved accuracy for fundamental vibrational frequencies compared to gas-phase data. Ch. 3 highlighted improvements to the F12-TZ level of theory by incorporating core electron correlation and scalar relativistic corrections, resulting in the F12-TcCR level of theory. This enhanced approach was used to predict novel rovibrational spectral constants for compounds containing the elusive fluorine atom in the ISM. In Ch. 4, a novel formation pathway and rovibrational spectral data for aluminum nitride compounds, starting from AlH_3 and NH_3, are predicted at the F12-TZ level of theory. These predictions are compared to available Ar matrix data to investigate a potential dust grain nucleating species in circumstellar environments contributing to the 13 μm dust feature. Ch. 5 presents a benchmark study of 10 different levels of theory on several aluminum-bearing molecules, identifying the hybrid F12-TcCR+TZ level as the most accurate for predicting rovibrational spectral data of aluminum molecules with a bond order

greater than one. Finally, Ch. 6 explores another aluminum nitride formation pathway, starting from AlH and NH_3. The corresponding rovibrational spectral data are predicted at the F12-TcCR+TZ level of theory when applicable and compared to available Ar matrix data, proposing an additional set of aluminum nitrides that may contribute to the composition of dust grains in circumstellar environments.

To better understand the chemical composition of Earth's atmosphere, the ISM, and the CSM, quantum chemical techniques must be employed to bridge the gap between laboratory spectroscopic capabilities and current observational telescopes. The advancements presented herein provide both novel and complementary rovibrational spectral data derived from highly accurate computational methods that have been benchmarked and refined over time to closely align with experimental data. In this way, computational quantum chemical techniques remain relevant and robust independent astrochemical tools, aiding in the deeper understanding of the physical world through chemical means.

BIBLIOGRAPHY

BIBLIOGRAPHY

[1] Song, X.; Fagiani, M. R.; Gewinner, S.; Schöllkopf, W.; Asmis, K. R.; Bischoff, F. A.; Berger, F.; Sauer, J. *J. Chem. Phys.* **2016**, *144*, 244305.

[2] Chertihin, G. V.; Andrews, L. *JPhCh* **1993**, *97*, 10295–10300.

[3] Himmel, H.-J.; Downs, A. J.; Greene, T. M. *ChCom* **2000**, 871–872.

[4] Trabelsi, T.; Esposito, V. J.; Francisco, J. S. *Acc. Chem. Res.* **2023**, *56*, 3045–3052.

[5] Beckers, H.; Esser, S.; Metzroth, T.; Behnke, M.; Willner, H.; Gauss, J.; Hahn, J. *Chem. Eur. J.* **2006**, *12*, 832–844.

[6] T. Dunham, J. *Publ. Astron. Soc. Pac.* **1937**, *49*, 26–28.

[7] Swings, P.; Rosenfield, L. *Astrophys. J.* **1937**, *86*, 483–486.

[8] McKellar, A. *Publ. Astron. Soc. Pac.* **1940**, *52*, 187–192.

[9] Klemperer, W. F. *Proc. Natl. Acad. Sci. U.S.A.* **2006**, *103*, 12232–12234.

[10] Snyder, L. E. *Proc. Natl. Acad. Sci. USA* **2006**, *103*, 12243–12248.

[11] Weinreb, S.; Barrett, A. H.; Meeks, M. L.; Henry, J. C. *Nature* **1963**, *200*, 829–831.

[12] Cheung, A. C.; Rank, D. M.; Townes, C. H.; Thornton, D. D.; Welch, W. J. *Phys. Rev. Lett.* **1968**, *21*, 1701–1705.

[13] Cheung, A. C.; Rank, D. M.; Townes, C. H.; Thornton, D. D.; Welch, W. J. *Nature* **1969**, *221*, 626.

[14] Tielens, A. G. G. M. *Rev. Mod. Phys.* **2013**, *85*, 1021–1081.

[15] Fortenberry, R. C. *J. Phys. Chem. Lett.* **2024**, *15*, 6528–6537.

[16] Barone, V.; Biczysko, M.; Puzzarini, C. *Acc. Chem. Res.* **2015**, *48*, 1413–1422.

[17] Belloche, A.; Garrod, R. T.; Müller, H. S. P.; Menten, K. M. *Science* **2014**, *345*, 1584–1587.

[18] Puzzarini, C.; Barone, V. *Phys. Chem. Chem. Phys.* **2020**, *22*, 6507–6523.

[19] McGuire, B. A. *Astrophys. J. Suppl. Ser.* **2018**, *239*, 17.

[20] McGuire, B. A. *Astrophys. J. Suppl. Ser.* **2021**, *259*, 51.

[21] Jakobsen, P. et al. *A&A* **2022**, *661*, A80.

[22] Labiano, A. et al. *A&A* **2021**, *656*, A57.

[23] Nickerson, S.; Rangwala, N.; Colgan, S. W. J.; DeWitt, C.; Huang, X.; Acharyya, K.; Drozdovskaya, M.; Fortenberry, R. C.; Herbst, E.; Lee, T. J. *Astrophys. J.* **2021**, *907*, 15.

[24] van Sheltinga, J. T.; Marcandalli, G.; McClure, M. K.; Hogerheijde, M. R.; Linnartz, H. *Astron. Astrophys.* **2021**, *651*, A95.

[25] Fortenberry, R. C.; Lee, T. J. *Vibrational Dynamics of Molecules*; World Scientific, 2022; Chapter 7, pp 235–295.

[26] Montzka, S. A. et al. *Nature* **2021**, *590*, 428–447.

[27] Plane, J. M. C. *Int. Rev. Phys. Chem.* **1991**, *10*, 55–106.

[28] Plane, J. M. C.; Feng, W.; Dawkins, E. C. M. *Chem. Rev.* **2015**, *115*, 4497–4541.

[29] Kramer, H. J. *CALIPSO (Cloud-Aerosol Lidar and Infrared Pathfinder Satellite Observations)*; 2023.

[30] Parkinson, C. L. *Earth Space Sci.* **2022**, *9*, e2022EA002481.

[31] Huang, X.; Schwenke, D. W.; Lee, T. J. *Acc. Chem. Res.* **2021**, *54*, 1311–1321.

[32] Turner, B. E. *Astrophys. J.* **1974**, *193*, L83–L84.

[33] Green, S.; Montgomery, J. A.; Thaddeus, P. *Astrophys. J.* **1974**, *193*, L89–L91.

[34] Tucker, K. D.; Kutner, M. L.; Thaddeus, P. *Astrophys. J.* **1974**, *193*, L115–L119.

[35] Guélin, M.; Green, S.; Thaddeus, P. *Astrophys. J.* **1978**, *224*, L27–L30.

[36] Wilson, S.; Green, S. *Astrophys. J.* **1977**, *212*, L87–L90.

[37] Fortenberry, R. C. *J. Phys. Chem. A* **2024**, *128*, 1555–1565.

[38] Puzzarini, C. *Int. J. Quantum Chem.* **2017**, *117*, 129–138.

[39] Fortenberry, R. C. *IJQC* **2017**, *117*, 81–91.

[40] Gardner, M. B.; Westbrook, B. R.; Fortenberry, R. C.; Lee, T. J. *AcSpA* **2021**, *248*, 119184.

[41] Watrous, A. G.; Westbrook, B. R.; Fortenberry, R. C. *JPCA* **2021**, *125*, 10532–10540.

[42] Watrous, A. G.; Westbrook, B. R.; Fortenberry, R. C. *PCCP* **2023**, (submitted).

[43] Zinner, E.; Amari, S.; Anders, E.; Lewis, R. *Nature* **1991**, *349*, 51–54.

[44] Szabo, A.; Ostlund, N. S. *Modern Quantum Chemistry: Introduction to Advanced Electronic Structure Theory*; Dover: Mineola, NY, 1996.

[45] Pilar, F. L. *Elementary Quantum Chemistry*, 2nd ed.; Dover: Mineola, NY, 1990.

[46] Levine, I. A. *Quantum Chemistry*; Pearson: New York, 2014.

[47] Hehre, W. J.; Stewart, R. F.; Pople, J. A. *J. Chem. Phys* **1969**, *51*, 2657–2664.

[48] Ditchfield, R.; Hehre, W. J.; Pople, J. A. *J. Chem. Phys.* **1971**, *54*, 724–728.

[49] Dunning, T. H. *J. Chem. Phys.* **1989**, *90*, 1007–1023.

[50] Roothan, C. C. J. *Rev. Mod. Phys.* **1951**, *23*, 69–89.

[51] Møller, C.; Plesset, M. S. *PhRv* **1934**, *46*, 618–622.

[52] Crawford, T. D.; Schaefer III, H. F. *Reviews in Computational Chemistry*; John Wiley and Sons, Inc.: New York, 2000; Vol. 14; Chapter 2, pp 33–136.

[53] Bartlett, R. J. *Ann. Rev. Phys. Chem.* **1981**, *32*, 359–401.

[54] Stanton, J. F.; Gauss, J.; Watts, J. D.; Bartlett, R. J. *J. Chem. Phys.* **1991**, *94*, 4334–4345.

[55] Noga, J.; Bartlett, R. J. *J. Chem. Phys.* **1987**, *86*, 7041–7050.

[56] Helgaker, T.; Ruden, T. A.; Jørgensen, P.; Olsen, J.; Klopper, W. *J. Phys. Org. Chem.* **2004**, *17*, 913–933.

[57] Bartlett, R. J. In *Modern Electronic Structure Theory*; Yarkony, D., Ed.; World Scientific: Singapore, 1995; pp 1047–1131.

[58] Raghavachari, K.; Trucks, G. W.; Pople, J. A.; Head-Gordon, M. *CPL* **1989**, *157*, 479–483.

[59] Shavitt, I.; Bartlett, R. J. *Many-Body Methods in Chemistry and Physics: MBPT and Coupled-Cluster Theory*; Cambridge University Press: Cambridge, UK, 2009.

[60] C++ Programming Tutorial in Chemistry. Accessed: 2023-03-06.

[61] Kutzelnigg, W.; Klopper, W. *J. Chem. Phys.* **1991**, *94*, 1985–2001.

[62] Adler, T. B.; Knizia, G.; Werner, H.-J. *J. Chem. Phys.* **2007**, *127*, 221106.

[63] Ten-no, S. *J. Chem. Phys.* **2004**, 117–129.

[64] Knizia, G.; Adler, T. B.; Werner, H.-J. *J. Chem. Phys.* **2009**, *130*, 054104.

[65] Györffy, W.; Werner, H.-J. *J. Chem. Phys.* **2018**, *148*, 114104.

[66] Fortenberry, R. C.; Lee, T. J. *Ann. Rep. Comput. Chem.* **2019**, *15*, 173–202.

[67] Watson, J. K. G. In *Vibrational Spectra and Structure*; During, J. R., Ed.; Elsevier: Amsterdam, 1977; pp 1–89.

[68] Gaw, J. F.; Willets, A.; Green, W. H.; Handy, N. C. In *Advances in Molecular Vibrations and Collision Dynamics*; Bowman, J. M., Ratner, M. A., Eds.; JAI Press, Inc.: Greenwich, Connecticut, 1991; pp 170–185.

[69] Lee, T. J.; Martin, J. M. L.; Taylor, P. R. *J. Chem. Phys.* **1995**, *102*, 254–261.

[70] Dateo, C. E.; Lee, T. J. *AcSpA* **1997**, *53*, 1065–1077.

[71] Morgan, W. J.; Fortenberry, R. C.; Schaefer III, H. F.; Lee, T. J. *Mol. Phys.* **2019**, *118*, 1.

[72] Westbrook, B. R.; Fortenberry, R. C. *J. Chem. Theory Comput.* **2023**, *19*, 2606–2615.

[73] Allen, W. D.; coworkers 2005; *INTDER* 2005 is a General Program Written by W. D. Allen and Coworkers, which Performs Vibrational Analysis and Higher-Order Non-Linear Transformations.

[74] Franke, P. R.; Stanton, J. F.; Douberly, G. E. *JPCA* **2021**, *125*, 1301–1324.

[75] Papousek, D.; Aliev, M. R. *Molecular Vibration-Rotation Spectra*; Elsevier: Amsterdam, 1982.

[76] Huang, X.; Lee, T. J. *J. Chem. Phys.* **2008**, *129*, 044312.

[77] Huang, X.; Lee, T. J. *J. Chem. Phys.* **2009**, *131*, 104301.

[78] Huang, X.; Taylor, P. R.; Lee, T. J. *JPCA* **2011**, *115*, 5005–5016.

[79] Huang, X.; Fortenberry, R. C.; Wang, Y.; Francisco, J. S.; Crawford, T. D.; Bowman, J. M.; Lee, T. J. *JPCA* **2013**, *117*, 6932–6939.

[80] Fortenberry, R. C.; Huang, X.; Crawford, T. D.; Lee, T. J. *JPCA* **2014**, *118*, 7034–7043.

[81] Inostroza-Pino, N.; Palmer, C. Z.; Lee, T. J.; Fortenberry, R. C. *JMoSp* **2020**, *369*, 111273.

[82] Oppenheimer, M.; Dalgarno, A. *Astrophys. J.* **1974**, 231–236.

[83] Penzias, A. A.; Solomon, P. M.; Wilson, R. W.; Jefferts, K. B. *Astrophys. J.* **1971**, *168*, L53–L58.

[84] Anderson, D. E.; Bergin, E. A.; Maret, S.; Wakelam, V. *Astrophys. J.* **2013**, *779*, 141–156.

[85] Plume, R.; Jaffe, D. T.; II, N. J. E.; Martín-Pintado, J.; Gómez-González, J. *Astrophys. J.* **1997**, *476*, 730–749.

[86] Kama, M.; Shorttle, O.; Jermyn, A. S.; Folsom, C. P.; Furuya, K.; Bergin, E. A.; Walsh, C.; Keller, L. *Astrophys. J.* **2019**, *885*, 114–121.

[87] Woods, P. M.; Occhiogrosso, A.; Viti, S.; Kaňuchová, Z.; Palumbo, M. E.; Price, S. D. *Mon. Not. Royal Astron. Soc.* **2015**, *450*, 1256–1267.

[88] Ruffle, D. P.; Hartquist, T. W.; Caselli, P.; Williams, D. A. *Mon. Not. Royal Astron. Soc.* **1999**, *306*, 691–695.

[89] Shingledecker, C. N.; Lamberts, T.; Laas, J. C.; Vasyunin, A.; Herbst, E.; Kästner, J.; Caselli, P. *Astrophys. J.* **2020**, *888*, 52–66.

[90] Vidal, T. H. G.; Loison, J.-C.; Jaziri, A. Y.; Ruaud, M.; Gratier, P.; Wakelam, V. *Mon. Not. Royal Astron. Soc.* **2017**, *469*, 435–447.

[91] Despois, D. *Earth, Moon, and Planets* **1997**, *79*, 103–124.

[92] Palumbo, M. E.; Geballe, T. R.; Tielens, A. G. G. M. *Astrophys. J.* **1997**, *479*, 839.

[93] Bergman, P.; Parise, B.; Liseau, R.; Larsson, B.; Olofsson, H.; Menten, K. M.; Güsten, R. *Astron. Astrophys.* **2011**, *531*, L8.

[94] Gottlieb, C. A.; Ball, J. *Astrophys. J.* **1973**, *184*, L59–L64.

[95] Matsuura, M. et al. *Mon. Not. Royal Astron. Soc.* **2017**, *469*, 3347–3362.

[96] Valiev, R. R.; Nasibullin, R. T.; Cherepanov, V. N.; Baryshnikov, G. V.; Sundholm, D.; Ågren, H.; Minaev, B. F.; Kurtén, T. *PCCP* **2020**, *22*, 22314–22323.

[97] Zhao, D.; Doney, K. D.; Linnartz, H. *Astrophys. J.l* **2014**, *791*, L28.

[98] Fortenberry, R. C.; Huang, X.; Francisco, J. S.; Crawford, T. D.; Lee, T. J. *J. Chem. Phys.* **2012**, *136*, 234309.

[99] Huang, X.; Fortenberry, R. C.; Lee, T. J. *J. Chem. Phys.* **2013**, *139*, 084313.

[100] Fortenberry, R. C.; Lee, T. J.; Müller, H. S. P. *MolAs* **2015**, *1*, 13–19.

[101] Kitchens, M. J. R.; Fortenberry, R. C. *CP* **2016**, *472*, 119–127.

[102] Bizzocchi, L.; Lattanzi, V.; Laas, J.; Spezzano, S.; Giuliano, B. M.; Prudenzano, D.; Endres, C.; Sipilä, O.; Caselli, P. *Astron. Astrophys.* **2017**, *602*, A34.

[103] Fortenberry, R. C.; Novak, C. M.; Layfield, J. P.; Matito, E.; Lee, T. J. *J. Chem. Theor. Comput.* **2018**, *14*, 2155–2164.

[104] Agbaglo, D.; Lee, T. J.; Thackston, R.; Fortenberry, R. C. *Astrophys. J.* **2019**, *871*, 236.

[105] Agbaglo, D.; Fortenberry, R. C. *IJQC* **2019**, *119*, e25899.

[106] Agbaglo, D.; Fortenberry, R. C. *CPL* **2019**, *734*, 136720.

[107] Werner, H.-J. et al. *WIREs Comput. Mol. Sci.* **2020**, see http://www.molpro.net.

[108] Martin, J. M. L.; Taylor, P. R. *CPL* **1994**, *225*, 473–479.

[109] Westbrook, B. R.; Dreux, K. M.; Tschumper, G. S.; Francisco, J. S.; Fortenberry, R. C. *PCCP* **2018**, *20*, 25967–25973.

[110] Hollman, D. S.; Schaefer, H. F. *J. Chem. Phys.* **2012**, *136*, 084302.

[111] Baraban, J. H.; Changala, P. B.; Stanton, J. F. *J. Mol. Spectrosc.* **2018**, *343*, 92–95.

[112] Petkie, D. T.; Goyette, T. M.; Lucia, F. C. D.; Helminger, P.; Belov, S. P.; Winnewisser, G. *JMoSp* **1998**, *192*, 25–31.

[113] Watts, J. D.; Francisco, J. S. *J. Chem. Phys.* **2006**, *125*, 104301.

[114] Perrin, A.; Flaud, J.-M.; Camy-Peyret, C.; Goldman, A.; Murcray, F. J.; Blatherwick *J. Mol. Spectrosc.* **1990**, *142*, 129–147.

[115] Camy-Peyret, C.; Flaud, J.-M.; Johns, J. W. C.; Noël, M. *JMoSp* **1992**, *155*, 84–104.

[116] Martin, J. M. L.; Lee, T. J. *CPL* **1996**, *258*, 136–143.

[117] Douglas, M.; Kroll, N. *Ann. Phys.* **1974**, *82*, 89–155.

[118] Mills, I. M. In *Molecular Spectroscopy - Modern Research*; Rao, K. N., Mathews, C. W., Eds.; Academic Press: New York, 1972; pp 115–140.

[119] Martin, J. M. L.; Taylor, P. R. *AcSpA* **1997**, *53*, 1039–1050.

[120] Frisch, M. J. et al. Gaussian 16 Revision C.01. 2016; Gaussian Inc. Wallingford CT.

[121] Finney, B.; Fortenberry, R. C.; Francisco, J. S.; Peterson, K. A. *J. Chem. Phys.* **2016**, *145*, 124311.

[122] Yu, Q.; Bowman, J. M.; Fortenberry, R. C.; Mancini, J. S.; Lee, T. J.; Crawford, T. D.; Klemperer, W.; Francisco, J. S. *JPCA* **2015**, *119*, 11623–11631.

[123] Olson, W. B.; Hunt, R. H.; Young, B. W.; Maki, A. G.; Brault, J. W. *JMoSp* **1988**, *127*, 12–34.

[124] Giguére, P. A.; Srinivasan, T. K. K. *J. Raman Spectrosc.* **1974**, *2*, 125–132.

[125] Klee, S.; Winnewisser, M.; Perrin, A.; Flaud, J.-M. *JMoSp* **1999**, *195*, 154–161.

[126] Halonen, L. *J. Chem. Phys.* **1987**, *86*, 3115.

[127] Giguére, P. A. *J. Chem. Phys.* **1950**, *18*, 88.

[128] Dzugan, L. C.; Matthews, J.; Sinha, A.; McCoy, A. B. *JPCA* **2017**, *121*, 9262–9274.

[129] Redington, R. L.; Olson, W. B.; Cross, P. C. *J. Chem. Phys.* **1962**, *36*, 1311–1326.

[130] Ghosh, D. C. *Int. J. Mol. Sci* **2006**, *7*, 289–319.

[131] Flaud, J.-M.; Camy-Peyret, C.; Johns, J. W. C.; Carli, B. *J. Chem. Phys.* **1989**, *91*, 1504.

[132] Trabelsi, T.; Davis, M. C.; Fortenberry, R. C.; Francisco, J. S. *J. Chem. Phys.* **2019**, *151*, 244303.

[133] Denis, P. A. *Molec. Phys.* **2008**, *106*, 2557–2567.

[134] Winnewisser, G.; Lewen, F.; Thorwirth, S.; Behnke, M.; Hahn, J.; Gauss, J.; Herbst, E. *Chem. Eur. J.* **2003**, *9*, 5501–5510.

[135] Baum, O.; Esser, S.; Gierse, N.; Brünken, S.; Lewen, F.; Hahn, J.; Gauss, J.; Schlemmer, S.; Giesen, T. F. *J. Mol. Struct.* **2006**, *795*, 256–262.

[136] Baum, O.; Giesen, T. F.; Schlemmer, S. *J. Mol. Struct.* **2008**, *247*, 25–29.

[137] Ovsyannikov, R. I.; Melnikov, V. V.; Thiel, W.; Jensen, P.; Baum, O.; Giesen, T. F.; Yurchenko, S. N. *J. Chem. Phys.* **2008**, *129*, 154314.

[138] Yurchenko, S. N.; Thiel, W.; Jensen, P. *J. Mol. Spectrosc.* **2007**, *245*, 126–140.

[139] Yurchenko, S. N.; Yachmenev, A.; Thiel, W.; Baum, O.; Giesen, T. F.; Melnikov, V. V.; Jensen, P. *J. Mol. Spectrosc.* **2009**, *257*, 57–65.

[140] Western, C. M. *J. Quant. Spectrosc. Radiat. Transf.* **2017**, *186*, 221–242.

[141] Turner, B. E. *Astron. Astrophys.* **1987**, *183*, L23–L26.

[142] Cernicharo, J.; Guèlin, M.; Agundez, M.; McCarthy, M. C.; Thaddeus, P. *Astrophys. J.* **2008**, *688*, L83–L86.

[143] Urban, S.; Herbst, E.; Mittler, P.; Winnewisser, G.; Yamada, K. M. T. *JMoSp* **1989**, *137*, 327–353.

[144] Maciel, G. S.; Barreto, P. R. P.; Palazzetti, F.; Lombardi, A.; Aquilanti, V. *J. Chem. Phys.* **2008**, *129*, 164302.

[145] Winnewisser, G.; Yamada, K. M. T. *Vib. Spectrosc.* **1991**, *1*, 263–272.

[146] Behrend, J.; Mittler, P.; Winnewisser, G.; Yamada, K. M. T. *JMoSp* **1990**, *141*, 265–280.

[147] Ye, H.; Mendolicchio, M.; Kruse, H.; Puzzarini, C.; Biczysko, M.; Barone, V. *J. Mol. Struct.* **2020**, *1211*, 127933.

[148] Mittler, P.; Yamada, K. M. T.; Winnewisser, G.; Birk, M. *J. Mol. Spectrosc.* **1994**, *164*, 390–394.

[149] Mittler, P.; Winnewisser, G.; Yamada, K. M. T.; Herbst, E. *J. Mol. Spectrosc.* **1990**, *140*, 259–268.

[150] Shimanouchi, T. *Tables of Molecular Vibrational Frequencies*, 39th ed.; National Standards Reference Data System: Washington, DC, 1972; Vol. 1.

[151] Herbst, E.; Klemperer, W. *Astrophys. J.* **1973**, *185*, 505–533.

[152] Herbst, E.; Cuppen, H. M. *Proc. Natl. Acad. Sci. U.S.A* **2006**, *133*, 12257–12262.

[153] Mahan, B. H. *Acc. Chem. Res.* **1975**, *8*, 55–61.

[154] Ziurys, L. M. *Proc. Natl. Acad. Sci. U.S.A.* **2006**, *103*, 12274–12279.

[155] Fehsenfeld, F. C.; Schmeltekopf, A. L.; Golden, P. D.; Schiff, H. I.; Ferguson, E. E. *J. Chem. Phys.* **1966**, *44*, 4087–4094.

[156] Cameron, A. G. W. *Space Science Rev.* **1970**, *15*, 121–146.

[157] Suess, H. E.; Urey, H. C. *Rev. Mod. Phys.* **1956**, *28*, 53–74.

[158] Snow, T. P.; York, D. G. *Astrophys. J.* **1981**, *247*, L39–L41.

[159] Ziurys, L. M.; Apponi, A. J.; Phillips, T. G. *Astrophys. J.* **1994**, *433*, 729–732.

[160] Neufeld, D. A.; Zmuidzinas, J.; Schilke, P.; Phillips, T. G. *Astrophys. J.* **1997**, *488*, L141–L144.

[161] Zhu, C.; Krems, R.; Dalgarno, A.; Balakrishnan, N. *Astrophys. J.* **2002**, *577*, 795–797.

[162] Kamiński, T.; Tylenda, R.; Menten, K. M.; Karakas, A.; Winters, J. M.; Breier, A. A.; Wong, K. T.; Giesen, T. F.; Patel, N. A. *NatAS* **2018**, *2*, 778–783.

[163] Woosley, S. E.; Haxton, W. C. *Nature* **1988**, *334*, 45–47.

[164] Woosley, S. E.; Weaver, T. A. *Astrophys. J.* **1995**, *101*, 181–235.

[165] Meynet, G.; Arnould, M. *Astron. Astrophys.* **2000**, *355*, 176–180.

[166] Forestini, M.; Goriely, S.; Jorissen, A.; Arnould, M. *Astron. Astrophys.* **1992**, *261*, 157–163.

[167] Parise, B.; Bergman, P.; Du, F. *Astron. Astrophys.* **2012**, *541*, L11.

[168] Mao, J. et al. *Atmos. Phys. Chem.* **2010**, *10*, 5823–5838.

[169] Cheng, M.-D. *J. Atmos. Chem.* **2017**, *75*, 1–16.

[170] Sakugawa, H.; Kaplan, I. R.; Tsai, W.; Cohen, Y. *Environ. Sci. Technol.* **1990**, *24*, 1452–1462.

[171] Francisco, J. S.; Findeis, M. A.; Steinfeld, J. I. *Int. J. Chem. Kins.* **1981**, *13*, 627–638.

[172] Theis, R. A.; Fortenberry, R. C. *Mol. Astrophys.* **2016**, *2*, 18–24.

[173] Wagner, J. P.; McDonald II, D. C.; Duncan, M. A. *Angew. Chem. Int. Ed* **2018**, *57*, 5081–5085.

[174] Peterson, K. A.; Adler, T. B.; Werner, H.-J. *J. Chem. Phys.* **2008**, *128*, 084102.

[175] Yousaf, K. E.; Peterson, K. A. *J. Chem. Phys.* **2008**, *129*, 184108.

[176] Martin, J. M. L.; Kesharwani, M. K. *J. Chem. Theor. Comput.* **2014**, *10*, 2085–2090.

[177] Hill, J. G.; Peterson, K. A. *PCCP* **2010**, *12*, 10460–10468.

[178] Huang, X.; Valeev, E. F.; Lee, T. J. *J. Chem. Phys.* **2010**, *133*, 244108.

[179] Watrous, A. G.; Davis, M. C.; Fortenberry, R. C. *FrASS* **2021**, *8*, 1–11.

[180] Westbrook, B. R.; Fortenberry, R. C. *Molecules* **2021**, *26*, 7348.

[181] Hehre, W. J.; Ditchfeld, R.; Pople, J. A. *J. Chem. Phys.* **1972**, *56*, 2257.

[182] Westbrook, B. R.; Patel, D. J.; Dallas, J. D.; Swartzfager, G. C.; Lee, T. J.; Fortenberry, R. C. *JPCA* **2021**, *125*, 8860–8868.

[183] Westbrook, B. R.; Fortenberry, R. C. *JPCA* **2020**, *124*, 3191–3204.

[184] Palmer, C. Z.; Fortenberry, R. C.; Fransisco, J. S. *Molecules* **2022**, *27(10)*, 3200.

[185] Lyman, J. L. *JPhCh Ref. Data* **1989**, *18*, 799–807.

[186] Gail, H.-P.; Sedlmayr, E. *FaDi* **1998**, *109*, 303–119.

[187] Gail, H.-P.; Sedlmayr, E. *Astron. Astrophys.* **1999**, *347*, 594–616.

[188] Gobrecht, D.; Cherchneff, I.; Sarangi, A.; Plane, J. M. C.; Bromley, S. T. *Astron. Astrophys.* **2016**, *585*, A6.

[189] Gobrecht, D.; Plane, J. M. C.; Bromley, S. T.; Decin, L.; Cristallo, S.; Sekaran, S. *Astron. Astrophys.* **2022**, *5658*, A167.

[190] Sloan, G. C.; Kraemer, K. E.; Goebel, J. H.; Price, S. D. *Astrophys. J.* **2003**, *594*, 483–495.

[191] Chang, C.; Patzer, A. B. C.; Sedlymayr, E.; Sülzle, D. *EPJD* **1998**, *2*, 57–63.

[192] Patzer, A. B. C.; Chang, C.; Sadlmayr, E.; Sülzle, D. *EPJD* **2005**, *32*, 329–337.

[193] Lodders, K. *Astrophys. J.* **2003**, *591*, 1220–1247.

[194] Nittler, L. R.; Alexander, C. M. O.; Gallino, R.; Hoppe, P.; Nguyen, A. N.; Stadermann, F. J.; Zinner, E. K. *Astrophys. J.* **2008**, *682*, 1450–1478.

[195] Hutcheon, I. D.; Huss, G. R.; Fahey, A. J.; Wasserburg, G. J. *Astrophys. J.* **1994**, *425*, L97–L100.

[196] Cernicharo, J.; Guélin, M. *Astron. Astrophys.* **1987**, *183*, L10–L12.

[197] Decin, L.; Richards, A. M. S.; Waters, L. B. F. M.; Danilovich, T.; Gobrecht, D.; Khouri, T.; Homan, W.; Bakker, J. M.; de Sande, M. V.; Nuth, J. A.; Beck, E. D. *A&A* **2017**, *608*, A55.

[198] Saberi, M.; Khouri, T.; Velilla-Prieto, L.; Fonfría, J. P.; Vlemmings, W. H. T.; Wedemeyer, S. *A&A* **2022**, *663*, A54.

[199] Danilovich, T. et al. *A&A* **2021**, *655*, A80.

[200] Ziurys, L. M.; Savage, C.; Highberger, J. L.; Apponi, A. J.; Guélin, M.; J.Cernicharo *Astrophys. J.* **2002**, *564*, L45–L48.

[201] Kamiński, T. *Nature* **2015**, *520*, 322–324.

[202] Doerksen, E. S.; Fortenberry, R. C. *ESC* **2020**, *4*, 812–816.

[203] Czyzak, S. J.; Hirth, J. P.; Tabak, R. G. *VA* **1982**, *25*, 337–382.

[204] Nuth, J. A. *Nature* **1985**, *318*, 166–168.

[205] Kamiński, T.; Wong, K. T.; Schmidt, M. R.; Müller, H. S. P.; Gottlieb, C. A.; Cherchneff, I.; Menten, K. M.; Keller, D.; Brünken, S.; Winters, J. M.; Patel, N. A. *A&A* **2016**, *592*, A42.

[206] Grosselin, D.; Fortenberry, R. C. *ESC* **2022**, *6*, 18–24.

[207] Flint, A.; Fortenberry, R. C. *ESC* **2023**, *7*, 2119–2128.

[208] Shavitt, I.; Bartlett, R. J. *Many-Body Methods in Chemistry and Physics: MBPT and Coupled-Cluster Theory*; Cambridge University Press: Cambridge, 2009.

[209] Crawford, T. D.; Schaefer III, H. F. In *Reviews in Computational Chemistry*; Lipkowitz, K. B., Boyd, D. B., Eds.; Wiley: New York, 2000; Vol. 14; pp 33–136.

[210] Yang, W. T.; Parr, R. G.; Lee, C. T. *Phys. Rev. A* **1986**, *34*, 4586–4590.

[211] Lee, C.; Yang, W. T.; Parr, R. G. *Phys. Rev. B.* **1988**, *37*, 785–789.

[212] Kendall, R. A.; Dunning, T. H.; Harrison, R. J. *J. Chem. Phys.* **1992**, *96*, 6796–6806.

[213] Ramal-Olmedo, J. C.; Menor-Salván, C. A.; Fortenberry, R. C. *A&A* **2021**, *656*, A148.

[214] Inostroza-Pino, N.; Palmer, C. Z.; Lee, T. J.; Fortenberry, R. C. *JMoSp* **2020**, *369*, 111273.

[215] Palmer, C. Z.; Fortenberry, R. C. *ESC* **2022**, *6*, 2032–2040.

[216] Martin, J. M. L.; Lee, T. J.; Taylor, P. R.; François, J.-P. *J. Chem. Phys.* **1995**, *103*, 2589–2602.

[217] Spanget-Larsen, J. Infrared Intensity and Lorentz Epsilon Curve from 'Gaussian' FREQ Output. 2015; Roskilde University, Roskilde Denmark.

[218] Boss, A. P. *AREPS* **1998**, *26*, 53–80.

[219] Maercker, M.; Khouri, T.; Mecina, M.; Beck, E. D. *Astron. Astrophys.* **2022**, *663*, A64.

[220] Höfner, S.; Olofsson, H. *A&ARv* **2018**, *26*, 1.

[221] Ferrarotti, A. S.; Gail, H.-P. *Astron. Astrophys.* **2006**, *447*, 553–576.

[222] Mayer, I. *JMoSt* **1989**, *186*, 43–52.

[223] Davy, R. D.; Jaffrey, K. L. *JPhCh* **1995**, *98*, 8930–8936.

[224] Leboeuf, M.; Russo, N.; Salahub, D. R.; Toscano, M. *J. Chem. Phys.* **1995**, *103*, 7408–7413.

[225] Marsh, C. M. B.; Hamilton, T. P.; Xie, Y.; III, H. F. S. *J. Chem. Phys.* **1992**, *96*, 5310–5317.

[226] Pimentel, G. C.; Charles, S. W. *PApCh* **1963**, *7*, 111–124.

[227] Fortenberry, R. C.; Trabelsi, T.; Francisco, J. S. *JPCA* **2020**, *124*, 8834–8841.

[228] Tenenbaum, E. D.; Ziurys, L. M. *Astrophys. J.* **2010**, L93–L97.

[229] Plane, J. M. C.; Daly, S. M.; Feng, W.; Gerding, M.; Martín, J. C. G. *J. Geophys. Res.: Space Phys.* **2021**, *126*.

[230] Krankowsky, D.; Arnold, F.; Wieder, H.; Kissel, J. *Int. J. Mass Spectrom. Ion Phys.* **1972**, *8*, 379–390.

[231] Mangan, T. P.; Harman-Thomas, J. M.; Lade, R. E.; Douglas, K. M.; Plane, J. M. C. *ESC* **2020**, *4*, 2007–2017.

[232] Ziurys, L. M.; Apponi, A. J.; Hollis, J. M.; Snyder, L. E. *Astrophys. J. Lett.* **1994**, *436*, 181–184.

[233] Tenenbaum, E. D.; Ziurys, L. M. *Astrophys. J.* **2009**, *693*, L59–L63.

[234] Huss, G. R.; Fahey, A. J.; Gallino, R.; Wasserburg, G. J. *Astrophys. J.s* **1994**, *430*, L81–L83.

[235] Nittler, L. R.; Alexander, C. M. O.; Gao, X.; Walker, R. M.; Zinner, E. K. *Nature* **1994**, *370*, 443–446.

[236] Fortenberry, R. C.; Yu, Q.; Mancini, J. S.; Bowman, J. M.; Lee, T. J.; Crawford, T. D.; Klemperer, W. F.; Francisco, J. S. *J. Chem. Phys.* **2015**, *143*, 071102.

[237] Bassett, M. K.; Fortenberry, R. C. *J. Chem. Phys.* **2017**, *146*, 224303.

[238] Fortenberry, R. C.; Thackston, R.; Francisco, J. S.; Lee, T. J. *J. Chem. Phys.* **2017**, *147*, 074303.

[239] Esposito, V. J.; Palmer, C. Z.; Fortenberry, R. C.; Francisco, J. S. *J. Phys. Chem. A* **2023**, *127*, 7618–7629.

[240] Woon, D. E.; Dunning, T. H. *J. Chem. Phys.* **1993**, *98*, 1358–1371.

[241] Woon, D. A.; Dunning, T. H. *J. Chem. Phys.* **1995**, *103*, 4572–4585.

[242] Peterson, K. A.; Dunning, T. H. *J. Chem. Phys.* **2002**, *117*, 10548–10560.

[243] Jansen, G.; Hess, B. A. *Phys. Rev. A* **1989**, *39*, 6016–6017.

[244] de Jong, W. A.; Harrison, R. J.; Dixon, D. A. *J. Chem. Phys.* **2001**, *114*, 48–53.

[245] Hill, J. G.; Mazumder, S.; Peterson, K. A. *J. Chem. Phys.* **2010**, *132*, 054108.

[246] Fortenberry, R. C.; Huang, X.; Francisco, J. S.; Crawford, T. D.; Lee, T. J. *J. Chem. Phys.* **2011**, *135*, 134301.

[247] Palmer, C. Z.; Fortenberry, R. C. *JPCA* **2018**, *122*, 7079–7088.

[248] Werner, H.-J.; Knowles, P. J.; Knizia, G.; Manby, F. R.; Schütz, M. *WIREs Comput. Mol. Sci.* **2012**, *2*, 242–253.

[249] Werner, H.-J. et al. MOLPRO, 2023.2, a package of ab initio programs. 2023.

[250] Watrous, A. G.; Westbrook, B. R.; Fortenberry, R. C. *Mon. Not. Royal Astron. Soc.* **2023**, (submitted).

[251] Garrett, N. R.; Davis, M. C.; Fortenberry, R. C. *J. Chem. Theory Comput.* **2024**, *20*, 1324–1336.

[252] Loginov, V. A. *Opt. Spectrosc. Engl. Transl.* **1964**, *16*, 220.

[253] L. B. Knight, J.; W. Weltner, J. *J. Chem. Phys.* **1971**, *55*, 5066–5077.

[254] Huang, X.; Fortenberry, R. C.; Lee, T. J. *Astrophys. J. Lett.* **2013**, *768*, 25.

[255] Botschwina, P.; Stein, C.; Sebald, P.; Schröder, B.; Oswald, R. *Astrophys. J.* **2014**, *787*, 72.

[256] Harwick, O. A.; Fortenberry, R. C. *J. Molec. Spectrosc.* **2023**, *391*, 111721.

[257] Berné, O. et al. *Nature* **2023**, *621*, 56–59.

[258] Hendrix, J.; Bera, P. P.; Lee, T. J.; Head-Gordon, M. *Mol. Phys.* **2023**, *122*, 7–8.

[259] Palmer, C. Z.; Fortenberry, R. C. *Astrophys. J.* **2024**, *962*, 148.

[260] Fortenberry, R. C.; Huang, X.; Francisco, J. S.; Crawford, T. D.; Lee, T. J. *JPCA.* **2012**, *116*, 9582–9590.

[261] Fortenberry, R. C.; Francisco, J. S. *Astrophys. J.* **2017**, *835*, 243.

[262] Werner, H.-J. et al. *J. Chem. Phys.* **2020**, *152*, see http://www.molpro.net.

[263] Palmer, C. Z.; Firth, R. A.; Fortenberry, R. C. *J. Comp. Chem.* **2024**, *26*, 27524.

[264] Gaw, J. F.; Willets, A.; Green, W. H.; Handy, N. C. 1996; *SPECTRO program*, version 3.0.

[265] Tosi, S.; Dell'Agli, F.; Kamath, D.; Ventura, P.; Winckel, H. V.; Martini, E. *Astron. Astrophys.* **2022**, *668*, A22.

[266] McMahon, R. J. *Science* **2003**, *299*, 833–834.

[267] Himmel, H.-J.; Downs, A. J.; Greene, T. M. *J. Am. Chem. Soc.* **2000**, 9793–9807.

[268] Firth, R. A.; Palmer, C. Z.; Franciscio, J. S.; Fortenberry, R. C. *J. Chem. Phys.* **2024**, *160*, 214304.

[269] Pei, L.; Min, Q.; Du, Y.; Wang, Z.; Yin, B.; Yang, K.; Disterhoft, P.; Pongetti, T.; Zhu1, L. *JGR Atmospheres* **2019**, *124*, 14310–14324.

APPENDICES

APPENDIX A

Supporting information for Chapter 2: "Spectral Signatures of Hydrogen Thioperoxide (HOSH) and Hydrogen Persulfide (HSSH): Possible Molecular Sulfur Sinks in the Dense ISM."

Table A1: Coordinates for Calculating HOSH Dipole Components

	A	B	C
H	-0.842633611	0.001714644	-1.417667570
O	0.063234434	-0.011889422	-1.095489670
S	-0.004570772	0.045997723	0.565839045
H	-0.015725052	-1.276059704	0.808878993

Table A2: The CcCR Force Constants for HOOH

$F_{1,1}$	0.339640	$F_{1,2}$	-0.086915	$F_{1,3}$	-0.227477	$F_{1,4}$	0.008298
$F_{1,5}$	-0.015014	$F_{1,6}$	-0.007013	$F_{1,7}$	-0.346860	$F_{1,8}$	0.101582
$F_{1,9}$	0.233069	$F_{1,10}$	-0.001079	$F_{1,11}$	0.000347	$F_{1,12}$	0.001421
$F_{1,13}$	-0.086915	$F_{2,1}$	0.093007	$F_{2,2}$	0.059326	$F_{2,3}$	0.035081
$F_{2,4}$	-0.033380	$F_{2,5}$	-0.018962	$F_{2,6}$	0.051487	$F_{2,7}$	-0.054071
$F_{2,8}$	-0.037614	$F_{2,9}$	0.000347	$F_{2,10}$	-0.005556	$F_{2,11}$	-0.002750
$F_{2,12}$	-0.227477	$F_{2,13}$	0.059326	$F_{3,1}$	0.156259	$F_{3,2}$	-0.004265
$F_{3,3}$	0.004660	$F_{3,4}$	0.001213	$F_{3,5}$	0.233163	$F_{3,6}$	-0.066736
$F_{3,7}$	-0.158782	$F_{3,8}$	-0.001421	$F_{3,9}$	0.002750	$F_{3,10}$	0.001311
$F_{3,11}$	0.008298	$F_{3,12}$	0.035081	$F_{3,13}$	-0.004265	$F_{4,1}$	0.392539
$F_{4,2}$	-0.087947	$F_{4,3}$	0.238755	$F_{4,4}$	-0.053978	$F_{4,5}$	0.001379
$F_{4,6}$	-0.001327	$F_{4,7}$	-0.346860	$F_{4,8}$	0.051487	$F_{4,9}$	-0.233163
$F_{4,10}$	-0.015014	$F_{4,11}$	-0.033380	$F_{4,12}$	0.004660	$F_{4,13}$	-0.087947
$F_{5,1}$	0.315174	$F_{5,2}$	-0.045024	$F_{5,3}$	0.001379	$F_{5,4}$	-0.227724
$F_{5,5}$	-0.026372	$F_{5,6}$	0.101582	$F_{5,7}$	-0.054071	$F_{5,8}$	0.066736
$F_{5,9}$	-0.007013	$F_{5,10}$	-0.018962	$F_{5,11}$	0.001213	$F_{5,12}$	0.238755
$F_{5,13}$	-0.045024	$F_{6,1}$	0.177890	$F_{6,2}$	0.001327	$F_{6,3}$	0.026372
$F_{6,4}$	-0.020321	$F_{6,5}$	-0.233069	$F_{6,6}$	0.037614	$F_{6,7}$	-0.158782
$F_{6,8}$	-0.346860	$F_{6,9}$	0.051487	$F_{6,10}$	0.233163	$F_{6,11}$	-0.053978
$F_{6,12}$	0.001379	$F_{6,13}$	0.001327	$F_{7,1}$	0.392539	$F_{7,2}$	-0.087947
$F_{7,3}$	-0.238755	$F_{7,4}$	0.008298	$F_{7,5}$	0.035081	$F_{7,6}$	0.004265
$F_{7,7}$	0.101582	$F_{7,8}$	-0.054071	$F_{7,9}$	-0.066736	$F_{7,10}$	0.001379
$F_{7,11}$	-0.227724	$F_{7,12}$	0.026372	$F_{7,13}$	-0.087947	$F_{8,1}$	0.315174
$F_{8,2}$	0.045024	$F_{8,3}$	-0.015014	$F_{8,4}$	-0.033380	$F_{8,5}$	-0.004660
$F_{8,6}$	0.233069	$F_{8,7}$	-0.037614	$F_{8,8}$	-0.158782	$F_{8,9}$	-0.001327
$F_{8,10}$	-0.026372	$F_{8,11}$	-0.020321	$F_{8,12}$	-0.238755	$F_{8,13}$	0.045024
$F_{9,1}$	0.177890	$F_{9,2}$	0.007013	$F_{9,3}$	0.018962	$F_{9,4}$	0.001213
$F_{9,5}$	-0.001079	$F_{9,6}$	0.000347	$F_{9,7}$	-0.001421	$F_{9,8}$	-0.346860
$F_{9,9}$	0.101582	$F_{9,10}$	-0.233069	$F_{9,11}$	0.008298	$F_{9,12}$	-0.015014
$F_{9,13}$	0.007013	$F_{10,1}$	0.339640	$F_{10,2}$	-0.086915	$F_{10,3}$	0.227477

Table A3: The CcCR Force Constants for HOOH (cont.)

$F_{10,4}$	0.000347	$F_{10,5}$	-0.005556	$F_{10,6}$	0.002750	$F_{10,7}$	0.051487
$F_{10,8}$	-0.054071	$F_{10,9}$	0.037614	$F_{10,10}$	0.035081	$F_{10,11}$	-0.033380
$F_{10,12}$	0.018962	$F_{10,13}$	-0.086915	$F_{11,1}$	0.093007	$F_{11,2}$	-0.059326
$F_{11,3}$	0.001421	$F_{11,4}$	-0.002750	$F_{11,5}$	0.001311	$F_{11,6}$	-0.233163
$F_{11,7}$	0.066736	$F_{11,8}$	-0.158782	$F_{11,9}$	0.004265	$F_{11,10}$	-0.004660
$F_{11,11}$	0.001213	$F_{11,12}$	0.227477	$F_{11,13}$	-0.059326	$F_{12,1}$	0.156259
$F_{1,1,1}$	-0.7736	$F_{1,1,2}$	0.3477	$F_{1,2,2}$	0.0480	$F_{2,2,2}$	-0.0894
$F_{1,1,3}$	0.8345	$F_{1,2,3}$	-0.2802	$F_{2,2,3}$	-0.0292	$F_{1,3,3}$	-0.4433
$F_{2,3,3}$	0.1306	$F_{3,3,3}$	-0.0095	$F_{1,1,4}$	-0.0030	$F_{1,2,4}$	-0.0085
$F_{2,2,4}$	0.0171	$F_{1,3,4}$	0.0055	$F_{2,3,4}$	0.0265	$F_{3,3,4}$	-0.0019
$F_{1,4,4}$	-0.0011	$F_{2,4,4}$	-0.0080	$F_{3,4,4}$	0.0175	$F_{4,4,4}$	-0.7921
$F_{1,1,5}$	0.0230	$F_{1,2,5}$	0.0002	$F_{2,2,5}$	-0.0713	$F_{1,3,5}$	-0.0200
$F_{2,3,5}$	0.0016	$F_{3,3,5}$	0.0034	$F_{1,4,5}$	-0.0098	$F_{2,4,5}$	-0.0377
$F_{3,4,5}$	-0.0034	$F_{4,4,5}$	0.3696	$F_{1,5,5}$	0.0047	$F_{2,5,5}$	0.0844
$F_{3,5,5}$	0.0094	$F_{4,5,5}$	0.0188	$F_{5,5,5}$	-1.0407	$F_{1,1,6}$	0.0084
$F_{1,2,6}$	0.0211	$F_{2,2,6}$	-0.0173	$F_{1,3,6}$	0.0017	$F_{2,3,6}$	0.0096
$F_{3,3,6}$	-0.0064	$F_{1,4,6}$	0.0064	$F_{2,4,6}$	-0.0074	$F_{3,4,6}$	0.0065
$F_{4,4,6}$	-0.8842	$F_{1,5,6}$	0.0015	$F_{2,5,6}$	0.0245	$F_{3,5,6}$	-0.0129
$F_{4,5,6}$	0.2618	$F_{5,5,6}$	-0.0152	$F_{1,6,6}$	-0.0132	$F_{2,6,6}$	-0.0080
$F_{3,6,6}$	-0.0095	$F_{4,6,6}$	-0.4559	$F_{5,6,6}$	0.2010	$F_{6,6,6}$	0.0572
$F_{1,1,7}$	0.7745	$F_{1,2,7}$	-0.3390	$F_{2,2,7}$	-0.0663	$F_{1,3,7}$	-0.8408
$F_{2,3,7}$	0.2550	$F_{3,3,7}$	0.4456	$F_{1,4,7}$	0.0013	$F_{2,4,7}$	0.0184
$F_{3,4,7}$	-0.0234	$F_{4,4,7}$	0.0201	$F_{1,5,7}$	-0.0124	$F_{2,5,7}$	0.0387
$F_{3,5,7}$	0.0197	$F_{4,5,7}$	-0.0103	$F_{5,5,7}$	0.0283	$F_{1,6,7}$	-0.0140
$F_{2,6,7}$	-0.0170	$F_{3,6,7}$	-0.0064	$F_{4,6,7}$	0.0234	$F_{5,6,7}$	0.0197
$F_{6,6,7}$	0.0121	$F_{1,7,7}$	-0.7731	$F_{2,7,7}$	0.3193	$F_{3,7,7}$	0.8658
$F_{4,7,7}$	-0.0201	$F_{5,7,7}$	0.0422	$F_{6,7,7}$	0.0009	$F_{7,7,7}$	0.7921
$F_{1,1,8}$	-0.3699	$F_{1,2,8}$	-0.0488	$F_{2,2,8}$	0.1622	$F_{1,3,8}$	0.3029
$F_{2,3,8}$	0.0330	$F_{3,3,8}$	-0.1359	$F_{1,4,8}$	0.0195	$F_{2,4,8}$	0.0214
$F_{3,4,8}$	-0.0201	$F_{4,4,8}$	-0.0422	$F_{1,5,8}$	-0.0042	$F_{2,5,8}$	-0.0144
$F_{3,5,8}$	-0.0091	$F_{4,5,8}$	0.0456	$F_{5,5,8}$	0.8099	$F_{1,6,8}$	-0.0235
$F_{2,6,8}$	-0.0126	$F_{3,6,8}$	0.0033	$F_{4,6,8}$	-0.0194	$F_{5,6,8}$	0.0091
$F_{6,6,8}$	-0.0493	$F_{1,7,8}$	0.3495	$F_{2,7,8}$	0.0267	$F_{3,7,8}$	-0.2811
$F_{4,7,8}$	0.0103	$F_{5,7,8}$	-0.0456	$F_{6,7,8}$	0.0227	$F_{7,7,8}$	-0.3696
$F_{1,8,8}$	0.0518	$F_{2,8,8}$	-0.1465	$F_{3,8,8}$	-0.0294	$F_{4,8,8}$	-0.0283
$F_{5,8,8}$	-0.8099	$F_{6,8,8}$	0.0351	$F_{7,8,8}$	-0.0188	$F_{8,8,8}$	1.0407
$F_{1,1,9}$	-0.8435	$F_{1,2,9}$	0.2596	$F_{2,2,9}$	0.0447	$F_{1,3,9}$	0.4438
$F_{2,3,9}$	-0.1410	$F_{3,3,9}$	0.0157	$F_{1,4,9}$	-0.0102	$F_{2,4,9}$	-0.0255
$F_{3,4,9}$	-0.0024	$F_{4,4,9}$	0.0009	$F_{1,5,9}$	0.0202	$F_{2,5,9}$	-0.0316
$F_{3,5,9}$	0.0087	$F_{4,5,9}$	0.0227	$F_{5,5,9}$	0.0351	$F_{1,6,9}$	0.0115
$F_{2,6,9}$	-0.0027	$F_{3,6,9}$	0.0161	$F_{4,6,9}$	0.0081	$F_{5,6,9}$	-0.0547
$F_{6,6,9}$	-0.0161	$F_{1,7,9}$	0.8545	$F_{2,7,9}$	-0.2350	$F_{3,7,9}$	-0.4413
$F_{4,7,9}$	0.0234	$F_{5,7,9}$	-0.0194	$F_{6,7,9}$	-0.0081	$F_{7,7,9}$	-0.8842
$F_{1,8,9}$	-0.2831	$F_{2,8,9}$	-0.0185	$F_{3,8,9}$	0.1333	$F_{4,8,9}$	0.0197

Table A4: The CcCR Force Constants for HOOH

$F_{1,1}$	0.339642	$F_{1,2}$	-0.086915	$F_{1,3}$	-0.227477	$F_{1,4}$	-0.346861	$F_{1,5}$	0.101584
$F_{1,6}$	0.233070	$F_{1,7}$	0.008299	$F_{1,8}$	-0.015015	$F_{1,9}$	-0.007015	$F_{1,10}$	-0.001079
$F_{1,11}$	0.000347	$F_{1,12}$	0.001422	$F_{1,13}$	-0.086915	$F_{2,1}$	0.093010	$F_{2,2}$	0.059326
$F_{2,3}$	0.051486	$F_{2,4}$	-0.054071	$F_{2,5}$	-0.037612	$F_{2,6}$	0.035082	$F_{2,7}$	-0.033382
$F_{2,8}$	-0.018962	$F_{2,9}$	0.000347	$F_{2,10}$	-0.005556	$F_{2,11}$	-0.002752	$F_{2,12}$	-0.227477
$F_{2,13}$	0.059326	$F_{3,1}$	0.156261	$F_{3,2}$	0.233165	$F_{3,3}$	-0.066734	$F_{3,4}$	-0.158785
$F_{3,5}$	-0.004265	$F_{3,6}$	0.004657	$F_{3,7}$	0.001212	$F_{3,8}$	-0.001422	$F_{3,9}$	0.002752
$F_{3,10}$	0.001311	$F_{3,11}$	-0.346861	$F_{3,12}$	0.051486	$F_{3,13}$	0.233165	$F_{4,1}$	0.392542
$F_{4,2}$	-0.087949	$F_{4,3}$	-0.238757	$F_{4,4}$	-0.053980	$F_{4,5}$	0.001381	$F_{4,6}$	0.001327
$F_{4,7}$	0.008299	$F_{4,8}$	0.035082	$F_{4,9}$	0.004265	$F_{4,10}$	0.101584	$F_{4,11}$	-0.054071
$F_{4,12}$	-0.066734	$F_{4,13}$	-0.087949	$F_{5,1}$	0.315182	$F_{5,2}$	0.045021	$F_{5,3}$	0.001381
$F_{5,4}$	-0.227729	$F_{5,5}$	0.026371	$F_{5,6}$	-0.015015	$F_{5,7}$	-0.033382	$F_{5,8}$	-0.004657
$F_{5,9}$	0.233070	$F_{5,10}$	-0.037612	$F_{5,11}$	-0.158785	$F_{5,12}$	-0.238757	$F_{5,13}$	0.045021
$F_{6,1}$	0.177893	$F_{6,2}$	-0.001327	$F_{6,3}$	-0.026371	$F_{6,4}$	-0.020321	$F_{6,5}$	0.007015
$F_{6,6}$	0.018962	$F_{6,7}$	0.001212	$F_{6,8}$	0.008299	$F_{6,9}$	0.035082	$F_{6,10}$	-0.004265
$F_{6,11}$	-0.053980	$F_{6,12}$	0.001381	$F_{6,13}$	-0.001327	$F_{7,1}$	0.392542	$F_{7,2}$	-0.087949
$F_{7,3}$	0.238757	$F_{7,4}$	-0.346861	$F_{7,5}$	0.051486	$F_{7,6}$	-0.233165	$F_{7,7}$	-0.015015
$F_{7,8}$	-0.033382	$F_{7,9}$	0.004657	$F_{7,10}$	0.001381	$F_{7,11}$	-0.227729	$F_{7,12}$	-0.026371
$F_{7,13}$	-0.087949	$F_{8,1}$	0.315182	$F_{8,2}$	-0.045021	$F_{8,3}$	0.101584	$F_{8,4}$	-0.054071
$F_{8,5}$	0.066734	$F_{8,6}$	-0.007015	$F_{8,7}$	-0.018962	$F_{8,8}$	0.001212	$F_{8,9}$	0.001327
$F_{8,10}$	0.026371	$F_{8,11}$	-0.020321	$F_{8,12}$	0.238757	$F_{8,13}$	-0.045021	$F_{9,1}$	0.177893
$F_{9,2}$	-0.233070	$F_{9,3}$	0.037612	$F_{9,4}$	-0.158785	$F_{9,5}$	-0.001079	$F_{9,6}$	0.000347
$F_{9,7}$	-0.001422	$F_{9,8}$	0.008299	$F_{9,9}$	-0.015015	$F_{9,10}$	0.007015	$F_{9,11}$	-0.346861
$F_{9,12}$	0.101584	$F_{9,13}$	-0.233070	$F_{10,1}$	0.339642	$F_{10,2}$	-0.086915	$F_{10,3}$	0.227477
$F_{10,4}$	0.000347	$F_{10,5}$	-0.005556	$F_{10,6}$	0.002752	$F_{10,7}$	0.035082	$F_{10,8}$	-0.033382
$F_{10,9}$	0.018962	$F_{10,10}$	0.051486	$F_{10,11}$	-0.054071	$F_{10,12}$	0.037612	$F_{10,13}$	-0.086915
$F_{11,1}$	0.093010	$F_{11,2}$	-0.059326	$F_{11,3}$	0.001422	$F_{11,4}$	-0.002752	$F_{11,5}$	0.001311
$F_{11,6}$	0.004265	$F_{11,7}$	-0.004657	$F_{11,8}$	0.001212	$F_{11,9}$	-0.233165	$F_{11,10}$	0.066734
$F_{11,11}$	-0.158785	$F_{11,12}$	0.227477	$F_{11,13}$	-0.059326	$F_{12,1}$	0.156261	$F_{1,1,1}$	-0.7734
$F_{1,1,2}$	0.3477	$F_{1,2,2}$	0.0478	$F_{2,2,2}$	-0.0895	$F_{1,1,3}$	0.8344	$F_{1,2,3}$	-0.2802
$F_{2,2,3}$	-0.0291	$F_{1,3,3}$	-0.4432	$F_{2,3,3}$	0.1306	$F_{3,3,3}$	-0.0096	$F_{1,1,4}$	0.7743
$F_{1,2,4}$	-0.3388	$F_{2,2,4}$	-0.0661	$F_{1,3,4}$	-0.8407	$F_{2,3,4}$	0.2550	$F_{3,3,4}$	0.4456
$F_{1,4,4}$	-0.7730	$F_{2,4,4}$	0.3191	$F_{3,4,4}$	0.8656	$F_{4,4,4}$	0.7923	$F_{1,1,5}$	-0.3696
$F_{1,2,5}$	-0.0487	$F_{2,2,5}$	0.1624	$F_{1,3,5}$	0.3028	$F_{2,3,5}$	0.0329	$F_{3,3,5}$	-0.1357
$F_{1,4,5}$	0.3492	$F_{2,4,5}$	0.0265	$F_{3,4,5}$	-0.2810	$F_{4,4,5}$	-0.3690	$F_{1,5,5}$	0.0519
$F_{2,5,5}$	-0.1466	$F_{3,5,5}$	-0.0294	$F_{4,5,5}$	-0.0189	$F_{5,5,5}$	1.0417	$F_{1,1,6}$	-0.8433
$F_{1,2,6}$	0.2596	$F_{2,2,6}$	0.0446	$F_{1,3,6}$	0.4437	$F_{2,3,6}$	-0.1409	$F_{3,3,6}$	0.0158
$F_{1,4,6}$	0.8543	$F_{2,4,6}$	-0.2349	$F_{3,4,6}$	-0.4413	$F_{4,4,6}$	-0.8840	$F_{1,5,6}$	-0.2830
$F_{2,5,6}$	-0.0183	$F_{3,5,6}$	0.1331	$F_{4,5,6}$	0.2617	$F_{5,5,6}$	-0.0153	$F_{1,6,6}$	-0.4570
$F_{2,6,6}$	0.1435	$F_{3,6,6}$	-0.0317	$F_{4,6,6}$	0.4559	$F_{5,6,6}$	-0.2006	$F_{6,6,6}$	0.0573
$F_{1,1,7}$	-0.0030	$F_{1,2,7}$	-0.0086	$F_{2,2,7}$	0.0171	$F_{1,3,7}$	0.0055	$F_{2,3,7}$	0.0266
$F_{3,3,7}$	-0.0020	$F_{1,4,7}$	0.0014	$F_{2,4,7}$	0.0186	$F_{3,4,7}$	-0.0233	$F_{4,4,7}$	-0.0204
$F_{1,5,7}$	0.0197	$F_{2,5,7}$	0.0216	$F_{3,5,7}$	-0.0200	$F_{4,5,7}$	0.0100	$F_{5,5,7}$	-0.0282
$F_{1,6,7}$	-0.0102	$F_{2,6,7}$	-0.0255	$F_{3,6,7}$	-0.0023	$F_{4,6,7}$	0.0233	$F_{5,6,7}$	0.0197
$F_{6,6,7}$	-0.0122	$F_{1,7,7}$	-0.0012	$F_{2,7,7}$	-0.0081	$F_{3,7,7}$	0.0175	$F_{4,7,7}$	0.0204
$F_{5,7,7}$	-0.0418	$F_{6,7,7}$	0.0009	$F_{7,7,7}$	-0.7923	$F_{1,1,8}$	0.0228	$F_{1,2,8}$	0.0003
$F_{2,2,8}$	-0.0714	$F_{1,3,8}$	-0.0199	$F_{2,3,8}$	0.0016	$F_{3,3,8}$	0.0032	$F_{1,4,8}$	-0.0121
$F_{2,4,8}$	0.0387	$F_{3,4,8}$	0.0197	$F_{4,4,8}$	0.0418	$F_{1,5,8}$	-0.0044	$F_{2,5,8}$	-0.0145
$F_{3,5,8}$	-0.0090	$F_{4,5,8}$	-0.0454	$F_{5,5,8}$	-0.8105	$F_{1,6,8}$	0.0201	$F_{2,6,8}$	-0.0316

Table A5: The CcCR Force Constants for HOOH (cont.)

$F_{3,6,8}$	0.0090	$F_{4,6,8}$	-0.0194	$F_{5,6,8}$	0.0090	$F_{6,6,8}$	0.0490	$F_{1,7,8}$	-0.0098
$F_{2,7,8}$	-0.0378	$F_{3,7,8}$	-0.0036	$F_{4,7,8}$	-0.0100	$F_{5,7,8}$	0.0454	$F_{6,7,8}$	0.0229
$F_{7,7,8}$	0.3690	$F_{1,8,8}$	0.0047	$F_{2,8,8}$	0.0846	$F_{3,8,8}$	0.0094	$F_{4,8,8}$	0.0282
$F_{5,8,8}$	0.8105	$F_{6,8,8}$	0.0352	$F_{7,8,8}$	0.0189	$F_{8,8,8}$	-1.0417	$F_{1,1,9}$	0.0084
$F_{1,2,9}$	0.0212	$F_{2,2,9}$	-0.0172	$F_{1,3,9}$	0.0017	$F_{2,3,9}$	0.0097	$F_{3,3,9}$	-0.0064
$F_{1,4,9}$	-0.0140	$F_{2,4,9}$	-0.0171	$F_{3,4,9}$	-0.0065	$F_{4,4,9}$	0.0009	$F_{1,5,9}$	-0.0236
$F_{2,5,9}$	-0.0126	$F_{3,5,9}$	0.0032	$F_{4,5,9}$	0.0229	$F_{5,5,9}$	0.0352	$F_{1,6,9}$	0.0115
$F_{2,6,9}$	-0.0027	$F_{3,6,9}$	0.0161	$F_{4,6,9}$	-0.0080	$F_{5,6,9}$	0.0548	$F_{6,6,9}$	-0.0161
$F_{1,7,9}$	0.0064	$F_{2,7,9}$	-0.0074	$F_{3,7,9}$	0.0066	$F_{4,7,9}$	0.0233	$F_{5,7,9}$	-0.0194
$F_{6,7,9}$	0.0080	$F_{7,7,9}$	-0.8840	$F_{1,8,9}$	0.0016	$F_{2,8,9}$	0.0245	$F_{3,8,9}$	-0.0128
$F_{4,8,9}$	0.0197	$F_{5,8,9}$	0.0090	$F_{6,8,9}$	-0.0548	$F_{7,8,9}$	0.2617	$F_{8,8,9}$	-0.0153
$F_{1,9,9}$	-0.0132	$F_{2,9,9}$	-0.0081	$F_{3,9,9}$	-0.0095	$F_{4,9,9}$	0.0122	$F_{5,9,9}$	-0.0490
$F_{6,9,9}$	-0.0161	$F_{7,9,9}$	-0.4559	$F_{8,9,9}$	0.2006	$F_{9,9,9}$	0.0573	$F_{1,1,10}$	0.0021
$F_{1,2,10}$	-0.0002	$F_{2,2,10}$	0.0012	$F_{1,3,10}$	0.0007	$F_{2,3,10}$	-0.0013	$F_{3,3,10}$	-0.0004
$F_{1,4,10}$	-0.0027	$F_{2,4,10}$	0.0012	$F_{3,4,10}$	-0.0017	$F_{4,4,10}$	0.0012	$F_{1,5,10}$	0.0008
$F_{2,5,10}$	0.0006	$F_{3,5,10}$	-0.0018	$F_{4,5,10}$	0.0098	$F_{5,5,10}$	-0.0047	$F_{1,6,10}$	-0.0007
$F_{2,6,10}$	0.0008	$F_{3,6,10}$	-0.0000	$F_{4,6,10}$	0.0064	$F_{5,6,10}$	0.0016	$F_{6,6,10}$	0.0132
$F_{1,7,10}$	0.0027	$F_{2,7,10}$	-0.0018	$F_{3,7,10}$	0.0004	$F_{4,7,10}$	-0.0014	$F_{5,7,10}$	0.0121
$F_{6,7,10}$	-0.0140	$F_{7,7,10}$	0.7730	$F_{1,8,10}$	-0.0008	$F_{2,8,10}$	-0.0012	$F_{3,8,10}$	0.0038
$F_{4,8,10}$	-0.0197	$F_{5,8,10}$	0.0044	$F_{6,8,10}$	-0.0236	$F_{7,8,10}$	-0.3492	$F_{8,8,10}$	-0.0519
$F_{1,9,10}$	-0.0007	$F_{2,9,10}$	0.0032	$F_{3,9,10}$	-0.0018	$F_{4,9,10}$	-0.0102	$F_{5,9,10}$	0.0201
$F_{6,9,10}$	-0.0115	$F_{7,9,10}$	0.8543	$F_{8,9,10}$	-0.2830	$F_{9,9,10}$	0.4570	$F_{1,10,10}$	-0.0021
$F_{2,10,10}$	0.0008	$F_{3,10,10}$	0.0006	$F_{4,10,10}$	0.0030	$F_{5,10,10}$	-0.0228	$F_{6,10,10}$	0.0084
$F_{7,10,10}$	-0.7743	$F_{8,10,10}$	0.3696	$F_{9,10,10}$	-0.8433	$F_{10,10,10}$	0.7734	$F_{1,1,11}$	-0.0008
$F_{1,2,11}$	0.0006	$F_{2,2,11}$	-0.0015	$F_{1,3,11}$	-0.0027	$F_{2,3,11}$	-0.0053	$F_{3,3,11}$	0.0019
$F_{1,4,11}$	0.0018	$F_{2,4,11}$	0.0009	$F_{3,4,11}$	0.0063	$F_{4,4,11}$	0.0081	$F_{1,5,11}$	0.0012
$F_{2,5,11}$	-0.0013	$F_{3,5,11}$	0.0055	$F_{4,5,11}$	0.0378	$F_{5,5,11}$	-0.0846	$F_{1,6,11}$	0.0032
$F_{2,6,11}$	0.0053	$F_{3,6,11}$	-0.0011	$F_{4,6,11}$	-0.0074	$F_{5,6,11}$	0.0245	$F_{6,6,11}$	0.0081
$F_{1,7,11}$	-0.0012	$F_{2,7,11}$	-0.0009	$F_{3,7,11}$	-0.0030	$F_{4,7,11}$	-0.0186	$F_{5,7,11}$	-0.0387
$F_{6,7,11}$	-0.0171	$F_{7,7,11}$	-0.3191	$F_{1,8,11}$	-0.0006	$F_{2,8,11}$	0.0013	$F_{3,8,11}$	-0.0020
$F_{4,8,11}$	-0.0216	$F_{5,8,11}$	0.0145	$F_{6,8,11}$	-0.0126	$F_{7,8,11}$	-0.0265	$F_{8,8,11}$	0.1466
$F_{1,9,11}$	0.0008	$F_{2,9,11}$	0.0053	$F_{3,9,11}$	-0.0001	$F_{4,9,11}$	-0.0255	$F_{5,9,11}$	-0.0316
$F_{6,9,11}$	0.0027	$F_{7,9,11}$	-0.2349	$F_{8,9,11}$	-0.0183	$F_{9,9,11}$	-0.1435	$F_{1,10,11}$	0.0002
$F_{2,10,11}$	-0.0006	$F_{3,10,11}$	-0.0006	$F_{4,10,11}$	0.0086	$F_{5,10,11}$	-0.0003	$F_{6,10,11}$	0.0212
$F_{7,10,11}$	0.3388	$F_{8,10,11}$	0.0487	$F_{9,10,11}$	0.2596	$F_{10,10,11}$	-0.3477	$F_{1,11,11}$	-0.0012
$F_{2,11,11}$	0.0015	$F_{3,11,11}$	0.0018	$F_{4,11,11}$	-0.0171	$F_{5,11,11}$	0.0714	$F_{6,11,11}$	-0.0172
$F_{7,11,11}$	0.0661	$F_{8,11,11}$	-0.1624	$F_{9,11,11}$	0.0446	$F_{10,11,11}$	-0.0478	$F_{11,11,11}$	0.0895
$F_{1,1,12}$	0.0006	$F_{1,2,12}$	-0.0006	$F_{2,2,12}$	0.0018	$F_{1,3,12}$	-0.0022	$F_{2,3,12}$	0.0007
$F_{3,3,12}$	0.0002	$F_{1,4,12}$	0.0004	$F_{2,4,12}$	-0.0030	$F_{3,4,12}$	0.0022	$F_{4,4,12}$	0.0175
$F_{1,5,12}$	0.0038	$F_{2,5,12}$	-0.0020	$F_{3,5,12}$	-0.0006	$F_{4,5,12}$	-0.0036	$F_{5,5,12}$	0.0094
$F_{1,6,12}$	0.0018	$F_{2,6,12}$	0.0001	$F_{3,6,12}$	-0.0002	$F_{4,6,12}$	-0.0066	$F_{5,6,12}$	0.0128
$F_{6,6,12}$	-0.0095	$F_{1,7,12}$	-0.0017	$F_{2,7,12}$	0.0063	$F_{3,7,12}$	-0.0022	$F_{4,7,12}$	-0.0233
$F_{5,7,12}$	0.0197	$F_{6,7,12}$	0.0065	$F_{7,7,12}$	0.8656	$F_{1,8,12}$	-0.0018	$F_{2,8,12}$	0.0055
$F_{3,8,12}$	0.0006	$F_{4,8,12}$	-0.0200	$F_{5,8,12}$	-0.0090	$F_{6,8,12}$	-0.0032	$F_{7,8,12}$	-0.2810
$F_{8,8,12}$	-0.0294	$F_{1,9,12}$	0.0000	$F_{2,9,12}$	0.0011	$F_{3,9,12}$	-0.0002	$F_{4,9,12}$	0.0023
$F_{5,9,12}$	-0.0090	$F_{6,9,12}$	0.0161	$F_{7,9,12}$	0.4413	$F_{8,9,12}$	-0.1331	$F_{9,9,12}$	-0.0317
$F_{1,10,12}$	0.0007	$F_{2,10,12}$	-0.0027	$F_{3,10,12}$	0.0022	$F_{4,10,12}$	0.0055	$F_{5,10,12}$	-0.0199
$F_{6,10,12}$	-0.0017	$F_{7,10,12}$	-0.8407	$F_{8,10,12}$	0.3028	$F_{9,10,12}$	-0.4437	$F_{10,10,12}$	0.8344
$F_{1,11,12}$	-0.0013	$F_{2,11,12}$	-0.0053	$F_{3,11,12}$	-0.0007	$F_{4,11,12}$	0.0266	$F_{5,11,12}$	0.0016

Table A6: The CcCR Force Constants for HOOH (cont.)

$F_{6,11,12}$	-0.0097	$F_{7,11,12}$	0.2550	$F_{8,11,12}$	0.0329	$F_{9,11,12}$	0.1409	$F_{10,11,12}$	-0.2802
$F_{11,11,12}$	-0.0291	$F_{1,12,12}$	0.0004	$F_{2,12,12}$	-0.0019	$F_{3,12,12}$	0.0002	$F_{4,12,12}$	0.0020
$F_{5,12,12}$	-0.0032	$F_{6,12,12}$	-0.0064	$F_{7,12,12}$	-0.4456	$F_{8,12,12}$	0.1357	$F_{9,12,12}$	0.0158
$F_{10,12,12}$	0.4432	$F_{11,12,12}$	-0.1306	$F_{12,12,12}$	-0.0096	$F_{1,1,1,1}$	0.80	$F_{1,1,1,2}$	-0.97
$F_{1,1,2,2}$	-0.34	$F_{1,2,2,2}$	0.59	$F_{2,2,2,2}$	-0.11	$F_{1,1,1,3}$	-2.25	$F_{1,1,2,3}$	1.04
$F_{1,2,2,3}$	0.25	$F_{2,2,2,3}$	-0.40	$F_{1,1,3,3}$	1.60	$F_{1,2,3,3}$	-0.56	$F_{2,2,3,3}$	-0.13
$F_{1,3,3,3}$	0.06	$F_{2,3,3,3}$	-0.01	$F_{3,3,3,3}$	-0.95	$F_{1,1,1,4}$	-0.80	$F_{1,1,2,4}$	0.98
$F_{1,2,2,4}$	0.35	$F_{2,2,2,4}$	-0.57	$F_{1,1,3,4}$	2.27	$F_{1,2,3,4}$	-1.02	$F_{2,2,3,4}$	-0.27
$F_{1,3,3,4}$	-1.62	$F_{2,3,3,4}$	0.55	$F_{3,3,3,4}$	-0.06	$F_{1,1,4,4}$	0.78	$F_{1,2,4,4}$	-1.01
$F_{2,2,4,4}$	-0.42	$F_{1,3,4,4}$	-2.29	$F_{2,3,4,4}$	1.01	$F_{3,3,4,4}$	1.63	$F_{1,4,4,4}$	-0.74
$F_{2,4,4,4}$	1.09	$F_{3,4,4,4}$	2.33	$F_{4,4,4,4}$	0.66	$F_{1,1,1,5}$	0.95	$F_{1,1,2,5}$	0.32
$F_{1,2,2,5}$	-0.67	$F_{2,2,2,5}$	0.18	$F_{1,1,3,5}$	-1.06	$F_{1,2,3,5}$	-0.25	$F_{2,2,3,5}$	0.46
$F_{1,3,3,5}$	0.55	$F_{2,3,3,5}$	0.13	$F_{3,3,3,5}$	0.04	$F_{1,1,4,5}$	-0.95	$F_{1,2,4,5}$	-0.33
$F_{2,2,4,5}$	0.62	$F_{1,3,4,5}$	1.04	$F_{2,3,4,5}$	0.24	$F_{3,3,4,5}$	-0.55	$F_{1,4,4,5}$	0.97
$F_{2,4,4,5}$	0.35	$F_{3,4,4,5}$	-1.01	$F_{4,4,4,5}$	-1.03	$F_{1,1,5,5}$	-0.36	$F_{1,2,5,5}$	0.71
$F_{2,2,5,5}$	-0.18	$F_{1,3,5,5}$	0.28	$F_{2,3,5,5}$	-0.49	$F_{3,3,5,5}$	-0.16	$F_{1,4,5,5}$	0.34
$F_{2,4,5,5}$	-0.69	$F_{3,4,5,5}$	-0.26	$F_{4,4,5,5}$	-0.64	$F_{1,5,5,5}$	-0.81	$F_{2,5,5,5}$	0.23
$F_{3,5,5,5}$	0.58	$F_{4,5,5,5}$	0.93	$F_{5,5,5,5}$	2.02	$F_{1,1,1,6}$	2.27	$F_{1,1,2,6}$	-1.02
$F_{1,2,2,6}$	-0.28	$F_{2,2,2,6}$	0.40	$F_{1,1,3,6}$	-1.61	$F_{1,2,3,6}$	0.56	$F_{2,2,3,6}$	0.14
$F_{1,3,3,6}$	-0.07	$F_{2,3,3,6}$	-0.02	$F_{3,3,3,6}$	0.96	$F_{1,1,4,6}$	-2.28	$F_{1,2,4,6}$	1.00
$F_{2,2,4,6}$	0.30	$F_{1,3,4,6}$	1.63	$F_{2,3,4,6}$	-0.56	$F_{3,3,4,6}$	0.09	$F_{1,4,4,6}$	2.30
$F_{2,4,4,6}$	-1.00	$F_{3,4,4,6}$	-1.65	$F_{4,4,4,6}$	-2.33	$F_{1,1,5,6}$	1.03	$F_{1,2,5,6}$	0.25
$F_{2,2,5,6}$	-0.43	$F_{1,3,5,6}$	-0.55	$F_{2,3,5,6}$	-0.15	$F_{3,3,5,6}$	-0.02	$F_{1,4,5,6}$	-1.01
$F_{2,4,5,6}$	-0.24	$F_{3,4,5,6}$	0.56	$F_{4,4,5,6}$	0.99	$F_{1,5,5,6}$	-0.27	$F_{2,5,5,6}$	0.49
$F_{3,5,5,6}$	0.15	$F_{4,5,5,6}$	0.25	$F_{5,5,5,6}$	-0.65	$F_{1,1,6,6}$	1.64	$F_{1,2,6,6}$	-0.57
$F_{2,2,6,6}$	-0.18	$F_{1,3,6,6}$	0.07	$F_{2,3,6,6}$	0.05	$F_{3,3,6,6}$	-0.97	$F_{1,4,6,6}$	-1.66
$F_{2,4,6,6}$	0.58	$F_{3,4,6,6}$	-0.12	$F_{4,4,6,6}$	1.68	$F_{1,5,6,6}$	0.55	$F_{2,5,6,6}$	0.17
$F_{3,5,6,6}$	-0.03	$F_{4,5,6,6}$	-0.57	$F_{5,5,6,6}$	-0.51	$F_{1,6,6,6}$	-0.09	$F_{2,6,6,6}$	-0.13
$F_{3,6,6,6}$	0.99	$F_{4,6,6,6}$	0.16	$F_{5,6,6,6}$	0.14	$F_{6,6,6,6}$	-0.99	$F_{1,1,1,7}$	-0.00
$F_{1,1,2,7}$	-0.02	$F_{1,2,2,7}$	-0.02	$F_{2,2,2,7}$	-0.03	$F_{1,1,3,7}$	-0.01	$F_{1,2,3,7}$	-0.02
$F_{2,2,3,7}$	0.03	$F_{1,3,3,7}$	0.01	$F_{2,3,3,7}$	0.01	$F_{3,3,3,7}$	0.00	$F_{1,1,4,7}$	0.01
$F_{1,2,4,7}$	0.02	$F_{2,2,4,7}$	0.06	$F_{1,3,4,7}$	0.03	$F_{2,3,4,7}$	0.01	$F_{3,3,4,7}$	-0.02
$F_{1,4,4,7}$	-0.03	$F_{2,4,4,7}$	-0.08	$F_{3,4,4,7}$	-0.04	$F_{4,4,4,7}$	0.09	$F_{1,1,5,7}$	0.01
$F_{1,2,5,7}$	0.01	$F_{2,2,5,7}$	0.05	$F_{1,3,5,7}$	0.01	$F_{2,3,5,7}$	0.00	$F_{3,3,5,7}$	-0.01
$F_{1,4,5,7}$	-0.02	$F_{2,4,5,7}$	-0.02	$F_{3,4,5,7}$	-0.02	$F_{4,4,5,7}$	0.05	$F_{1,5,5,7}$	0.02
$F_{2,5,5,7}$	-0.03	$F_{3,5,5,7}$	-0.01	$F_{4,5,5,7}$	0.27	$F_{5,5,5,7}$	-0.18	$F_{1,1,6,7}$	0.01
$F_{1,2,6,7}$	0.02	$F_{2,2,6,7}$	-0.02	$F_{1,3,6,7}$	-0.01	$F_{2,3,6,7}$	-0.00	$F_{3,3,6,7}$	-0.02
$F_{1,4,6,7}$	-0.02	$F_{2,4,6,7}$	-0.01	$F_{3,4,6,7}$	0.02	$F_{4,4,6,7}$	0.03	$F_{1,5,6,7}$	-0.02
$F_{2,5,6,7}$	-0.00	$F_{3,5,6,7}$	-0.00	$F_{4,5,6,7}$	0.02	$F_{5,5,6,7}$	0.02	$F_{1,6,6,7}$	0.02
$F_{2,6,6,7}$	-0.01	$F_{3,6,6,7}$	0.04	$F_{4,6,6,7}$	-0.02	$F_{5,6,6,7}$	0.00	$F_{6,6,6,7}$	-0.06
$F_{1,1,7,7}$	-0.01	$F_{1,2,7,7}$	-0.00	$F_{2,2,7,7}$	-0.04	$F_{1,3,7,7}$	-0.01	$F_{2,3,7,7}$	0.01
$F_{3,3,7,7}$	0.01	$F_{1,4,7,7}$	0.02	$F_{2,4,7,7}$	0.06	$F_{3,4,7,7}$	0.01	$F_{4,4,7,7}$	-0.08
$F_{1,5,7,7}$	0.00	$F_{2,5,7,7}$	0.01	$F_{3,5,7,7}$	0.01	$F_{4,5,7,7}$	-0.03	$F_{5,5,7,7}$	-0.33
$F_{1,6,7,7}$	0.01	$F_{2,6,7,7}$	-0.01	$F_{3,6,7,7}$	0.00	$F_{4,6,7,7}$	-0.02	$F_{5,6,7,7}$	0.01
$F_{6,6,7,7}$	0.01	$F_{1,7,7,7}$	-0.01	$F_{2,7,7,7}$	-0.06	$F_{3,7,7,7}$	-0.00	$F_{4,7,7,7}$	0.09
$F_{5,7,7,7}$	-0.00	$F_{6,7,7,7}$	0.00	$F_{7,7,7,7}$	0.66	$F_{1,1,1,8}$	0.02	$F_{1,1,2,8}$	0.02
$F_{1,2,2,8}$	0.07	$F_{2,2,2,8}$	-0.07	$F_{1,1,3,8}$	0.02	$F_{1,2,3,8}$	-0.00	$F_{2,2,3,8}$	-0.05
$F_{1,3,3,8}$	0.01	$F_{2,3,3,8}$	0.01	$F_{3,3,3,8}$	-0.03	$F_{1,1,4,8}$	-0.03	$F_{1,2,4,8}$	-0.02
$F_{2,2,4,8}$	-0.04	$F_{1,3,4,8}$	-0.02	$F_{2,3,4,8}$	0.03	$F_{3,3,4,8}$	-0.01	$F_{1,4,4,8}$	0.03

Table A7: The CcCR Force Constants for HOOH (cont.)

$F_{2,4,4,8}$	0.05	$F_{3,4,4,8}$	0.00	$F_{4,4,4,8}$	-0.00	$F_{1,1,5,8}$	0.04	$F_{1,2,5,8}$	-0.05
$F_{2,2,5,8}$	0.00	$F_{1,3,5,8}$	-0.03	$F_{2,3,5,8}$	0.03	$F_{3,3,5,8}$	0.02	$F_{1,4,5,8}$	-0.01
$F_{2,4,5,8}$	0.06	$F_{3,4,5,8}$	0.01	$F_{4,4,5,8}$	0.27	$F_{1,5,5,8}$	0.09	$F_{2,5,5,8}$	-0.06
$F_{3,5,5,8}$	-0.09	$F_{4,5,5,8}$	-0.27	$F_{5,5,5,8}$	-2.11	$F_{1,1,6,8}$	-0.01	$F_{1,2,6,8}$	0.03
$F_{2,2,6,8}$	0.03	$F_{1,3,6,8}$	-0.01	$F_{2,3,6,8}$	0.01	$F_{3,3,6,8}$	0.03	$F_{1,4,6,8}$	0.01
$F_{2,4,6,8}$	-0.06	$F_{3,4,6,8}$	0.01	$F_{4,4,6,8}$	0.02	$F_{1,5,6,8}$	0.02	$F_{2,5,6,8}$	-0.06
$F_{3,5,6,8}$	-0.00	$F_{4,5,6,8}$	0.00	$F_{5,5,6,8}$	0.12	$F_{1,6,6,8}$	0.03	$F_{2,6,6,8}$	0.01
$F_{3,6,6,8}$	-0.02	$F_{4,6,6,8}$	-0.01	$F_{5,6,6,8}$	0.30	$F_{6,6,6,8}$	0.02	$F_{1,1,7,8}$	0.01
$F_{1,2,7,8}$	0.01	$F_{2,2,7,8}$	-0.03	$F_{1,3,7,8}$	0.00	$F_{2,3,7,8}$	-0.03	$F_{3,3,7,8}$	0.00
$F_{1,4,7,8}$	-0.01	$F_{2,4,7,8}$	-0.03	$F_{3,4,7,8}$	0.01	$F_{4,4,7,8}$	-0.03	$F_{1,5,7,8}$	-0.03
$F_{2,5,7,8}$	-0.01	$F_{3,5,7,8}$	0.01	$F_{4,5,7,8}$	-0.23	$F_{5,5,7,8}$	0.22	$F_{1,6,7,8}$	0.00
$F_{2,6,7,8}$	0.02	$F_{3,6,7,8}$	0.00	$F_{4,6,7,8}$	-0.02	$F_{5,6,7,8}$	0.01	$F_{6,6,7,8}$	-0.01
$F_{1,7,7,8}$	0.00	$F_{2,7,7,8}$	0.02	$F_{3,7,7,8}$	-0.01	$F_{4,7,7,8}$	0.05	$F_{5,7,7,8}$	0.27
$F_{6,7,7,8}$	-0.01	$F_{7,7,7,8}$	-1.03	$F_{1,1,8,8}$	-0.05	$F_{1,2,8,8}$	-0.02	$F_{2,2,8,8}$	0.06
$F_{1,3,8,8}$	0.04	$F_{2,3,8,8}$	0.02	$F_{3,3,8,8}$	-0.02	$F_{1,4,8,8}$	0.03	$F_{2,4,8,8}$	-0.02
$F_{3,4,8,8}$	-0.05	$F_{4,4,8,8}$	-0.33	$F_{1,5,8,8}$	-0.04	$F_{2,5,8,8}$	0.06	$F_{3,5,8,8}$	0.06
$F_{4,5,8,8}$	0.22	$F_{5,5,8,8}$	2.11	$F_{1,6,8,8}$	-0.05	$F_{2,6,8,8}$	0.03	$F_{3,6,8,8}$	-0.01
$F_{4,6,8,8}$	0.06	$F_{5,6,8,8}$	-0.03	$F_{6,6,8,8}$	-0.32	$F_{1,7,8,8}$	0.02	$F_{2,7,8,8}$	0.03
$F_{3,7,8,8}$	0.03	$F_{4,7,8,8}$	0.27	$F_{5,7,8,8}$	-0.27	$F_{6,7,8,8}$	-0.04	$F_{7,7,8,8}$	-0.64
$F_{1,8,8,8}$	0.06	$F_{2,8,8,8}$	-0.13	$F_{3,8,8,8}$	-0.08	$F_{4,8,8,8}$	-0.18	$F_{5,8,8,8}$	-2.11
$F_{6,8,8,8}$	0.02	$F_{7,8,8,8}$	0.93	$F_{8,8,8,8}$	2.02	$F_{1,1,1,9}$	-0.02	$F_{1,1,2,9}$	-0.01
$F_{1,2,2,9}$	0.03	$F_{2,2,2,9}$	0.00	$F_{1,1,3,9}$	0.01	$F_{1,2,3,9}$	-0.00	$F_{2,2,3,9}$	-0.00
$F_{1,3,3,9}$	0.01	$F_{2,3,3,9}$	0.03	$F_{3,3,3,9}$	-0.00	$F_{1,1,4,9}$	0.01	$F_{1,2,4,9}$	0.01
$F_{2,2,4,9}$	-0.02	$F_{1,3,4,9}$	-0.01	$F_{2,3,4,9}$	0.01	$F_{3,3,4,9}$	-0.03	$F_{1,4,4,9}$	-0.01
$F_{2,4,4,9}$	-0.01	$F_{3,4,4,9}$	0.01	$F_{4,4,4,9}$	-0.00	$F_{1,1,5,9}$	0.02	$F_{1,2,5,9}$	0.00
$F_{2,2,5,9}$	-0.03	$F_{1,3,5,9}$	0.00	$F_{2,3,5,9}$	0.01	$F_{3,3,5,9}$	-0.02	$F_{1,4,5,9}$	-0.03
$F_{2,4,5,9}$	-0.01	$F_{3,4,5,9}$	-0.01	$F_{4,4,5,9}$	0.01	$F_{1,5,5,9}$	-0.03	$F_{2,5,5,9}$	0.01
$F_{3,5,5,9}$	0.01	$F_{4,5,5,9}$	0.04	$F_{5,5,5,9}$	-0.02	$F_{1,1,6,9}$	-0.02	$F_{1,2,6,9}$	0.01
$F_{2,2,6,9}$	0.04	$F_{1,3,6,9}$	-0.01	$F_{2,3,6,9}$	-0.03	$F_{3,3,6,9}$	0.01	$F_{1,4,6,9}$	0.02
$F_{2,4,6,9}$	-0.03	$F_{3,4,6,9}$	0.03	$F_{4,4,6,9}$	-0.02	$F_{1,5,6,9}$	0.01	$F_{2,5,6,9}$	-0.02
$F_{3,5,6,9}$	0.05	$F_{4,5,6,9}$	0.02	$F_{5,5,6,9}$	0.32	$F_{1,6,6,9}$	0.02	$F_{2,6,6,9}$	0.07
$F_{3,6,6,9}$	-0.02	$F_{4,6,6,9}$	-0.04	$F_{5,6,6,9}$	-0.09	$F_{6,6,6,9}$	0.01	$F_{1,1,7,9}$	0.01
$F_{1,2,7,9}$	0.00	$F_{2,2,7,9}$	-0.01	$F_{1,3,7,9}$	0.00	$F_{2,3,7,9}$	-0.01	$F_{3,3,7,9}$	0.02
$F_{1,4,7,9}$	-0.01	$F_{2,4,7,9}$	-0.01	$F_{3,4,7,9}$	0.01	$F_{4,4,7,9}$	0.02	$F_{1,5,7,9}$	0.01
$F_{2,5,7,9}$	0.00	$F_{3,5,7,9}$	0.01	$F_{4,5,7,9}$	0.02	$F_{5,5,7,9}$	-0.06	$F_{1,6,7,9}$	0.00
$F_{2,6,7,9}$	0.02	$F_{3,6,7,9}$	-0.02	$F_{4,6,7,9}$	-0.00	$F_{5,6,7,9}$	-0.01	$F_{6,6,7,9}$	0.01
$F_{1,7,7,9}$	-0.00	$F_{2,7,7,9}$	0.01	$F_{3,7,7,9}$	-0.01	$F_{4,7,7,9}$	-0.03	$F_{5,7,7,9}$	-0.02
$F_{6,7,7,9}$	-0.02	$F_{7,7,7,9}$	2.33	$F_{1,1,8,9}$	-0.00	$F_{1,2,8,9}$	-0.03	$F_{2,2,8,9}$	0.02
$F_{1,3,8,9}$	-0.00	$F_{2,3,8,9}$	-0.01	$F_{3,3,8,9}$	-0.00	$F_{1,4,8,9}$	0.01	$F_{2,4,8,9}$	0.02
$F_{3,4,8,9}$	0.01	$F_{4,4,8,9}$	-0.01	$F_{1,5,8,9}$	0.02	$F_{2,5,8,9}$	0.02	$F_{3,5,8,9}$	-0.02
$F_{4,5,8,9}$	-0.01	$F_{5,5,8,9}$	0.03	$F_{1,6,8,9}$	-0.02	$F_{2,6,8,9}$	-0.02	$F_{3,6,8,9}$	-0.02
$F_{4,6,8,9}$	-0.01	$F_{5,6,8,9}$	-0.28	$F_{6,6,8,9}$	-0.03	$F_{1,7,8,9}$	-0.01	$F_{2,7,8,9}$	0.01
$F_{3,7,8,9}$	-0.01	$F_{4,7,8,9}$	-0.02	$F_{5,7,8,9}$	-0.00	$F_{6,7,8,9}$	0.02	$F_{7,7,8,9}$	-0.99
$F_{1,8,8,9}$	0.00	$F_{2,8,8,9}$	-0.04	$F_{3,8,8,9}$	0.04	$F_{4,8,8,9}$	-0.02	$F_{5,8,8,9}$	-0.12
$F_{6,8,8,9}$	0.32	$F_{7,8,8,9}$	-0.25	$F_{8,8,8,9}$	0.65	$F_{1,1,9,9}$	0.01	$F_{1,2,9,9}$	-0.01
$F_{2,2,9,9}$	-0.03	$F_{1,3,9,9}$	0.00	$F_{2,3,9,9}$	0.00	$F_{3,3,9,9}$	-0.00	$F_{1,4,9,9}$	-0.01
$F_{2,4,9,9}$	0.02	$F_{3,4,9,9}$	-0.00	$F_{4,4,9,9}$	0.01	$F_{1,5,9,9}$	-0.01	$F_{2,5,9,9}$	0.01
$F_{3,5,9,9}$	-0.02	$F_{4,5,9,9}$	-0.01	$F_{5,5,9,9}$	-0.32	$F_{1,6,9,9}$	-0.01	$F_{2,6,9,9}$	-0.04
$F_{3,6,9,9}$	0.02	$F_{4,6,9,9}$	-0.01	$F_{5,6,9,9}$	0.03	$F_{6,6,9,9}$	-0.00	$F_{1,7,9,9}$	-0.01

Table A8: The CcCR Force Constants for HOOH (cont.)

$F_{2,7,9,9}$	-0.00	$F_{3,7,9,9}$	0.00	$F_{4,7,9,9}$	-0.02	$F_{5,7,9,9}$	-0.01	$F_{6,7,9,9}$	0.04
$F_{7,7,9,9}$	1.68	$F_{1,8,9,9}$	0.02	$F_{2,8,9,9}$	0.04	$F_{3,8,9,9}$	0.02	$F_{4,8,9,9}$	0.00
$F_{5,8,9,9}$	0.30	$F_{6,8,9,9}$	0.09	$F_{7,8,9,9}$	-0.57	$F_{8,8,9,9}$	-0.51	$F_{1,9,9,9}$	0.01
$F_{2,9,9,9}$	0.03	$F_{3,9,9,9}$	-0.01	$F_{4,9,9,9}$	0.06	$F_{5,9,9,9}$	-0.02	$F_{6,9,9,9}$	0.01
$F_{7,9,9,9}$	-0.16	$F_{8,9,9,9}$	-0.14	$F_{9,9,9,9}$	-0.99	$F_{1,1,1,10}$	-0.00	$F_{1,1,2,10}$	0.00
$F_{1,2,2,10}$	-0.00	$F_{2,2,2,10}$	0.00	$F_{1,1,3,10}$	0.00	$F_{1,2,3,10}$	0.00	$F_{2,2,3,10}$	-0.00
$F_{1,3,3,10}$	0.00	$F_{2,3,3,10}$	-0.00	$F_{3,3,3,10}$	0.00	$F_{1,1,4,10}$	0.00	$F_{1,2,4,10}$	-0.00
$F_{2,2,4,10}$	0.00	$F_{1,3,4,10}$	-0.00	$F_{2,3,4,10}$	-0.00	$F_{3,3,4,10}$	-0.00	$F_{1,4,4,10}$	-0.00
$F_{2,4,4,10}$	-0.00	$F_{3,4,4,10}$	-0.00	$F_{4,4,4,10}$	-0.01	$F_{1,1,5,10}$	0.00	$F_{1,2,5,10}$	0.00
$F_{2,2,5,10}$	0.00	$F_{1,3,5,10}$	0.00	$F_{2,3,5,10}$	0.00	$F_{3,3,5,10}$	0.00	$F_{1,4,5,10}$	-0.00
$F_{2,4,5,10}$	-0.00	$F_{3,4,5,10}$	-0.01	$F_{4,4,5,10}$	0.00	$F_{1,5,5,10}$	-0.00	$F_{2,5,5,10}$	0.00
$F_{3,5,5,10}$	-0.01	$F_{4,5,5,10}$	0.02	$F_{5,5,5,10}$	0.06	$F_{1,1,6,10}$	-0.00	$F_{1,2,6,10}$	-0.00
$F_{2,2,6,10}$	-0.00	$F_{1,3,6,10}$	-0.00	$F_{2,3,6,10}$	0.00	$F_{3,3,6,10}$	-0.00	$F_{1,4,6,10}$	0.00
$F_{2,4,6,10}$	0.00	$F_{3,4,6,10}$	0.00	$F_{4,4,6,10}$	0.00	$F_{1,5,6,10}$	-0.00	$F_{2,5,6,10}$	-0.00
$F_{3,5,6,10}$	-0.00	$F_{4,5,6,10}$	0.01	$F_{5,5,6,10}$	-0.00	$F_{1,6,6,10}$	0.00	$F_{2,6,6,10}$	-0.00
$F_{3,6,6,10}$	0.00	$F_{4,6,6,10}$	-0.01	$F_{5,6,6,10}$	0.02	$F_{6,6,6,10}$	-0.01	$F_{1,1,7,10}$	0.00
$F_{1,2,7,10}$	-0.00	$F_{2,2,7,10}$	-0.00	$F_{1,3,7,10}$	0.00	$F_{2,3,7,10}$	-0.00	$F_{3,3,7,10}$	0.00
$F_{1,4,7,10}$	0.00	$F_{2,4,7,10}$	0.00	$F_{3,4,7,10}$	-0.00	$F_{4,4,7,10}$	0.02	$F_{1,5,7,10}$	0.01
$F_{2,5,7,10}$	0.00	$F_{3,5,7,10}$	0.00	$F_{4,5,7,10}$	-0.01	$F_{5,5,7,10}$	0.03	$F_{1,6,7,10}$	-0.00
$F_{2,6,7,10}$	-0.00	$F_{3,6,7,10}$	-0.00	$F_{4,6,7,10}$	0.01	$F_{5,6,7,10}$	-0.01	$F_{6,6,7,10}$	-0.01
$F_{1,7,7,10}$	-0.00	$F_{2,7,7,10}$	0.01	$F_{3,7,7,10}$	-0.00	$F_{4,7,7,10}$	-0.03	$F_{5,7,7,10}$	0.03
$F_{6,7,7,10}$	0.01	$F_{7,7,7,10}$	-0.74	$F_{1,1,8,10}$	-0.00	$F_{1,2,8,10}$	-0.00	$F_{2,2,8,10}$	-0.00
$F_{1,3,8,10}$	-0.00	$F_{2,3,8,10}$	0.00	$F_{3,3,8,10}$	0.00	$F_{1,4,8,10}$	0.01	$F_{2,4,8,10}$	-0.00
$F_{3,4,8,10}$	0.01	$F_{4,4,8,10}$	0.00	$F_{1,5,8,10}$	0.00	$F_{2,5,8,10}$	-0.00	$F_{3,5,8,10}$	0.01
$F_{4,5,8,10}$	-0.03	$F_{5,5,8,10}$	-0.04	$F_{1,6,8,10}$	0.00	$F_{2,6,8,10}$	0.00	$F_{3,6,8,10}$	0.00
$F_{4,6,8,10}$	-0.01	$F_{5,6,8,10}$	-0.02	$F_{6,6,8,10}$	-0.01	$F_{1,7,8,10}$	-0.00	$F_{2,7,8,10}$	0.00
$F_{3,7,8,10}$	0.00	$F_{4,7,8,10}$	-0.02	$F_{5,7,8,10}$	-0.01	$F_{6,7,8,10}$	0.03	$F_{7,7,8,10}$	0.97
$F_{1,8,8,10}$	-0.00	$F_{2,8,8,10}$	0.01	$F_{3,8,8,10}$	-0.02	$F_{4,8,8,10}$	0.02	$F_{5,8,8,10}$	0.09
$F_{6,8,8,10}$	0.03	$F_{7,8,8,10}$	0.34	$F_{8,8,8,10}$	-0.81	$F_{1,1,9,10}$	-0.00	$F_{1,2,9,10}$	-0.00
$F_{2,2,9,10}$	0.00	$F_{1,3,9,10}$	0.00	$F_{2,3,9,10}$	0.00	$F_{3,3,9,10}$	-0.00	$F_{1,4,9,10}$	0.00
$F_{2,4,9,10}$	0.00	$F_{3,4,9,10}$	-0.00	$F_{4,4,9,10}$	-0.01	$F_{1,5,9,10}$	-0.00	$F_{2,5,9,10}$	-0.00
$F_{3,5,9,10}$	-0.00	$F_{4,5,9,10}$	-0.00	$F_{5,5,9,10}$	0.05	$F_{1,6,9,10}$	-0.00	$F_{2,6,9,10}$	-0.00
$F_{3,6,9,10}$	0.00	$F_{4,6,9,10}$	0.00	$F_{5,6,9,10}$	-0.02	$F_{6,6,9,10}$	0.01	$F_{1,7,9,10}$	-0.00
$F_{2,7,9,10}$	-0.00	$F_{3,7,9,10}$	0.00	$F_{4,7,9,10}$	0.02	$F_{5,7,9,10}$	-0.01	$F_{6,7,9,10}$	0.02
$F_{7,7,9,10}$	-2.30	$F_{1,8,9,10}$	0.00	$F_{2,8,9,10}$	-0.00	$F_{3,8,9,10}$	0.00	$F_{4,8,9,10}$	0.02
$F_{5,8,9,10}$	-0.02	$F_{6,8,9,10}$	0.01	$F_{7,8,9,10}$	1.01	$F_{8,8,9,10}$	0.27	$F_{1,9,9,10}$	0.00
$F_{2,9,9,10}$	-0.01	$F_{3,9,9,10}$	0.00	$F_{4,9,9,10}$	0.02	$F_{5,9,9,10}$	0.03	$F_{6,9,9,10}$	-0.02
$F_{7,9,9,10}$	-1.66	$F_{8,9,9,10}$	0.55	$F_{9,9,9,10}$	0.09	$F_{1,1,10,10}$	-0.00	$F_{1,2,10,10}$	-0.00
$F_{2,2,10,10}$	0.00	$F_{1,3,10,10}$	-0.00	$F_{2,3,10,10}$	-0.00	$F_{3,3,10,10}$	-0.00	$F_{1,4,10,10}$	0.00
$F_{2,4,10,10}$	0.00	$F_{3,4,10,10}$	0.00	$F_{4,4,10,10}$	-0.01	$F_{1,5,10,10}$	-0.00	$F_{2,5,10,10}$	-0.00
$F_{3,5,10,10}$	0.00	$F_{4,5,10,10}$	0.01	$F_{5,5,10,10}$	-0.05	$F_{1,6,10,10}$	0.00	$F_{2,6,10,10}$	0.00
$F_{3,6,10,10}$	0.00	$F_{4,6,10,10}$	-0.01	$F_{5,6,10,10}$	0.00	$F_{6,6,10,10}$	0.01	$F_{1,7,10,10}$	0.00
$F_{2,7,10,10}$	-0.01	$F_{3,7,10,10}$	0.00	$F_{4,7,10,10}$	0.01	$F_{5,7,10,10}$	-0.03	$F_{6,7,10,10}$	-0.01
$F_{7,7,10,10}$	0.78	$F_{1,8,10,10}$	0.00	$F_{2,8,10,10}$	-0.00	$F_{3,8,10,10}$	-0.00	$F_{4,8,10,10}$	0.01
$F_{5,8,10,10}$	0.04	$F_{6,8,10,10}$	-0.02	$F_{7,8,10,10}$	-0.95	$F_{8,8,10,10}$	-0.36	$F_{1,9,10,10}$	0.00
$F_{2,9,10,10}$	0.00	$F_{3,9,10,10}$	-0.00	$F_{4,9,10,10}$	-0.01	$F_{5,9,10,10}$	0.01	$F_{6,9,10,10}$	-0.02
$F_{7,9,10,10}$	2.28	$F_{8,9,10,10}$	-1.03	$F_{9,9,10,10}$	1.64	$F_{1,10,10,10}$	-0.00	$F_{2,10,10,10}$	0.00
$F_{3,10,10,10}$	-0.00	$F_{4,10,10,10}$	-0.00	$F_{5,10,10,10}$	0.02	$F_{6,10,10,10}$	0.02	$F_{7,10,10,10}$	-0.80
$F_{8,10,10,10}$	0.95	$F_{9,10,10,10}$	-2.27	$F_{10,10,10,10}$	0.80	$F_{1,1,1,11}$	0.00	$F_{1,1,2,11}$	0.00

Table A9: The CcCR Force Constants for HOOH (cont.)

$F_{1,2,2,11}$	0.00	$F_{2,2,2,11}$	0.01	$F_{1,1,3,11}$	0.00	$F_{1,2,3,11}$	0.00	$F_{2,2,3,11}$	-0.00
$F_{1,3,3,11}$	-0.00	$F_{2,3,3,11}$	-0.00	$F_{3,3,3,11}$	-0.00	$F_{1,1,4,11}$	-0.01	$F_{1,2,4,11}$	-0.00
$F_{2,2,4,11}$	-0.01	$F_{1,3,4,11}$	-0.00	$F_{2,3,4,11}$	-0.00	$F_{3,3,4,11}$	0.01	$F_{1,4,4,11}$	0.01
$F_{2,4,4,11}$	0.01	$F_{3,4,4,11}$	0.00	$F_{4,4,4,11}$	-0.06	$F_{1,1,5,11}$	-0.00	$F_{1,2,5,11}$	-0.00
$F_{2,2,5,11}$	-0.01	$F_{1,3,5,11}$	-0.00	$F_{2,3,5,11}$	0.00	$F_{3,3,5,11}$	0.01	$F_{1,4,5,11}$	0.00
$F_{2,4,5,11}$	0.01	$F_{3,4,5,11}$	0.01	$F_{4,4,5,11}$	0.02	$F_{1,5,5,11}$	0.01	$F_{2,5,5,11}$	0.01
$F_{3,5,5,11}$	0.00	$F_{4,5,5,11}$	0.03	$F_{5,5,5,11}$	-0.13	$F_{1,1,6,11}$	-0.00	$F_{1,2,6,11}$	-0.00
$F_{2,2,6,11}$	-0.00	$F_{1,3,6,11}$	0.00	$F_{2,3,6,11}$	0.00	$F_{3,3,6,11}$	0.00	$F_{1,4,6,11}$	0.00
$F_{2,4,6,11}$	0.01	$F_{3,4,6,11}$	-0.01	$F_{4,4,6,11}$	-0.01	$F_{1,5,6,11}$	0.00	$F_{2,5,6,11}$	0.00
$F_{3,5,6,11}$	-0.01	$F_{4,5,6,11}$	-0.01	$F_{5,5,6,11}$	0.04	$F_{1,6,6,11}$	-0.01	$F_{2,6,6,11}$	-0.01
$F_{3,6,6,11}$	-0.01	$F_{4,6,6,11}$	-0.00	$F_{5,6,6,11}$	0.04	$F_{6,6,6,11}$	-0.03	$F_{1,1,7,11}$	0.00
$F_{1,2,7,11}$	0.00	$F_{2,2,7,11}$	0.01	$F_{1,3,7,11}$	0.00	$F_{2,3,7,11}$	0.00	$F_{3,3,7,11}$	-0.00
$F_{1,4,7,11}$	0.00	$F_{2,4,7,11}$	-0.01	$F_{3,4,7,11}$	-0.00	$F_{4,4,7,11}$	0.06	$F_{1,5,7,11}$	-0.00
$F_{2,5,7,11}$	-0.01	$F_{3,5,7,11}$	-0.00	$F_{4,5,7,11}$	-0.03	$F_{5,5,7,11}$	-0.02	$F_{1,6,7,11}$	-0.00
$F_{2,6,7,11}$	-0.00	$F_{3,6,7,11}$	0.00	$F_{4,6,7,11}$	0.01	$F_{5,6,7,11}$	-0.02	$F_{6,6,7,11}$	0.02
$F_{1,7,7,11}$	-0.00	$F_{2,7,7,11}$	0.01	$F_{3,7,7,11}$	0.00	$F_{4,7,7,11}$	-0.08	$F_{5,7,7,11}$	0.05
$F_{6,7,7,11}$	0.01	$F_{7,7,7,11}$	1.09	$F_{1,1,8,11}$	-0.00	$F_{1,2,8,11}$	0.00	$F_{2,2,8,11}$	0.01
$F_{1,3,8,11}$	-0.00	$F_{2,3,8,11}$	0.00	$F_{3,3,8,11}$	-0.00	$F_{1,4,8,11}$	0.00	$F_{2,4,8,11}$	-0.01
$F_{3,4,8,11}$	0.00	$F_{4,4,8,11}$	0.01	$F_{1,5,8,11}$	-0.00	$F_{2,5,8,11}$	-0.01	$F_{3,5,8,11}$	-0.00
$F_{4,5,8,11}$	-0.01	$F_{5,5,8,11}$	0.06	$F_{1,6,8,11}$	0.00	$F_{2,6,8,11}$	0.00	$F_{3,6,8,11}$	0.00
$F_{4,6,8,11}$	-0.00	$F_{5,6,8,11}$	-0.02	$F_{6,6,8,11}$	0.01	$F_{1,7,8,11}$	-0.00	$F_{2,7,8,11}$	0.01
$F_{3,7,8,11}$	-0.01	$F_{4,7,8,11}$	-0.02	$F_{5,7,8,11}$	0.06	$F_{6,7,8,11}$	0.01	$F_{7,7,8,11}$	0.35
$F_{1,8,8,11}$	0.00	$F_{2,8,8,11}$	0.01	$F_{3,8,8,11}$	0.00	$F_{4,8,8,11}$	-0.03	$F_{5,8,8,11}$	-0.06
$F_{6,8,8,11}$	-0.01	$F_{7,8,8,11}$	-0.69	$F_{8,8,8,11}$	0.23	$F_{1,1,9,11}$	-0.00	$F_{1,2,9,11}$	-0.00
$F_{2,2,9,11}$	0.00	$F_{1,3,9,11}$	0.00	$F_{2,3,9,11}$	0.00	$F_{3,3,9,11}$	-0.00	$F_{1,4,9,11}$	0.00
$F_{2,4,9,11}$	0.00	$F_{3,4,9,11}$	-0.00	$F_{4,4,9,11}$	0.01	$F_{1,5,9,11}$	-0.00	$F_{2,5,9,11}$	-0.00
$F_{3,5,9,11}$	-0.00	$F_{4,5,9,11}$	-0.02	$F_{5,5,9,11}$	-0.03	$F_{1,6,9,11}$	-0.00	$F_{2,6,9,11}$	-0.00
$F_{3,6,9,11}$	0.00	$F_{4,6,9,11}$	0.02	$F_{5,6,9,11}$	-0.02	$F_{6,6,9,11}$	0.04	$F_{1,7,9,11}$	-0.00
$F_{2,7,9,11}$	-0.01	$F_{3,7,9,11}$	0.00	$F_{4,7,9,11}$	0.01	$F_{5,7,9,11}$	0.06	$F_{6,7,9,11}$	-0.03
$F_{7,7,9,11}$	1.00	$F_{1,8,9,11}$	0.00	$F_{2,8,9,11}$	-0.00	$F_{3,8,9,11}$	-0.00	$F_{4,8,9,11}$	0.00
$F_{5,8,9,11}$	0.06	$F_{6,8,9,11}$	-0.02	$F_{7,8,9,11}$	0.24	$F_{8,8,9,11}$	-0.49	$F_{1,9,9,11}$	-0.00
$F_{2,9,9,11}$	-0.01	$F_{3,9,9,11}$	-0.00	$F_{4,9,9,11}$	-0.01	$F_{5,9,9,11}$	0.01	$F_{6,9,9,11}$	-0.07
$F_{7,9,9,11}$	0.58	$F_{8,9,9,11}$	0.17	$F_{9,9,9,11}$	0.13	$F_{1,1,10,11}$	-0.00	$F_{1,2,10,11}$	0.00
$F_{2,2,10,11}$	0.00	$F_{1,3,10,11}$	-0.00	$F_{2,3,10,11}$	-0.00	$F_{3,3,10,11}$	-0.00	$F_{1,4,10,11}$	-0.00
$F_{2,4,10,11}$	0.00	$F_{3,4,10,11}$	0.00	$F_{4,4,10,11}$	-0.00	$F_{1,5,10,11}$	-0.00	$F_{2,5,10,11}$	0.00
$F_{3,5,10,11}$	-0.00	$F_{4,5,10,11}$	0.01	$F_{5,5,10,11}$	-0.02	$F_{1,6,10,11}$	0.00	$F_{2,6,10,11}$	0.00
$F_{3,6,10,11}$	0.00	$F_{4,6,10,11}$	-0.00	$F_{5,6,10,11}$	0.03	$F_{6,6,10,11}$	-0.01	$F_{1,7,10,11}$	-0.00
$F_{2,7,10,11}$	-0.00	$F_{3,7,10,11}$	-0.00	$F_{4,7,10,11}$	0.02	$F_{5,7,10,11}$	-0.02	$F_{6,7,10,11}$	-0.01
$F_{7,7,10,11}$	-1.01	$F_{1,8,10,11}$	0.00	$F_{2,8,10,11}$	-0.00	$F_{3,8,10,11}$	0.01	$F_{4,8,10,11}$	0.01
$F_{5,8,10,11}$	-0.05	$F_{6,8,10,11}$	-0.00	$F_{7,8,10,11}$	-0.33	$F_{8,8,10,11}$	0.71	$F_{1,9,10,11}$	0.00
$F_{2,9,10,11}$	0.00	$F_{3,9,10,11}$	0.00	$F_{4,9,10,11}$	-0.02	$F_{5,9,10,11}$	-0.03	$F_{6,9,10,11}$	0.01
$F_{7,9,10,11}$	-1.00	$F_{8,9,10,11}$	-0.25	$F_{9,9,10,11}$	-0.57	$F_{1,10,10,11}$	0.00	$F_{2,10,10,11}$	0.00
$F_{3,10,10,11}$	0.00	$F_{4,10,10,11}$	-0.02	$F_{5,10,10,11}$	0.02	$F_{6,10,10,11}$	0.01	$F_{7,10,10,11}$	0.98
$F_{8,10,10,11}$	0.32	$F_{9,10,10,11}$	1.02	$F_{10,10,10,11}$	-0.97	$F_{1,1,11,11}$	0.00	$F_{1,2,11,11}$	0.00
$F_{2,2,11,11}$	-0.01	$F_{1,3,11,11}$	0.00	$F_{2,3,11,11}$	0.00	$F_{3,3,11,11}$	0.00	$F_{1,4,11,11}$	-0.00
$F_{2,4,11,11}$	0.01	$F_{3,4,11,11}$	-0.00	$F_{4,4,11,11}$	-0.04	$F_{1,5,11,11}$	-0.00	$F_{2,5,11,11}$	0.01
$F_{3,5,11,11}$	0.00	$F_{4,5,11,11}$	-0.03	$F_{5,5,11,11}$	0.06	$F_{1,6,11,11}$	-0.00	$F_{2,6,11,11}$	-0.00
$F_{3,6,11,11}$	-0.00	$F_{4,6,11,11}$	0.01	$F_{5,6,11,11}$	-0.02	$F_{6,6,11,11}$	-0.03	$F_{1,7,11,11}$	0.00
$F_{2,7,11,11}$	-0.01	$F_{3,7,11,11}$	0.00	$F_{4,7,11,11}$	0.06	$F_{5,7,11,11}$	-0.04	$F_{6,7,11,11}$	0.02

Table A10: The CcCR Force Constants for HOOH (cont.)

$F_{7,7,11,11}$	-0.42	$F_{1,8,11,11}$	0.00	$F_{2,8,11,11}$	-0.01	$F_{3,8,11,11}$	-0.00	$F_{4,8,11,11}$	0.05
$F_{5,8,11,11}$	0.00	$F_{6,8,11,11}$	0.03	$F_{7,8,11,11}$	0.62	$F_{8,8,11,11}$	-0.18	$F_{1,9,11,11}$	0.00
$F_{2,9,11,11}$	0.00	$F_{3,9,11,11}$	0.00	$F_{4,9,11,11}$	0.02	$F_{5,9,11,11}$	-0.03	$F_{6,9,11,11}$	0.04
$F_{7,9,11,11}$	-0.30	$F_{8,9,11,11}$	0.43	$F_{9,9,11,11}$	-0.18	$F_{1,10,11,11}$	-0.00	$F_{2,10,11,11}$	0.00
$F_{3,10,11,11}$	-0.00	$F_{4,10,11,11}$	-0.02	$F_{5,10,11,11}$	0.07	$F_{6,10,11,11}$	-0.03	$F_{7,10,11,11}$	0.35
$F_{8,10,11,11}$	-0.67	$F_{9,10,11,11}$	0.28	$F_{10,10,11,11}$	-0.34	$F_{1,11,11,11}$	0.00	$F_{2,11,11,11}$	0.01
$F_{3,11,11,11}$	-0.00	$F_{4,11,11,11}$	-0.03	$F_{5,11,11,11}$	-0.07	$F_{6,11,11,11}$	-0.00	$F_{7,11,11,11}$	-0.57
$F_{8,11,11,11}$	0.18	$F_{9,11,11,11}$	-0.40	$F_{10,11,11,11}$	0.59	$F_{11,11,11,11}$	-0.11	$F_{1,1,1,12}$	0.00
$F_{1,1,2,12}$	-0.00	$F_{1,2,2,12}$	0.00	$F_{2,2,2,12}$	0.00	$F_{1,1,3,12}$	0.00	$F_{1,2,3,12}$	-0.00
$F_{2,2,3,12}$	0.00	$F_{1,3,3,12}$	-0.00	$F_{2,3,3,12}$	0.00	$F_{3,3,3,12}$	-0.00	$F_{1,1,4,12}$	-0.00
$F_{1,2,4,12}$	0.00	$F_{2,2,4,12}$	-0.00	$F_{1,3,4,12}$	-0.00	$F_{2,3,4,12}$	-0.00	$F_{3,3,4,12}$	0.00
$F_{1,4,4,12}$	0.00	$F_{2,4,4,12}$	-0.00	$F_{3,4,4,12}$	0.01	$F_{4,4,4,12}$	0.00	$F_{1,1,5,12}$	0.00
$F_{1,2,5,12}$	-0.01	$F_{2,2,5,12}$	0.00	$F_{1,3,5,12}$	-0.00	$F_{2,3,5,12}$	0.00	$F_{3,3,5,12}$	-0.00
$F_{1,4,5,12}$	-0.00	$F_{2,4,5,12}$	0.01	$F_{3,4,5,12}$	0.00	$F_{4,4,5,12}$	0.01	$F_{1,5,5,12}$	0.02
$F_{2,5,5,12}$	-0.00	$F_{3,5,5,12}$	-0.01	$F_{4,5,5,12}$	-0.03	$F_{5,5,5,12}$	0.08	$F_{1,1,6,12}$	-0.00
$F_{1,2,6,12}$	0.00	$F_{2,2,6,12}$	0.00	$F_{1,3,6,12}$	0.00	$F_{2,3,6,12}$	-0.00	$F_{3,3,6,12}$	0.00
$F_{1,4,6,12}$	0.00	$F_{2,4,6,12}$	0.00	$F_{3,4,6,12}$	-0.00	$F_{4,4,6,12}$	-0.01	$F_{1,5,6,12}$	0.00
$F_{2,5,6,12}$	-0.00	$F_{3,5,6,12}$	0.00	$F_{4,5,6,12}$	-0.01	$F_{5,5,6,12}$	0.04	$F_{1,6,6,12}$	-0.00
$F_{2,6,6,12}$	0.00	$F_{3,6,6,12}$	-0.00	$F_{4,6,6,12}$	-0.00	$F_{5,6,6,12}$	-0.02	$F_{6,6,6,12}$	-0.01
$F_{1,1,7,12}$	-0.00	$F_{1,2,7,12}$	-0.00	$F_{2,2,7,12}$	0.00	$F_{1,3,7,12}$	0.00	$F_{2,3,7,12}$	0.00
$F_{3,3,7,12}$	-0.00	$F_{1,4,7,12}$	0.00	$F_{2,4,7,12}$	0.00	$F_{3,4,7,12}$	-0.01	$F_{4,4,7,12}$	-0.01
$F_{1,5,7,12}$	-0.01	$F_{2,5,7,12}$	-0.00	$F_{3,5,7,12}$	-0.00	$F_{4,5,7,12}$	-0.01	$F_{5,5,7,12}$	0.05
$F_{1,6,7,12}$	-0.00	$F_{2,6,7,12}$	-0.00	$F_{3,6,7,12}$	0.00	$F_{4,6,7,12}$	0.01	$F_{5,6,7,12}$	0.01
$F_{6,6,7,12}$	0.00	$F_{1,7,7,12}$	0.00	$F_{2,7,7,12}$	-0.00	$F_{3,7,7,12}$	0.01	$F_{4,7,7,12}$	0.04
$F_{5,7,7,12}$	-0.00	$F_{6,7,7,12}$	0.01	$F_{7,7,7,12}$	-2.33	$F_{1,1,8,12}$	-0.00	$F_{1,2,8,12}$	0.00
$F_{2,2,8,12}$	-0.00	$F_{1,3,8,12}$	0.00	$F_{2,3,8,12}$	0.00	$F_{3,3,8,12}$	0.00	$F_{1,4,8,12}$	-0.00
$F_{2,4,8,12}$	0.00	$F_{3,4,8,12}$	-0.00	$F_{4,4,8,12}$	-0.01	$F_{1,5,8,12}$	-0.01	$F_{2,5,8,12}$	0.00
$F_{3,5,8,12}$	0.00	$F_{4,5,8,12}$	-0.01	$F_{5,5,8,12}$	-0.06	$F_{1,6,8,12}$	-0.00	$F_{2,6,8,12}$	-0.00
$F_{3,6,8,12}$	-0.00	$F_{4,6,8,12}$	0.01	$F_{5,6,8,12}$	-0.02	$F_{6,6,8,12}$	0.02	$F_{1,7,8,12}$	0.01
$F_{2,7,8,12}$	-0.01	$F_{3,7,8,12}$	0.00	$F_{4,7,8,12}$	0.02	$F_{5,7,8,12}$	-0.01	$F_{6,7,8,12}$	-0.01
$F_{7,7,8,12}$	1.01	$F_{1,8,8,12}$	0.01	$F_{2,8,8,12}$	-0.00	$F_{3,8,8,12}$	-0.01	$F_{4,8,8,12}$	0.01
$F_{5,8,8,12}$	0.09	$F_{6,8,8,12}$	0.01	$F_{7,8,8,12}$	0.26	$F_{8,8,8,12}$	-0.58	$F_{1,1,9,12}$	0.00
$F_{1,2,9,12}$	0.00	$F_{2,2,9,12}$	-0.00	$F_{1,3,9,12}$	0.00	$F_{2,3,9,12}$	-0.00	$F_{3,3,9,12}$	0.00
$F_{1,4,9,12}$	-0.00	$F_{2,4,9,12}$	0.00	$F_{3,4,9,12}$	-0.00	$F_{4,4,9,12}$	0.00	$F_{1,5,9,12}$	0.00
$F_{2,5,9,12}$	0.00	$F_{3,5,9,12}$	0.00	$F_{4,5,9,12}$	0.00	$F_{5,5,9,12}$	-0.01	$F_{1,6,9,12}$	-0.00
$F_{2,6,9,12}$	-0.00	$F_{3,6,9,12}$	-0.00	$F_{4,6,9,12}$	0.02	$F_{5,6,9,12}$	0.02	$F_{6,6,9,12}$	0.02
$F_{1,7,9,12}$	0.00	$F_{2,7,9,12}$	-0.01	$F_{3,7,9,12}$	0.00	$F_{4,7,9,12}$	0.02	$F_{5,7,9,12}$	0.01
$F_{6,7,9,12}$	-0.03	$F_{7,7,9,12}$	-1.65	$F_{1,8,9,12}$	-0.00	$F_{2,8,9,12}$	-0.01	$F_{3,8,9,12}$	-0.00
$F_{4,8,9,12}$	-0.00	$F_{5,8,9,12}$	-0.00	$F_{6,8,9,12}$	-0.05	$F_{7,8,9,12}$	0.56	$F_{8,8,9,12}$	0.15
$F_{1,9,9,12}$	-0.00	$F_{2,9,9,12}$	0.01	$F_{3,9,9,12}$	-0.00	$F_{4,9,9,12}$	-0.04	$F_{5,9,9,12}$	0.02
$F_{6,9,9,12}$	-0.02	$F_{7,9,9,12}$	0.12	$F_{8,9,9,12}$	0.03	$F_{9,9,9,12}$	0.99	$F_{1,1,10,12}$	0.00
$F_{1,2,10,12}$	0.00	$F_{2,2,10,12}$	-0.00	$F_{1,3,10,12}$	-0.00	$F_{2,3,10,12}$	-0.00	$F_{3,3,10,12}$	0.00
$F_{1,4,10,12}$	-0.00	$F_{2,4,10,12}$	-0.00	$F_{3,4,10,12}$	0.00	$F_{4,4,10,12}$	0.01	$F_{1,5,10,12}$	0.00
$F_{2,5,10,12}$	0.00	$F_{3,5,10,12}$	0.00	$F_{4,5,10,12}$	-0.00	$F_{5,5,10,12}$	-0.04	$F_{1,6,10,12}$	0.00
$F_{2,6,10,12}$	0.00	$F_{3,6,10,12}$	-0.00	$F_{4,6,10,12}$	0.00	$F_{5,6,10,12}$	-0.00	$F_{6,6,10,12}$	-0.00
$F_{1,7,10,12}$	0.00	$F_{2,7,10,12}$	0.00	$F_{3,7,10,12}$	-0.00	$F_{4,7,10,12}$	-0.03	$F_{5,7,10,12}$	0.02
$F_{6,7,10,12}$	-0.01	$F_{7,7,10,12}$	2.29	$F_{1,8,10,12}$	-0.00	$F_{2,8,10,12}$	0.00	$F_{3,8,10,12}$	-0.00
$F_{4,8,10,12}$	-0.01	$F_{5,8,10,12}$	0.03	$F_{6,8,10,12}$	0.00	$F_{7,8,10,12}$	-1.04	$F_{8,8,10,12}$	-0.28
$F_{1,9,10,12}$	-0.00	$F_{2,9,10,12}$	0.00	$F_{3,9,10,12}$	-0.00	$F_{4,9,10,12}$	-0.01	$F_{5,9,10,12}$	-0.01

Table A11: The CcCR Force Constants for HOOH (cont.)

$F_{6,9,10,12}$	0.01	$F_{7,9,10,12}$	1.63	$F_{8,9,10,12}$	-0.55	$F_{9,9,10,12}$	-0.07	$F_{1,10,10,12}$	-0.00
$F_{2,10,10,12}$	-0.00	$F_{3,10,10,12}$	0.00	$F_{4,10,10,12}$	0.01	$F_{5,10,10,12}$	-0.02	$F_{6,10,10,12}$	0.01
$F_{7,10,10,12}$	-2.27	$F_{8,10,10,12}$	1.06	$F_{9,10,10,12}$	-1.61	$F_{10,10,10,12}$	2.25	$F_{1,1,11,12}$	0.00
$F_{1,2,11,12}$	0.00	$F_{2,2,11,12}$	-0.00	$F_{1,3,11,12}$	-0.00	$F_{2,3,11,12}$	-0.00	$F_{3,3,11,12}$	-0.00
$F_{1,4,11,12}$	0.00	$F_{2,4,11,12}$	-0.00	$F_{3,4,11,12}$	0.00	$F_{4,4,11,12}$	-0.01	$F_{1,5,11,12}$	-0.00
$F_{2,5,11,12}$	-0.00	$F_{3,5,11,12}$	0.00	$F_{4,5,11,12}$	0.03	$F_{5,5,11,12}$	-0.02	$F_{1,6,11,12}$	0.00
$F_{2,6,11,12}$	0.00	$F_{3,6,11,12}$	0.00	$F_{4,6,11,12}$	-0.01	$F_{5,6,11,12}$	-0.01	$F_{6,6,11,12}$	-0.00
$F_{1,7,11,12}$	0.00	$F_{2,7,11,12}$	0.00	$F_{3,7,11,12}$	-0.00	$F_{4,7,11,12}$	-0.01	$F_{5,7,11,12}$	-0.03
$F_{6,7,11,12}$	0.01	$F_{7,7,11,12}$	-1.01	$F_{1,8,11,12}$	-0.00	$F_{2,8,11,12}$	-0.00	$F_{3,8,11,12}$	0.00
$F_{4,8,11,12}$	-0.00	$F_{5,8,11,12}$	-0.03	$F_{6,8,11,12}$	0.01	$F_{7,8,11,12}$	-0.24	$F_{8,8,11,12}$	0.49
$F_{1,9,11,12}$	0.00	$F_{2,9,11,12}$	0.00	$F_{3,9,11,12}$	0.00	$F_{4,9,11,12}$	-0.00	$F_{5,9,11,12}$	0.01
$F_{6,9,11,12}$	0.03	$F_{7,9,11,12}$	-0.56	$F_{8,9,11,12}$	-0.15	$F_{9,9,11,12}$	-0.05	$F_{1,10,11,12}$	-0.00
$F_{2,10,11,12}$	-0.00	$F_{3,10,11,12}$	-0.00	$F_{4,10,11,12}$	0.02	$F_{5,10,11,12}$	0.00	$F_{6,10,11,12}$	-0.00
$F_{7,10,11,12}$	1.02	$F_{8,10,11,12}$	0.25	$F_{9,10,11,12}$	0.56	$F_{10,10,11,12}$	-1.04	$F_{1,11,11,12}$	0.00
$F_{2,11,11,12}$	0.00	$F_{3,11,11,12}$	0.00	$F_{4,11,11,12}$	-0.03	$F_{5,11,11,12}$	0.05	$F_{6,11,11,12}$	-0.00
$F_{7,11,11,12}$	0.27	$F_{8,11,11,12}$	-0.46	$F_{9,11,11,12}$	0.14	$F_{10,11,11,12}$	-0.25	$F_{11,11,11,12}$	0.40
$F_{1,1,12,12}$	-0.00	$F_{1,2,12,12}$	-0.00	$F_{2,2,12,12}$	0.00	$F_{1,3,12,12}$	-0.00	$F_{2,3,12,12}$	0.00
$F_{3,3,12,12}$	0.00	$F_{1,4,12,12}$	0.00	$F_{2,4,12,12}$	-0.00	$F_{3,4,12,12}$	0.00	$F_{4,4,12,12}$	0.01
$F_{1,5,12,12}$	0.00	$F_{2,5,12,12}$	-0.00	$F_{3,5,12,12}$	-0.00	$F_{4,5,12,12}$	0.00	$F_{5,5,12,12}$	-0.02
$F_{1,6,12,12}$	0.00	$F_{2,6,12,12}$	0.00	$F_{3,6,12,12}$	0.00	$F_{4,6,12,12}$	-0.02	$F_{5,6,12,12}$	0.00
$F_{6,6,12,12}$	-0.00	$F_{1,7,12,12}$	-0.00	$F_{2,7,12,12}$	0.01	$F_{3,7,12,12}$	-0.00	$F_{4,7,12,12}$	-0.02
$F_{5,7,12,12}$	-0.01	$F_{6,7,12,12}$	0.03	$F_{7,7,12,12}$	1.63	$F_{1,8,12,12}$	0.00	$F_{2,8,12,12}$	0.01
$F_{3,8,12,12}$	0.00	$F_{4,8,12,12}$	-0.01	$F_{5,8,12,12}$	0.02	$F_{6,8,12,12}$	0.02	$F_{7,8,12,12}$	-0.55
$F_{8,8,12,12}$	-0.16	$F_{1,9,12,12}$	0.00	$F_{2,9,12,12}$	-0.00	$F_{3,9,12,12}$	0.00	$F_{4,9,12,12}$	0.02
$F_{5,9,12,12}$	-0.03	$F_{6,9,12,12}$	0.01	$F_{7,9,12,12}$	-0.09	$F_{8,9,12,12}$	0.02	$F_{9,9,12,12}$	-0.97
$F_{1,10,12,12}$	0.00	$F_{2,10,12,12}$	-0.00	$F_{3,10,12,12}$	0.00	$F_{4,10,12,12}$	0.01	$F_{5,10,12,12}$	0.01
$F_{6,10,12,12}$	-0.01	$F_{7,10,12,12}$	-1.62	$F_{8,10,12,12}$	0.55	$F_{9,10,12,12}$	0.07	$F_{10,10,12,12}$	1.60
$F_{1,11,12,12}$	-0.00	$F_{2,11,12,12}$	-0.00	$F_{3,11,12,12}$	-0.00	$F_{4,11,12,12}$	0.01	$F_{5,11,12,12}$	0.01
$F_{6,11,12,12}$	-0.03	$F_{7,11,12,12}$	0.55	$F_{8,11,12,12}$	0.13	$F_{9,11,12,12}$	0.02	$F_{10,11,12,12}$	-0.56
$F_{11,11,12,12}$	-0.13	$F_{1,12,12,12}$	-0.00	$F_{2,12,12,12}$	0.00	$F_{3,12,12,12}$	-0.00	$F_{4,12,12,12}$	-0.00
$F_{5,12,12,12}$	0.03	$F_{6,12,12,12}$	-0.00	$F_{7,12,12,12}$	0.06	$F_{8,12,12,12}$	-0.04	$F_{9,12,12,12}$	0.96
$F_{10,12,12,12}$	-0.06	$F_{11,12,12,12}$	0.01	$F_{12,12,12,12}$	-0.95				

Table A12: The CcCR Force Constants for HOSH (cont.)

$F_{5,8,9}$	-0.0240	$F_{6,8,9}$	0.0387	$F_{7,8,9}$	0.0057	$F_{8,8,9}$	0.1844
$F_{1,9,9}$	0.0039	$F_{2,9,9}$	0.0017	$F_{3,9,9}$	0.0481	$F_{4,9,9}$	-0.0045
$F_{5,9,9}$	0.0457	$F_{6,9,9}$	0.7295	$F_{7,9,9}$	0.0020	$F_{8,9,9}$	-0.0133
$F_{9,9,9}$	-0.8199	$F_{1,1,10}$	0.0006	$F_{1,2,10}$	0.0020	$F_{2,2,10}$	-0.0007
$F_{1,3,10}$	-0.0004	$F_{2,3,10}$	0.0002	$F_{3,3,10}$	0.0000	$F_{1,4,10}$	-0.0010
$F_{2,4,10}$	-0.0032	$F_{3,4,10}$	0.0008	$F_{4,4,10}$	0.0012	$F_{1,5,10}$	-0.0022
$F_{2,5,10}$	0.0026	$F_{3,5,10}$	-0.0010	$F_{4,5,10}$	-0.0062	$F_{5,5,10}$	-0.0050
$F_{1,6,10}$	0.0002	$F_{2,6,10}$	0.0036	$F_{3,6,10}$	-0.0000	$F_{4,6,10}$	0.0055
$F_{5,6,10}$	-0.0052	$F_{6,6,10}$	0.0021	$F_{1,7,10}$	0.0004	$F_{2,7,10}$	0.0016
$F_{3,7,10}$	-0.0006	$F_{4,7,10}$	0.0000	$F_{5,7,10}$	0.0098	$F_{6,7,10}$	-0.0072
$F_{7,7,10}$	-0.0032	$F_{1,8,10}$	0.0004	$F_{2,8,10}$	-0.0027	$F_{3,8,10}$	0.0017
$F_{4,8,10}$	0.0127	$F_{5,8,10}$	0.0033	$F_{6,8,10}$	0.0016	$F_{7,8,10}$	-0.1155
$F_{8,8,10}$	0.0077	$F_{1,9,10}$	-0.0001	$F_{2,9,10}$	-0.0053	$F_{3,9,10}$	0.0023
$F_{4,9,10}$	0.0059	$F_{5,9,10}$	0.0076	$F_{6,9,10}$	-0.0025	$F_{7,9,10}$	0.0120
$F_{8,9,10}$	-0.0047	$F_{9,9,10}$	-0.0015	$F_{1,10,10}$	0.0001	$F_{2,10,10}$	-0.0004
$F_{3,10,10}$	0.0002	$F_{4,10,10}$	-0.0002	$F_{5,10,10}$	-0.0014	$F_{6,10,10}$	0.0015
$F_{7,10,10}$	0.0027	$F_{8,10,10}$	0.1024	$F_{9,10,10}$	-0.0178	$F_{10,10,10}$	-0.0026
$F_{1,1,11}$	0.0000	$F_{1,2,11}$	-0.0005	$F_{2,2,11}$	-0.0008	$F_{1,3,11}$	0.0001
$F_{2,3,11}$	-0.0008	$F_{3,3,11}$	0.0011	$F_{1,4,11}$	0.0001	$F_{2,4,11}$	0.0003
$F_{3,4,11}$	0.0002	$F_{4,4,11}$	-0.0012	$F_{1,5,11}$	0.0007	$F_{2,5,11}$	0.0009
$F_{3,5,11}$	0.0003	$F_{4,5,11}$	-0.0009	$F_{5,5,11}$	0.0007	$F_{1,6,11}$	-0.0015
$F_{2,6,11}$	-0.0002	$F_{3,6,11}$	-0.0009	$F_{4,6,11}$	0.0010	$F_{5,6,11}$	0.0049
$F_{6,6,11}$	0.0142	$F_{1,7,11}$	0.0001	$F_{2,7,11}$	-0.0006	$F_{3,7,11}$	0.0007
$F_{4,7,11}$	0.0044	$F_{5,7,11}$	0.0011	$F_{6,7,11}$	0.0005	$F_{7,7,11}$	-0.1087
$F_{1,8,11}$	-0.0015	$F_{2,8,11}$	-0.0007	$F_{3,8,11}$	0.0006	$F_{4,8,11}$	0.0016
$F_{5,8,11}$	-0.0066	$F_{6,8,11}$	0.0088	$F_{7,8,11}$	0.0082	$F_{8,8,11}$	0.7203
$F_{1,9,11}$	0.0009	$F_{2,9,11}$	0.0001	$F_{3,9,11}$	0.0007	$F_{4,9,11}$	-0.0002
$F_{5,9,11}$	-0.0176	$F_{6,9,11}$	-0.0104	$F_{7,9,11}$	-0.0031	$F_{8,9,11}$	-0.1481
$F_{9,9,11}$	-0.0342	$F_{1,10,11}$	-0.0002	$F_{2,10,11}$	0.0008	$F_{3,10,11}$	-0.0009
$F_{4,10,11}$	-0.0034	$F_{5,10,11}$	-0.0009	$F_{6,10,11}$	0.0001	$F_{7,10,11}$	0.1042
$F_{8,10,11}$	-0.0083	$F_{9,10,11}$	0.0024	$F_{10,10,11}$	-0.1006	$F_{1,11,11}$	0.0013
$F_{2,11,11}$	0.0005	$F_{3,11,11}$	-0.0002	$F_{4,11,11}$	-0.0010	$F_{5,11,11}$	0.0049
$F_{6,11,11}$	-0.0136	$F_{7,11,11}$	-0.0087	$F_{8,11,11}$	-0.7131	$F_{9,11,11}$	0.1657

Table A13: The CcCR Force Constants for HOSH (cont.)

$F_{10,11,11}$	0.0084	$F_{11,11,11}$	0.7077	$F_{1,1,12}$	0.0015	$F_{1,2,12}$	0.0017
$F_{2,2,12}$	0.0011	$F_{1,3,12}$	-0.0002	$F_{2,3,12}$	-0.0033	$F_{3,3,12}$	-0.0016
$F_{1,4,12}$	-0.0016	$F_{2,4,12}$	-0.0024	$F_{3,4,12}$	-0.0008	$F_{4,4,12}$	0.0054
$F_{1,5,12}$	-0.0013	$F_{2,5,12}$	-0.0013	$F_{3,5,12}$	0.0051	$F_{4,5,12}$	0.0014
$F_{5,5,12}$	0.0014	$F_{1,6,12}$	0.0013	$F_{2,6,12}$	0.0030	$F_{3,6,12}$	0.0011
$F_{4,6,12}$	0.0007	$F_{5,6,12}$	0.0264	$F_{6,6,12}$	-0.0333	$F_{1,7,12}$	-0.0001
$F_{2,7,12}$	-0.0008	$F_{3,7,12}$	0.0033	$F_{4,7,12}$	0.0084	$F_{5,7,12}$	0.0012
$F_{6,7,12}$	-0.0024	$F_{7,7,12}$	-0.0041	$F_{1,8,12}$	-0.0010	$F_{2,8,12}$	-0.0007
$F_{3,8,12}$	-0.0010	$F_{4,8,12}$	0.0019	$F_{5,8,12}$	-0.0124	$F_{6,8,12}$	-0.0264
$F_{7,8,12}$	-0.0024	$F_{8,8,12}$	-0.1256	$F_{1,9,12}$	-0.0020	$F_{2,9,12}$	0.0007
$F_{3,9,12}$	-0.0004	$F_{4,9,12}$	0.0019	$F_{5,9,12}$	-0.0170	$F_{6,9,12}$	0.0038
$F_{7,9,12}$	-0.0015	$F_{8,9,12}$	-0.0276	$F_{9,9,12}$	0.0423	$F_{1,10,12}$	0.0002
$F_{2,10,12}$	0.0015	$F_{3,10,12}$	-0.0023	$F_{4,10,12}$	-0.0122	$F_{5,10,12}$	-0.0013
$F_{6,10,12}$	0.0004	$F_{7,10,12}$	-0.0042	$F_{8,10,12}$	0.0014	$F_{9,10,12}$	0.0017
$F_{10,10,12}$	0.0161	$F_{1,11,12}$	0.0006	$F_{2,11,12}$	0.0009	$F_{3,11,12}$	-0.0009
$F_{4,11,12}$	-0.0009	$F_{5,11,12}$	0.0123	$F_{6,11,12}$	-0.0029	$F_{7,11,12}$	0.0020
$F_{8,11,12}$	0.1387	$F_{9,11,12}$	0.0439	$F_{10,11,12}$	-0.0016	$F_{11,11,12}$	-0.1519
$F_{1,12,12}$	0.0010	$F_{2,12,12}$	-0.0004	$F_{3,12,12}$	0.0008	$F_{4,12,12}$	-0.0019
$F_{5,12,12}$	-0.0146	$F_{6,12,12}$	0.0284	$F_{7,12,12}$	0.0007	$F_{8,12,12}$	0.0550
$F_{9,12,12}$	-0.0457	$F_{10,12,12}$	0.0002	$F_{11,12,12}$	-0.0401	$F_{12,12,12}$	0.0165
$F_{1,1,1,1}$	4.27	$F_{1,1,1,2}$	-0.12	$F_{1,1,2,2}$	-1.23	$F_{1,2,2,2}$	0.06
$F_{2,2,2,2}$	0.46	$F_{1,1,1,3}$	2.75	$F_{1,1,2,3}$	-0.05	$F_{1,2,2,3}$	-0.47
$F_{2,2,2,3}$	0.02	$F_{1,1,3,3}$	0.11	$F_{1,2,3,3}$	-0.00	$F_{2,2,3,3}$	-0.04
$F_{1,3,3,3}$	-0.81	$F_{2,3,3,3}$	0.01	$F_{3,3,3,3}$	-0.39	$F_{1,1,1,4}$	-4.29
$F_{1,1,2,4}$	0.12	$F_{1,2,2,4}$	1.24	$F_{2,2,2,4}$	-0.06	$F_{1,1,3,4}$	-2.76
$F_{1,2,3,4}$	0.05	$F_{2,2,3,4}$	0.45	$F_{1,3,3,4}$	-0.08	$F_{2,3,3,4}$	0.00
$F_{3,3,3,4}$	0.81	$F_{1,1,4,4}$	4.31	$F_{1,2,4,4}$	-0.12	$F_{2,2,4,4}$	-1.26
$F_{1,3,4,4}$	2.78	$F_{2,3,4,4}$	-0.06	$F_{3,3,4,4}$	0.03	$F_{1,4,4,4}$	-4.32
$F_{2,4,4,4}$	0.11	$F_{3,4,4,4}$	-2.84	$F_{4,4,4,4}$	4.35	$F_{1,1,1,5}$	0.12
$F_{1,1,2,5}$	1.24	$F_{1,2,2,5}$	-0.06	$F_{2,2,2,5}$	-0.46	$F_{1,1,3,5}$	0.05
$F_{1,2,3,5}$	0.45	$F_{2,2,3,5}$	-0.02	$F_{1,3,3,5}$	0.00	$F_{2,3,3,5}$	0.02
$F_{3,3,3,5}$	-0.01	$F_{1,1,4,5}$	-0.12	$F_{1,2,4,5}$	-1.25	$F_{2,2,4,5}$	0.06
$F_{1,3,4,5}$	-0.05	$F_{2,3,4,5}$	-0.44	$F_{3,3,4,5}$	-0.00	$F_{1,4,4,5}$	0.12
$F_{2,4,4,5}$	1.29	$F_{3,4,4,5}$	0.05	$F_{4,4,4,5}$	-0.11	$F_{1,1,5,5}$	-1.24
$F_{1,2,5,5}$	0.06	$F_{2,2,5,5}$	0.48	$F_{1,3,5,5}$	-0.43	$F_{2,3,5,5}$	0.02
$F_{3,3,5,5}$	-0.03	$F_{1,4,5,5}$	1.26	$F_{2,4,5,5}$	-0.06	$F_{3,4,5,5}$	0.41
$F_{4,4,5,5}$	-1.30	$F_{1,5,5,5}$	-0.07	$F_{2,5,5,5}$	-0.49	$F_{3,5,5,5}$	-0.03
$F_{4,5,5,5}$	0.07	$F_{5,5,5,5}$	0.53	$F_{1,1,1,6}$	-2.75	$F_{1,1,2,6}$	0.06
$F_{1,2,2,6}$	0.50	$F_{2,2,2,6}$	-0.02	$F_{1,1,3,6}$	-0.12	$F_{1,2,3,6}$	0.00
$F_{2,2,3,6}$	0.03	$F_{1,3,3,6}$	0.86	$F_{2,3,3,6}$	-0.02	$F_{3,3,3,6}$	0.44
$F_{1,1,4,6}$	2.76	$F_{1,2,4,6}$	-0.06	$F_{2,2,4,6}$	-0.49	$F_{1,3,4,6}$	0.09

Table A14: The CcCR Force Constants for HOSH (cont.)

$F_{2,3,4,6}$	-0.00	$F_{3,3,4,6}$	-0.84	$F_{1,4,4,6}$	-2.78	$F_{2,4,4,6}$	0.06
$F_{3,4,4,6}$	-0.07	$F_{4,4,4,6}$	2.83	$F_{1,1,5,6}$	-0.06	$F_{1,2,5,6}$	-0.48
$F_{2,2,5,6}$	0.03	$F_{1,3,5,6}$	-0.00	$F_{2,3,5,6}$	-0.03	$F_{3,3,5,6}$	0.02
$F_{1,4,5,6}$	0.06	$F_{2,4,5,6}$	0.47	$F_{3,4,5,6}$	0.00	$F_{4,4,5,6}$	-0.05
$F_{1,5,5,6}$	0.46	$F_{2,5,5,6}$	-0.04	$F_{3,5,5,6}$	0.04	$F_{4,5,5,6}$	-0.43
$F_{5,5,5,6}$	0.04	$F_{1,1,6,6}$	0.08	$F_{1,2,6,6}$	0.00	$F_{2,2,6,6}$	-0.03
$F_{1,3,6,6}$	-0.91	$F_{2,3,6,6}$	0.02	$F_{3,3,6,6}$	-0.47	$F_{1,4,6,6}$	-0.08
$F_{2,4,6,6}$	0.00	$F_{3,4,6,6}$	0.89	$F_{4,4,6,6}$	-0.20	$F_{1,5,6,6}$	-0.00
$F_{2,5,6,6}$	0.02	$F_{3,5,6,6}$	-0.02	$F_{4,5,6,6}$	-0.01	$F_{5,5,6,6}$	-0.25
$F_{1,6,6,6}$	0.99	$F_{2,6,6,6}$	-0.03	$F_{3,6,6,6}$	0.52	$F_{4,6,6,6}$	-1.06
$F_{5,6,6,6}$	0.07	$F_{6,6,6,6}$	1.25	$F_{1,1,1,7}$	0.02	$F_{1,1,2,7}$	-0.00
$F_{1,2,2,7}$	-0.01	$F_{2,2,2,7}$	0.01	$F_{1,1,3,7}$	0.01	$F_{1,2,3,7}$	-0.01
$F_{2,2,3,7}$	0.02	$F_{1,3,3,7}$	-0.03	$F_{2,3,3,7}$	-0.00	$F_{3,3,3,7}$	-0.00
$F_{1,1,4,7}$	-0.02	$F_{1,2,4,7}$	-0.00	$F_{2,2,4,7}$	0.03	$F_{1,3,4,7}$	-0.02
$F_{2,3,4,7}$	0.00	$F_{3,3,4,7}$	0.04	$F_{1,4,4,7}$	0.00	$F_{2,4,4,7}$	0.01
$F_{3,4,4,7}$	0.06	$F_{4,4,4,7}$	-0.03	$F_{1,1,5,7}$	0.00	$F_{1,2,5,7}$	0.02
$F_{2,2,5,7}$	-0.01	$F_{1,3,5,7}$	0.01	$F_{2,3,5,7}$	-0.01	$F_{3,3,5,7}$	0.00
$F_{1,4,5,7}$	0.00	$F_{2,4,5,7}$	-0.03	$F_{3,4,5,7}$	-0.00	$F_{4,4,5,7}$	-0.01
$F_{1,5,5,7}$	-0.02	$F_{2,5,5,7}$	0.01	$F_{3,5,5,7}$	0.02	$F_{4,5,5,7}$	0.04
$F_{5,5,5,7}$	-0.02	$F_{1,1,6,7}$	-0.01	$F_{1,2,6,7}$	0.00	$F_{2,2,6,7}$	-0.01
$F_{1,3,6,7}$	0.02	$F_{2,3,6,7}$	0.01	$F_{3,3,6,7}$	-0.01	$F_{1,4,6,7}$	0.02
$F_{2,4,6,7}$	0.00	$F_{3,4,6,7}$	-0.02	$F_{4,4,6,7}$	-0.06	$F_{1,5,6,7}$	-0.00
$F_{2,5,6,7}$	0.01	$F_{3,5,6,7}$	-0.01	$F_{4,5,6,7}$	0.01	$F_{5,5,6,7}$	-0.02
$F_{1,6,6,7}$	-0.00	$F_{2,6,6,7}$	-0.01	$F_{3,6,6,7}$	0.01	$F_{4,6,6,7}$	0.26
$F_{5,6,6,7}$	0.02	$F_{6,6,6,7}$	0.07	$F_{1,1,7,7}$	-0.00	$F_{1,2,7,7}$	0.01
$F_{2,2,7,7}$	-0.02	$F_{1,3,7,7}$	0.02	$F_{2,3,7,7}$	0.00	$F_{3,3,7,7}$	-0.01
$F_{1,4,7,7}$	0.02	$F_{2,4,7,7}$	-0.01	$F_{3,4,7,7}$	-0.03	$F_{4,4,7,7}$	0.02
$F_{1,5,7,7}$	-0.01	$F_{2,5,7,7}$	0.02	$F_{3,5,7,7}$	-0.00	$F_{4,5,7,7}$	0.01
$F_{5,5,7,7}$	-0.03	$F_{1,6,7,7}$	-0.02	$F_{2,6,7,7}$	-0.01	$F_{3,6,7,7}$	-0.01
$F_{4,6,7,7}$	0.03	$F_{5,6,7,7}$	-0.01	$F_{6,6,7,7}$	-0.24	$F_{1,7,7,7}$	-0.02
$F_{2,7,7,7}$	0.01	$F_{3,7,7,7}$	0.01	$F_{4,7,7,7}$	-0.05	$F_{5,7,7,7}$	-0.01
$F_{6,7,7,7}$	-0.01	$F_{7,7,7,7}$	0.21	$F_{1,1,1,8}$	0.00	$F_{1,1,2,8}$	-0.01

Table A15: The CcCR Force Constants for HOSH (cont.)

$F_{1,2,2,8}$	0.00	$F_{2,2,2,8}$	0.00	$F_{1,1,3,8}$	-0.00	$F_{1,2,3,8}$	0.02
$F_{2,2,3,8}$	-0.00	$F_{1,3,3,8}$	-0.00	$F_{2,3,3,8}$	0.02	$F_{3,3,3,8}$	-0.01
$F_{1,1,4,8}$	-0.00	$F_{1,2,4,8}$	0.01	$F_{2,2,4,8}$	-0.00	$F_{1,3,4,8}$	0.00
$F_{2,3,4,8}$	-0.02	$F_{3,3,4,8}$	-0.00	$F_{1,4,4,8}$	0.00	$F_{2,4,4,8}$	-0.02
$F_{3,4,4,8}$	-0.00	$F_{4,4,4,8}$	-0.00	$F_{1,1,5,8}$	-0.00	$F_{1,2,5,8}$	-0.01
$F_{2,2,5,8}$	-0.01	$F_{1,3,5,8}$	-0.02	$F_{2,3,5,8}$	0.00	$F_{3,3,5,8}$	0.01
$F_{1,4,5,8}$	-0.01	$F_{2,4,5,8}$	0.01	$F_{3,4,5,8}$	0.03	$F_{4,4,5,8}$	0.01
$F_{1,5,5,8}$	0.01	$F_{2,5,5,8}$	0.01	$F_{3,5,5,8}$	0.00	$F_{4,5,5,8}$	-0.01
$F_{5,5,5,8}$	-0.03	$F_{1,1,6,8}$	-0.00	$F_{1,2,6,8}$	-0.02	$F_{2,2,6,8}$	-0.00
$F_{1,3,6,8}$	0.01	$F_{2,3,6,8}$	-0.01	$F_{3,3,6,8}$	0.01	$F_{1,4,6,8}$	0.01
$F_{2,4,6,8}$	0.02	$F_{3,4,6,8}$	-0.00	$F_{4,4,6,8}$	-0.00	$F_{1,5,6,8}$	0.02
$F_{2,5,6,8}$	0.01	$F_{3,5,6,8}$	-0.00	$F_{4,5,6,8}$	-0.03	$F_{5,5,6,8}$	-0.00
$F_{1,6,6,8}$	-0.01	$F_{2,6,6,8}$	0.02	$F_{3,6,6,8}$	-0.01	$F_{4,6,6,8}$	0.01
$F_{5,6,6,8}$	0.23	$F_{6,6,6,8}$	-0.07	$F_{1,1,7,8}$	0.00	$F_{1,2,7,8}$	-0.01
$F_{2,2,7,8}$	0.00	$F_{1,3,7,8}$	-0.00	$F_{2,3,7,8}$	-0.00	$F_{3,3,7,8}$	0.00
$F_{1,4,7,8}$	-0.00	$F_{2,4,7,8}$	0.01	$F_{3,4,7,8}$	0.00	$F_{4,4,7,8}$	0.01
$F_{1,5,7,8}$	0.01	$F_{2,5,7,8}$	-0.00	$F_{3,5,7,8}$	-0.01	$F_{4,5,7,8}$	-0.01
$F_{5,5,7,8}$	0.01	$F_{1,6,7,8}$	-0.00	$F_{2,6,7,8}$	0.00	$F_{3,6,7,8}$	0.00
$F_{4,6,7,8}$	-0.01	$F_{5,6,7,8}$	0.01	$F_{6,6,7,8}$	-0.01	$F_{1,7,7,8}$	0.00
$F_{2,7,7,8}$	-0.00	$F_{3,7,7,8}$	0.00	$F_{4,7,7,8}$	-0.01	$F_{5,7,7,8}$	0.02
$F_{6,7,7,8}$	0.01	$F_{7,7,7,8}$	-0.00	$F_{1,1,8,8}$	0.01	$F_{1,2,8,8}$	0.01
$F_{2,2,8,8}$	0.01	$F_{1,3,8,8}$	0.01	$F_{2,3,8,8}$	-0.00	$F_{3,3,8,8}$	-0.03
$F_{1,4,8,8}$	-0.01	$F_{2,4,8,8}$	-0.01	$F_{3,4,8,8}$	-0.02	$F_{4,4,8,8}$	0.02
$F_{1,5,8,8}$	-0.01	$F_{2,5,8,8}$	-0.00	$F_{3,5,8,8}$	0.00	$F_{4,5,8,8}$	0.01
$F_{5,5,8,8}$	0.01	$F_{1,6,8,8}$	0.00	$F_{2,6,8,8}$	-0.01	$F_{3,6,8,8}$	0.01
$F_{4,6,8,8}$	0.01	$F_{5,6,8,8}$	0.01	$F_{6,6,8,8}$	-0.27	$F_{1,7,8,8}$	-0.01
$F_{2,7,8,8}$	-0.00	$F_{3,7,8,8}$	0.01	$F_{4,7,8,8}$	0.01	$F_{5,7,8,8}$	-0.00
$F_{6,7,8,8}$	-0.00	$F_{7,7,8,8}$	-0.40	$F_{1,8,8,8}$	0.00	$F_{2,8,8,8}$	-0.01
$F_{3,8,8,8}$	-0.00	$F_{4,8,8,8}$	-0.01	$F_{5,8,8,8}$	-0.01	$F_{6,8,8,8}$	-0.01
$F_{7,8,8,8}$	0.03	$F_{8,8,8,8}$	1.60	$F_{1,1,1,9}$	0.00	$F_{1,1,2,9}$	-0.00
$F_{1,2,2,9}$	-0.03	$F_{2,2,2,9}$	0.01	$F_{1,1,3,9}$	0.01	$F_{1,2,3,9}$	0.00
$F_{2,2,3,9}$	0.00	$F_{1,3,3,9}$	-0.05	$F_{2,3,3,9}$	0.00	$F_{3,3,3,9}$	-0.04
$F_{1,1,4,9}$	0.00	$F_{1,2,4,9}$	0.01	$F_{2,2,4,9}$	0.04	$F_{1,3,4,9}$	-0.02
$F_{2,3,4,9}$	-0.00	$F_{3,3,4,9}$	0.03	$F_{1,4,4,9}$	-0.01	$F_{2,4,4,9}$	-0.00
$F_{3,4,4,9}$	0.04	$F_{4,4,4,9}$	0.01	$F_{1,1,5,9}$	0.01	$F_{1,2,5,9}$	0.03
$F_{2,2,5,9}$	-0.01	$F_{1,3,5,9}$	-0.00	$F_{2,3,5,9}$	0.01	$F_{3,3,5,9}$	0.00
$F_{1,4,5,9}$	-0.01	$F_{2,4,5,9}$	-0.03	$F_{3,4,5,9}$	0.00	$F_{4,4,5,9}$	0.02
$F_{1,5,5,9}$	-0.04	$F_{2,5,5,9}$	0.02	$F_{3,5,5,9}$	-0.00	$F_{4,5,5,9}$	0.03
$F_{5,5,5,9}$	-0.00	$F_{1,1,6,9}$	0.04	$F_{1,2,6,9}$	-0.01	$F_{2,2,6,9}$	-0.01
$F_{1,3,6,9}$	0.05	$F_{2,3,6,9}$	-0.00	$F_{3,3,6,9}$	0.03	$F_{1,4,6,9}$	-0.02
$F_{2,4,6,9}$	0.00	$F_{3,4,6,9}$	-0.04	$F_{4,4,6,9}$	0.26	$F_{1,5,6,9}$	0.01
$F_{2,5,6,9}$	0.02	$F_{3,5,6,9}$	-0.00	$F_{4,5,6,9}$	-0.00	$F_{5,5,6,9}$	0.21

Table A16: The CcCR Force Constants for HOSH (cont.)

$F_{1,6,6,9}$	-0.08	$F_{2,6,6,9}$	0.00	$F_{3,6,6,9}$	-0.06	$F_{4,6,6,9}$	0.16
$F_{5,6,6,9}$	-0.08	$F_{6,6,6,9}$	-1.74	$F_{1,1,7,9}$	-0.00	$F_{1,2,7,9}$	0.00
$F_{2,2,7,9}$	-0.01	$F_{1,3,7,9}$	0.01	$F_{2,3,7,9}$	-0.00	$F_{3,3,7,9}$	0.02
$F_{1,4,7,9}$	0.00	$F_{2,4,7,9}$	-0.01	$F_{3,4,7,9}$	-0.02	$F_{4,4,7,9}$	0.00
$F_{1,5,7,9}$	-0.00	$F_{2,5,7,9}$	0.01	$F_{3,5,7,9}$	0.00	$F_{4,5,7,9}$	-0.01
$F_{5,5,7,9}$	-0.01	$F_{1,6,7,9}$	-0.02	$F_{2,6,7,9}$	0.01	$F_{3,6,7,9}$	0.00
$F_{4,6,7,9}$	-0.25	$F_{5,6,7,9}$	-0.02	$F_{6,6,7,9}$	-0.08	$F_{1,7,7,9}$	0.00
$F_{2,7,7,9}$	0.01	$F_{3,7,7,9}$	0.01	$F_{4,7,7,9}$	-0.00	$F_{5,7,7,9}$	0.03
$F_{6,7,7,9}$	0.26	$F_{7,7,7,9}$	0.00	$F_{1,1,8,9}$	0.00	$F_{1,2,8,9}$	-0.00
$F_{2,2,8,9}$	0.01	$F_{1,3,8,9}$	-0.00	$F_{2,3,8,9}$	-0.01	$F_{3,3,8,9}$	-0.01
$F_{1,4,8,9}$	-0.01	$F_{2,4,8,9}$	-0.01	$F_{3,4,8,9}$	0.00	$F_{4,4,8,9}$	-0.01
$F_{1,5,8,9}$	0.00	$F_{2,5,8,9}$	-0.01	$F_{3,5,8,9}$	-0.01	$F_{4,5,8,9}$	0.00
$F_{5,5,8,9}$	-0.02	$F_{1,6,8,9}$	0.00	$F_{2,6,8,9}$	-0.02	$F_{3,6,8,9}$	0.01
$F_{4,6,8,9}$	-0.01	$F_{5,6,8,9}$	-0.22	$F_{6,6,8,9}$	0.09	$F_{1,7,8,9}$	0.00
$F_{2,7,8,9}$	-0.00	$F_{3,7,8,9}$	0.00	$F_{4,7,8,9}$	0.04	$F_{5,7,8,9}$	0.01
$F_{6,7,8,9}$	0.01	$F_{7,7,8,9}$	0.01	$F_{1,8,8,9}$	-0.01	$F_{2,8,8,9}$	0.01
$F_{3,8,8,9}$	0.02	$F_{4,8,8,9}$	0.01	$F_{5,8,8,9}$	0.02	$F_{6,8,8,9}$	0.24
$F_{7,8,8,9}$	-0.01	$F_{8,8,8,9}$	-0.47	$F_{1,1,9,9}$	-0.04	$F_{1,2,9,9}$	0.01
$F_{2,2,9,9}$	0.00	$F_{1,3,9,9}$	0.01	$F_{2,3,9,9}$	0.00	$F_{3,3,9,9}$	0.01
$F_{1,4,9,9}$	0.03	$F_{2,4,9,9}$	-0.00	$F_{3,4,9,9}$	0.01	$F_{4,4,9,9}$	-0.31
$F_{1,5,9,9}$	-0.01	$F_{2,5,9,9}$	-0.03	$F_{3,5,9,9}$	-0.00	$F_{4,5,9,9}$	-0.00
$F_{5,5,9,9}$	-0.21	$F_{1,6,9,9}$	0.04	$F_{2,6,9,9}$	0.00	$F_{3,6,9,9}$	0.03
$F_{4,6,9,9}$	-0.12	$F_{5,6,9,9}$	0.10	$F_{6,6,9,9}$	1.80	$F_{1,7,9,9}$	0.01
$F_{2,7,9,9}$	-0.01	$F_{3,7,9,9}$	-0.02	$F_{4,7,9,9}$	0.28	$F_{5,7,9,9}$	0.02
$F_{6,7,9,9}$	0.08	$F_{7,7,9,9}$	-0.27	$F_{1,8,9,9}$	-0.00	$F_{2,8,9,9}$	0.03
$F_{3,8,9,9}$	-0.00	$F_{4,8,9,9}$	0.01	$F_{5,8,9,9}$	0.23	$F_{6,8,9,9}$	-0.12
$F_{7,8,9,9}$	-0.02	$F_{8,8,9,9}$	-0.47	$F_{1,9,9,9}$	-0.04	$F_{2,9,9,9}$	0.00
$F_{3,9,9,9}$	-0.03	$F_{4,9,9,9}$	0.11	$F_{5,9,9,9}$	-0.09	$F_{6,9,9,9}$	-1.83
$F_{7,9,9,9}$	-0.07	$F_{8,9,9,9}$	0.30	$F_{9,9,9,9}$	1.84	$F_{1,1,1,10}$	0.00
$F_{1,1,2,10}$	0.00	$F_{1,2,2,10}$	0.00	$F_{2,2,2,10}$	-0.01	$F_{1,1,3,10}$	0.00
$F_{1,2,3,10}$	0.01	$F_{2,2,3,10}$	-0.00	$F_{1,3,3,10}$	-0.00	$F_{2,3,3,10}$	0.00
$F_{3,3,3,10}$	0.00	$F_{1,1,4,10}$	-0.00	$F_{1,2,4,10}$	0.00	$F_{2,2,4,10}$	-0.00
$F_{1,3,4,10}$	-0.00	$F_{2,3,4,10}$	-0.00	$F_{3,3,4,10}$	0.00	$F_{1,4,4,10}$	0.00
$F_{2,4,4,10}$	-0.00	$F_{3,4,4,10}$	0.00	$F_{4,4,4,10}$	-0.01	$F_{1,1,5,10}$	-0.00
$F_{1,2,5,10}$	-0.00	$F_{2,2,5,10}$	0.01	$F_{1,3,5,10}$	-0.01	$F_{2,3,5,10}$	-0.00
$F_{3,3,5,10}$	-0.00	$F_{1,4,5,10}$	-0.00	$F_{2,4,5,10}$	0.00	$F_{3,4,5,10}$	0.00
$F_{4,4,5,10}$	0.01	$F_{1,5,5,10}$	0.00	$F_{2,5,5,10}$	-0.01	$F_{3,5,5,10}$	0.00
$F_{4,5,5,10}$	-0.00	$F_{5,5,5,10}$	0.01	$F_{1,1,6,10}$	0.00	$F_{1,2,6,10}$	-0.00
$F_{2,2,6,10}$	-0.00	$F_{1,3,6,10}$	0.00	$F_{2,3,6,10}$	-0.00	$F_{3,3,6,10}$	-0.00
$F_{1,4,6,10}$	-0.00	$F_{2,4,6,10}$	-0.00	$F_{3,4,6,10}$	-0.00	$F_{4,4,6,10}$	0.00

Table A17: The CcCR Force Constants for HOSH (cont.)

$F_{1,5,6,10}$	0.00	$F_{2,5,6,10}$	0.01	$F_{3,5,6,10}$	0.00	$F_{4,5,6,10}$	-0.01
$F_{5,5,6,10}$	-0.01	$F_{1,6,6,10}$	0.00	$F_{2,6,6,10}$	0.01	$F_{3,6,6,10}$	0.01
$F_{4,6,6,10}$	0.01	$F_{5,6,6,10}$	-0.01	$F_{6,6,6,10}$	-0.01	$F_{1,1,7,10}$	0.00
$F_{1,2,7,10}$	-0.00	$F_{2,2,7,10}$	0.00	$F_{1,3,7,10}$	-0.00	$F_{2,3,7,10}$	-0.00
$F_{3,3,7,10}$	-0.00	$F_{1,4,7,10}$	-0.00	$F_{2,4,7,10}$	0.01	$F_{3,4,7,10}$	0.00
$F_{4,4,7,10}$	0.00	$F_{1,5,7,10}$	0.00	$F_{2,5,7,10}$	-0.00	$F_{3,5,7,10}$	0.00
$F_{4,5,7,10}$	-0.01	$F_{5,5,7,10}$	0.01	$F_{1,6,7,10}$	0.00	$F_{2,6,7,10}$	0.00
$F_{3,6,7,10}$	0.00	$F_{4,6,7,10}$	0.00	$F_{5,6,7,10}$	0.00	$F_{6,6,7,10}$	-0.02
$F_{1,7,7,10}$	0.01	$F_{2,7,7,10}$	-0.01	$F_{3,7,7,10}$	0.00	$F_{4,7,7,10}$	0.01
$F_{5,7,7,10}$	0.01	$F_{6,7,7,10}$	-0.01	$F_{7,7,7,10}$	-0.14	$F_{1,1,8,10}$	0.00
$F_{1,2,8,10}$	0.00	$F_{2,2,8,10}$	-0.00	$F_{1,3,8,10}$	0.00	$F_{2,3,8,10}$	0.00
$F_{3,3,8,10}$	0.00	$F_{1,4,8,10}$	0.00	$F_{2,4,8,10}$	-0.00	$F_{3,4,8,10}$	-0.00
$F_{4,4,8,10}$	-0.00	$F_{1,5,8,10}$	-0.00	$F_{2,5,8,10}$	0.00	$F_{3,5,8,10}$	-0.00
$F_{4,5,8,10}$	0.01	$F_{5,5,8,10}$	-0.00	$F_{1,6,8,10}$	-0.00	$F_{2,6,8,10}$	-0.00
$F_{3,6,8,10}$	-0.00	$F_{4,6,8,10}$	0.01	$F_{5,6,8,10}$	0.01	$F_{6,6,8,10}$	0.01
$F_{1,7,8,10}$	-0.00	$F_{2,7,8,10}$	0.00	$F_{3,7,8,10}$	-0.00	$F_{4,7,8,10}$	0.01
$F_{5,7,8,10}$	-0.02	$F_{6,7,8,10}$	0.00	$F_{7,7,8,10}$	0.01	$F_{1,8,8,10}$	0.00
$F_{2,8,8,10}$	0.00	$F_{3,8,8,10}$	-0.00	$F_{4,8,8,10}$	-0.02	$F_{5,8,8,10}$	0.00
$F_{6,8,8,10}$	-0.01	$F_{7,8,8,10}$	0.40	$F_{8,8,8,10}$	-0.03	$F_{1,1,9,10}$	-0.00
$F_{1,2,9,10}$	-0.00	$F_{2,2,9,10}$	0.00	$F_{1,3,9,10}$	0.00	$F_{2,3,9,10}$	0.00
$F_{3,3,9,10}$	0.00	$F_{1,4,9,10}$	0.00	$F_{2,4,9,10}$	0.01	$F_{3,4,9,10}$	-0.00
$F_{4,4,9,10}$	-0.00	$F_{1,5,9,10}$	0.00	$F_{2,5,9,10}$	-0.01	$F_{3,5,9,10}$	-0.00
$F_{4,5,9,10}$	0.00	$F_{5,5,9,10}$	0.01	$F_{1,6,9,10}$	-0.00	$F_{2,6,9,10}$	-0.01
$F_{3,6,9,10}$	-0.00	$F_{4,6,9,10}$	0.00	$F_{5,6,9,10}$	0.01	$F_{6,6,9,10}$	0.00
$F_{1,7,9,10}$	-0.00	$F_{2,7,9,10}$	-0.00	$F_{3,7,9,10}$	-0.00	$F_{4,7,9,10}$	-0.00
$F_{5,7,9,10}$	-0.01	$F_{6,7,9,10}$	0.00	$F_{7,7,9,10}$	-0.00	$F_{1,8,9,10}$	0.00
$F_{2,8,9,10}$	0.01	$F_{3,8,9,10}$	0.00	$F_{4,8,9,10}$	-0.02	$F_{5,8,9,10}$	-0.01
$F_{6,8,9,10}$	-0.01	$F_{7,8,9,10}$	-0.05	$F_{8,8,9,10}$	0.01	$F_{1,9,9,10}$	0.00
$F_{2,9,9,10}$	0.01	$F_{3,9,9,10}$	-0.00	$F_{4,9,9,10}$	-0.01	$F_{5,9,9,10}$	-0.01
$F_{6,9,9,10}$	-0.00	$F_{7,9,9,10}$	-0.01	$F_{8,9,9,10}$	0.01	$F_{9,9,9,10}$	0.00
$F_{1,1,10,10}$	-0.00	$F_{1,2,10,10}$	0.00	$F_{2,2,10,10}$	-0.00	$F_{1,3,10,10}$	0.00
$F_{2,3,10,10}$	-0.00	$F_{3,3,10,10}$	0.00	$F_{1,4,10,10}$	0.00	$F_{2,4,10,10}$	-0.00
$F_{3,4,10,10}$	-0.00	$F_{4,4,10,10}$	0.00	$F_{1,5,10,10}$	-0.00	$F_{2,5,10,10}$	0.00
$F_{3,5,10,10}$	-0.00	$F_{4,5,10,10}$	0.00	$F_{5,5,10,10}$	-0.01	$F_{1,6,10,10}$	-0.00

Table A18: The CcCR Force Constants for HOSH (cont.)

$F_{2,6,10,10}$	-0.00	$F_{3,6,10,10}$	-0.00	$F_{4,6,10,10}$	0.00	$F_{5,6,10,10}$	0.01
$F_{6,6,10,10}$	-0.00	$F_{1,7,10,10}$	-0.00	$F_{2,7,10,10}$	0.00	$F_{3,7,10,10}$	-0.00
$F_{4,7,10,10}$	-0.01	$F_{5,7,10,10}$	-0.00	$F_{6,7,10,10}$	0.00	$F_{7,7,10,10}$	0.13
$F_{1,8,10,10}$	0.00	$F_{2,8,10,10}$	-0.00	$F_{3,8,10,10}$	-0.00	$F_{4,8,10,10}$	-0.00
$F_{5,8,10,10}$	0.01	$F_{6,8,10,10}$	-0.01	$F_{7,8,10,10}$	-0.01	$F_{8,8,10,10}$	-0.38
$F_{1,9,10,10}$	-0.00	$F_{2,9,10,10}$	0.00	$F_{3,9,10,10}$	0.00	$F_{4,9,10,10}$	0.00
$F_{5,9,10,10}$	0.00	$F_{6,9,10,10}$	-0.00	$F_{7,9,10,10}$	0.00	$F_{8,9,10,10}$	0.07
$F_{9,9,10,10}$	0.02	$F_{1,10,10,10}$	0.00	$F_{2,10,10,10}$	-0.00	$F_{3,10,10,10}$	0.00
$F_{4,10,10,10}$	0.00	$F_{5,10,10,10}$	0.00	$F_{6,10,10,10}$	-0.00	$F_{7,10,10,10}$	-0.12
$F_{8,10,10,10}$	0.01	$F_{9,10,10,10}$	-0.00	$F_{10,10,10,10}$	0.12	$F_{1,1,1,11}$	-0.00
$F_{1,1,2,11}$	-0.00	$F_{1,2,2,11}$	-0.00	$F_{2,2,2,11}$	0.00	$F_{1,1,3,11}$	0.00
$F_{1,2,3,11}$	-0.00	$F_{2,2,3,11}$	0.00	$F_{1,3,3,11}$	0.00	$F_{2,3,3,11}$	-0.00
$F_{3,3,3,11}$	0.00	$F_{1,1,4,11}$	0.00	$F_{1,2,4,11}$	0.00	$F_{2,2,4,11}$	0.00
$F_{1,3,4,11}$	-0.00	$F_{2,3,4,11}$	0.00	$F_{3,3,4,11}$	0.00	$F_{1,4,4,11}$	-0.00
$F_{2,4,4,11}$	-0.00	$F_{3,4,4,11}$	0.00	$F_{4,4,4,11}$	0.01	$F_{1,1,5,11}$	0.00
$F_{1,2,5,11}$	0.01	$F_{2,2,5,11}$	-0.00	$F_{1,3,5,11}$	0.00	$F_{2,3,5,11}$	-0.00
$F_{3,3,5,11}$	0.00	$F_{1,4,5,11}$	-0.00	$F_{2,4,5,11}$	-0.01	$F_{3,4,5,11}$	-0.00
$F_{4,4,5,11}$	-0.00	$F_{1,5,5,11}$	-0.01	$F_{2,5,5,11}$	0.00	$F_{3,5,5,11}$	0.00
$F_{4,5,5,11}$	0.01	$F_{5,5,5,11}$	-0.01	$F_{1,1,6,11}$	0.00	$F_{1,2,6,11}$	0.00
$F_{2,2,6,11}$	-0.00	$F_{1,3,6,11}$	-0.01	$F_{2,3,6,11}$	0.00	$F_{3,3,6,11}$	-0.01
$F_{1,4,6,11}$	-0.00	$F_{2,4,6,11}$	0.00	$F_{3,4,6,11}$	0.00	$F_{4,4,6,11}$	0.00
$F_{1,5,6,11}$	0.00	$F_{2,5,6,11}$	0.00	$F_{3,5,6,11}$	-0.00	$F_{4,5,6,11}$	-0.00
$F_{5,5,6,11}$	-0.00	$F_{1,6,6,11}$	0.01	$F_{2,6,6,11}$	-0.01	$F_{3,6,6,11}$	0.01
$F_{4,6,6,11}$	-0.01	$F_{5,6,6,11}$	0.00	$F_{6,6,6,11}$	0.03	$F_{1,1,7,11}$	-0.00
$F_{1,2,7,11}$	0.00	$F_{2,2,7,11}$	-0.00	$F_{1,3,7,11}$	0.00	$F_{2,3,7,11}$	-0.00
$F_{3,3,7,11}$	-0.00	$F_{1,4,7,11}$	0.00	$F_{2,4,7,11}$	-0.00	$F_{3,4,7,11}$	-0.00
$F_{4,4,7,11}$	-0.00	$F_{1,5,7,11}$	-0.00	$F_{2,5,7,11}$	0.00	$F_{3,5,7,11}$	0.00
$F_{4,5,7,11}$	0.01	$F_{5,5,7,11}$	-0.00	$F_{1,6,7,11}$	0.00	$F_{2,6,7,11}$	-0.00
$F_{3,6,7,11}$	-0.00	$F_{4,6,7,11}$	0.00	$F_{5,6,7,11}$	0.00	$F_{6,6,7,11}$	0.00
$F_{1,7,7,11}$	-0.00	$F_{2,7,7,11}$	0.00	$F_{3,7,7,11}$	0.00	$F_{4,7,7,11}$	0.00
$F_{5,7,7,11}$	-0.02	$F_{6,7,7,11}$	0.01	$F_{7,7,7,11}$	0.01	$F_{1,1,8,11}$	-0.00
$F_{1,2,8,11}$	-0.00	$F_{2,2,8,11}$	0.00	$F_{1,3,8,11}$	0.00	$F_{2,3,8,11}$	0.00
$F_{3,3,8,11}$	0.00	$F_{1,4,8,11}$	0.00	$F_{2,4,8,11}$	0.00	$F_{3,4,8,11}$	0.00
$F_{4,4,8,11}$	-0.01	$F_{1,5,8,11}$	0.00	$F_{2,5,8,11}$	-0.00	$F_{3,5,8,11}$	-0.00
$F_{4,5,8,11}$	-0.01	$F_{5,5,8,11}$	0.01	$F_{1,6,8,11}$	-0.00	$F_{2,6,8,11}$	0.00
$F_{3,6,8,11}$	0.00	$F_{4,6,8,11}$	0.00	$F_{5,6,8,11}$	-0.01	$F_{6,6,8,11}$	0.02
$F_{1,7,8,11}$	0.00	$F_{2,7,8,11}$	0.00	$F_{3,7,8,11}$	-0.00	$F_{4,7,8,11}$	-0.01
$F_{5,7,8,11}$	0.00	$F_{6,7,8,11}$	-0.00	$F_{7,7,8,11}$	0.39	$F_{1,8,8,11}$	-0.00
$F_{2,8,8,11}$	0.00	$F_{3,8,8,11}$	0.00	$F_{4,8,8,11}$	0.00	$F_{5,8,8,11}$	-0.01
$F_{6,8,8,11}$	0.01	$F_{7,8,8,11}$	-0.03	$F_{8,8,8,11}$	-1.58	$F_{1,1,9,11}$	-0.01
$F_{1,2,9,11}$	-0.00	$F_{2,2,9,11}$	-0.00	$F_{1,3,9,11}$	0.00	$F_{2,3,9,11}$	-0.00

Table A19: The CcCR Force Constants for HOSH (cont.)

$F_{3,3,9,11}$	0.00	$F_{1,4,9,11}$	0.01	$F_{2,4,9,11}$	0.00	$F_{3,4,9,11}$	-0.00
$F_{4,4,9,11}$	-0.01	$F_{1,5,9,11}$	0.00	$F_{2,5,9,11}$	0.00	$F_{3,5,9,11}$	-0.00
$F_{4,5,9,11}$	0.00	$F_{5,5,9,11}$	-0.00	$F_{1,6,9,11}$	-0.00	$F_{2,6,9,11}$	0.00
$F_{3,6,9,11}$	-0.00	$F_{4,6,9,11}$	0.00	$F_{5,6,9,11}$	-0.01	$F_{6,6,9,11}$	-0.01
$F_{1,7,9,11}$	-0.00	$F_{2,7,9,11}$	0.00	$F_{3,7,9,11}$	-0.00	$F_{4,7,9,11}$	-0.01
$F_{5,7,9,11}$	-0.00	$F_{6,7,9,11}$	-0.00	$F_{7,7,9,11}$	-0.05	$F_{1,8,9,11}$	0.00
$F_{2,8,9,11}$	-0.00	$F_{3,8,9,11}$	-0.00	$F_{4,8,9,11}$	-0.00	$F_{5,8,9,11}$	0.01
$F_{6,8,9,11}$	-0.00	$F_{7,8,9,11}$	0.01	$F_{8,8,9,11}$	0.45	$F_{1,9,9,11}$	0.00
$F_{2,9,9,11}$	-0.00	$F_{3,9,9,11}$	0.00	$F_{4,9,9,11}$	-0.00	$F_{5,9,9,11}$	0.01
$F_{6,9,9,11}$	0.02	$F_{7,9,9,11}$	0.00	$F_{8,9,9,11}$	0.21	$F_{9,9,9,11}$	-0.21
$F_{1,1,10,11}$	-0.00	$F_{1,2,10,11}$	-0.00	$F_{2,2,10,11}$	0.00	$F_{1,3,10,11}$	-0.00
$F_{2,3,10,11}$	0.00	$F_{3,3,10,11}$	-0.00	$F_{1,4,10,11}$	-0.00	$F_{2,4,10,11}$	0.00
$F_{3,4,10,11}$	0.00	$F_{4,4,10,11}$	0.00	$F_{1,5,10,11}$	0.00	$F_{2,5,10,11}$	-0.00
$F_{3,5,10,11}$	-0.00	$F_{4,5,10,11}$	-0.01	$F_{5,5,10,11}$	-0.00	$F_{1,6,10,11}$	0.00
$F_{2,6,10,11}$	0.00	$F_{3,6,10,11}$	0.00	$F_{4,6,10,11}$	0.00	$F_{5,6,10,11}$	-0.00
$F_{6,6,10,11}$	-0.00	$F_{1,7,10,11}$	0.00	$F_{2,7,10,11}$	-0.00	$F_{3,7,10,11}$	-0.00
$F_{4,7,10,11}$	-0.00	$F_{5,7,10,11}$	0.01	$F_{6,7,10,11}$	-0.01	$F_{7,7,10,11}$	-0.01
$F_{1,8,10,11}$	-0.00	$F_{2,8,10,11}$	-0.00	$F_{3,8,10,11}$	0.00	$F_{4,8,10,11}$	0.01
$F_{5,8,10,11}$	0.00	$F_{6,8,10,11}$	0.00	$F_{7,8,10,11}$	-0.38	$F_{8,8,10,11}$	0.03
$F_{1,9,10,11}$	-0.00	$F_{2,9,10,11}$	-0.00	$F_{3,9,10,11}$	0.00	$F_{4,9,10,11}$	0.01
$F_{5,9,10,11}$	0.00	$F_{6,9,10,11}$	0.00	$F_{7,9,10,11}$	0.07	$F_{8,9,10,11}$	-0.01
$F_{9,9,10,11}$	-0.00	$F_{1,10,10,11}$	-0.00	$F_{2,10,10,11}$	0.00	$F_{3,10,10,11}$	0.00
$F_{4,10,10,11}$	0.00	$F_{5,10,10,11}$	-0.00	$F_{6,10,10,11}$	0.01	$F_{7,10,10,11}$	0.01
$F_{8,10,10,11}$	0.37	$F_{9,10,10,11}$	-0.08	$F_{10,10,10,11}$	-0.01	$F_{1,1,11,11}$	0.00
$F_{1,2,11,11}$	0.00	$F_{2,2,11,11}$	-0.00	$F_{1,3,11,11}$	-0.00	$F_{2,3,11,11}$	0.00
$F_{3,3,11,11}$	-0.00	$F_{1,4,11,11}$	-0.00	$F_{2,4,11,11}$	-0.00	$F_{3,4,11,11}$	-0.00
$F_{4,4,11,11}$	0.01	$F_{1,5,11,11}$	-0.00	$F_{2,5,11,11}$	0.00	$F_{3,5,11,11}$	0.00
$F_{4,5,11,11}$	0.00	$F_{5,5,11,11}$	-0.00	$F_{1,6,11,11}$	0.00	$F_{2,6,11,11}$	-0.00
$F_{3,6,11,11}$	-0.00	$F_{4,6,11,11}$	-0.00	$F_{5,6,11,11}$	0.01	$F_{6,6,11,11}$	-0.01
$F_{1,7,11,11}$	-0.00	$F_{2,7,11,11}$	-0.00	$F_{3,7,11,11}$	0.00	$F_{4,7,11,11}$	0.00
$F_{5,7,11,11}$	0.00	$F_{6,7,11,11}$	0.00	$F_{7,7,11,11}$	-0.37	$F_{1,8,11,11}$	0.00
$F_{2,8,11,11}$	-0.00	$F_{3,8,11,11}$	-0.00	$F_{4,8,11,11}$	-0.00	$F_{5,8,11,11}$	0.00
$F_{6,8,11,11}$	-0.00	$F_{7,8,11,11}$	0.03	$F_{8,8,11,11}$	1.59	$F_{1,9,11,11}$	-0.00

Table A20: The CcCR Force Constants for HOSH (cont.)

$F_{2,9,11,11}$	0.00	$F_{3,9,11,11}$	0.00	$F_{4,9,11,11}$	0.00	$F_{5,9,11,11}$	-0.02
$F_{6,9,11,11}$	0.01	$F_{7,9,11,11}$	-0.01	$F_{8,9,11,11}$	-0.46	$F_{9,9,11,11}$	-0.23
$F_{1,10,11,11}$	0.00	$F_{2,10,11,11}$	0.00	$F_{3,10,11,11}$	-0.00	$F_{4,10,11,11}$	-0.01
$F_{5,10,11,11}$	-0.00	$F_{6,10,11,11}$	-0.00	$F_{7,10,11,11}$	0.37	$F_{8,10,11,11}$	-0.03
$F_{9,10,11,11}$	0.01	$F_{10,10,11,11}$	-0.36	$F_{1,11,11,11}$	-0.00	$F_{2,11,11,11}$	0.00
$F_{3,11,11,11}$	0.00	$F_{4,11,11,11}$	0.00	$F_{5,11,11,11}$	-0.00	$F_{6,11,11,11}$	-0.00
$F_{7,11,11,11}$	-0.03	$F_{8,11,11,11}$	-1.59	$F_{9,11,11,11}$	0.48	$F_{10,11,11,11}$	0.03
$F_{11,11,11,11}$	1.59	$F_{1,1,1,12}$	0.00	$F_{1,1,2,12}$	0.00	$F_{1,2,2,12}$	0.00
$F_{2,2,2,12}$	-0.00	$F_{1,1,3,12}$	-0.00	$F_{1,2,3,12}$	-0.00	$F_{2,2,3,12}$	-0.00
$F_{1,3,3,12}$	-0.00	$F_{2,3,3,12}$	-0.00	$F_{3,3,3,12}$	0.00	$F_{1,1,4,12}$	-0.00
$F_{1,2,4,12}$	-0.00	$F_{2,2,4,12}$	-0.00	$F_{1,3,4,12}$	0.00	$F_{2,3,4,12}$	0.00
$F_{3,3,4,12}$	0.00	$F_{1,4,4,12}$	0.00	$F_{2,4,4,12}$	0.00	$F_{3,4,4,12}$	-0.00
$F_{4,4,4,12}$	-0.00	$F_{1,1,5,12}$	-0.00	$F_{1,2,5,12}$	0.00	$F_{2,2,5,12}$	0.00
$F_{1,3,5,12}$	0.00	$F_{2,3,5,12}$	0.00	$F_{3,3,5,12}$	-0.00	$F_{1,4,5,12}$	0.00
$F_{2,4,5,12}$	0.00	$F_{3,4,5,12}$	-0.01	$F_{4,4,5,12}$	-0.02	$F_{1,5,5,12}$	-0.00
$F_{2,5,5,12}$	-0.01	$F_{3,5,5,12}$	-0.00	$F_{4,5,5,12}$	-0.00	$F_{5,5,5,12}$	-0.02
$F_{1,1,6,12}$	0.00	$F_{1,2,6,12}$	0.00	$F_{2,2,6,12}$	0.00	$F_{1,3,6,12}$	0.00
$F_{2,3,6,12}$	-0.00	$F_{3,3,6,12}$	-0.00	$F_{1,4,6,12}$	-0.00	$F_{2,4,6,12}$	-0.00
$F_{3,4,6,12}$	-0.00	$F_{4,4,6,12}$	0.01	$F_{1,5,6,12}$	-0.00	$F_{2,5,6,12}$	-0.01
$F_{3,5,6,12}$	0.00	$F_{4,5,6,12}$	0.00	$F_{5,5,6,12}$	0.01	$F_{1,6,6,12}$	-0.00
$F_{2,6,6,12}$	0.00	$F_{3,6,6,12}$	0.00	$F_{4,6,6,12}$	0.01	$F_{5,6,6,12}$	0.03
$F_{6,6,6,12}$	-0.03	$F_{1,1,7,12}$	-0.00	$F_{1,2,7,12}$	-0.00	$F_{2,2,7,12}$	0.00
$F_{1,3,7,12}$	0.00	$F_{2,3,7,12}$	-0.00	$F_{3,3,7,12}$	-0.00	$F_{1,4,7,12}$	0.00
$F_{2,4,7,12}$	0.00	$F_{3,4,7,12}$	-0.00	$F_{4,4,7,12}$	-0.00	$F_{1,5,7,12}$	-0.00
$F_{2,5,7,12}$	-0.00	$F_{3,5,7,12}$	0.00	$F_{4,5,7,12}$	0.01	$F_{5,5,7,12}$	0.01
$F_{1,6,7,12}$	-0.00	$F_{2,6,7,12}$	-0.00	$F_{3,6,7,12}$	0.00	$F_{4,6,7,12}$	0.00
$F_{5,6,7,12}$	0.01	$F_{6,6,7,12}$	-0.00	$F_{1,7,7,12}$	-0.00	$F_{2,7,7,12}$	-0.00
$F_{3,7,7,12}$	0.00	$F_{4,7,7,12}$	0.00	$F_{5,7,7,12}$	-0.02	$F_{6,7,7,12}$	-0.01
$F_{7,7,7,12}$	-0.00	$F_{1,1,8,12}$	-0.00	$F_{1,2,8,12}$	-0.00	$F_{2,2,8,12}$	-0.00
$F_{1,3,8,12}$	-0.00	$F_{2,3,8,12}$	0.00	$F_{3,3,8,12}$	0.00	$F_{1,4,8,12}$	0.00
$F_{2,4,8,12}$	0.00	$F_{3,4,8,12}$	0.00	$F_{4,4,8,12}$	0.01	$F_{1,5,8,12}$	0.00
$F_{2,5,8,12}$	0.00	$F_{3,5,8,12}$	-0.00	$F_{4,5,8,12}$	-0.00	$F_{5,5,8,12}$	0.02
$F_{1,6,8,12}$	-0.00	$F_{2,6,8,12}$	0.00	$F_{3,6,8,12}$	-0.01	$F_{4,6,8,12}$	-0.00
$F_{5,6,8,12}$	-0.01	$F_{6,6,8,12}$	-0.01	$F_{1,7,8,12}$	0.00	$F_{2,7,8,12}$	0.00
$F_{3,7,8,12}$	-0.00	$F_{4,7,8,12}$	-0.02	$F_{5,7,8,12}$	-0.00	$F_{6,7,8,12}$	0.00
$F_{7,7,8,12}$	-0.03	$F_{1,8,8,12}$	-0.00	$F_{2,8,8,12}$	0.00	$F_{3,8,8,12}$	0.00
$F_{4,8,8,12}$	0.00	$F_{5,8,8,12}$	-0.02	$F_{6,8,8,12}$	0.03	$F_{7,8,8,12}$	0.00
$F_{8,8,8,12}$	0.49	$F_{1,1,9,12}$	-0.00	$F_{1,2,9,12}$	-0.00	$F_{2,2,9,12}$	-0.00
$F_{1,3,9,12}$	-0.00	$F_{2,3,9,12}$	0.00	$F_{3,3,9,12}$	0.00	$F_{1,4,9,12}$	0.00
$F_{2,4,9,12}$	-0.00	$F_{3,4,9,12}$	0.00	$F_{4,4,9,12}$	0.01	$F_{1,5,9,12}$	0.00
$F_{2,5,9,12}$	0.00	$F_{3,5,9,12}$	0.00	$F_{4,5,9,12}$	0.00	$F_{5,5,9,12}$	0.00
$F_{1,6,9,12}$	0.00	$F_{2,6,9,12}$	0.00	$F_{3,6,9,12}$	-0.00	$F_{4,6,9,12}$	-0.00
$F_{5,6,9,12}$	-0.02	$F_{6,6,9,12}$	0.00	$F_{1,7,9,12}$	0.00	$F_{2,7,9,12}$	0.00
$F_{3,7,9,12}$	-0.00	$F_{4,7,9,12}$	-0.01	$F_{5,7,9,12}$	-0.01	$F_{6,7,9,12}$	-0.00

Table A21: The CcCR Force Constants for HOSH (cont.)

$F_{7,7,9,12}$	-0.00	$F_{1,8,9,12}$	0.00	$F_{2,8,9,12}$	-0.00	$F_{3,8,9,12}$	0.00
$F_{4,8,9,12}$	-0.00	$F_{5,8,9,12}$	-0.00	$F_{6,8,9,12}$	0.02	$F_{7,8,9,12}$	0.01
$F_{8,8,9,12}$	0.22	$F_{1,9,9,12}$	-0.00	$F_{2,9,9,12}$	-0.00	$F_{3,9,9,12}$	-0.01
$F_{4,9,9,12}$	-0.00	$F_{5,9,9,12}$	-0.01	$F_{6,9,9,12}$	-0.00	$F_{7,9,9,12}$	0.00
$F_{8,9,9,12}$	-0.18	$F_{9,9,9,12}$	0.02	$F_{1,1,10,12}$	0.00	$F_{1,2,10,12}$	0.00
$F_{2,2,10,12}$	0.00	$F_{1,3,10,12}$	-0.00	$F_{2,3,10,12}$	-0.00	$F_{3,3,10,12}$	0.00
$F_{1,4,10,12}$	-0.00	$F_{2,4,10,12}$	-0.00	$F_{3,4,10,12}$	0.00	$F_{4,4,10,12}$	0.00
$F_{1,5,10,12}$	-0.00	$F_{2,5,10,12}$	0.00	$F_{3,5,10,12}$	0.00	$F_{4,5,10,12}$	0.00
$F_{5,5,10,12}$	-0.00	$F_{1,6,10,12}$	0.00	$F_{2,6,10,12}$	0.00	$F_{3,6,10,12}$	-0.00
$F_{4,6,10,12}$	-0.01	$F_{5,6,10,12}$	-0.01	$F_{6,6,10,12}$	-0.00	$F_{1,7,10,12}$	0.00
$F_{2,7,10,12}$	0.00	$F_{3,7,10,12}$	0.00	$F_{4,7,10,12}$	-0.00	$F_{5,7,10,12}$	0.01
$F_{6,7,10,12}$	0.01	$F_{7,7,10,12}$	0.00	$F_{1,8,10,12}$	-0.00	$F_{2,8,10,12}$	-0.00
$F_{3,8,10,12}$	0.00	$F_{4,8,10,12}$	0.01	$F_{5,8,10,12}$	0.00	$F_{6,8,10,12}$	0.00
$F_{7,8,10,12}$	0.05	$F_{8,8,10,12}$	-0.00	$F_{1,9,10,12}$	-0.00	$F_{2,9,10,12}$	-0.00
$F_{3,9,10,12}$	0.00	$F_{4,9,10,12}$	0.01	$F_{5,9,10,12}$	0.00	$F_{6,9,10,12}$	0.00
$F_{7,9,10,12}$	0.01	$F_{8,9,10,12}$	-0.00	$F_{9,9,10,12}$	-0.00	$F_{1,10,10,12}$	-0.00
$F_{2,10,10,12}$	-0.00	$F_{3,10,10,12}$	-0.00	$F_{4,10,10,12}$	-0.00	$F_{5,10,10,12}$	-0.01
$F_{6,10,10,12}$	0.00	$F_{7,10,10,12}$	-0.00	$F_{8,10,10,12}$	-0.06	$F_{9,10,10,12}$	-0.02
$F_{10,10,10,12}$	0.00	$F_{1,1,11,12}$	0.00	$F_{1,2,11,12}$	0.00	$F_{2,2,11,12}$	0.00
$F_{1,3,11,12}$	-0.00	$F_{2,3,11,12}$	-0.00	$F_{3,3,11,12}$	-0.00	$F_{1,4,11,12}$	-0.00
$F_{2,4,11,12}$	-0.00	$F_{3,4,11,12}$	-0.00	$F_{4,4,11,12}$	0.00	$F_{1,5,11,12}$	-0.00
$F_{2,5,11,12}$	-0.00	$F_{3,5,11,12}$	0.00	$F_{4,5,11,12}$	0.00	$F_{5,5,11,12}$	-0.00
$F_{1,6,11,12}$	0.00	$F_{2,6,11,12}$	0.00	$F_{3,6,11,12}$	0.00	$F_{4,6,11,12}$	0.00
$F_{5,6,11,12}$	0.01	$F_{6,6,11,12}$	-0.03	$F_{1,7,11,12}$	-0.00	$F_{2,7,11,12}$	-0.00
$F_{3,7,11,12}$	0.00	$F_{4,7,11,12}$	0.01	$F_{5,7,11,12}$	0.00	$F_{6,7,11,12}$	-0.00
$F_{7,7,11,12}$	0.05	$F_{1,8,11,12}$	-0.00	$F_{2,8,11,12}$	-0.00	$F_{3,8,11,12}$	-0.00
$F_{4,8,11,12}$	0.00	$F_{5,8,11,12}$	-0.00	$F_{6,8,11,12}$	-0.02	$F_{7,8,11,12}$	-0.01
$F_{8,8,11,12}$	-0.47	$F_{1,9,11,12}$	-0.00	$F_{2,9,11,12}$	-0.00	$F_{3,9,11,12}$	-0.00
$F_{4,9,11,12}$	0.00	$F_{5,9,11,12}$	-0.00	$F_{6,9,11,12}$	-0.00	$F_{7,9,11,12}$	-0.00
$F_{8,9,11,12}$	-0.21	$F_{9,9,11,12}$	0.19	$F_{1,10,11,12}$	0.00	$F_{2,10,11,12}$	0.00

Table A22: The CcCR Force Constants for HOSH (cont.)

$F_{3,10,11,12}$	-0.00	$F_{4,10,11,12}$	-0.01	$F_{5,10,11,12}$	-0.00	$F_{6,10,11,12}$	0.00
$F_{7,10,11,12}$	-0.06	$F_{8,10,11,12}$	0.01	$F_{9,10,11,12}$	0.00	$F_{10,10,11,12}$	0.07
$F_{1,11,11,12}$	-0.00	$F_{2,11,11,12}$	0.00	$F_{3,11,11,12}$	0.00	$F_{4,11,11,12}$	0.00
$F_{5,11,11,12}$	0.00	$F_{6,11,11,12}$	0.01	$F_{7,11,11,12}$	0.01	$F_{8,11,11,12}$	0.47
$F_{9,11,11,12}$	0.22	$F_{10,11,11,12}$	-0.01	$F_{11,11,11,12}$	-0.47	$F_{1,1,12,12}$	-0.00
$F_{1,2,12,12}$	0.00	$F_{2,2,12,12}$	-0.00	$F_{1,3,12,12}$	0.00	$F_{2,3,12,12}$	0.00
$F_{3,3,12,12}$	-0.00	$F_{1,4,12,12}$	0.00	$F_{2,4,12,12}$	0.00	$F_{3,4,12,12}$	-0.00
$F_{4,4,12,12}$	-0.02	$F_{1,5,12,12}$	-0.00	$F_{2,5,12,12}$	0.00	$F_{3,5,12,12}$	-0.00
$F_{4,5,12,12}$	0.00	$F_{5,5,12,12}$	-0.01	$F_{1,6,12,12}$	-0.00	$F_{2,6,12,12}$	-0.00
$F_{3,6,12,12}$	-0.00	$F_{4,6,12,12}$	-0.00	$F_{5,6,12,12}$	-0.02	$F_{6,6,12,12}$	0.02
$F_{1,7,12,12}$	-0.00	$F_{2,7,12,12}$	-0.00	$F_{3,7,12,12}$	0.00	$F_{4,7,12,12}$	0.01
$F_{5,7,12,12}$	0.00	$F_{6,7,12,12}$	0.00	$F_{7,7,12,12}$	0.01	$F_{1,8,12,12}$	0.00
$F_{2,8,12,12}$	-0.00	$F_{3,8,12,12}$	-0.00	$F_{4,8,12,12}$	-0.00	$F_{5,8,12,12}$	0.02
$F_{6,8,12,12}$	-0.01	$F_{7,8,12,12}$	-0.00	$F_{8,8,12,12}$	-0.25	$F_{1,9,12,12}$	0.00
$F_{2,9,12,12}$	0.00	$F_{3,9,12,12}$	0.00	$F_{4,9,12,12}$	0.00	$F_{5,9,12,12}$	0.02
$F_{6,9,12,12}$	0.00	$F_{7,9,12,12}$	-0.00	$F_{8,9,12,12}$	0.16	$F_{9,9,12,12}$	-0.02
$F_{1,10,12,12}$	0.00	$F_{2,10,12,12}$	-0.00	$F_{3,10,12,12}$	0.00	$F_{4,10,12,12}$	0.01
$F_{5,10,12,12}$	0.00	$F_{6,10,12,12}$	-0.00	$F_{7,10,12,12}$	-0.02	$F_{8,10,12,12}$	0.00
$F_{9,10,12,12}$	-0.00	$F_{10,10,12,12}$	0.02	$F_{1,11,12,12}$	0.00	$F_{2,11,12,12}$	0.00
$F_{3,11,12,12}$	0.00	$F_{4,11,12,12}$	-0.00	$F_{5,11,12,12}$	-0.01	$F_{6,11,12,12}$	0.03
$F_{7,11,12,12}$	0.00	$F_{8,11,12,12}$	0.23	$F_{9,11,12,12}$	-0.18	$F_{10,11,12,12}$	-0.00
$F_{11,11,12,12}$	-0.22	$F_{1,12,12,12}$	-0.00	$F_{2,12,12,12}$	-0.00	$F_{3,12,12,12}$	0.00
$F_{4,12,12,12}$	0.00	$F_{5,12,12,12}$	-0.01	$F_{6,12,12,12}$	-0.02	$F_{7,12,12,12}$	-0.00
$F_{8,12,12,12}$	-0.15	$F_{9,12,12,12}$	0.01	$F_{10,12,12,12}$	0.00	$F_{11,12,12,12}$	0.16
$F_{12,12,12,12}$	0.01						

Table A23: The CcCR Force Constants for HSSH

$F_{1,1}$	0.035389	$F_{1,2}$	0.025097	$F_{1,3}$	-0.024657	$F_{1,4}$	-0.020648
$F_{1,5}$	-0.012017	$F_{1,6}$	0.011507	$F_{1,7}$	-0.014332	$F_{1,8}$	-0.012646
$F_{1,9}$	0.012252	$F_{1,10}$	-0.000408	$F_{1,11}$	-0.000435	$F_{1,12}$	0.000898
$F_{1,13}$	0.025097	$F_{2,1}$	0.132705	$F_{2,2}$	-0.128366	$F_{2,3}$	-0.025124
$F_{2,4}$	-0.135663	$F_{2,5}$	0.131307	$F_{2,6}$	0.000462	$F_{2,7}$	0.004713
$F_{2,8}$	-0.004840	$F_{2,9}$	-0.000435	$F_{2,10}$	-0.001755	$F_{2,11}$	0.001899
$F_{2,12}$	-0.024657	$F_{2,13}$	-0.128366	$F_{3,1}$	0.131327	$F_{3,2}$	0.024639
$F_{3,3}$	0.131267	$F_{3,4}$	-0.133790	$F_{3,5}$	0.000916	$F_{3,6}$	-0.001001
$F_{3,7}$	0.000755	$F_{3,8}$	-0.000898	$F_{3,9}$	-0.001899	$F_{3,10}$	0.001708
$F_{3,11}$	-0.020648	$F_{3,12}$	-0.025124	$F_{3,13}$	0.024639	$F_{4,1}$	0.189553
$F_{4,2}$	0.019266	$F_{4,3}$	-0.011489	$F_{4,4}$	-0.154572	$F_{4,5}$	0.005396
$F_{4,6}$	-0.012234	$F_{4,7}$	-0.014332	$F_{4,8}$	0.000462	$F_{4,9}$	-0.000916
$F_{4,10}$	-0.012017	$F_{4,11}$	-0.135663	$F_{4,12}$	0.131267	$F_{4,13}$	0.019266
$F_{5,1}$	0.150976	$F_{5,2}$	-0.134207	$F_{5,3}$	0.005396	$F_{5,4}$	-0.020025
$F_{5,5}$	0.001939	$F_{5,6}$	-0.012646	$F_{5,7}$	0.004713	$F_{5,8}$	0.001001
$F_{5,9}$	0.011507	$F_{5,10}$	0.131307	$F_{5,11}$	-0.133790	$F_{5,12}$	-0.011489
$F_{5,13}$	-0.134207	$F_{6,1}$	0.148767	$F_{6,2}$	0.012234	$F_{6,3}$	-0.001939
$F_{6,4}$	-0.015732	$F_{6,5}$	-0.012252	$F_{6,6}$	0.004840	$F_{6,7}$	0.000755
$F_{6,8}$	-0.014332	$F_{6,9}$	0.000462	$F_{6,10}$	0.000916	$F_{6,11}$	-0.154572
$F_{6,12}$	0.005396	$F_{6,13}$	0.012234	$F_{7,1}$	0.189553	$F_{7,2}$	0.019266
$F_{7,3}$	0.011489	$F_{7,4}$	-0.020648	$F_{7,5}$	-0.025124	$F_{7,6}$	-0.024639
$F_{7,7}$	-0.012646	$F_{7,8}$	0.004713	$F_{7,9}$	-0.001001	$F_{7,10}$	0.005396
$F_{7,11}$	-0.020025	$F_{7,12}$	-0.001939	$F_{7,13}$	0.019266	$F_{8,1}$	0.150976
$F_{8,2}$	0.134207	$F_{8,3}$	-0.012017	$F_{8,4}$	-0.135663	$F_{8,5}$	-0.131267
$F_{8,6}$	0.012252	$F_{8,7}$	-0.004840	$F_{8,8}$	0.000755	$F_{8,9}$	-0.012234
$F_{8,10}$	0.001939	$F_{8,11}$	-0.015732	$F_{8,12}$	0.011489	$F_{8,13}$	0.134207
$F_{9,1}$	0.148767	$F_{9,2}$	-0.011507	$F_{9,3}$	-0.131307	$F_{9,4}$	-0.133790
$F_{9,5}$	-0.000408	$F_{9,6}$	-0.000435	$F_{9,7}$	-0.000898	$F_{9,8}$	-0.014332
$F_{9,9}$	-0.012646	$F_{9,10}$	-0.012252	$F_{9,11}$	-0.020648	$F_{9,12}$	-0.012017
$F_{9,13}$	-0.011507	$F_{10,1}$	0.035389	$F_{10,2}$	0.025097	$F_{10,3}$	0.024657
$F_{10,4}$	-0.000435	$F_{10,5}$	-0.001755	$F_{10,6}$	-0.001899	$F_{10,7}$	0.000462

Table A24: The CcCR Force Constants for HSSH (cont.)

$F_{10,8}$	0.004713	$F_{10,9}$	0.004840	$F_{10,10}$	-0.025124	$F_{10,11}$	-0.135663
$F_{10,12}$	-0.131307	$F_{10,13}$	0.025097	$F_{11,1}$	0.132705	$F_{11,2}$	0.128366
$F_{11,3}$	0.000898	$F_{11,4}$	0.001899	$F_{11,5}$	0.001708	$F_{11,6}$	-0.000916
$F_{11,7}$	0.001001	$F_{11,8}$	0.000755	$F_{11,9}$	-0.024639	$F_{11,10}$	-0.131267
$F_{11,11}$	-0.133790	$F_{11,12}$	0.024657	$F_{11,13}$	0.128366	$F_{12,1}$	0.131327
$F_{1,1,1}$	0.0248	$F_{1,1,2}$	0.0380	$F_{1,2,2}$	-0.0661	$F_{2,2,2}$	-0.1493
$F_{1,1,3}$	-0.0370	$F_{1,2,3}$	0.0812	$F_{2,2,3}$	0.2918	$F_{1,3,3}$	-0.0651
$F_{2,3,3}$	-0.2902	$F_{3,3,3}$	0.1459	$F_{1,1,4}$	-0.0440	$F_{1,2,4}$	-0.0369
$F_{2,2,4}$	0.0696	$F_{1,3,4}$	0.0367	$F_{2,3,4}$	-0.0888	$F_{3,3,4}$	0.0692
$F_{1,4,4}$	0.0372	$F_{2,4,4}$	0.0303	$F_{3,4,4}$	-0.0301	$F_{4,4,4}$	-0.4571
$F_{1,1,5}$	-0.0433	$F_{1,2,5}$	0.0659	$F_{2,2,5}$	0.1483	$F_{1,3,5}$	-0.0731
$F_{2,3,5}$	-0.2924	$F_{3,3,5}$	0.2925	$F_{1,4,5}$	0.0308	$F_{2,4,5}$	-0.0642
$F_{3,4,5}$	0.0805	$F_{4,4,5}$	-0.0238	$F_{1,5,5}$	-0.0636	$F_{2,5,5}$	-0.1442
$F_{3,5,5}$	0.2968	$F_{4,5,5}$	0.0899	$F_{5,5,5}$	0.1407	$F_{1,1,6}$	0.0423
$F_{1,2,6}$	-0.0736	$F_{2,2,6}$	-0.2935	$F_{1,3,6}$	0.0651	$F_{2,3,6}$	0.2914
$F_{3,3,6}$	-0.1441	$F_{1,4,6}$	-0.0297	$F_{2,4,6}$	0.0807	$F_{3,4,6}$	-0.0655
$F_{4,4,6}$	0.0110	$F_{1,5,6}$	0.0659	$F_{2,5,6}$	0.2944	$F_{3,5,6}$	-0.2939
$F_{4,5,6}$	-0.0728	$F_{5,5,6}$	-0.2991	$F_{1,6,6}$	-0.0631	$F_{2,6,6}$	-0.2962
$F_{3,6,6}$	0.1387	$F_{4,6,6}$	0.0919	$F_{5,6,6}$	0.3005	$F_{6,6,6}$	-0.1296
$F_{1,1,7}$	0.0186	$F_{1,2,7}$	-0.0001	$F_{2,2,7}$	-0.0034	$F_{1,3,7}$	0.0021
$F_{2,3,7}$	0.0080	$F_{3,3,7}$	-0.0027	$F_{1,4,7}$	0.0074	$F_{2,4,7}$	0.0057
$F_{3,4,7}$	-0.0086	$F_{4,4,7}$	0.3933	$F_{1,5,7}$	0.0105	$F_{2,5,7}$	-0.0017
$F_{3,5,7}$	-0.0073	$F_{4,5,7}$	-0.0166	$F_{5,5,7}$	-0.0242	$F_{1,6,7}$	-0.0143
$F_{2,6,7}$	-0.0074	$F_{3,6,7}$	-0.0012	$F_{4,6,7}$	0.0086	$F_{5,6,7}$	0.0063
$F_{6,6,7}$	-0.0252	$F_{1,7,7}$	-0.0267	$F_{2,7,7}$	-0.0059	$F_{3,7,7}$	0.0074
$F_{4,7,7}$	-0.3933	$F_{5,7,7}$	0.0124	$F_{6,7,7}$	0.0117	$F_{7,7,7}$	0.4571
$F_{1,1,8}$	0.0052	$F_{1,2,8}$	0.0004	$F_{2,2,8}$	-0.0000	$F_{1,3,8}$	-0.0074
$F_{2,3,8}$	0.0005	$F_{3,3,8}$	-0.0014	$F_{1,4,8}$	0.0063	$F_{2,4,8}$	-0.0075
$F_{3,4,8}$	0.0054	$F_{4,4,8}$	-0.0124	$F_{1,5,8}$	-0.0025	$F_{2,5,8}$	-0.0024
$F_{3,5,8}$	-0.0034	$F_{4,5,8}$	-0.0183	$F_{5,5,8}$	0.0041	$F_{1,6,8}$	0.0070
$F_{2,6,8}$	-0.0008	$F_{3,6,8}$	0.0016	$F_{4,6,8}$	-0.0044	$F_{5,6,8}$	0.0034
$F_{6,6,8}$	-0.0069	$F_{1,7,8}$	-0.0095	$F_{2,7,8}$	0.0073	$F_{3,7,8}$	0.0021
$F_{4,7,8}$	0.0166	$F_{5,7,8}$	0.0183	$F_{6,7,8}$	-0.0099	$F_{7,7,8}$	0.0238
$F_{1,8,8}$	0.0021	$F_{2,8,8}$	0.0007	$F_{3,8,8}$	0.0010	$F_{4,8,8}$	0.0242
$F_{5,8,8}$	-0.0041	$F_{6,8,8}$	0.0012	$F_{7,8,8}$	-0.0899	$F_{8,8,8}$	-0.1407
$F_{1,1,9}$	-0.0058	$F_{1,2,9}$	-0.0082	$F_{2,2,9}$	0.0026	$F_{1,3,9}$	-0.0010
$F_{2,3,9}$	-0.0009	$F_{3,3,9}$	-0.0025	$F_{1,4,9}$	-0.0060	$F_{2,4,9}$	0.0110
$F_{3,4,9}$	-0.0013	$F_{4,4,9}$	0.0117	$F_{1,5,9}$	0.0073	$F_{2,5,9}$	-0.0038
$F_{3,5,9}$	0.0002	$F_{4,5,9}$	-0.0099	$F_{5,5,9}$	0.0012	$F_{1,6,9}$	-0.0011
$F_{2,6,9}$	0.0044	$F_{3,6,9}$	0.0062	$F_{4,6,9}$	-0.0251	$F_{5,6,9}$	-0.0055
$F_{6,6,9}$	-0.0062	$F_{1,7,9}$	0.0101	$F_{2,7,9}$	-0.0035	$F_{3,7,9}$	0.0014
$F_{4,7,9}$	0.0086	$F_{5,7,9}$	-0.0044	$F_{6,7,9}$	0.0251	$F_{7,7,9}$	0.0110
$F_{1,8,9}$	0.0005	$F_{2,8,9}$	0.0013	$F_{3,8,9}$	0.0011	$F_{4,8,9}$	0.0063

Table A25: The CcCR Force Constants for HSSH (cont.)

$F_{5,8,9}$	0.0034	$F_{6,8,9}$	0.0055	$F_{7,8,9}$	-0.0728	$F_{8,8,9}$	-0.2991
$F_{1,9,9}$	0.0036	$F_{2,9,9}$	-0.0026	$F_{3,9,9}$	-0.0029	$F_{4,9,9}$	0.0252
$F_{5,9,9}$	0.0069	$F_{6,9,9}$	-0.0062	$F_{7,9,9}$	-0.0919	$F_{8,9,9}$	-0.3005
$F_{9,9,9}$	-0.1296	$F_{1,1,10}$	0.0006	$F_{1,2,10}$	-0.0010	$F_{2,2,10}$	-0.0001
$F_{1,3,10}$	-0.0017	$F_{2,3,10}$	-0.0004	$F_{3,3,10}$	-0.0014	$F_{1,4,10}$	-0.0006
$F_{2,4,10}$	0.0009	$F_{3,4,10}$	0.0021	$F_{4,4,10}$	0.0267	$F_{1,5,10}$	0.0020
$F_{2,5,10}$	0.0001	$F_{3,5,10}$	-0.0001	$F_{4,5,10}$	0.0095	$F_{5,5,10}$	-0.0021
$F_{1,6,10}$	0.0017	$F_{2,6,10}$	0.0003	$F_{3,6,10}$	0.0015	$F_{4,6,10}$	0.0101
$F_{5,6,10}$	0.0005	$F_{6,6,10}$	-0.0036	$F_{1,7,10}$	0.0006	$F_{2,7,10}$	0.0003
$F_{3,7,10}$	-0.0009	$F_{4,7,10}$	-0.0074	$F_{5,7,10}$	-0.0063	$F_{6,7,10}$	-0.0060
$F_{7,7,10}$	-0.0372	$F_{1,8,10}$	-0.0020	$F_{2,8,10}$	-0.0002	$F_{3,8,10}$	-0.0002
$F_{4,8,10}$	-0.0105	$F_{5,8,10}$	0.0025	$F_{6,8,10}$	0.0073	$F_{7,8,10}$	-0.0308
$F_{8,8,10}$	0.0636	$F_{1,9,10}$	0.0017	$F_{2,9,10}$	0.0007	$F_{3,9,10}$	0.0009
$F_{4,9,10}$	-0.0143	$F_{5,9,10}$	0.0070	$F_{6,9,10}$	0.0011	$F_{7,9,10}$	-0.0297
$F_{8,9,10}$	0.0659	$F_{9,9,10}$	0.0631	$F_{1,10,10}$	-0.0006	$F_{2,10,10}$	-0.0001
$F_{3,10,10}$	0.0005	$F_{4,10,10}$	-0.0186	$F_{5,10,10}$	-0.0052	$F_{6,10,10}$	-0.0058
$F_{7,10,10}$	0.0440	$F_{8,10,10}$	0.0433	$F_{9,10,10}$	0.0423	$F_{10,10,10}$	-0.0248
$F_{1,1,11}$	0.0001	$F_{1,2,11}$	-0.0002	$F_{2,2,11}$	0.0010	$F_{1,3,11}$	-0.0007
$F_{2,3,11}$	0.0000	$F_{3,3,11}$	-0.0008	$F_{1,4,11}$	-0.0003	$F_{2,4,11}$	0.0022
$F_{3,4,11}$	0.0029	$F_{4,4,11}$	0.0059	$F_{1,5,11}$	0.0002	$F_{2,5,11}$	-0.0018
$F_{3,5,11}$	-0.0010	$F_{4,5,11}$	-0.0073	$F_{5,5,11}$	-0.0007	$F_{1,6,11}$	0.0007
$F_{2,6,11}$	-0.0000	$F_{3,6,11}$	0.0009	$F_{4,6,11}$	-0.0035	$F_{5,6,11}$	0.0013
$F_{6,6,11}$	0.0026	$F_{1,7,11}$	-0.0009	$F_{2,7,11}$	-0.0022	$F_{3,7,11}$	-0.0028
$F_{4,7,11}$	-0.0057	$F_{5,7,11}$	0.0075	$F_{6,7,11}$	0.0110	$F_{7,7,11}$	-0.0303
$F_{1,8,11}$	-0.0001	$F_{2,8,11}$	0.0018	$F_{3,8,11}$	0.0018	$F_{4,8,11}$	0.0017
$F_{5,8,11}$	0.0024	$F_{6,8,11}$	-0.0038	$F_{7,8,11}$	0.0642	$F_{8,8,11}$	0.1442
$F_{1,9,11}$	0.0003	$F_{2,9,11}$	-0.0000	$F_{3,9,11}$	-0.0003	$F_{4,9,11}$	-0.0074
$F_{5,9,11}$	-0.0008	$F_{6,9,11}$	-0.0044	$F_{7,9,11}$	0.0807	$F_{8,9,11}$	0.2944
$F_{9,9,11}$	0.2962	$F_{1,10,11}$	0.0010	$F_{2,10,11}$	0.0002	$F_{3,10,11}$	0.0006
$F_{4,10,11}$	0.0001	$F_{5,10,11}$	-0.0004	$F_{6,10,11}$	-0.0082	$F_{7,10,11}$	0.0369
$F_{8,10,11}$	-0.0659	$F_{9,10,11}$	-0.0736	$F_{10,10,11}$	-0.0380	$F_{1,11,11}$	0.0001
$F_{2,11,11}$	-0.0010	$F_{3,11,11}$	-0.0009	$F_{4,11,11}$	0.0034	$F_{5,11,11}$	0.0000
$F_{6,11,11}$	0.0026	$F_{7,11,11}$	-0.0696	$F_{8,11,11}$	-0.1483	$F_{9,11,11}$	-0.2935
$F_{10,11,11}$	0.0661	$F_{11,11,11}$	0.1493	$F_{1,1,12}$	0.0005	$F_{1,2,12}$	0.0006

Table A26: The CcCR Force Constants for HSSH (cont.)

$F_{2,2,12}$	-0.0009	$F_{1,3,12}$	0.0009	$F_{2,3,12}$	-0.0003	$F_{3,3,12}$	0.0008
$F_{1,4,12}$	-0.0009	$F_{2,4,12}$	-0.0028	$F_{3,4,12}$	-0.0025	$F_{4,4,12}$	0.0074
$F_{1,5,12}$	-0.0002	$F_{2,5,12}$	0.0018	$F_{3,5,12}$	0.0013	$F_{4,5,12}$	0.0021
$F_{5,5,12}$	0.0010	$F_{1,6,12}$	-0.0009	$F_{2,6,12}$	0.0003	$F_{3,6,12}$	-0.0008
$F_{4,6,12}$	-0.0014	$F_{5,6,12}$	-0.0011	$F_{6,6,12}$	-0.0029	$F_{1,7,12}$	0.0021
$F_{2,7,12}$	0.0029	$F_{3,7,12}$	0.0025	$F_{4,7,12}$	-0.0086	$F_{5,7,12}$	0.0054
$F_{6,7,12}$	0.0013	$F_{7,7,12}$	-0.0301	$F_{1,8,12}$	-0.0001	$F_{2,8,12}$	-0.0010
$F_{3,8,12}$	-0.0013	$F_{4,8,12}$	-0.0073	$F_{5,8,12}$	-0.0034	$F_{6,8,12}$	-0.0002
$F_{7,8,12}$	0.0805	$F_{8,8,12}$	0.2968	$F_{1,9,12}$	-0.0015	$F_{2,9,12}$	-0.0009
$F_{3,9,12}$	-0.0008	$F_{4,9,12}$	0.0012	$F_{5,9,12}$	-0.0016	$F_{6,9,12}$	0.0062
$F_{7,9,12}$	0.0655	$F_{8,9,12}$	0.2939	$F_{9,9,12}$	0.1387	$F_{1,10,12}$	-0.0017
$F_{2,10,12}$	-0.0007	$F_{3,10,12}$	-0.0009	$F_{4,10,12}$	0.0021	$F_{5,10,12}$	-0.0074
$F_{6,10,12}$	0.0010	$F_{7,10,12}$	0.0367	$F_{8,10,12}$	-0.0731	$F_{9,10,12}$	-0.0651
$F_{10,10,12}$	-0.0370	$F_{1,11,12}$	-0.0004	$F_{2,11,12}$	0.0000	$F_{3,11,12}$	0.0003
$F_{4,11,12}$	0.0080	$F_{5,11,12}$	0.0005	$F_{6,11,12}$	0.0009	$F_{7,11,12}$	-0.0888
$F_{8,11,12}$	-0.2924	$F_{9,11,12}$	-0.2914	$F_{10,11,12}$	0.0812	$F_{11,11,12}$	0.2918
$F_{1,12,12}$	0.0014	$F_{2,12,12}$	0.0008	$F_{3,12,12}$	0.0008	$F_{4,12,12}$	0.0027
$F_{5,12,12}$	0.0014	$F_{6,12,12}$	-0.0025	$F_{7,12,12}$	-0.0692	$F_{8,12,12}$	-0.2925
$F_{9,12,12}$	-0.1441	$F_{10,12,12}$	0.0651	$F_{11,12,12}$	0.2902	$F_{12,12,12}$	0.1459
$F_{1,1,1,1}$	0.02	$F_{1,1,1,2}$	-0.12	$F_{1,1,2,2}$	-0.12	$F_{1,2,2,2}$	0.09
$F_{2,2,2,2}$	-0.12	$F_{1,1,1,3}$	0.11	$F_{1,1,2,3}$	0.14	$F_{1,2,2,3}$	-0.18
$F_{2,2,2,3}$	-0.38	$F_{1,1,3,3}$	-0.12	$F_{1,2,3,3}$	0.18	$F_{2,2,3,3}$	0.62
$F_{1,3,3,3}$	-0.09	$F_{2,3,3,3}$	-0.37	$F_{3,3,3,3}$	-0.12	$F_{1,1,1,4}$	-0.01
$F_{1,1,2,4}$	0.13	$F_{1,2,2,4}$	0.11	$F_{2,2,2,4}$	-0.08	$F_{1,1,3,4}$	-0.13
$F_{1,2,3,4}$	-0.14	$F_{2,2,3,4}$	0.18	$F_{1,3,3,4}$	0.12	$F_{2,3,3,4}$	-0.18
$F_{3,3,3,4}$	0.08	$F_{1,1,4,4}$	0.01	$F_{1,2,4,4}$	-0.14	$F_{2,2,4,4}$	-0.12
$F_{1,3,4,4}$	0.14	$F_{2,3,4,4}$	0.14	$F_{3,3,4,4}$	-0.12	$F_{1,4,4,4}$	0.01
$F_{2,4,4,4}$	0.16	$F_{3,4,4,4}$	-0.16	$F_{4,4,4,4}$	0.81	$F_{1,1,1,5}$	0.11
$F_{1,1,2,5}$	0.12	$F_{1,2,2,5}$	-0.10	$F_{2,2,2,5}$	0.12	$F_{1,1,3,5}$	-0.14
$F_{1,2,3,5}$	0.18	$F_{2,2,3,5}$	0.38	$F_{1,3,3,5}$	-0.18	$F_{2,3,3,5}$	-0.62
$F_{3,3,3,5}$	0.37	$F_{1,1,4,5}$	-0.12	$F_{1,2,4,5}$	-0.11	$F_{2,2,4,5}$	0.08
$F_{1,3,4,5}$	0.13	$F_{2,3,4,5}$	-0.18	$F_{3,3,4,5}$	0.18	$F_{1,4,4,5}$	0.13
$F_{2,4,4,5}$	0.11	$F_{3,4,4,5}$	-0.14	$F_{4,4,4,5}$	-0.17	$F_{1,1,5,5}$	-0.13
$F_{1,2,5,5}$	0.10	$F_{2,2,5,5}$	-0.12	$F_{1,3,5,5}$	-0.18	$F_{2,3,5,5}$	-0.38
$F_{3,3,5,5}$	0.62	$F_{1,4,5,5}$	0.12	$F_{2,4,5,5}$	-0.09	$F_{3,4,5,5}$	0.17
$F_{4,4,5,5}$	-0.22	$F_{1,5,5,5}$	-0.12	$F_{2,5,5,5}$	0.13	$F_{3,5,5,5}$	0.38
$F_{4,5,5,5}$	0.10	$F_{5,5,5,5}$	-0.14	$F_{1,1,1,6}$	-0.11	$F_{1,1,2,6}$	-0.14
$F_{1,2,2,6}$	0.18	$F_{2,2,2,6}$	0.38	$F_{1,1,3,6}$	0.12	$F_{1,2,3,6}$	-0.18
$F_{2,2,3,6}$	-0.62	$F_{1,3,3,6}$	0.10	$F_{2,3,3,6}$	0.37	$F_{3,3,3,6}$	0.12
$F_{1,1,4,6}$	0.12	$F_{1,2,4,6}$	0.13	$F_{2,2,4,6}$	-0.18	$F_{1,3,4,6}$	-0.12

Table A27: The CcCR Force Constants for HSSH (cont.)

$F_{2,3,4,6}$	0.18	$F_{3,3,4,6}$	-0.09	$F_{1,4,4,6}$	-0.13	$F_{2,4,4,6}$	-0.14
$F_{3,4,4,6}$	0.12	$F_{4,4,4,6}$	0.18	$F_{1,1,5,6}$	0.14	$F_{1,2,5,6}$	-0.18
$F_{2,2,5,6}$	-0.38	$F_{1,3,5,6}$	0.17	$F_{2,3,5,6}$	0.62	$F_{3,3,5,6}$	-0.37
$F_{1,4,5,6}$	-0.13	$F_{2,4,5,6}$	0.17	$F_{3,4,5,6}$	-0.17	$F_{4,4,5,6}$	0.13
$F_{1,5,5,6}$	0.18	$F_{2,5,5,6}$	0.37	$F_{3,5,5,6}$	-0.63	$F_{4,5,5,6}$	-0.17
$F_{5,5,5,6}$	-0.37	$F_{1,1,6,6}$	-0.12	$F_{1,2,6,6}$	0.18	$F_{2,2,6,6}$	0.63
$F_{1,3,6,6}$	-0.10	$F_{2,3,6,6}$	-0.38	$F_{3,3,6,6}$	-0.13	$F_{1,4,6,6}$	0.12
$F_{2,4,6,6}$	-0.18	$F_{3,4,6,6}$	0.10	$F_{4,4,6,6}$	-0.23	$F_{1,5,6,6}$	-0.17
$F_{2,5,6,6}$	-0.63	$F_{3,5,6,6}$	0.37	$F_{4,5,6,6}$	0.17	$F_{5,5,6,6}$	0.64
$F_{1,6,6,6}$	0.12	$F_{2,6,6,6}$	0.38	$F_{3,6,6,6}$	0.14	$F_{4,6,6,6}$	-0.13
$F_{5,6,6,6}$	-0.37	$F_{6,6,6,6}$	-0.14	$F_{1,1,1,7}$	-0.02	$F_{1,1,2,7}$	-0.01
$F_{1,2,2,7}$	0.00	$F_{2,2,2,7}$	-0.01	$F_{1,1,3,7}$	0.01	$F_{1,2,3,7}$	-0.00
$F_{2,2,3,7}$	-0.00	$F_{1,3,3,7}$	0.00	$F_{2,3,3,7}$	0.00	$F_{3,3,3,7}$	0.01
$F_{1,1,4,7}$	0.00	$F_{1,2,4,7}$	0.01	$F_{2,2,4,7}$	0.01	$F_{1,3,4,7}$	-0.01
$F_{2,3,4,7}$	-0.01	$F_{3,3,4,7}$	0.00	$F_{1,4,4,7}$	-0.02	$F_{2,4,4,7}$	-0.03
$F_{3,4,4,7}$	0.03	$F_{4,4,4,7}$	-0.79	$F_{1,1,5,7}$	0.00	$F_{1,2,5,7}$	-0.00
$F_{2,2,5,7}$	0.02	$F_{1,3,5,7}$	0.01	$F_{2,3,5,7}$	-0.00	$F_{3,3,5,7}$	0.00
$F_{1,4,5,7}$	-0.01	$F_{2,4,5,7}$	0.00	$F_{3,4,5,7}$	0.00	$F_{4,4,5,7}$	0.05
$F_{1,5,5,7}$	0.01	$F_{2,5,5,7}$	-0.02	$F_{3,5,5,7}$	0.00	$F_{4,5,5,7}$	0.10
$F_{5,5,5,7}$	0.01	$F_{1,1,6,7}$	-0.01	$F_{1,2,6,7}$	0.01	$F_{2,2,6,7}$	0.00
$F_{1,3,6,7}$	-0.00	$F_{2,3,6,7}$	-0.00	$F_{3,3,6,7}$	-0.01	$F_{1,4,6,7}$	0.02
$F_{2,4,6,7}$	0.00	$F_{3,4,6,7}$	0.00	$F_{4,4,6,7}$	-0.04	$F_{1,5,6,7}$	-0.01
$F_{2,5,6,7}$	0.00	$F_{3,5,6,7}$	-0.00	$F_{4,5,6,7}$	0.00	$F_{5,5,6,7}$	-0.01
$F_{1,6,6,7}$	0.01	$F_{2,6,6,7}$	0.00	$F_{3,6,6,7}$	0.00	$F_{4,6,6,7}$	0.10
$F_{5,6,6,7}$	0.00	$F_{6,6,6,7}$	-0.00	$F_{1,1,7,7}$	0.01	$F_{1,2,7,7}$	0.00
$F_{2,2,7,7}$	-0.00	$F_{1,3,7,7}$	-0.00	$F_{2,3,7,7}$	0.01	$F_{3,3,7,7}$	-0.01
$F_{1,4,7,7}$	0.02	$F_{2,4,7,7}$	0.02	$F_{3,4,7,7}$	-0.02	$F_{4,4,7,7}$	0.79
$F_{1,5,7,7}$	0.01	$F_{2,5,7,7}$	-0.01	$F_{3,5,7,7}$	-0.01	$F_{4,5,7,7}$	-0.04
$F_{5,5,7,7}$	-0.10	$F_{1,6,7,7}$	-0.01	$F_{2,6,7,7}$	-0.01	$F_{3,6,7,7}$	0.00
$F_{4,6,7,7}$	0.01	$F_{5,6,7,7}$	0.00	$F_{6,6,7,7}$	-0.11	$F_{1,7,7,7}$	-0.04
$F_{2,7,7,7}$	-0.02	$F_{3,7,7,7}$	0.03	$F_{4,7,7,7}$	-0.79	$F_{5,7,7,7}$	0.03
$F_{6,7,7,7}$	-0.01	$F_{7,7,7,7}$	0.81	$F_{1,1,1,8}$	0.01	$F_{1,1,2,8}$	-0.00
$F_{1,2,2,8}$	0.01	$F_{2,2,2,8}$	-0.00	$F_{1,1,3,8}$	0.00	$F_{1,2,3,8}$	0.00

Table A28: The CcCR Force Constants for HSSH (cont.)

$F_{2,2,3,8}$	-0.00	$F_{1,3,3,8}$	-0.01	$F_{2,3,3,8}$	-0.00	$F_{3,3,3,8}$	0.00
$F_{1,1,4,8}$	-0.01	$F_{1,2,4,8}$	-0.00	$F_{2,2,4,8}$	-0.00	$F_{1,3,4,8}$	0.00
$F_{2,3,4,8}$	-0.00	$F_{3,3,4,8}$	0.01	$F_{1,4,4,8}$	0.01	$F_{2,4,4,8}$	0.01
$F_{3,4,4,8}$	-0.00	$F_{4,4,4,8}$	0.03	$F_{1,1,5,8}$	0.01	$F_{1,2,5,8}$	-0.01
$F_{2,2,5,8}$	0.01	$F_{1,3,5,8}$	-0.00	$F_{2,3,5,8}$	0.00	$F_{3,3,5,8}$	-0.00
$F_{1,4,5,8}$	0.00	$F_{2,4,5,8}$	0.01	$F_{3,4,5,8}$	0.00	$F_{4,4,5,8}$	0.10
$F_{1,5,5,8}$	0.02	$F_{2,5,5,8}$	-0.01	$F_{3,5,5,8}$	-0.00	$F_{4,5,5,8}$	-0.02
$F_{5,5,5,8}$	0.01	$F_{1,1,6,8}$	-0.00	$F_{1,2,6,8}$	-0.00	$F_{2,2,6,8}$	-0.00
$F_{1,3,6,8}$	0.01	$F_{2,3,6,8}$	0.00	$F_{3,3,6,8}$	-0.00	$F_{1,4,6,8}$	-0.00
$F_{2,4,6,8}$	0.00	$F_{3,4,6,8}$	-0.01	$F_{4,4,6,8}$	0.00	$F_{1,5,6,8}$	-0.00
$F_{2,5,6,8}$	0.00	$F_{3,5,6,8}$	0.00	$F_{4,5,6,8}$	-0.00	$F_{5,5,6,8}$	0.00
$F_{1,6,6,8}$	-0.00	$F_{2,6,6,8}$	-0.00	$F_{3,6,6,8}$	0.00	$F_{4,6,6,8}$	0.01
$F_{5,6,6,8}$	-0.01	$F_{6,6,6,8}$	-0.00	$F_{1,1,7,8}$	0.01	$F_{1,2,7,8}$	0.00
$F_{2,2,7,8}$	-0.00	$F_{1,3,7,8}$	-0.01	$F_{2,3,7,8}$	0.00	$F_{3,3,7,8}$	-0.00
$F_{1,4,7,8}$	0.00	$F_{2,4,7,8}$	-0.01	$F_{3,4,7,8}$	0.00	$F_{4,4,7,8}$	-0.04
$F_{1,5,7,8}$	-0.01	$F_{2,5,7,8}$	0.00	$F_{3,5,7,8}$	-0.00	$F_{4,5,7,8}$	-0.09
$F_{5,5,7,8}$	0.01	$F_{1,6,7,8}$	0.00	$F_{2,6,7,8}$	-0.00	$F_{3,6,7,8}$	0.00
$F_{4,6,7,8}$	0.00	$F_{5,6,7,8}$	0.00	$F_{6,6,7,8}$	-0.00	$F_{1,7,7,8}$	-0.01
$F_{2,7,7,8}$	0.01	$F_{3,7,7,8}$	0.00	$F_{4,7,7,8}$	0.05	$F_{5,7,7,8}$	0.10
$F_{6,7,7,8}$	-0.01	$F_{7,7,7,8}$	-0.17	$F_{1,1,8,8}$	-0.01	$F_{1,2,8,8}$	0.00
$F_{2,2,8,8}$	-0.00	$F_{1,3,8,8}$	-0.00	$F_{2,3,8,8}$	-0.00	$F_{3,3,8,8}$	0.00
$F_{1,4,8,8}$	-0.01	$F_{2,4,8,8}$	-0.00	$F_{3,4,8,8}$	0.01	$F_{4,4,8,8}$	-0.10
$F_{1,5,8,8}$	-0.01	$F_{2,5,8,8}$	0.01	$F_{3,5,8,8}$	0.00	$F_{4,5,8,8}$	0.01
$F_{5,5,8,8}$	-0.01	$F_{1,6,8,8}$	0.01	$F_{2,6,8,8}$	0.00	$F_{3,6,8,8}$	-0.00
$F_{4,6,8,8}$	-0.01	$F_{5,6,8,8}$	-0.01	$F_{6,6,8,8}$	0.01	$F_{1,7,8,8}$	0.01
$F_{2,7,8,8}$	0.00	$F_{3,7,8,8}$	-0.00	$F_{4,7,8,8}$	0.10	$F_{5,7,8,8}$	-0.02
$F_{6,7,8,8}$	0.01	$F_{7,7,8,8}$	-0.22	$F_{1,8,8,8}$	0.01	$F_{2,8,8,8}$	-0.01
$F_{3,8,8,8}$	0.00	$F_{4,8,8,8}$	0.01	$F_{5,8,8,8}$	0.01	$F_{6,8,8,8}$	0.01
$F_{7,8,8,8}$	0.10	$F_{8,8,8,8}$	-0.14	$F_{1,1,1,9}$	-0.00	$F_{1,1,2,9}$	0.01
$F_{1,2,2,9}$	0.00	$F_{2,2,2,9}$	0.00	$F_{1,1,3,9}$	0.00	$F_{1,2,3,9}$	-0.00
$F_{2,2,3,9}$	0.00	$F_{1,3,3,9}$	-0.01	$F_{2,3,3,9}$	0.00	$F_{3,3,3,9}$	-0.01
$F_{1,1,4,9}$	0.01	$F_{1,2,4,9}$	0.00	$F_{2,2,4,9}$	-0.01	$F_{1,3,4,9}$	-0.00
$F_{2,3,4,9}$	0.00	$F_{3,3,4,9}$	0.01	$F_{1,4,4,9}$	-0.01	$F_{2,4,4,9}$	-0.01
$F_{3,4,4,9}$	0.01	$F_{4,4,4,9}$	0.01	$F_{1,1,5,9}$	-0.00	$F_{1,2,5,9}$	-0.00
$F_{2,2,5,9}$	-0.00	$F_{1,3,5,9}$	0.00	$F_{2,3,5,9}$	-0.00	$F_{3,3,5,9}$	-0.01
$F_{1,4,5,9}$	-0.00	$F_{2,4,5,9}$	0.01	$F_{3,4,5,9}$	-0.00	$F_{4,4,5,9}$	0.01
$F_{1,5,5,9}$	0.00	$F_{2,5,5,9}$	0.01	$F_{3,5,5,9}$	0.01	$F_{4,5,5,9}$	-0.01
$F_{5,5,5,9}$	-0.01	$F_{1,1,6,9}$	0.01	$F_{1,2,6,9}$	0.00	$F_{2,2,6,9}$	-0.01
$F_{1,3,6,9}$	0.01	$F_{2,3,6,9}$	0.00	$F_{3,3,6,9}$	0.01	$F_{1,4,6,9}$	-0.00
$F_{2,4,6,9}$	-0.00	$F_{3,4,6,9}$	-0.01	$F_{4,4,6,9}$	0.11	$F_{1,5,6,9}$	0.00
$F_{2,5,6,9}$	0.01	$F_{3,5,6,9}$	0.00	$F_{4,5,6,9}$	0.00	$F_{5,5,6,9}$	-0.01

Table A29: The CcCR Force Constants for HSSH (cont.)

$F_{1,6,6,9}$	-0.02	$F_{2,6,6,9}$	-0.00	$F_{3,6,6,9}$	-0.01	$F_{4,6,6,9}$	0.02
$F_{5,6,6,9}$	-0.00	$F_{6,6,6,9}$	0.00	$F_{1,1,7,9}$	-0.01	$F_{1,2,7,9}$	-0.01
$F_{2,2,7,9}$	0.00	$F_{1,3,7,9}$	0.00	$F_{2,3,7,9}$	0.00	$F_{3,3,7,9}$	-0.00
$F_{1,4,7,9}$	-0.01	$F_{2,4,7,9}$	0.01	$F_{3,4,7,9}$	-0.00	$F_{4,4,7,9}$	-0.01
$F_{1,5,7,9}$	0.01	$F_{2,5,7,9}$	-0.01	$F_{3,5,7,9}$	-0.00	$F_{4,5,7,9}$	-0.00
$F_{5,5,7,9}$	0.01	$F_{1,6,7,9}$	-0.01	$F_{2,6,7,9}$	0.00	$F_{3,6,7,9}$	0.01
$F_{4,6,7,9}$	-0.10	$F_{5,6,7,9}$	-0.00	$F_{6,6,7,9}$	0.00	$F_{1,7,7,9}$	0.01
$F_{2,7,7,9}$	-0.00	$F_{3,7,7,9}$	0.00	$F_{4,7,7,9}$	0.04	$F_{5,7,7,9}$	-0.00
$F_{6,7,7,9}$	0.11	$F_{7,7,7,9}$	-0.18	$F_{1,1,8,9}$	0.00	$F_{1,2,8,9}$	0.00
$F_{2,2,8,9}$	0.00	$F_{1,3,8,9}$	-0.00	$F_{2,3,8,9}$	0.00	$F_{3,3,8,9}$	0.00
$F_{1,4,8,9}$	-0.00	$F_{2,4,8,9}$	-0.00	$F_{3,4,8,9}$	0.00	$F_{4,4,8,9}$	-0.00
$F_{1,5,8,9}$	0.00	$F_{2,5,8,9}$	-0.01	$F_{3,5,8,9}$	-0.00	$F_{4,5,8,9}$	-0.00
$F_{5,5,8,9}$	0.01	$F_{1,6,8,9}$	-0.00	$F_{2,6,8,9}$	-0.00	$F_{3,6,8,9}$	-0.00
$F_{4,6,8,9}$	-0.00	$F_{5,6,8,9}$	0.01	$F_{6,6,8,9}$	0.00	$F_{1,7,8,9}$	0.00
$F_{2,7,8,9}$	0.00	$F_{3,7,8,9}$	-0.00	$F_{4,7,8,9}$	-0.00	$F_{5,7,8,9}$	0.00
$F_{6,7,8,9}$	0.00	$F_{7,7,8,9}$	-0.13	$F_{1,8,8,9}$	0.00	$F_{2,8,8,9}$	0.00
$F_{3,8,8,9}$	-0.00	$F_{4,8,8,9}$	0.01	$F_{5,8,8,9}$	-0.00	$F_{6,8,8,9}$	-0.01
$F_{7,8,8,9}$	0.17	$F_{8,8,8,9}$	0.37	$F_{1,1,9,9}$	-0.01	$F_{1,2,9,9}$	0.00
$F_{2,2,9,9}$	0.00	$F_{1,3,9,9}$	0.00	$F_{2,3,9,9}$	-0.00	$F_{3,3,9,9}$	-0.00
$F_{1,4,9,9}$	0.00	$F_{2,4,9,9}$	-0.00	$F_{3,4,9,9}$	0.00	$F_{4,4,9,9}$	-0.11
$F_{1,5,9,9}$	-0.00	$F_{2,5,9,9}$	0.00	$F_{3,5,9,9}$	0.00	$F_{4,5,9,9}$	-0.00
$F_{5,5,9,9}$	0.01	$F_{1,6,9,9}$	0.01	$F_{2,6,9,9}$	-0.00	$F_{3,6,9,9}$	0.00
$F_{4,6,9,9}$	-0.00	$F_{5,6,9,9}$	-0.00	$F_{6,6,9,9}$	0.01	$F_{1,7,9,9}$	0.01
$F_{2,7,9,9}$	-0.00	$F_{3,7,9,9}$	-0.01	$F_{4,7,9,9}$	0.10	$F_{5,7,9,9}$	0.01
$F_{6,7,9,9}$	-0.02	$F_{7,7,9,9}$	-0.23	$F_{1,8,9,9}$	0.00	$F_{2,8,9,9}$	-0.00
$F_{3,8,9,9}$	-0.00	$F_{4,8,9,9}$	0.00	$F_{5,8,9,9}$	-0.01	$F_{6,8,9,9}$	0.00
$F_{7,8,9,9}$	0.17	$F_{8,8,9,9}$	0.64	$F_{1,9,9,9}$	-0.01	$F_{2,9,9,9}$	0.00
$F_{3,9,9,9}$	-0.00	$F_{4,9,9,9}$	0.00	$F_{5,9,9,9}$	0.00	$F_{6,9,9,9}$	0.00
$F_{7,9,9,9}$	0.13	$F_{8,9,9,9}$	0.37	$F_{9,9,9,9}$	-0.14	$F_{1,1,1,10}$	0.00
$F_{1,1,2,10}$	0.00	$F_{1,2,2,10}$	0.00	$F_{2,2,2,10}$	0.00	$F_{1,1,3,10}$	0.00
$F_{1,2,3,10}$	-0.00	$F_{2,2,3,10}$	0.00	$F_{1,3,3,10}$	-0.00	$F_{2,3,3,10}$	-0.00
$F_{3,3,3,10}$	-0.00	$F_{1,1,4,10}$	-0.00	$F_{1,2,4,10}$	-0.00	$F_{2,2,4,10}$	0.00

Table A30: The CcCR Force Constants for HSSH (cont.)

$F_{1,3,4,10}$	0.00	$F_{2,3,4,10}$	-0.00	$F_{3,3,4,10}$	0.00	$F_{1,4,4,10}$	0.00
$F_{2,4,4,10}$	0.00	$F_{3,4,4,10}$	-0.00	$F_{4,4,4,10}$	-0.04	$F_{1,1,5,10}$	0.00
$F_{1,2,5,10}$	-0.00	$F_{2,2,5,10}$	-0.00	$F_{1,3,5,10}$	0.00	$F_{2,3,5,10}$	-0.00
$F_{3,3,5,10}$	-0.00	$F_{1,4,5,10}$	-0.00	$F_{2,4,5,10}$	-0.00	$F_{3,4,5,10}$	0.00
$F_{4,4,5,10}$	-0.01	$F_{1,5,5,10}$	0.00	$F_{2,5,5,10}$	0.00	$F_{3,5,5,10}$	0.00
$F_{4,5,5,10}$	0.01	$F_{5,5,5,10}$	0.01	$F_{1,1,6,10}$	0.00	$F_{1,2,6,10}$	-0.00
$F_{2,2,6,10}$	-0.00	$F_{1,3,6,10}$	0.00	$F_{2,3,6,10}$	0.00	$F_{3,3,6,10}$	0.00
$F_{1,4,6,10}$	-0.00	$F_{2,4,6,10}$	0.00	$F_{3,4,6,10}$	-0.00	$F_{4,4,6,10}$	-0.01
$F_{1,5,6,10}$	-0.00	$F_{2,5,6,10}$	0.00	$F_{3,5,6,10}$	-0.00	$F_{4,5,6,10}$	-0.00
$F_{5,5,6,10}$	-0.00	$F_{1,6,6,10}$	-0.00	$F_{2,6,6,10}$	-0.00	$F_{3,6,6,10}$	-0.00
$F_{4,6,6,10}$	0.01	$F_{5,6,6,10}$	0.00	$F_{6,6,6,10}$	0.01	$F_{1,1,7,10}$	0.00
$F_{1,2,7,10}$	0.00	$F_{2,2,7,10}$	-0.00	$F_{1,3,7,10}$	-0.00	$F_{2,3,7,10}$	0.00
$F_{3,3,7,10}$	-0.00	$F_{1,4,7,10}$	-0.01	$F_{2,4,7,10}$	-0.00	$F_{3,4,7,10}$	0.00
$F_{4,4,7,10}$	0.02	$F_{1,5,7,10}$	0.00	$F_{2,5,7,10}$	0.01	$F_{3,5,7,10}$	-0.00
$F_{4,5,7,10}$	0.00	$F_{5,5,7,10}$	-0.01	$F_{1,6,7,10}$	-0.00	$F_{2,6,7,10}$	-0.00
$F_{3,6,7,10}$	0.00	$F_{4,6,7,10}$	0.01	$F_{5,6,7,10}$	0.00	$F_{6,6,7,10}$	0.00
$F_{1,7,7,10}$	0.00	$F_{2,7,7,10}$	0.00	$F_{3,7,7,10}$	-0.00	$F_{4,7,7,10}$	-0.02
$F_{5,7,7,10}$	0.01	$F_{6,7,7,10}$	0.01	$F_{7,7,7,10}$	0.01	$F_{1,1,8,10}$	-0.00
$F_{1,2,8,10}$	0.00	$F_{2,2,8,10}$	0.00	$F_{1,3,8,10}$	-0.00	$F_{2,3,8,10}$	-0.00
$F_{3,3,8,10}$	0.00	$F_{1,4,8,10}$	0.00	$F_{2,4,8,10}$	0.00	$F_{3,4,8,10}$	0.00
$F_{4,4,8,10}$	0.01	$F_{1,5,8,10}$	-0.00	$F_{2,5,8,10}$	-0.00	$F_{3,5,8,10}$	0.00
$F_{4,5,8,10}$	-0.01	$F_{5,5,8,10}$	-0.01	$F_{1,6,8,10}$	0.00	$F_{2,6,8,10}$	0.00
$F_{3,6,8,10}$	0.00	$F_{4,6,8,10}$	-0.01	$F_{5,6,8,10}$	-0.00	$F_{6,6,8,10}$	-0.00
$F_{1,7,8,10}$	-0.00	$F_{2,7,8,10}$	-0.00	$F_{3,7,8,10}$	0.00	$F_{4,7,8,10}$	-0.01
$F_{5,7,8,10}$	0.00	$F_{6,7,8,10}$	0.00	$F_{7,7,8,10}$	0.13	$F_{1,8,8,10}$	0.00
$F_{2,8,8,10}$	0.00	$F_{3,8,8,10}$	0.00	$F_{4,8,8,10}$	0.01	$F_{5,8,8,10}$	0.02
$F_{6,8,8,10}$	-0.00	$F_{7,8,8,10}$	0.12	$F_{8,8,8,10}$	-0.12	$F_{1,1,9,10}$	-0.00
$F_{1,2,9,10}$	0.00	$F_{2,2,9,10}$	0.00	$F_{1,3,9,10}$	0.00	$F_{2,3,9,10}$	-0.00
$F_{3,3,9,10}$	0.00	$F_{1,4,9,10}$	0.00	$F_{2,4,9,10}$	-0.00	$F_{3,4,9,10}$	-0.00
$F_{4,4,9,10}$	0.01	$F_{1,5,9,10}$	-0.00	$F_{2,5,9,10}$	0.00	$F_{3,5,9,10}$	0.00
$F_{4,5,9,10}$	-0.00	$F_{5,5,9,10}$	-0.01	$F_{1,6,9,10}$	0.00	$F_{2,6,9,10}$	0.00
$F_{3,6,9,10}$	-0.00	$F_{4,6,9,10}$	-0.01	$F_{5,6,9,10}$	-0.00	$F_{6,6,9,10}$	-0.01
$F_{1,7,9,10}$	0.00	$F_{2,7,9,10}$	0.00	$F_{3,7,9,10}$	-0.00	$F_{4,7,9,10}$	-0.02
$F_{5,7,9,10}$	0.00	$F_{6,7,9,10}$	-0.00	$F_{7,7,9,10}$	0.13	$F_{1,8,9,10}$	0.00
$F_{2,8,9,10}$	0.00	$F_{3,8,9,10}$	-0.00	$F_{4,8,9,10}$	0.01	$F_{5,8,9,10}$	0.00
$F_{6,8,9,10}$	0.00	$F_{7,8,9,10}$	0.13	$F_{8,8,9,10}$	-0.18	$F_{1,9,9,10}$	-0.00
$F_{2,9,9,10}$	0.00	$F_{3,9,9,10}$	-0.00	$F_{4,9,9,10}$	0.01	$F_{5,9,9,10}$	-0.00
$F_{6,9,9,10}$	0.02	$F_{7,9,9,10}$	0.12	$F_{8,9,9,10}$	-0.17	$F_{9,9,9,10}$	-0.12
$F_{1,1,10,10}$	-0.00	$F_{1,2,10,10}$	-0.00	$F_{2,2,10,10}$	0.00	$F_{1,3,10,10}$	-0.00
$F_{2,3,10,10}$	-0.00	$F_{3,3,10,10}$	0.00	$F_{1,4,10,10}$	0.00	$F_{2,4,10,10}$	0.00
$F_{3,4,10,10}$	-0.00	$F_{4,4,10,10}$	0.01	$F_{1,5,10,10}$	-0.00	$F_{2,5,10,10}$	-0.00
$F_{3,5,10,10}$	0.00	$F_{4,5,10,10}$	0.01	$F_{5,5,10,10}$	-0.01	$F_{1,6,10,10}$	0.00

Table A31: The CcCR Force Constants for HSSH (cont.)

$F_{2,6,10,10}$	0.00	$F_{3,6,10,10}$	0.00	$F_{4,6,10,10}$	0.01	$F_{5,6,10,10}$	-0.00
$F_{6,6,10,10}$	-0.01	$F_{1,7,10,10}$	-0.00	$F_{2,7,10,10}$	-0.00	$F_{3,7,10,10}$	0.00
$F_{4,7,10,10}$	0.00	$F_{5,7,10,10}$	-0.01	$F_{6,7,10,10}$	-0.01	$F_{7,7,10,10}$	0.01
$F_{1,8,10,10}$	0.00	$F_{2,8,10,10}$	0.00	$F_{3,8,10,10}$	-0.00	$F_{4,8,10,10}$	0.00
$F_{5,8,10,10}$	0.01	$F_{6,8,10,10}$	0.00	$F_{7,8,10,10}$	-0.12	$F_{8,8,10,10}$	-0.13
$F_{1,9,10,10}$	-0.00	$F_{2,9,10,10}$	0.00	$F_{3,9,10,10}$	0.00	$F_{4,9,10,10}$	0.01
$F_{5,9,10,10}$	0.00	$F_{6,9,10,10}$	0.01	$F_{7,9,10,10}$	-0.12	$F_{8,9,10,10}$	-0.14
$F_{9,9,10,10}$	-0.12	$F_{1,10,10,10}$	0.00	$F_{2,10,10,10}$	0.00	$F_{3,10,10,10}$	0.00
$F_{4,10,10,10}$	-0.02	$F_{5,10,10,10}$	0.01	$F_{6,10,10,10}$	0.00	$F_{7,10,10,10}$	-0.01
$F_{8,10,10,10}$	0.11	$F_{9,10,10,10}$	0.11	$F_{10,10,10,10}$	0.02	$F_{1,1,1,11}$	0.00
$F_{1,1,2,11}$	0.00	$F_{1,2,2,11}$	0.00	$F_{2,2,2,11}$	0.00	$F_{1,1,3,11}$	0.00
$F_{1,2,3,11}$	-0.00	$F_{2,2,3,11}$	0.00	$F_{1,3,3,11}$	0.00	$F_{2,3,3,11}$	0.00
$F_{3,3,3,11}$	-0.00	$F_{1,1,4,11}$	-0.00	$F_{1,2,4,11}$	0.00	$F_{2,2,4,11}$	-0.00
$F_{1,3,4,11}$	0.00	$F_{2,3,4,11}$	0.00	$F_{3,3,4,11}$	-0.00	$F_{1,4,4,11}$	0.00
$F_{2,4,4,11}$	-0.00	$F_{3,4,4,11}$	-0.00	$F_{4,4,4,11}$	-0.02	$F_{1,1,5,11}$	0.00
$F_{1,2,5,11}$	0.00	$F_{2,2,5,11}$	-0.00	$F_{1,3,5,11}$	-0.00	$F_{2,3,5,11}$	-0.00
$F_{3,3,5,11}$	-0.00	$F_{1,4,5,11}$	-0.00	$F_{2,4,5,11}$	0.00	$F_{3,4,5,11}$	0.00
$F_{4,4,5,11}$	0.01	$F_{1,5,5,11}$	0.00	$F_{2,5,5,11}$	0.00	$F_{3,5,5,11}$	0.00
$F_{4,5,5,11}$	0.00	$F_{5,5,5,11}$	-0.01	$F_{1,1,6,11}$	-0.00	$F_{1,2,6,11}$	0.00
$F_{2,2,6,11}$	-0.00	$F_{1,3,6,11}$	-0.00	$F_{2,3,6,11}$	-0.00	$F_{3,3,6,11}$	0.00
$F_{1,4,6,11}$	-0.00	$F_{2,4,6,11}$	-0.00	$F_{3,4,6,11}$	0.00	$F_{4,4,6,11}$	0.00
$F_{1,5,6,11}$	-0.00	$F_{2,5,6,11}$	0.00	$F_{3,5,6,11}$	0.00	$F_{4,5,6,11}$	-0.00
$F_{5,5,6,11}$	-0.00	$F_{1,6,6,11}$	0.00	$F_{2,6,6,11}$	0.00	$F_{3,6,6,11}$	0.00
$F_{4,6,6,11}$	-0.00	$F_{5,6,6,11}$	-0.00	$F_{6,6,6,11}$	-0.00	$F_{1,1,7,11}$	0.00
$F_{1,2,7,11}$	0.00	$F_{2,2,7,11}$	0.00	$F_{1,3,7,11}$	-0.00	$F_{2,3,7,11}$	-0.00
$F_{3,3,7,11}$	0.00	$F_{1,4,7,11}$	-0.00	$F_{2,4,7,11}$	0.00	$F_{3,4,7,11}$	0.00
$F_{4,4,7,11}$	0.02	$F_{1,5,7,11}$	0.00	$F_{2,5,7,11}$	-0.00	$F_{3,5,7,11}$	-0.00
$F_{4,5,7,11}$	-0.01	$F_{5,5,7,11}$	-0.00	$F_{1,6,7,11}$	0.00	$F_{2,6,7,11}$	0.00
$F_{3,6,7,11}$	0.00	$F_{4,6,7,11}$	-0.01	$F_{5,6,7,11}$	0.00	$F_{6,6,7,11}$	-0.00
$F_{1,7,7,11}$	0.00	$F_{2,7,7,11}$	-0.00	$F_{3,7,7,11}$	-0.00	$F_{4,7,7,11}$	-0.03
$F_{5,7,7,11}$	0.01	$F_{6,7,7,11}$	0.01	$F_{7,7,7,11}$	0.16	$F_{1,1,8,11}$	-0.00
$F_{1,2,8,11}$	-0.00	$F_{2,2,8,11}$	0.00	$F_{1,3,8,11}$	0.00	$F_{2,3,8,11}$	0.00
$F_{3,3,8,11}$	0.00	$F_{1,4,8,11}$	0.01	$F_{2,4,8,11}$	-0.00	$F_{3,4,8,11}$	-0.01
$F_{4,4,8,11}$	-0.01	$F_{1,5,8,11}$	-0.00	$F_{2,5,8,11}$	-0.00	$F_{3,5,8,11}$	-0.00
$F_{4,5,8,11}$	0.00	$F_{5,5,8,11}$	0.01	$F_{1,6,8,11}$	-0.00	$F_{2,6,8,11}$	-0.00
$F_{3,6,8,11}$	-0.00	$F_{4,6,8,11}$	0.01	$F_{5,6,8,11}$	0.01	$F_{6,6,8,11}$	0.00
$F_{1,7,8,11}$	-0.00	$F_{2,7,8,11}$	0.00	$F_{3,7,8,11}$	0.00	$F_{4,7,8,11}$	0.00
$F_{5,7,8,11}$	0.01	$F_{6,7,8,11}$	-0.01	$F_{7,7,8,11}$	0.11	$F_{1,8,8,11}$	0.00
$F_{2,8,8,11}$	0.00	$F_{3,8,8,11}$	-0.00	$F_{4,8,8,11}$	-0.02	$F_{5,8,8,11}$	-0.01
$F_{6,8,8,11}$	-0.01	$F_{7,8,8,11}$	-0.09	$F_{8,8,8,11}$	0.13	$F_{1,1,9,11}$	-0.00
$F_{1,2,9,11}$	0.00	$F_{2,2,9,11}$	-0.00	$F_{1,3,9,11}$	-0.00	$F_{2,3,9,11}$	-0.00

Table A32: The CcCR Force Constants for HSSH (cont.)

$F_{3,3,9,11}$	0.00	$F_{1,4,9,11}$	0.00	$F_{2,4,9,11}$	-0.00	$F_{3,4,9,11}$	0.00
$F_{4,4,9,11}$	0.01	$F_{1,5,9,11}$	-0.00	$F_{2,5,9,11}$	0.00	$F_{3,5,9,11}$	0.00
$F_{4,5,9,11}$	0.00	$F_{5,5,9,11}$	-0.00	$F_{1,6,9,11}$	0.00	$F_{2,6,9,11}$	0.00
$F_{3,6,9,11}$	-0.00	$F_{4,6,9,11}$	0.00	$F_{5,6,9,11}$	-0.00	$F_{6,6,9,11}$	0.00
$F_{1,7,9,11}$	-0.00	$F_{2,7,9,11}$	0.00	$F_{3,7,9,11}$	-0.00	$F_{4,7,9,11}$	-0.00
$F_{5,7,9,11}$	-0.00	$F_{6,7,9,11}$	-0.00	$F_{7,7,9,11}$	0.14	$F_{1,8,9,11}$	-0.00
$F_{2,8,9,11}$	-0.00	$F_{3,8,9,11}$	-0.00	$F_{4,8,9,11}$	-0.00	$F_{5,8,9,11}$	-0.00
$F_{6,8,9,11}$	0.01	$F_{7,8,9,11}$	-0.17	$F_{8,8,9,11}$	-0.37	$F_{1,9,9,11}$	-0.00
$F_{2,9,9,11}$	0.00	$F_{3,9,9,11}$	0.00	$F_{4,9,9,11}$	0.00	$F_{5,9,9,11}$	-0.00
$F_{6,9,9,11}$	0.00	$F_{7,9,9,11}$	-0.18	$F_{8,9,9,11}$	-0.63	$F_{9,9,9,11}$	-0.38
$F_{1,1,10,11}$	-0.00	$F_{1,2,10,11}$	-0.00	$F_{2,2,10,11}$	-0.00	$F_{1,3,10,11}$	0.00
$F_{2,3,10,11}$	0.00	$F_{3,3,10,11}$	0.00	$F_{1,4,10,11}$	0.00	$F_{2,4,10,11}$	0.00
$F_{3,4,10,11}$	-0.00	$F_{4,4,10,11}$	0.00	$F_{1,5,10,11}$	0.00	$F_{2,5,10,11}$	-0.00
$F_{3,5,10,11}$	-0.00	$F_{4,5,10,11}$	0.00	$F_{5,5,10,11}$	0.00	$F_{1,6,10,11}$	-0.00
$F_{2,6,10,11}$	-0.00	$F_{3,6,10,11}$	-0.00	$F_{4,6,10,11}$	0.01	$F_{5,6,10,11}$	-0.00
$F_{6,6,10,11}$	0.00	$F_{1,7,10,11}$	-0.00	$F_{2,7,10,11}$	0.00	$F_{3,7,10,11}$	-0.00
$F_{4,7,10,11}$	0.01	$F_{5,7,10,11}$	-0.00	$F_{6,7,10,11}$	-0.00	$F_{7,7,10,11}$	-0.14
$F_{1,8,10,11}$	-0.00	$F_{2,8,10,11}$	0.00	$F_{3,8,10,11}$	-0.00	$F_{4,8,10,11}$	-0.00
$F_{5,8,10,11}$	-0.01	$F_{6,8,10,11}$	0.00	$F_{7,8,10,11}$	-0.11	$F_{8,8,10,11}$	0.10
$F_{1,9,10,11}$	0.00	$F_{2,9,10,11}$	-0.00	$F_{3,9,10,11}$	0.00	$F_{4,9,10,11}$	-0.01
$F_{5,9,10,11}$	0.00	$F_{6,9,10,11}$	0.00	$F_{7,9,10,11}$	-0.13	$F_{8,9,10,11}$	0.18
$F_{9,9,10,11}$	0.18	$F_{1,10,10,11}$	0.00	$F_{2,10,10,11}$	0.00	$F_{3,10,10,11}$	0.00
$F_{4,10,10,11}$	-0.01	$F_{5,10,10,11}$	-0.00	$F_{6,10,10,11}$	-0.01	$F_{7,10,10,11}$	0.13
$F_{8,10,10,11}$	0.12	$F_{9,10,10,11}$	0.14	$F_{10,10,10,11}$	-0.12	$F_{1,1,11,11}$	0.00
$F_{1,2,11,11}$	-0.00	$F_{2,2,11,11}$	-0.00	$F_{1,3,11,11}$	-0.00	$F_{2,3,11,11}$	-0.00
$F_{3,3,11,11}$	-0.00	$F_{1,4,11,11}$	-0.00	$F_{2,4,11,11}$	0.00	$F_{3,4,11,11}$	0.00
$F_{4,4,11,11}$	-0.00	$F_{1,5,11,11}$	0.00	$F_{2,5,11,11}$	0.00	$F_{3,5,11,11}$	0.00
$F_{4,5,11,11}$	-0.00	$F_{5,5,11,11}$	-0.00	$F_{1,6,11,11}$	-0.00	$F_{2,6,11,11}$	0.00
$F_{3,6,11,11}$	0.00	$F_{4,6,11,11}$	-0.00	$F_{5,6,11,11}$	-0.00	$F_{6,6,11,11}$	0.00
$F_{1,7,11,11}$	0.00	$F_{2,7,11,11}$	-0.00	$F_{3,7,11,11}$	-0.00	$F_{4,7,11,11}$	0.01
$F_{5,7,11,11}$	-0.00	$F_{6,7,11,11}$	0.01	$F_{7,7,11,11}$	-0.12	$F_{1,8,11,11}$	-0.00
$F_{2,8,11,11}$	-0.00	$F_{3,8,11,11}$	0.00	$F_{4,8,11,11}$	0.02	$F_{5,8,11,11}$	0.01
$F_{6,8,11,11}$	0.00	$F_{7,8,11,11}$	0.08	$F_{8,8,11,11}$	-0.12	$F_{1,9,11,11}$	0.00

Table A33: The CcCR Force Constants for HSSH (cont.)

$F_{2,9,11,11}$	0.00	$F_{3,9,11,11}$	0.00	$F_{4,9,11,11}$	-0.00	$F_{5,9,11,11}$	0.00
$F_{6,9,11,11}$	-0.01	$F_{7,9,11,11}$	0.18	$F_{8,9,11,11}$	0.38	$F_{9,9,11,11}$	0.63
$F_{1,10,11,11}$	0.00	$F_{2,10,11,11}$	0.00	$F_{3,10,11,11}$	0.00	$F_{4,10,11,11}$	0.00
$F_{5,10,11,11}$	0.01	$F_{6,10,11,11}$	-0.00	$F_{7,10,11,11}$	0.11	$F_{8,10,11,11}$	-0.10
$F_{9,10,11,11}$	-0.18	$F_{10,10,11,11}$	-0.12	$F_{1,11,11,11}$	0.00	$F_{2,11,11,11}$	0.00
$F_{3,11,11,11}$	0.00	$F_{4,11,11,11}$	-0.01	$F_{5,11,11,11}$	-0.00	$F_{6,11,11,11}$	-0.00
$F_{7,11,11,11}$	-0.08	$F_{8,11,11,11}$	0.12	$F_{9,11,11,11}$	-0.38	$F_{10,11,11,11}$	0.09
$F_{11,11,11,11}$	-0.12	$F_{1,1,1,12}$	-0.00	$F_{1,1,2,12}$	-0.00	$F_{1,2,2,12}$	-0.00
$F_{2,2,2,12}$	-0.00	$F_{1,1,3,12}$	-0.00	$F_{1,2,3,12}$	0.00	$F_{2,2,3,12}$	-0.00
$F_{1,3,3,12}$	0.00	$F_{2,3,3,12}$	-0.00	$F_{3,3,3,12}$	0.00	$F_{1,1,4,12}$	-0.00
$F_{1,2,4,12}$	0.00	$F_{2,2,4,12}$	0.00	$F_{1,3,4,12}$	0.00	$F_{2,3,4,12}$	-0.00
$F_{3,3,4,12}$	-0.00	$F_{1,4,4,12}$	0.00	$F_{2,4,4,12}$	0.00	$F_{3,4,4,12}$	-0.00
$F_{4,4,4,12}$	-0.03	$F_{1,1,5,12}$	0.00	$F_{1,2,5,12}$	0.00	$F_{2,2,5,12}$	-0.00
$F_{1,3,5,12}$	0.00	$F_{2,3,5,12}$	0.00	$F_{3,3,5,12}$	0.00	$F_{1,4,5,12}$	-0.00
$F_{2,4,5,12}$	-0.00	$F_{3,4,5,12}$	0.00	$F_{4,4,5,12}$	-0.00	$F_{1,5,5,12}$	-0.00
$F_{2,5,5,12}$	0.00	$F_{3,5,5,12}$	-0.00	$F_{4,5,5,12}$	0.00	$F_{5,5,5,12}$	-0.00
$F_{1,1,6,12}$	0.00	$F_{1,2,6,12}$	0.00	$F_{2,2,6,12}$	0.00	$F_{1,3,6,12}$	-0.00
$F_{2,3,6,12}$	0.00	$F_{3,3,6,12}$	-0.00	$F_{1,4,6,12}$	-0.00	$F_{2,4,6,12}$	-0.00
$F_{3,4,6,12}$	0.00	$F_{4,4,6,12}$	0.00	$F_{1,5,6,12}$	-0.00	$F_{2,5,6,12}$	-0.00
$F_{3,5,6,12}$	-0.00	$F_{4,5,6,12}$	-0.00	$F_{5,5,6,12}$	-0.00	$F_{1,6,6,12}$	0.00
$F_{2,6,6,12}$	-0.00	$F_{3,6,6,12}$	-0.00	$F_{4,6,6,12}$	0.01	$F_{5,6,6,12}$	0.00
$F_{6,6,6,12}$	-0.00	$F_{1,1,7,12}$	0.00	$F_{1,2,7,12}$	0.00	$F_{2,2,7,12}$	-0.00
$F_{1,3,7,12}$	0.00	$F_{2,3,7,12}$	-0.00	$F_{3,3,7,12}$	0.00	$F_{1,4,7,12}$	-0.00
$F_{2,4,7,12}$	-0.00	$F_{3,4,7,12}$	-0.00	$F_{4,4,7,12}$	0.02	$F_{1,5,7,12}$	-0.00
$F_{2,5,7,12}$	0.01	$F_{3,5,7,12}$	0.00	$F_{4,5,7,12}$	-0.00	$F_{5,5,7,12}$	-0.01
$F_{1,6,7,12}$	-0.00	$F_{2,6,7,12}$	0.00	$F_{3,6,7,12}$	-0.00	$F_{4,6,7,12}$	-0.00
$F_{5,6,7,12}$	0.00	$F_{6,6,7,12}$	-0.00	$F_{1,7,7,12}$	0.00	$F_{2,7,7,12}$	0.00
$F_{3,7,7,12}$	-0.00	$F_{4,7,7,12}$	-0.03	$F_{5,7,7,12}$	0.00	$F_{6,7,7,12}$	0.01
$F_{7,7,7,12}$	0.16	$F_{1,1,8,12}$	-0.00	$F_{1,2,8,12}$	0.00	$F_{2,2,8,12}$	-0.00
$F_{1,3,8,12}$	-0.00	$F_{2,3,8,12}$	-0.00	$F_{3,3,8,12}$	-0.00	$F_{1,4,8,12}$	0.00
$F_{2,4,8,12}$	0.00	$F_{3,4,8,12}$	0.00	$F_{4,4,8,12}$	0.01	$F_{1,5,8,12}$	-0.00
$F_{2,5,8,12}$	0.00	$F_{3,5,8,12}$	0.00	$F_{4,5,8,12}$	0.00	$F_{5,5,8,12}$	-0.00
$F_{1,6,8,12}$	0.00	$F_{2,6,8,12}$	0.00	$F_{3,6,8,12}$	0.00	$F_{4,6,8,12}$	-0.00
$F_{5,6,8,12}$	-0.00	$F_{6,6,8,12}$	-0.00	$F_{1,7,8,12}$	-0.00	$F_{2,7,8,12}$	-0.00
$F_{3,7,8,12}$	0.00	$F_{4,7,8,12}$	-0.00	$F_{5,7,8,12}$	-0.00	$F_{6,7,8,12}$	-0.00
$F_{7,7,8,12}$	0.14	$F_{1,8,8,12}$	-0.00	$F_{2,8,8,12}$	-0.00	$F_{3,8,8,12}$	-0.00
$F_{4,8,8,12}$	-0.00	$F_{5,8,8,12}$	0.00	$F_{6,8,8,12}$	0.01	$F_{7,8,8,12}$	-0.17
$F_{8,8,8,12}$	-0.38	$F_{1,1,9,12}$	0.00	$F_{1,2,9,12}$	-0.00	$F_{2,2,9,12}$	0.00

Table A34: The CcCR Force Constants for HSSH (cont.)

$F_{1,3,9,12}$	-0.00	$F_{2,3,9,12}$	0.00	$F_{3,3,9,12}$	-0.00	$F_{1,4,9,12}$	0.00
$F_{2,4,9,12}$	0.00	$F_{3,4,9,12}$	0.00	$F_{4,4,9,12}$	0.00	$F_{1,5,9,12}$	0.00
$F_{2,5,9,12}$	-0.00	$F_{3,5,9,12}$	-0.00	$F_{4,5,9,12}$	0.00	$F_{5,5,9,12}$	-0.00
$F_{1,6,9,12}$	0.00	$F_{2,6,9,12}$	0.00	$F_{3,6,9,12}$	0.00	$F_{4,6,9,12}$	-0.01
$F_{5,6,9,12}$	0.00	$F_{6,6,9,12}$	0.00	$F_{1,7,9,12}$	-0.00	$F_{2,7,9,12}$	0.00
$F_{3,7,9,12}$	-0.00	$F_{4,7,9,12}$	0.00	$F_{5,7,9,12}$	-0.01	$F_{6,7,9,12}$	0.01
$F_{7,7,9,12}$	0.12	$F_{1,8,9,12}$	-0.00	$F_{2,8,9,12}$	0.00	$F_{3,8,9,12}$	0.00
$F_{4,8,9,12}$	-0.00	$F_{5,8,9,12}$	0.00	$F_{6,8,9,12}$	-0.00	$F_{7,8,9,12}$	-0.17
$F_{8,8,9,12}$	-0.63	$F_{1,9,9,12}$	0.00	$F_{2,9,9,12}$	-0.00	$F_{3,9,9,12}$	-0.00
$F_{4,9,9,12}$	-0.00	$F_{5,9,9,12}$	-0.00	$F_{6,9,9,12}$	-0.01	$F_{7,9,9,12}$	-0.10
$F_{8,9,9,12}$	-0.37	$F_{9,9,9,12}$	0.14	$F_{1,1,10,12}$	0.00	$F_{1,2,10,12}$	-0.00
$F_{2,2,10,12}$	0.00	$F_{1,3,10,12}$	-0.00	$F_{2,3,10,12}$	0.00	$F_{3,3,10,12}$	-0.00
$F_{1,4,10,12}$	0.00	$F_{2,4,10,12}$	0.00	$F_{3,4,10,12}$	0.00	$F_{4,4,10,12}$	0.00
$F_{1,5,10,12}$	0.00	$F_{2,5,10,12}$	-0.00	$F_{3,5,10,12}$	-0.00	$F_{4,5,10,12}$	0.01
$F_{5,5,10,12}$	0.00	$F_{1,6,10,12}$	0.00	$F_{2,6,10,12}$	-0.00	$F_{3,6,10,12}$	0.00
$F_{4,6,10,12}$	0.00	$F_{5,6,10,12}$	-0.00	$F_{6,6,10,12}$	-0.00	$F_{1,7,10,12}$	-0.00
$F_{2,7,10,12}$	-0.00	$F_{3,7,10,12}$	0.00	$F_{4,7,10,12}$	0.01	$F_{5,7,10,12}$	-0.00
$F_{6,7,10,12}$	-0.00	$F_{7,7,10,12}$	-0.14	$F_{1,8,10,12}$	-0.00	$F_{2,8,10,12}$	0.00
$F_{3,8,10,12}$	0.00	$F_{4,8,10,12}$	-0.01	$F_{5,8,10,12}$	0.00	$F_{6,8,10,12}$	0.00
$F_{7,8,10,12}$	-0.13	$F_{8,8,10,12}$	0.18	$F_{1,9,10,12}$	0.00	$F_{2,9,10,12}$	-0.00
$F_{3,9,10,12}$	0.00	$F_{4,9,10,12}$	-0.00	$F_{5,9,10,12}$	0.01	$F_{6,9,10,12}$	-0.01
$F_{7,9,10,12}$	-0.12	$F_{8,9,10,12}$	0.17	$F_{9,9,10,12}$	0.10	$F_{1,10,10,12}$	-0.00
$F_{2,10,10,12}$	-0.00	$F_{3,10,10,12}$	-0.00	$F_{4,10,10,12}$	-0.01	$F_{5,10,10,12}$	-0.00
$F_{6,10,10,12}$	0.00	$F_{7,10,10,12}$	0.13	$F_{8,10,10,12}$	0.14	$F_{9,10,10,12}$	0.12
$F_{10,10,10,12}$	-0.11	$F_{1,1,11,12}$	0.00	$F_{1,2,11,12}$	-0.00	$F_{2,2,11,12}$	0.00
$F_{1,3,11,12}$	0.00	$F_{2,3,11,12}$	0.00	$F_{3,3,11,12}$	0.00	$F_{1,4,11,12}$	-0.00
$F_{2,4,11,12}$	0.00	$F_{3,4,11,12}$	-0.00	$F_{4,4,11,12}$	-0.01	$F_{1,5,11,12}$	0.00
$F_{2,5,11,12}$	-0.00	$F_{3,5,11,12}$	-0.00	$F_{4,5,11,12}$	-0.00	$F_{5,5,11,12}$	0.00
$F_{1,6,11,12}$	-0.00	$F_{2,6,11,12}$	-0.00	$F_{3,6,11,12}$	-0.00	$F_{4,6,11,12}$	0.00
$F_{5,6,11,12}$	0.00	$F_{6,6,11,12}$	0.00	$F_{1,7,11,12}$	0.00	$F_{2,7,11,12}$	-0.00
$F_{3,7,11,12}$	-0.00	$F_{4,7,11,12}$	0.01	$F_{5,7,11,12}$	0.00	$F_{6,7,11,12}$	0.00
$F_{7,7,11,12}$	-0.14	$F_{1,8,11,12}$	0.00	$F_{2,8,11,12}$	0.00	$F_{3,8,11,12}$	0.00
$F_{4,8,11,12}$	0.00	$F_{5,8,11,12}$	-0.00	$F_{6,8,11,12}$	-0.00	$F_{7,8,11,12}$	0.18
$F_{8,8,11,12}$	0.38	$F_{1,9,11,12}$	0.00	$F_{2,9,11,12}$	-0.00	$F_{3,9,11,12}$	-0.00
$F_{4,9,11,12}$	-0.00	$F_{5,9,11,12}$	0.00	$F_{6,9,11,12}$	-0.00	$F_{7,9,11,12}$	0.18
$F_{8,9,11,12}$	0.62	$F_{9,9,11,12}$	0.38	$F_{1,10,11,12}$	0.00	$F_{2,10,11,12}$	0.00

Table A35: The CcCR Force Constants for HSSH (cont.)

$F_{3,10,11,12}$	0.00	$F_{4,10,11,12}$	0.00	$F_{5,10,11,12}$	-0.00	$F_{6,10,11,12}$	-0.00
$F_{7,10,11,12}$	0.14	$F_{8,10,11,12}$	-0.18	$F_{9,10,11,12}$	-0.18	$F_{10,10,11,12}$	-0.14
$F_{1,11,11,12}$	-0.00	$F_{2,11,11,12}$	-0.00	$F_{3,11,11,12}$	-0.00	$F_{4,11,11,12}$	0.00
$F_{5,11,11,12}$	0.00	$F_{6,11,11,12}$	0.00	$F_{7,11,11,12}$	-0.18	$F_{8,11,11,12}$	-0.38
$F_{9,11,11,12}$	-0.62	$F_{10,11,11,12}$	0.18	$F_{11,11,11,12}$	0.38	$F_{1,1,12,12}$	0.00
$F_{1,2,12,12}$	0.00	$F_{2,2,12,12}$	-0.00	$F_{1,3,12,12}$	0.00	$F_{2,3,12,12}$	-0.00
$F_{3,3,12,12}$	0.00	$F_{1,4,12,12}$	-0.00	$F_{2,4,12,12}$	0.00	$F_{3,4,12,12}$	-0.00
$F_{4,4,12,12}$	-0.01	$F_{1,5,12,12}$	0.00	$F_{2,5,12,12}$	0.00	$F_{3,5,12,12}$	0.00
$F_{4,5,12,12}$	-0.00	$F_{5,5,12,12}$	0.00	$F_{1,6,12,12}$	-0.00	$F_{2,6,12,12}$	-0.00
$F_{3,6,12,12}$	-0.00	$F_{4,6,12,12}$	0.00	$F_{5,6,12,12}$	-0.00	$F_{6,6,12,12}$	-0.00
$F_{1,7,12,12}$	0.00	$F_{2,7,12,12}$	-0.00	$F_{3,7,12,12}$	0.00	$F_{4,7,12,12}$	0.00
$F_{5,7,12,12}$	0.01	$F_{6,7,12,12}$	-0.01	$F_{7,7,12,12}$	-0.12	$F_{1,8,12,12}$	-0.00
$F_{2,8,12,12}$	-0.00	$F_{3,8,12,12}$	-0.00	$F_{4,8,12,12}$	0.00	$F_{5,8,12,12}$	-0.00
$F_{6,8,12,12}$	0.01	$F_{7,8,12,12}$	0.18	$F_{8,8,12,12}$	0.62	$F_{1,9,12,12}$	-0.00
$F_{2,9,12,12}$	-0.00	$F_{3,9,12,12}$	-0.00	$F_{4,9,12,12}$	0.01	$F_{5,9,12,12}$	0.00
$F_{6,9,12,12}$	0.01	$F_{7,9,12,12}$	0.09	$F_{8,9,12,12}$	0.37	$F_{9,9,12,12}$	-0.13
$F_{1,10,12,12}$	-0.00	$F_{2,10,12,12}$	0.00	$F_{3,10,12,12}$	-0.00	$F_{4,10,12,12}$	0.00
$F_{5,10,12,12}$	-0.01	$F_{6,10,12,12}$	0.01	$F_{7,10,12,12}$	0.12	$F_{8,10,12,12}$	-0.18
$F_{9,10,12,12}$	-0.10	$F_{10,10,12,12}$	-0.12	$F_{1,11,12,12}$	-0.00	$F_{2,11,12,12}$	0.00
$F_{3,11,12,12}$	0.00	$F_{4,11,12,12}$	0.00	$F_{5,11,12,12}$	-0.00	$F_{6,11,12,12}$	-0.00
$F_{7,11,12,12}$	-0.18	$F_{8,11,12,12}$	-0.62	$F_{9,11,12,12}$	-0.37	$F_{10,11,12,12}$	0.18
$F_{11,11,12,12}$	0.62	$F_{1,12,12,12}$	0.00	$F_{2,12,12,12}$	0.00	$F_{3,12,12,12}$	0.00
$F_{4,12,12,12}$	-0.01	$F_{5,12,12,12}$	-0.00	$F_{6,12,12,12}$	-0.01	$F_{7,12,12,12}$	-0.08
$F_{8,12,12,12}$	-0.37	$F_{9,12,12,12}$	0.12	$F_{10,12,12,12}$	0.09	$F_{11,12,12,12}$	0.37
$F_{12,12,12,12}$	-0.12						

Table A36: The CcCR Vibrational Frequencies (cm^{-1}) for the Isotopologues of HOOH

Mode	$H^{18}OOH$	DOOH	DOOD	$D^{18}O^{18}OD$
ω_1	3805.6	3805.6	2774.7	2756.4
ω_2	3792.8	2773.1	2771.3	2753.9
ω_3	1438.5	1392.0	1056.3	1048.6
ω_4	1329.8	1017.1	986.5	977.0
ω_5	889.1	913.7	912.7	860.9
ω_6	379.5	333.3	278.2	276.3
ν_1	3609.7	3609.2	2670.1	2653.1
ν_2	3598.1	2669.5	2668.1	2652.0
ν_3	1395.2	1375.0	1030.3	1023.2
ν_4	1275.6	986.9	953.1	945.0
ν_5	854.0	879.6	880.9	832.1
ν_6	314.2	282.6	242.7	241.4
ZPT	5717.7	5038.4	4333.5	4281.6

Table A37: The CcCR Geometrical Parameters and Spectroscopic Constants for the Isotopologues of HOOH

	Units	$H^{18}OOH$	DOOH	DOOD	$D^{18}O^{18}OH$
$R_e(H_1\text{-}O_1)$	Å	0.96198	0.96198	0.96198	0.96198
$R_e(O_1\text{-}O_2)$	Å	1.44803	1.44803	1.44803	1.44803
$R_e(O_2\text{-}H_2)$	Å	0.96198	0.96198	0.96198	0.96198
$\angle_e(O_1\text{-}H_1\text{-}O_2)$	°	100.15	100.15	100.15	100.15
$\angle_e(O_1\text{-}H_1\text{-}H_2)$	°	100.15	100.15	100.15	100.15
A_e	MHz	303372.3	214618.4	166303.9	163164.1
B_e	MHz	25260.8	25186.5	23592.5	21519.7
C_e	MHz	24500.5	23899.2	22466.1	20550.5
$R_0(H_1\text{-}O_1)$	Å	0.96232	0.96615	0.96248	0.96242
$R_0(O_1\text{-}O_2)$	Å	1.46144	1.46086	1.46001	1.45955
$R_0(O_2\text{-}H_2)$	Å	0.96218	0.95638	0.96248	0.96242
$\angle_0(O_1\text{-}H_1\text{-}O_2)$	°	100.06	99.92	100.02	100.03
$\angle_0(O_1\text{-}H_1\text{-}H_2)$	°	100.06	100.17	100.02	100.03
A_0	MHz	300658.7	213127.0	165402.4	162243.3
B_0	MHz	24975.6	24934.3	23402.6	21346.0
C_0	MHz	24073.8	23515.9	22119.0	20244.6
A_1	MHz	295067.1	210320.8	163191.4	160092.0
B_1	MHz	24939.6	24886.4	23347.2	21302.0
C_1	MHz	24071.7	23523.2	22105.1	20234.2
A_2	MHz	294991.1	209441.7	163165.0	160048.6
B_2	MHz	24942.3	24893.6	23342.3	21297.1
C_2	MHz	24073.3	23477.8	22103.4	20233.1
A_3	MHz	304196.9	214844.4	166783.4	163610.8
B_3	MHz	24803.7	24784.5	23271.2	21229.2
C_3	MHz	23999.5	23426.4	22167.4	20263.9
A_4	MHz	304871.3	215974.7	167278.3	164013.5
B_4	MHz	24910.9	24916.9	23462.9	21374.3
C_4	MHz	23846.0	23405.7	21924.9	20076.4
A_5	MHz	300056.7	212650.6	164940.0	161855.4
B_5	MHz	24680.1	24646.8	23118.6	21108.9
C_5	MHz	23773.8	23191.6	21822.2	19996.1
A_6	MHz	299342.1	212547.0	165253.7	161998.4
B_6	MHz	24982.7	24969.3	23473.0	21400.0
C_6	MHz	23849.2	23308.5	21916.9	20069.3
Δ_J	kHz	87.665	79.369	78.605	64.488
Δ_K	MHz	10.882	6.325	3.696	3.427
Δ_{JK}	kHz	1.057 (MHz)	921.464	641.912	566.125
δ_J	Hz	-25.078	1.513 (kHz)	-642.400	-322.349
δ_K	MHz	6.164	1.283	5.306	4.411
Φ_j	mHz	-7.464	-72.613	158.252	90.267
Φ_k	kHz	1.659	1.463	772.462 (Hz)	586.836 (Hz)
Φ_{jk}	Hz	64.402	226.725	89.392	62.262
Φ_{kj}	Hz	-175.364	-795.880	-417.549	-278.660
ϕ_j	mHz	894.134 (μHz)	85.821	19.711	13.179
ϕ_{jk}	Hz	95.243	-33.217	94.518	67.211
ϕ_k	kHz	-47.806	49.734	-26.123	-20.668

Table A38: The CcCR Vibrational Frequencies (cm^{-1}) for the Isotopologues of HOSH

Mode	$H^{18}OSH$	$HO^{34}SH$	DOSH	DOSD	$H^{18}O^{34}SH$
ω_1	3812.7	3825.5	2786.5	2786.5	3812.7
ω_2	2661.9	2659.5	2661.9	1912.7	2659.5
ω_3	1207.5	1210.2	1032.6	885.6	1206.8
ω_4	1030.7	1032.7	885.5	791.0	1029.8
ω_5	757.1	777.9	783.3	749.6	748.8
ω_6	478.2	479.6	397.1	350.7	478.0
ν_1	3617.2	3628.6	2682.3	2682.1	3617.2
ν_2	2546.7	2544.5	2546.2	1853.7	2544.5
ν_3	1171.7	1174.1	1008.2	865.2	1171.0
ν_4	1006.7	1008.4	864.5	774.3	1005.8
ν_5	736.9	756.3	768.7	737.3	729.2
ν_6	436.7	437.8	368.5	327.9	436.6
ZPT	4898.2	4916.4	4219.5	3696.7	4892.1

Table A39: The CcCR Geometrical Parameters and Spectroscopic Constants for the Isotopologues of HOSH

	Units	$H^{18}OSH$	$HO^{34}SH$	DOSH	DOSD	$H^{18}O^{34}SH$
$R_e(H_1\text{-}O)$	Å	0.96012	0.96012	0.9601	0.96012	0.96012
R_e(O-S)	Å	1.66051	1.66051	1.6605	1.66051	1.66051
$R_e(S\text{-}H_2)$	Å	1.34273	1.34273	1.3427	1.34273	1.34273
$\angle_e(O\text{-}H_1\text{-}S)$	°	107.21	107.21	107.2	107.21	107.21
$\angle_e(S\text{-}O\text{-}H_2)$	°	98.45	98.45	98.4	98.45	98.45
A_e	MHz	202735.5	203009.3	160886.3	107317.0	202408.2
B_e	MHz	14405.9	15134.4	14256.6	13970.6	14120.2
C_e	MHz	14037.2	14723.1	14147.5	13294.0	13764.1
$R_0(H_1\text{-}O)$	Å	0.95807	0.95803	0.96175	0.95875	0.95805
R_0(O-S)	Å	1.66903	1.66919	1.66873	1.66840	1.66897
$R_0(S\text{-}H_2)$	Å	1.35220	1.35226	1.34914	1.34992	1.35219
$\angle_0(O\text{-}H_1\text{-}S)$	°	107.51	107.51	107.32	107.40	107.51
$\angle_0(S\text{-}O\text{-}H_2)$	°	98.51	98.51	98.56	98.46	98.51
A_0	MHz	201383.8	201658.1	159997.7	106836.0	201056.8
B_0	MHz	14295.3	15016.5	14139.0	13879.6	14012.2
C_0	MHz	13913.7	14591.1	14044.4	13187.5	13643.8
A_1	MHz	198955.8	199241.9	157995.9	105943.8	198636.4
B_1	MHz	14274.3	14992.7	14108.6	13850.0	13991.9
C_1	MHz	13904.2	14580.0	14028.1	13172.6	13634.6
A_2	MHz	197367.4	197622.3	157472.0	105310.3	197044.2
B_2	MHz	14313.0	15035.3	14155.4	13886.0	14029.9
C_2	MHz	13914.3	14590.9	14044.0	13173.5	13645.0
A_3	MHz	204379.6	204672.2	161452.2	108096.8	204043.2
B_3	MHz	14256.7	14975.4	14126.0	13855.6	13974.5
C_3	MHz	13913.3	14591.7	13988.6	13200.4	13642.9
A_4	MHz	203693.4	203968.7	162636.1	106801.3	203356.3
B_4	MHz	14280.5	15002.3	14113.6	13768.9	13997.2
C_4	MHz	13854.7	14529.8	14059.9	13146.7	13586.1
A_5	MHz	201193.8	201463.2	159727.0	107600.3	200869.8
B_5	MHz	14176.4	14889.1	14012.9	13876.9	13897.0
C_5	MHz	13797.4	14465.2	13925.1	13075.6	13531.0
A_6	MHz	200009.2	200278.2	158925.6	106301.8	199688.2
B_6	MHz	14252.8	14972.3	14101.0	13860.6	13970.2
C_6	MHz	13848.2	14521.7	13996.2	13140.4	13579.6
Δ_J	kHz	20.814	22.740	19.434	17.060	20.059
Δ_K	MHz	5.472	5.474	3.848	1.514	5.453
Δ_{JK}	kHz	345.443	373.986	291.004	254.383	334.341
δ_J	Hz	562.175	645.367	154.134	828.194	532.699
δ_K	MHz	-0.739	-0.790	-4.578	-0.567	-0.707
Φ_j	mHz	-11.755	-13.644	-9.287	-6.770	-11.073
Φ_k	Hz	431.584	429.231	409.595	64.083	427.003
Φ_{jk}	Hz	-7.034	-8.407	-10.995	-9.819	-6.485
Φ_{kj}	Hz	49.217	55.355	40.910	37.261	46.653
ϕ_j	μHz	387.635	378.666	-26.850	203.398	359.204
ϕ_{jk}	mHz	-428.852	-624.312	-8.519 (Hz)	-1.905 (Hz)	-364.575
ϕ_k	kHz	-7.280	-7.642	-400.589	-2.523	-6.946

Table A40: The CcCR Vibrational Frequencies (cm^{-1}) for the Isotopologues of HSSH

Mode	$H^{34}SSH$	DSSH	DSSD	$D^{34}S^{34}SD$
ω_1	2682.4	2681.8	1927.4	1923.9
ω_2	2678.8	1926.5	1925.6	1922.2
ω_3	907.8	907.5	660.3	658.1
ω_4	906.6	656.1	651.3	650.2
ω_5	522.1	529.7	529.5	513.7
ω_6	443.4	386.8	319.8	319.1
ν_1	2568.9	2567.3	1869.0	1865.7
ν_2	2564.8	1868.3	1866.8	1863.5
ν_3	886.8	884.5	647.6	645.6
ν_4	883.4	642.4	646.4	645.0
ν_5	510.6	518.8	519.0	503.9
ν_6	405.6	357.7	299.7	299.1
ZPT	4014.4	3500.9	2977.1	2964.0

Table A41: The CcCR Geometrical Parameters and Spectroscopic Constants for the Isotopologues of HSSH

	Units	$H^{34}SSH$	DSSH	DSSD	$D^{34}S^{34}SH$
$R_e(H_1\text{-}S_1)$	Å	1.34066	1.34066	1.34066	1.34066
$R_e(S_1\text{-}S_2)$	Å	2.05016	2.05016	2.05016	2.05016
$R_e(S_2\text{-}H_2)$	Å	2.60447	2.60447	2.60447	2.60447
$\angle_e(S_1\text{-}H_1\text{-}S_2)$	°	98.19	98.19	98.19	98.19
$\angle_e(S_1\text{-}H_1\text{-}H_2)$	°	97.36	97.36	97.36	97.36
$\angle_e(S_1\text{-}S_2\text{-}H_1)$	°	30.63	30.63	30.63	30.63
A_e	MHz	147710.1	101104.7	76807.7	76473.5
B_e	MHz	6830.8	6872.4	6586.1	6244.7
C_e	MHz	6829.3	6727.6	6584.3	6243.8
$R_0(H_1\text{-}S_1)$	Å	1.34588	1.34676	1.34457	1.34454
$R_0(S_1\text{-}S_2)$	Å	2.05876	2.05830	2.05772	2.05758
$R_0(S_2\text{-}H_2)$	Å	2.61586	2.61411	2.61355	2.61345
$\angle_0(S_1\text{-}H_1\text{-}S_2)$	°	98.23	98.15	98.19	98.20
$\angle_0(S_1\text{-}H_1\text{-}H_2)$	°	97.46	97.39	97.43	97.43
$\angle_0(S_1\text{-}S_2\text{-}H_1)$	°	30.61	30.54	30.61	30.61
A_0	MHz	146591.3	100493.2	76402.5	76069.3
B_0	MHz	6811.4	6831.0	6591.1	6264.8
C_0	MHz	6754.2	6683.0	6503.6	6152.8
A_1	MHz	144529.4	99522.0	75650.1	75319.7
B_1	MHz	6816.8	6835.0	6592.5	6266.4
C_1	MHz	6760.9	6690.7	6503.9	6153.4
A_2	MHz	144479.6	99162.5	75621.4	75291.9
B_2	MHz	6818.0	6834.9	6592.9	6266.8
C_2	MHz	6760.8	6681.5	6504.2	6153.7
A_3	MHz	148835.0	101151.1	77173.2	76830.5
B_3	MHz	6797.9	6805.8	6575.2	6249.8
C_3	MHz	6741.2	6671.9	6499.0	6147.8
A_4	MHz	147207.7	101469.1	76743.4	76408.6
B_4	MHz	6786.7	6829.8	6589.6	6262.3
C_4	MHz	6731.1	6665.1	6487.9	6137.8
A_5	MHz	146523.7	100439.3	76357.8	76027.6
B_5	MHz	6772.1	6791.5	6552.0	6229.1
C_5	MHz	6715.9	6642.9	6464.7	6117.1
A_6	MHz	145735.0	99992.6	76058.4	75729.4
B_6	MHz	6783.7	6807.1	6567.4	6242.3
C_6	MHz	6720.2	6655.6	6487.2	6137.0
Δ_J	kHz	5.058	4.736	4.529	4.079
Δ_K	MHz	2.264	1.177	0.602	0.598
Δ_{JK}	kHz	81.461	79.432	62.643	57.252
δ_J	Hz	-7.487	97.988	16.875	13.766
δ_K	MHz	13.766	-0.153	21.741	27.986
Φ_j	mHz	-1.117	-1.297	-723.733 (μHz)	-672.823 (μHz)
Φ_k	kHz	1.515	39.617	-11.978 (Hz)	-17.027 (Hz)
Φ_{jk}	Hz	610.693	-517.843 (mHz)	-11.773	-13.693
Φ_{kj}	kHz	-2.032	3.581 (Hz)	40.319 (Hz)	46.657 (Hz)
ϕ_j	μHz	4.575	29.504	-13.924	-11.863 (μHz)
ϕ_{jk}	Hz	283.132	38.949 (mHz)	-821.738	-1.391 (kHz)
ϕ_k	GHz	-0.180	-762.307 (Hz)	-0.570	-1.489

APPENDIX B

Supporting information for Chapter 3: "Fluoro Hydrogen Peroxide: A Plausible Molecular Form of Naturally-Occuring Fluorine."

Table B1: Coordinates for Calculating HOOF Dipole Components

	A	B	C
H	-0.858147111	-0.543257826	-1.275575535
O	0.065956113	-0.281576321	-1.143862823
O	-0.016364993	0.595474778	-0.093146211
F	0.003765192	-0.235525885	1.109414614

Table B2: F12-TZ Force Constants for HOOF

$F_{1,1}$	0.455391	$F_{1,2}$	0.112669	$F_{1,3}$	0.048769
$F_{1,4}$	-0.470780	$F_{1,5}$	-0.117691	$F_{1,6}$	-0.053500
$F_{1,7}$	0.016700	$F_{1,8}$	0.006814	$F_{1,9}$	0.000994
$F_{1,10}$	-0.001311	$F_{1,11}$	-0.001792	$F_{1,12}$	0.003737
$F_{1,13}$	0.112669	$F_{2,1}$	0.064974	$F_{2,2}$	0.045770
$F_{2,3}$	-0.083500	$F_{2,4}$	-0.044431	$F_{2,5}$	-0.027343
$F_{2,6}$	-0.033108	$F_{2,7}$	-0.021167	$F_{2,8}$	-0.019934
$F_{2,9}$	0.003939	$F_{2,10}$	0.000624	$F_{2,11}$	0.001506
$F_{2,12}$	0.048769	$F_{2,13}$	0.045770	$F_{3,1}$	0.055785
$F_{3,2}$	-0.013085	$F_{3,3}$	-0.018755	$F_{3,4}$	-0.033061
$F_{3,5}$	-0.030871	$F_{3,6}$	-0.027636	$F_{3,7}$	-0.021687
$F_{3,8}$	-0.004812	$F_{3,9}$	0.000621	$F_{3,10}$	-0.001037
$F_{3,11}$	-0.470780	$F_{3,12}$	-0.083500	$F_{3,13}$	-0.013085
$F_{4,1}$	0.519758	$F_{4,2}$	0.099616	$F_{4,3}$	0.025009
$F_{4,4}$	-0.051063	$F_{4,5}$	-0.016110	$F_{4,6}$	-0.010609
$F_{4,7}$	0.002085	$F_{4,8}$	-0.000006	$F_{4,9}$	-0.001315
$F_{4,10}$	-0.117691	$F_{4,11}$	-0.044431	$F_{4,12}$	-0.018755
$F_{4,13}$	0.099616	$F_{5,1}$	0.173583	$F_{5,2}$	0.126764
$F_{5,3}$	0.025237	$F_{5,4}$	-0.174260	$F_{5,5}$	-0.090893
$F_{5,6}$	-0.007161	$F_{5,7}$	0.045108	$F_{5,8}$	-0.017116
$F_{5,9}$	-0.053500	$F_{5,10}$	-0.027343	$F_{5,11}$	-0.033061
$F_{5,12}$	0.025009	$F_{5,13}$	0.126764	$F_{6,1}$	0.225979
$F_{6,2}$	0.021769	$F_{6,3}$	-0.096864	$F_{6,4}$	-0.124782
$F_{6,5}$	0.006722	$F_{6,6}$	-0.002557	$F_{6,7}$	-0.068136
$F_{6,8}$	0.016700	$F_{6,9}$	-0.033108	$F_{6,10}$	-0.030871
$F_{6,11}$	-0.051063	$F_{6,12}$	0.025237	$F_{6,13}$	0.021769
$F_{7,1}$	0.039517	$F_{7,2}$	0.002562	$F_{7,3}$	0.012656
$F_{7,4}$	-0.005154	$F_{7,5}$	0.005309	$F_{7,6}$	-0.003553
$F_{7,7}$	0.006814	$F_{7,8}$	-0.021167	$F_{7,9}$	-0.027636
$F_{7,10}$	-0.016110	$F_{7,11}$	-0.174260	$F_{7,12}$	-0.096864
$F_{7,13}$	0.002562	$F_{8,1}$	0.329360	$F_{8,2}$	0.041028
$F_{8,3}$	0.006734	$F_{8,4}$	-0.133934	$F_{8,5}$	0.083471
$F_{8,6}$	0.000994	$F_{8,7}$	-0.019934	$F_{8,8}$	-0.021687
$F_{8,9}$	-0.010609	$F_{8,10}$	-0.090893	$F_{8,11}$	-0.124782
$F_{8,12}$	0.012656	$F_{8,13}$	0.041028	$F_{9,1}$	0.229324
$F_{9,2}$	-0.003041	$F_{9,3}$	0.069798	$F_{9,4}$	-0.082855
$F_{9,5}$	-0.001311	$F_{9,6}$	0.003939	$F_{9,7}$	-0.004812
$F_{9,8}$	0.002085	$F_{9,9}$	-0.007161	$F_{9,10}$	0.006722
$F_{9,11}$	-0.005154	$F_{9,12}$	0.006734	$F_{9,13}$	-0.003041
$F_{10,1}$	0.004380	$F_{10,2}$	-0.003512	$F_{10,3}$	0.001131
$F_{10,4}$	-0.001792	$F_{10,5}$	0.000624	$F_{10,6}$	0.000621
$F_{10,7}$	-0.000006	$F_{10,8}$	0.045108	$F_{10,9}$	-0.002557
$F_{10,10}$	0.005309	$F_{10,11}$	-0.133934	$F_{10,12}$	0.069798
$F_{10,13}$	-0.003512	$F_{11,1}$	0.088202	$F_{11,2}$	-0.067861
$F_{11,3}$	0.003737	$F_{11,4}$	0.001506	$F_{11,5}$	-0.001037
$F_{11,6}$	-0.001315	$F_{11,7}$	-0.017116	$F_{11,8}$	-0.068136
$F_{11,9}$	-0.003553	$F_{11,10}$	0.083471	$F_{11,11}$	-0.082855
$F_{11,12}$	0.001131	$F_{11,13}$	-0.067861	$F_{12,1}$	0.152028
$F_{1,1,1}$	1.5652	$F_{1,1,2}$	0.5599	$F_{1,2,2}$	-0.0519

Table B3: F12-TZ Force Constants for HOOF (cont.)

$F_{2,2,2}$	-0.1238	$F_{1,1,3}$	0.2648	$F_{1,2,3}$	0.1164
$F_{2,2,3}$	0.0205	$F_{1,3,3}$	-0.1644	$F_{2,3,3}$	-0.0258
$F_{3,3,3}$	-0.0606	$F_{1,1,4}$	-1.5752	$F_{1,2,4}$	-0.5478
$F_{2,2,4}$	0.0725	$F_{1,3,4}$	-0.2457	$F_{2,3,4}$	-0.1001
$F_{3,3,4}$	0.1803	$F_{1,4,4}$	1.5880	$F_{2,4,4}$	0.5332
$F_{3,4,4}$	0.2180	$F_{4,4,4}$	-1.6158	$F_{1,1,5}$	-0.5911
$F_{1,2,5}$	0.0535	$F_{2,2,5}$	0.1317	$F_{1,3,5}$	-0.1118
$F_{2,3,5}$	-0.0084	$F_{3,3,5}$	0.0797	$F_{1,4,5}$	0.5690
$F_{2,4,5}$	-0.0590	$F_{3,4,5}$	0.1296	$F_{4,4,5}$	-0.5876
$F_{1,5,5}$	-0.0367	$F_{2,5,5}$	-0.1299	$F_{3,5,5}$	0.0446
$F_{4,5,5}$	0.0309	$F_{5,5,5}$	0.3360	$F_{1,1,6}$	-0.2965
$F_{1,2,6}$	-0.1295	$F_{2,2,6}$	0.0243	$F_{1,3,6}$	0.1684
$F_{2,3,6}$	0.0516	$F_{3,3,6}$	0.0792	$F_{1,4,6}$	0.2622
$F_{2,4,6}$	0.1536	$F_{3,4,6}$	-0.1589	$F_{4,4,6}$	-0.2661
$F_{1,5,6}$	0.1414	$F_{2,5,6}$	0.0020	$F_{3,5,6}$	-0.0627
$F_{4,5,6}$	-0.1928	$F_{5,5,6}$	0.2768	$F_{1,6,6}$	-0.1559
$F_{2,6,6}$	-0.0287	$F_{3,6,6}$	-0.0750	$F_{4,6,6}$	0.1185
$F_{5,6,6}$	0.4290	$F_{6,6,6}$	0.5660	$F_{1,1,7}$	0.0100
$F_{1,2,7}$	-0.0138	$F_{2,2,7}$	-0.0203	$F_{1,3,7}$	-0.0154
$F_{2,3,7}$	-0.0151	$F_{3,3,7}$	-0.0167	$F_{1,4,7}$	-0.0121
$F_{2,4,7}$	0.0189	$F_{3,4,7}$	0.0234	$F_{4,4,7}$	0.0266
$F_{1,5,7}$	0.0263	$F_{2,5,7}$	-0.0016	$F_{3,5,7}$	-0.0130
$F_{4,5,7}$	0.0205	$F_{5,5,7}$	0.0272	$F_{1,6,7}$	0.0325
$F_{2,6,7}$	-0.0298	$F_{3,6,7}$	-0.0050	$F_{4,6,7}$	-0.0116
$F_{5,6,7}$	0.0519	$F_{6,6,7}$	0.0200	$F_{1,7,7}$	0.0029
$F_{2,7,7}$	-0.0078	$F_{3,7,7}$	-0.0079	$F_{4,7,7}$	-0.0136
$F_{5,7,7}$	-0.0631	$F_{6,7,7}$	-0.0149	$F_{7,7,7}$	0.0032
$F_{1,1,8}$	0.0332	$F_{1,2,8}$	-0.0013	$F_{2,2,8}$	-0.0051
$F_{1,3,8}$	-0.0044	$F_{2,3,8}$	-0.0122	$F_{3,3,8}$	-0.0580
$F_{1,4,8}$	-0.0227	$F_{2,4,8}$	-0.0131	$F_{3,4,8}$	-0.0294
$F_{4,4,8}$	0.0698	$F_{1,5,8}$	-0.0154	$F_{2,5,8}$	-0.0046
$F_{3,5,8}$	-0.0364	$F_{4,5,8}$	0.0306	$F_{5,5,8}$	-0.2489
$F_{1,6,8}$	-0.0108	$F_{2,6,8}$	-0.0247	$F_{3,6,8}$	0.0155
$F_{4,6,8}$	0.0391	$F_{5,6,8}$	-0.3132	$F_{6,6,8}$	-0.3807
$F_{1,7,8}$	-0.0134	$F_{2,7,8}$	0.0202	$F_{3,7,8}$	0.0251
$F_{4,7,8}$	-0.0665	$F_{5,7,8}$	-0.0315	$F_{6,7,8}$	-0.0221
$F_{7,7,8}$	0.1520	$F_{1,8,8}$	0.0166	$F_{2,8,8}$	0.0114
$F_{3,8,8}$	0.0490	$F_{4,8,8}$	-0.0242	$F_{5,8,8}$	0.3217
$F_{6,8,8}$	0.3559	$F_{7,8,8}$	0.0265	$F_{8,8,8}$	-0.5257
$F_{1,1,9}$	0.0294	$F_{1,2,9}$	0.0105	$F_{2,2,9}$	-0.0438
$F_{1,3,9}$	-0.0043	$F_{2,3,9}$	-0.0195	$F_{3,3,9}$	-0.0179
$F_{1,4,9}$	-0.0143	$F_{2,4,9}$	-0.0495	$F_{3,4,9}$	-0.0167
$F_{4,4,9}$	0.0277	$F_{1,5,9}$	-0.0313	$F_{2,5,9}$	0.0073
$F_{3,5,9}$	-0.0255	$F_{4,5,9}$	0.0624	$F_{5,5,9}$	-0.3077
$F_{1,6,9}$	-0.0173	$F_{2,6,9}$	-0.0292	$F_{3,6,9}$	-0.0047
$F_{4,6,9}$	0.0364	$F_{5,6,9}$	-0.3360	$F_{6,6,9}$	-0.3649
$F_{1,7,9}$	-0.0163	$F_{2,7,9}$	0.0456	$F_{3,7,9}$	0.0147
$F_{4,7,9}$	-0.0054	$F_{5,7,9}$	-0.0395	$F_{6,7,9}$	-0.0079
$F_{7,7,9}$	-0.0302	$F_{1,8,9}$	0.0185	$F_{2,8,9}$	0.0349

Table B4: F12-TZ Force Constants for HOOF (cont.)

$F_{3,8,9}$	0.0424	$F_{4,8,9}$	-0.0123	$F_{5,8,9}$	0.3111
$F_{6,8,9}$	0.3582	$F_{7,8,9}$	-0.0110	$F_{8,8,9}$	-0.1588
$F_{1,9,9}$	0.0298	$F_{2,9,9}$	0.0470	$F_{3,9,9}$	0.0264
$F_{4,9,9}$	-0.0238	$F_{5,9,9}$	0.3036	$F_{6,9,9}$	0.3352
$F_{7,9,9}$	-0.0014	$F_{8,9,9}$	-0.6146	$F_{9,9,9}$	0.0120
$F_{1,1,10}$	0.0000	$F_{1,2,10}$	0.0017	$F_{2,2,10}$	-0.0004
$F_{1,3,10}$	-0.0036	$F_{2,3,10}$	-0.0011	$F_{3,3,10}$	0.0008
$F_{1,4,10}$	-0.0007	$F_{2,4,10}$	-0.0043	$F_{3,4,10}$	0.0043
$F_{4,4,10}$	0.0012	$F_{1,5,10}$	-0.0043	$F_{2,5,10}$	0.0071
$F_{3,5,10}$	-0.0048	$F_{4,5,10}$	-0.0019	$F_{5,5,10}$	-0.0215
$F_{1,6,10}$	0.0018	$F_{2,6,10}$	0.0057	$F_{3,6,10}$	-0.0045
$F_{4,6,10}$	0.0155	$F_{5,6,10}$	-0.0005	$F_{6,6,10}$	0.0174
$F_{1,7,10}$	-0.0009	$F_{2,7,10}$	0.0027	$F_{3,7,10}$	-0.0001
$F_{4,7,10}$	-0.0009	$F_{5,7,10}$	0.0164	$F_{6,7,10}$	-0.0059
$F_{7,7,10}$	0.0075	$F_{1,8,10}$	0.0029	$F_{2,8,10}$	-0.0058
$F_{3,8,10}$	0.0087	$F_{4,8,10}$	0.0194	$F_{5,8,10}$	0.0163
$F_{6,8,10}$	-0.0062	$F_{7,8,10}$	-0.0721	$F_{8,8,10}$	-0.0189
$F_{1,9,10}$	0.0012	$F_{2,9,10}$	-0.0067	$F_{3,9,10}$	0.0064
$F_{4,9,10}$	-0.0080	$F_{5,9,10}$	0.0084	$F_{6,9,10}$	-0.0112
$F_{7,9,10}$	0.0519	$F_{8,9,10}$	0.0048	$F_{9,9,10}$	-0.0045
$F_{1,10,10}$	0.0016	$F_{2,10,10}$	-0.0001	$F_{3,10,10}$	-0.0006
$F_{4,10,10}$	0.0005	$F_{5,10,10}$	-0.0101	$F_{6,10,10}$	-0.0113
$F_{7,10,10}$	-0.0057	$F_{8,10,10}$	0.0499	$F_{9,10,10}$	-0.0451
$F_{10,10,10}$	0.0036	$F_{1,1,11}$	-0.0020	$F_{1,2,11}$	-0.0004
$F_{2,2,11}$	-0.0028	$F_{1,3,11}$	-0.0002	$F_{2,3,11}$	0.0000
$F_{3,3,11}$	0.0041	$F_{1,4,11}$	0.0015	$F_{2,4,11}$	-0.0004
$F_{3,4,11}$	-0.0001	$F_{4,4,11}$	-0.0155	$F_{1,5,11}$	-0.0014
$F_{2,5,11}$	0.0028	$F_{3,5,11}$	0.0001	$F_{4,5,11}$	-0.0026
$F_{5,5,11}$	0.0428	$F_{1,6,11}$	-0.0011	$F_{2,6,11}$	-0.0016
$F_{3,6,11}$	-0.0044	$F_{4,6,11}$	0.0001	$F_{5,6,11}$	0.0343
$F_{6,6,11}$	-0.0196	$F_{1,7,11}$	0.0008	$F_{2,7,11}$	0.0017
$F_{3,7,11}$	0.0030	$F_{4,7,11}$	0.0272	$F_{5,7,11}$	0.0058
$F_{6,7,11}$	0.0000	$F_{7,7,11}$	-0.0811	$F_{1,8,11}$	0.0001
$F_{2,8,11}$	-0.0017	$F_{3,8,11}$	-0.0004	$F_{4,8,11}$	0.0067
$F_{5,8,11}$	-0.0683	$F_{6,8,11}$	-0.0180	$F_{7,8,11}$	-0.0152
$F_{8,8,11}$	0.1926	$F_{1,9,11}$	0.0023	$F_{2,9,11}$	0.0016
$F_{3,9,11}$	0.0025	$F_{4,9,11}$	-0.0006	$F_{5,9,11}$	-0.0107
$F_{6,9,11}$	0.0071	$F_{7,9,11}$	0.0048	$F_{8,9,11}$	-0.1872
$F_{9,9,11}$	0.2640	$F_{1,10,11}$	-0.0003	$F_{2,10,11}$	-0.0009
$F_{3,10,11}$	-0.0027	$F_{4,10,11}$	-0.0132	$F_{5,10,11}$	-0.0018
$F_{6,10,11}$	0.0010	$F_{7,10,11}$	0.0531	$F_{8,10,11}$	0.0084
$F_{9,10,11}$	-0.0065	$F_{10,10,11}$	-0.0396	$F_{1,11,11}$	0.0017
$F_{2,11,11}$	0.0018	$F_{3,11,11}$	0.0003	$F_{4,11,11}$	-0.0037
$F_{5,11,11}$	0.0227	$F_{6,11,11}$	-0.0147	$F_{7,11,11}$	0.0077
$F_{8,11,11}$	-0.1225	$F_{9,11,11}$	0.1963	$F_{10,11,11}$	-0.0058
$F_{11,11,11}$	0.0980	$F_{1,1,12}$	0.0023	$F_{1,2,12}$	0.0026
$F_{2,2,12}$	-0.0010	$F_{1,3,12}$	0.0003	$F_{2,3,12}$	-0.0063
$F_{3,3,12}$	-0.0008	$F_{1,4,12}$	-0.0022	$F_{2,4,12}$	-0.0041
$F_{3,4,12}$	-0.0047	$F_{4,4,12}$	0.0203	$F_{1,5,12}$	0.0017

Table B5: F12-TZ Force Constants for HOOF (cont.)

$F_{2,5,12}$	-0.0009	$F_{3,5,12}$	0.0084	$F_{4,5,12}$	0.0008
$F_{5,5,12}$	-0.0138	$F_{1,6,12}$	0.0048	$F_{2,6,12}$	0.0064
$F_{3,6,12}$	0.0006	$F_{4,6,12}$	0.0040	$F_{5,6,12}$	-0.0304
$F_{6,6,12}$	-0.1260	$F_{1,7,12}$	-0.0008	$F_{2,7,12}$	-0.0007
$F_{3,7,12}$	0.0070	$F_{4,7,12}$	-0.0064	$F_{5,7,12}$	0.0005
$F_{6,7,12}$	-0.0071	$F_{7,7,12}$	0.0530	$F_{1,8,12}$	-0.0033
$F_{2,8,12}$	0.0020	$F_{3,8,12}$	0.0002	$F_{4,8,12}$	0.0026
$F_{5,8,12}$	0.0385	$F_{6,8,12}$	0.0071	$F_{7,8,12}$	0.0080
$F_{8,8,12}$	-0.2461	$F_{1,9,12}$	-0.0081	$F_{2,9,12}$	0.0017
$F_{3,9,12}$	-0.0038	$F_{4,9,12}$	0.0042	$F_{5,9,12}$	0.0579
$F_{6,9,12}$	0.0344	$F_{7,9,12}$	-0.0054	$F_{8,9,12}$	0.2141
$F_{9,9,12}$	-0.3735	$F_{1,10,12}$	0.0007	$F_{2,10,12}$	0.0021
$F_{3,10,12}$	-0.0027	$F_{4,10,12}$	-0.0118	$F_{5,10,12}$	-0.0030
$F_{6,10,12}$	-0.0017	$F_{7,10,12}$	-0.0459	$F_{8,10,12}$	-0.0073
$F_{9,10,12}$	0.0093	$F_{10,10,12}$	0.0570	$F_{1,11,12}$	-0.0010
$F_{2,11,12}$	-0.0000	$F_{3,11,12}$	-0.0023	$F_{4,11,12}$	0.0006
$F_{5,11,12}$	-0.0238	$F_{6,11,12}$	0.0169	$F_{7,11,12}$	-0.0078
$F_{8,11,12}$	0.2057	$F_{9,11,12}$	-0.2737	$F_{10,11,12}$	0.0082
$F_{11,11,12}$	-0.1819	$F_{1,12,12}$	0.0031	$F_{2,12,12}$	-0.0018
$F_{3,12,12}$	0.0040	$F_{4,12,12}$	-0.0036	$F_{5,12,12}$	-0.0359
$F_{6,12,12}$	0.0910	$F_{7,12,12}$	0.0055	$F_{8,12,12}$	-0.2214
$F_{9,12,12}$	0.3428	$F_{10,12,12}$	-0.0050	$F_{11,12,12}$	0.2590
$F_{12,12,12}$	-0.4379	$F_{1,1,1,1}$	4.47	$F_{1,1,1,2}$	2.20
$F_{1,1,2,2}$	-0.33	$F_{1,2,2,2}$	-0.77	$F_{2,2,2,2}$	-0.15
$F_{1,1,1,3}$	1.07	$F_{1,1,2,3}$	0.43	$F_{1,2,2,3}$	0.00
$F_{2,2,2,3}$	-0.13	$F_{1,1,3,3}$	-0.93	$F_{1,2,3,3}$	-0.25
$F_{2,2,3,3}$	0.03	$F_{1,3,3,3}$	-0.43	$F_{2,3,3,3}$	-0.16
$F_{3,3,3,3}$	0.17	$F_{1,1,1,4}$	-4.49	$F_{1,1,2,4}$	-2.21
$F_{1,2,2,4}$	0.37	$F_{2,2,2,4}$	0.74	$F_{1,1,3,4}$	-1.06
$F_{1,2,3,4}$	-0.42	$F_{2,2,3,4}$	-0.00	$F_{1,3,3,4}$	0.95
$F_{2,3,3,4}$	0.25	$F_{3,3,3,4}$	0.39	$F_{1,1,4,4}$	4.51
$F_{1,2,4,4}$	2.23	$F_{2,2,4,4}$	-0.43	$F_{1,3,4,4}$	1.06
$F_{2,3,4,4}$	0.39	$F_{3,3,4,4}$	-1.01	$F_{1,4,4,4}$	-4.52
$F_{2,4,4,4}$	-2.32	$F_{3,4,4,4}$	-1.12	$F_{4,4,4,4}$	4.49
$F_{1,1,1,5}$	-2.21	$F_{1,1,2,5}$	0.33	$F_{1,2,2,5}$	0.79
$F_{2,2,2,5}$	0.15	$F_{1,1,3,5}$	-0.44	$F_{1,2,3,5}$	0.01
$F_{2,2,3,5}$	0.14	$F_{1,3,3,5}$	0.32	$F_{2,3,3,5}$	-0.00
$F_{3,3,3,5}$	0.18	$F_{1,1,4,5}$	2.21	$F_{1,2,4,5}$	-0.36
$F_{2,2,4,5}$	-0.76	$F_{1,3,4,5}$	0.44	$F_{2,3,4,5}$	0.01
$F_{3,3,4,5}$	-0.32	$F_{1,4,4,5}$	-2.24	$F_{2,4,4,5}$	0.41
$F_{3,4,4,5}$	-0.45	$F_{4,4,4,5}$	2.34	$F_{1,1,5,5}$	-0.37
$F_{1,2,5,5}$	-0.81	$F_{2,2,5,5}$	-0.16	$F_{1,3,5,5}$	0.01
$F_{2,3,5,5}$	-0.15	$F_{3,3,5,5}$	-0.01	$F_{1,4,5,5}$	0.38
$F_{2,4,5,5}$	0.79	$F_{3,4,5,5}$	-0.03	$F_{4,4,5,5}$	-0.57
$F_{1,5,5,5}$	0.89	$F_{2,5,5,5}$	0.15	$F_{3,5,5,5}$	0.19
$F_{4,5,5,5}$	-0.90	$F_{5,5,5,5}$	-0.15	$F_{1,1,1,6}$	-1.06
$F_{1,1,2,6}$	-0.46	$F_{1,2,2,6}$	0.05	$F_{2,2,2,6}$	0.18
$F_{1,1,3,6}$	0.92	$F_{1,2,3,6}$	0.27	$F_{2,2,3,6}$	-0.00
$F_{1,3,3,6}$	0.47	$F_{2,3,3,6}$	0.18	$F_{3,3,3,6}$	-0.17

Table B6: F12-TZ Force Constants for HOOF (cont.)

$F_{1,1,4,6}$	1.05	$F_{1,2,4,6}$	0.46	$F_{2,2,4,6}$	-0.03
$F_{1,3,4,6}$	-0.94	$F_{2,3,4,6}$	-0.26	$F_{3,3,4,6}$	-0.42
$F_{1,4,4,6}$	-1.05	$F_{2,4,4,6}$	-0.47	$F_{3,4,4,6}$	0.97
$F_{4,4,4,6}$	1.11	$F_{1,1,5,6}$	0.41	$F_{1,2,5,6}$	-0.07
$F_{2,2,5,6}$	-0.17	$F_{1,3,5,6}$	-0.34	$F_{2,3,5,6}$	0.00
$F_{3,3,5,6}$	-0.17	$F_{1,4,5,6}$	-0.44	$F_{2,4,5,6}$	0.06
$F_{3,4,5,6}$	0.35	$F_{4,4,5,6}$	0.32	$F_{1,5,5,6}$	0.13
$F_{2,5,5,6}$	0.20	$F_{3,5,5,6}$	0.04	$F_{4,5,5,6}$	-0.20
$F_{5,5,5,6}$	0.26	$F_{1,1,6,6}$	-0.97	$F_{1,2,6,6}$	-0.29
$F_{2,2,6,6}$	0.02	$F_{1,3,6,6}$	-0.49	$F_{2,3,6,6}$	-0.20
$F_{3,3,6,6}$	0.14	$F_{1,4,6,6}$	0.96	$F_{2,4,6,6}$	0.30
$F_{3,4,6,6}$	0.43	$F_{4,4,6,6}$	-1.20	$F_{1,5,6,6}$	0.43
$F_{2,5,6,6}$	0.03	$F_{3,5,6,6}$	0.19	$F_{4,5,6,6}$	-0.55
$F_{5,5,6,6}$	0.77	$F_{1,6,6,6}$	0.57	$F_{2,6,6,6}$	0.27
$F_{3,6,6,6}$	-0.13	$F_{4,6,6,6}$	-0.58	$F_{5,6,6,6}$	0.70
$F_{6,6,6,6}$	0.82	$F_{1,1,1,7}$	0.02	$F_{1,1,2,7}$	0.00
$F_{1,2,2,7}$	-0.04	$F_{2,2,2,7}$	0.03	$F_{1,1,3,7}$	0.00
$F_{1,2,3,7}$	-0.02	$F_{2,2,3,7}$	-0.00	$F_{1,3,3,7}$	-0.02
$F_{2,3,3,7}$	-0.00	$F_{3,3,3,7}$	0.04	$F_{1,1,4,7}$	-0.03
$F_{1,2,4,7}$	-0.02	$F_{2,2,4,7}$	0.07	$F_{1,3,4,7}$	-0.00
$F_{2,3,4,7}$	0.02	$F_{3,3,4,7}$	0.06	$F_{1,4,4,7}$	0.00
$F_{2,4,4,7}$	0.09	$F_{3,4,4,7}$	0.05	$F_{4,4,4,7}$	0.03
$F_{1,1,5,7}$	0.00	$F_{1,2,5,7}$	0.03	$F_{2,2,5,7}$	-0.03
$F_{1,3,5,7}$	0.01	$F_{2,3,5,7}$	-0.01	$F_{3,3,5,7}$	-0.01
$F_{1,4,5,7}$	0.03	$F_{2,4,5,7}$	-0.04	$F_{3,4,5,7}$	0.01
$F_{4,4,5,7}$	-0.10	$F_{1,5,5,7}$	-0.01	$F_{2,5,5,7}$	0.02
$F_{3,5,5,7}$	0.01	$F_{4,5,5,7}$	0.18	$F_{5,5,5,7}$	0.05
$F_{1,1,6,7}$	0.01	$F_{1,2,6,7}$	-0.00	$F_{2,2,6,7}$	-0.02
$F_{1,3,6,7}$	0.01	$F_{2,3,6,7}$	-0.02	$F_{3,3,6,7}$	-0.05
$F_{1,4,6,7}$	0.01	$F_{2,4,6,7}$	0.02	$F_{3,4,6,7}$	-0.04
$F_{4,4,6,7}$	-0.06	$F_{1,5,6,7}$	0.04	$F_{2,5,6,7}$	-0.01
$F_{3,5,6,7}$	-0.00	$F_{4,5,6,7}$	0.11	$F_{5,5,6,7}$	0.11
$F_{1,6,6,7}$	0.01	$F_{2,6,6,7}$	-0.01	$F_{3,6,6,7}$	0.06
$F_{4,6,6,7}$	0.20	$F_{5,6,6,7}$	0.10	$F_{6,6,6,7}$	-0.02
$F_{1,1,7,7}$	0.01	$F_{1,2,7,7}$	0.02	$F_{2,2,7,7}$	-0.03
$F_{1,3,7,7}$	0.01	$F_{2,3,7,7}$	-0.00	$F_{3,3,7,7}$	-0.04
$F_{1,4,7,7}$	0.03	$F_{2,4,7,7}$	-0.08	$F_{3,4,7,7}$	-0.05
$F_{4,4,7,7}$	-0.03	$F_{1,5,7,7}$	-0.04	$F_{2,5,7,7}$	0.01
$F_{3,5,7,7}$	-0.02	$F_{4,5,7,7}$	0.09	$F_{5,5,7,7}$	-0.19
$F_{1,6,7,7}$	-0.02	$F_{2,6,7,7}$	-0.02	$F_{3,6,7,7}$	0.03
$F_{4,6,7,7}$	0.05	$F_{5,6,7,7}$	-0.15	$F_{6,6,7,7}$	-0.21
$F_{1,7,7,7}$	-0.05	$F_{2,7,7,7}$	0.05	$F_{3,7,7,7}$	0.03
$F_{4,7,7,7}$	-0.03	$F_{5,7,7,7}$	-0.07	$F_{6,7,7,7}$	-0.02
$F_{7,7,7,7}$	0.21	$F_{1,1,1,8}$	0.00	$F_{1,1,2,8}$	-0.00
$F_{1,2,2,8}$	-0.02	$F_{2,2,2,8}$	0.01	$F_{1,1,3,8}$	0.00
$F_{1,2,3,8}$	-0.01	$F_{2,2,3,8}$	-0.01	$F_{1,3,3,8}$	-0.08
$F_{2,3,3,8}$	-0.03	$F_{3,3,3,8}$	-0.02	$F_{1,1,4,8}$	-0.00
$F_{1,2,4,8}$	-0.00	$F_{2,2,4,8}$	0.02	$F_{1,3,4,8}$	-0.02
$F_{2,3,4,8}$	-0.01	$F_{3,3,4,8}$	0.07	$F_{1,4,4,8}$	0.01

Table B7: F12-TZ Force Constants for HOOF (cont.)

$F_{2,4,4,8}$	0.02	$F_{3,4,4,8}$	0.06	$F_{4,4,4,8}$	-0.02
$F_{1,1,5,8}$	0.04	$F_{1,2,5,8}$	0.02	$F_{2,2,5,8}$	0.01
$F_{1,3,5,8}$	-0.02	$F_{2,3,5,8}$	0.01	$F_{3,3,5,8}$	0.00
$F_{1,4,5,8}$	-0.02	$F_{2,4,5,8}$	-0.03	$F_{3,4,5,8}$	0.01
$F_{4,4,5,8}$	0.19	$F_{1,5,5,8}$	-0.07	$F_{2,5,5,8}$	0.01
$F_{3,5,5,8}$	-0.05	$F_{4,5,5,8}$	0.12	$F_{5,5,5,8}$	-0.00
$F_{1,1,6,8}$	0.06	$F_{1,2,6,8}$	0.02	$F_{2,2,6,8}$	-0.01
$F_{1,3,6,8}$	0.07	$F_{2,3,6,8}$	-0.00	$F_{3,3,6,8}$	-0.01
$F_{1,4,6,8}$	-0.02	$F_{2,4,6,8}$	-0.04	$F_{3,4,6,8}$	-0.10
$F_{4,4,6,8}$	0.15	$F_{1,5,6,8}$	-0.06	$F_{2,5,6,8}$	-0.02
$F_{3,5,6,8}$	-0.04	$F_{4,5,6,8}$	0.14	$F_{5,5,6,8}$	-0.51
$F_{1,6,6,8}$	-0.14	$F_{2,6,6,8}$	-0.04	$F_{3,6,6,8}$	0.00
$F_{4,6,6,8}$	0.25	$F_{5,6,6,8}$	-0.85	$F_{6,6,6,8}$	-0.97
$F_{1,1,7,8}$	-0.00	$F_{1,2,7,8}$	0.00	$F_{2,2,7,8}$	-0.00
$F_{1,3,7,8}$	0.01	$F_{2,3,7,8}$	0.02	$F_{3,3,7,8}$	0.02
$F_{1,4,7,8}$	-0.01	$F_{2,4,7,8}$	-0.02	$F_{3,4,7,8}$	-0.03
$F_{4,4,7,8}$	0.03	$F_{1,5,7,8}$	-0.02	$F_{2,5,7,8}$	0.02
$F_{3,5,7,8}$	0.00	$F_{4,5,7,8}$	-0.18	$F_{5,5,7,8}$	-0.09
$F_{1,6,7,8}$	-0.04	$F_{2,6,7,8}$	0.04	$F_{3,6,7,8}$	0.02
$F_{4,6,7,8}$	-0.14	$F_{5,6,7,8}$	-0.10	$F_{6,6,7,8}$	-0.10
$F_{1,7,7,8}$	0.01	$F_{2,7,7,8}$	0.02	$F_{3,7,7,8}$	0.02
$F_{4,7,7,8}$	-0.03	$F_{5,7,7,8}$	0.24	$F_{6,7,7,8}$	0.17
$F_{7,7,7,8}$	0.04	$F_{1,1,8,8}$	-0.04	$F_{1,2,8,8}$	-0.00
$F_{2,2,8,8}$	-0.03	$F_{1,3,8,8}$	0.02	$F_{2,3,8,8}$	-0.01
$F_{3,3,8,8}$	0.03	$F_{1,4,8,8}$	0.03	$F_{2,4,8,8}$	0.00
$F_{3,4,8,8}$	-0.00	$F_{4,4,8,8}$	-0.25	$F_{1,5,8,8}$	0.05
$F_{2,5,8,8}$	-0.01	$F_{3,5,8,8}$	0.04	$F_{4,5,8,8}$	-0.11
$F_{5,5,8,8}$	0.01	$F_{1,6,8,8}$	0.05	$F_{2,6,8,8}$	0.04
$F_{3,6,8,8}$	0.04	$F_{4,6,8,8}$	-0.10	$F_{5,6,8,8}$	0.56
$F_{6,6,8,8}$	0.85	$F_{1,7,8,8}$	0.02	$F_{2,7,8,8}$	-0.01
$F_{3,7,8,8}$	-0.01	$F_{4,7,8,8}$	0.27	$F_{5,7,8,8}$	0.08
$F_{6,7,8,8}$	0.06	$F_{7,7,8,8}$	-0.49	$F_{1,8,8,8}$	-0.05
$F_{2,8,8,8}$	0.04	$F_{3,8,8,8}$	-0.03	$F_{4,8,8,8}$	0.13
$F_{5,8,8,8}$	-0.05	$F_{6,8,8,8}$	-0.66	$F_{7,8,8,8}$	-0.11
$F_{8,8,8,8}$	-0.07	$F_{1,1,1,9}$	-0.00	$F_{1,1,2,9}$	0.02
$F_{1,2,2,9}$	-0.05	$F_{2,2,2,9}$	-0.05	$F_{1,1,3,9}$	0.00
$F_{1,2,3,9}$	-0.02	$F_{2,2,3,9}$	-0.02	$F_{1,3,3,9}$	-0.04
$F_{2,3,3,9}$	-0.02	$F_{3,3,3,9}$	0.01	$F_{1,1,4,9}$	0.01
$F_{1,2,4,9}$	-0.04	$F_{2,2,4,9}$	0.03	$F_{1,3,4,9}$	-0.01
$F_{2,3,4,9}$	-0.00	$F_{3,3,4,9}$	0.03	$F_{1,4,4,9}$	-0.01
$F_{2,4,4,9}$	0.08	$F_{3,4,4,9}$	0.04	$F_{4,4,4,9}$	-0.00
$F_{1,1,5,9}$	0.03	$F_{1,2,5,9}$	0.06	$F_{2,2,5,9}$	0.03
$F_{1,3,5,9}$	0.01	$F_{2,3,5,9}$	-0.00	$F_{3,3,5,9}$	0.01
$F_{1,4,5,9}$	0.01	$F_{2,4,5,9}$	-0.08	$F_{3,4,5,9}$	-0.02
$F_{4,4,5,9}$	0.11	$F_{1,5,5,9}$	-0.14	$F_{2,5,5,9}$	-0.04
$F_{3,5,5,9}$	-0.03	$F_{4,5,5,9}$	0.24	$F_{5,5,5,9}$	-0.45
$F_{1,1,6,9}$	0.05	$F_{1,2,6,9}$	0.01	$F_{2,2,6,9}$	-0.01
$F_{1,3,6,9}$	0.03	$F_{2,3,6,9}$	0.02	$F_{3,3,6,9}$	0.02
$F_{1,4,6,9}$	-0.02	$F_{2,4,6,9}$	-0.04	$F_{3,4,6,9}$	-0.02

Table B8: F12-TZ Force Constants for HOOF (cont.)

$F_{4,4,6,9}$	0.18	$F_{1,5,6,9}$	-0.09	$F_{2,5,6,9}$	-0.04
$F_{3,5,6,9}$	-0.04	$F_{4,5,6,9}$	0.19	$F_{5,5,6,9}$	-0.81
$F_{1,6,6,9}$	-0.10	$F_{2,6,6,9}$	-0.08	$F_{3,6,6,9}$	-0.01
$F_{4,6,6,9}$	0.15	$F_{5,6,6,9}$	-0.83	$F_{6,6,6,9}$	-0.43
$F_{1,1,7,9}$	-0.01	$F_{1,2,7,9}$	0.02	$F_{2,2,7,9}$	0.02
$F_{1,3,7,9}$	0.01	$F_{2,3,7,9}$	0.02	$F_{3,3,7,9}$	0.01
$F_{1,4,7,9}$	-0.00	$F_{2,4,7,9}$	-0.04	$F_{3,4,7,9}$	-0.02
$F_{4,4,7,9}$	0.01	$F_{1,5,7,9}$	-0.05	$F_{2,5,7,9}$	0.04
$F_{3,5,7,9}$	0.01	$F_{4,5,7,9}$	-0.10	$F_{5,5,7,9}$	-0.13
$F_{1,6,7,9}$	-0.02	$F_{2,6,7,9}$	0.02	$F_{3,6,7,9}$	-0.01
$F_{4,6,7,9}$	-0.16	$F_{5,6,7,9}$	-0.09	$F_{6,6,7,9}$	-0.03
$F_{1,7,7,9}$	0.01	$F_{2,7,7,9}$	0.02	$F_{3,7,7,9}$	0.01
$F_{4,7,7,9}$	-0.00	$F_{5,7,7,9}$	0.13	$F_{6,7,7,9}$	0.18
$F_{7,7,7,9}$	-0.02	$F_{1,1,8,9}$	-0.05	$F_{1,2,8,9}$	-0.01
$F_{2,2,8,9}$	0.02	$F_{1,3,8,9}$	0.01	$F_{2,3,8,9}$	0.03
$F_{3,3,8,9}$	0.02	$F_{1,4,8,9}$	0.03	$F_{2,4,8,9}$	0.06
$F_{3,4,8,9}$	0.02	$F_{4,4,8,9}$	-0.19	$F_{1,5,8,9}$	0.07
$F_{2,5,8,9}$	-0.00	$F_{3,5,8,9}$	0.03	$F_{4,5,8,9}$	-0.16
$F_{5,5,8,9}$	0.50	$F_{1,6,8,9}$	0.07	$F_{2,6,8,9}$	0.04
$F_{3,6,8,9}$	0.02	$F_{4,6,8,9}$	-0.15	$F_{5,6,8,9}$	0.86
$F_{6,6,8,9}$	0.96	$F_{1,7,8,9}$	0.03	$F_{2,7,8,9}$	-0.07
$F_{3,7,8,9}$	-0.03	$F_{4,7,8,9}$	0.13	$F_{5,7,8,9}$	0.10
$F_{6,7,8,9}$	0.07	$F_{7,7,8,9}$	0.01	$F_{1,8,8,9}$	-0.06
$F_{2,8,8,9}$	-0.02	$F_{3,8,8,9}$	-0.07	$F_{4,8,8,9}$	0.10
$F_{5,8,8,9}$	-0.51	$F_{6,8,8,9}$	-0.87	$F_{7,8,8,9}$	-0.03
$F_{8,8,8,9}$	0.38	$F_{1,1,9,9}$	-0.05	$F_{1,2,9,9}$	-0.00
$F_{2,2,9,9}$	0.03	$F_{1,3,9,9}$	0.01	$F_{2,3,9,9}$	-0.00
$F_{3,3,9,9}$	-0.05	$F_{1,4,9,9}$	0.03	$F_{2,4,9,9}$	0.04
$F_{3,4,9,9}$	-0.02	$F_{4,4,9,9}$	-0.19	$F_{1,5,9,9}$	0.10
$F_{2,5,9,9}$	0.05	$F_{3,5,9,9}$	0.03	$F_{4,5,9,9}$	-0.18
$F_{5,5,9,9}$	0.82	$F_{1,6,9,9}$	0.08	$F_{2,6,9,9}$	0.07
$F_{3,6,9,9}$	0.00	$F_{4,6,9,9}$	-0.13	$F_{5,6,9,9}$	0.84
$F_{6,6,9,9}$	0.40	$F_{1,7,9,9}$	0.02	$F_{2,7,9,9}$	-0.04
$F_{3,7,9,9}$	0.01	$F_{4,7,9,9}$	0.13	$F_{5,7,9,9}$	0.07
$F_{6,7,9,9}$	0.03	$F_{7,7,9,9}$	-0.32	$F_{1,8,9,9}$	-0.09
$F_{2,8,9,9}$	-0.07	$F_{3,8,9,9}$	-0.04	$F_{4,8,9,9}$	0.13
$F_{5,8,9,9}$	-0.78	$F_{6,8,9,9}$	-0.92	$F_{7,8,9,9}$	-0.04
$F_{8,8,9,9}$	1.29	$F_{1,9,9,9}$	-0.10	$F_{2,9,9,9}$	-0.08
$F_{3,9,9,9}$	0.05	$F_{4,9,9,9}$	0.16	$F_{5,9,9,9}$	-0.99
$F_{6,9,9,9}$	-0.50	$F_{7,9,9,9}$	-0.02	$F_{8,9,9,9}$	0.19
$F_{9,9,9,9}$	1.47	$F_{1,1,1,10}$	0.00	$F_{1,1,2,10}$	0.00
$F_{1,2,2,10}$	0.01	$F_{2,2,2,10}$	-0.00	$F_{1,1,3,10}$	-0.00
$F_{1,2,3,10}$	-0.00	$F_{2,2,3,10}$	0.00	$F_{1,3,3,10}$	-0.00
$F_{2,3,3,10}$	-0.00	$F_{3,3,3,10}$	0.00	$F_{1,1,4,10}$	0.00
$F_{1,2,4,10}$	-0.00	$F_{2,2,4,10}$	-0.00	$F_{1,3,4,10}$	0.00
$F_{2,3,4,10}$	0.00	$F_{3,3,4,10}$	0.00	$F_{1,4,4,10}$	0.00
$F_{2,4,4,10}$	-0.00	$F_{3,4,4,10}$	0.00	$F_{4,4,4,10}$	-0.01
$F_{1,1,5,10}$	-0.00	$F_{1,2,5,10}$	-0.00	$F_{2,2,5,10}$	0.00
$F_{1,3,5,10}$	-0.00	$F_{2,3,5,10}$	-0.01	$F_{3,3,5,10}$	0.01

Table B9: F12-TZ Force Constants for HOOF (cont.)

$F_{1,4,5,10}$	-0.00	$F_{2,4,5,10}$	-0.00	$F_{3,4,5,10}$	0.00
$F_{4,4,5,10}$	0.01	$F_{1,5,5,10}$	-0.00	$F_{2,5,5,10}$	0.01
$F_{3,5,5,10}$	0.01	$F_{4,5,5,10}$	0.00	$F_{5,5,5,10}$	-0.04
$F_{1,1,6,10}$	0.00	$F_{1,2,6,10}$	0.00	$F_{2,2,6,10}$	-0.01
$F_{1,3,6,10}$	0.00	$F_{2,3,6,10}$	0.00	$F_{3,3,6,10}$	-0.00
$F_{1,4,6,10}$	-0.00	$F_{2,4,6,10}$	-0.01	$F_{3,4,6,10}$	0.00
$F_{4,4,6,10}$	-0.00	$F_{1,5,6,10}$	-0.00	$F_{2,5,6,10}$	0.02
$F_{3,5,6,10}$	-0.01	$F_{4,5,6,10}$	0.01	$F_{5,5,6,10}$	-0.04
$F_{1,6,6,10}$	0.00	$F_{2,6,6,10}$	-0.00	$F_{3,6,6,10}$	-0.00
$F_{4,6,6,10}$	0.04	$F_{5,6,6,10}$	0.02	$F_{6,6,6,10}$	0.04
$F_{1,1,7,10}$	-0.00	$F_{1,2,7,10}$	-0.01	$F_{2,2,7,10}$	-0.00
$F_{1,3,7,10}$	-0.00	$F_{2,3,7,10}$	-0.00	$F_{3,3,7,10}$	0.01
$F_{1,4,7,10}$	-0.00	$F_{2,4,7,10}$	0.01	$F_{3,4,7,10}$	-0.00
$F_{4,4,7,10}$	-0.01	$F_{1,5,7,10}$	0.01	$F_{2,5,7,10}$	0.00
$F_{3,5,7,10}$	0.00	$F_{4,5,7,10}$	-0.01	$F_{5,5,7,10}$	0.02
$F_{1,6,7,10}$	0.00	$F_{2,6,7,10}$	0.01	$F_{3,6,7,10}$	-0.01
$F_{4,6,7,10}$	0.01	$F_{5,6,7,10}$	-0.01	$F_{6,6,7,10}$	-0.01
$F_{1,7,7,10}$	0.01	$F_{2,7,7,10}$	-0.00	$F_{3,7,7,10}$	0.01
$F_{4,7,7,10}$	0.03	$F_{5,7,7,10}$	0.01	$F_{6,7,7,10}$	-0.01
$F_{7,7,7,10}$	-0.13	$F_{1,1,8,10}$	-0.00	$F_{1,2,8,10}$	-0.00
$F_{2,2,8,10}$	0.00	$F_{1,3,8,10}$	0.01	$F_{2,3,8,10}$	0.00
$F_{3,3,8,10}$	-0.00	$F_{1,4,8,10}$	0.00	$F_{2,4,8,10}$	0.01
$F_{3,4,8,10}$	-0.01	$F_{4,4,8,10}$	-0.01	$F_{1,5,8,10}$	0.01
$F_{2,5,8,10}$	-0.01	$F_{3,5,8,10}$	-0.00	$F_{4,5,8,10}$	0.01
$F_{5,5,8,10}$	0.04	$F_{1,6,8,10}$	-0.00	$F_{2,6,8,10}$	-0.01
$F_{3,6,8,10}$	0.01	$F_{4,6,8,10}$	0.00	$F_{5,6,8,10}$	0.02
$F_{6,6,8,10}$	-0.02	$F_{1,7,8,10}$	-0.00	$F_{2,7,8,10}$	-0.01
$F_{3,7,8,10}$	-0.00	$F_{4,7,8,10}$	0.01	$F_{5,7,8,10}$	-0.05
$F_{6,7,8,10}$	0.01	$F_{7,7,8,10}$	-0.03	$F_{1,8,8,10}$	-0.01
$F_{2,8,8,10}$	0.01	$F_{3,8,8,10}$	-0.01	$F_{4,8,8,10}$	-0.04
$F_{5,8,8,10}$	-0.03	$F_{6,8,8,10}$	-0.00	$F_{7,8,8,10}$	0.20
$F_{8,8,8,10}$	0.03	$F_{1,1,9,10}$	0.00	$F_{1,2,9,10}$	-0.00
$F_{2,2,9,10}$	0.00	$F_{1,3,9,10}$	0.00	$F_{2,3,9,10}$	-0.00
$F_{3,3,9,10}$	-0.00	$F_{1,4,9,10}$	0.00	$F_{2,4,9,10}$	0.00
$F_{3,4,9,10}$	-0.01	$F_{4,4,9,10}$	-0.00	$F_{1,5,9,10}$	0.01
$F_{2,5,9,10}$	-0.01	$F_{3,5,9,10}$	0.00	$F_{4,5,9,10}$	-0.02
$F_{5,5,9,10}$	0.03	$F_{1,6,9,10}$	-0.00	$F_{2,6,9,10}$	-0.00
$F_{3,6,9,10}$	0.01	$F_{4,6,9,10}$	-0.00	$F_{5,6,9,10}$	-0.01
$F_{6,6,9,10}$	-0.03	$F_{1,7,9,10}$	0.00	$F_{2,7,9,10}$	-0.00
$F_{3,7,9,10}$	0.00	$F_{4,7,9,10}$	-0.00	$F_{5,7,9,10}$	0.02
$F_{6,7,9,10}$	0.00	$F_{7,7,9,10}$	0.01	$F_{1,8,9,10}$	-0.00
$F_{2,8,9,10}$	0.02	$F_{3,8,9,10}$	-0.00	$F_{4,8,9,10}$	0.03
$F_{5,8,9,10}$	-0.02	$F_{6,8,9,10}$	0.01	$F_{7,8,9,10}$	-0.17
$F_{8,8,9,10}$	-0.01	$F_{1,9,9,10}$	-0.00	$F_{2,9,9,10}$	0.00
$F_{3,9,9,10}$	0.00	$F_{4,9,9,10}$	0.02	$F_{5,9,9,10}$	0.01
$F_{6,9,9,10}$	0.01	$F_{7,9,9,10}$	0.17	$F_{8,9,9,10}$	0.01
$F_{9,9,9,10}$	-0.04	$F_{1,1,10,10}$	0.00	$F_{1,2,10,10}$	0.00
$F_{2,2,10,10}$	-0.00	$F_{1,3,10,10}$	0.00	$F_{2,3,10,10}$	-0.00
$F_{3,3,10,10}$	-0.00	$F_{1,4,10,10}$	0.00	$F_{2,4,10,10}$	-0.00

Table B10: F12-TZ Force Constants for HOOF (cont.)

$F_{3,4,10,10}$	0.00	$F_{4,4,10,10}$	0.02	$F_{1,5,10,10}$	-0.00
$F_{2,5,10,10}$	0.00	$F_{3,5,10,10}$	-0.00	$F_{4,5,10,10}$	0.01
$F_{5,5,10,10}$	-0.02	$F_{1,6,10,10}$	0.00	$F_{2,6,10,10}$	-0.00
$F_{3,6,10,10}$	0.00	$F_{4,6,10,10}$	0.00	$F_{5,6,10,10}$	0.00
$F_{6,6,10,10}$	-0.03	$F_{1,7,10,10}$	-0.00	$F_{2,7,10,10}$	0.00
$F_{3,7,10,10}$	-0.00	$F_{4,7,10,10}$	-0.02	$F_{5,7,10,10}$	-0.01
$F_{6,7,10,10}$	0.00	$F_{7,7,10,10}$	0.10	$F_{1,8,10,10}$	-0.00
$F_{2,8,10,10}$	0.00	$F_{3,8,10,10}$	0.00	$F_{4,8,10,10}$	-0.00
$F_{5,8,10,10}$	0.03	$F_{6,8,10,10}$	-0.01	$F_{7,8,10,10}$	0.02
$F_{8,8,10,10}$	-0.15	$F_{1,9,10,10}$	-0.00	$F_{2,9,10,10}$	0.00
$F_{3,9,10,10}$	-0.00	$F_{4,9,10,10}$	0.00	$F_{5,9,10,10}$	0.00
$F_{6,9,10,10}$	0.01	$F_{7,9,10,10}$	-0.01	$F_{8,9,10,10}$	0.15
$F_{9,9,10,10}$	-0.19	$F_{1,10,10,10}$	0.00	$F_{2,10,10,10}$	0.00
$F_{3,10,10,10}$	0.00	$F_{4,10,10,10}$	-0.00	$F_{5,10,10,10}$	0.00
$F_{6,10,10,10}$	-0.00	$F_{7,10,10,10}$	-0.08	$F_{8,10,10,10}$	-0.01
$F_{9,10,10,10}$	0.01	$F_{10,10,10,10}$	0.08	$F_{1,1,1,11}$	0.00
$F_{1,1,2,11}$	0.00	$F_{1,2,2,11}$	-0.00	$F_{2,2,2,11}$	-0.00
$F_{1,1,3,11}$	-0.00	$F_{1,2,3,11}$	-0.00	$F_{2,2,3,11}$	-0.00
$F_{1,3,3,11}$	0.00	$F_{2,3,3,11}$	0.00	$F_{3,3,3,11}$	0.00
$F_{1,1,4,11}$	-0.00	$F_{1,2,4,11}$	-0.00	$F_{2,2,4,11}$	0.00
$F_{1,3,4,11}$	-0.00	$F_{2,3,4,11}$	0.00	$F_{3,3,4,11}$	-0.00
$F_{1,4,4,11}$	0.00	$F_{2,4,4,11}$	0.00	$F_{3,4,4,11}$	0.00
$F_{4,4,4,11}$	0.01	$F_{1,1,5,11}$	-0.00	$F_{1,2,5,11}$	0.00
$F_{2,2,5,11}$	0.00	$F_{1,3,5,11}$	-0.00	$F_{2,3,5,11}$	0.00
$F_{3,3,5,11}$	0.00	$F_{1,4,5,11}$	0.00	$F_{2,4,5,11}$	0.00
$F_{3,4,5,11}$	0.00	$F_{4,4,5,11}$	-0.03	$F_{1,5,5,11}$	-0.00
$F_{2,5,5,11}$	0.00	$F_{3,5,5,11}$	0.00	$F_{4,5,5,11}$	-0.01
$F_{5,5,5,11}$	0.00	$F_{1,1,6,11}$	-0.00	$F_{1,2,6,11}$	-0.00
$F_{2,2,6,11}$	0.00	$F_{1,3,6,11}$	-0.00	$F_{2,3,6,11}$	0.00
$F_{3,3,6,11}$	0.00	$F_{1,4,6,11}$	0.00	$F_{2,4,6,11}$	0.01
$F_{3,4,6,11}$	0.00	$F_{4,4,6,11}$	-0.00	$F_{1,5,6,11}$	-0.00
$F_{2,5,6,11}$	-0.01	$F_{3,5,6,11}$	-0.01	$F_{4,5,6,11}$	-0.01
$F_{5,5,6,11}$	0.05	$F_{1,6,6,11}$	0.00	$F_{2,6,6,11}$	-0.01
$F_{3,6,6,11}$	0.00	$F_{4,6,6,11}$	-0.00	$F_{5,6,6,11}$	0.05
$F_{6,6,6,11}$	0.01	$F_{1,1,7,11}$	-0.00	$F_{1,2,7,11}$	0.00
$F_{2,2,7,11}$	0.00	$F_{1,3,7,11}$	0.00	$F_{2,3,7,11}$	0.00
$F_{3,3,7,11}$	-0.00	$F_{1,4,7,11}$	0.00	$F_{2,4,7,11}$	0.00
$F_{3,4,7,11}$	-0.00	$F_{4,4,7,11}$	-0.01	$F_{1,5,7,11}$	0.00
$F_{2,5,7,11}$	-0.00	$F_{3,5,7,11}$	0.00	$F_{4,5,7,11}$	0.04
$F_{5,5,7,11}$	0.02	$F_{1,6,7,11}$	-0.00	$F_{2,6,7,11}$	-0.01
$F_{3,6,7,11}$	-0.00	$F_{4,6,7,11}$	0.00	$F_{5,6,7,11}$	0.01
$F_{6,6,7,11}$	0.00	$F_{1,7,7,11}$	-0.00	$F_{2,7,7,11}$	-0.01
$F_{3,7,7,11}$	-0.00	$F_{4,7,7,11}$	0.01	$F_{5,7,7,11}$	-0.06
$F_{6,7,7,11}$	0.00	$F_{7,7,7,11}$	-0.03	$F_{1,1,8,11}$	0.00
$F_{1,2,8,11}$	0.00	$F_{2,2,8,11}$	0.01	$F_{1,3,8,11}$	0.00
$F_{2,3,8,11}$	0.00	$F_{3,3,8,11}$	-0.00	$F_{1,4,8,11}$	-0.00
$F_{2,4,8,11}$	0.00	$F_{3,4,8,11}$	0.00	$F_{4,4,8,11}$	0.05
$F_{1,5,8,11}$	-0.00	$F_{2,5,8,11}$	-0.01	$F_{3,5,8,11}$	-0.00
$F_{4,5,8,11}$	0.01	$F_{5,5,8,11}$	-0.02	$F_{1,6,8,11}$	-0.00

Table B11: F12-TZ Force Constants for HOOF (cont.)

$F_{2,6,8,11}$	-0.00	$F_{3,6,8,11}$	0.00	$F_{4,6,8,11}$	0.00
$F_{5,6,8,11}$	-0.03	$F_{6,6,8,11}$	0.04	$F_{1,7,8,11}$	-0.00
$F_{2,7,8,11}$	-0.01	$F_{3,7,8,11}$	-0.01	$F_{4,7,8,11}$	-0.07
$F_{5,7,8,11}$	-0.01	$F_{6,7,8,11}$	0.00	$F_{7,7,8,11}$	0.22
$F_{1,8,8,11}$	0.01	$F_{2,8,8,11}$	0.00	$F_{3,8,8,11}$	-0.00
$F_{4,8,8,11}$	-0.02	$F_{5,8,8,11}$	0.05	$F_{6,8,8,11}$	0.06
$F_{7,8,8,11}$	0.03	$F_{8,8,8,11}$	0.08	$F_{1,1,9,11}$	-0.00
$F_{1,2,9,11}$	0.00	$F_{2,2,9,11}$	-0.01	$F_{1,3,9,11}$	0.00
$F_{2,3,9,11}$	-0.00	$F_{3,3,9,11}$	-0.01	$F_{1,4,9,11}$	0.00
$F_{2,4,9,11}$	-0.01	$F_{3,4,9,11}$	-0.00	$F_{4,4,9,11}$	-0.00
$F_{1,5,9,11}$	0.01	$F_{2,5,9,11}$	0.01	$F_{3,5,9,11}$	-0.00
$F_{4,5,9,11}$	0.00	$F_{5,5,9,11}$	-0.01	$F_{1,6,9,11}$	0.01
$F_{2,6,9,11}$	0.01	$F_{3,6,9,11}$	0.00	$F_{4,6,9,11}$	-0.00
$F_{5,6,9,11}$	-0.01	$F_{6,6,9,11}$	-0.05	$F_{1,7,9,11}$	-0.00
$F_{2,7,9,11}$	0.01	$F_{3,7,9,11}$	0.00	$F_{4,7,9,11}$	0.01
$F_{5,7,9,11}$	-0.01	$F_{6,7,9,11}$	0.00	$F_{7,7,9,11}$	-0.16
$F_{1,8,9,11}$	-0.00	$F_{2,8,9,11}$	-0.00	$F_{3,8,9,11}$	0.00
$F_{4,8,9,11}$	0.00	$F_{5,8,9,11}$	0.01	$F_{6,8,9,11}$	-0.03
$F_{7,8,9,11}$	-0.01	$F_{8,8,9,11}$	0.16	$F_{1,9,9,11}$	-0.00
$F_{2,9,9,11}$	-0.01	$F_{3,9,9,11}$	0.01	$F_{4,9,9,11}$	0.01
$F_{5,9,9,11}$	-0.09	$F_{6,9,9,11}$	0.00	$F_{7,9,9,11}$	0.01
$F_{8,9,9,11}$	-0.43	$F_{9,9,9,11}$	0.89	$F_{1,1,10,11}$	0.00
$F_{1,2,10,11}$	-0.00	$F_{2,2,10,11}$	-0.00	$F_{1,3,10,11}$	-0.00
$F_{2,3,10,11}$	-0.00	$F_{3,3,10,11}$	0.00	$F_{1,4,10,11}$	-0.00
$F_{2,4,10,11}$	-0.00	$F_{3,4,10,11}$	0.00	$F_{4,4,10,11}$	0.00
$F_{1,5,10,11}$	-0.00	$F_{2,5,10,11}$	0.00	$F_{3,5,10,11}$	-0.00
$F_{4,5,10,11}$	-0.01	$F_{5,5,10,11}$	-0.01	$F_{1,6,10,11}$	0.00
$F_{2,6,10,11}$	0.00	$F_{3,6,10,11}$	0.00	$F_{4,6,10,11}$	-0.00
$F_{5,6,10,11}$	-0.00	$F_{6,6,10,11}$	-0.00	$F_{1,7,10,11}$	0.00
$F_{2,7,10,11}$	0.00	$F_{3,7,10,11}$	0.00	$F_{4,7,10,11}$	-0.00
$F_{5,7,10,11}$	0.03	$F_{6,7,10,11}$	-0.00	$F_{7,7,10,11}$	0.02
$F_{1,8,10,11}$	0.00	$F_{2,8,10,11}$	0.00	$F_{3,8,10,11}$	0.01
$F_{4,8,10,11}$	0.03	$F_{5,8,10,11}$	0.01	$F_{6,8,10,11}$	-0.00
$F_{7,8,10,11}$	-0.14	$F_{8,8,10,11}$	-0.01	$F_{1,9,10,11}$	-0.00
$F_{2,9,10,11}$	-0.00	$F_{3,9,10,11}$	0.00	$F_{4,9,10,11}$	-0.01
$F_{5,9,10,11}$	0.01	$F_{6,9,10,11}$	-0.00	$F_{7,9,10,11}$	0.16
$F_{8,9,10,11}$	0.01	$F_{9,9,10,11}$	-0.02	$F_{1,10,10,11}$	-0.00
$F_{2,10,10,11}$	-0.00	$F_{3,10,10,11}$	-0.00	$F_{4,10,10,11}$	0.00
$F_{5,10,10,11}$	-0.02	$F_{6,10,10,11}$	0.01	$F_{7,10,10,11}$	-0.01
$F_{8,10,10,11}$	0.11	$F_{9,10,10,11}$	-0.15	$F_{10,10,10,11}$	0.01
$F_{1,1,11,11}$	-0.00	$F_{1,2,11,11}$	0.00	$F_{2,2,11,11}$	-0.01
$F_{1,3,11,11}$	-0.00	$F_{2,3,11,11}$	-0.00	$F_{3,3,11,11}$	-0.00
$F_{1,4,11,11}$	0.00	$F_{2,4,11,11}$	-0.01	$F_{3,4,11,11}$	-0.00
$F_{4,4,11,11}$	-0.02	$F_{1,5,11,11}$	0.00	$F_{2,5,11,11}$	0.01
$F_{3,5,11,11}$	0.00	$F_{4,5,11,11}$	-0.00	$F_{5,5,11,11}$	0.02
$F_{1,6,11,11}$	0.00	$F_{2,6,11,11}$	0.00	$F_{3,6,11,11}$	-0.00
$F_{4,6,11,11}$	-0.00	$F_{5,6,11,11}$	-0.01	$F_{6,6,11,11}$	-0.08
$F_{1,7,11,11}$	0.00	$F_{2,7,11,11}$	0.01	$F_{3,7,11,11}$	0.01
$F_{4,7,11,11}$	0.04	$F_{5,7,11,11}$	0.00	$F_{6,7,11,11}$	-0.00

Table B12: F12-TZ Force Constants for HOOF (cont.)

$F_{7,7,11,11}$	-0.15	$F_{1,8,11,11}$	-0.01	$F_{2,8,11,11}$	0.00
$F_{3,8,11,11}$	0.00	$F_{4,8,11,11}$	0.01	$F_{5,8,11,11}$	-0.01
$F_{6,8,11,11}$	-0.02	$F_{7,8,11,11}$	-0.02	$F_{8,8,11,11}$	-0.13
$F_{1,9,11,11}$	-0.00	$F_{2,9,11,11}$	-0.00	$F_{3,9,11,11}$	0.00
$F_{4,9,11,11}$	0.00	$F_{5,9,11,11}$	-0.00	$F_{6,9,11,11}$	0.03
$F_{7,9,11,11}$	0.01	$F_{8,9,11,11}$	-0.17	$F_{9,9,11,11}$	0.53
$F_{1,10,11,11}$	-0.00	$F_{2,10,11,11}$	-0.00	$F_{3,10,11,11}$	-0.00
$F_{4,10,11,11}$	-0.02	$F_{5,10,11,11}$	-0.00	$F_{6,10,11,11}$	0.00
$F_{7,10,11,11}$	0.11	$F_{8,10,11,11}$	0.01	$F_{9,10,11,11}$	-0.01
$F_{10,10,11,11}$	-0.09	$F_{1,11,11,11}$	0.00	$F_{2,11,11,11}$	-0.00
$F_{3,11,11,11}$	-0.00	$F_{4,11,11,11}$	-0.01	$F_{5,11,11,11}$	-0.01
$F_{6,11,11,11}$	0.03	$F_{7,11,11,11}$	0.01	$F_{8,11,11,11}$	0.14
$F_{9,11,11,11}$	0.17	$F_{10,11,11,11}$	-0.00	$F_{11,11,11,11}$	-0.13
$F_{1,1,1,12}$	-0.00	$F_{1,1,2,12}$	0.00	$F_{1,2,2,12}$	-0.00
$F_{2,2,2,12}$	-0.00	$F_{1,1,3,12}$	0.00	$F_{1,2,3,12}$	-0.00
$F_{2,2,3,12}$	-0.00	$F_{1,3,3,12}$	0.00	$F_{2,3,3,12}$	-0.00
$F_{3,3,3,12}$	-0.00	$F_{1,1,4,12}$	0.01	$F_{1,2,4,12}$	-0.00
$F_{2,2,4,12}$	-0.00	$F_{1,3,4,12}$	-0.00	$F_{2,3,4,12}$	0.00
$F_{3,3,4,12}$	-0.01	$F_{1,4,4,12}$	-0.01	$F_{2,4,4,12}$	0.00
$F_{3,4,4,12}$	0.00	$F_{4,4,4,12}$	0.01	$F_{1,1,5,12}$	0.00
$F_{1,2,5,12}$	-0.00	$F_{2,2,5,12}$	0.01	$F_{1,3,5,12}$	0.01
$F_{2,3,5,12}$	-0.00	$F_{3,3,5,12}$	-0.01	$F_{1,4,5,12}$	-0.00
$F_{2,4,5,12}$	0.01	$F_{3,4,5,12}$	-0.01	$F_{4,4,5,12}$	0.02
$F_{1,5,5,12}$	0.01	$F_{2,5,5,12}$	-0.01	$F_{3,5,5,12}$	-0.00
$F_{4,5,5,12}$	-0.02	$F_{5,5,5,12}$	0.00	$F_{1,1,6,12}$	-0.00
$F_{1,2,6,12}$	0.00	$F_{2,2,6,12}$	-0.00	$F_{1,3,6,12}$	-0.01
$F_{2,3,6,12}$	-0.00	$F_{3,3,6,12}$	0.00	$F_{1,4,6,12}$	-0.00
$F_{2,4,6,12}$	-0.01	$F_{3,4,6,12}$	0.00	$F_{4,4,6,12}$	0.05
$F_{1,5,6,12}$	0.00	$F_{2,5,6,12}$	0.01	$F_{3,5,6,12}$	0.02
$F_{4,5,6,12}$	0.01	$F_{5,5,6,12}$	0.00	$F_{1,6,6,12}$	0.02
$F_{2,6,6,12}$	0.01	$F_{3,6,6,12}$	-0.00	$F_{4,6,6,12}$	0.00
$F_{5,6,6,12}$	-0.06	$F_{6,6,6,12}$	-0.26	$F_{1,1,7,12}$	-0.00
$F_{1,2,7,12}$	-0.00	$F_{2,2,7,12}$	-0.00	$F_{1,3,7,12}$	0.00
$F_{2,3,7,12}$	0.00	$F_{3,3,7,12}$	0.00	$F_{1,4,7,12}$	0.00
$F_{2,4,7,12}$	0.00	$F_{3,4,7,12}$	-0.00	$F_{4,4,7,12}$	-0.00
$F_{1,5,7,12}$	0.00	$F_{2,5,7,12}$	-0.01	$F_{3,5,7,12}$	0.01
$F_{4,5,7,12}$	-0.03	$F_{5,5,7,12}$	0.01	$F_{1,6,7,12}$	-0.00
$F_{2,6,7,12}$	0.00	$F_{3,6,7,12}$	0.00	$F_{4,6,7,12}$	-0.01
$F_{5,6,7,12}$	-0.01	$F_{6,6,7,12}$	-0.01	$F_{1,7,7,12}$	-0.00
$F_{2,7,7,12}$	0.00	$F_{3,7,7,12}$	0.00	$F_{4,7,7,12}$	-0.00
$F_{5,7,7,12}$	0.04	$F_{6,7,7,12}$	0.00	$F_{7,7,7,12}$	0.02
$F_{1,1,8,12}$	-0.01	$F_{1,2,8,12}$	-0.00	$F_{2,2,8,12}$	-0.01
$F_{1,3,8,12}$	0.00	$F_{2,3,8,12}$	0.01	$F_{3,3,8,12}$	0.01
$F_{1,4,8,12}$	0.01	$F_{2,4,8,12}$	-0.00	$F_{3,4,8,12}$	0.01
$F_{4,4,8,12}$	-0.02	$F_{1,5,8,12}$	0.00	$F_{2,5,8,12}$	0.01
$F_{3,5,8,12}$	-0.00	$F_{4,5,8,12}$	0.00	$F_{5,5,8,12}$	0.05
$F_{1,6,8,12}$	-0.00	$F_{2,6,8,12}$	-0.00	$F_{3,6,8,12}$	-0.01
$F_{4,6,8,12}$	-0.01	$F_{5,6,8,12}$	0.03	$F_{6,6,8,12}$	0.01
$F_{1,7,8,12}$	0.00	$F_{2,7,8,12}$	0.01	$F_{3,7,8,12}$	-0.01

Table B13: F12-TZ Force Constants for HOOF (cont.)

$F_{4,7,8,12}$	0.03	$F_{5,7,8,12}$	-0.01	$F_{6,7,8,12}$	0.01
$F_{7,7,8,12}$	-0.20	$F_{1,8,8,12}$	-0.00	$F_{2,8,8,12}$	-0.01
$F_{3,8,8,12}$	-0.00	$F_{4,8,8,12}$	0.01	$F_{5,8,8,12}$	-0.09
$F_{6,8,8,12}$	-0.01	$F_{7,8,8,12}$	-0.02	$F_{8,8,8,12}$	0.31
$F_{1,1,9,12}$	-0.00	$F_{1,2,9,12}$	0.00	$F_{2,2,9,12}$	0.01
$F_{1,3,9,12}$	-0.00	$F_{2,3,9,12}$	0.00	$F_{3,3,9,12}$	0.02
$F_{1,4,9,12}$	0.00	$F_{2,4,9,12}$	-0.00	$F_{3,4,9,12}$	0.01
$F_{4,4,9,12}$	-0.03	$F_{1,5,9,12}$	-0.01	$F_{2,5,9,12}$	-0.01
$F_{3,5,9,12}$	0.00	$F_{4,5,9,12}$	0.01	$F_{5,5,9,12}$	0.02
$F_{1,6,9,12}$	-0.01	$F_{2,6,9,12}$	-0.01	$F_{3,6,9,12}$	-0.01
$F_{4,6,9,12}$	-0.00	$F_{5,6,9,12}$	0.03	$F_{6,6,9,12}$	0.05
$F_{1,7,9,12}$	-0.00	$F_{2,7,9,12}$	0.00	$F_{3,7,9,12}$	-0.00
$F_{4,7,9,12}$	0.04	$F_{5,7,9,12}$	0.01	$F_{6,7,9,12}$	0.01
$F_{7,7,9,12}$	0.14	$F_{1,8,9,12}$	0.01	$F_{2,8,9,12}$	0.00
$F_{3,8,9,12}$	-0.00	$F_{4,8,9,12}$	-0.01	$F_{5,8,9,12}$	-0.11
$F_{6,8,9,12}$	-0.06	$F_{7,8,9,12}$	0.01	$F_{8,8,9,12}$	-0.35
$F_{1,9,9,12}$	0.00	$F_{2,9,9,12}$	0.01	$F_{3,9,9,12}$	-0.01
$F_{4,9,9,12}$	-0.01	$F_{5,9,9,12}$	0.12	$F_{6,9,9,12}$	0.09
$F_{7,9,9,12}$	-0.02	$F_{8,9,9,12}$	0.77	$F_{9,9,9,12}$	-1.03
$F_{1,1,10,12}$	-0.00	$F_{1,2,10,12}$	0.00	$F_{2,2,10,12}$	0.00
$F_{1,3,10,12}$	-0.00	$F_{2,3,10,12}$	-0.00	$F_{3,3,10,12}$	0.00
$F_{1,4,10,12}$	0.00	$F_{2,4,10,12}$	0.00	$F_{3,4,10,12}$	0.00
$F_{4,4,10,12}$	0.00	$F_{1,5,10,12}$	-0.00	$F_{2,5,10,12}$	0.00
$F_{3,5,10,12}$	0.00	$F_{4,5,10,12}$	0.01	$F_{5,5,10,12}$	0.00
$F_{1,6,10,12}$	0.00	$F_{2,6,10,12}$	0.00	$F_{3,6,10,12}$	-0.00
$F_{4,6,10,12}$	-0.03	$F_{5,6,10,12}$	-0.00	$F_{6,6,10,12}$	-0.01
$F_{1,7,10,12}$	-0.00	$F_{2,7,10,12}$	-0.00	$F_{3,7,10,12}$	-0.00
$F_{4,7,10,12}$	0.00	$F_{5,7,10,12}$	-0.01	$F_{6,7,10,12}$	0.01
$F_{7,7,10,12}$	-0.01	$F_{1,8,10,12}$	-0.00	$F_{2,8,10,12}$	-0.01
$F_{3,8,10,12}$	-0.00	$F_{4,8,10,12}$	-0.02	$F_{5,8,10,12}$	0.00
$F_{6,8,10,12}$	0.00	$F_{7,8,10,12}$	0.16	$F_{8,8,10,12}$	0.02
$F_{1,9,10,12}$	0.00	$F_{2,9,10,12}$	0.00	$F_{3,9,10,12}$	-0.01
$F_{4,9,10,12}$	-0.01	$F_{5,9,10,12}$	-0.01	$F_{6,9,10,12}$	0.00
$F_{7,9,10,12}$	-0.17	$F_{8,9,10,12}$	-0.01	$F_{9,9,10,12}$	0.03
$F_{1,10,10,12}$	0.00	$F_{2,10,10,12}$	0.00	$F_{3,10,10,12}$	0.00
$F_{4,10,10,12}$	-0.00	$F_{5,10,10,12}$	-0.00	$F_{6,10,10,12}$	0.02
$F_{7,10,10,12}$	0.01	$F_{8,10,10,12}$	-0.14	$F_{9,10,10,12}$	0.19
$F_{10,10,10,12}$	-0.01	$F_{1,1,11,12}$	0.00	$F_{1,2,11,12}$	0.00
$F_{2,2,11,12}$	0.00	$F_{1,3,11,12}$	-0.00	$F_{2,3,11,12}$	-0.00
$F_{3,3,11,12}$	0.00	$F_{1,4,11,12}$	-0.00	$F_{2,4,11,12}$	-0.00
$F_{3,4,11,12}$	0.00	$F_{4,4,11,12}$	-0.00	$F_{1,5,11,12}$	-0.00
$F_{2,5,11,12}$	-0.00	$F_{3,5,11,12}$	0.00	$F_{4,5,11,12}$	0.01
$F_{5,5,11,12}$	-0.04	$F_{1,6,11,12}$	-0.00	$F_{2,6,11,12}$	-0.00
$F_{3,6,11,12}$	-0.00	$F_{4,6,11,12}$	0.00	$F_{5,6,11,12}$	-0.04
$F_{6,6,11,12}$	0.04	$F_{1,7,11,12}$	-0.00	$F_{2,7,11,12}$	-0.00
$F_{3,7,11,12}$	0.00	$F_{4,7,11,12}$	-0.01	$F_{5,7,11,12}$	0.00
$F_{6,7,11,12}$	-0.00	$F_{7,7,11,12}$	0.16	$F_{1,8,11,12}$	0.00
$F_{2,8,11,12}$	0.00	$F_{3,8,11,12}$	-0.00	$F_{4,8,11,12}$	-0.01
$F_{5,8,11,12}$	0.03	$F_{6,8,11,12}$	-0.01	$F_{7,8,11,12}$	0.02

Table B14: F12-TZ Force Constants for HOOF (cont.)

$F_{8,8,11,12}$	-0.22	$F_{1,9,11,12}$	-0.00	$F_{2,9,11,12}$	0.00
$F_{3,9,11,12}$	-0.01	$F_{4,9,11,12}$	-0.00	$F_{5,9,11,12}$	0.10
$F_{6,9,11,12}$	0.05	$F_{7,9,11,12}$	-0.01	$F_{8,9,11,12}$	0.46
$F_{9,9,11,12}$	-0.90	$F_{1,10,11,12}$	0.00	$F_{2,10,11,12}$	0.00
$F_{3,10,11,12}$	-0.00	$F_{4,10,11,12}$	0.01	$F_{5,10,11,12}$	-0.00
$F_{6,10,11,12}$	0.00	$F_{7,10,11,12}$	-0.15	$F_{8,10,11,12}$	-0.01
$F_{9,10,11,12}$	0.02	$F_{10,10,11,12}$	0.14	$F_{1,11,11,12}$	-0.00
$F_{2,11,11,12}$	-0.00	$F_{3,11,11,12}$	-0.00	$F_{4,11,11,12}$	0.00
$F_{5,11,11,12}$	0.01	$F_{6,11,11,12}$	0.05	$F_{7,11,11,12}$	-0.01
$F_{8,11,11,12}$	0.18	$F_{9,11,11,12}$	-0.56	$F_{10,11,11,12}$	0.01
$F_{11,11,11,12}$	-0.20	$F_{1,1,12,12}$	-0.00	$F_{1,2,12,12}$	-0.00
$F_{2,2,12,12}$	0.00	$F_{1,3,12,12}$	0.00	$F_{2,3,12,12}$	0.00
$F_{3,3,12,12}$	-0.02	$F_{1,4,12,12}$	0.00	$F_{2,4,12,12}$	0.01
$F_{3,4,12,12}$	-0.01	$F_{4,4,12,12}$	-0.01	$F_{1,5,12,12}$	0.00
$F_{2,5,12,12}$	0.00	$F_{3,5,12,12}$	-0.01	$F_{4,5,12,12}$	-0.01
$F_{5,5,12,12}$	-0.03	$F_{1,6,12,12}$	-0.00	$F_{2,6,12,12}$	0.00
$F_{3,6,12,12}$	0.01	$F_{4,6,12,12}$	-0.00	$F_{5,6,12,12}$	0.02
$F_{6,6,12,12}$	0.22	$F_{1,7,12,12}$	0.00	$F_{2,7,12,12}$	-0.00
$F_{3,7,12,12}$	-0.00	$F_{4,7,12,12}$	-0.03	$F_{5,7,12,12}$	-0.00
$F_{6,7,12,12}$	-0.00	$F_{7,7,12,12}$	-0.14	$F_{1,8,12,12}$	-0.01
$F_{2,8,12,12}$	-0.00	$F_{3,8,12,12}$	0.00	$F_{4,8,12,12}$	0.00
$F_{5,8,12,12}$	0.09	$F_{6,8,12,12}$	0.07	$F_{7,8,12,12}$	-0.01
$F_{8,8,12,12}$	0.37	$F_{1,9,12,12}$	0.01	$F_{2,9,12,12}$	-0.00
$F_{3,9,12,12}$	0.00	$F_{4,9,12,12}$	-0.00	$F_{5,9,12,12}$	-0.15
$F_{6,9,12,12}$	-0.12	$F_{7,9,12,12}$	0.01	$F_{8,9,12,12}$	-0.71
$F_{9,9,12,12}$	0.94	$F_{1,10,12,12}$	-0.00	$F_{2,10,12,12}$	-0.00
$F_{3,10,12,12}$	0.01	$F_{4,10,12,12}$	0.05	$F_{5,10,12,12}$	0.01
$F_{6,10,12,12}$	0.00	$F_{7,10,12,12}$	0.17	$F_{8,10,12,12}$	0.01
$F_{9,10,12,12}$	-0.02	$F_{10,10,12,12}$	-0.21	$F_{1,11,12,12}$	0.01
$F_{2,11,12,12}$	0.00	$F_{3,11,12,12}$	0.00	$F_{4,11,12,12}$	-0.00
$F_{5,11,12,12}$	-0.06	$F_{6,11,12,12}$	-0.08	$F_{7,11,12,12}$	0.01
$F_{8,11,12,12}$	-0.45	$F_{9,11,12,12}$	0.86	$F_{10,11,12,12}$	-0.02
$F_{11,11,12,12}$	0.51	$F_{1,12,12,12}$	-0.02	$F_{2,12,12,12}$	-0.00
$F_{3,12,12,12}$	-0.00	$F_{4,12,12,12}$	0.01	$F_{5,12,12,12}$	0.14
$F_{6,12,12,12}$	-0.11	$F_{7,12,12,12}$	-0.01	$F_{8,12,12,12}$	0.64
$F_{9,12,12,12}$	-0.82	$F_{10,12,12,12}$	0.01	$F_{11,12,12,12}$	-0.78
$F_{12,12,12,12}$	0.94				

Table B15: F12-TZ Harmonic and Anharmonic Vibrational Frequencies for HOOF Isotopologues

Mode	$HOO^{18}F$	$HO^{18}O^{18}F$	DOOF	$DOO^{18}F$	$DO^{18}O^{18}F$
ω_1	3709.8	3697.3	2702.9	2702.8	2685.5
ω_2	1458.8	1454.6	1088.4	1080.8	1076.2
ω_3	951.1	926.7	975.1	949.6	924.3
ω_4	733.6	729.4	759.1	732.8	728.7
ω_5	541.9	536.3	494.4	491.3	479.2
ω_6	462.0	455.4	379.4	377.3	376.8
ν_1	3508.5	3497.4	2596.1	2596.1	2580.0
ν_2	1410.7	1423.0	1055.2	1043.1	1039.8
ν_3	916.5	896.8	945.6	922.8	899.4
ν_4	713.4	709.0	1099.7	707.3	703.2
ν_5	515.1	509.4	481.6	478.7	467.1
ν_6	451.3	445.4	365.9	364.1	363.8
ZPT	3868.3	3840.3	3163.3	3131.4	3100.1

Table B16: Spectroscopic Constants and Geometrical Parameters of HOOF Isotopologues

Constant	Units	$HOO^{18}F$	$HO^{18}O^{18}F$	DOOF	$DOO^{18}F$	$DO^{18}O^{18}F$
R_e(H-O_1)	Å	0.96940	0.96940	0.96940	0.96940	0.96940
R_e(O_1-O_2)	Å	1.37112	1.37112	1.37112	1.37112	1.37112
R_e(O_2-F)	Å	1.46187	1.46187	1.46187	1.46187	1.46187
$\angle_e$(H-O_1-O_2)	°	102.68	102.68	102.68	102.68	102.68
$\angle_e$(O_1-O_2-F)	°	105.42	105.42	105.42	105.42	105.42
A_e	MHz	51603.6	50681.1	50083.6	46791.6	46111.1
B_e	MHz	10770.0	10220.2	10267.0	10264.9	9777.4
C_e	MHz	9174.5	8747.9	8971.0	8858.9	8478.4
R_0(H-O_1)	Å	0.96702	0.96700	0.96899	0.96884	0.96882
R_0(O_1-O_2)	Å	1.38044	1.38020	1.37967	1.37952	1.37928
R_0(O_2-F)	Å	1.46865	1.46868	1.46914	1.46894	1.46896
$\angle_0$(H-O_1-O_2)	°	102.87	102.88	102.77	102.77	102.78
$\angle_0$(O_1-O_2-F)	°	105.41	105.40	105.43	105.43	105.43
A_0	MHz	51392.6	50476.6	49909.0	46636.0	45956.9
B_0	MHz	10685.0	10139.8	10182.6	10183.2	9700.0
C_0	MHz	9083.1	8661.5	8882.8	8773.2	8397.3
A_1	MHz	51287.8	50377.3	49700.1	46454.4	45783.8
B_1	MHz	10675.6	10132.1	10172.6	10173.2	9691.2
C_1	MHz	9081.6	8660.9	8878.6	8769.1	8394.3
A_2	MHz	51314.4	50407.0	50082.0	46745.5	46048.7
B_2	MHz	10657.6	10112.3	10159.7	10162.1	9678.1
C_2	MHz	9070.2	8648.1	8874.7	8766.7	8389.9
A_3	MHz	51163.7	50297.8	49550.9	46337.4	45712.5
B_3	MHz	10639.2	10094.3	10137.5	10137.9	9656.3
C_3	MHz	9060.5	8641.0	8862.7	8751.8	8378.1
A_4	MHz	51099.4	50153.9	49591.6	46353.1	45656.0
B_4	MHz	10615.8	10076.3	10115.2	10118.8	9640.0
C_4	MHz	9003.3	8583.9	8799.8	8697.5	8323.6
A_5	MHz	51321.0	50364.7	50284.7	46992.0	46304.3
B_5	MHz	10690.2	10149.5	10132.2	10133.4	9656.0
C_5	MHz	9063.9	8647.2	8826.4	8715.9	8345.3
A_6	MHz	51747.0	50849.8	49895.6	46621.9	45928.1
B_6	MHz	10661.8	10113.3	10209.8	10210.3	9723.2
C_6	MHz	9035.7	8615.0	8878.1	8766.9	8390.9
Δ_J	kHz	14.678	13.209	13.822	13.565	12.233
Δ_K	MHz	1.123	1.088	965.823	856.841	826.792
Δ_{JK}	kHz	-48.394	-46.566	-48.181	-42.534	-39.954
δ_J	kHz	3.057	2.685	2.652	2.779	2.432
δ_K	kHz	47.181	43.376	25.399	26.950	24.204
Φ_J	mHz	15.521	13.512	21.363	21.041	16.985
Φ_K	Hz	82.930	78.389	62.991	53.536	49.965
Φ_{JK}	mHz	108.982	97.364	-56.214	-63.672	-59.437
Φ_{KJ}	Hz	-13.289	-12.263	-10.098	-8.876	-8.146
ϕ_j	mHz	9.522	8.037	11.690	11.714	9.387
ϕ_{jk}	mHz	-49.011	-42.515	86.564	61.258	37.420
ϕ_k	Hz	13.339	12.184	8.577	7.972	6.673

Table B17: F12-TZ-cCR Force Constants for HOOF

$F_{1,1}$	0.455617	$F_{1,2}$	0.112890	$F_{1,3}$	0.049044
$F_{1,4}$	-0.471061	$F_{1,5}$	-0.117972	$F_{1,6}$	-0.053860
$F_{1,7}$	0.016750	$F_{1,8}$	0.006865	$F_{1,9}$	0.001062
$F_{1,10}$	-0.001306	$F_{1,11}$	-0.001784	$F_{1,12}$	0.003753
$F_{1,13}$	0.112890	$F_{2,1}$	0.065141	$F_{2,2}$	0.045942
$F_{2,3}$	-0.083673	$F_{2,4}$	-0.044568	$F_{2,5}$	-0.027485
$F_{2,6}$	-0.033148	$F_{2,7}$	-0.021195	$F_{2,8}$	-0.019963
$F_{2,9}$	0.003932	$F_{2,10}$	0.000622	$F_{2,11}$	0.001507
$F_{2,12}$	0.049044	$F_{2,13}$	0.045942	$F_{3,1}$	0.055931
$F_{3,2}$	-0.013304	$F_{3,3}$	-0.018883	$F_{3,4}$	-0.033169
$F_{3,5}$	-0.030928	$F_{3,6}$	-0.027675	$F_{3,7}$	-0.021723
$F_{3,8}$	-0.004812	$F_{3,9}$	0.000616	$F_{3,10}$	-0.001039
$F_{3,11}$	-0.471061	$F_{3,12}$	-0.083673	$F_{3,13}$	-0.013304
$F_{4,1}$	0.520163	$F_{4,2}$	0.099837	$F_{4,3}$	0.025303
$F_{4,4}$	-0.051180	$F_{4,5}$	-0.016134	$F_{4,6}$	-0.010678
$F_{4,7}$	0.002078	$F_{4,8}$	-0.000029	$F_{4,9}$	-0.001321
$F_{4,10}$	-0.117972	$F_{4,11}$	-0.044568	$F_{4,12}$	-0.018883
$F_{4,13}$	0.099837	$F_{5,1}$	0.173892	$F_{5,2}$	0.126976
$F_{5,3}$	0.025302	$F_{5,4}$	-0.174491	$F_{5,5}$	-0.090913
$F_{5,6}$	-0.007168	$F_{5,7}$	0.045167	$F_{5,8}$	-0.017180
$F_{5,9}$	-0.053860	$F_{5,10}$	-0.027485	$F_{5,11}$	-0.033169
$F_{5,12}$	0.025303	$F_{5,13}$	0.126976	$F_{6,1}$	0.226263
$F_{6,2}$	0.021820	$F_{6,3}$	-0.096874	$F_{6,4}$	-0.124906
$F_{6,5}$	0.006737	$F_{6,6}$	-0.002617	$F_{6,7}$	-0.068188
$F_{6,8}$	0.016750	$F_{6,9}$	-0.033148	$F_{6,10}$	-0.030928
$F_{6,11}$	-0.051180	$F_{6,12}$	0.025302	$F_{6,13}$	0.021820
$F_{7,1}$	0.039579	$F_{7,2}$	0.002509	$F_{7,3}$	0.012666
$F_{7,4}$	-0.005148	$F_{7,5}$	0.005337	$F_{7,6}$	-0.003559
$F_{7,7}$	0.006865	$F_{7,8}$	-0.021195	$F_{7,9}$	-0.027675
$F_{7,10}$	-0.016134	$F_{7,11}$	-0.174491	$F_{7,12}$	-0.096874
$F_{7,13}$	0.002509	$F_{8,1}$	0.329595	$F_{8,2}$	0.041157
$F_{8,3}$	0.006760	$F_{8,4}$	-0.133909	$F_{8,5}$	0.083393
$F_{8,6}$	0.001062	$F_{8,7}$	-0.019963	$F_{8,8}$	-0.021723
$F_{8,9}$	-0.010678	$F_{8,10}$	-0.090913	$F_{8,11}$	-0.124906
$F_{8,12}$	0.012666	$F_{8,13}$	0.041157	$F_{9,1}$	0.229299
$F_{9,2}$	-0.003050	$F_{9,3}$	0.069720	$F_{9,4}$	-0.082670
$F_{9,5}$	-0.001306	$F_{9,6}$	0.003932	$F_{9,7}$	-0.004812
$F_{9,8}$	0.002078	$F_{9,9}$	-0.007168	$F_{9,10}$	0.006737
$F_{9,11}$	-0.005148	$F_{9,12}$	0.006760	$F_{9,13}$	-0.003050
$F_{10,1}$	0.004376	$F_{10,2}$	-0.003524	$F_{10,3}$	0.001126
$F_{10,4}$	-0.001784	$F_{10,5}$	0.000622	$F_{10,6}$	0.000616
$F_{10,7}$	-0.000029	$F_{10,8}$	0.045167	$F_{10,9}$	-0.002617
$F_{10,10}$	0.005337	$F_{10,11}$	-0.133909	$F_{10,12}$	0.069720
$F_{10,13}$	-0.003524	$F_{11,1}$	0.088121	$F_{11,2}$	-0.067719
$F_{11,3}$	0.003753	$F_{11,4}$	0.001507	$F_{11,5}$	-0.001039
$F_{11,6}$	-0.001321	$F_{11,7}$	-0.017180	$F_{11,8}$	-0.068188
$F_{11,9}$	-0.003559	$F_{11,10}$	0.083393	$F_{11,11}$	-0.082670
$F_{11,12}$	0.001126	$F_{11,13}$	-0.067719	$F_{12,1}$	0.151897
$F_{1,1,1}$	1.5660	$F_{1,1,2}$	0.5612	$F_{1,2,2}$	-0.0515

Table B18: F12-TZ-cCR Force Constants for HOOF (cont.)

$F_{2,2,2}$	-0.1241	$F_{1,1,3}$	0.2662	$F_{1,2,3}$	0.1171
$F_{2,2,3}$	0.0207	$F_{1,3,3}$	-0.1642	$F_{2,3,3}$	-0.0257
$F_{3,3,3}$	-0.0610	$F_{1,1,4}$	-1.5761	$F_{1,2,4}$	-0.5491
$F_{2,2,4}$	0.0722	$F_{1,3,4}$	-0.2472	$F_{2,3,4}$	-0.1007
$F_{3,3,4}$	0.1802	$F_{1,4,4}$	1.5890	$F_{2,4,4}$	0.5345
$F_{3,4,4}$	0.2194	$F_{4,4,4}$	-1.6170	$F_{1,1,5}$	-0.5924
$F_{1,2,5}$	0.0531	$F_{2,2,5}$	0.1320	$F_{1,3,5}$	-0.1125
$F_{2,3,5}$	-0.0085	$F_{3,3,5}$	0.0798	$F_{1,4,5}$	0.5703
$F_{2,4,5}$	-0.0586	$F_{3,4,5}$	0.1303	$F_{4,4,5}$	-0.5888
$F_{1,5,5}$	-0.0362	$F_{2,5,5}$	-0.1302	$F_{3,5,5}$	0.0448
$F_{4,5,5}$	0.0304	$F_{5,5,5}$	0.3368	$F_{1,1,6}$	-0.2980
$F_{1,2,6}$	-0.1302	$F_{2,2,6}$	0.0243	$F_{1,3,6}$	0.1682
$F_{2,3,6}$	0.0516	$F_{3,3,6}$	0.0796	$F_{1,4,6}$	0.2636
$F_{2,4,6}$	0.1544	$F_{3,4,6}$	-0.1588	$F_{4,4,6}$	-0.2674
$F_{1,5,6}$	0.1422	$F_{2,5,6}$	0.0021	$F_{3,5,6}$	-0.0627
$F_{4,5,6}$	-0.1938	$F_{5,5,6}$	0.2772	$F_{1,6,6}$	-0.1557
$F_{2,6,6}$	-0.0286	$F_{3,6,6}$	-0.0754	$F_{4,6,6}$	0.1182
$F_{5,6,6}$	0.4295	$F_{6,6,6}$	0.5670	$F_{1,1,7}$	0.0101
$F_{1,2,7}$	-0.0138	$F_{2,2,7}$	-0.0203	$F_{1,3,7}$	-0.0154
$F_{2,3,7}$	-0.0152	$F_{3,3,7}$	-0.0168	$F_{1,4,7}$	-0.0122
$F_{2,4,7}$	0.0189	$F_{3,4,7}$	0.0234	$F_{4,4,7}$	0.0268
$F_{1,5,7}$	0.0264	$F_{2,5,7}$	-0.0015	$F_{3,5,7}$	-0.0130
$F_{4,5,7}$	0.0204	$F_{5,5,7}$	0.0273	$F_{1,6,7}$	0.0326
$F_{2,6,7}$	-0.0298	$F_{3,6,7}$	-0.0050	$F_{4,6,7}$	-0.0117
$F_{5,6,7}$	0.0521	$F_{6,6,7}$	0.0200	$F_{1,7,7}$	0.0030
$F_{2,7,7}$	-0.0078	$F_{3,7,7}$	-0.0079	$F_{4,7,7}$	-0.0136
$F_{5,7,7}$	-0.0633	$F_{6,7,7}$	-0.0149	$F_{7,7,7}$	0.0032
$F_{1,1,8}$	0.0332	$F_{1,2,8}$	-0.0012	$F_{2,2,8}$	-0.0051
$F_{1,3,8}$	-0.0044	$F_{2,3,8}$	-0.0122	$F_{3,3,8}$	-0.0582
$F_{1,4,8}$	-0.0227	$F_{2,4,8}$	-0.0131	$F_{3,4,8}$	-0.0295
$F_{4,4,8}$	0.0699	$F_{1,5,8}$	-0.0155	$F_{2,5,8}$	-0.0046
$F_{3,5,8}$	-0.0365	$F_{4,5,8}$	0.0308	$F_{5,5,8}$	-0.2495
$F_{1,6,8}$	-0.0109	$F_{2,6,8}$	-0.0248	$F_{3,6,8}$	0.0155
$F_{4,6,8}$	0.0393	$F_{5,6,8}$	-0.3137	$F_{6,6,8}$	-0.3813
$F_{1,7,8}$	-0.0134	$F_{2,7,8}$	0.0202	$F_{3,7,8}$	0.0252
$F_{4,7,8}$	-0.0666	$F_{5,7,8}$	-0.0317	$F_{6,7,8}$	-0.0223
$F_{7,7,8}$	0.1522	$F_{1,8,8}$	0.0166	$F_{2,8,8}$	0.0114
$F_{3,8,8}$	0.0491	$F_{4,8,8}$	-0.0244	$F_{5,8,8}$	0.3225
$F_{6,8,8}$	0.3565	$F_{7,8,8}$	0.0268	$F_{8,8,8}$	-0.5264
$F_{1,1,9}$	0.0295	$F_{1,2,9}$	0.0106	$F_{2,2,9}$	-0.0439
$F_{1,3,9}$	-0.0043	$F_{2,3,9}$	-0.0195	$F_{3,3,9}$	-0.0179
$F_{1,4,9}$	-0.0143	$F_{2,4,9}$	-0.0496	$F_{3,4,9}$	-0.0167
$F_{4,4,9}$	0.0277	$F_{1,5,9}$	-0.0314	$F_{2,5,9}$	0.0073
$F_{3,5,9}$	-0.0255	$F_{4,5,9}$	0.0627	$F_{5,5,9}$	-0.3082
$F_{1,6,9}$	-0.0173	$F_{2,6,9}$	-0.0294	$F_{3,6,9}$	-0.0047
$F_{4,6,9}$	0.0365	$F_{5,6,9}$	-0.3365	$F_{6,6,9}$	-0.3654
$F_{1,7,9}$	-0.0164	$F_{2,7,9}$	0.0457	$F_{3,7,9}$	0.0147
$F_{4,7,9}$	-0.0053	$F_{5,7,9}$	-0.0397	$F_{6,7,9}$	-0.0079
$F_{7,7,9}$	-0.0302	$F_{1,8,9}$	0.0185	$F_{2,8,9}$	0.0350

Table B19: F12-TZ-cCR Force Constants for HOOF (cont.)

$F_{3,8,9}$	0.0425	$F_{4,8,9}$	-0.0124	$F_{5,8,9}$	0.3115
$F_{6,8,9}$	0.3587	$F_{7,8,9}$	-0.0109	$F_{8,8,9}$	-0.1597
$F_{1,9,9}$	0.0298	$F_{2,9,9}$	0.0471	$F_{3,9,9}$	0.0264
$F_{4,9,9}$	-0.0240	$F_{5,9,9}$	0.3042	$F_{6,9,9}$	0.3357
$F_{7,9,9}$	-0.0014	$F_{8,9,9}$	-0.6144	$F_{9,9,9}$	0.0104
$F_{1,1,10}$	0.0000	$F_{1,2,10}$	0.0017	$F_{2,2,10}$	-0.0004
$F_{1,3,10}$	-0.0036	$F_{2,3,10}$	-0.0011	$F_{3,3,10}$	0.0008
$F_{1,4,10}$	-0.0007	$F_{2,4,10}$	-0.0043	$F_{3,4,10}$	0.0044
$F_{4,4,10}$	0.0012	$F_{1,5,10}$	-0.0043	$F_{2,5,10}$	0.0071
$F_{3,5,10}$	-0.0049	$F_{4,5,10}$	-0.0019	$F_{5,5,10}$	-0.0216
$F_{1,6,10}$	0.0018	$F_{2,6,10}$	0.0057	$F_{3,6,10}$	-0.0045
$F_{4,6,10}$	0.0155	$F_{5,6,10}$	-0.0005	$F_{6,6,10}$	0.0175
$F_{1,7,10}$	-0.0009	$F_{2,7,10}$	0.0027	$F_{3,7,10}$	-0.0001
$F_{4,7,10}$	-0.0010	$F_{5,7,10}$	0.0164	$F_{6,7,10}$	-0.0059
$F_{7,7,10}$	0.0075	$F_{1,8,10}$	0.0029	$F_{2,8,10}$	-0.0058
$F_{3,8,10}$	0.0087	$F_{4,8,10}$	0.0194	$F_{5,8,10}$	0.0163
$F_{6,8,10}$	-0.0062	$F_{7,8,10}$	-0.0722	$F_{8,8,10}$	-0.0190
$F_{1,9,10}$	0.0012	$F_{2,9,10}$	-0.0067	$F_{3,9,10}$	0.0064
$F_{4,9,10}$	-0.0081	$F_{5,9,10}$	0.0084	$F_{6,9,10}$	-0.0113
$F_{7,9,10}$	0.0519	$F_{8,9,10}$	0.0048	$F_{9,9,10}$	-0.0044
$F_{1,10,10}$	0.0016	$F_{2,10,10}$	-0.0001	$F_{3,10,10}$	-0.0006
$F_{4,10,10}$	0.0005	$F_{5,10,10}$	-0.0102	$F_{6,10,10}$	-0.0113
$F_{7,10,10}$	-0.0057	$F_{8,10,10}$	0.0499	$F_{9,10,10}$	-0.0450
$F_{10,10,10}$	0.0036	$F_{1,1,11}$	-0.0020	$F_{1,2,11}$	-0.0004
$F_{2,2,11}$	-0.0028	$F_{1,3,11}$	-0.0002	$F_{2,3,11}$	0.0000
$F_{3,3,11}$	0.0041	$F_{1,4,11}$	0.0015	$F_{2,4,11}$	-0.0004
$F_{3,4,11}$	-0.0001	$F_{4,4,11}$	-0.0155	$F_{1,5,11}$	-0.0014
$F_{2,5,11}$	0.0028	$F_{3,5,11}$	0.0002	$F_{4,5,11}$	-0.0026
$F_{5,5,11}$	0.0429	$F_{1,6,11}$	-0.0011	$F_{2,6,11}$	-0.0016
$F_{3,6,11}$	-0.0044	$F_{4,6,11}$	0.0000	$F_{5,6,11}$	0.0343
$F_{6,6,11}$	-0.0197	$F_{1,7,11}$	0.0008	$F_{2,7,11}$	0.0017
$F_{3,7,11}$	0.0030	$F_{4,7,11}$	0.0272	$F_{5,7,11}$	0.0059
$F_{6,7,11}$	0.0000	$F_{7,7,11}$	-0.0812	$F_{1,8,11}$	0.0001
$F_{2,8,11}$	-0.0017	$F_{3,8,11}$	-0.0004	$F_{4,8,11}$	0.0068
$F_{5,8,11}$	-0.0685	$F_{6,8,11}$	-0.0180	$F_{7,8,11}$	-0.0153
$F_{8,8,11}$	0.1925	$F_{1,9,11}$	0.0023	$F_{2,9,11}$	0.0016
$F_{3,9,11}$	0.0025	$F_{4,9,11}$	-0.0006	$F_{5,9,11}$	-0.0106
$F_{6,9,11}$	0.0072	$F_{7,9,11}$	0.0048	$F_{8,9,11}$	-0.1868
$F_{9,9,11}$	0.2631	$F_{1,10,11}$	-0.0003	$F_{2,10,11}$	-0.0009
$F_{3,10,11}$	-0.0027	$F_{4,10,11}$	-0.0132	$F_{5,10,11}$	-0.0018
$F_{6,10,11}$	0.0010	$F_{7,10,11}$	0.0531	$F_{8,10,11}$	0.0085
$F_{9,10,11}$	-0.0065	$F_{10,10,11}$	-0.0395	$F_{1,11,11}$	0.0017
$F_{2,11,11}$	0.0018	$F_{3,11,11}$	0.0003	$F_{4,11,11}$	-0.0037
$F_{5,11,11}$	0.0228	$F_{6,11,11}$	-0.0147	$F_{7,11,11}$	0.0078
$F_{8,11,11}$	-0.1222	$F_{9,11,11}$	0.1957	$F_{10,11,11}$	-0.0058
$F_{11,11,11}$	0.0977	$F_{1,1,12}$	0.0023	$F_{1,2,12}$	0.0026
$F_{2,2,12}$	-0.0010	$F_{1,3,12}$	0.0003	$F_{2,3,12}$	-0.0063
$F_{3,3,12}$	-0.0008	$F_{1,4,12}$	-0.0021	$F_{2,4,12}$	-0.0041
$F_{3,4,12}$	-0.0047	$F_{4,4,12}$	0.0203	$F_{1,5,12}$	0.0017

Table B20: F12-TZ-cCR Force Constants for HOOF (cont.)

$F_{2,5,12}$	-0.0009	$F_{3,5,12}$	0.0084	$F_{4,5,12}$	0.0008
$F_{5,5,12}$	-0.0138	$F_{1,6,12}$	0.0048	$F_{2,6,12}$	0.0064
$F_{3,6,12}$	0.0006	$F_{4,6,12}$	0.0040	$F_{5,6,12}$	-0.0304
$F_{6,6,12}$	-0.1262	$F_{1,7,12}$	-0.0008	$F_{2,7,12}$	-0.0007
$F_{3,7,12}$	0.0071	$F_{4,7,12}$	-0.0064	$F_{5,7,12}$	0.0005
$F_{6,7,12}$	-0.0071	$F_{7,7,12}$	0.0531	$F_{1,8,12}$	-0.0033
$F_{2,8,12}$	0.0020	$F_{3,8,12}$	0.0002	$F_{4,8,12}$	0.0026
$F_{5,8,12}$	0.0387	$F_{6,8,12}$	0.0071	$F_{7,8,12}$	0.0080
$F_{8,8,12}$	-0.2459	$F_{1,9,12}$	-0.0081	$F_{2,9,12}$	0.0017
$F_{3,9,12}$	-0.0038	$F_{4,9,12}$	0.0042	$F_{5,9,12}$	0.0578
$F_{6,9,12}$	0.0344	$F_{7,9,12}$	-0.0054	$F_{8,9,12}$	0.2132
$F_{9,9,12}$	-0.3725	$F_{1,10,12}$	0.0007	$F_{2,10,12}$	0.0021
$F_{3,10,12}$	-0.0027	$F_{4,10,12}$	-0.0118	$F_{5,10,12}$	-0.0030
$F_{6,10,12}$	-0.0017	$F_{7,10,12}$	-0.0458	$F_{8,10,12}$	-0.0073
$F_{9,10,12}$	0.0093	$F_{10,10,12}$	0.0570	$F_{1,11,12}$	-0.0010
$F_{2,11,12}$	-0.0000	$F_{3,11,12}$	-0.0023	$F_{4,11,12}$	0.0007
$F_{5,11,12}$	-0.0239	$F_{6,11,12}$	0.0169	$F_{7,11,12}$	-0.0078
$F_{8,11,12}$	0.2052	$F_{9,11,12}$	-0.2728	$F_{10,11,12}$	0.0082
$F_{11,11,12}$	-0.1813	$F_{1,12,12}$	0.0030	$F_{2,12,12}$	-0.0018
$F_{3,12,12}$	0.0040	$F_{4,12,12}$	-0.0035	$F_{5,12,12}$	-0.0358
$F_{6,12,12}$	0.0912	$F_{7,12,12}$	0.0055	$F_{8,12,12}$	-0.2205
$F_{9,12,12}$	0.3419	$F_{10,12,12}$	-0.0050	$F_{11,12,12}$	0.2581
$F_{12,12,12}$	-0.4371	$F_{1,1,1,1}$	4.48	$F_{1,1,1,2}$	2.21
$F_{1,1,2,2}$	-0.33	$F_{1,2,2,2}$	-0.77	$F_{2,2,2,2}$	-0.15
$F_{1,1,1,3}$	1.07	$F_{1,1,2,3}$	0.44	$F_{1,2,2,3}$	0.00
$F_{2,2,2,3}$	-0.13	$F_{1,1,3,3}$	-0.92	$F_{1,2,3,3}$	-0.25
$F_{2,2,3,3}$	0.03	$F_{1,3,3,3}$	-0.44	$F_{2,3,3,3}$	-0.16
$F_{3,3,3,3}$	0.17	$F_{1,1,1,4}$	-4.50	$F_{1,1,2,4}$	-2.22
$F_{1,2,2,4}$	0.37	$F_{2,2,2,4}$	0.75	$F_{1,1,3,4}$	-1.07
$F_{1,2,3,4}$	-0.42	$F_{2,2,3,4}$	-0.00	$F_{1,3,3,4}$	0.95
$F_{2,3,3,4}$	0.25	$F_{3,3,3,4}$	0.40	$F_{1,1,4,4}$	4.53
$F_{1,2,4,4}$	2.24	$F_{2,2,4,4}$	-0.43	$F_{1,3,4,4}$	1.07
$F_{2,3,4,4}$	0.40	$F_{3,3,4,4}$	-1.01	$F_{1,4,4,4}$	-4.53
$F_{2,4,4,4}$	-2.33	$F_{3,4,4,4}$	-1.13	$F_{4,4,4,4}$	4.50
$F_{1,1,1,5}$	-2.22	$F_{1,1,2,5}$	0.33	$F_{1,2,2,5}$	0.79
$F_{2,2,2,5}$	0.15	$F_{1,1,3,5}$	-0.44	$F_{1,2,3,5}$	0.01
$F_{2,2,3,5}$	0.14	$F_{1,3,3,5}$	0.33	$F_{2,3,3,5}$	-0.00
$F_{3,3,3,5}$	0.18	$F_{1,1,4,5}$	2.22	$F_{1,2,4,5}$	-0.36
$F_{2,2,4,5}$	-0.76	$F_{1,3,4,5}$	0.44	$F_{2,3,4,5}$	0.01
$F_{3,3,4,5}$	-0.32	$F_{1,4,4,5}$	-2.25	$F_{2,4,4,5}$	0.41
$F_{3,4,4,5}$	-0.46	$F_{4,4,4,5}$	2.35	$F_{1,1,5,5}$	-0.36
$F_{1,2,5,5}$	-0.81	$F_{2,2,5,5}$	-0.16	$F_{1,3,5,5}$	0.01
$F_{2,3,5,5}$	-0.15	$F_{3,3,5,5}$	-0.01	$F_{1,4,5,5}$	0.38
$F_{2,4,5,5}$	0.79	$F_{3,4,5,5}$	-0.03	$F_{4,4,5,5}$	-0.57
$F_{1,5,5,5}$	0.89	$F_{2,5,5,5}$	0.15	$F_{3,5,5,5}$	0.20
$F_{4,5,5,5}$	-0.91	$F_{5,5,5,5}$	-0.15	$F_{1,1,1,6}$	-1.07
$F_{1,1,2,6}$	-0.46	$F_{1,2,2,6}$	0.05	$F_{2,2,2,6}$	0.18
$F_{1,1,3,6}$	0.92	$F_{1,2,3,6}$	0.27	$F_{2,2,3,6}$	-0.00
$F_{1,3,3,6}$	0.47	$F_{2,3,3,6}$	0.18	$F_{3,3,3,6}$	-0.17

Table B21: F12-TZ-cCR Force Constants for HOOF (cont.)

$F_{1,1,4,6}$	1.05	$F_{1,2,4,6}$	0.46	$F_{2,2,4,6}$	-0.03
$F_{1,3,4,6}$	-0.94	$F_{2,3,4,6}$	-0.26	$F_{3,3,4,6}$	-0.42
$F_{1,4,4,6}$	-1.06	$F_{2,4,4,6}$	-0.48	$F_{3,4,4,6}$	0.97
$F_{4,4,4,6}$	1.12	$F_{1,1,5,6}$	0.41	$F_{1,2,5,6}$	-0.07
$F_{2,2,5,6}$	-0.17	$F_{1,3,5,6}$	-0.34	$F_{2,3,5,6}$	0.00
$F_{3,3,5,6}$	-0.17	$F_{1,4,5,6}$	-0.45	$F_{2,4,5,6}$	0.06
$F_{3,4,5,6}$	0.35	$F_{4,4,5,6}$	0.33	$F_{1,5,5,6}$	0.13
$F_{2,5,5,6}$	0.20	$F_{3,5,5,6}$	0.04	$F_{4,5,5,6}$	-0.20
$F_{5,5,5,6}$	0.26	$F_{1,1,6,6}$	-0.97	$F_{1,2,6,6}$	-0.29
$F_{2,2,6,6}$	0.02	$F_{1,3,6,6}$	-0.49	$F_{2,3,6,6}$	-0.20
$F_{3,3,6,6}$	0.14	$F_{1,4,6,6}$	0.96	$F_{2,4,6,6}$	0.30
$F_{3,4,6,6}$	0.44	$F_{4,4,6,6}$	-1.20	$F_{1,5,6,6}$	0.43
$F_{2,5,6,6}$	0.03	$F_{3,5,6,6}$	0.19	$F_{4,5,6,6}$	-0.55
$F_{5,5,6,6}$	0.77	$F_{1,6,6,6}$	0.57	$F_{2,6,6,6}$	0.27
$F_{3,6,6,6}$	-0.13	$F_{4,6,6,6}$	-0.59	$F_{5,6,6,6}$	0.70
$F_{6,6,6,6}$	0.83	$F_{1,1,1,7}$	0.02	$F_{1,1,2,7}$	0.00
$F_{1,2,2,7}$	-0.04	$F_{2,2,2,7}$	0.02	$F_{1,1,3,7}$	0.00
$F_{1,2,3,7}$	-0.02	$F_{2,2,3,7}$	-0.00	$F_{1,3,3,7}$	-0.02
$F_{2,3,3,7}$	-0.00	$F_{3,3,3,7}$	0.04	$F_{1,1,4,7}$	-0.03
$F_{1,2,4,7}$	-0.02	$F_{2,2,4,7}$	0.07	$F_{1,3,4,7}$	-0.00
$F_{2,3,4,7}$	0.02	$F_{3,3,4,7}$	0.06	$F_{1,4,4,7}$	0.00
$F_{2,4,4,7}$	0.09	$F_{3,4,4,7}$	0.05	$F_{4,4,4,7}$	0.03
$F_{1,1,5,7}$	0.00	$F_{1,2,5,7}$	0.03	$F_{2,2,5,7}$	-0.03
$F_{1,3,5,7}$	0.01	$F_{2,3,5,7}$	-0.01	$F_{3,3,5,7}$	-0.01
$F_{1,4,5,7}$	0.03	$F_{2,4,5,7}$	-0.05	$F_{3,4,5,7}$	0.01
$F_{4,4,5,7}$	-0.11	$F_{1,5,5,7}$	-0.01	$F_{2,5,5,7}$	0.02
$F_{3,5,5,7}$	0.01	$F_{4,5,5,7}$	0.19	$F_{5,5,5,7}$	0.05
$F_{1,1,6,7}$	0.01	$F_{1,2,6,7}$	-0.00	$F_{2,2,6,7}$	-0.02
$F_{1,3,6,7}$	0.01	$F_{2,3,6,7}$	-0.02	$F_{3,3,6,7}$	-0.05
$F_{1,4,6,7}$	0.01	$F_{2,4,6,7}$	0.02	$F_{3,4,6,7}$	-0.04
$F_{4,4,6,7}$	-0.06	$F_{1,5,6,7}$	0.04	$F_{2,5,6,7}$	-0.01
$F_{3,5,6,7}$	-0.00	$F_{4,5,6,7}$	0.11	$F_{5,5,6,7}$	0.11
$F_{1,6,6,7}$	0.01	$F_{2,6,6,7}$	-0.01	$F_{3,6,6,7}$	0.06
$F_{4,6,6,7}$	0.20	$F_{5,6,6,7}$	0.10	$F_{6,6,6,7}$	-0.02
$F_{1,1,7,7}$	0.01	$F_{1,2,7,7}$	0.02	$F_{2,2,7,7}$	-0.02
$F_{1,3,7,7}$	0.01	$F_{2,3,7,7}$	-0.00	$F_{3,3,7,7}$	-0.04
$F_{1,4,7,7}$	0.03	$F_{2,4,7,7}$	-0.08	$F_{3,4,7,7}$	-0.05
$F_{4,4,7,7}$	-0.03	$F_{1,5,7,7}$	-0.04	$F_{2,5,7,7}$	0.01
$F_{3,5,7,7}$	-0.02	$F_{4,5,7,7}$	0.09	$F_{5,5,7,7}$	-0.19
$F_{1,6,7,7}$	-0.02	$F_{2,6,7,7}$	-0.02	$F_{3,6,7,7}$	0.03
$F_{4,6,7,7}$	0.05	$F_{5,6,7,7}$	-0.15	$F_{6,6,7,7}$	-0.21
$F_{1,7,7,7}$	-0.05	$F_{2,7,7,7}$	0.05	$F_{3,7,7,7}$	0.03
$F_{4,7,7,7}$	-0.03	$F_{5,7,7,7}$	-0.07	$F_{6,7,7,7}$	-0.02
$F_{7,7,7,7}$	0.21	$F_{1,1,1,8}$	0.00	$F_{1,1,2,8}$	-0.00
$F_{1,2,2,8}$	-0.02	$F_{2,2,2,8}$	0.01	$F_{1,1,3,8}$	0.00
$F_{1,2,3,8}$	-0.01	$F_{2,2,3,8}$	-0.01	$F_{1,3,3,8}$	-0.08
$F_{2,3,3,8}$	-0.03	$F_{3,3,3,8}$	-0.02	$F_{1,1,4,8}$	-0.00
$F_{1,2,4,8}$	-0.00	$F_{2,2,4,8}$	0.02	$F_{1,3,4,8}$	-0.02
$F_{2,3,4,8}$	-0.01	$F_{3,3,4,8}$	0.07	$F_{1,4,4,8}$	0.01

Table B22: F12-TZ-cCR Force Constants for HOOF (cont.)

$F_{2,4,4,8}$	0.02	$F_{3,4,4,8}$	0.06	$F_{4,4,4,8}$	-0.03
$F_{1,1,5,8}$	0.04	$F_{1,2,5,8}$	0.02	$F_{2,2,5,8}$	0.01
$F_{1,3,5,8}$	-0.02	$F_{2,3,5,8}$	0.01	$F_{3,3,5,8}$	0.00
$F_{1,4,5,8}$	-0.02	$F_{2,4,5,8}$	-0.02	$F_{3,4,5,8}$	0.01
$F_{4,4,5,8}$	0.19	$F_{1,5,5,8}$	-0.07	$F_{2,5,5,8}$	0.01
$F_{3,5,5,8}$	-0.05	$F_{4,5,5,8}$	0.12	$F_{5,5,5,8}$	-0.00
$F_{1,1,6,8}$	0.06	$F_{1,2,6,8}$	0.02	$F_{2,2,6,8}$	-0.01
$F_{1,3,6,8}$	0.07	$F_{2,3,6,8}$	-0.00	$F_{3,3,6,8}$	-0.01
$F_{1,4,6,8}$	-0.02	$F_{2,4,6,8}$	-0.04	$F_{3,4,6,8}$	-0.10
$F_{4,4,6,8}$	0.15	$F_{1,5,6,8}$	-0.06	$F_{2,5,6,8}$	-0.02
$F_{3,5,6,8}$	-0.04	$F_{4,5,6,8}$	0.14	$F_{5,5,6,8}$	-0.51
$F_{1,6,6,8}$	-0.14	$F_{2,6,6,8}$	-0.04	$F_{3,6,6,8}$	0.00
$F_{4,6,6,8}$	0.25	$F_{5,6,6,8}$	-0.85	$F_{6,6,6,8}$	-0.98
$F_{1,1,7,8}$	-0.00	$F_{1,2,7,8}$	0.00	$F_{2,2,7,8}$	0.00
$F_{1,3,7,8}$	0.01	$F_{2,3,7,8}$	0.02	$F_{3,3,7,8}$	0.02
$F_{1,4,7,8}$	-0.01	$F_{2,4,7,8}$	-0.02	$F_{3,4,7,8}$	-0.03
$F_{4,4,7,8}$	0.03	$F_{1,5,7,8}$	-0.02	$F_{2,5,7,8}$	0.02
$F_{3,5,7,8}$	0.00	$F_{4,5,7,8}$	-0.18	$F_{5,5,7,8}$	-0.09
$F_{1,6,7,8}$	-0.04	$F_{2,6,7,8}$	0.04	$F_{3,6,7,8}$	0.02
$F_{4,6,7,8}$	-0.14	$F_{5,6,7,8}$	-0.10	$F_{6,6,7,8}$	-0.10
$F_{1,7,7,8}$	0.01	$F_{2,7,7,8}$	0.02	$F_{3,7,7,8}$	0.02
$F_{4,7,7,8}$	-0.03	$F_{5,7,7,8}$	0.25	$F_{6,7,7,8}$	0.17
$F_{7,7,7,8}$	0.04	$F_{1,1,8,8}$	-0.04	$F_{1,2,8,8}$	-0.00
$F_{2,2,8,8}$	-0.03	$F_{1,3,8,8}$	0.02	$F_{2,3,8,8}$	-0.01
$F_{3,3,8,8}$	0.03	$F_{1,4,8,8}$	0.03	$F_{2,4,8,8}$	0.00
$F_{3,4,8,8}$	-0.00	$F_{4,4,8,8}$	-0.25	$F_{1,5,8,8}$	0.05
$F_{2,5,8,8}$	-0.01	$F_{3,5,8,8}$	0.04	$F_{4,5,8,8}$	-0.11
$F_{5,5,8,8}$	0.02	$F_{1,6,8,8}$	0.05	$F_{2,6,8,8}$	0.04
$F_{3,6,8,8}$	0.04	$F_{4,6,8,8}$	-0.10	$F_{5,6,8,8}$	0.57
$F_{6,6,8,8}$	0.85	$F_{1,7,8,8}$	0.02	$F_{2,7,8,8}$	-0.01
$F_{3,7,8,8}$	-0.01	$F_{4,7,8,8}$	0.27	$F_{5,7,8,8}$	0.08
$F_{6,7,8,8}$	0.06	$F_{7,7,8,8}$	-0.49	$F_{1,8,8,8}$	-0.05
$F_{2,8,8,8}$	0.04	$F_{3,8,8,8}$	-0.03	$F_{4,8,8,8}$	0.13
$F_{5,8,8,8}$	-0.05	$F_{6,8,8,8}$	-0.67	$F_{7,8,8,8}$	-0.11
$F_{8,8,8,8}$	-0.06	$F_{1,1,1,9}$	-0.00	$F_{1,1,2,9}$	0.02
$F_{1,2,2,9}$	-0.06	$F_{2,2,2,9}$	-0.05	$F_{1,1,3,9}$	0.00
$F_{1,2,3,9}$	-0.02	$F_{2,2,3,9}$	-0.02	$F_{1,3,3,9}$	-0.04
$F_{2,3,3,9}$	-0.02	$F_{3,3,3,9}$	0.01	$F_{1,1,4,9}$	0.01
$F_{1,2,4,9}$	-0.04	$F_{2,2,4,9}$	0.03	$F_{1,3,4,9}$	-0.01
$F_{2,3,4,9}$	-0.00	$F_{3,3,4,9}$	0.03	$F_{1,4,4,9}$	-0.01
$F_{2,4,4,9}$	0.08	$F_{3,4,4,9}$	0.04	$F_{4,4,4,9}$	-0.00
$F_{1,1,5,9}$	0.03	$F_{1,2,5,9}$	0.06	$F_{2,2,5,9}$	0.03
$F_{1,3,5,9}$	0.01	$F_{2,3,5,9}$	-0.00	$F_{3,3,5,9}$	0.01
$F_{1,4,5,9}$	0.01	$F_{2,4,5,9}$	-0.08	$F_{3,4,5,9}$	-0.02
$F_{4,4,5,9}$	0.11	$F_{1,5,5,9}$	-0.14	$F_{2,5,5,9}$	-0.04
$F_{3,5,5,9}$	-0.03	$F_{4,5,5,9}$	0.24	$F_{5,5,5,9}$	-0.46
$F_{1,1,6,9}$	0.05	$F_{1,2,6,9}$	0.02	$F_{2,2,6,9}$	-0.01
$F_{1,3,6,9}$	0.03	$F_{2,3,6,9}$	0.02	$F_{3,3,6,9}$	0.02
$F_{1,4,6,9}$	-0.02	$F_{2,4,6,9}$	-0.04	$F_{3,4,6,9}$	-0.02

Table B23: F12-TZ-cCR Force Constants for HOOF (cont.)

$F_{4,4,6,9}$	0.18	$F_{1,5,6,9}$	-0.09	$F_{2,5,6,9}$	-0.04
$F_{3,5,6,9}$	-0.04	$F_{4,5,6,9}$	0.19	$F_{5,5,6,9}$	-0.82
$F_{1,6,6,9}$	-0.10	$F_{2,6,6,9}$	-0.08	$F_{3,6,6,9}$	-0.01
$F_{4,6,6,9}$	0.15	$F_{5,6,6,9}$	-0.84	$F_{6,6,6,9}$	-0.44
$F_{1,1,7,9}$	-0.01	$F_{1,2,7,9}$	0.02	$F_{2,2,7,9}$	0.02
$F_{1,3,7,9}$	0.01	$F_{2,3,7,9}$	0.02	$F_{3,3,7,9}$	0.01
$F_{1,4,7,9}$	-0.00	$F_{2,4,7,9}$	-0.04	$F_{3,4,7,9}$	-0.02
$F_{4,4,7,9}$	0.01	$F_{1,5,7,9}$	-0.05	$F_{2,5,7,9}$	0.03
$F_{3,5,7,9}$	0.01	$F_{4,5,7,9}$	-0.10	$F_{5,5,7,9}$	-0.13
$F_{1,6,7,9}$	-0.03	$F_{2,6,7,9}$	0.02	$F_{3,6,7,9}$	-0.01
$F_{4,6,7,9}$	-0.16	$F_{5,6,7,9}$	-0.09	$F_{6,6,7,9}$	-0.03
$F_{1,7,7,9}$	0.01	$F_{2,7,7,9}$	0.02	$F_{3,7,7,9}$	0.01
$F_{4,7,7,9}$	-0.00	$F_{5,7,7,9}$	0.13	$F_{6,7,7,9}$	0.18
$F_{7,7,7,9}$	-0.02	$F_{1,1,8,9}$	-0.05	$F_{1,2,8,9}$	-0.01
$F_{2,2,8,9}$	0.03	$F_{1,3,8,9}$	0.01	$F_{2,3,8,9}$	0.03
$F_{3,3,8,9}$	0.02	$F_{1,4,8,9}$	0.03	$F_{2,4,8,9}$	0.06
$F_{3,4,8,9}$	0.02	$F_{4,4,8,9}$	-0.19	$F_{1,5,8,9}$	0.08
$F_{2,5,8,9}$	-0.00	$F_{3,5,8,9}$	0.03	$F_{4,5,8,9}$	-0.16
$F_{5,5,8,9}$	0.51	$F_{1,6,8,9}$	0.07	$F_{2,6,8,9}$	0.04
$F_{3,6,8,9}$	0.02	$F_{4,6,8,9}$	-0.15	$F_{5,6,8,9}$	0.87
$F_{6,6,8,9}$	0.97	$F_{1,7,8,9}$	0.03	$F_{2,7,8,9}$	-0.07
$F_{3,7,8,9}$	-0.03	$F_{4,7,8,9}$	0.13	$F_{5,7,8,9}$	0.10
$F_{6,7,8,9}$	0.07	$F_{7,7,8,9}$	0.01	$F_{1,8,8,9}$	-0.06
$F_{2,8,8,9}$	-0.02	$F_{3,8,8,9}$	-0.07	$F_{4,8,8,9}$	0.10
$F_{5,8,8,9}$	-0.52	$F_{6,8,8,9}$	-0.88	$F_{7,8,8,9}$	-0.03
$F_{8,8,8,9}$	0.38	$F_{1,1,9,9}$	-0.05	$F_{1,2,9,9}$	-0.00
$F_{2,2,9,9}$	0.03	$F_{1,3,9,9}$	0.01	$F_{2,3,9,9}$	-0.00
$F_{3,3,9,9}$	-0.05	$F_{1,4,9,9}$	0.03	$F_{2,4,9,9}$	0.04
$F_{3,4,9,9}$	-0.02	$F_{4,4,9,9}$	-0.19	$F_{1,5,9,9}$	0.10
$F_{2,5,9,9}$	0.05	$F_{3,5,9,9}$	0.03	$F_{4,5,9,9}$	-0.18
$F_{5,5,9,9}$	0.83	$F_{1,6,9,9}$	0.08	$F_{2,6,9,9}$	0.07
$F_{3,6,9,9}$	0.00	$F_{4,6,9,9}$	-0.13	$F_{5,6,9,9}$	0.85
$F_{6,6,9,9}$	0.40	$F_{1,7,9,9}$	0.02	$F_{2,7,9,9}$	-0.04
$F_{3,7,9,9}$	0.01	$F_{4,7,9,9}$	0.13	$F_{5,7,9,9}$	0.07
$F_{6,7,9,9}$	0.03	$F_{7,7,9,9}$	-0.32	$F_{1,8,9,9}$	-0.10
$F_{2,8,9,9}$	-0.07	$F_{3,8,9,9}$	-0.04	$F_{4,8,9,9}$	0.13
$F_{5,8,9,9}$	-0.79	$F_{6,8,9,9}$	-0.92	$F_{7,8,9,9}$	-0.04
$F_{8,8,9,9}$	1.29	$F_{1,9,9,9}$	-0.10	$F_{2,9,9,9}$	-0.08
$F_{3,9,9,9}$	0.05	$F_{4,9,9,9}$	0.16	$F_{5,9,9,9}$	-1.00
$F_{6,9,9,9}$	-0.50	$F_{7,9,9,9}$	-0.02	$F_{8,9,9,9}$	0.19
$F_{9,9,9,9}$	1.49	$F_{1,1,1,10}$	0.00	$F_{1,1,2,10}$	0.00
$F_{1,2,2,10}$	0.01	$F_{2,2,2,10}$	-0.00	$F_{1,1,3,10}$	-0.00
$F_{1,2,3,10}$	-0.00	$F_{2,2,3,10}$	0.00	$F_{1,3,3,10}$	-0.00
$F_{2,3,3,10}$	-0.00	$F_{3,3,3,10}$	0.00	$F_{1,1,4,10}$	0.00
$F_{1,2,4,10}$	-0.00	$F_{2,2,4,10}$	-0.00	$F_{1,3,4,10}$	0.00
$F_{2,3,4,10}$	0.00	$F_{3,3,4,10}$	0.00	$F_{1,4,4,10}$	0.00
$F_{2,4,4,10}$	-0.00	$F_{3,4,4,10}$	0.00	$F_{4,4,4,10}$	-0.01
$F_{1,1,5,10}$	-0.00	$F_{1,2,5,10}$	-0.00	$F_{2,2,5,10}$	0.00
$F_{1,3,5,10}$	-0.00	$F_{2,3,5,10}$	-0.01	$F_{3,3,5,10}$	0.01

Table B24: F12-TZ-cCR Force Constants for HOOF (cont.)

$F_{1,4,5,10}$	-0.00	$F_{2,4,5,10}$	-0.00	$F_{3,4,5,10}$	0.00
$F_{4,4,5,10}$	0.01	$F_{1,5,5,10}$	-0.00	$F_{2,5,5,10}$	0.01
$F_{3,5,5,10}$	0.01	$F_{4,5,5,10}$	0.00	$F_{5,5,5,10}$	-0.04
$F_{1,1,6,10}$	0.00	$F_{1,2,6,10}$	0.00	$F_{2,2,6,10}$	-0.00
$F_{1,3,6,10}$	0.00	$F_{2,3,6,10}$	0.00	$F_{3,3,6,10}$	-0.00
$F_{1,4,6,10}$	-0.00	$F_{2,4,6,10}$	-0.01	$F_{3,4,6,10}$	0.00
$F_{4,4,6,10}$	-0.00	$F_{1,5,6,10}$	-0.00	$F_{2,5,6,10}$	0.02
$F_{3,5,6,10}$	-0.01	$F_{4,5,6,10}$	0.01	$F_{5,5,6,10}$	-0.04
$F_{1,6,6,10}$	0.00	$F_{2,6,6,10}$	-0.00	$F_{3,6,6,10}$	-0.00
$F_{4,6,6,10}$	0.04	$F_{5,6,6,10}$	0.02	$F_{6,6,6,10}$	0.04
$F_{1,1,7,10}$	-0.00	$F_{1,2,7,10}$	-0.01	$F_{2,2,7,10}$	-0.00
$F_{1,3,7,10}$	-0.00	$F_{2,3,7,10}$	-0.00	$F_{3,3,7,10}$	0.01
$F_{1,4,7,10}$	-0.00	$F_{2,4,7,10}$	0.01	$F_{3,4,7,10}$	-0.00
$F_{4,4,7,10}$	-0.01	$F_{1,5,7,10}$	0.01	$F_{2,5,7,10}$	0.00
$F_{3,5,7,10}$	0.00	$F_{4,5,7,10}$	-0.01	$F_{5,5,7,10}$	0.02
$F_{1,6,7,10}$	0.00	$F_{2,6,7,10}$	0.01	$F_{3,6,7,10}$	-0.01
$F_{4,6,7,10}$	0.01	$F_{5,6,7,10}$	-0.01	$F_{6,6,7,10}$	-0.01
$F_{1,7,7,10}$	0.01	$F_{2,7,7,10}$	-0.00	$F_{3,7,7,10}$	0.01
$F_{4,7,7,10}$	0.03	$F_{5,7,7,10}$	0.01	$F_{6,7,7,10}$	-0.01
$F_{7,7,7,10}$	-0.13	$F_{1,1,8,10}$	-0.00	$F_{1,2,8,10}$	-0.00
$F_{2,2,8,10}$	0.00	$F_{1,3,8,10}$	0.01	$F_{2,3,8,10}$	0.00
$F_{3,3,8,10}$	-0.00	$F_{1,4,8,10}$	0.00	$F_{2,4,8,10}$	0.01
$F_{3,4,8,10}$	-0.01	$F_{4,4,8,10}$	-0.01	$F_{1,5,8,10}$	0.01
$F_{2,5,8,10}$	-0.01	$F_{3,5,8,10}$	-0.00	$F_{4,5,8,10}$	0.01
$F_{5,5,8,10}$	0.04	$F_{1,6,8,10}$	-0.00	$F_{2,6,8,10}$	-0.01
$F_{3,6,8,10}$	0.01	$F_{4,6,8,10}$	0.00	$F_{5,6,8,10}$	0.02
$F_{6,6,8,10}$	-0.02	$F_{1,7,8,10}$	-0.00	$F_{2,7,8,10}$	-0.01
$F_{3,7,8,10}$	-0.00	$F_{4,7,8,10}$	0.01	$F_{5,7,8,10}$	-0.05
$F_{6,7,8,10}$	0.01	$F_{7,7,8,10}$	-0.03	$F_{1,8,8,10}$	-0.01
$F_{2,8,8,10}$	0.01	$F_{3,8,8,10}$	-0.01	$F_{4,8,8,10}$	-0.04
$F_{5,8,8,10}$	-0.03	$F_{6,8,8,10}$	-0.00	$F_{7,8,8,10}$	0.20
$F_{8,8,8,10}$	0.04	$F_{1,1,9,10}$	0.00	$F_{1,2,9,10}$	-0.00
$F_{2,2,9,10}$	0.00	$F_{1,3,9,10}$	0.00	$F_{2,3,9,10}$	-0.00
$F_{3,3,9,10}$	-0.00	$F_{1,4,9,10}$	0.00	$F_{2,4,9,10}$	0.00
$F_{3,4,9,10}$	-0.01	$F_{4,4,9,10}$	-0.00	$F_{1,5,9,10}$	0.01
$F_{2,5,9,10}$	-0.01	$F_{3,5,9,10}$	0.00	$F_{4,5,9,10}$	-0.02
$F_{5,5,9,10}$	0.03	$F_{1,6,9,10}$	-0.00	$F_{2,6,9,10}$	-0.00
$F_{3,6,9,10}$	0.01	$F_{4,6,9,10}$	-0.00	$F_{5,6,9,10}$	-0.01
$F_{6,6,9,10}$	-0.03	$F_{1,7,9,10}$	0.00	$F_{2,7,9,10}$	-0.00
$F_{3,7,9,10}$	0.00	$F_{4,7,9,10}$	-0.00	$F_{5,7,9,10}$	0.02
$F_{6,7,9,10}$	0.00	$F_{7,7,9,10}$	0.01	$F_{1,8,9,10}$	-0.00
$F_{2,8,9,10}$	0.02	$F_{3,8,9,10}$	-0.00	$F_{4,8,9,10}$	0.03
$F_{5,8,9,10}$	-0.02	$F_{6,8,9,10}$	0.01	$F_{7,8,9,10}$	-0.17
$F_{8,8,9,10}$	-0.01	$F_{1,9,9,10}$	-0.00	$F_{2,9,9,10}$	0.00
$F_{3,9,9,10}$	0.00	$F_{4,9,9,10}$	0.02	$F_{5,9,9,10}$	0.01
$F_{6,9,9,10}$	0.01	$F_{7,9,9,10}$	0.17	$F_{8,9,9,10}$	0.01
$F_{9,9,9,10}$	-0.04	$F_{1,1,10,10}$	0.00	$F_{1,2,10,10}$	0.00
$F_{2,2,10,10}$	-0.00	$F_{1,3,10,10}$	0.00	$F_{2,3,10,10}$	-0.00
$F_{3,3,10,10}$	-0.00	$F_{1,4,10,10}$	0.00	$F_{2,4,10,10}$	-0.00

Table B25: F12-TZ-cCR Force Constants for HOOF (cont.)

$F_{3,4,10,10}$	0.00	$F_{4,4,10,10}$	0.02	$F_{1,5,10,10}$	-0.00
$F_{2,5,10,10}$	-0.00	$F_{3,5,10,10}$	-0.00	$F_{4,5,10,10}$	0.01
$F_{5,5,10,10}$	-0.02	$F_{1,6,10,10}$	0.00	$F_{2,6,10,10}$	-0.00
$F_{3,6,10,10}$	0.00	$F_{4,6,10,10}$	0.00	$F_{5,6,10,10}$	0.00
$F_{6,6,10,10}$	-0.03	$F_{1,7,10,10}$	-0.00	$F_{2,7,10,10}$	-0.00
$F_{3,7,10,10}$	-0.00	$F_{4,7,10,10}$	-0.02	$F_{5,7,10,10}$	-0.00
$F_{6,7,10,10}$	0.00	$F_{7,7,10,10}$	0.10	$F_{1,8,10,10}$	-0.00
$F_{2,8,10,10}$	0.00	$F_{3,8,10,10}$	0.00	$F_{4,8,10,10}$	-0.00
$F_{5,8,10,10}$	0.03	$F_{6,8,10,10}$	-0.01	$F_{7,8,10,10}$	0.02
$F_{8,8,10,10}$	-0.15	$F_{1,9,10,10}$	-0.00	$F_{2,9,10,10}$	0.00
$F_{3,9,10,10}$	-0.00	$F_{4,9,10,10}$	0.00	$F_{5,9,10,10}$	0.00
$F_{6,9,10,10}$	0.01	$F_{7,9,10,10}$	-0.01	$F_{8,9,10,10}$	0.15
$F_{9,9,10,10}$	-0.19	$F_{1,10,10,10}$	0.00	$F_{2,10,10,10}$	0.00
$F_{3,10,10,10}$	0.00	$F_{4,10,10,10}$	-0.00	$F_{5,10,10,10}$	0.00
$F_{6,10,10,10}$	-0.00	$F_{7,10,10,10}$	-0.08	$F_{8,10,10,10}$	-0.01
$F_{9,10,10,10}$	0.01	$F_{10,10,10,10}$	0.08	$F_{1,1,1,11}$	0.00
$F_{1,1,2,11}$	0.00	$F_{1,2,2,11}$	-0.00	$F_{2,2,2,11}$	-0.00
$F_{1,1,3,11}$	-0.00	$F_{1,2,3,11}$	-0.00	$F_{2,2,3,11}$	-0.00
$F_{1,3,3,11}$	0.00	$F_{2,3,3,11}$	0.00	$F_{3,3,3,11}$	0.00
$F_{1,1,4,11}$	-0.00	$F_{1,2,4,11}$	-0.00	$F_{2,2,4,11}$	0.00
$F_{1,3,4,11}$	-0.00	$F_{2,3,4,11}$	0.00	$F_{3,3,4,11}$	-0.00
$F_{1,4,4,11}$	0.00	$F_{2,4,4,11}$	0.00	$F_{3,4,4,11}$	0.00
$F_{4,4,4,11}$	0.01	$F_{1,1,5,11}$	-0.00	$F_{1,2,5,11}$	0.00
$F_{2,2,5,11}$	0.00	$F_{1,3,5,11}$	-0.00	$F_{2,3,5,11}$	0.00
$F_{3,3,5,11}$	0.00	$F_{1,4,5,11}$	0.00	$F_{2,4,5,11}$	0.00
$F_{3,4,5,11}$	0.00	$F_{4,4,5,11}$	-0.03	$F_{1,5,5,11}$	-0.00
$F_{2,5,5,11}$	-0.00	$F_{3,5,5,11}$	0.00	$F_{4,5,5,11}$	-0.01
$F_{5,5,5,11}$	0.01	$F_{1,1,6,11}$	-0.00	$F_{1,2,6,11}$	-0.00
$F_{2,2,6,11}$	0.00	$F_{1,3,6,11}$	-0.00	$F_{2,3,6,11}$	0.00
$F_{3,3,6,11}$	0.00	$F_{1,4,6,11}$	0.00	$F_{2,4,6,11}$	0.01
$F_{3,4,6,11}$	0.01	$F_{4,4,6,11}$	-0.00	$F_{1,5,6,11}$	-0.00
$F_{2,5,6,11}$	-0.01	$F_{3,5,6,11}$	-0.00	$F_{4,5,6,11}$	-0.01
$F_{5,5,6,11}$	0.05	$F_{1,6,6,11}$	0.00	$F_{2,6,6,11}$	-0.01
$F_{3,6,6,11}$	0.00	$F_{4,6,6,11}$	-0.00	$F_{5,6,6,11}$	0.05
$F_{6,6,6,11}$	0.01	$F_{1,1,7,11}$	-0.00	$F_{1,2,7,11}$	0.00
$F_{2,2,7,11}$	0.00	$F_{1,3,7,11}$	0.00	$F_{2,3,7,11}$	0.00
$F_{3,3,7,11}$	-0.00	$F_{1,4,7,11}$	0.00	$F_{2,4,7,11}$	0.00
$F_{3,4,7,11}$	-0.00	$F_{4,4,7,11}$	-0.01	$F_{1,5,7,11}$	-0.00
$F_{2,5,7,11}$	-0.00	$F_{3,5,7,11}$	0.00	$F_{4,5,7,11}$	0.04
$F_{5,5,7,11}$	0.02	$F_{1,6,7,11}$	-0.00	$F_{2,6,7,11}$	-0.01
$F_{3,6,7,11}$	-0.00	$F_{4,6,7,11}$	0.00	$F_{5,6,7,11}$	0.01
$F_{6,6,7,11}$	0.00	$F_{1,7,7,11}$	-0.00	$F_{2,7,7,11}$	-0.01
$F_{3,7,7,11}$	-0.00	$F_{4,7,7,11}$	0.01	$F_{5,7,7,11}$	-0.06
$F_{6,7,7,11}$	0.00	$F_{7,7,7,11}$	-0.03	$F_{1,1,8,11}$	0.00
$F_{1,2,8,11}$	0.00	$F_{2,2,8,11}$	0.01	$F_{1,3,8,11}$	0.00
$F_{2,3,8,11}$	0.00	$F_{3,3,8,11}$	-0.00	$F_{1,4,8,11}$	-0.00
$F_{2,4,8,11}$	0.00	$F_{3,4,8,11}$	0.00	$F_{4,4,8,11}$	0.05
$F_{1,5,8,11}$	-0.00	$F_{2,5,8,11}$	-0.01	$F_{3,5,8,11}$	-0.01
$F_{4,5,8,11}$	0.01	$F_{5,5,8,11}$	-0.02	$F_{1,6,8,11}$	-0.00

Table B26: F12-TZ-cCR Force Constants for HOOF (cont.)

$F_{2,6,8,11}$	-0.00	$F_{3,6,8,11}$	0.00	$F_{4,6,8,11}$	0.00
$F_{5,6,8,11}$	-0.03	$F_{6,6,8,11}$	0.04	$F_{1,7,8,11}$	-0.00
$F_{2,7,8,11}$	-0.01	$F_{3,7,8,11}$	-0.01	$F_{4,7,8,11}$	-0.07
$F_{5,7,8,11}$	-0.01	$F_{6,7,8,11}$	0.00	$F_{7,7,8,11}$	0.22
$F_{1,8,8,11}$	0.01	$F_{2,8,8,11}$	0.00	$F_{3,8,8,11}$	0.00
$F_{4,8,8,11}$	-0.02	$F_{5,8,8,11}$	0.05	$F_{6,8,8,11}$	0.06
$F_{7,8,8,11}$	0.03	$F_{8,8,8,11}$	0.08	$F_{1,1,9,11}$	-0.00
$F_{1,2,9,11}$	0.00	$F_{2,2,9,11}$	-0.01	$F_{1,3,9,11}$	0.00
$F_{2,3,9,11}$	-0.00	$F_{3,3,9,11}$	-0.01	$F_{1,4,9,11}$	0.00
$F_{2,4,9,11}$	-0.01	$F_{3,4,9,11}$	-0.00	$F_{4,4,9,11}$	-0.00
$F_{1,5,9,11}$	0.01	$F_{2,5,9,11}$	0.01	$F_{3,5,9,11}$	-0.00
$F_{4,5,9,11}$	0.00	$F_{5,5,9,11}$	-0.01	$F_{1,6,9,11}$	0.01
$F_{2,6,9,11}$	0.01	$F_{3,6,9,11}$	0.00	$F_{4,6,9,11}$	-0.00
$F_{5,6,9,11}$	-0.01	$F_{6,6,9,11}$	-0.05	$F_{1,7,9,11}$	-0.00
$F_{2,7,9,11}$	0.01	$F_{3,7,9,11}$	0.00	$F_{4,7,9,11}$	0.01
$F_{5,7,9,11}$	-0.01	$F_{6,7,9,11}$	0.00	$F_{7,7,9,11}$	-0.16
$F_{1,8,9,11}$	-0.00	$F_{2,8,9,11}$	-0.00	$F_{3,8,9,11}$	0.00
$F_{4,8,9,11}$	0.00	$F_{5,8,9,11}$	0.01	$F_{6,8,9,11}$	-0.03
$F_{7,8,9,11}$	-0.01	$F_{8,8,9,11}$	0.16	$F_{1,9,9,11}$	-0.00
$F_{2,9,9,11}$	-0.01	$F_{3,9,9,11}$	0.01	$F_{4,9,9,11}$	0.01
$F_{5,9,9,11}$	-0.09	$F_{6,9,9,11}$	0.00	$F_{7,9,9,11}$	0.01
$F_{8,9,9,11}$	-0.43	$F_{9,9,9,11}$	0.89	$F_{1,1,10,11}$	0.00
$F_{1,2,10,11}$	-0.00	$F_{2,2,10,11}$	-0.00	$F_{1,3,10,11}$	-0.00
$F_{2,3,10,11}$	-0.00	$F_{3,3,10,11}$	0.00	$F_{1,4,10,11}$	-0.00
$F_{2,4,10,11}$	-0.00	$F_{3,4,10,11}$	0.00	$F_{4,4,10,11}$	0.00
$F_{1,5,10,11}$	-0.00	$F_{2,5,10,11}$	0.00	$F_{3,5,10,11}$	-0.00
$F_{4,5,10,11}$	-0.01	$F_{5,5,10,11}$	-0.01	$F_{1,6,10,11}$	0.00
$F_{2,6,10,11}$	0.00	$F_{3,6,10,11}$	0.00	$F_{4,6,10,11}$	-0.00
$F_{5,6,10,11}$	-0.00	$F_{6,6,10,11}$	-0.00	$F_{1,7,10,11}$	0.00
$F_{2,7,10,11}$	0.00	$F_{3,7,10,11}$	0.00	$F_{4,7,10,11}$	-0.00
$F_{5,7,10,11}$	0.03	$F_{6,7,10,11}$	-0.00	$F_{7,7,10,11}$	0.02
$F_{1,8,10,11}$	0.00	$F_{2,8,10,11}$	0.00	$F_{3,8,10,11}$	0.01
$F_{4,8,10,11}$	0.03	$F_{5,8,10,11}$	0.01	$F_{6,8,10,11}$	-0.00
$F_{7,8,10,11}$	-0.14	$F_{8,8,10,11}$	-0.02	$F_{1,9,10,11}$	-0.00
$F_{2,9,10,11}$	-0.00	$F_{3,9,10,11}$	0.00	$F_{4,9,10,11}$	-0.01
$F_{5,9,10,11}$	0.01	$F_{6,9,10,11}$	-0.00	$F_{7,9,10,11}$	0.16
$F_{8,9,10,11}$	0.01	$F_{9,9,10,11}$	-0.02	$F_{1,10,10,11}$	-0.00
$F_{2,10,10,11}$	-0.00	$F_{3,10,10,11}$	-0.00	$F_{4,10,10,11}$	0.00
$F_{5,10,10,11}$	-0.02	$F_{6,10,10,11}$	0.01	$F_{7,10,10,11}$	-0.01
$F_{8,10,10,11}$	0.11	$F_{9,10,10,11}$	-0.15	$F_{10,10,10,11}$	0.01
$F_{1,1,11,11}$	-0.00	$F_{1,2,11,11}$	0.00	$F_{2,2,11,11}$	-0.01
$F_{1,3,11,11}$	-0.00	$F_{2,3,11,11}$	-0.00	$F_{3,3,11,11}$	-0.00
$F_{1,4,11,11}$	0.00	$F_{2,4,11,11}$	-0.01	$F_{3,4,11,11}$	-0.00
$F_{4,4,11,11}$	-0.02	$F_{1,5,11,11}$	0.00	$F_{2,5,11,11}$	0.01
$F_{3,5,11,11}$	0.00	$F_{4,5,11,11}$	-0.00	$F_{5,5,11,11}$	0.02
$F_{1,6,11,11}$	0.00	$F_{2,6,11,11}$	0.00	$F_{3,6,11,11}$	-0.00
$F_{4,6,11,11}$	-0.00	$F_{5,6,11,11}$	-0.01	$F_{6,6,11,11}$	-0.08
$F_{1,7,11,11}$	0.00	$F_{2,7,11,11}$	0.01	$F_{3,7,11,11}$	0.01
$F_{4,7,11,11}$	0.04	$F_{5,7,11,11}$	0.00	$F_{6,7,11,11}$	-0.00

Table B27: F12-TZ-cCR Force Constants for HOOF (cont.)

$F_{7,7,11,11}$	-0.15	$F_{1,8,11,11}$	-0.01	$F_{2,8,11,11}$	0.00
$F_{3,8,11,11}$	0.00	$F_{4,8,11,11}$	0.01	$F_{5,8,11,11}$	-0.01
$F_{6,8,11,11}$	-0.02	$F_{7,8,11,11}$	-0.02	$F_{8,8,11,11}$	-0.12
$F_{1,9,11,11}$	-0.00	$F_{2,9,11,11}$	-0.00	$F_{3,9,11,11}$	0.00
$F_{4,9,11,11}$	0.00	$F_{5,9,11,11}$	-0.00	$F_{6,9,11,11}$	0.03
$F_{7,9,11,11}$	0.01	$F_{8,9,11,11}$	-0.17	$F_{9,9,11,11}$	0.53
$F_{1,10,11,11}$	-0.00	$F_{2,10,11,11}$	-0.00	$F_{3,10,11,11}$	-0.00
$F_{4,10,11,11}$	-0.02	$F_{5,10,11,11}$	-0.00	$F_{6,10,11,11}$	0.00
$F_{7,10,11,11}$	0.11	$F_{8,10,11,11}$	0.01	$F_{9,10,11,11}$	-0.01
$F_{10,10,11,11}$	-0.09	$F_{1,11,11,11}$	0.00	$F_{2,11,11,11}$	-0.00
$F_{3,11,11,11}$	-0.00	$F_{4,11,11,11}$	-0.01	$F_{5,11,11,11}$	-0.01
$F_{6,11,11,11}$	0.03	$F_{7,11,11,11}$	0.01	$F_{8,11,11,11}$	0.14
$F_{9,11,11,11}$	0.17	$F_{10,11,11,11}$	-0.00	$F_{11,11,11,11}$	-0.13
$F_{1,1,1,12}$	-0.00	$F_{1,1,2,12}$	0.00	$F_{1,2,2,12}$	0.00
$F_{2,2,2,12}$	-0.00	$F_{1,1,3,12}$	0.00	$F_{1,2,3,12}$	-0.00
$F_{2,2,3,12}$	-0.00	$F_{1,3,3,12}$	0.00	$F_{2,3,3,12}$	-0.00
$F_{3,3,3,12}$	-0.00	$F_{1,1,4,12}$	0.01	$F_{1,2,4,12}$	-0.00
$F_{2,2,4,12}$	-0.00	$F_{1,3,4,12}$	-0.00	$F_{2,3,4,12}$	0.00
$F_{3,3,4,12}$	-0.01	$F_{1,4,4,12}$	-0.01	$F_{2,4,4,12}$	0.00
$F_{3,4,4,12}$	0.00	$F_{4,4,4,12}$	0.01	$F_{1,1,5,12}$	0.00
$F_{1,2,5,12}$	-0.00	$F_{2,2,5,12}$	0.01	$F_{1,3,5,12}$	0.01
$F_{2,3,5,12}$	-0.00	$F_{3,3,5,12}$	-0.01	$F_{1,4,5,12}$	-0.00
$F_{2,4,5,12}$	0.01	$F_{3,4,5,12}$	-0.01	$F_{4,4,5,12}$	0.02
$F_{1,5,5,12}$	0.01	$F_{2,5,5,12}$	-0.01	$F_{3,5,5,12}$	-0.00
$F_{4,5,5,12}$	-0.02	$F_{5,5,5,12}$	0.00	$F_{1,1,6,12}$	-0.00
$F_{1,2,6,12}$	0.00	$F_{2,2,6,12}$	-0.00	$F_{1,3,6,12}$	-0.01
$F_{2,3,6,12}$	-0.00	$F_{3,3,6,12}$	0.00	$F_{1,4,6,12}$	-0.00
$F_{2,4,6,12}$	-0.01	$F_{3,4,6,12}$	0.00	$F_{4,4,6,12}$	0.05
$F_{1,5,6,12}$	0.00	$F_{2,5,6,12}$	0.01	$F_{3,5,6,12}$	0.02
$F_{4,5,6,12}$	0.01	$F_{5,5,6,12}$	0.00	$F_{1,6,6,12}$	0.02
$F_{2,6,6,12}$	0.01	$F_{3,6,6,12}$	-0.00	$F_{4,6,6,12}$	0.00
$F_{5,6,6,12}$	-0.06	$F_{6,6,6,12}$	-0.27	$F_{1,1,7,12}$	-0.00
$F_{1,2,7,12}$	-0.00	$F_{2,2,7,12}$	-0.00	$F_{1,3,7,12}$	0.00
$F_{2,3,7,12}$	0.00	$F_{3,3,7,12}$	0.00	$F_{1,4,7,12}$	0.00
$F_{2,4,7,12}$	0.00	$F_{3,4,7,12}$	-0.00	$F_{4,4,7,12}$	-0.00
$F_{1,5,7,12}$	0.00	$F_{2,5,7,12}$	-0.01	$F_{3,5,7,12}$	0.01
$F_{4,5,7,12}$	-0.03	$F_{5,5,7,12}$	0.01	$F_{1,6,7,12}$	0.00
$F_{2,6,7,12}$	0.00	$F_{3,6,7,12}$	0.00	$F_{4,6,7,12}$	-0.01
$F_{5,6,7,12}$	-0.01	$F_{6,6,7,12}$	-0.01	$F_{1,7,7,12}$	-0.00
$F_{2,7,7,12}$	0.00	$F_{3,7,7,12}$	0.00	$F_{4,7,7,12}$	-0.00
$F_{5,7,7,12}$	0.04	$F_{6,7,7,12}$	0.00	$F_{7,7,7,12}$	0.02
$F_{1,1,8,12}$	-0.01	$F_{1,2,8,12}$	-0.00	$F_{2,2,8,12}$	-0.01
$F_{1,3,8,12}$	0.00	$F_{2,3,8,12}$	0.01	$F_{3,3,8,12}$	0.01
$F_{1,4,8,12}$	0.01	$F_{2,4,8,12}$	-0.00	$F_{3,4,8,12}$	0.01
$F_{4,4,8,12}$	-0.02	$F_{1,5,8,12}$	0.00	$F_{2,5,8,12}$	0.01
$F_{3,5,8,12}$	-0.00	$F_{4,5,8,12}$	0.01	$F_{5,5,8,12}$	0.05
$F_{1,6,8,12}$	-0.00	$F_{2,6,8,12}$	-0.00	$F_{3,6,8,12}$	-0.01
$F_{4,6,8,12}$	-0.01	$F_{5,6,8,12}$	0.03	$F_{6,6,8,12}$	0.01
$F_{1,7,8,12}$	0.00	$F_{2,7,8,12}$	0.01	$F_{3,7,8,12}$	-0.01

Table B28: F12-TZ-cCR Force Constants for HOOF (cont.)

$F_{4,7,8,12}$	0.03	$F_{5,7,8,12}$	-0.01	$F_{6,7,8,12}$	0.01
$F_{7,7,8,12}$	-0.20	$F_{1,8,8,12}$	-0.00	$F_{2,8,8,12}$	-0.01
$F_{3,8,8,12}$	-0.00	$F_{4,8,8,12}$	0.01	$F_{5,8,8,12}$	-0.09
$F_{6,8,8,12}$	-0.01	$F_{7,8,8,12}$	-0.02	$F_{8,8,8,12}$	0.31
$F_{1,1,9,12}$	-0.00	$F_{1,2,9,12}$	0.00	$F_{2,2,9,12}$	0.01
$F_{1,3,9,12}$	-0.00	$F_{2,3,9,12}$	0.00	$F_{3,3,9,12}$	0.02
$F_{1,4,9,12}$	0.00	$F_{2,4,9,12}$	-0.00	$F_{3,4,9,12}$	0.01
$F_{4,4,9,12}$	-0.03	$F_{1,5,9,12}$	-0.01	$F_{2,5,9,12}$	-0.01
$F_{3,5,9,12}$	0.00	$F_{4,5,9,12}$	0.01	$F_{5,5,9,12}$	0.02
$F_{1,6,9,12}$	-0.01	$F_{2,6,9,12}$	-0.01	$F_{3,6,9,12}$	-0.01
$F_{4,6,9,12}$	-0.00	$F_{5,6,9,12}$	0.02	$F_{6,6,9,12}$	0.05
$F_{1,7,9,12}$	-0.00	$F_{2,7,9,12}$	0.00	$F_{3,7,9,12}$	-0.00
$F_{4,7,9,12}$	0.04	$F_{5,7,9,12}$	0.01	$F_{6,7,9,12}$	0.01
$F_{7,7,9,12}$	0.14	$F_{1,8,9,12}$	0.01	$F_{2,8,9,12}$	0.00
$F_{3,8,9,12}$	-0.00	$F_{4,8,9,12}$	-0.01	$F_{5,8,9,12}$	-0.11
$F_{6,8,9,12}$	-0.06	$F_{7,8,9,12}$	0.01	$F_{8,8,9,12}$	-0.35
$F_{1,9,9,12}$	0.00	$F_{2,9,9,12}$	0.01	$F_{3,9,9,12}$	-0.01
$F_{4,9,9,12}$	-0.01	$F_{5,9,9,12}$	0.12	$F_{6,9,9,12}$	0.09
$F_{7,9,9,12}$	-0.02	$F_{8,9,9,12}$	0.77	$F_{9,9,9,12}$	-1.04
$F_{1,1,10,12}$	-0.00	$F_{1,2,10,12}$	0.00	$F_{2,2,10,12}$	0.00
$F_{1,3,10,12}$	-0.00	$F_{2,3,10,12}$	-0.00	$F_{3,3,10,12}$	-0.00
$F_{1,4,10,12}$	0.00	$F_{2,4,10,12}$	0.00	$F_{3,4,10,12}$	0.00
$F_{4,4,10,12}$	0.00	$F_{1,5,10,12}$	-0.00	$F_{2,5,10,12}$	0.00
$F_{3,5,10,12}$	0.00	$F_{4,5,10,12}$	0.01	$F_{5,5,10,12}$	0.00
$F_{1,6,10,12}$	0.00	$F_{2,6,10,12}$	0.00	$F_{3,6,10,12}$	-0.00
$F_{4,6,10,12}$	-0.03	$F_{5,6,10,12}$	-0.00	$F_{6,6,10,12}$	-0.01
$F_{1,7,10,12}$	-0.00	$F_{2,7,10,12}$	-0.00	$F_{3,7,10,12}$	-0.00
$F_{4,7,10,12}$	0.00	$F_{5,7,10,12}$	-0.01	$F_{6,7,10,12}$	0.01
$F_{7,7,10,12}$	-0.01	$F_{1,8,10,12}$	-0.00	$F_{2,8,10,12}$	-0.01
$F_{3,8,10,12}$	-0.00	$F_{4,8,10,12}$	-0.02	$F_{5,8,10,12}$	0.00
$F_{6,8,10,12}$	0.00	$F_{7,8,10,12}$	0.16	$F_{8,8,10,12}$	0.02
$F_{1,9,10,12}$	0.00	$F_{2,9,10,12}$	0.00	$F_{3,9,10,12}$	-0.01
$F_{4,9,10,12}$	-0.01	$F_{5,9,10,12}$	-0.01	$F_{6,9,10,12}$	0.00
$F_{7,9,10,12}$	-0.17	$F_{8,9,10,12}$	-0.01	$F_{9,9,10,12}$	0.03
$F_{1,10,10,12}$	0.00	$F_{2,10,10,12}$	0.00	$F_{3,10,10,12}$	0.00
$F_{4,10,10,12}$	-0.00	$F_{5,10,10,12}$	-0.00	$F_{6,10,10,12}$	0.02
$F_{7,10,10,12}$	0.01	$F_{8,10,10,12}$	-0.14	$F_{9,10,10,12}$	0.19
$F_{10,10,10,12}$	-0.01	$F_{1,1,11,12}$	0.00	$F_{1,2,11,12}$	0.00
$F_{2,2,11,12}$	0.00	$F_{1,3,11,12}$	-0.00	$F_{2,3,11,12}$	-0.00
$F_{3,3,11,12}$	0.00	$F_{1,4,11,12}$	-0.00	$F_{2,4,11,12}$	-0.00
$F_{3,4,11,12}$	0.00	$F_{4,4,11,12}$	-0.00	$F_{1,5,11,12}$	-0.00
$F_{2,5,11,12}$	-0.00	$F_{3,5,11,12}$	0.00	$F_{4,5,11,12}$	0.01
$F_{5,5,11,12}$	-0.04	$F_{1,6,11,12}$	-0.00	$F_{2,6,11,12}$	-0.00
$F_{3,6,11,12}$	-0.00	$F_{4,6,11,12}$	0.00	$F_{5,6,11,12}$	-0.04
$F_{6,6,11,12}$	0.04	$F_{1,7,11,12}$	-0.00	$F_{2,7,11,12}$	-0.00
$F_{3,7,11,12}$	0.00	$F_{4,7,11,12}$	-0.01	$F_{5,7,11,12}$	0.00
$F_{6,7,11,12}$	-0.00	$F_{7,7,11,12}$	0.16	$F_{1,8,11,12}$	0.00
$F_{2,8,11,12}$	0.00	$F_{3,8,11,12}$	-0.00	$F_{4,8,11,12}$	-0.01
$F_{5,8,11,12}$	0.03	$F_{6,8,11,12}$	-0.01	$F_{7,8,11,12}$	0.02

Table B29: F12-TZ-cCR Force Constants for HOOF (cont.)

$F_{8,8,11,12}$	-0.22	$F_{1,9,11,12}$	-0.00	$F_{2,9,11,12}$	0.00
$F_{3,9,11,12}$	-0.01	$F_{4,9,11,12}$	-0.00	$F_{5,9,11,12}$	0.10
$F_{6,9,11,12}$	0.05	$F_{7,9,11,12}$	-0.01	$F_{8,9,11,12}$	0.46
$F_{9,9,11,12}$	-0.90	$F_{1,10,11,12}$	0.00	$F_{2,10,11,12}$	0.00
$F_{3,10,11,12}$	-0.00	$F_{4,10,11,12}$	0.01	$F_{5,10,11,12}$	-0.00
$F_{6,10,11,12}$	0.00	$F_{7,10,11,12}$	-0.15	$F_{8,10,11,12}$	-0.01
$F_{9,10,11,12}$	0.02	$F_{10,10,11,12}$	0.14	$F_{1,11,11,12}$	-0.00
$F_{2,11,11,12}$	-0.00	$F_{3,11,11,12}$	-0.00	$F_{4,11,11,12}$	0.00
$F_{5,11,11,12}$	0.01	$F_{6,11,11,12}$	0.05	$F_{7,11,11,12}$	-0.01
$F_{8,11,11,12}$	0.19	$F_{9,11,11,12}$	-0.56	$F_{10,11,11,12}$	0.01
$F_{11,11,11,12}$	-0.20	$F_{1,1,12,12}$	-0.00	$F_{1,2,12,12}$	-0.00
$F_{2,2,12,12}$	0.00	$F_{1,3,12,12}$	0.00	$F_{2,3,12,12}$	0.00
$F_{3,3,12,12}$	-0.02	$F_{1,4,12,12}$	0.00	$F_{2,4,12,12}$	0.01
$F_{3,4,12,12}$	-0.01	$F_{4,4,12,12}$	-0.01	$F_{1,5,12,12}$	0.00
$F_{2,5,12,12}$	0.00	$F_{3,5,12,12}$	-0.01	$F_{4,5,12,12}$	-0.01
$F_{5,5,12,12}$	-0.03	$F_{1,6,12,12}$	-0.00	$F_{2,6,12,12}$	0.00
$F_{3,6,12,12}$	0.01	$F_{4,6,12,12}$	-0.00	$F_{5,6,12,12}$	0.02
$F_{6,6,12,12}$	0.22	$F_{1,7,12,12}$	0.00	$F_{2,7,12,12}$	-0.00
$F_{3,7,12,12}$	-0.00	$F_{4,7,12,12}$	-0.03	$F_{5,7,12,12}$	-0.00
$F_{6,7,12,12}$	-0.00	$F_{7,7,12,12}$	-0.14	$F_{1,8,12,12}$	-0.01
$F_{2,8,12,12}$	-0.00	$F_{3,8,12,12}$	0.00	$F_{4,8,12,12}$	0.00
$F_{5,8,12,12}$	0.09	$F_{6,8,12,12}$	0.07	$F_{7,8,12,12}$	-0.01
$F_{8,8,12,12}$	0.37	$F_{1,9,12,12}$	0.01	$F_{2,9,12,12}$	-0.00
$F_{3,9,12,12}$	0.00	$F_{4,9,12,12}$	-0.00	$F_{5,9,12,12}$	-0.15
$F_{6,9,12,12}$	-0.13	$F_{7,9,12,12}$	0.01	$F_{8,9,12,12}$	-0.71
$F_{9,9,12,12}$	0.95	$F_{1,10,12,12}$	-0.00	$F_{2,10,12,12}$	-0.00
$F_{3,10,12,12}$	0.01	$F_{4,10,12,12}$	0.05	$F_{5,10,12,12}$	0.01
$F_{6,10,12,12}$	0.00	$F_{7,10,12,12}$	0.17	$F_{8,10,12,12}$	0.01
$F_{9,10,12,12}$	-0.02	$F_{10,10,12,12}$	-0.21	$F_{1,11,12,12}$	0.01
$F_{2,11,12,12}$	0.00	$F_{3,11,12,12}$	0.00	$F_{4,11,12,12}$	-0.00
$F_{5,11,12,12}$	-0.06	$F_{6,11,12,12}$	-0.08	$F_{7,11,12,12}$	0.01
$F_{8,11,12,12}$	-0.45	$F_{9,11,12,12}$	0.86	$F_{10,11,12,12}$	-0.02
$F_{11,11,12,12}$	0.51	$F_{1,12,12,12}$	-0.02	$F_{2,12,12,12}$	-0.00
$F_{3,12,12,12}$	-0.00	$F_{4,12,12,12}$	0.01	$F_{5,12,12,12}$	0.15
$F_{6,12,12,12}$	-0.11	$F_{7,12,12,12}$	-0.01	$F_{8,12,12,12}$	0.64
$F_{9,12,12,12}$	-0.83	$F_{10,12,12,12}$	0.01	$F_{11,12,12,12}$	-0.78
$F_{12,12,12,12}$	0.95				

Table B30: F12-TZ-cCR Harmonic and Anharmonic Vibrational Frequencies for HOOF Isotopologues

Mode	$HOO^{18}F$	$HO^{18}O^{18}F$	DOOF	$DOO^{18}F$	$DO^{18}O^{18}F$
ω_1	3711.3	3698.9	2704.0	2704.0	2686.7
ω_2	1460.2	1456.0	1089.4	1081.8	1077.1
ω_3	951.5	927.0	975.5	949.9	924.7
ω_4	733.4	729.2	758.9	732.6	728.5
ω_5	541.8	536.2	494.6	491.4	479.4
ω_6	462.2	455.5	379.3	377.2	376.7
ν_1	3510.3	3499.1	2597.3	2597.3	2581.2
ν_2	1411.6	1424.0	1055.9	1043.4	1040.1
ν_3	917.0	897.3	946.0	923.2	899.8
ν_4	713.4	708.9	1161.2	707.2	703.1
ν_5	515.5	509.8	481.9	479.0	467.5
ν_6	451.6	445.7	366.0	364.2	363.9
ZPT	3870.1	3842.0	3164.7	3132.7	3101.5

Table B31: Spectroscopic Constants and Geometrical Parameters of HOOF Isotopologues

Constant	Units	$HOO^{18}F$	$HO^{18}O^{18}F$	DOOF	$DOO^{18}F$	$DO^{18}O^{18}F$
R_e(H-O_1)	Å	0.96864	0.96864	0.96864	0.96864	0.96864
R_e(O_1-O_2)	Å	1.36969	1.36969	1.36969	1.36969	1.36969
R_e(O_2-F)	Å	1.46121	1.46121	1.46121	1.46121	1.46121
$\angle_e$(H-O_1-O_2)	°	102.71	102.71	102.71	102.71	102.71
$\angle_e$(O_1-O_2-F)	°	105.43	105.43	105.43	105.43	105.43
A_e	MHz	51697.4	50772.3	50173.0	46875.2	46192.9
B_e	MHz	10783.5	10233.1	10279.6	10277.8	9789.7
C_e	MHz	9186.8	8759.6	8982.7	8870.3	8489.5
R_0(H-O_1)	Å	0.96625	0.96623	0.96822	0.96807	0.96806
R_0(O_1-O_2)	Å	1.37902	1.37878	1.37825	1.37810	1.37786
R_0(O_2-F)	Å	1.46798	1.46801	1.46847	1.46827	1.46829
$\angle_0$(H-O_1-O_2)	°	102.90	102.91	102.80	102.80	102.81
$\angle_0$(O_1-O_2-F)	°	105.42	105.42	105.44	105.44	105.44
A_0	MHz	51485.8	50567.3	49998.2	46719.4	46038.6
B_0	MHz	10698.3	10152.7	10195.3	10195.8	9712.2
C_0	MHz	9095.1	8673.1	8894.3	8784.6	8408.4
A_1	MHz	51381.0	50468.0	49788.9	46537.5	45865.2
B_1	MHz	10688.8	10144.8	10185.2	10185.7	9703.4
C_1	MHz	9093.5	8672.4	8890.0	8780.5	8405.3
A_2	MHz	51406.8	50497.0	50170.6	46828.5	46130.0
B_2	MHz	10670.9	10125.1	10172.3	10174.7	9690.4
C_2	MHz	9082.2	8659.7	8886.2	8778.2	8401.0
A_3	MHz	51255.7	50387.5	49639.3	46420.0	45793.3
B_3	MHz	10652.5	10107.1	10150.1	10150.5	9668.5
C_3	MHz	9072.6	8652.6	8874.3	8763.3	8389.1
A_4	MHz	51193.3	50245.3	49681.1	46437.0	45738.1
B_4	MHz	10629.1	10089.1	10127.8	10131.4	9652.2
C_4	MHz	9015.3	8595.4	8811.4	8709.0	8334.7
A_5	MHz	51414.7	50455.6	50375.0	47076.5	46386.9
B_5	MHz	10703.4	10162.3	10144.6	10145.8	9668.0
C_5	MHz	9075.8	8658.7	8837.7	8727.1	8356.2
A_6	MHz	51839.9	50940.5	49984.9	46705.2	46009.7
B_6	MHz	10675.1	10126.1	10222.6	10223.0	9735.5
C_6	MHz	9047.6	8626.5	8889.7	8778.4	8402.0
Δ_J	kHz	14.730	13.256	13.871	13.613	12.277
Δ_K	MHz	1.127	1.092	970.104	860.606	830.384
Δ_{JK}	kHz	-0.000	-0.000	-0.000	-0.000	-0.000
δ_J	kHz	3.066	2.693	2.659	2.787	2.439
δ_K	kHz	47.391	43.568	25.511	27.070	24.310
Φ_J	mHz	15.547	13.538	21.446	21.121	17.049
Φ_K	Hz	83.469	78.894	63.441	53.915	50.313
Φ_{JK}	mHz	110.812	98.804	-55.867	-63.370	-59.328
Φ_{KJ}	Hz	-13.368	-12.335	-10.161	-8.930	-8.195
ϕ_j	mHz	9.551	8.062	11.743	11.766	9.428
ϕ_{jk}	mHz	-49.231	-42.761	87.164	61.721	37.643
ϕ_k	Hz	13.433	12.269	8.646	8.035	6.723

APPENDIX C

Supporting information for Chapter 5: "Computing Accurate Rovibrational Spectral Data for Relevant Aluminum-bearing Species in Interstellar and Atmospheric Chemistry"

Table C1: Harmonic frequencies (in cm^{-1}) and zero-point (ZPT) energies for AlH, AlO^- and AlO.

	AlH		AlO^-		AlO	
Level of Theory	ω	ZPT	ω	ZPT	ω	ZPT
aTZ	1665.3	826.9	931.6	2.7	955.5	487.5
aCTZ	1663.0	826.0	940.2	1.8	953.4	478.8
awCTZ	1668.0	828.5	948.8	0.9	960.8	481.3
F12-TZ	1688.5	838.2	955.2	0.2	980.3	491.5
F12-TcC	1688.3	838.9	950.9	0.6	981.4	491.5
F12-TZR	1687.2	837.3	951.0	0.6	981.2	495.3
F12-TcCR	1686.9	837.3	945.2	1.2	981.7	493.4
F12-TcCR+TZ	1686.9	836.8	958.5	0.2	981.7	492.2
Split basis TcC	1688.5	838.2	977.6	2.2	981.3	494.6
Split basis TcCR	1687.2	837.2	954.5	0.3	980.4	491.3

Table C2: Spectroscopic constants (MHz) and dipole moment (D) for AlH.

Const.	aTZ	aCTZ	awCTZ	F12−TZ	F12−TcC
B_e	189027.9	190497.6	191605.1	191040.5	192149.4
B_0	186333.4	187788.6	188761.9	188294.2	189360.6
B_1	180944.4	182370.7	183075.5	182801.6	183783.1
D_e	10.843	11.128	11.256	10.886	11.080
Dipole				0.09	

F12−TZR	F12−TcCR	F12−TcCR+TZ	Split basis TcC	Split basis TcCR
191040.5	192149.4	192149.4	191040.5	191040.5
188292.0	189357.0	189285.2	188289.2	188294.2
182794.8	183772.2	183556.9	182786.5	182801.6
10.904	11.098	11.098	10.904	10.886

Table C3: Spectroscopic constants (MHz) and dipole moment (D) for AlO

Const.	aTZ	aCTZ	awCTZ	F12-TZ	F12-TcC	F12-TZR
B_e	18661.2	18906.1	19041.9	19046.7	19182.5	19052.7
B_0	18609.9	18832.6	18963.3	18973.4	19106.5	18986.4
B_1	18507.5	18685.7	18805.9	18826.7	18954.4	18853.9
D_e	31.686	33.095	33.294	32.007	32.621	31.981
H_e	32.091	2.474	−4.742	1.131	−1.389	11.352
Dipole				4.42		

F12-TcCR	F12-TcCR+TZ	Split Basis TcC	Split Basis TcCR
19188.8	19188.8	19055.1	19048.8
19117.7	19115.2	18988.8	18975.4
18975.3	18968.0	18856.0	18828.5
32.639	32.639	31.986	32.014
5.852	2.232	11.236	0.984

Const.	Units	aTZ	aCTZ	awCTZ	F12-TZ	F12-TcC
B_e	MHz	18245.5	18497.1	18623.0	18576.8	18732.6
B_0	MHz	18173.8	18424.1	18549.5	18504.5	18659.2
B_1	MHz	18030.4	18278.2	18402.6	18359.9	18512.4
D_e	kHz	30.491	31.180	31.257	30.620	30.978
Dipole	D					1.34

Const.	Units	F12-TZR	F12-TcCR	F12-TcCR+TZ	Split Basis TcC	Split Basis TcCR
B_e	MHz	18576.8	18732.6	18732.6	19048.3	18579.0
B_0	MHz	18504.3	18658.6	18657.3	18974.4	18506.5
B_1	MHz	18359.1	18510.4	18506.5	18826.7	18361.4
D_e	kHz	30.758	31.121	31.121	32.003	30.760

Table C4: Spectroscopic rotational constants (MHz), centrifugal distortion constants (kHz), and dipole moment (D) for AlO^-

Table C5: Rotational spectral constants for AlO_2^-

Const.	Units	aTZ	aCTZ	awCTZ	F12−TZ
B_e	MHz	5793.7	5869.3	5906.6	5887.8
B_0	MHz	5779.3	5855.0	5892.1	5873.6
B_1	MHz	5747.9	5823.1	5860.1	5842.0
B_2	MHz	5762.2	5837.7	5874.7	5856.5
B_3	MHz	5789.0	5865.2	5902.3	5883.8
D_e	kHz	1.428	1.459	1.463	1.433
H_e	μHz	9.725	9.804	7.871	12.012
F12−TcC	F12−TZR	F12−TcCR	F12−TcCR+TZ	Split Basis TcC	
5941.4	5887.8	5941.4	5941.4	5888.5	
5924.6	5873.6	5926.0	5927.2	5874.3	
5892.3	5841.9	5894.4	5894.5	5842.7	
5905.7	5856.3	5908.8	5909.4	5857.2	
5933.2	5883.7	5935.0	5938.3	5884.5	
1.450	10.324	1.456	1.456	1.433	
−49.637	1.439	19.558	−6.619	11.096	

Table C6: Harmonic vibrational frequencies and zero-point energies (in cm^{-1}) for AlO_3^-

Mode	Symm.	aTZ	aCTZ	awCTZ	F12-TZ	F12-TcC
ω_1	a_1	1086.9	1080.1	1057.9	1106.6	1116.4
ω_2	b_2	736.8	733.4	697.0	751.8	756.9
ω_3	a_1	661.5	659.8	692.8	680.3	687.4
ω_4	a_1	535.5	535.0	390.7	544.9	546.9
ω_5	b_1	270.1	276.7	284.5	269.8	271.1
ω_6	b_2	258.3	264.4	275.6	258.6	260.0
ZPT		1769.1	1663.1	1652.4	1816.4	1829.2
F12-TZR	F12-TcCR	F12-TcCR+TZ	Split Basis TcC	Split Basis TcCR		
1104.4	1114.1	1114.1	1106.8	1057.8		
751.5	756.5	756.5	751.9	769.3		
678.6	685.6	685.7	680.4	723.3		
545.6	547.6	547.6	545.0	544.0		
270.1	271.4	271.4	269.8	292.6		
258.9	260.4	260.4	258.7	284.9		
1785.0	2635.9	1809.7	1836.2	1806.4		

Table C7: Equilibrium, ground, and vibrationally-excited rotational constants for AlO_3^-

Const.	Units	aTZ	aCTZ	awCTZ	F12-TZ	F12-TcC
A_e	MHz	23630.6	23664.6	20952.8	23921.8	23985.6
B_e	MHz	4460.8	4497.3	4606.1	4539.2	4588.1
C_e	MHz	3752.4	3779.1	3776.0	3815.3	3851.4
A_0	MHz	23452.2	23484.6	20596.1	23747.9	23796.3
B_0	MHz	4453.3	4489.0	4606.6	4531.8	4582.5
C_0	MHz	3737.1	3763.0	3758.2	3800.0	3836.8
A_1	MHz	23430.1	23462.4	20553.6	23725.5	23772.3
B_1	MHz	4432.5	4467.7	4585.0	4510.7	4561.4
C_1	MHz	3722.0	3747.6	3742.6	3784.8	3821.6
A_2	MHz	23295.9	23324.4	20503.4	23598.0	23647.9
B_2	MHz	4449.4	4485.0	4598.5	4527.5	4578.3
C_2	MHz	3730.1	3755.8	3750.5	3792.8	3829.8
A_3	MHz	23565.7	23599.2	20681.7	23860.3	23906.6
B_3	MHz	4436.7	4471.9	4588.7	4514.9	4565.9
C_3	MHz	3723.1	3748.6	3749.0	3785.8	3822.8
A_4	MHz	23177.0	23212.3	19938.6	23474.5	23513.7
B_4	MHz	4464.6	4500.2	4640.7	4543.3	4595.3
C_4	MHz	3734.0	3759.9	3746.2	3796.9	3834.3
A_5	MHz	23385.6	23415.4	20552.1	23681.1	23719.1
B_5	MHz	4456.7	4492.4	4609.3	4535.7	4587.0
C_5	MHz	3744.3	3770.2	3765.3	3807.6	3844.7
A_6	MHz	23501.8	23534.2	20633.4	23800.4	23839.5
B_6	MHz	4464.5	4500.2	4618.6	4543.5	4595.8
C_6	MHz	3738.3	3764.0	3759.9	3801.3	3838.9

Table C8: Equilibrium, ground, and vibrationally-excited rotational constants for AlO_3^- *cont.*

Const.	Units	F12-TZR	F12-TcCR	F12-TcCR+TZ	Split Basis TcC	Split Basis TcCR
A_e	MHz	23921.8	23985.6	23985.5	23926.3	24095.2
B_e	MHz	4539.2	4588.1	4588.1	4539.7	4520.1
C_e	MHz	3815.3	3851.4	3851.4	3815.7	3806.1
A_0	MHz	23750.6	23853.0	23810.8	23751.8	23957.1
B_0	MHz	4531.7	4584.5	4580.5	4532.3	4516.9
C_0	MHz	3799.9	3839.7	3835.8	3800.4	3792.1
A_1	MHz	23727.7	23840.9	23787.7	23729.3	23912.5
B_1	MHz	4510.7	4563.3	4558.7	4511.3	4496.2
C_1	MHz	3784.8	3824.7	3820.1	3785.3	3776.6
A_2	MHz	23597.6	23715.0	23662.0	23601.9	24045.9
B_2	MHz	4527.6	4580.8	4575.9	4528.1	4501.9
C_2	MHz	3792.8	3833.2	3828.4	3793.3	3785.9
A_3	MHz	23865.9	23981.5	23923.2	23863.6	23822.2
B_3	MHz	4514.7	4568.2	4562.9	4515.5	4511.0
C_3	MHz	3785.7	3826.3	3821.1	3786.2	3783.3
A_4	MHz	23480.9	23598.8	23536.4	23478.0	23676.8
B_4	MHz	4543.0	4596.2	4592.3	4543.8	4528.2
C_4	MHz	3796.9	3837.2	3832.8	3797.4	3784.1
A_5	MHz	23683.8	23793.3	23743.5	23684.8	23948.3
B_5	MHz	4535.7	4590.5	4585.0	4536.3	4518.8
C_5	MHz	3807.7	3849.0	3843.9	3808.1	3802.6
A_6	MHz	23805.3	23923.2	23862.5	23803.7	24060.4
B_6	MHz	4543.3	4601.2	4592.9	4544.2	4539.1
C_6	MHz	3801.2	3844.8	3837.4	3801.8	3792.0

Table C9: A- and S-reduced Hamiltonian spectroscopic constants for AlO_3^-

Const.	Units	aTZ	aCTZ	awCTZ	F12-TZ	F12-TcC
Δ_J	Hz	748.365	773.707	891.309	754.697	767.414
Δ_K	kHz	135.560	136.011	206.947	135.561	135.711
Δ_{JK}	kHz	17.207	17.317	13.192	17.919	18.109
δ_J	Hz	135.122	139.932	198.191	136.957	140.335
δ_K	kHz	11.257	11.350	9.745	11.635	11.775
Φ_J	μHz	87.305	86.810	480.381	90.241	119.631
Φ_K	Hz	13.942	13.883	25.538	13.872	13.819
Φ_{JK}	mHz	171.443	169.895	94.074	184.110	193.105
Φ_{KJ}	Hz	1.376	1.429	2.295	1.374	1.312
ϕ_j	μHz	120.517	125.940	322.309	121.535	133.993
ϕ_{jk}	mHz	88.863	88.184	53.807	95.192	100.125
ϕ_k	Hz	3.072	3.043	2.414	3.193	3.204
D_J	Hz	646.263	669.341	770.661	648.042	657.695
D_{JK}	kHz	17.820	17.943	13.916	18.559	18.767
D_K	kHz	135.050	135.489	206.344	135.028	135.163
d_1	Hz	−135.122	−139.932	−198.191	−136.957	−140.335
d_2	Hz	−51.051	−52.183	−60.324	−53.327	−54.860
H_J	μHz	−713.651	−720.060	−219.685	−773.782	−804.342
H_{JK}	mHz	87.200	85.287	9.076	95.603	103.087
H_{KJ}	Hz	1.668	1.723	2.589	1.682	1.626
H_K	Hz	13.735	13.674	25.330	13.653	13.596
h_1	μHz	19.556	23.127	184.264	14.183	22.689
h_2	μHz	400.478	403.435	350.033	432.011	461.987
h_3	μHz	100.962	102.813	138.045	107.352	111.305

Table C10: A- and S-reduced Hamiltonian spectroscopic constants for AlO_3^- *cont.*

Const.	Units	F12-TZR	F12-TcCR	F12-TcCR+TZ	Split Basis TcC	Split Basis TcCR
Δ_J	Hz	757.112	769.909	769.887	754.722	786.810
Δ_K	kHz	134.485	134.628	134.616	135.599	83.411
Δ_{JK}	kHz	18.152	18.341	18.355	17.919	72.387
δ_J	Hz	137.263	140.657	140.654	136.947	143.223
δ_K	kHz	11.750	11.889	11.896	11.635	23.784
Φ_J	μHz	91.535	124.481	90.738	89.764	−1.333 (mHZ)
Φ_K	Hz	13.677	13.718	13.616	13.882	16.298
Φ_{JK}	mHz	186.613	204.450	193.028	184.622	1.367 (Hz)
Φ_{KJ}	Hz	1.400	1.419	1.363	1.369	−1.743
ϕ_j	μHz	122.519	133.390	125.282	121.359	−172.278
ϕ_{jk}	mHz	96.483	105.641	99.754	95.441	631.359
ϕ_k	Hz	3.229	3.280	3.239	3.193	8.260
D_J	Hz	649.409	659.127	659.037	648.087	573.814
D_{JK}	kHz	18.799	19.005	19.020	18.559	73.665
D_K	kHz	133.947	134.074	134.062	135.066	82.346
d_1	Hz	−137.263	−140.657	−140.654	−136.947	−143.223
d_2	Hz	−53.851	−55.391	−55.425	−53.317	−106.498
H_J	μHz	−783.148	−849.823	−828.491	−776.400	−6.401 (mHz)
H_{JK}	mHz	97.004	112.422	101.821	96.147	1.138 (Hz)
H_{KJ}	Hz	1.712	1.740	1.681	1.677	−904.879 (mHz)
H_K	Hz	13.456	13.490	13.390	13.663	15.693
h_1	μHz	13.831	19.393	12.625	14.048	−462.340
h_2	μHz	437.341	487.152	459.615	433.082	2.534 (mHZ)
h_3	μHz	108.688	113.998	112.657	107.311	290.061

Table C11: Spectroscopic Constants of AlH_3

Const.	Units	aTZ	aCTZ	awCTZ	F12-TZ	F12-TcC
A_e	MHz	132971.1	134298.7	134955.2	133833.5	135026.8
C_e	MHz	66485.6	67149.4	67477.6	66916.7	67513.4
A_0	MHz	131553.4	132865.1	133444.3	132407.7	134772.5
C_0	MHz	65605.9	66257.2	66547.9	66034.4	66540.9
A_1	MHz	130526.0	131823.6	132363.4	131377.0	133731.5
C_1	MHz	65091.9	65736.1	66007.1	65518.7	66020.0
A_2	MHz	130792.9	132093.2	132666.0	131652.2	134020.9
C_2	MHz	65907.4	66567.9	66858.5	66346.7	66864.1
A_3	MHz	130607.6	131919.6	132447.1	131458.1	133824.1
C_3	MHz	64620.0	65259.0	65523.7	65043.5	66128.0
A_4	MHz	131975.3	133283.7	133860.1	132824.7	136362.7
C_4	MHz	65818.2	66468.3	66757.5	66244.7	66080.1
D_J	MHz	6.342	6.467	6.468	6.338	6.433
D_{JK}	MHz	−11.283	−11.501	−11.496	−11.275	−11.440
D_K	MHz	5.291	5.392	5.388	5.287	5.364
d_1	Hz	−32.285	−32.613	−33.854	−32.026	−37.416
d_2	Hz	158.395	161.410	164.255	158.379	784.463
H_J	kHz	0.894	0.917	0.910	0.885	1.368
H_{JK}	kHz	−3.323	−3.411	−3.385	−3.292	−4.659
H_{KJ}	kHz	3.974	4.081	4.051	3.939	5.219
H_K	kHz	−1.543	−1.585	−1.574	−1.530	−1.929
h_1	Hz	0.041	0.042	0.021	0.088	−232.077
h_2	mHz	−24.581	−27.979	−29.201	−20.386	−729.895
h_3	Hz	−56.372	−55.850	−54.639	−52.839	−51.767

Table C12: Spectroscopic Constants of AlH_3 *cont.*

Const.	Units	F12-TZR	F12-TcCR	F12-TcCR+TZ	Split Basis TcC	Split Basis TcCR
A_e	MHz	133833.5	135026.8	135026.8	133833.5	133833.5
C_e	MHz	66916.7	67513.4	67513.4	66916.7	66916.7
A_0	MHz	132400.2	133576.6	133570.1	132407.4	133542.9
C_0	MHz	66029.8	66613.4	66612.7	66034.4	65940.3
A_1	MHz	131366.3	132524.3	132499.6	131376.7	132509.4
C_1	MHz	65512.5	66086.8	66077.1	65518.7	65423.2
A_2	MHz	131641.7	132807.1	132827.8	131651.9	132784.9
C_2	MHz	66340.6	66927.4	66940.2	66346.6	66251.3
A_3	MHz	131448.9	132620.3	132579.2	131457.5	132590.6
C_3	MHz	65037.1	65609.1	65593.8	65043.3	65529.4
A_4	MHz	132814.5	133993.4	134010.7	132824.4	135100.2
C_4	MHz	66238.7	66824.0	66834.9	66244.7	65477.7
D_J	MHz	6.327	6.421	6.421	6.338	6.327
D_{JK}	MHz	−11.250	−11.414	−11.414	−11.275	−11.250
D_K	MHz	5.274	5.350	5.350	5.287	5.274
d_1	Hz	−20.657	−133.708	−520.197	−31.393	−22.221
d_2	Hz	98.918	438.198	528.413	151.612	376.035
H_J	kHz	0.881	1.356	1.364	885.251	881.100
H_{JK}	kHz	−3.274	−4.623	−4.641	−3.292	−3.276
H_{KJ}	kHz	3.917	5.181	5.196	3.939	3.918
H_K	kHz	−1.521	−1.916	−1.919	−1.530	−1.522
h_1	Hz	0.019	−226.770	−228.453	0.026	0.468
h_2	mHz	−91.688	−322.341	−95.157	−25.965	−166.770
h_3	Hz	−52.400	−53.248	−54.900	−52.816	−52.652

Table C13: Harmonic vibrational frequencies and zero-point energies (in cm^{-1}) for $AlNH_4$

Mode	Symm.	aTZ	aCTZ	awCTZ	F12-TZ	F12-TcC
ω_1	b_2	3663.9	3668.9	3671.1	3673.6	3681.1
ω_2	a_1	3574.1	3578.6	3581.0	3582.7	3589.6
ω_3	b_2	1948.6	1953.6	1960.8	1961.2	1971.8
ω_4	a_1	1943.6	1949.3	1956.3	1957.5	1967.8
ω_5	a_1	1581.6	1582.6	1584.3	1582.0	1582.5
ω_6	a_1	824.8	832.6	836.7	836.9	842.9
ω_7	a_1	752.1	757.0	760.2	757.2	762.7
ω_8	b_2	729.6	730.4	732.3	732.6	736.5
ω_9	b_1	619.1	618.7	619.2	614.4	617.7
ω_{10}	a_2	497.2	497.7	499.6	495.0	498.3
ω_{11}	b_1	439.4	449.1	457.0	448.9	456.7
ω_{12}	b_2	424.6	425.3	426.2	426.0	428.3
ZPT		8393.5	8417.3	8432.1	8426.7	8495.6
F12-TZR	F12-TcCR	F12-TcCR+TZ	Split Basis TcC	Split Basis TcCR		
3672.3	3679.9	3679.8	3673.9	3672.7		
3580.9	3587.8	3587.8	3583.1	3581.3		
1958.8	1969.4	1969.3	1961.2	1958.7		
1955.1	1965.4	1965.4	1957.5	1955.1		
1581.9	1582.4	1582.4	1582.1	1582.0		
835.9	841.9	841.9	836.9	835.9		
758.0	763.8	763.6	757.2	758.0		
733.8	737.8	737.7	732.6	733.8		
616.1	619.5	619.3	614.3	616.1		
495.6	499.6	498.8	495.0	495.5		
445.2	453.3	453.3	448.7	445.0		
427.8	430.5	430.0	426.0	427.8		
8438.6	7605.3	8455.9	8439.0	8433.6		

Table C14: Equilibrium, ground, and vibrationally-excited rotational constants for $AlNH_4$

Const.	Units	aTZ	aCTZ	awCTZ	F12-TZ	F12-TcC
A_e	MHz	94884.7	95576.3	95954.9	95478.0	96110.8
B_e	MHz	12933.0	13080.2	13145.8	13074.1	13194.3
C_e	MHz	11381.7	11505.6	11561.8	11499.5	11601.6
A_0	MHz	94520.7	95218.3	95550.5	95063.4	95674.0
B_0	MHz	12870.8	13018.8	13082.5	13015.9	13143.5
C_0	MHz	11310.5	11434.6	11488.4	11430.3	11537.5
A_1	MHz	94271.0	94964.8	95293.2	94810.9	95418.4
B_1	MHz	12849.4	12997.0	13060.5	12994.8	13122.5
C_1	MHz	11292.5	11416.2	11469.8	11412.4	11519.6
A_2	MHz	94098.3	94791.9	95119.6	94636.2	95242.0
B_2	MHz	12854.0	13001.8	13065.4	12999.7	13127.5
C_2	MHz	11291.5	11415.4	11469.0	11411.7	11518.9
A_3	MHz	93917.3	94607.5	94896.5	94432.0	95039.0
B_3	MHz	12863.3	13011.5	13075.6	13009.2	13136.7
C_3	MHz	11298.1	11422.4	11475.9	11418.4	11525.5
A_4	MHz	93690.1	94376.4	94673.7	94214.4	94816.2
B_4	MHz	12866.8	13015.3	13079.1	13012.7	13140.6
C_4	MHz	11295.9	11419.9	11473.2	11415.5	11522.8
A_5	MHz	94913.4	95616.8	95951.7	95437.2	96056.3
B_5	MHz	12887.3	13035.9	13099.3	13034.3	13162.7
C_5	MHz	11300.4	11424.4	11477.7	11420.7	11528.1
A_6	MHz	94681.6	95382.8	95721.2	95225.0	95832.1
B_6	MHz	12837.7	12985.5	13050.5	12981.6	13109.4
C_6	MHz	11249.9	11373.6	11427.4	11369.6	11477.2
A_7	MHz	95066.3	95753.2	96064.0	95582.9	96191.6
B_7	MHz	12871.0	13018.9	13082.1	13017.0	13146.4
C_7	MHz	11322.3	11443.0	11496.4	11441.5	11547.8
A_8	MHz	96994.5	97762.8	98124.8	97565.3	98225.5
B_8	MHz	12907.2	13055.6	13118.4	13052.9	13181.4
C_8	MHz	11277.6	11404.5	11457.1	11398.1	11507.4
A_9	MHz	93380.1	94051.3	94388.4	93906.7	94485.5
B_9	MHz	12834.1	12982.4	13045.8	12981.3	13110.9
C_9	MHz	11323.9	11448.5	11502.6	11444.5	11552.9
A_{10}	MHz	94170.3	94869.6	95197.3	94707.2	95307.0
B_{10}	MHz	12831.6	12979.9	13042.9	12976.9	13107.4
C_{10}	MHz	11312.7	11437.2	11490.7	11433.0	11542.4
A_{11}	MHz	92709.7	93381.6	93679.4	93227.5	93793.6
B_{11}	MHz	12829.3	12977.7	13039.8	12975.5	13106.1
C_{11}	MHz	11308.4	11433.2	11485.8	11429.2	11538.5
A_{12}	MHz	95627.7	96345.5	96687.3	96185.9	96807.0
B_{12}	MHz	12892.7	13040.8	13103.8	13038.4	13169.3
C_{12}	MHz	11310.8	11435.2	11488.4	11430.9	11540.8

Table C15: Equilibrium, ground, and vibrationally-excited rotational constants for $AlNH_4$ *cont.*

Const.	Units	F12-TZR	F12-TcCR	F12-TcCR+TZ	Split Basis TcC	Split Basis TcCR
A_e	MHz	95478.0	96110.8	96110.8	95481.8	95481.8
B_e	MHz	13074.1	13194.3	13194.3	13075.0	13075.0
C_e	MHz	11499.5	11601.6	11601.6	11500.2	11500.2
A_0	MHz	95049.0	95697.1	95698.0	95068.2	95053.0
B_0	MHz	13015.2	13101.9	13135.0	13016.6	13016.2
C_0	MHz	11429.9	11506.0	11531.6	11431.0	11430.8
A_1	MHz	94795.7	95445.2	95440.0	94816.0	94799.8
B_1	MHz	12994.1	13079.1	13113.6	12995.5	12995.1
C_1	MHz	11412.0	11486.8	11513.4	11413.1	11412.9
A_2	MHz	94620.3	95266.6	95262.4	94641.2	94624.3
B_2	MHz	12999.0	13084.1	13118.6	13000.4	13000.0
C_2	MHz	11411.3	11486.1	11512.7	11412.3	11412.1
A_3	MHz	94418.3	95069.4	95041.1	94436.9	94422.1
B_3	MHz	13008.5	13092.4	13128.0	13009.9	13009.5
C_3	MHz	11418.0	11492.0	11519.1	11419.1	11418.9
A_4	MHz	94200.9	94840.3	94825.2	94219.3	94204.9
B_4	MHz	13012.0	13096.4	13131.6	13013.4	13013.0
C_4	MHz	11415.1	11489.3	11516.3	11416.1	11416.0
A_5	MHz	95419.7	96064.7	96075.6	95442.1	95423.5
B_5	MHz	13033.6	13118.8	13153.8	13035.0	13034.6
C_5	MHz	11420.3	11494.7	11521.9	11421.4	11421.2
A_6	MHz	95220.8	95847.1	95869.7	95229.9	95224.3
B_6	MHz	12983.1	13063.8	13099.8	12982.3	12984.1
C_6	MHz	11369.6	11440.8	11469.1	11370.2	11370.4
A_7	MHz	95558.0	96214.8	96225.3	95588.2	95561.9
B_7	MHz	13015.3	13097.9	13135.1	13017.8	13016.3
C_7	MHz	11442.1	11512.8	11541.7	11442.1	11442.9
A_8	MHz	97531.3	98233.9	98230.1	97569.7	97534.8
B_8	MHz	13051.8	13131.1	13172.4	13053.6	13052.9
C_8	MHz	11396.0	11468.1	11499.9	11398.8	11396.9
A_9	MHz	93888.3	94486.8	94541.9	93910.9	93891.5
B_9	MHz	12978.9	13061.7	13099.2	12982.0	12980.0
C_9	MHz	11444.0	11516.6	11546.3	11445.1	11444.9
A_{10}	MHz	94689.8	95342.0	95339.8	94712.3	94694.4
B_{10}	MHz	12976.6	13055.0	13096.4	12977.7	12977.5
C_{10}	MHz	11432.7	11502.6	11534.6	11433.7	11433.4
A_{11}	MHz	93224.5	93880.0	93858.0	93233.5	93230.1
B_{11}	MHz	12974.4	13044.3	13095.0	12976.1	12975.4
C_{11}	MHz	11428.6	11492.2	11531.2	11429.7	11429.5
A_{12}	MHz	96162.2	96846.9	96841.9	96191.2	96166.1
B_{12}	MHz	13037.2	13112.8	13157.3	13039.1	13038.4
C_{12}	MHz	11430.5	11498.5	11532.7	11431.6	11431.4

Table C16: A- and S-reduced Hamiltonian spectroscopic constants for $AlNH_4$

Const.	Units	aTZ	aCTZ	awCTZ	F12-TZ	F12-TcC
Δ_J	kHz	12.023	12.245	12.344	12.151	12.290
Δ_K	MHz	1.616	1.633	1.639	1.630	1.640
Δ_{JK}	kHz	190.774	192.663	194.322	192.296	193.450
δ_J	kHz	1.589	1.628	1.644	1.621	1.643
δ_K	kHz	138.309	140.377	141.733	140.576	141.516
Φ_J	mHz	2.654	2.902	2.890	2.957	3.743
Φ_K	Hz	122.012	122.338	121.747	122.502	122.215
Φ_{JK}	Hz	2.193	2.231	2.261	2.262	2.295
Φ_{KJ}	Hz	−8.833	−8.660	−8.697	−9.068	−8.707
ϕ_j	mHz	2.521	2.630	2.656	2.639	2.822
ϕ_{jk}	Hz	1.152	1.172	1.188	1.189	1.212
ϕ_k	Hz	80.109	81.269	82.375	81.820	82.115
D_J	kHz	11.375	11.582	11.673	11.486	11.617
D_{JK}	kHz	194.665	196.644	198.350	196.288	197.488
D_K	MHz	1.613	1.630	1.636	1.627	1.637
d_1	kHz	−1.589	−1.628	−1.644	−1.621	−1.643
d_2	Hz	−324.206	−331.759	−335.671	−332.607	−336.553
H_J	mHz	−3.929	−3.867	−3.981	−3.890	−3.261
H_{JK}	mHz	834.508	842.004	850.634	863.605	885.769
H_{KJ}	Hz	−4.207	−3.930	−3.891	−4.303	−3.904
H_K	Hz	118.751	119.003	118.359	119.143	118.829
h_1	mHz	1.702	1.785	1.797	1.787	1.959
h_2	mHz	3.291	3.384	3.435	3.423	3.502
h_3	μHz	818.983	844.433	859.700	851.555	862.934

Table C17: A- and S-reduced Hamiltonian spectroscopic constants for $AlNH_4$ *cont.*

Const.	Units	F12-TZR	F12-TcCR	F12-TcCR+TZ	Split Basis TcC	Split Basis TcCR
Δ_J	kHz	12.190	12.329	12.330	12.152	12.191
Δ_K	MHz	1.632	1.642	1.642	1.630	1.632
Δ_{JK}	kHz	187.437	188.192	188.785	192.313	187.446
δ_J	kHz	1.625	1.646	1.646	1.621	1.625
δ_K	kHz	138.077	138.788	139.108	140.591	138.088
Φ_J	mHz	2.938	605.624 (μHz)	2.387	2.956	2.940
Φ_K	Hz	121.375	118.794	122.668	122.542	121.405
Φ_{JK}	Hz	2.188	1.902	2.211	2.262	2.191
Φ_{KJ}	Hz	−9.723	−7.558	−9.228	−9.057	−9.750
ϕ_j	mHz	2.626	2.238	2.561	2.638	2.625
ϕ_{jk}	Hz	1.150	995.189 (mHz)	1.160	1.189	1.151
ϕ_k	Hz	79.539	78.562	79.746	81.836	79.554
D_J	kHz	11.536	11.668	11.668	11.486	11.537
D_{JK}	kHz	191.357	192.153	192.755	196.305	191.367
D_K	MHz	1.628	1.638	1.638	1.627	1.629
d_1	kHz	−1.625	−1.646	−1.646	−1.621	−1.625
d_2	Hz	−326.695	−330.065	−330.826	−332.661	−326.740
H_J	mHz	−3.748	−5.392	−4.391	−3.890	−3.752
H_{JK}	mHz	832.206	549.541	845.026	862.783	834.471
H_{KJ}	Hz	−5.103	−2.960	−4.572	−4.292	−5.129
H_K	Hz	118.118	115.554	119.386	119.182	118.147
h_1	mHz	1.800	1.412	1.724	1.786	1.799
h_2	mHz	3.343	2.999	3.389	3.423	3.346
h_3	μHz	825.752	825.514	836.401	851.799	825.978
0.000						

Table C18: Harmonic and anharmonic vibrational frequencies (in cm^{-1}) and IR intensities (in parentheses in km mol^{-1} computed at B3LYP/aTZ) for $HAlO_2$

Mode	Symm.	Desc.	aTZ	aCTZ	awCTZ	F12-TZ
ω_1	a_1	S(AlH)	2049.7 (63)	2053.3	2061.3	2057.1
ω_2	a_1	SS (AlO)	923.0 (51)	931.0	937.7	943.2
ω_3	b_2	AS (AlO)	758.0 (24)	768.2	774.8	777.9
ω_4	a_1	S (OO)	512.6 (24)	516.4	519.3	525.0
ω_5	b_2	Bend (HAlO)	521.7 (86)	521.2	522.6	520.9
ω_6	b_1	OPB (HAlO)	487.5 (138)	484.9	482.2	477.1
ν_1	a_1	S(AlH)	1987.1	1990.7	1995.4	1994.8
ν_2	a_1	SS (AlO)	905.9	912.3	918.6	929.2
ν_3	b_2	AS (AlO)	750.9	762.4	767.6	772.1
ν_4	a_1	S (OO)	494.8	496.2	499.7	511.9
ν_5	b_2	Bend (HAlO)	521.8	520.6	522.5	524.4
ν_6	b_1	OPB (HAlO)	487.2	481.4	479.4	480.6
Mode	F12-TcC	F12-TZR	F12-TcCR	F12-TcCR+TZ	Split Basis TcC	Split Basis TcCR
ω_1	2069.4	2055.8	2068.2	2068.2	2057.1	2055.8
ω_2	950.0	941.8	948.5	948.5	943.3	941.9
ω_3	784.9	776.2	783.2	783.2	777.9	776.2
ω_4	526.7	526.5	528.2	528.2	525.2	526.7
ω_5	523.3	523.1	525.6	525.6	521.0	523.2
ω_6	479.3	478.3	480.5	480.5	477.1	478.2
ν_1	2089.8	1996.0	2042.1	2005.3	1995.6	1993.6
ν_2	940.5	934.8	935.3	926.5	928.2	921.2
ν_3	799.6	789.2	783.9	771.8	769.1	770.2
ν_4	510.9	529.3	534.0	508.2	514.4	508.4
ν_5	652.5	553.8	823.7	520.2	520.5	532.0
ν_6	861.3	505.0	556.0	474.0	484.2	490.7
Mode	Al=1 TcC	Al=1 TcCR	Al=2 TcC	Al=2 TcCR	Al=21 TcC	Al=21 TcCR
ω_1	2069.6	2068.4	2068.9	2067.6	2057.6	2056.3
ω_2	949.0	947.6	948.2	946.8	943.4	942.0
ω_3	784.2	782.4	783.2	781.4	777.9	776.3
ω_4	525.7	527.3	525.6	527.1	525.3	526.9
ω_5	523.4	525.7	523.3	525.6	520.6	522.8
ω_6	478.9	480.1	478.9	480.0	477.5	478.6
ν_1	2036.3	1991.1	2010.4	2018.2	1996.3	1986.1
ν_2	972.8	865.0	922.6	962.4	928.2	898.7
ν_3	873.3	742.6	799.0	795.0	776.6	742.5
ν_4	612.7	466.3	530.5	569.7	515.3	476.9
ν_5	534.8	381.3	496.4	559.5	526.9	500.8
ν_6	626.7	447.4	479.2	506.6	483.3	456.9

Table C19: Rotational Spectroscopic Constants for $HAlO_2$ with A- and S-reduced Hamiltonian spectroscopic constants

Const.	Units	atz	actz	awctz	F12-TZ	F12-TcC
A_e	MHz	22735.4	22829.5	22866.0	23033.5	23091.1
B_e	MHz	13132.5	13355.2	13459.7	13367.8	13519.3
C_e	MHz	8324.2	8426.0	8472.5	8458.7	8527.0
A_0	MHz	22529.7	22625.9	22664.0	22838.3	22851.6
B_0	MHz	13122.6	13344.9	13448.7	13356.0	13509.6
C_0	MHz	8269.9	8371.1	8417.3	8404.8	8467.4
A_1	MHz	22514.3	22610.8	22649.4	22824.2	22833.6
B_1	MHz	13090.7	13312.3	13414.9	13323.4	13476.8
C_1	MHz	8255.1	8356.2	8402.0	8390.0	8452.0
A_2	MHz	22458.6	22555.3	22592.8	22768.5	22775.3
B_2	MHz	13073.7	13294.4	13398.1	13306.0	13457.5
C_2	MHz	8242.3	8343.1	8389.2	8377.0	8438.0
A_3	MHz	22630.9	22726.2	22763.0	22935.9	22927.6
B_3	MHz	13055.1	13275.4	13378.7	13287.7	13442.9
C_3	MHz	8269.7	8369.8	8415.7	8404.0	8464.2
A_4	MHz	22562.1	22660.0	22698.9	22421.4	22425.3
B_4	MHz	13142.9	13365.9	13469.8	13470.5	13625.9
C_4	MHz	8312.0	8459.0	8548.6	8428.8	8515.5
A_5	MHz	22098.5	22196.8	22236.6	22873.4	22876.1
B_5	MHz	13244.5	13466.5	13569.7	13377.1	13529.6
C_5	MHz	8150.2	8205.1	8207.8	8303.8	8338.6
A_6	MHz	22502.5	22599.2	22639.1	22815.8	22792.6
B_6	MHz	13108.9	13333.9	13439.1	13348.1	13505.4
C_6	MHz	8281.6	8383.4	8429.9	8417.5	8476.7

Table C20: A- and S-reduced Hamiltonian spectroscopic constants and dipole moment for $HAlO_2$

Const.	Units	atz	actz	awctz	F12-TZ	F12-TcC
Δ_J	kHz	10.005	10.320	10.405	10.064	10.282
Δ_K	kHz	153.525	153.220	152.389	151.877	152.467
Δ_{JK}	kHz	5.119	4.826	4.565	5.429	4.751
δ_J	kHz	3.432	3.553	3.589	3.452	3.541
δ_K	kHz	15.683	15.744	15.618	15.770	15.643
Φ_J	mHz	29.708	31.151	31.642	29.131	29.573
Φ_K	Hz	-1.969	-1.945	-1.921	-1.769	-1.729
Φ_{JK}	mHz	-388.824	-400.902	-405.642	-372.292	-367.842
Φ_{KJ}	Hz	1.599	1.617	1.617	1.522	1.387
ϕ_j	mHz	15.132	15.870	16.126	14.826	15.139
ϕ_{jk}	mHz	-117.467	-121.197	-122.743	-111.697	-108.557
ϕ_k	Hz	2.069	2.076	2.056	2.002	1.976
D_J	kHz	8.435	8.695	8.769	8.468	8.664
D_{JK}	kHz	14.540	14.577	14.383	15.010	14.458
D_K	kHz	145.674	145.095	144.207	143.893	144.378
d_1	kHz	−3.432	−3.553	−3.589	−3.452	−3.541
d_2	Hz	−785.047	−812.520	−818.182	−798.414	−808.909
D_e	μHz	0.000	0.000	0.000	0.000	0.000
H_J	mHz	31.987	33.411	33.971	31.033	30.944
H_{JK}	mHz	−920.472	−948.013	−955.195	−888.861	−882.541
H_{KJ}	Hz	3.337	3.407	3.413	3.216	3.082
H_K	Hz	−3.178	−3.190	−3.171	−2.948	−2.911
h_1	mHz	8.650	8.986	9.111	8.432	8.591
h_2	mHz	−1.140	−1.130	−1.164	−0.951	−0.685
h_3	mHz	6.482	6.884	7.014	6.394	6.548
H_e	μHz	0.000	0.000	0.000	0.000	0.000
Dipole	D				4.55	

Table C21: Equilibrium, ground, and vibrationally-excited rotational constants $HAlO_2$ *cont.*

Const.	Units	F12-TZR	F12-TcCR	F12-TcCR+TZ	Split Basis TcC	Split Basis TcCR
A_e	MHz	23033.5	23091.1	23091.1	23038.2	23038.2
B_e	MHz	13367.8	13519.3	13519.3	13368.8	13368.8
C_e	MHz	8458.7	8527.0	8527.0	8459.7	8459.7
A_0	MHz	22835.0	22898.1	22898.0	22843.5	22844.6
B_0	MHz	13354.6	13503.7	13506.2	13357.0	13355.9
C_0	MHz	8403.8	8471.4	8472.3	8405.9	8405.6
A_1	MHz	22819.9	22880.3	22883.4	22829.4	22830.4
B_1	MHz	13321.9	13470.3	13472.2	13324.4	13323.0
C_1	MHz	8388.8	8455.8	8456.9	8391.1	8390.7
A_2	MHz	22763.7	22827.2	22828.3	22773.9	22774.4
B_2	MHz	13304.2	13453.1	13453.4	13307.0	13305.6
C_2	MHz	8375.6	8443.3	8443.6	8378.2	8377.7
A_3	MHz	22930.1	23003.9	22996.6	22941.4	22942.5
B_3	MHz	13286.2	13431.6	13434.4	13288.7	13287.0
C_3	MHz	8403.0	8470.5	8470.6	8405.1	8405.1
A_4	MHz	22419.3	22493.2	22484.1	22427.2	22431.4
B_4	MHz	13468.0	13617.1	13622.7	13471.4	13469.4
C_4	MHz	8449.3	8559.6	8561.2	8429.1	8450.5
A_5	MHz	22869.5	22933.0	22933.4	22878.9	22880.1
B_5	MHz	13374.8	13525.3	13528.6	13378.1	13377.0
C_5	MHz	8280.3	8305.9	8306.7	8305.8	8283.7
A_6	MHz	22810.7	22865.2	22876.0	22820.9	22821.6
B_6	MHz	13346.4	13493.5	13499.2	13349.2	13347.5
C_6	MHz	8416.1	8481.9	8485.7	8418.6	8418.0

Table C22: A- and S-reduced Hamiltonian spectroscopic constants and dipole moment for $HAlO_2$ *cont.*

Const.	Units	F12-TZR	F12-TcCR	F12-TcCR+TZ	Split Basis TcC	Split Basis TcCR
Δ_J	kHz	10.078	10.296	10.296	10.063	10.076
Δ_K	kHz	150.442	151.018	151.025	151.874	150.438
Δ_{JK}	kHz	5.767	5.099	5.093	5.450	5.789
δ_J	kHz	3.457	3.546	3.547	3.451	3.456
δ_K	kHz	15.968	15.846	15.843	15.779	15.977
Φ_J	mHz	28.723	29.794	30.291	29.128	28.933
Φ_K	Hz	−1.739	−1.523	−1.762	−1.764	−1.733
Φ_{JK}	mHz	−363.458	−350.845	−390.942	−372.390	−367.481
Φ_{KJ}	Hz	1.476	1.329	1.564	1.524	1.502
ϕ_j	mHz	14.630	15.160	15.419	14.822	14.719
ϕ_{jk}	mHz	−108.681	−100.962	−119.151	−111.771	−110.220
ϕ_k	Hz	1.982	1.939	2.001	2.002	1.986
D_J	kHz	8.461	8.657	8.657	8.466	8.459
D_{JK}	kHz	15.468	14.932	14.924	15.034	15.492
D_K	kHz	142.358	142.824	142.832	143.888	142.352
d_1	kHz	−3.457	−3.546	−3.547	−3.451	−3.456
d_2	Hz	−808.420	−819.427	−819.278	−798.637	−808.635
D_e	μHz	0.000	0.000	0.000	0.000	0.000
H_J	mHz	30.399	30.532	32.660	31.042	30.755
H_{JK}	mHz	−873.376	−851.081	−919.677	−888.827	−879.267
H_{KJ}	Hz	3.150	2.985	3.291	3.216	3.180
H_K	Hz	−2.905	−2.680	−2.962	−2.942	−2.902
h_1	mHz	8.303	8.750	8.767	8.432	8.381
h_2	mHz	−837.906	−0.369	−1.184	−0.957	−0.911
h_3	mHz	6.327	6.410	6.652	6.389	6.337
H_e	μHz	0.000	0.000	0.000	0.000	0.000

Mode	Symm.	Desc.	aTZ	aCTZ	awCTZ	F12-TZ
ω_1	a'	S (OH)	3922.5 (73)	3927.2	3930.7	3946.3
ω_2	a'	S (AlH)	1971.5 (176)	1977.3	1985.7	1984.7
ω_3	a'	S (AlH)	1941.0 (163)	1946.1	1954.5	1954.2
ω_4	a'	S (AlO)	851.1 (160)	860.9	868.4	868.2
ω_5	a'	Bend (HAlH)	767.2 (96)	773.5	778.5	774.8
ω_6	a'	Bend (HOAl)	674.9 (212)	666.6	666.3	665.0
ω_7	a''	OPB (HAlH)	630.6 (224)	630.3	631.5	624.8
ω_8	a'	Bend (HAlH)	492.9 (81)	493.9	495.9	494.0
ω_9	a''	τ (HOAl)	435.9 (104)	436.4	439.4	434.4
ν_1	a'	S (OH)	3748.4	3753.8	3755.6	3769.5
ν_2	a'	S (AlH)	1907.3	1912.2	1917.6	1920.0
ν_3	a'	S (AlH)	1878.5	1883.2	1888.6	1892.1
ν_4	a'	S (AlO)	839.9	848.3	855.2	858.9
ν_5	a'	Bend (HAlH)	762.0	759.4	765.6	767.0
ν_6	a'	Bend (HOAl)	621.8	610.5	614.2	615.7
ν_7	a''	OPB (HAlH)	625.6	624.7	626.3	626.2
ν_8	a'	Bend (HAlH)	489.1	485.3	489.1	493.8
ν_9	a''	τ (HOAl)	405.9	405.2	408.9	412.6

Mode	F12-TcC	F12-TZR	F12-TcCR	F12-TcCR+TZ	Split Basis TcC	Split Basis TcCR
ω_1	3952.7	3943.4	3949.8	3949.8	3946.7	3943.8
ω_2	1995.7	1982.4	1993.3	1993.3	1984.7	1982.4
ω_3	1964.5	1951.8	1962.0	1962.0	1954.2	1951.8
ω_4	874.9	866.9	873.5	873.5	868.3	867.0
ω_5	780.7	775.6	781.5	781.5	774.8	775.7
ω_6	665.5	665.0	665.6	665.6	664.8	664.7
ω_7	628.7	626.4	630.2	630.2	624.8	626.4
ω_8	496.6	494.8	497.4	497.4	494.0	494.8
ω_9	437.7	431.2	434.6	434.6	434.4	431.3
ν_1	3784.4	3767.3	3725.5	3772.3	3769.0	3764.9
ν_2	1842.9	1914.5	1932.2	1926.0	1918.0	1914.0
ν_3	1801.5	1893.0	1802.4	1897.3	1890.0	1886.8
ν_4	675.4	867.3	682.2	859.6	854.4	849.8
ν_5	616.3	780.4	559.5	766.4	761.9	760.5
ν_6	396.8	627.9	330.4	613.2	611.3	599.4
ν_7	460.4	636.7	328.1	627.7	621.1	616.3
ν_8	113.8	507.2	261.7	488.8	487.8	467.4
ν_9	332.2	416.3	-53.6	403.3	406.6	375.2

Table C23: Harmonic and anharmonic vibrational frequencies (in cm^{-1}) and IR intensities (in parentheses in km mol^{-1} computed at B3LYP/aTZ) for AlH_2OH

Table C24: Rotational Spectroscopic Constants for AlH_2OH with A- and S-reduced Hamiltonian spectroscopic constants

Const.	Units	atz	actz	awctz	F12-TZ	F12-TcC
A_e	MHz	111831.2	113041.8	113764.3	113030.1	113969.8
B_e	MHz	14092.8	14281.3	14360.4	14284.5	14414.8
C_e	MHz	12515.6	12679.5	12750.9	12681.8	12796.4
A_0	MHz	112481.5	113785.7	114372.2	113739.0	114717.0
B_0	MHz	14036.3	14224.4	14304.7	14230.6	14348.8
C_0	MHz	12445.9	12609.8	12680.2	12614.2	12719.3
A_1	MHz	111255.3	112509.0	113069.4	112456.8	113418.0
B_1	MHz	14012.5	14199.9	14280.2	14207.1	14324.9
C_1	MHz	12411.9	12574.6	12644.6	12579.6	12684.2
A_2	MHz	111583.3	112869.3	113402.7	112809.4	113783.5
B_2	MHz	14027.5	14215.7	14296.1	14222.3	14340.0
C_2	MHz	12429.4	12593.2	12663.0	12597.8	12702.4
A_3	MHz	111422.4	112717.1	113237.6	112647.7	113619.5
B_3	MHz	14030.5	14218.8	14299.5	14225.6	14342.3
C_3	MHz	12429.5	12593.5	12663.3	12598.0	12701.9
A_4	MHz	112578.5	113852.2	114424.5	113785.9	114729.6
B_4	MHz	13989.6	14174.9	14254.3	14178.5	14292.0
C_4	MHz	12373.7	12535.1	12612.9	12547.5	12649.0
A_5	MHz	113115.8	114411.9	114965.7	114353.3	115334.3
B_5	MHz	14039.4	14227.5	14309.0	14235.4	14351.0
C_5	MHz	12429.7	12592.6	12663.2	12597.9	12700.3
A_6	MHz	118897.0	118196.9	118809.0	118134.6	119151.8
B_6	MHz	14082.2	14271.1	14352.1	14278.1	14394.6
C_6	MHz	12447.2	12612.1	12673.8	12608.9	12712.1
A_7	MHz	109372.1	112887.4	113447.9	112851.2	113853.8
B_7	MHz	13994.8	14183.0	14264.3	14191.9	14307.9
C_7	MHz	12461.0	12625.5	12696.2	12630.3	12734.1
A_8	MHz	116113.9	117972.9	118733.0	117991.0	119343.4
B_8	MHz	14060.5	14247.9	14329.0	14255.6	14370.3
C_8	MHz	12437.4	12603.2	12673.9	12608.8	12713.0
A_9	MHz	109295.7	110141.9	110476.1	110039.3	110713.4
B_9	MHz	13977.1	14166.7	14246.8	14173.1	14283.7
C_9	MHz	12454.5	12619.2	12689.4	12623.9	12722.2

Table C25: Equilibrium, ground, and vibrationally-excited rotational constants AlH_2OH.

Table C26: A- and S-reduced Hamiltonian spectroscopic constants and dipole moment for AlH_2OH.

Const.	Units	atz	actz	awctz	F12-TZ	F12-TcC
Δ_J	kHz	15.036	15.322	15.332	15.105	15.260
Δ_K	MHz	3.650	3.801	3.871	3.824	3.896
Δ_{JK}	kHz	334.352	341.754	344.627	340.926	342.966
δ_J	kHz	1.825	1.866	1.867	1.848	1.867
δ_K	kHz	218.208	223.067	224.831	223.139	224.447
Φ_J	mHz	1.821	1.880	1.996	2.174	0.010
Φ_K	Hz	596.509	646.690	657.578	650.453	668.868
Φ_{JK}	Hz	4.304	4.421	4.477	4.473	4.194
Φ_{KJ}	Hz	−1.730	0.347	0.276	−0.360	2.660
ϕ_j	mHz	3.589	3.731	3.787	3.758	3.355
ϕ_{jk}	Hz	2.343	2.412	2.448	2.441	2.278
ϕ_k	Hz	190.594	196.802	199.485	197.500	197.768
D_J	kHz	14.163	14.425	14.429	14.207	14.355
D_{JK}	kHz	339.592	347.138	350.044	346.315	348.395
D_K	MHz	3.645	3.797	3.867	3.819	3.892
d_1	kHz	−1.825	−1.866	−1.867	−1.848	−1.867
d_2	Hz	−436.627	−448.626	−451.400	−449.064	−452.431
D_e	μHz	0.000	0.000	0.000	0.000	0.000
H_J	mHz	−8.660	−8.950	−8.944	−8.743	−10.282
H_{JK}	Hz	1.548	1.567	1.592	1.611	1.322
H_{KJ}	Hz	7.615	10.022	10.056	9.346	12.389
H_K	Hz	589.931	639.880	650.694	643.621	662.022
h_1	mHz	2.179	2.264	2.306	2.284	1.876
h_2	mHz	5.240	5.415	5.470	5.458	5.146
h_3	mHz	1.410	1.468	1.481	1.473	1.479
H_e	μHz	0.000	0.000	0.000	0.000	0.000
Dipole	D				1.21	

Table C27: Rotational Spectroscopic Constants for AlH_2OH with A- and S-reduced Hamiltonian spectroscopic constants *cont.*

Const.	Units	F12-TZR	F12-TcCR	F12-TcCR+TZ	Split Basis TcC	Split Basis TcCR
A_e	MHz	113030.1	113969.8	113969.8	113045.2	113045.2
B_e	MHz	14284.5	14414.8	14414.8	14285.9	14285.9
C_e	MHz	12681.8	12796.4	12796.4	12683.1	12683.1
A_0	MHz	113731.1	114650.1	114677.1	113754.4	113755.2
B_0	MHz	14230.5	14359.8	14358.7	14232.0	14231.0
C_0	MHz	12614.4	12727.4	12727.0	12615.5	12615.1
A_1	MHz	112450.8	113351.4	113374.0	112472.0	112475.4
B_1	MHz	14206.7	14335.8	14334.7	14208.5	14207.1
C_1	MHz	12579.7	12692.4	12691.8	12580.9	12580.4
A_2	MHz	112802.5	113713.6	113714.8	112824.5	112827.5
B_2	MHz	14222.2	14349.7	14350.0	14223.7	14222.7
C_2	MHz	12598.0	12709.6	12709.8	12599.1	12598.7
A_3	MHz	112641.2	113545.0	113545.2	112662.7	112666.5
B_3	MHz	14225.6	14354.3	14353.5	14227.0	14226.0
C_3	MHz	12598.3	12710.7	12710.1	12599.3	12598.9
A_4	MHz	113790.2	114694.7	114715.0	113800.2	113814.3
B_4	MHz	14180.3	14306.2	14304.1	14179.8	14180.5
C_4	MHz	12548.0	12658.7	12657.3	12548.7	12548.4
A_5	MHz	114334.3	115280.8	115304.2	114369.2	114358.9
B_5	MHz	14234.7	14364.1	14363.1	14236.9	14235.0
C_5	MHz	12597.8	12710.6	12710.1	12599.2	12598.3
A_6	MHz	118072.9	119009.3	119068.9	118154.0	118105.5
B_6	MHz	14277.1	14407.9	14405.1	14279.6	14277.1
C_6	MHz	12609.0	12722.3	12720.9	12610.3	12609.4
A_7	MHz	112836.7	113743.2	113803.4	112866.4	112865.5
B_7	MHz	14190.9	14318.3	14319.3	14193.3	14190.8
C_7	MHz	12630.7	12742.3	12743.8	12631.6	12631.0
A_8	MHz	117829.6	119026.1	119092.3	118017.8	117865.2
B_8	MHz	14254.8	14385.7	14383.0	14257.0	14255.5
C_8	MHz	12609.2	12724.3	12723.0	12610.1	12610.1
A_9	MHz	110223.5	110847.7	110890.4	110041.2	110237.6
B_9	MHz	14174.5	14305.4	14303.4	14174.5	14174.7
C_9	MHz	12624.6	12738.2	12737.2	12625.2	12625.1

Table C28: A- and S-reduced Hamiltonian spectroscopic constants and dipole moment for AlH_2OH *cont.*

Const.	Units	F12-TZR	F12-TcCR	F12-TcCR+TZ	Split Basis TcC	Split Basis TcCR
Δ_J	kHz	15.162	15.318	15.317	15.105	15.161
Δ_K	MHz	3.825	3.896	3.897	3.827	3.828
Δ_{JK}	kHz	333.994	337.006	336.833	341.050	334.099
δ_J	kHz	1.852	1.871	1.871	1.848	1.852
δ_K	kHz	219.412	221.206	221.076	223.193	219.453
Φ_J	mHz	2.206	1.229	1.153	2.160	1.965
Φ_K	Hz	662.296	690.483	687.690	651.461	662.729
Φ_{JK}	Hz	4.297	4.533	4.347	4.474	4.301
Φ_{KJ}	Hz	−1.829	−3.074	−555.521	−0.339	−1.630
ϕ_j	mHz	3.755	3.609	3.653	3.758	3.718
ϕ_{jk}	Hz	2.347	2.459	2.374	2.442	2.348
ϕ_k	Hz	191.243	193.367	193.075	197.598	191.383
D_J	kHz	14.279	14.426	14.426	14.207	14.278
D_{JK}	kHz	339.293	342.357	342.180	346.440	339.398
D_K	MHz	3.821	3.892	3.892	3.822	3.824
d_1	kHz	−1.852	−1.871	−1.871	−1.848	−1.852
d_2	Hz	−441.562	−445.898	−445.635	−449.144	−441.618
D_e	μHz	0.000	0.000	0.000	0.000	0.000
H_J	mHz	−8.386	−9.840	−9.575	−8.758	−8.630
H_{JK}	Hz	1.530	1.737	1.554	1.611	1.532
H_{KJ}	Hz	7.555	6.412	8.917	9.370	7.759
H_K	Hz	655.690	683.804	681.021	644.627	656.119
h_1	mHz	2.331	2.166	2.213	2.284	2.293
h_2	mHz	5.296	5.534	5.364	5.459	5.297
h_3	mHz	1.424	1.442	1.440	1.474	1.425
H_e	μHz	0.000	0.000	0.000	0.000	0.000

APPENDIX D

Copyright Releases

D.1 Copyright Release for Chapter 2

MDPI Open Access Information and Policy

All articles published by MDPI are made immediately available worldwide under an open access license. This means:

- everyone has free and unlimited access to the full-text of *all* articles published in MDPI journals;
- everyone is free to re-use the published material if proper accreditation/citation of the original publication is given;
- open access publication is supported by the authors' institutes or research funding agencies by payment of a comparatively low **Article Processing Charge (APC) (/about/apc)** for accepted articles.

Permissions

No special permission is required to reuse all or part of article published by MDPI, including figures and tables. For articles published under an open access Creative Common CC BY license, any part of the article may be reused without permission provided that the original article is clearly cited. Reuse of an article does not imply endorsement by the authors or MDPI. Furthermore, no special permission is required for authors to submit their work to external repositories. This policy extends to all versions of a paper: submitted, accepted, and published.

D.2 Copyright Release for Chapter 3

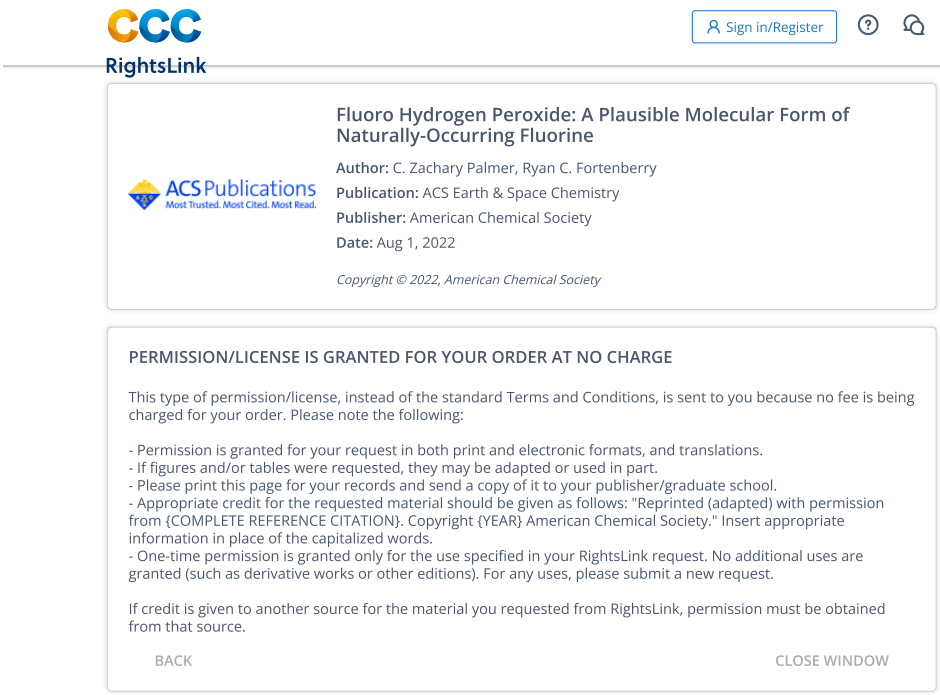

RightsLink

Sign in/Register

Fluoro Hydrogen Peroxide: A Plausible Molecular Form of Naturally-Occurring Fluorine

Author: C. Zachary Palmer, Ryan C. Fortenberry

Publication: ACS Earth & Space Chemistry

Publisher: American Chemical Society

Date: Aug 1, 2022

Copyright © 2022, American Chemical Society

PERMISSION/LICENSE IS GRANTED FOR YOUR ORDER AT NO CHARGE

This type of permission/license, instead of the standard Terms and Conditions, is sent to you because no fee is being charged for your order. Please note the following:

- Permission is granted for your request in both print and electronic formats, and translations.
- If figures and/or tables were requested, they may be adapted or used in part.
- Please print this page for your records and send a copy of it to your publisher/graduate school.
- Appropriate credit for the requested material should be given as follows: "Reprinted (adapted) with permission from {COMPLETE REFERENCE CITATION}. Copyright {YEAR} American Chemical Society." Insert appropriate information in place of the capitalized words.
- One-time permission is granted only for the use specified in your RightsLink request. No additional uses are granted (such as derivative works or other editions). For any uses, please submit a new request.

If credit is given to another source for the material you requested from RightsLink, permission must be obtained from that source.

BACK CLOSE WINDOW

© 2025 Copyright - All Rights Reserved | Copyright Clearance Center, Inc. | Privacy statement | Data Security and Privacy | For California Residents | Terms and ConditionsComments? We would like to hear from you. E-mail us at customercare@copyright.com

D.3 Copyright Release for Chapter 4

AAS PUBLISHING American Astronomical Society (https://journals.aas.org)

SUBMIT (HTTPS://JOURNALS.AAS.ORG/SUBMISSION/) |
AUTHOR TOOLS (HTTPS://JOURNALS.AAS.ORG/AUTHOR-RESOURCES/) |
ABOUT AAS JOURNALS (HTTPS://JOURNALS.AAS.ORG/WHY-AAS-JOURNALS/) |
POLICIES (HTTPS://JOURNALS.AAS.ORG/POLICIES/)

Navigate: AAS Journals

Home (https://journals.aas.org) › Author Instructions (https://journals.aas.org/author-resources/) › Article Publication Charges and Licensing Agreements

Article Publication Charges and Licensing Agreements

Publication fees are required for publication in the refereed journals of the American Astronomical Society (the *Astronomical Journal* (https://iopscience.iop.org/journal/1538-3881), the *Astrophysical Journal* (https://iopscience.iop.org/journal/0004-637X), *Astrophysical Journal Letters* (https://iopscience.iop.org/journal/2041-8205), the *Astrophysical Journal Supplement Series* (https://iopscience.iop.org/journal/0067-0049), and the *Planetary Science Journal* (https://iopscience.iop.org/journal/2632-3338)*)*. Please be aware that the journals do not receive direct funding from any external agencies.

Research Notes of the AAS (http://rnaas.aas.org/) and the *Bulletin of the AAS* (https://baas.aas.org/) are fully open access (OA) publications and have no article publication charges.

Note that, effective 1 January 2022, all AAS journals are fully open access.

For information about article publication charges and licensing agreements after 1 January 2022, please see our open access FAQ (https://journals.aas.org/oa/). Authors that have submitted prior to 1 January 2022 are subject to the old article publication charges. Please contact the editorial office at journals.manager@aas.org for details on the prior author publication fees.

D.4 Copyright Release for Chapter 5

THE UNIVERSITY of MISSISSIPPI

Charles Palmer <cpalmer5@go.olemiss.edu>

Thank you for your order with RightsLink / John Wiley and Sons

no-reply@email.copyright.com <no-reply@email.copyright.com> Wed, Feb 12, 2025 at 1:01 PM
To: cpalmer5@go.olemiss.edu

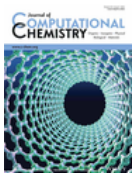

Thank you for your order!

Dear Mr. Charles Palmer,

Thank you for placing your order through Copyright Clearance Center's RightsLink® service.

Order Summary

Licensee:	Mr. Charles Palmer
Order Date:	Feb 12, 2025
Order Number:	5966611480858
Publication:	Journal of Computational Chemistry
Title:	Computing Accurate & Reliable Rovibrational Spectral Data for Aluminum-Bearing Molecules
Type of Use:	Dissertation/Thesis
Order Total:	0.00 USD

View or print complete details of your order and the publisher's terms and conditions.

Sincerely,

Copyright Clearance Center

customercare@copyright.com
https://myaccount.copyright.com

CCC RightsLink

D.5 Copyright Release for Chapter 6

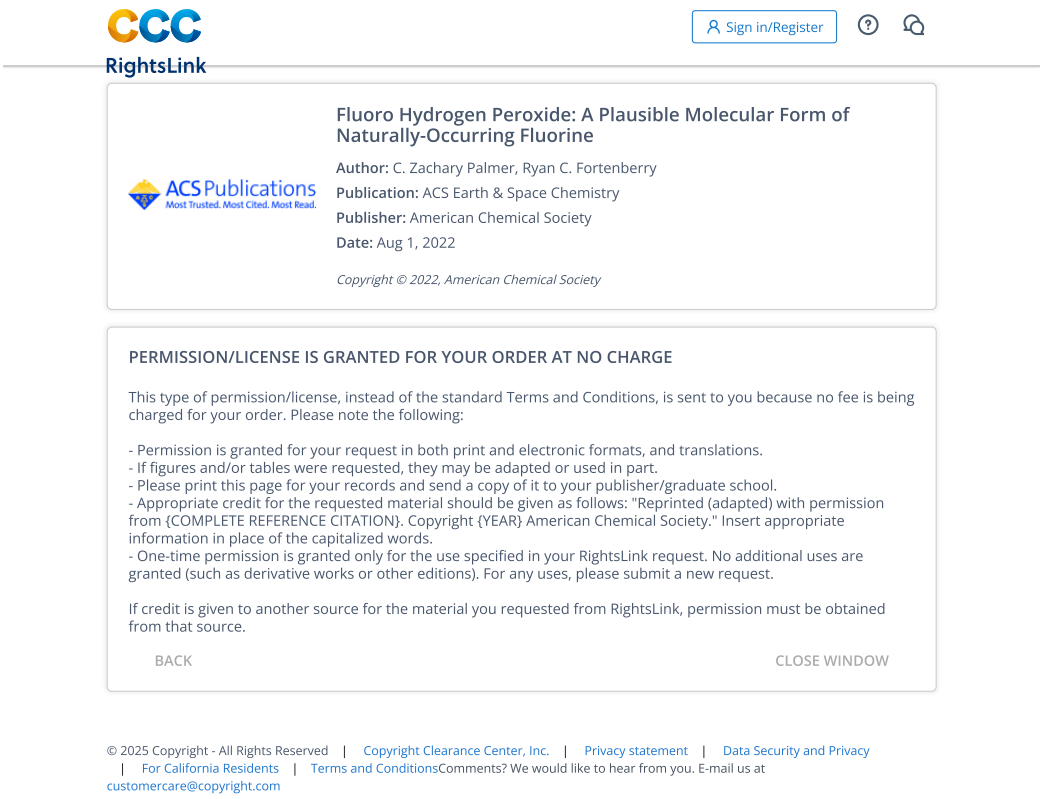

Figure D.1: [THIS IS A PLACEHOLDER UNTIL PAPER IS PUBLISHED]

VITA

Education

- B.S. in Chemistry, Georgia Southern University, July 2020

Published Research

15. "Investigating the Spectral Constants and Formation Pathway of Aluminum Nitrides from AlH and NH_3" **C. Z. Palmer**, J. A. Johns, R. C. Fortenberry. *J. Phys. Chem. A*, **2025**, (*submitted*).

14. "Pinpointing the CN stretch frequency of neutral cyano-polycyclic aromatic hydrocarbons: a laboratory and quantum chemical spectroscopic study of 9-cyanoanthracene" V. J. Esposito, P. Ferrari, **C. Z. Palmer**, C. Boersma, A. Candian, R. C. Fortenberry, W. J. Bauma, A. G. G. M. Tielens. *J. Phys. Chem. Lett.*, **2025**, 16(1296-1304)

13. "Computing Accurate Rovibrational Spectral Data for Relevant Aluminum-bearing Species in Interstellar and Atmospheric Chemistry" **C. Z. Palmer**, R. A. Firth, R. C. Fortenberry. *J. Comp. Chem.*, **2024**, 46(27524)

12. "Spectral Features for Systematic Aluminum Replacement in N_2H_2 and c-N_4H_4 Isomers" J. R. Dotson, **C. Z. Palmer**, R. C. Fortenberry. *J. Molec. Spectrosc.*, **2024**, 406(111956)

11. "Rovibrational Analysis of $AlCO_3$, $OAlO_2$, and $HOAlO_2$ for Possible Atmospheric Detection." R. A. Firth, **C. Z. Palmer**, J. S. Francisco, R. C. Forten-

berry. *J. Chem. Phys.*, **2024**, 160(214304)

10. "Reaction Pathway and Rovibrational Analysis of Aluminum Nitride Species as Potential Dust Grain Nucleation Agents." **OleRed**C. Z. Palmer, R. C. Fortenberry. *Astrophys. J.*, **2024**, 962:148

9. "Rotational Spectroscopic Characteriztion of [D_2,C,S] System: An Update from the Laboratory and Theory." N. Inostroza-Pino, V. Lattanzi, **C. Z. Palmer**, R. C. Fortenberry, T. J. Lee, P. Caselli, and D. Mardones. *Mol. Phys.*, **2023**, 122

8. "Spectroscopy and Photochemistry of OAlNO and Implications for New Metal Chemistry in the Atmosphere." V. Esposito, **C. Z. Palmer**, R. C. Fortenberry, J. S. Francisco. *J. Phys. Chem. A*, **2023**, 127(7618-7629)

7. "The Spectral Features and Detectability of Small, Cyclic Silicon Carbide Clusters." C. M. Sehring, **C. Z. Palmer**, B. R. Westrbook, R. C. Fortenberry. *Front. Astron. Space Sci.*, **2022**, 9(1074879)

6. "Fluoro Hydrogen Peroxide: A Plausible Molecular Form of Naturally-Occuring Fluorine." **C. Z. Palmer**, R. C. Fortenberry, *ACS Earth & Space*, **2022**, 6(2032-2040)

5. "Spectral Signatures of Hydrogen Thioperoxide (HOSH) and Hydrogen Persulfide (HSSH): Possible Molecular Sulfur Sinks in the Dense ISM." **C. Z. Palmer**, R. C. Fortenberry, J. S. Francisco, *Molecules*, **2022**, 27(10) 3200

4. "On the Formation and Spectral Signatures of Magnesacyclopropene (c-MgC_2H_2)." Kimberly N. Poland, **C. Z. Palmer**, A. Chard, S. R. Davis, R. C. Fortenberry, *J. Molec. Spectrosc.*, **2021**, 382(111514)

3. "Effect of 'X' Ligands on the Photocatalytic Reduction of CO2 to CO with Re(pyridylNHC-CF3)(CO)3X Complexes." H. Shirley, T. M. Sexton, N. P. Liyange, **C. Z. Palmer**, L. E. McNamara, N. I. Hammer, G. S. Tschumper, J. H. Delcamp, *Eur. J. Inorg. Chem.*, **2020**, 2020(1844-1851)

2. "Theoretical Rovibrational Characterization of the cis/trans-HCSH and H2SC Isomers of the Known Interstellar Molecule Thioformaldehyde." N. Inostroza-Pino, **C. Z. Palmer**, T. J. Lee, R. C. Fortenberry, *J. Molec. Spectrosc.*, **2020**, 369(111273)

1. "Rovibrational Considerations for the Monomers and Dimers of Magnesium Hydride (MgH_2) and Magnesium Fluoride (MgF_2)." **C. Z. Palmer**, R. C. Fortenberry, *J. Phys. Chem. A*, **2018**, 122(7079-7088)

Oral Presentations

- **C. Z. Palmer**, and R. C. Fortenberry, "Computational Chemistry & Undergraduate Research," Research Conference for High Schoolers, Oxford, GA, June 12, 2024.

Poster Presentations

- **C. Z. Palmer**, and R. C. Fortenberry, "Formation and Spectral Analysis of Larger Aluminum Nitride Clusters," ACS National Meeting Spring 2025, San Diego, CA, March 25, 2025.

- **C. Z. Palmer**, and R. C. Fortenberry, "Aluminum Nitrides as Dust Nucleating Species," Southeastern Regional Meeting of the ACS, Atlanta, GA, October 23, 2024.

- **C. Z. Palmer**, and R. C. Fortenberry, "Alternative Dust Grain Formation Pathways with Alane and Ammonia," ACS National Meeting Spring 2025, New Orleans, LA, March 19, 2024.

- **C. Z. Palmer**, and R. C. Fortenberry, "Alternative Dust Grain Formation Pathways with Alane and Ammonia," Origin and Fate of the Dust in Our Universe, Gothenburg, Sweden, September 26, 2023.

- **C. Z. Palmer**, and R. C. Fortenberry, "Alternative Dust Grain Formation Pathways with Alane and Ammonia," International Astronomical Union, Traverse City, MI, July 12, 2023.

- **C. Z. Palmer**, and R. C. Fortenberry, "Fluoro Hydrogen Peroxide and Other Substituted Peroxides as Sinks for the Elusive Fluorine and Sulfur Atoms," Southeastern Section of the American Physical Society, Oxford, MS, November, 2022.

- **C. Z. Palmer**, and R. C. Fortenberry, "Fluoro Hydrogen Peroxide and Other Substituted Peroxides as Sinks for the Elusive Fluorine and Sulfur Atoms," Southeastern Theoretical Chemistry Association, Atlanta, GA, May 18, 2022.

- **C. Z. Palmer**, and R. C. Fortenberry, "Fluoro Hydrogen Peroxide and Other Substituted Peroxides as Sinks for the Elusive Fluorine and Sulfur Atoms," Sanibel Symposium, St. Simons, GA, February 15, 2022.

Courses Taught

- UM: LIBA 150 (Interdisciplinary Science I) – Fall '24 & Spr. '25

Other Professional Experience

- UM: Graduate Teaching Assistant for General Chemistry I & II Laboratory (CHEM 115 & 116)
- UM: Graduate Teaching Assistant for Survey of Chemistry I Laboratory (CHEM 113)
- UM: Graduate Teaching Assistant for Physical Chemistry Laboratory (CHEM 331 & 332)
- UM: Graduate Teaching Assistant for Interdisciplinary Science I (LIBA 150)
- UM: Guest Lecturer for Physical Chemistry I (CHEM 331)

Students Supervised

- Jacob Johns, University of Mississippi, BS Chemistry, Expected 2025
- Jonathan Dotson, University of Mississippi, BA Chemistry, 2024
- Chris Sehring, University of Mississippi, NSF REU, Summer 2022 & 2023
- Rebecca Firth, University of Mississippi, NSF REU, Summer 2022

Awards

- Outstanding Student Poster Award for Exemplary Research, Spring National ACS Meeting, 2025
- Outstanding Student Poster Award for Exemplary Research, Spring National ACS Meeting, 2024
- Outstanding Early Physical Chemistry Graduate Student Award, University of Mississippi, Department of Chemistry & Biochemistry, 2022